HAL open science

Impact of the surrounding subduction zones on the tectonic evolution of the South China Sea

Sung-Ping Chang

To cite this version:

Sung-Ping Chang. Impact of the surrounding subduction zones on the tectonic evolution of the South China Sea. Earth Sciences. Université Paris sciences et lettres, 2020. English. NNT : 2020UPSLE038 . tel-03541984

HAL Id: tel-03541984

https://theses.hal.science/tel-03541984v1

Submitted on 25 Jan 2022

HAL is a multi-disciplinary open access archive for the deposit and dissemination of scientific research documents, whether they are published or not. The documents may come from teaching and research institutions in France or abroad, or from public or private research centers.

L'archive ouverte pluridisciplinaire **HAL**, est destinée au dépôt et à la diffusion de documents scientifiques de niveau recherche, publiés ou non, émanant des établissements d'enseignement et de recherche français ou étrangers, des laboratoires publics ou privés.

PSL UNIVERSITÉ PARIS

THÈSE DE DOCTORAT
DE L'UNIVERSITÉ PSL

l'École normale supérieure

Impact of the surrounding subduction zones on the tectonic evolution of the South China Sea

Impact des zones de subduction environnantes sur l'évolution tectonique de la Mer de Chine méridionale

Soutenue par

Sung-Ping CHANG

Le 09 06 2020

Ecole doctorale n° 560

STEP'UP

Sciences de la Terre et de l'Environnement et Physique de l'Univers de Paris

Spécialité

Sciences de la Terre et de l'environnement

Composition du jury :

Philippe HUCHON
Professeur, Sorbonne Université — *Rapporteur*

Frederic MOUTHEREAU
Professeur, Université Toulouse III-Paul Sabatier — *Rapporteur*

Javier ESCARTIN
Directeur de recherche, CNRS — *Examinateur*

Gwenn PERON-PINVIDIC
Professeur, Norges Geologiske Undersøkelse — *Présidente*

Geoffroy MOHN
Maître de conférences, Université de Cergy-Pontoise — *Examinateur*

Jean LETOUZEY
Chercheur émérite, Sorbonne Université — *Invité*

Manuel PUBELLIER
DR1, CNRS — *Directeur de thèse*

Matthias DELESCLUSE
Maître de conférences, École normale supérieure — *Co-directeur de thèse*

ENS | PSL

Acknowledgement

I would like to express my deepest gratitude to my supervisors, Manuel Pubellier and Matthias Delescluse, who guided this research into an accomplishment that I never imagined to have been clinched in three years. Having the privilege to stand on the shoulders of giants, I have discovered a new horizon. They were also acting like friends, who encouraged me and tolerated my stubbornness. Without their persistent help, the goal of this project would not be realized.

I have been benefited richly from the insightful discussions with Nicolas Chamot-Rooke, concerning marine geology and geophysics. His abundant experiences have also crafted one of the most important pillars to support this study.

I want to thank all the people whose assistance was a milestone in the completion of this project – Vivien Bailly, Chee Meng Choong, Ho-Han Hsu, Fathiyah Jamaludin, Char-Shine Liu, Geoffroy Mohn, Michael Nirrengarten, Jean-Claude Ringenbach, François Sapin, Benjamin Sautter, Chih-Chieh Su, and Jonny Wu. Also, Afiqah, Nabilah, and Sofiyah supported me considerably in the field. Their inputs have enriched this study.

I would also like to thank the members of my jury: Javier Escartin, Philippe Huchon, Jean Letouzey, Geoffroy Mohn again, Frédéric Mouthereau, Gwenn Péron-Pinvidic. The Covid-19 was a little obstacle but the discussion was fruitful yet. Your perceptive suggestions have polished my research and made it shiner.

I would love to thank the École Normale Supérieure and the CNRS to fund my research and travels between Europe and Asia. Moreover, the Malaysian Petroleum Management of PETRONAS provided the data in offshore Sabah through YUTP Project. This robust collaboration with Universiti Teknologi PETRONAS has been under a MoU for several years. Seismic profiles in the South China Sea were also provided by Guangzhou Marine Geological Survey in China.

I would like to express my sincere gratitude to the best people from the ENS and the IPGP – (in alphabetical order) Alexandre, Amin, Mme. Archat, Arefeh, Ariel, M. Bacha, Cédric Bailly, Cédric Bulois, Chao, Claire, Damian, Damien, M. Dubernet, Elenora, Eva, Han-Jun, Hélène Lyon-Caen, Hélène Rouby, Jan, Jara, Jean-Arthur, Jérôme, Jia-Lan, John Dale, Juan, Harsha, Kurama, Lavinia, Louise, Mme. Manchon, Manon Bouvard, Manon Dalaison, Mathieu, Meng-Lan, M. Oubellouch, Ouissem, Paoline, Pierre-Henri, Mme. Rialet, Sam, Samson, Simon, Ssu-Ting, Sylvain, Thomas Chartier, Thomas Ferrand, Valentin, Valentine, Zhi, and Zhi-Kai. Your friendship and kindness have colored my days in Paris and have smoothened my tough moments in the past years.

My wife, Chih-Yi Chiu, and our parents have been supporting me every single day, not because of what achievement I have but who I am. Additionally, Lok Man, Michael Chiu, Tien-Jen, Tong Wa, Yi-Chen, Yu-Chun kept me in mind no matter how busy they were.

Last but not least, while sailing on the ocean of knowledge, I thank God for every lightbulb moment to keep my passion for discovering the aesthetic earth.

RÉSUMÉ

Cette étude se concentre sur la configuration d'un exemple rare de l'ouverture d'un bassin sur la plaque plongeante d'une zone de subduction. Les étapes, la naissance et la cessation de l'activité du bassin de la mer de Chine méridionale (MDC) au Cénozoïque semblent être liées à la disparition de la Proto Mer Chine du Sud (PMDC), par subduction à Bornéo et à Palawan. Cependant, les mécanismes régissant les forces liées au système de subduction sont encore mal contraints. La MDC, étroite, permet d'établir une corrélation aisée en termes de remplissage sédimentaire, de style structural et d'activité magmatique. Les études régionales sur la base de données sismiques, dont le premier profil académique couvrant les marges opposées (ENS-GMGS), combinées à l'observation sur le terrain permettent de comprendre la relation entre l'ouverture océanique et la zone de subduction adjacente.

L'étirement et l'amincissement de la croûte continentale de la MDC se sont traduits par un rifting et un breakup diachrones, d'Est en Ouest, à mesure qu'avançait le propagateur. Pour illustrer les géométries précédant l'éclatement des marges de la MDC, nous restaurons deux sections conjuguées près de la première anomalie magnétique océanique. La configuration COT montre non seulement l'hyper-extension, mais apparaît également comme ayant une forme de losanges contrôlés par des segments abrupts N-S et des segments hyper-étirés E-W. La variation spatiale des structures crustales enregistre une extension initiale N-S simultanément avec la première phase d'accrétion dans l'est de la MCS, et un changement de direction d'extension peu de temps après (~23Ma) vers le NW-SE. Pendant la période post-accrétion océanique, images sismiques montrent qu'un soulèvement local sur quelques kilomètres de diamètre s'accompagne de magmatisme, ce qui témoignerait de périodes de subsidence épisodique à l'échelle régionale.

Cependant, une collision amorcée depuis la fin de l'Oligocène par la fin the la subduction de la PMDC, est marquée, outre des dépôts de delta, par des mélanges principalement sédimentaires argileux accumulant les résidus de l'érosion des zones émergées pendant la collision. Cette unité a été occasionnellement remontée à la surface et les strates sus-jacentes se déforment en synclinaux et anticlinaux circulaires. Je soupçonne donc que le mécanisme d'exposition du mélange impliquait un processus diapirique. L'ensemble du processus illustrerait ainsi une évolution tectonique impliquant une argilocinèse autour de la période syn et post-collision du nord de Bornéo, délimitant un âge de fin d'orogenèse synchrone de la fin de l'accrétion océanique de la MDC, il y a 16 Ma.

L'évolution du rifting, de la propagation et de la cessation du rifting en mer de Chine méridionale semble donc être contrôlée par l'effet de la subduction de la PMDC. Sa fermeture subit en outre une plus longue période de raccourcissement à Palawan et Sabah où le

domaine océanique est large - croûte continentale nulle ou très limitée - alors que le raccourcissement est limité à la pointe du bassin dans la région du Sarawak, ou la PMDC n'était qu'un rift continental fortement sédimenté (pas d'ophiolite présente). L'hétérogénéité lithosphérique de la plaque inférieure (croûte continentale épaisse au sud et mince à océanique au nord) a induit une rotation dans le sens antihoraire de la subduction, alors que simultanément, la MDC changeait, elle, d'une extension passant de NS à NW-SE à 23Ma. La lithosphère de la PMDC s'est finalement rompue au Miocène supérieur pour induire du magmatisme dans la marge, une forte subsidence, et enfin des intrusions magmatiques locales dans la MDC pendant la période post-rifting, suggérant que la lithosphère détachée a provoqué une remontée de matériel mantellique profond vers la surface. Cette évolution reflète la configuration tectonique deux marges opposées, sous l'influence des forces en champ lointain d'une subduction voisine.

MOTS CLÉS

Mer de Chine du Sud; Proto Mer chine du Sud; Marge déchirée; Subduction; Géophysique marine; Géologie

ABSTRACT

This study focuses on the tectonic configuration of a rare example of the subduction-related opening on the downgoing plate of a subduction zone. The birth, the stages, and the cessation, of activity of the South China Sea (SCS) basin in Cenozoic seem to be related with the decay of the Proto-South China Sea (PSCS), by subduction in Borneo and Palawan. However, the mechanisms are still poorly constrained in terms of leading parameter and fundamental mechanism. Being narrow, the SCS margin offers the advantage of easily feasible correlation of sedimentary infill, structural styles and magmatic activities. The comprehensive and regional tectono-stratigraphic studies on subsurface seismic data and field observation could help better understanding the genetic relation between the ocean opening and the adjacent subduction zone.

The SCS continental crust stretching and thinning by ubiquitous large extensional detachment faults were expressed in a diachronous rifting and breakup, initiated in the east while rifting continued in the west until the propagator's arrival. To illustrate the pre-breakup geometries of the southwestern SCS margins, we restore two conjugate sections near the first oceanic magnetic anomaly. The COT configuration, not only illustrates local asymmetrical hyper-extension, but also appears in map view to have a rhomb-shape controlled by N-S abrupt segments and E-W hyper-extended ones. The spatial variation of the crustal structures records an initial N-S extension simultaneous with the first phase of seafloor spreading in the eastern SCS, and a significant change of extensional direction shortly later (circa 23Ma) to NW-SE. During the post-spreading period, in the ocean floor, few key seismic images show that the local uplift in diameter of few kilometers goes with important magma production, interestingly within an episodic subsidence period at regional scale. This large global subsidence is anomalous compared to the theoretical thermal subsidence of post-rifting basins.

Meanwhile, collision initiated since Late Oligocene in the PSCS, and mélange and shale-prone delta deposits characterize the shallow part of the accretionary wedge. This unit was occasionally brought to the surface and the overlying strata were deformed as circular synclines and anticlines. I, therefore, suspect that the mechanism of exposing the mélange involved a diapiric process that pushed this low viscosity material upward. Accordingly, the entire process illustrates a tectonic evolution involving shale tectonics from the end of the collision to the post-collision setting of northern Borneo, delineating an age of termination of orogeny, when the seafloor spreading also ceased, at ca. 16 Ma.

The evolution of the rifting, spreading and cessation of rifting in the South China Sea seems to be controlled by the effect of subduction of the PSCS margin. The closure of the PSCS underwent a longer period of shortening in front of Palawan and Sabah where the oceanic domain is wide – none or very limited continental crust - whereas we had a limited shortening to the tip of the basin in the Sarawak region. The lithospheric heterogeneity of lower plate in the PSCS margin (thick continental crust in the south and thin one to oceanic in the north)

induced a counterclockwise rotation off the subduction zone, and simultaneously, a change of the extensional direction from N-S to NW-SE in the contiguous SCS margin around 23Ma. The slab ultimately broke off in the Late Miocene resulting in large plutons along the PSCS margin in the vicinity of Borneo and Palawan. In the SCS, we also see local magmatic intrusions and dramatic subsidence during the post-spreading period. This suggests a slab detachment which provoked deep mantle upwelling to the surface. This dual tectonic evolution on two opposite margins therefore illustrates how far-field subduction process may impact the regional tectonics.

KEYWORDS

South China Sea; Proto-South China Sea; Rifted margin; Subduction; Marine geophysics; Geology

摘要

南中國海被認為是少數案例位於隱沒帶之上覆板塊的拉張盆地，從拉張作用的起源到終止，南中國海（南海）的大地構造演化皆強烈受到古南中國海（古南海）的隱沒作用影響。然而，這兩個被動與主動邊緣之間相對比的地質事件，以及區域性的地體動力與大地構造的機制仍然缺乏充分了解。固本研究利用構造地層學（tectono-stratigraphy）分析對比多頻道震測剖面（multichannel seismic, MCS）與野外露頭的觀察。利用南海與古南海的研究，提供詳細橫跨兩個邊緣的地層對比、地質構造描述以及岩漿作用。嘗試了解海盆擴張與比鄰的隱沒作用之間的關聯。

南海大陸地殼的拉張與剪薄作用受到底拖（detachment）斷層主導，並且可將同拉張地層區分 syn-rift I 和 syn-rift II 兩個單位。syn-rift II 的底部與大陸地殼破裂（breakup）的年代皆從南海的東部開始，往西南部越年輕，在地層表上形成不等時（diachronism）的現象。本研究描繪了西南部的南海大陸地殼破裂前的地殼構造，重建到此地區最早海洋磁力異常條帶的位置。兩條剖面展現同張裂的沉積層厚度有側向變化，較厚的沉積盆地呈現菱形狀的形貌，暗示受到南北向平移斷層的張裂盆地（pull-apart basin）。此南北向的拉張方向持續到陸殼破裂前（約 20 百萬年前），伴隨的海底擴張方向則變成西北-東南向。在後拉張時期的海洋地殼與沉積盆地中皆出現小規模的岩漿活動，岩漿的侵入在震測剖面上顯示地殼與上覆的沉積物受到伴隨的抬升作用。此岩漿作用導致在後張裂時期的熱沉降呈現多次事件，並總沉降量也異常高於理論的沉降值。

在古南海的主動大陸邊緣中，大陸地殼在晚漸新世開始隱沒，開始碰撞造山運動。在淺層的增積岩體主要以泥質的混同層與三角洲沉積物組成，並在南海南端覆蓋在同張裂地層之上，成為與南海被動大陸邊緣地層對比的重要指標層。本研究在震測剖面中辨識一塑性變形的泥灌入體，並透過野外觀察確認其岩性為基質支持的混同層，確認碰撞作用在 14 百萬年前左右結束。在後碰撞時期的泥灌入體持續活動，活動的時間點與沙巴的京那巴魯山（Mount Kinabalu）的岩漿入侵年代一致。此抬升作用影響上覆的地層，並沿著泥質的混同層變形，地層呈現相斜與背斜型的構造特徵。

本研究發現南海海底擴張方向的改變可與婆羅洲的逆時鐘旋轉時間對應，並兩者地質作用皆在中中新世終止，顯示被動大陸邊緣的南海與古南海的主動大陸邊緣相互影響。本研究提出隱沒帶的岩石圈有側向變化有關。在 23 百萬年前，巴拉望與婆羅洲北部地區的下伏板塊為海洋岩石圈，持續進行隱沒作用。然而在婆羅洲南部下伏板塊以大陸岩石圈為主形成碰撞造山運動，導致隱沒帶引發逆時針的旋轉，影響南海的海底擴張作用從南北擴張方向漸變成西北-東南向。此下伏板塊最終在晚中新世拆離沿著隱沒帶形成大量的岩漿入侵。南海同時也形成許多後擴張時期來自深部地函的岩漿活動，並可能與板塊拆離和隨後的板塊沉沒導致岩漿作用有關。此研究描繪出兩種不同類型的大陸邊緣受到隱沒作用影響，兩邊的地質作用可以相互對比。

關鍵字

南中國海、古南中國海、被動大陸邊緣、隱沒作用、海洋地質、地質

Contents

Contents 1
CHAPTER 1. Introduction 3
1.1 Marginal seas opening: two types of setting 4
1.2 Subduction-related forces, V-shaped opening and closure, implications on lateral variation 9
1.3 Marginal seas in SE Asia: examples of recent analogues 11
1.4 Problem statement 14
1.5 Thesis structure 14
CHAPTER 2. Geodynamic background of SE Asia 17
2.1 Subducting plate and marginal basins in SE Asia 17
2.2 Crustal evolution prior to basin opening 23
2.2.1 Cretaceous Yanshanian Orogeny in South China 27
2.2.2 Reactivation of structures and mountain collapse 28
2.3 Rift margin developing along inherited structures 33
2.3.1 Crustal structure of SCS Margin 36
2.3.2 Differences between N and S margin 45
2.4 Closure of PSCS: accretionary wedge, fold-and-thrust belt 49
2.4.1 Active subduction-collision boundary in the SCS 49
2.4.2 The inactive subduction-collision zone of the PSCS 52
2.4.3 Relics of subduction: the igneous rocks in the PSCS 62
2.4.4 The deep tomography image of the PSCS slab 65
2.5 Objectives: tectonic link between the SCS and the PSCS 67
CHAPTER 3. The crustal architecture of the southwestern South China Sea: implications on breakup setting 71
3.1 Introduction 71
3.2 Geological Background 74
3.3 Data acquisition and processing 79
3.4 Rifting architecture in the SW South China Sea 82
3.4.1 East Vietnam-South Hainan Margin of the SW sub-basin 82
3.4.2 Northwest Borneo margin of the SW Sub-basin 87
3.5 COT configuration prior to the break-up 91
3.5.1 N-S trending segments of the margin 92
3.5.2 E-W trending segments of the margins 94
3.5.3 Lateral variation of COT structures 98
3.6. Discussion 101
3.6.1 Breakup process in the SW margin 101
3.6.2 Implication for the margin configuration just before breakup 103
3.7 Synthetic rifting evolution in the South China Sea 105
3.8. Conclusion 109
CHAPTER 4. Collision, mélange and circular basins in north Borneo: a genetic link? 113
4.1 Introduction 113
4.2 Geological Background 115
4.3 Geological observations 122
4.3.1 Integration of offshore and onshore multichannel seismic profiles 122

4.3.2 Onshore subsurface field observations 129
4.3.3 Morphological expression of the deformation 143
4.4 Different significances of the mélange of Kudat Peninsula 145
4.5 Discussion 147
4.5.1 Mélange and the termination of the orogeny 147
4.5.2 A review of the mélange in Sabah 152
4.6 Conclusion 156
CHAPTER 5. Late Miocene vertical movements; Slab detachment and plumes consequence 157
5.1 Post-rift thermal subsidence 157
5.2 Post-spreading magmatism in the SCS 159
5.3 Thermal subsidence post-rift succession 162
5.4 Post-spreading uplifts and intrusions 166
5.5 Discussion and conclusion 171
Chapter 6. Discussion 173
6.1 Introduction: recalling the main relevant observations in the SCS and Borneo 173
6.2 Correlation of SCS and PSCS 174
6.2.1 Paleogene: N-S extension and N-S Subduction 176
6.2.2 Early Miocene (23-16 Ma): collision-induced counterclockwise change of direction 182
6.2.3 Middle Miocene to present day (16-0 Ma): regional subsidence and local vertical intrusion 194
6.3 Geometry of PSCS Margin 208
6.3.1 Shortening a V-shaped margin 209
6.3.2 Subduction polarity of the PSCS 212
6.3.3 Mesozoic ophiolite in Borneo 214
Conclusion 217
Reference 219
Appendix 239
A.1 Re-interpretation of MCS profiles in Pearl River Mouth Basin, Phu Khanh Basin, and Nam Con Son Basin 240
A.2 Bio-stratigraphy results in Kudat Peninsula 241
A.3 Sediment analyses in sedimentary mélange 247

CHAPTER 1. Introduction

During plate convergence, subduction zones form at the expense of basins floored by oceanic crust or thinned continental crust. There, shallow sediments blanketing the oceanic crust are involved into the accretionary wedge whereas the lithosphere is driven into the mantle and sinks. As light continental material from drifted blocks or from the conjugate margin arrives, the buoyant lithosphere resists the penetration so that rocks gets stacked and are later exhumed to the surface; thus, creating a mountain belt around the suture zone. The forces driving the subduction, chiefly traction, may affect neighboring regions, inducing the birth of new basins and even oceans. However, the leading forces and parameters which control the opening are difficult to evaluate in large deformed zones, and correlation of boundary forces across large oceans are also uncertain because the opposite margins are far apart.

In past few decades, paleo-geography and plate reconstructions attempted to illustrate the earth evolution through geological times. However, the ancient cases, based on crumpled and crushed strata in the convergent margins, lack the clear traces of the vanished slab to reconstruct the entire process. For subduction zone, boundary forces such as slab pull, ridge push, and mantle convection have been proposed to establish geodynamic settings, but many uncertainties still remain due to poor understanding of the interactions between oceans evolution and mountain building.

Marginal seas are among the most useful tools to approach the mechanism of plate tectonics. They are often formed and deformed by the interactions with adjacent boundary forces, for instance, trench retreat, block rotations or collision (Zhou, 2014; Chenin et al., 2017). Regional-scale and short-lived tectonic processes are distinctively observe in spatial and temporal variations. Their thermal condition and heterogeneous lithospheric structure within a narrow belt may dominate the processes of opening and closure which may not be seen properly in large ocean margins. These are sensitive to the boundary forces and have unique features in the convergent and divergent settings. They are therefore good material to examine the interaction between tectonic forces and deformation.

1.1 Marginal seas opening: two types of setting

We therefore need to explore the state of the crust and its evolution during the extension of marginal basins. Continental extension may be due to mantellic processes such as mantle plumes and are not the focus of this work. In most region, convergence results in compression, deforms and thickens the lithosphere with its overlying sediments. In the framework of this convergence, extension becomes the principal stress in some region, especially in the back-arc region of the upper plate (Karig et al., 1978; Taylor, 1979). This extensional movement is observed in several plate convergence margins. If most basins and seas open initially in convergent or very oblique tectonic environment within the upper, the lower plate might be impacted as well. We therefore discriminate two types; supra-subduction and subducting-plate basins, based on the position of the developing extensional basins. The genetic boundary forces are mainly slab retreats and slab pull respectively (Figure 1- 1).

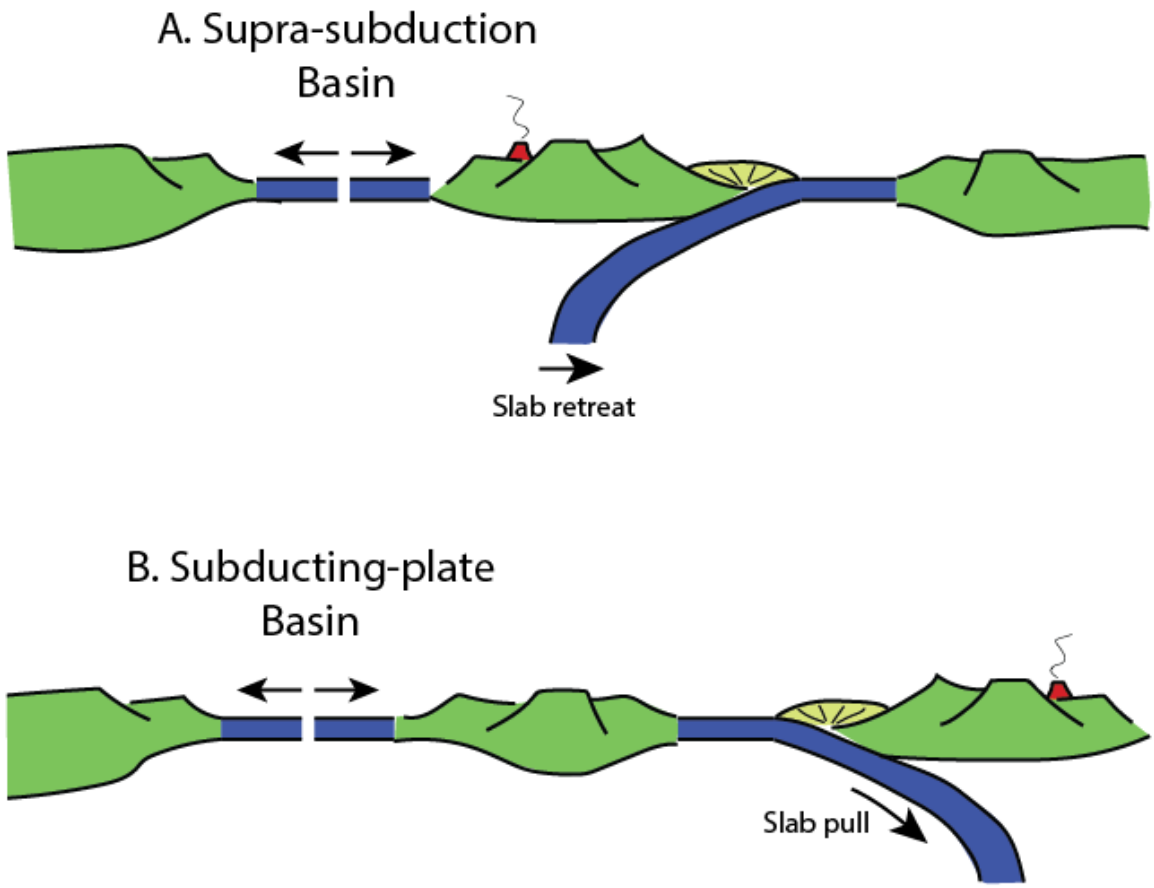

Figure 1- 1 Conceptual models describing two main types of genetic forces, which are induced by the subducting plate, and create extensional basins. The main different relies on the extension taking place in either (A) overriding or upper plate or (B) subducting or lower plate.

The Type A develops along the upper plate, and is the classical as the back-arc basin. The slab retreat leads migration of the trench and the cause of back-arc extension (Figure 1- 2); however, several mechanisms proposed for back-arc extension include subduction-induced mantle flow (Sleep and Toksoz, 1971; Schellart and Moresi, 2013), slab-rollback-induced trench suction at the subduction zone interface (Shemenda, 1993) and overriding plate collapse due to excess potential energy (Gautier et al., 1999)(Figure 1- 3). This extension initiates within the volcanic arc and forms a back-arc basin. Many examples exist in the western Pacific Ocean (Karig et al., 1978; Jolivet et al., 1989; Rangin et al., 1990).

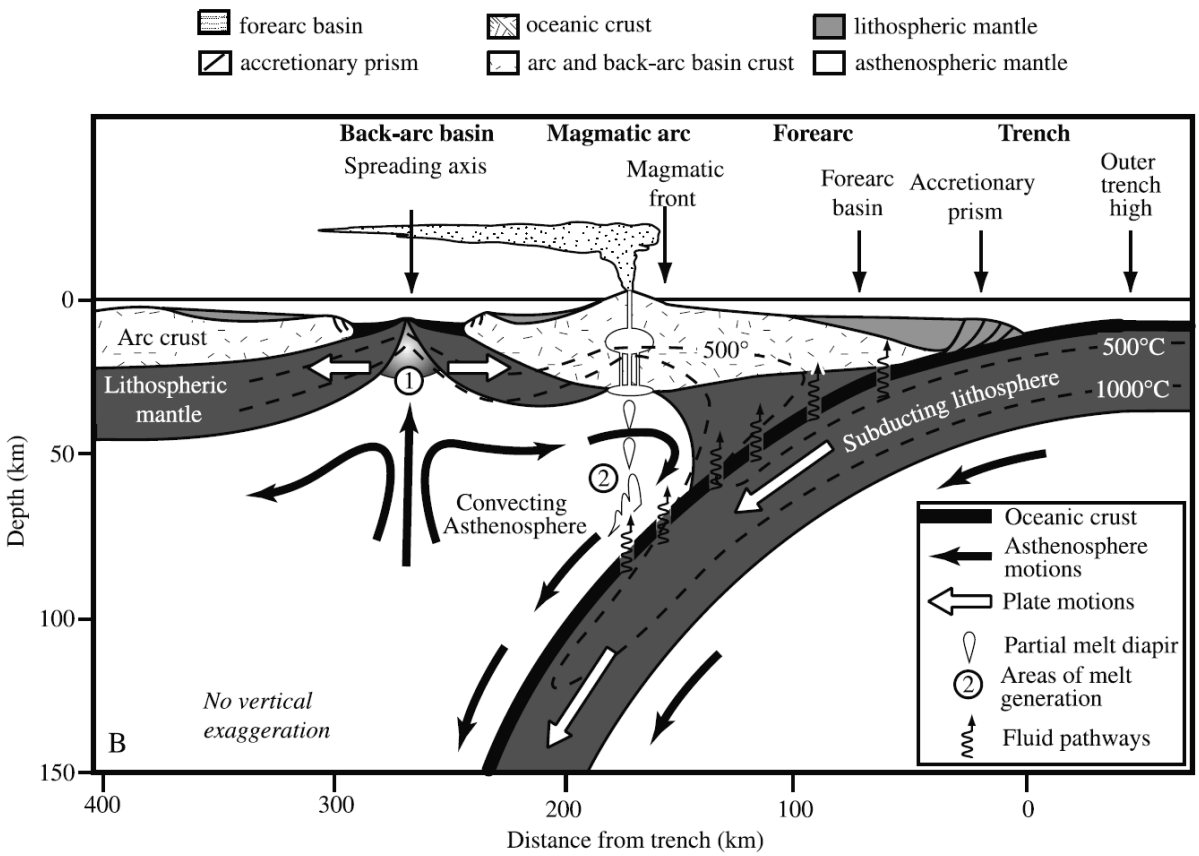

Figure 1- 2. An extension environment in a type-A configuration (Stern, 2002). The subduction wedge introduces the asthenosphere flows and diverge behind the volcanic arc to produce the "back-arc" extension.

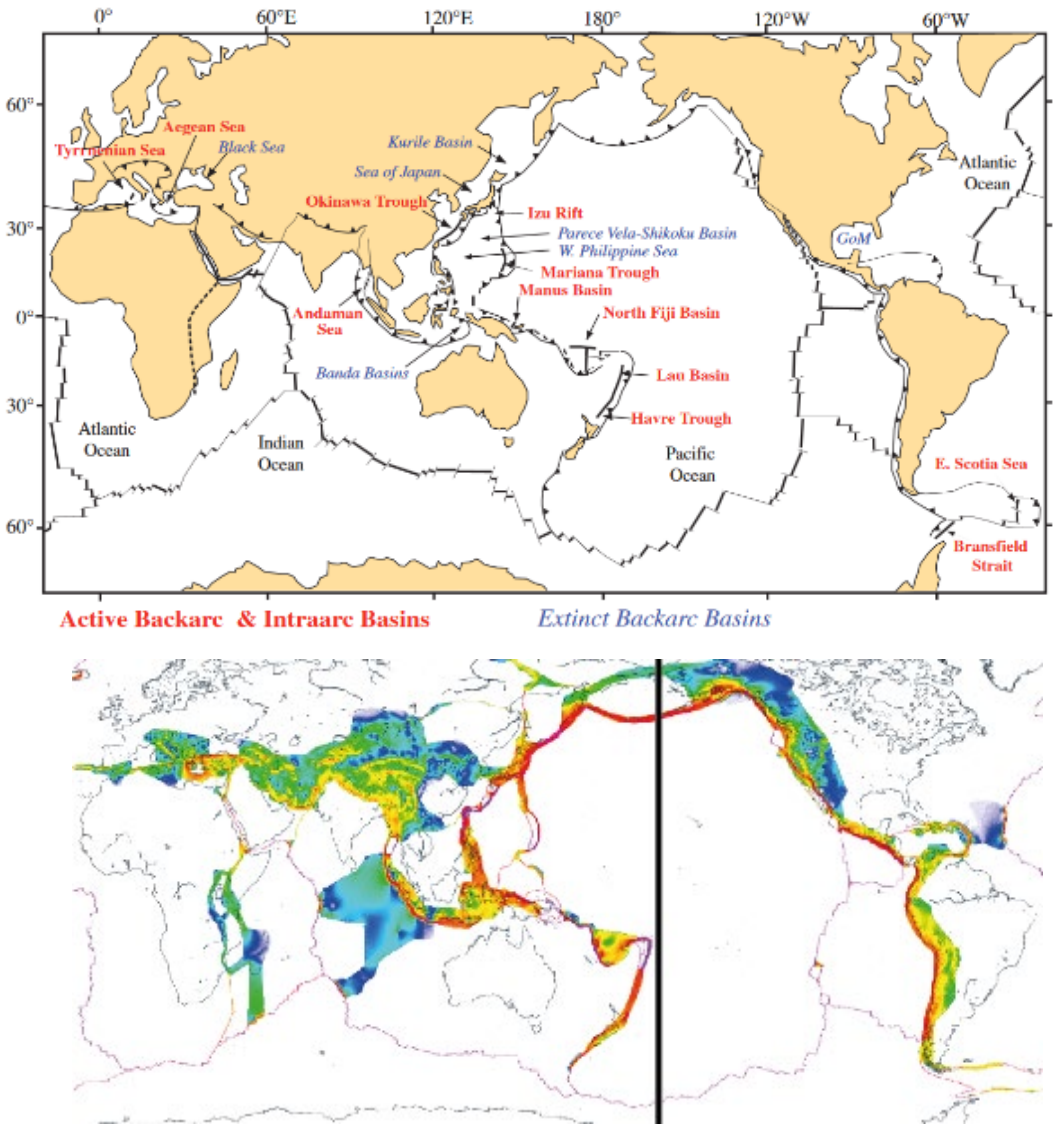

Figure 1- 3 (Top) Tectonic map and distribution of back-arc basins in the vicinity of subduction or collision zone (Stern and Dickinson, 2010). (Bottom) Strain rate along the tectonic plate boundaries. Extension zones are very narrow indicating more localized deformation whereas convergent zones result in deformation zones which vary in width as shown by the distribution of the strain rate. They indicate that more complex processes are involved including opening and closure of marginal basins such as back-arc basins. Figure from UNAVCO, https://gsrm2.unavco.org/gsrm2.html).

Oppositely, the Type B extensional basins should develop on the lower plate (Figure 1- 4). Indeed, most of the lower plates document the extensional stress induced by the plate bending or flexure. However, the trench pull invoked for the stretching of the upper plate may also apply to the downgoing plate. This is rarely reported for the development of ocean in the present–day geodynamic settings but is invoked at larger scale for the paired Paleo-Tethys/Neo-Tethys based on the observation of many extensional basins (Stampfli and Borel, 2002). During the

closure of the Tethys ocean, the southern margin (Gondwana) was experiencing rifting that formed the Neo-Tethys and allowed small fragments or slivers to separate and drift away toward the north (Figure 1- 4). Consequently, the Paleo-Tethys was in the process of closure meanwhile the Neotethys was created between the fragment and the main block. We will further see similar process for the opening of the SCS as the PSCS was closing. The South China Sea is one of the basins opened in this context, although there are other alternative tectonic models in debate (Tapponnier et al., 1982; Peltzer and Tapponnier, 1988).

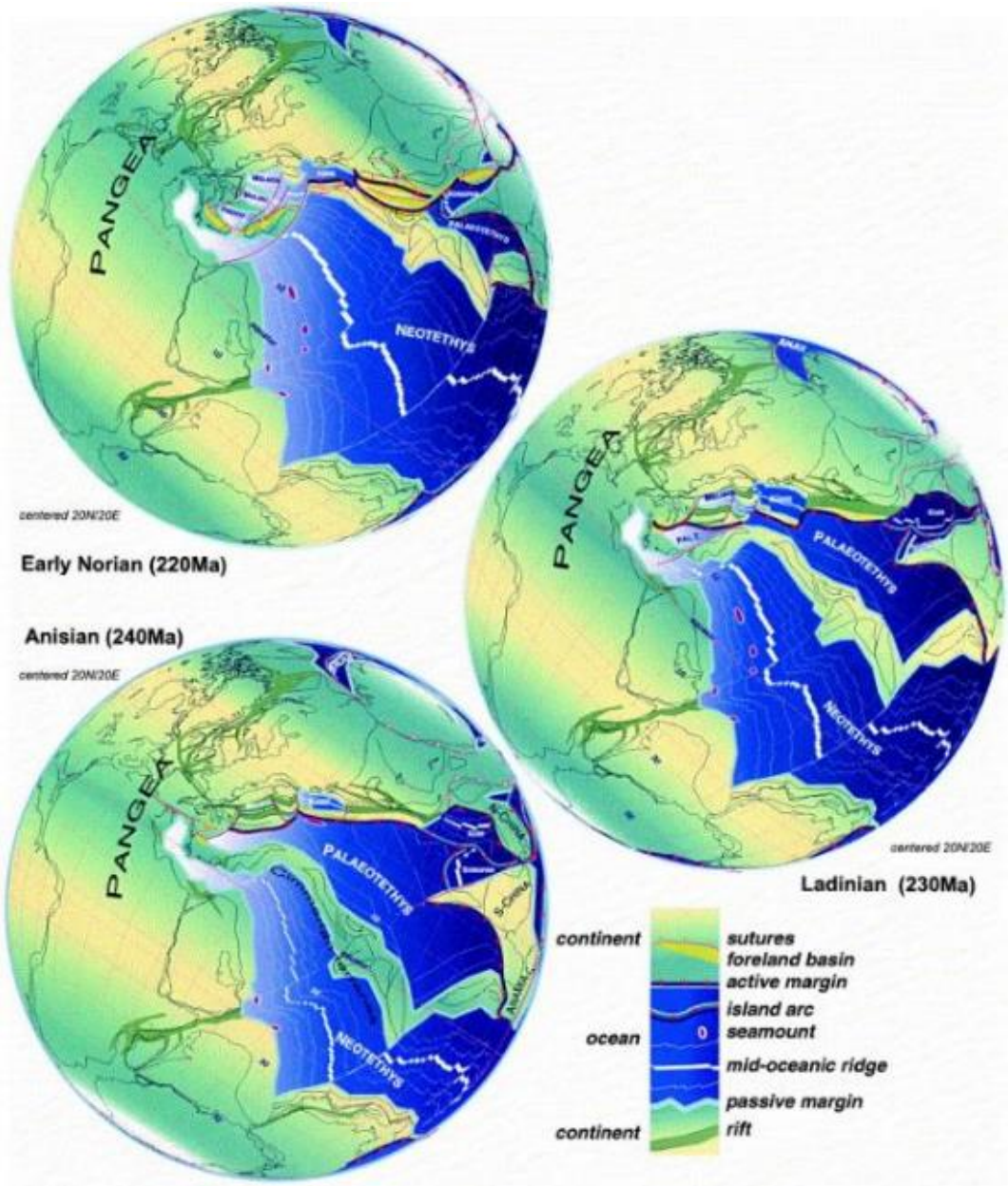

Figure 1- 4 Example of type B extension along the margin of the Pangea (Stampfli and Borel, 2002). The neo-Tethys opened initially at the lower plate and coeval with the closure of the paleo-Tethys.

When reviewing the marginal basins of the world, it appears that most of them have actually opened as a “V-shape” (Figure 1- 5); the cylindrical opening being in fact a special case. Some examples have been very much explored such as the Woodlark basin (Taylor et al., 1999), the South China Sea, or the Gulf of Aden (Manighetti et al., 1997; Huchon and Khanbari, 2003).

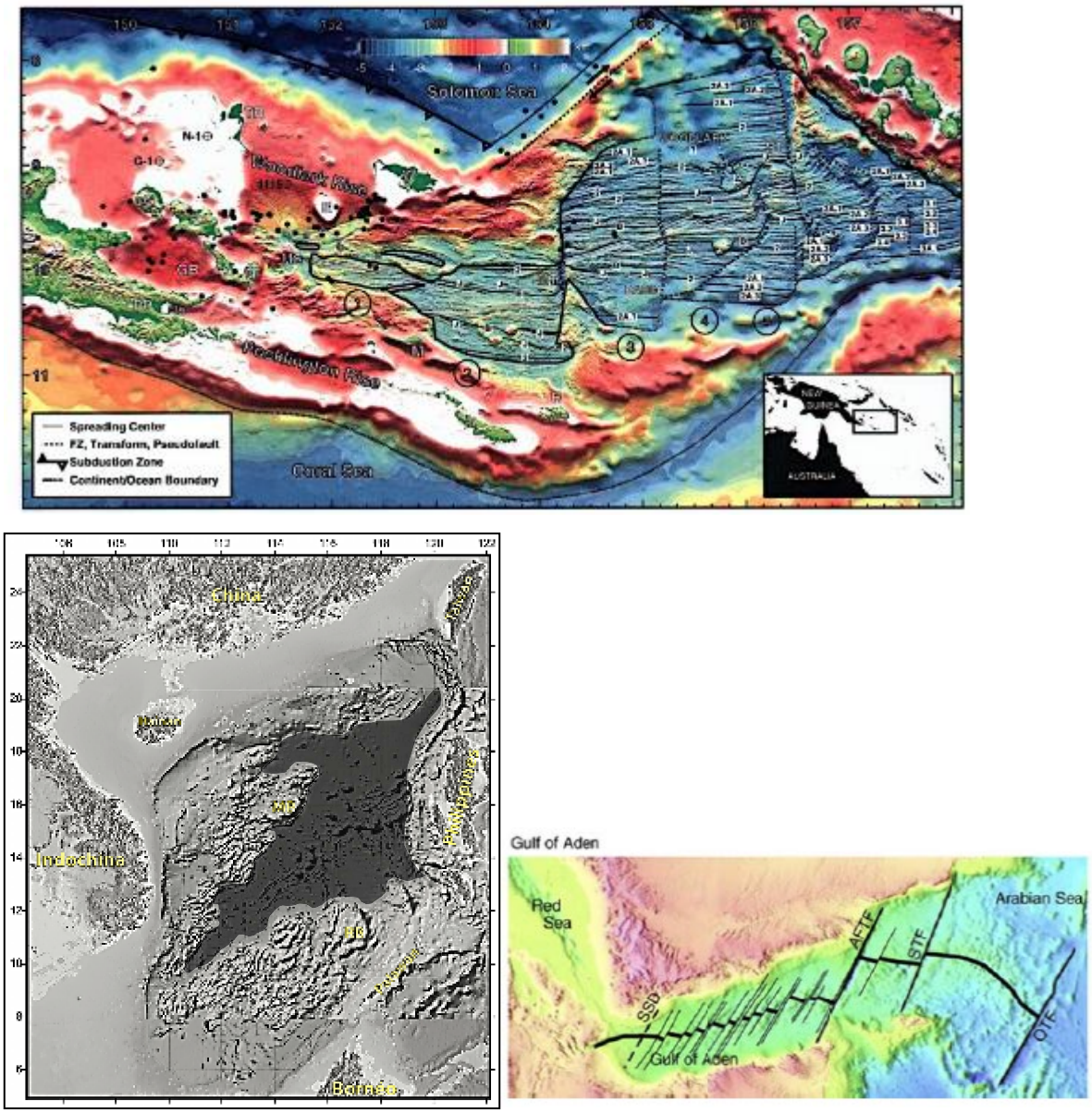

Figure 1- 5. Detail of the Woodlark basin at the tip of (upper) New Guinea Island (Taylor et al., 1999), (lower left) the South China Sea (Savva, 2013) and (lower right) the Gulf of Aden (Manighetti et al., 1997; Huchon and Khanbari, 2003). The tip preserved the location of the propagators which are the latest location of breakup and cessation of the seafloor formation.

1.2 Subduction-related forces, V-shaped opening and closure, implications on lateral variation

We thus need to recall the importance of the subduction in terms of forces (Figure 1- 6). The negative buoyancy of the lithosphere at the subducting front, and the density increase due to the dehydration, drags the subducting plate to the front, despite the mantle resistance from the surrounding mantle. Friction also exists at the interface between the two plates, allowing the strain to accumulate and subsequently be released during the co-seismic periods. In the asthenosphere, the mantle convection contributes to coupling forces at the interface of lithosphere and asthenosphere. Convection flows may stall at the corner of the subduction wedge beneath the overriding plate, inducing poloidal flows due to down-dip convection along the surface of the subducting plate, whereas horizontally toroidal flows are related to the trench migration along the slab edge (Figure 1- 6). We may have to invoke these processes when discussing possible asthenospheric windows in Borneo during the last tectonic events.

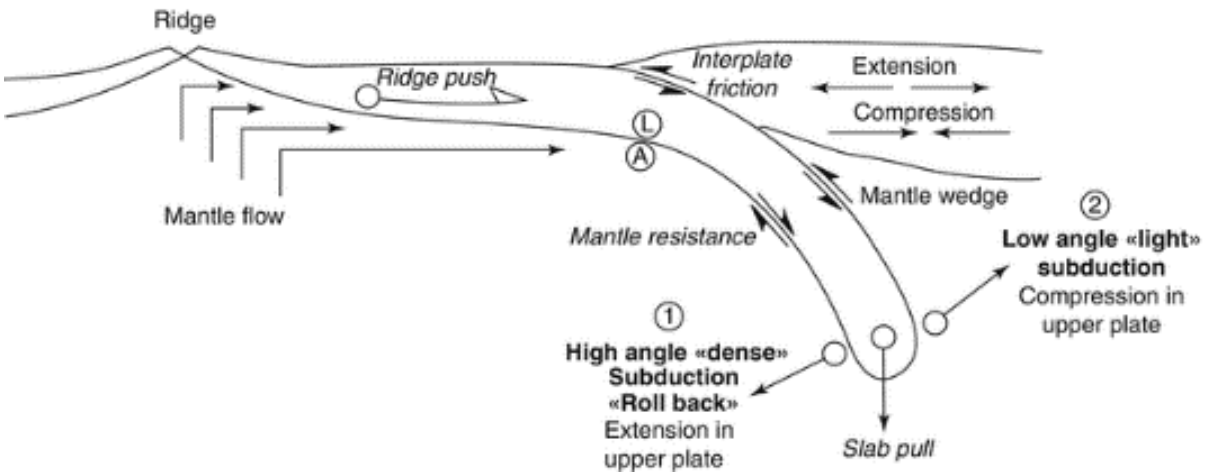

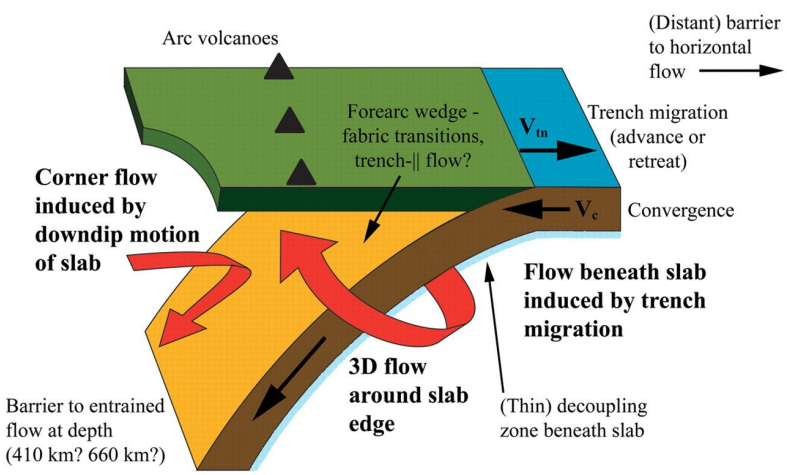

Figure 1- 6 (Upper) Driving forces prompted by mantle convection in convergent and divergent tectonic margins. More comprehensive forces display along a subducting slab in the shallow depth (Schulmann and Whitechurch, 2014). (Lower) subduction-related forces in the deep asthenosphere illustrate poloidal and toroidal flows induced by the subducting slab distribute along the slab (Long and Silver, 2008).

The toroidal flow in the asthenosphere also has influence on the rotation on the overriding crust. (Menant et al., 2016; Magni et al., 2017). Therefore, geological objects display different stages of evolution along strike. This has been described early for the collision of Taiwan migrating along the China margin for example (Lu and Malavieille, 1994; Gautier et al., 2019), the eastern Mediterranean Sea (Armijo et al., 1996; Menant et al., 2016) and also in New Guinea for the collision of the Finisterre Terrane along the Australian margin (Silver et al., 1991), and others as Tonga and Marianas, etc. (Wallace et al., 2005; Wallace et al., 2009). There, block rotation is also observed. Although they are not necessary present for scissor-shape closure, they are common mechanisms (Figure 1- 7) (Wallace et al., 2005; Duretz et al., 2014; Menant et al., 2016; Brune, 2018). The rotation and asthenospheric flows may occur when a morpho-structure constituting a "buoyant indentor" collides with the upper plate, meanwhile, a part of the down-going slab continues subducting. Wrenching and rotation localized at the transition between continental and oceanic crust become important. In addition, this happens sometimes at very high velocity such as for the rotation of the N Arm of Sulawesi which started less than 10 Ma ago (Otofuji et al., 1981) and is nowadays controlled by GPS with 4.5 mm/y along the Palu-Koro fault (Walpersdorf et al., 1998; Vigny et al., 2002).

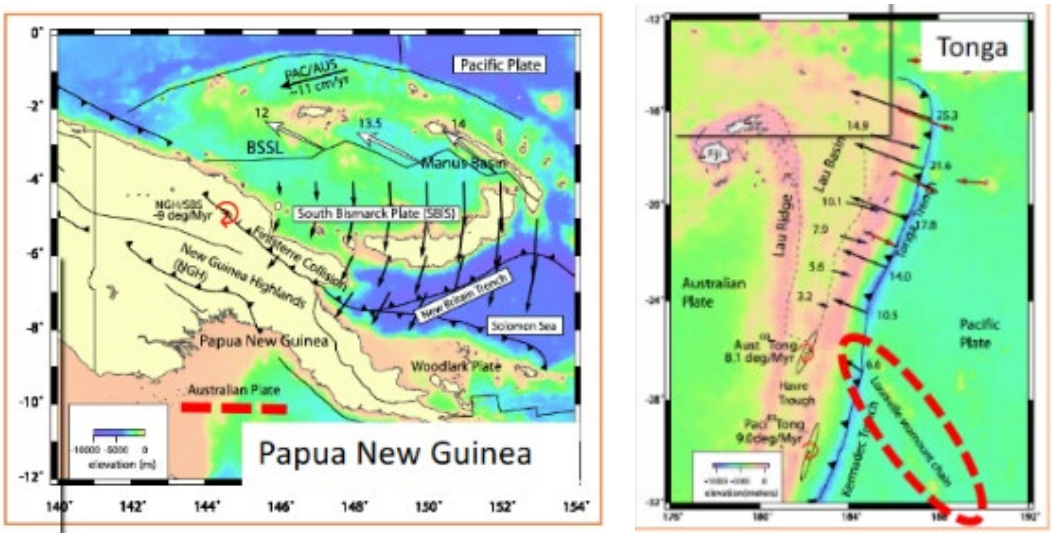

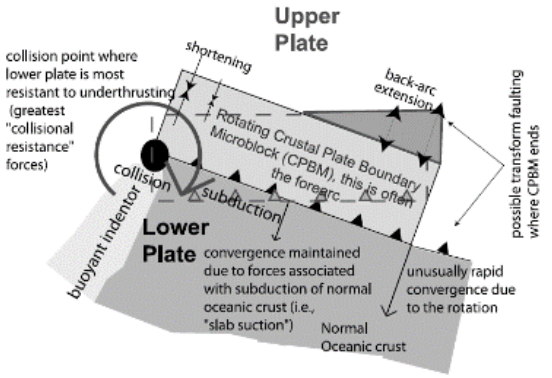

Figure 1- 7 (Upper) Examples of block rotation at the closure zone. The "buoyant indentor" reaches the subduction zone and triggers rotation and extension of the overriding plate in Papua New Guinea and Tonga (Wallace et al., 2009). (Lower) Conceptual model illustrates that heterogeneous lithosphere of the subducting plate drives the rotational movement and the back-arc extension (Wallace et al., 2009).

The lateral changes, along the downgoing plate may be inherited from heterogeneity and geometry of the crust of which in turn, comes from the previous tectonic events. According to commonly scissor shape in the opening of marginal seas, the closure of these basins will also display structures which laterally vary in time and space. Many examples of former back-arc basins ending as propagators into the continental margins have been later undergoing shortening, leading ultimately to the formation of spectacular mountain range (Pubellier and Meresse, 2013). For example, the closure of a V-shaped margin at the Solomon Sea has been described (Cooper and Brian, 1989; Abbott et al., 1994; Holm and Richards, 2013). The Pyrenées in Europe also result from the closure of the narrowest part of propagating basin. Other less mature examples, such as the Celebes Sea, only involve an accretionary wedge to observe the shortening (in addition to the rotation described above), and the closure is not complete yet.

1.3 Marginal seas in SE Asia: examples of recent analogues

The topic of investigation has to be located in a region where a coeval tectonic settings of rifting and subduction with well-preserved geological structures are present so that we can observe the present-day configuration and correlate movement with both geological and geophysical tools, for example using, multichannel seismic images, industrial and academic drillings, seismic tomography, in addition to field observation. For these reasons, SE Asia is a good playground where many different examples can be seen and compared.

SE Asia is located at the junction between the Eurasia Plate, the Philippine Sea Plate, the Indian-Australian Plate, and the Pacific Plate. Since the Cretaceous period, a northward subduction beneath the Eurasia Plate, initiated extensional environments to form several intra-plate marginal seas (Figure 1- 8) (Karig et al., 1978; Jolivet et al., 1989; Rangin et al., 1990). The subduction-related forces dominated both the surface deformation and the asthenospheric flows in the mantle (Figure 1- 9) (Schellart et al., 2019). The marginal seas are often floored by oceanic material, which were accreted along spreading centers developing above subduction zones (supra-subduction zone, SSZ). Their sequence of opening follows the migration and retreat of the subducting plate without overlap (Pubellier and Meresse, 2013).

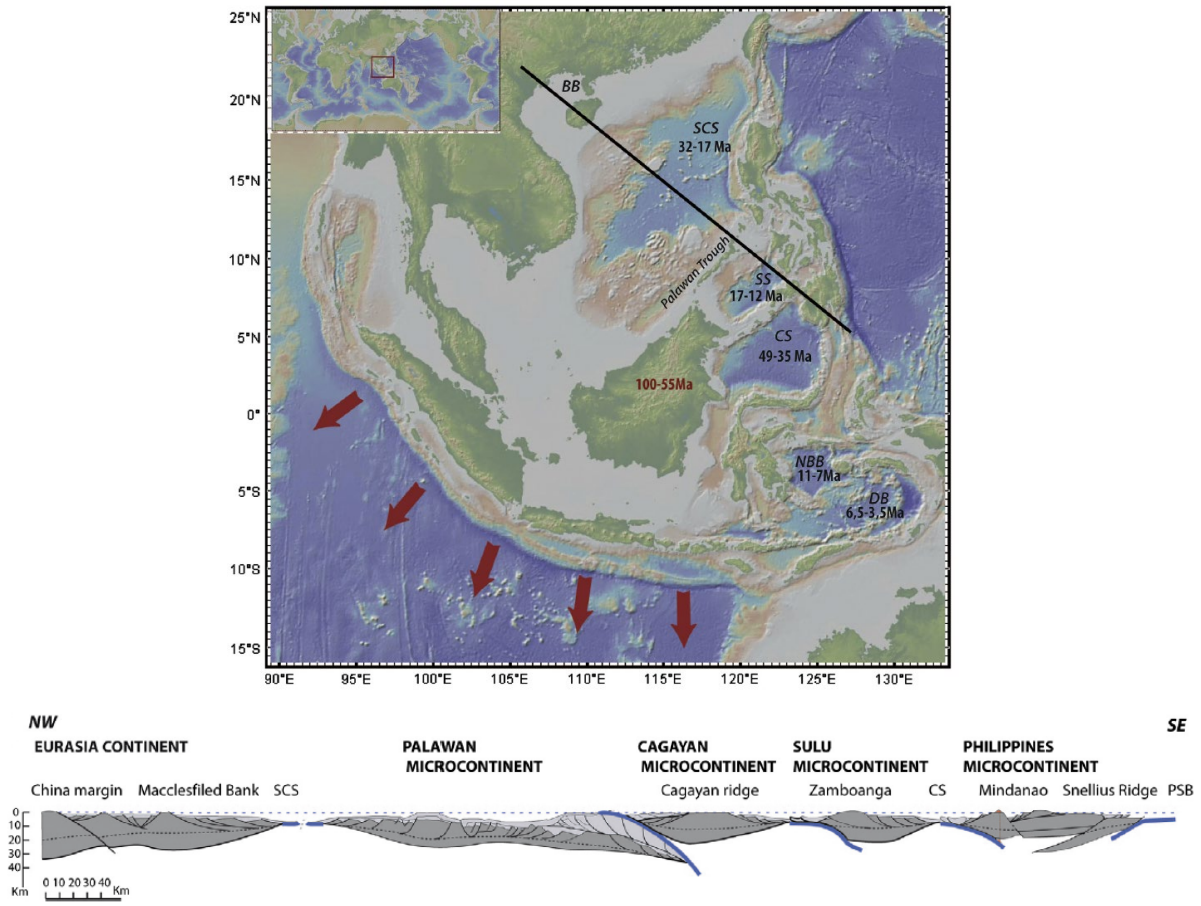

Figure 1- 8. Detailed marginal basins in SE Asia. Figures are from (Pubellier and Meresse, 2013; Schellart et al., 2019). This area underwent openings and closures. The marginal seas opened since late Mesozoic time. When shortened, the basins and continental slivers result in a complex chain of accreted micro-blocks.

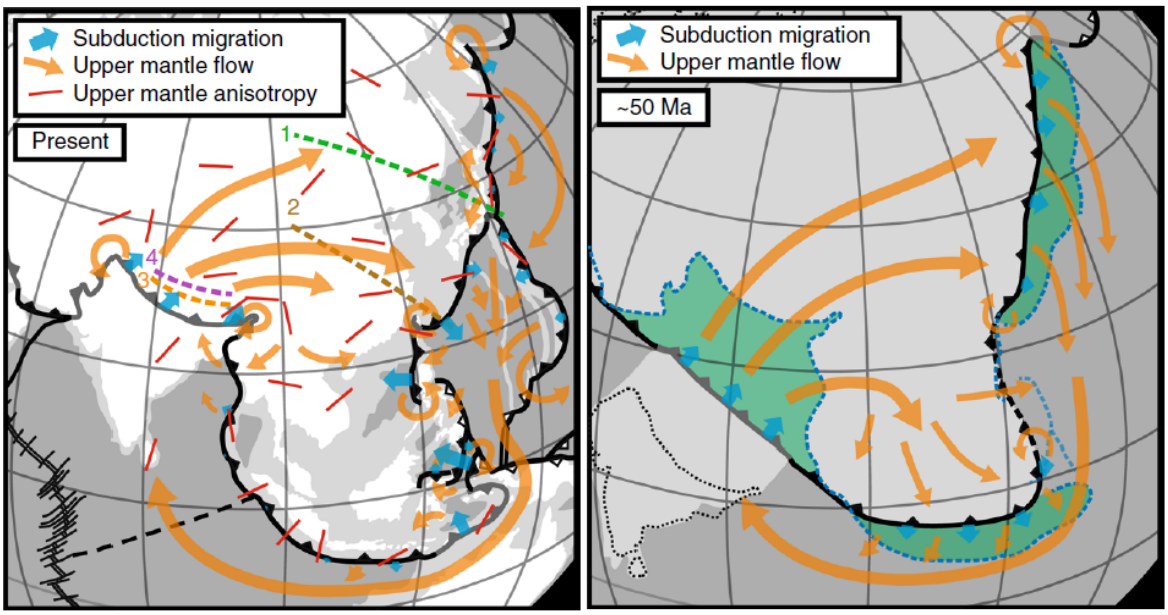

Figure 1- 9 Large-scale upper mantle flows proposed by (Schellart et al., 2019) and the relation with the opening of marginal basins in SE Asia, Himalaya-Tibet region and East China. The subduction-related forces dominated both the surface deformation and the asthenospheric flows in the mantle.

However, one exception is not visible in this context and concerns the vanishing of the Proto-South China Sea. The existence of this ancient closure is based on ophiolite complexes which crop out in North Sabah and Palawan, in the midst of a mountain range in Borneo and Palawan which results from the shortening of the relics of the PSCS. Many studies had suggested a link between these two marginal seas (Lunt, 2019) although correlations of the tectonic events are still debated and hypotheses are sometimes conflicting in many aspects. Different boundary forces have been invoked, such as the India-Eurasia collision induced extrusion of the Indo-China Block (middle on Figure 1- 10) (Tapponnier et al., 1982; Briais et al., 1993; Leloup et al., 2001), a supra-subduction basin opened in the South China Sea (right on Figure 1- 10) (Wu and Suppe, 2017), or basins opening on the downgoing plate (left on Figure 1- 10) (Taylor and Hayes, 1983; Hall, 2002; Pubellier et al., 2003; Morley, 2016). The interaction between convergent and divergent margins or even the influence of inherited structures have captured geologists' attention in the past years, and indeed, the South China Sea which opened apparently at the same time as the PSCS closed during the Cenozoic may be a good candidate to explore the relation between the two mechanisms. Therefore, the southern margin of the SCS may have recorded both the rifting structures and the echo of the closure of the neighboring PSCS, despite thick sediments of the Borneo-Palawan fold-and-thrust belt and despite the post-orogenic sediments overlying the southern rift margin.

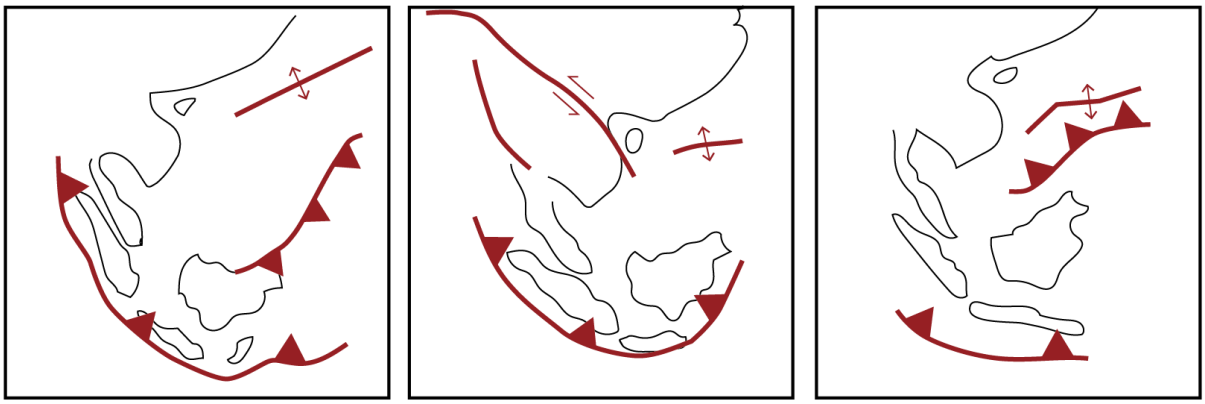

Figure 1- 10 Possible boundary forces are proposed as (Left) the SCS situated on the lower plate opened by the slab pull resulting from the subduction of the PSCS (Hall, 2002; Pubellier et al., 2003), (Middle) block extrusion of Indochina block induced from the collision in Tibet (Briais et al., 1993; Leloup et al., 2001), and (Right) the opening initiate by the back-arc extension in the upper plate (Wu and Suppe, 2017).

The South China Sea is spectacular by its wide stretched margins and a significant V-shaped ocean formation. On the other hand, the NW Borneo wedge has attracted a lot of studies from

academic institutions as well as the industry. These two areas accumulate sophisticated multichannel seismic data from academia or industrial companies in the SCS, Palawan and Borneo. Several tectonostratigraphic studies are generally compiled tectonic events between the extensional and convergent marginal seas. Therefore, this area could give us a good opportunity to get a comprehensive correlation in the different tectonic event and further approach the possible mechanism and driving forces in the system.

1.4 Problem statement

The global question I am posing is the following: **is there a genetic link between the subduction of the PSCS and the opening of the SCS?**

I try to explore this hypothesis by addressing the questions below:

- What is the relationship of the tectono-stratigraphy between the subduction and rifted basins? I will handle this by correlating the syn-rift successions and key bed of "mélange" respectively.
- What are the directions of extension during the rifting and the spreading? This will done so that we can compare them with the directions and modalities of the closure of the neighboring basin (PSCS)
- What mechanism and driving forces could lead to these coeval tectonic events, and what is the implication of the opening and closure in the world, in terms of formation of orogens?

1.5 Thesis structure

Chapter 2 Geological Background will to briefly introduce the geological evolution and geodynamics in the SE Asia, and emphasize on the aspect which are relevant for the thesis, namely the presence of the nearby subduction and the reactivation of pre-existing features such as the granite-sediments boundaries, limbs of broad folds or former crustal thrusts.

Chapter 3 Crustal architecture of the western SCS displays the structures of the rifting margins. I put a lot of emphasis on the change of extensional direction around a critical age in the SCS for the sake of correlation.

Chapter 4 Genetic link among collision, mélange and circular basins shows my results of differentiating the syn- and post-orogeny in the context of shale tectonics. The seismic and field observations identify a ductile deformation constituted by the sedimentary mélange. This would have a better age constrain in order to identify when is the end of the closure PSCS.

Chapter 5 Post-spreading magmatism in the southwest SCS margin will focus on the recent tectonic evolution during the post-spreading period. This chapter will describe the local uplifts induced by magmatism as well as the regional subsidence. The result will link to the relation of the magmatism and coeval thermal subsidence since Late Miocene.

Chapter 6 Synthesis of Geodynamics in the SE Asia and discussion will attempt to pin-point tectonic correlations between the subduction/collision and the rifting and offer a possibility to compare the mechanisms of rifting of the marginal basins and explore how this can help resolve issue regarding the rifting of large oceans for which the initial parameter is difficult to evaluate.

Appendix: A display of several types of data mentioned in the text. First, the re-interpreted seismic profiles from Phu Khank and Nam Con Son basins. The entire profiles have been published in some literature but we interpret them in different tectonic aspects. Second, bio-stratigraphy results on nannofossils collected from Kudat Peninsula. Third, raw analysis results on matrix of mélange from North Sabah, including XRD, XRF, and SEM images.

CHAPTER 2. Geodynamic background of SE Asia

This chapter will not discuss extensively all the geodynamic characteristics of SE Asia. I will focus on some of the aspects, which will be relevant for the topic of this research. Since I want to discuss the opening and closure of marginal basins, I will describe more in details the basins surrounding the Sunda Plate in conjunction with the evolution of the subduction of the Indian Ocean and the Paleo-Pacific Plate. I will then discuss how these basins closed and what is the deformation associated with the closure.

2.1 Subducting plate and marginal basins in SE Asia

Southeast Asia (SEA) is situated at the plate boundary of the southeastern part of Eurasia and converging Pacific Plate, Philippine Sea Plate, and Indo-Australia Plate. Intense seismicity shows that two subduction/collision zones (Figure 2- 1D). Two subduction/collision zones are highlighted by intense seismicity. These active plate boundaries involve the Indo-Australian Plate in the south and the Philippines Sea Plate as well as the Pacific Plate in the east (Figure 2- 1B), define the active plate boundaries. Each active plate boundary appears differently on the width of the strain rate zones, which indicates various closure characteristics (Figure 2- 1C). These convergent boundaries have been robustly active since the beginning of the Mesozoic subduction way north of its current position. Slab rollback followed, inducing micro-blocks to drift away from South China. The origin of the slab retreat invoked is not clear, nor are the origins of subducting plate, such as the Pacific Plate, Izanagi Plate, or Proto-South China Sea (Cullen, 2010; Savva et al., 2014; Zahirovic et al., 2014; Pubellier et al., 2016; Li et al., 2018; Schellart et al., 2019). However the significant extension took place during the mountain collapse of the Yanshanian Range from Late Cretaceous to Paleocene with development of narrow molassic basins (Ding et al., 2013b; Morley, 2016), and evolved to a widely distributed rifting event in South China (Chan et al., 2010) and in Palawan (Schlüter et al., 1996) and Borneo (Sapin, 2010). Hence, the intense tectonic activity of this region, which involves small marginal basins and continental slivers is a good setting to approach the parameters of the subduction/collision processes.

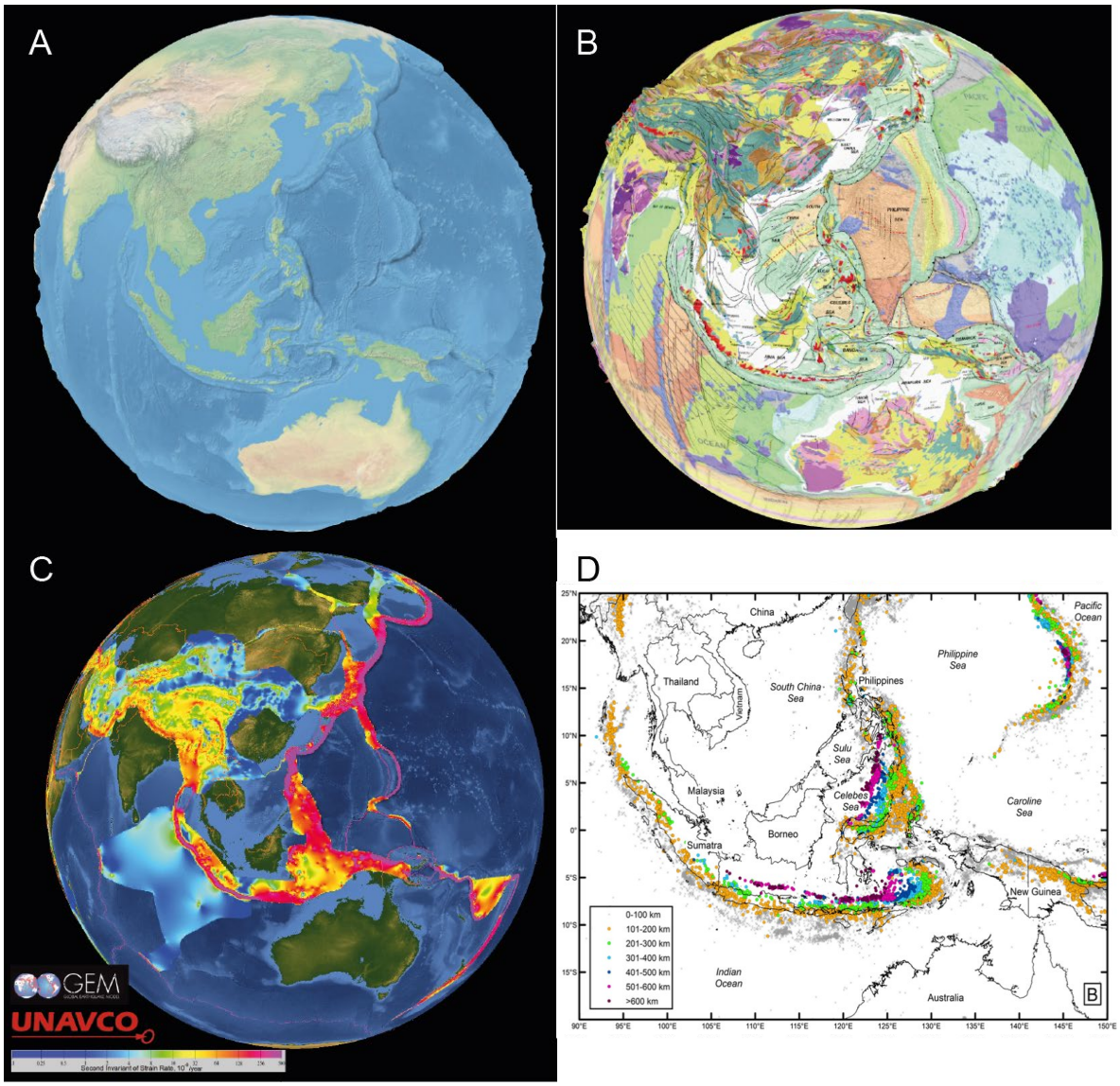

Figure 2- 1. (A) Altimetry of the E Asia and Australia. (B) The tectonic structural map illustrates the SE Asia surrounded by the Indo-Australian Plate in the south and Philippines Sea Plate and the Philippines Mobile Belt in the east (Zahirovic et al., 2014). The Sundaland promontory received several accreted micro-blocks. (C) The strain rate displays the active divergent zone with varying deformation widths. The pure subduction zones tend to display a narrow belt with higher strain rate, contrarily to the collision zones which have a diffused the strain rate within a larger deformation belt. (D) Only few earthquakes locate at the South China Sea and the Borneo-Palawan, showing they are inactive regions. Figure is from Hall and Spakman (2015).

The extensional features are distributed along the edge of the Cretaceous boundaries of the core of the Sunda Plate (formerly part of Eurasia), which is often referred to as "Sundaland" in the literature (Metcalfe, 2011; Pubellier and Morley, 2014). Subduction activity around Sundaland triggered mostly opening of rifted basins with or without oceanic floor underlined by the onset of deposition since the beginning of the Tertiary, and even the Late Cretaceous (Figure 2- 2).

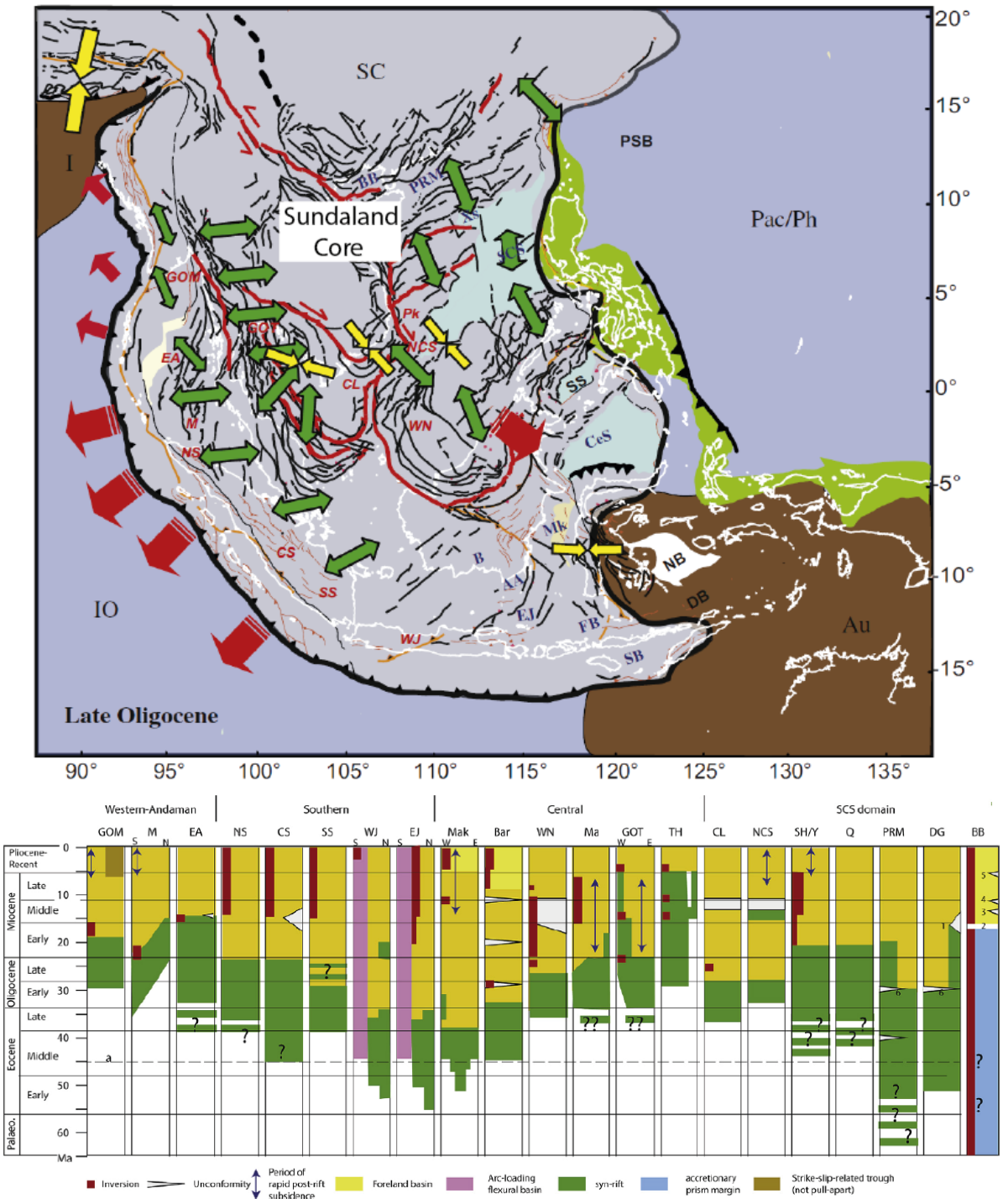

Figure 2- 2. Map of the Sundaland and extensional basins (Pubellier and Morley, 2014). (Upper) Several marginal seas opened during the Early Tertiary, some of which floored by oceanic crust developed on the eastern side of the plate. They are namely the South China Sea (SCS), Sulu Sea (SS), the Celebes Sea (CeS), and the Banda Sea (NB and DB). On the opposite side, the Sundaland Core also amalgamated numerous blocks of various origins with extensional intra-continental basins and only one marginal sea with oceanic crust; the Andaman Sea. The extension pattern, which was associated with the subduction-related forces from the Indo-Australian Plate, follows an orientation perpendicular the trench. (Lower) stratigraphic chart shows basins formed mainly since Eocene.

The opening of these marginal seas was followed by shortening induced by the Cenozoic subduction and collision of Australia and Philippine Sea Plate (right on Figure 2- 3). The current slab geometry is displayed on the cross section of Figure 2- 4. To study the parameters which controlled the rifted architecture, a group of marginal seas, South China Sea (SCS), Sulu Sea (SS), Celebes Sea (CS), and a vanished Proto-South China Sea (PSCS), therefore display good indicators; having a well-ordered chronology of closing, and being all contained within a relatively narrow time bracket.

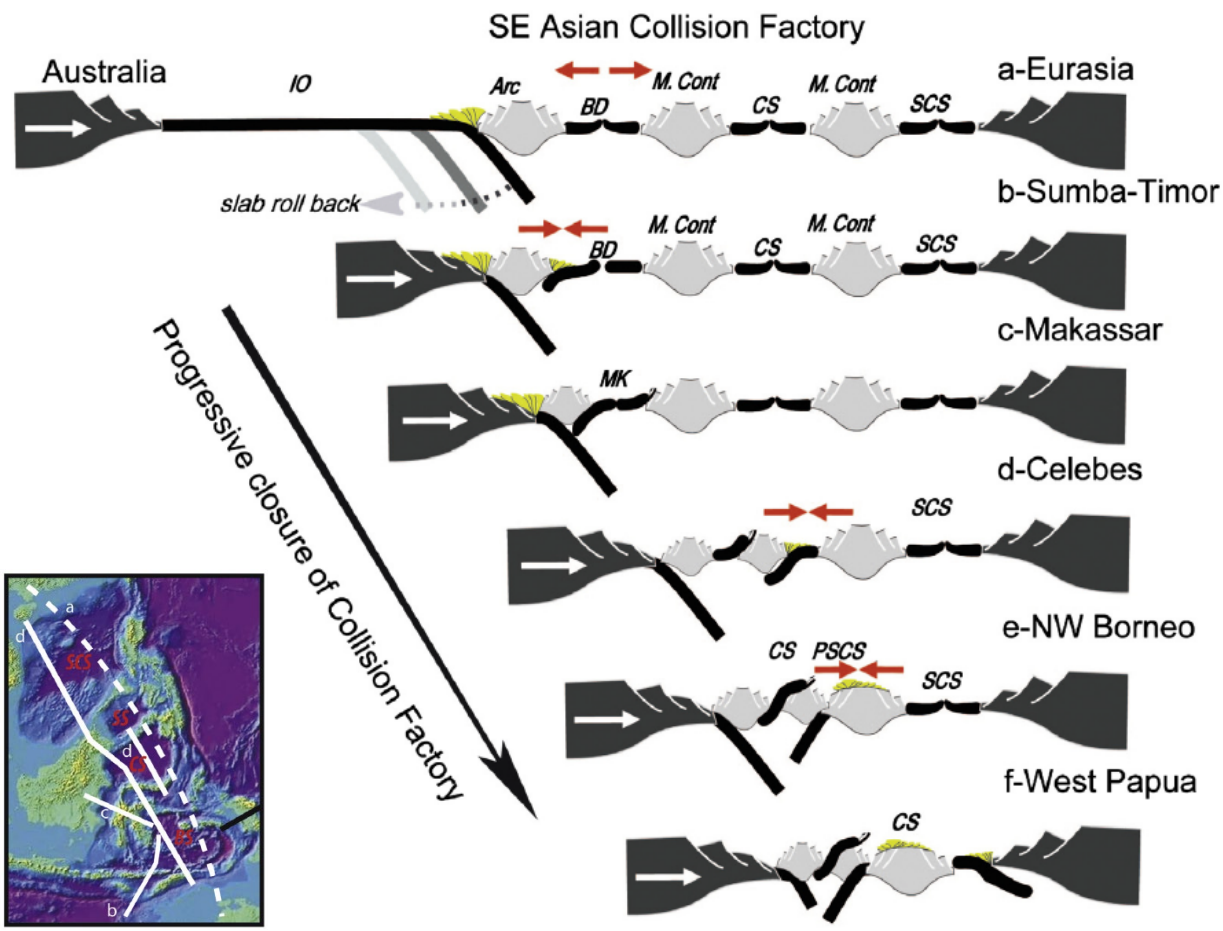

Figure 2- 3. The series of marginal seas in the SE Asia and their history of opening and closure related to the shortening with neighboring Australia Plate (Pubellier and Meresse, 2013). The main idea is that subduction initiated the opening of marginal basins by slab roll-back, and it is again the subduction; if it is difficult with more coupling, which contracts the supra-subduction area; thus, closing the basins one after another.

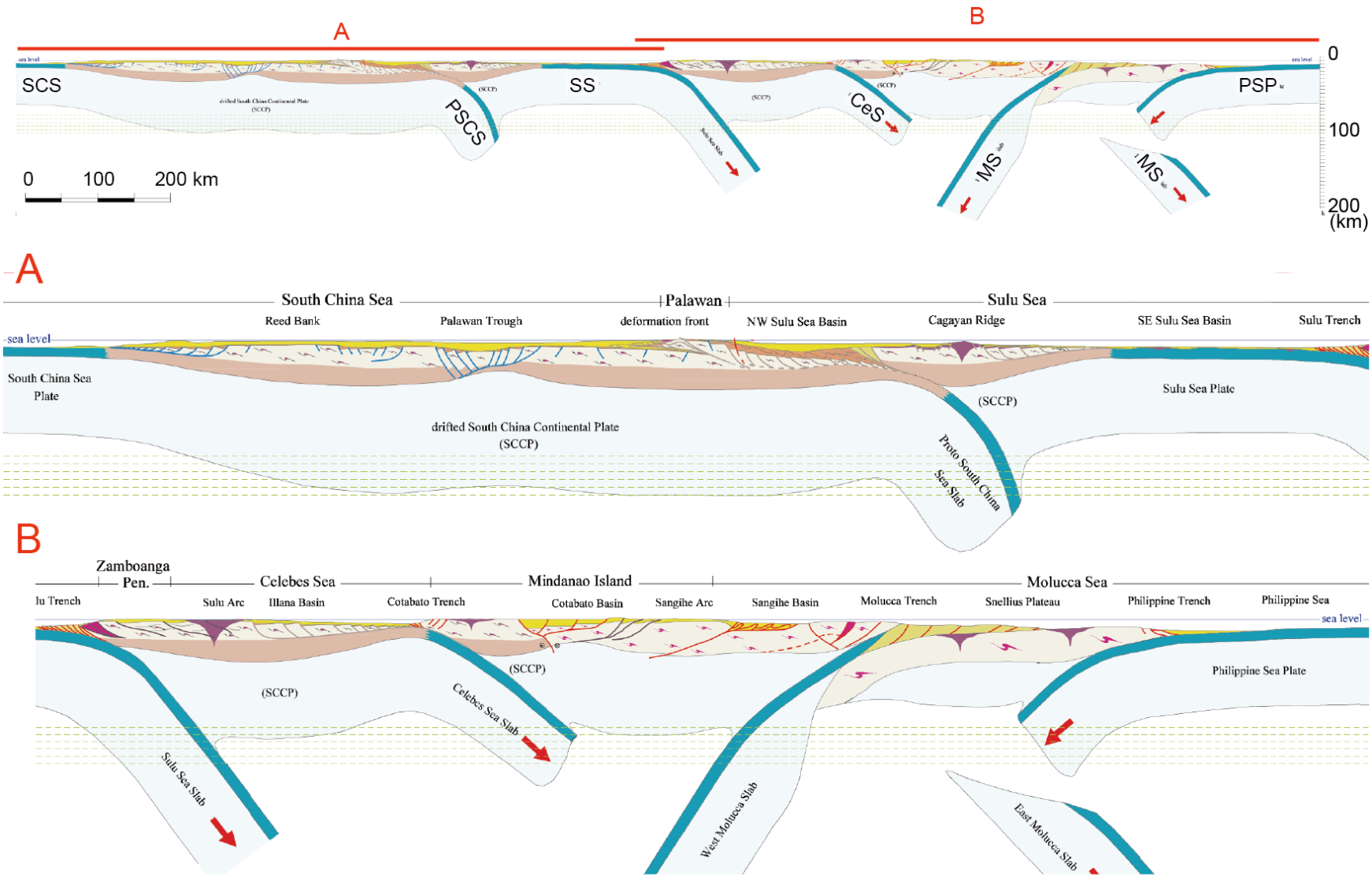

Figure 2- 4. Cross-section of the tectonic of the SCS, SS, CS, and PSCS (Pubellier et al., 2001). Numerous subducting slabs vary in time and scale of the tectonic evolution. The supra-subduction area yields marginal basins which are nowadays at varying state of contraction.

The ages of the marginal seas with oceanic floor are mostly identified by the magnetic anomalies, and by samples collected from drilling, including deep-sea drilling, and analysis and dating of the surrounding volcanic arcs (Silver and Rangin, 1991). The Celebes Sea opened possibly via back-arc extension from 35 to 45 Ma and may have a genetic link with Molucca Sea (Bader et al., 1999; Zhang et al., 2017). The ages of Celebes Sea accretions identified by the marine magnetic anomalies are younger than the ages of PSCS. Indeed, the PSCS is Early to Middle Cretaceous, as dated by the radiometric methods on ultramafic and mafic rocks as well as bio-stratigraphic data from radiolarite (Jasin and Geologi, 1992; Jasin and S, 1993; Asis and Jasin, 2012; Jasin and Tongkul, 2013). Yet the SCS is not exactly a back-arc basin; being developed within the downgoing plate (Type B of this study; see in Chapter 1). Several authors have established a link between the opening of the SCS and the apparent coeval closure of the PSCS (Taylor and Hayes, 1983; Hall, 2002; Pubellier et al., 2004). The identified magnetic anomalies and ages dated from basalts indicate that oceanic floor initiated from 32 Ma ago and terminated 16 Ma ago (Briais et al., 1993; Li et al., 2015; Larsen et al., 2018), although some differences have been proposed for the end of the spreading by Barckhausen et al. (2014), leading to a different evolution of the spreading rate through time. The Sulu Sea (SS on Figure 2- 3 and Figure 2- 4) was formed from 17 to 12 Ma as a back-arc opening with in the system of the PSCS closure (Rangin, 1989).

The mechanism which removed crustal material by “peeling off” a continental mass is not specific to the Sunda Plate. Basins opened around the Australian Continent seems to behavior the similar manner (Figure 2- 5B). The orientation of opening is parallel to the continental margin (Eyles et al., 2003; Brakel et al., 2009; Doig and Stanmore, 2012), although the extensional stress did not develop until ocean spreading. The similarities with the Sunda Plate evolution suggest a common mechanism of basin opening, closely linked to subduction-related forces (Figure 2- 5A).

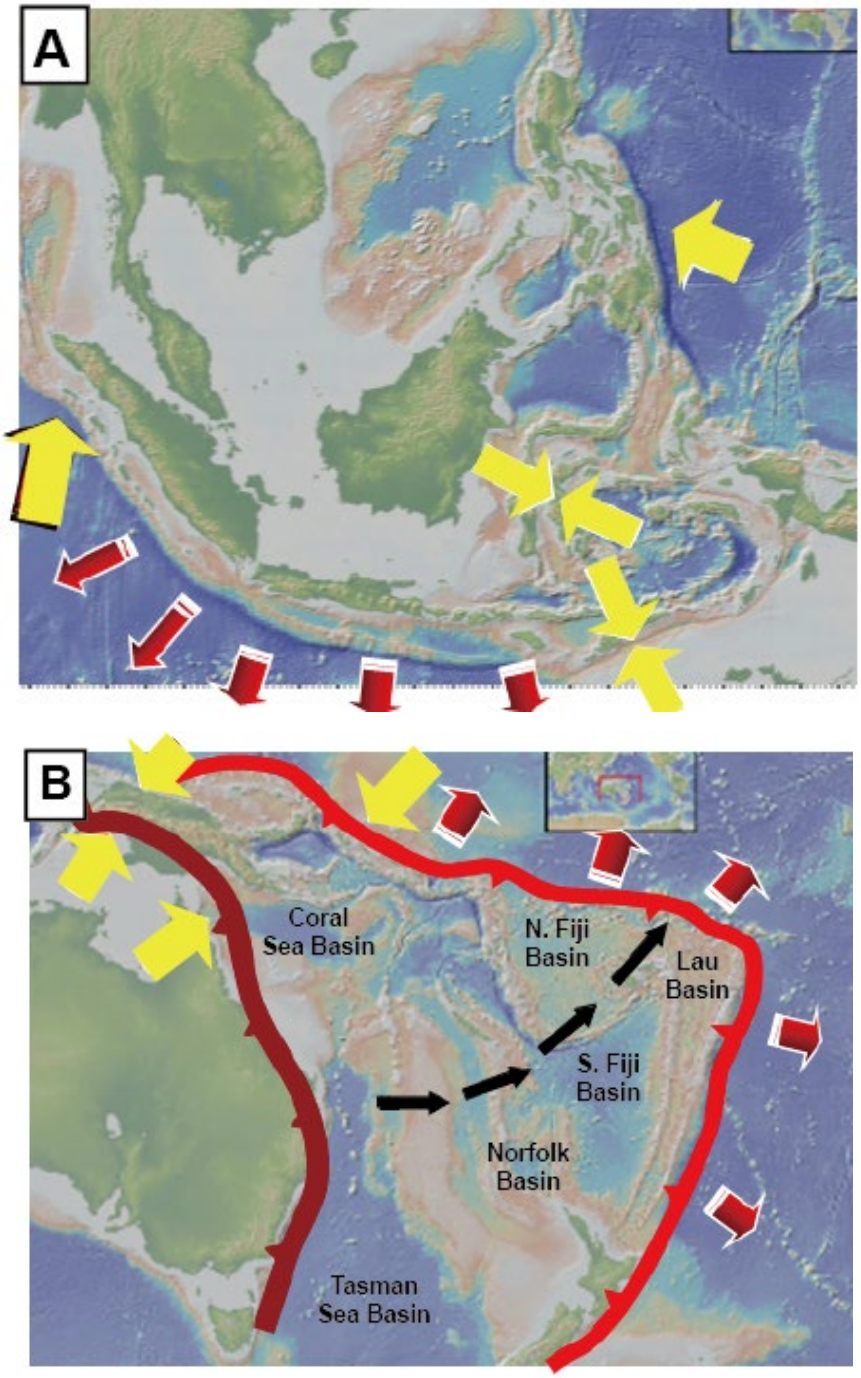

Figure 2- 5. The marginal basins opened in both SE Asia side and Australia side. Extensional directions due to trench pull during the Cenozoic (red arrows), convergence in SE Asia (yellow arrows).

2.2 Crustal evolution prior to basin opening

The crustal structure of basins and marginal seas can favor the development of structures along the existing weak zones intrinsic to the continental margin, which inherited from the previous tectonic settings. Many micro-plates (or rather crustal blocks) were incorporated to the East

Laurasia continent following the closure of the Neo- and Paleo-Tethys and associated marginal oceanic basins (Figure 2- 6) (Audley-Charles et al., 1979; Hall, 2002; Metcalfe, 2011; Zahirovic et al., 2014). Two main subduction systems accommodate the plate convergence toward SE Asia, and the resulting collage of micro-blocks nowadays compose the South China block and the Sundaland Core (Metcalfe, 2011; Li et al., 2015; Faure et al., 2018; Sautter et al., 2019; Zhang et al., 2019b).

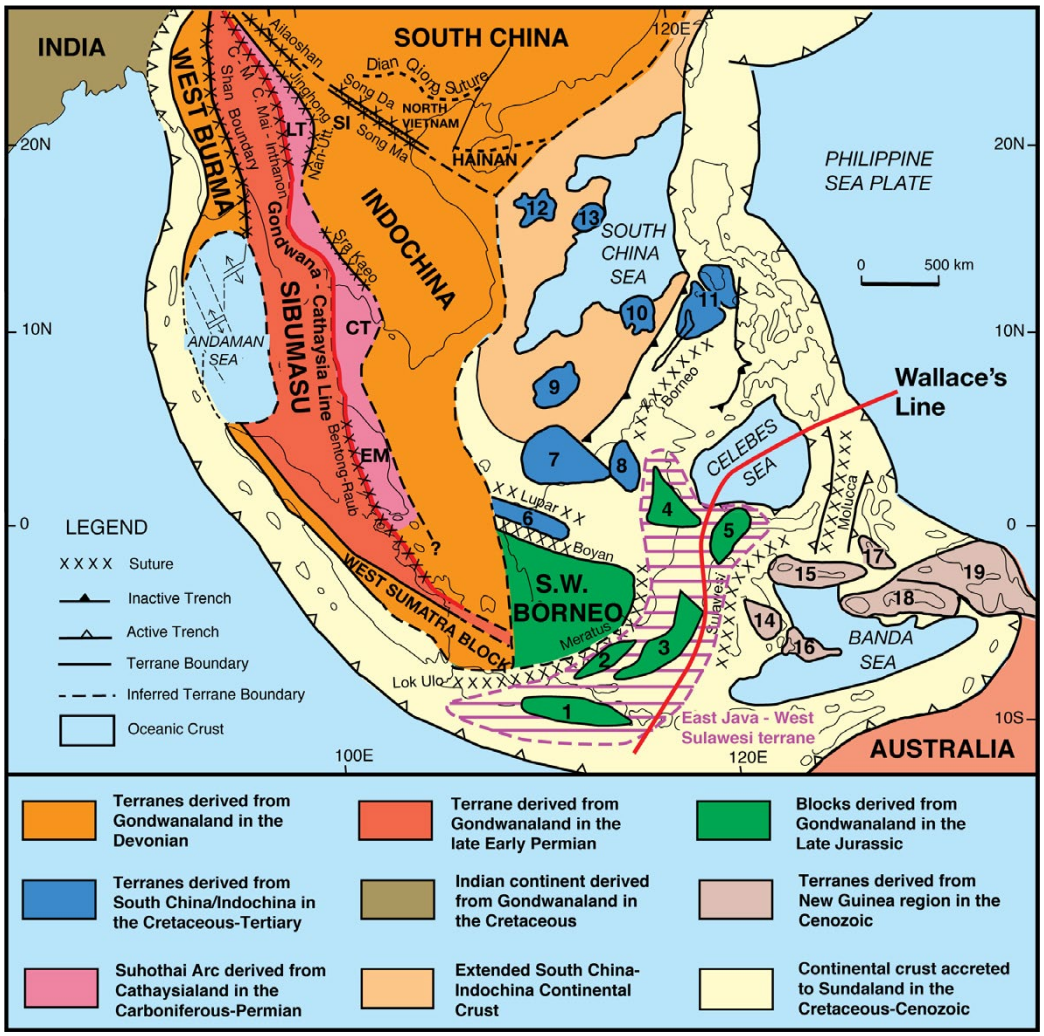

Figure 2- 6 Assembling micro-continent and blocks compose the SE Asia (Metcalfe, 2011). Large accreted continental slivers concentrate to the western part and compose the Sundaland Core since the Triassic. Scattered continental block abutted marginal seas in the eastern part due to the opening of the marginal seas.

In the south, neo-Tethys and present-day Indo-Australian Plate move northward carrying blocks of West Burma and West Sumatra Block derived from Gondwanaland (Figure 2- 6). To the eastern side, the subduction of paleo-Pacific Plate reached the Cathaysia Block of South China

and the coastal sliver was dragged with sinistral motion (Khanchuk et al., 2019) until the Cretaceous. The long-lasting convergent scenario resulted in periodic stages of Mesozoic–Cenozoic plutonic/volcanic activities along the South China to SE Asia during 90Ma in Cretaceous, well-dated by many literatures and within a narrow age span (Figure 2- 9B) (Barber et al., 2005; Hall, 2012; Zhang et al., 2019b). Both northward Neo-Tethyan subduction and westward Paleo-Pacific subduction resulted in an Andean-type convergent margin with extensive arc magmatism (Chung et al., 2005; Chu et al., 2006; Ji et al., 2009; Clements and Hall, 2011; Pubellier and Morley, 2014). These stages of magmatic intrusion and extrusion have been well-documented in the onshore (Huang et al., 2012; Xu et al., 2017) as well as in the offshore (Kudrass et al., 1986; Yan et al., 2010; Xu et al., 2015; Xu et al., 2017; Xiao et al., 2019).

Based on stratigraphic correlations and structural studies, regional syntheses have been performed (van Bemmelen, 1949; Hamilton, 1979) numerous plate reconstructions have been attempted (Lee and Lawver, 1995; Pubellier et al., 2003; Metcalfe, 2011; Hall, 2012; Seton et al., 2012; Zahirovic et al., 2014; Gibbons et al., 2015). According to most of them, the opening and closure of marginal seas happened dominantly on the eastern side (Figure 2- 7). The extension generated oceanic floor in some basins whereas others aborted. However, it has been proposed that the PSCS subduction and initiated the SCS opening.

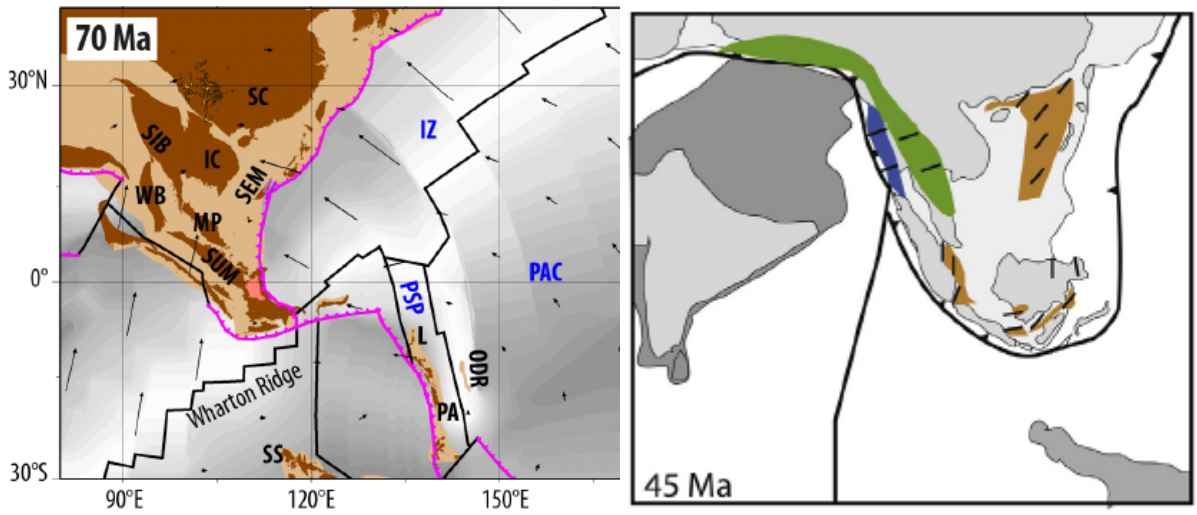

Figure 2- 7 Plate reconstructions of the SE Asia with marginal seas opening by roll-back of a northward subducting Izanagi (IZ) slab: Proto-South China Sea above proto-Sunda Trench (Zahirovic et al., 2014) and the South China Sea (Pubellier and Morley, 2014). Green for compression and brown for extension.

Thus, somehow the opening of the SCS is not directly the result from the subduction of the Neo-tethys or the Indian Ocean, but rather the consequence of an intra-plate convergence of the paired system PSCS/SCS. The final consumption of the PSCS left compressional structures on the surface, and yet, subducted slabs are still visible at depth on tomographic images (Figure 2-8). Pieces of slabs are deciphered by the higher velocity anomaly (cold colors of Figure 2- 8) representing the denser and colder material such as a subducted slab in the deep depth (Wu et al., 2016; Wu and Suppe, 2017). This has proven to be a useful tool to detect slabs deeper than the actual seismic Benioff zone, and allowed to obtain comprehensive slab geometry. Within the SE Asia, the Sunda slabs and Molucca Sea slab are significant subducted slabs, and the active subduction zone is shown down to the 640 km, near the transition zone between upper and lower mantle. An inactive high velocity anomaly of PSCS is located beneath the present-day SCS (Rangin et al., 1999; Hall and Spakman, 2015; Wu et al., 2016; Fan et al., 2017; Wu and Suppe, 2017; Zenonos et al., 2019), which is interpreted the relic slabs of the subduction the PSCS (Wu et al., 2016; Wu and Suppe, 2017).

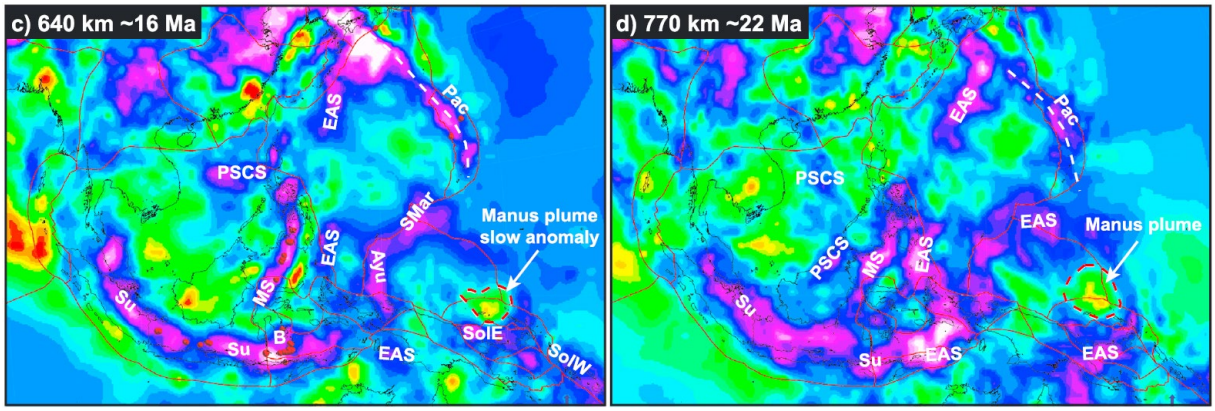

Figure 2- 8 Tomography images of SE illustrating the distinct subducted slabs in the SE Asia (Wu et al., 2016). Several small-size slabs are identified below the main subduction zones and flatten around the bottom of upper mantle (~640 km). Ayu, deep Ayu detached slab; B, Banda; EAS, East Asian Sea; MS, Molucca Sea; Pac, Pacific slabs; PSCS, Proto-South China Sea; SMar, southern Marianas detached slab; Su, Sunda slabs; SolE, Solomon east; SolW, Solomon west. The active subduction zones are connected to trenches on the surface, while others high velocity slabs could represent other and probably the detached slabs. Furthermore, the tomography images could refer to different even subduction scenario in different ages presenting through depth.

2.2.1 Cretaceous Yanshanian Orogeny in South China

Continental extension often follows closely mountain formation; when the horizontal compressional forces begin to relax and the vertical stress becomes dominant. It is actually difficult to discriminate the orogenic collapse from the subsequent rifting. The geological history of the studied area has benefited from numerous studies onshore South China by characterizing a Yanshanian Orogen and the subsequent mountain collapse.

The Yanshanian Orogeny configuration dates back from the Middle Jurassic (Dong et al. (2018b) and reference therein). Large magmatism was attributed to an Andean-type convergent margin related to the northward subduction of paleo-Pacific Plate, which was active during Jurassic to Cretaceous time with magmatic flare-ups and lulls (Figure 2- 9) (Hamilton, 1979; Taylor and Hayes, 1983; Li et al., 2012; Xu et al., 2017). Patchy distribution of plutonic granitoids along the coast of South China implying arc magmatism had contributed to the tectonic crustal thickening along the SE boundary of the South China Block (Figure 2- 9) (Jiawei et al., 1989; Langford, 1989; Zhao et al., 2004; Zhou et al., 2006; Xu et al., 2010). Even in the middle of the SCS, dredging encountered granitic samples dated at 119 Ma (Kudrass et al., 1986; Yan et al., 2010; Xu et al., 2015; Xu et al., 2017; Xiao et al., 2019).

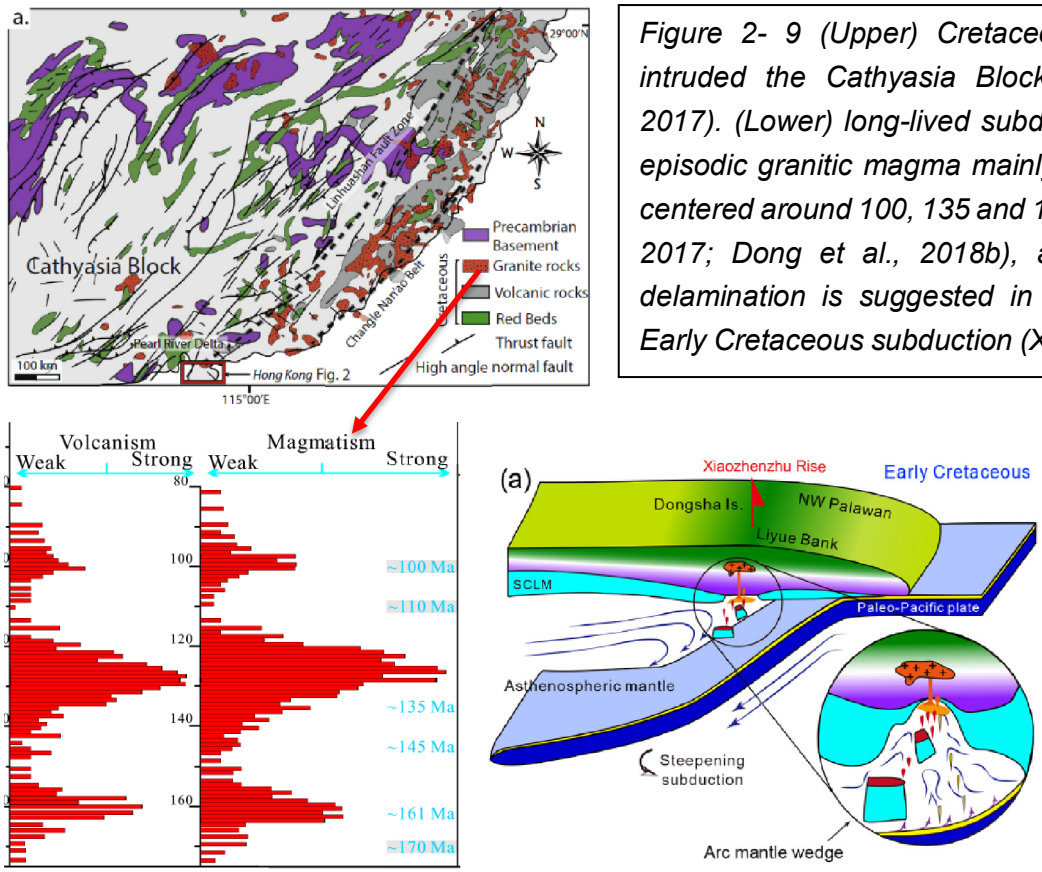

Figure 2- 9 (Upper) Cretaceous magmatism intruded the Cathyasia Block (Nanni et al., 2017). (Lower) long-lived subduction produced episodic granitic magma mainly in three peaks centered around 100, 135 and 161 Ma (Xu et al., 2017; Dong et al., 2018b), and lower crust delamination is suggested in the scenario of Early Cretaceous subduction (Xiao et al., 2019).

Geochemical analysis as well as compiled evidence of regional magmatism, metamorphism, crustal structures such as the thickness and lithology, and sedimentary sequences suggests the magma was formed by the hybrid of sub-continental mantle and arc lower crust in the Early Cretaceous (Xiao et al., 2019), which implies the lithospheric delamination may have weakened the crust and terminated the Yanshanian Orogeny. The subsequent uplift and erosional denudation of the remaining arc crust in the Late Cretaceous could have provided weak crustal conditions for the rifting of the South China Sea (Xiao et al., 2019).

2.2.2 Reactivation of structures and mountain collapse

The importance of the transition from the orogeny to the extension determines the crustal structure of marginal seas, such as crustal exhumation and mountain collapse (Hsü et al., 1990). In South China, widespread extension in the vicinity of the Cretaceous granitic rocks led to crustal subsidence, causing a large volume of red fluvial and lacustrine deposits to accumulate in the extensional basins (Shu et al., 2009).

The region of extension in the Mesozoic arc area affected the previous compressional structures, implying probable reactivation of the previous structures (Figure 2- 10) (Pubellier et al., 2008; Pubellier et al., 2016; Nanni et al., 2017). The morphology and structure of the Cretaceous folds delineate locally the early extension which is globally perpendicular to the Yenshanian range, and early mollassic basins witness the erosion and the collapse of the Yenshanian orogen (Pubellier et al., 2008; Chan et al., 2010; Nanni et al., 2017).

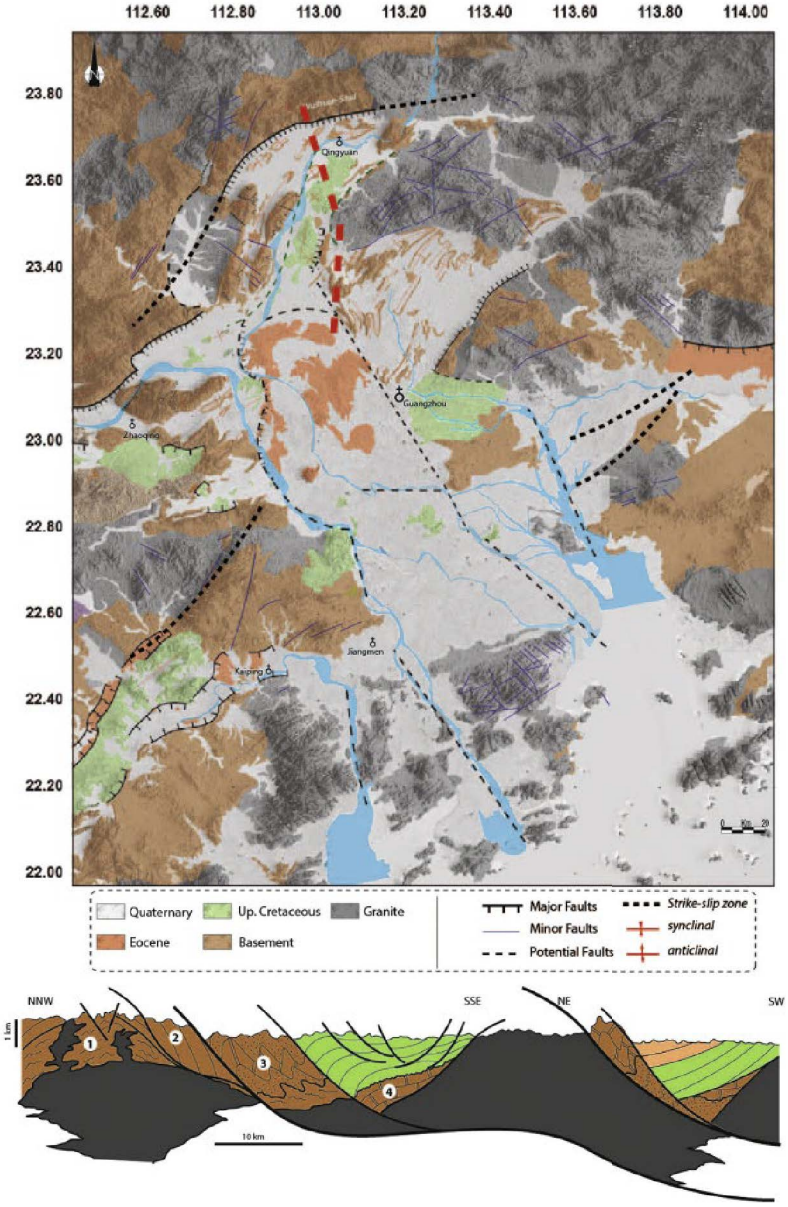

Figure 2- 10 Collapsing structures shown by satellite images (figure from SRTM with Structural Map of the SCS (Pubellier et al., 2016) draped on Visioterra VtWeb tool) and structural lineation on the geological map (Savva et al., 2014).

This mountain collapse setting is also expressed offshore on the Northern margin of the SCS. A system of half-grabens and tilted horst structures from Late Cretaceous to Early Cenozoic is nicely preserved. The granitic massif is widespread South China, South China Sea and Vietnam (Figure 2- 11). Drills and dredged rocks in the SCS encountered Early Jurassic–Early Cretaceous intermediate-acidic magma with arc-related geochemical features, which and is linked to the presence of this Mesozoic marginal arc (Kudrass et al., 1986; Yan et al., 2014b; Xu et al., 2015; Xu et al., 2017; Xiao et al., 2019).

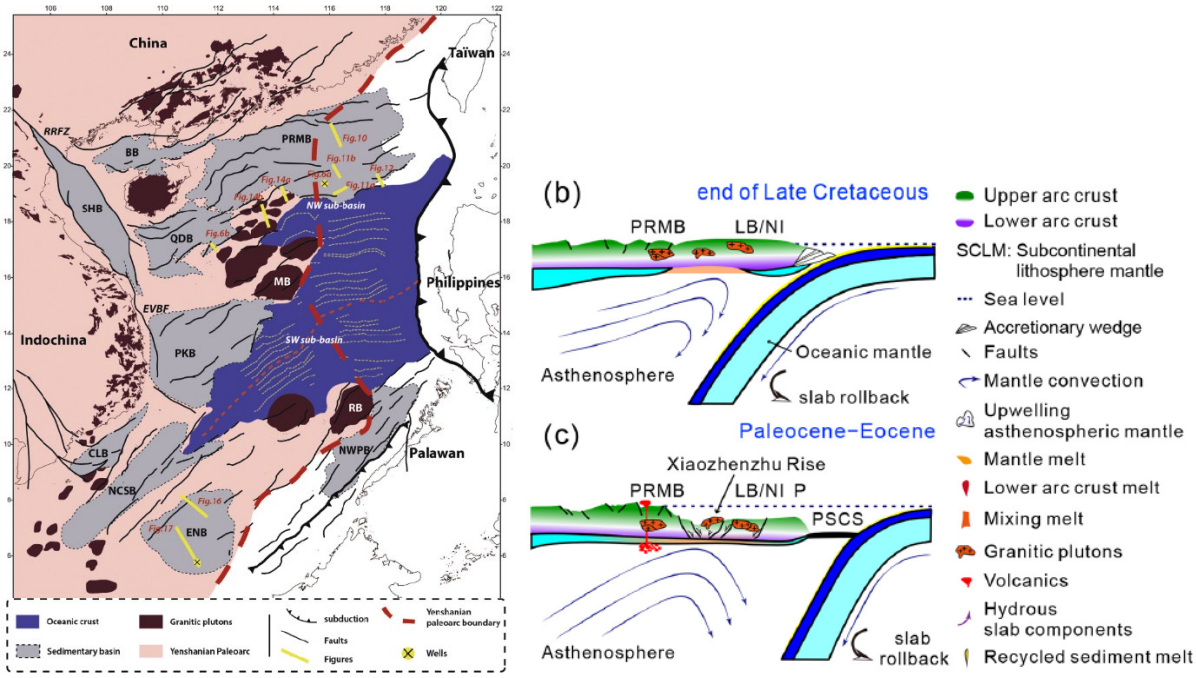

Figure 2- 11. Boundary of Yenshanian Orogeny in the South China Sea (Savva et al., 2014). Red dash line delineates the south limit of distribution of granitic plutons offshore. (Right) Cretaceous granite stretched into the SCS (Xiao et al., 2019).

Significant detachment faults were identified on the offshore northern margin of the South China Sea, and the offshore Vietnam (Cullen et al., 2010; Savva et al., 2013), as well as offshore Palawan (Nirrengarten et al., 2020a) which characterized by faults rooted between the Paleozoic cover and the basement possibly down to the base of granitic plutons (Savva et al., 2014). Just like onshore mainland China, extensional structures offshore have been revealed by seismic lines and show compressional folding and intrusive granitoid bodies being re-used by the low angle normal faults (Figure 2- 12 and Figure 2- 13). The inherited structures offered preferred detachment planes to develop along the folds (Savva et al., 2014). The overlying syn-rift strata are, therefore, influenced by the structure and deformed along the detachment level.

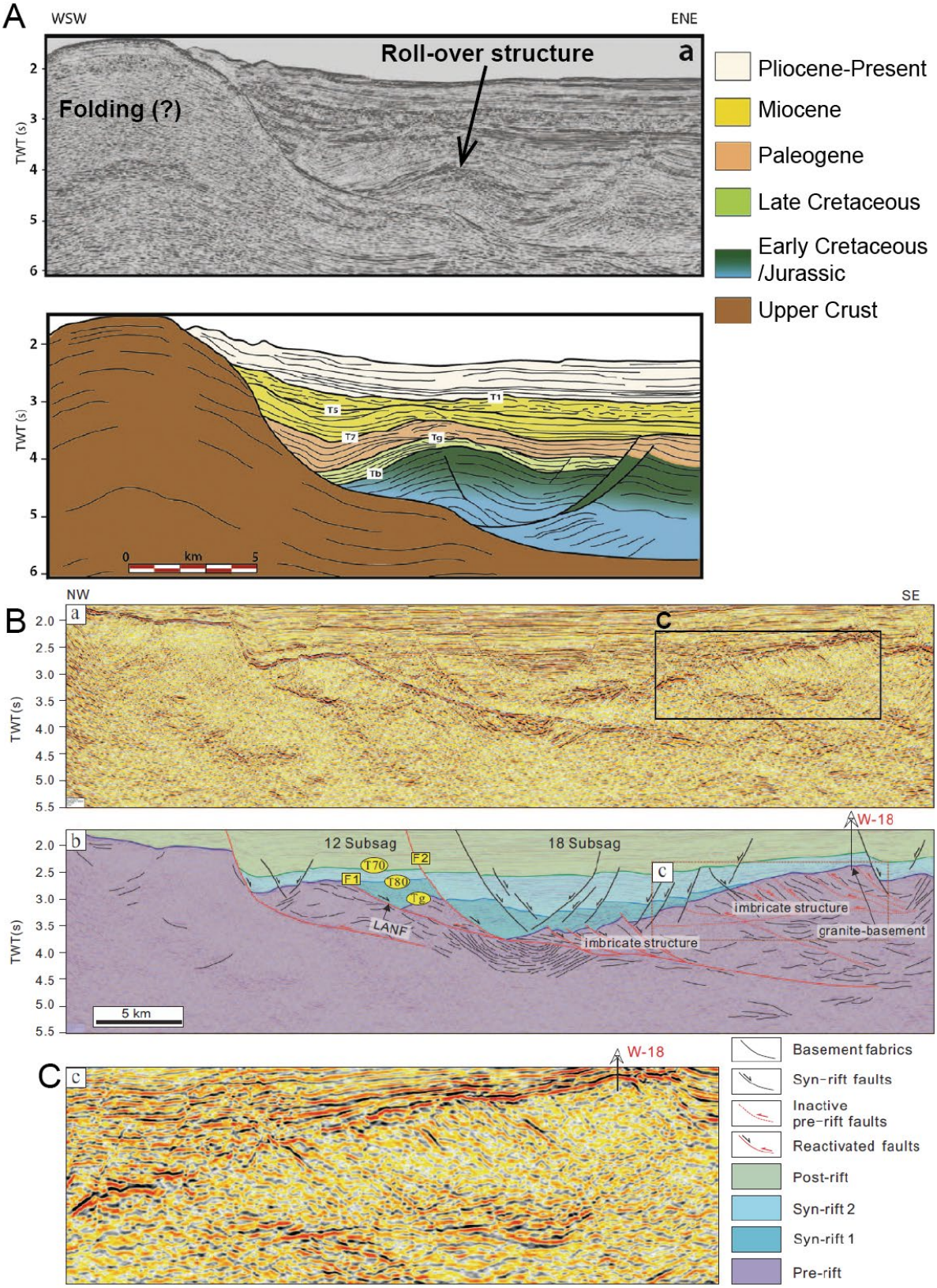

Figure 2- 12 Seismic image shows a structural contact with a low-angle normal fault and roll-over between the Paleozoic basement and overlying Mesozoic and Cenozoic sedimentary strata (Savva et al., 2014). Contact parallel to inferred fault plane within the imbricated basement, favoring reactivation later along the preexisting weak shear zone (Ye et al., 2018).

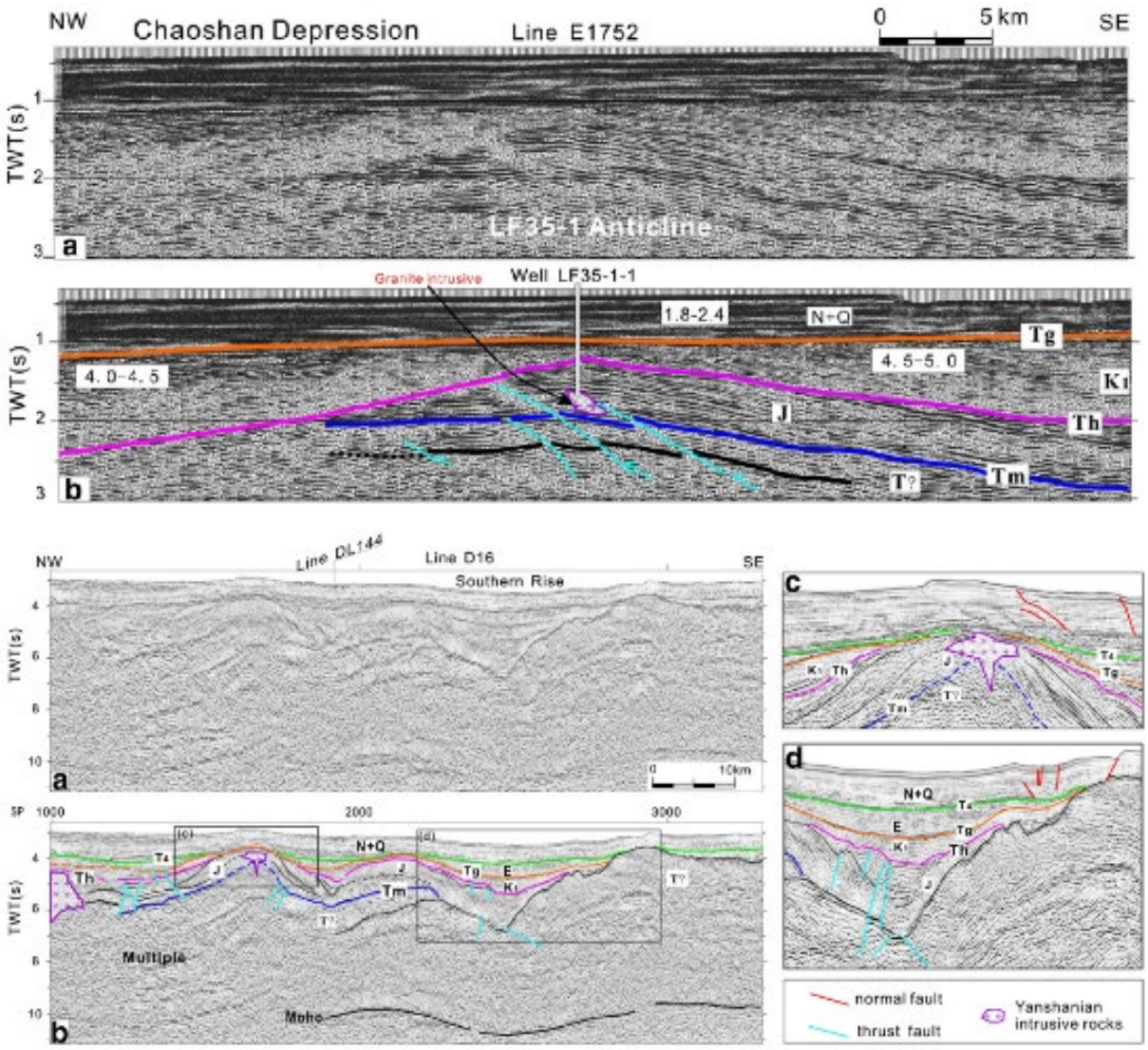

Figure 2- 13. Mesozoic basement with folding structures cored by Yanshanian intrusive rocks in the Pearl River Mouth Basin (Yan et al., 2014a). The age of the tectonics is within the Early Cretaceous below the Tg (orange horizon).

These widely distributed morphostructures of the margin of the South China Sea play an important role in the evolution of the basin formation. For example, the large wavelength crustal boudinage shown in Pichot et al. (2014) seems to be controlled by the location of the Cretaceous batholiths. Globally, the complexity of the composition of the crust has shown in many places, including in the Alpine rifted margin, where the observed structures have been modelled by thermo-mechanical modelling (Duretz et al., 2016). The strain is able to localize alongside the boundary of the intrusive or metamorphic bodies to control the crustal structure (Duretz et al., 2016; Petri et al., 2019).

2.3 Extension processes beyond reactivations of pre-existing structures

We have seen that extensive deformation in the SCS area localized on pre-existing sutures related to the previous orogenic phase. In this context, the rifting structures also developed according to various parameters among which the thermal condition, lithospheric rheology, and extension rate play a noticeable role. Two end-members have been proposed for the last decade in the world: magma-poor and magma-rich margins (Figure 2- 14) (Whitmarsh et al., 2001; Péron-Pinvidic and Manatschal, 2009; Masini et al., 2011; Franke, 2013; Tugend et al., 2018), and this first-order observation has been applied worldwide such as for the Atlantic, Indian, Antarctic and Australian margins, and to some marginal basins including the South China Sea (Whitmarsh et al., 2001; Péron-Pinvidic et al., 2007; Franke, 2013; Péron-Pinvidic et al., 2013; Gillard et al., 2015; Tugend et al., 2018).

The magma-poor type characterizes mainly the lack of significant magmatic activity during the breakup due to a slow and cold rifted margin (Ros et al., 2017). The significant serpentinized sub-continent mantle is supposedly resulting from the exhumation of sub-continental mantle rising to the seafloor prior to the breakup initiation, and juxtaposed to the oceanic floor when the system generates continuous partial melting. For instance, the Iberia margin exhibits serpentinite altered from the lithospheric mantle through a fault plane pathway filling water from the seafloor to the mantle (middle on Figure 2- 14). The similarity has been proposed in the rifted margin nowadays exposed onshore in the Alps (Masini et al., 2011; Mohn et al., 2012). The thermal condition and the detailed characteristics are revealed in field outcrops (Lavier et al., 2019). A large low-angle shear zone, - detachment fault – is responsible for the exhumation of the mantle to shallow depth (Whitmarsh et al., 2001; Lavier and Manatschal, 2006; Péron-Pinvidic et al., 2007).

On the opposite end member case, the magma-rich margin term characterizes the noteworthy magmatism of intrusion and extrusion involved during the latest rifting to the breakup (lower on Figure 2- 14). Seaward Dipping Reflectors (SDRs) are significant features which suggest higher thermal condition, and might result from the presence of a mantle plume or inherited back-arc context. At the great depth, the magma may be underplated beneath the bottom of crust and accumulate a high velocity pocket layer has been image, sometimes referred to as the "Lower Crustal Body" (Gernigon et al., 2012; Gao et al., 2015; Sun et al., 2019).

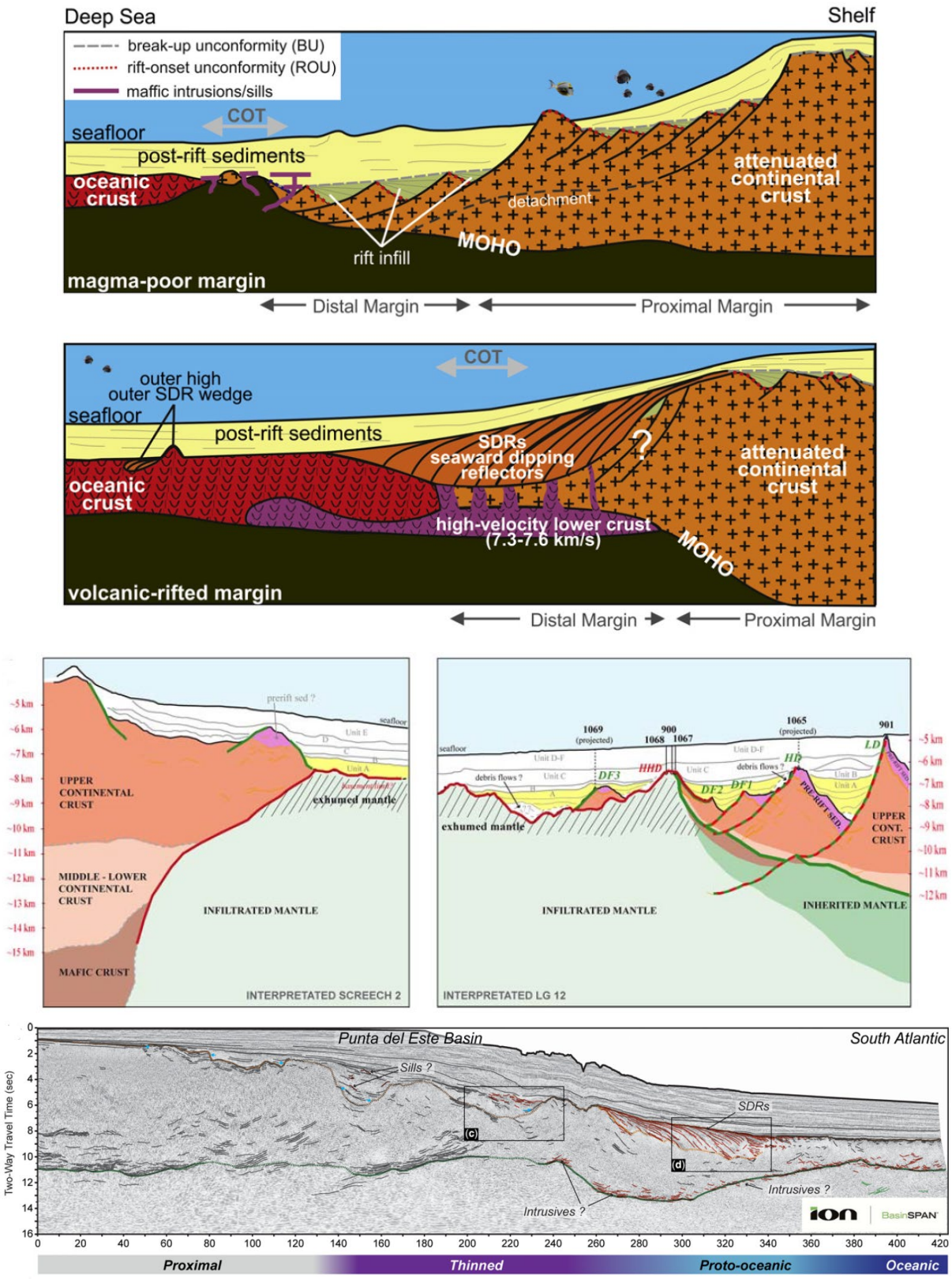

Figure 2- 14 (Upper) the conceptual models describe the main difference between magma-poor and magma-rich margin (Franke, 2013). (Middle) Magma-poor margin of the Iberia-Newfoundland Margin in the northern Atlantic (Péron-Pinvidic and Manatschal, 2008). (Lower) Magma-rich margin of Uruguayan margin in the south Atlantic, showing the SDRs (Tugend et al., 2018).

In the past decade, more parameters were allowed in numerical simulations. Various rheologies may be assigned to each crustal layer and be critical to explain the different crustal structure in the rifted margins. Whether the upper crust and lithospheric mantle are coupled, it has consequences on the width of the margin and therefore, its thickness (Figure 2- 15) (Huismans and Beaumont, 2011; Ros et al., 2017). The strength of the lower crust may impact the magma evolution in the crust near the COT in a result of serpentinite-like magma-poor margins or magmatism-like magma-rich margins. If the strength of the lower crust decreases, the decoupled mantle uplifts to heat the crust at the COT to produce extensive magma underneath the continental crust, instead of serpentinizing the sub-continental mantle. This type of margin characterizes a wider rifting margin and longer period of stretching and thinning (Ros et al., 2017).

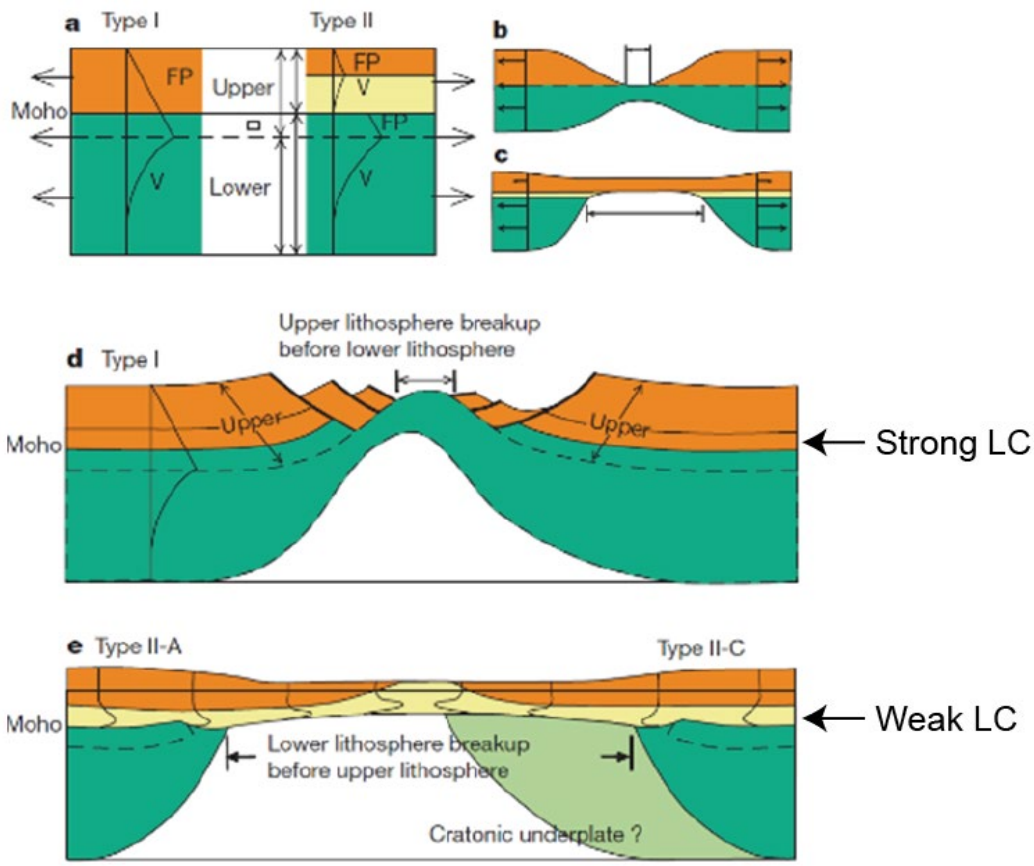

Figure 2- 15. Two end-member types of rifting insight from the different rheology of lower crust that have a decoupling or coupling during the rifting process (Huismans and Beaumont, 2011). Type II-A has always been regarded as fitting many of the specific characteristics of the SCS; such as the wide rifted zone, the homogenously thinned crust, the warm thermal conditions, and the shallow elevation of the crust for long time; prior to the crustal breakup. Note that the mantle breaks up long before the crust.

2.3.1 Crustal structure of SCS Margin

The SCS has been debated and qualified as a magma-poor, a magma-rich, or even an in-between case due to the wide stretching margins and lack of efficient magmatic aggregation nor serpentinite mantle in the COT (Franke, 2013; Ding et al., 2016; Chang et al., 2017). The regional structures, dynamic formation mechanism and tectonic evolution of the SCS have been extensively studied to achieve better understandings of the deformation of continental margins, the formation of marginal seas, and the potential for hydrocarbons (Taylor and Hayes, 1980; Holloway, 1982; Taylor and Hayes, 1983; Mitchell et al., 1986; Hayes and Nissen, 2005; Franke et al., 2011; Savva et al., 2013; Gao et al., 2016; Sibuet et al., 2016; Shi et al., 2017; Zhang et al., 2019c; Ding et al., 2020).

The first-order image is the long stretching margins across 500 km length for each side of margin. The Moho is flat across most of the rifted margins and ascends rapidly near the COT (Figure 2- 16D, (Pichot et al., 2014)). Exhumed mantle has been identified in several basins by the geophysical investigation (Franke et al., 2011; Savva et al., 2013; McIntosh et al., 2014; Ding et al., 2016; Lei and Ren, 2016; Pubellier et al., 2016). Magmatism is still identified in several basins and at the COT (Yan et al., 2006; Franke et al., 2011; Zhao et al., 2016; Deng et al., 2018; Sun et al., 2019), and a high velocity or density layer (HVL) (McIntosh et al., 2014; Pichot et al., 2014; Gao et al., 2015; Chang et al., 2017) is deduced from seismic refraction data in the northern margin. In addition, inherited structure of the continental margin such as granitoid bodies scattered in the margin are also a parameter controlling the crustal and thermal structure (Ding and Li, 2016b). Yet the other parameters mentioned above are still needed to explore the crustal rheology and deformation behavior during the rifting. These may have an impact on breakup process (Huismans and Beaumont, 2011; Clift, 2015).

Figure 2- 16 Figure from Nirrengarten et al. (2020a). (A) Topographic map of the SCS associated with the oceanic magnetic anomalies (Briais et al., 1993). (B) Crustal thickness map determined by 3D gravity anomaly inversion with the free-air gravity anomaly in shaded relief (Gozzard et al., 2018) and the location of profile C-C') Profile extracted from the crustal thickness map determined by 3D gravity anomaly inversion (Gozzard et al., 2018) crossing the SCS from SE China to NW Palawan coast. BB: Baiyun Basin, CC: Continental Crust EP: Enping Sub-Basin, ESB: East sub-basin IC: Indochina, QB: Qiongdongnan Basin, LB: Liwan Sub-Basin, NWPB: Northwest Palawan Basin, NWSB: Northwestern Sub-Basin, OC: Oceanic crust, P: Philippines, PKB: Phu Khan Basin, PRMB: Pearl River Mouth Basin, PW: Palawan, SHB: Song Hong-Yinggehai Basin, SWSB: Southwest Sub-Basin, TB: Tainan Basin, TW: Taiwan, V: Volcano, ZI: Zhu I Basin (Nirrengarten et al., 2020a). (D) Extended continental crust

across more than 1000 kilometers width with relatively flat Moho fluctuation imply a ductile lower crust along the South China Sea margin (Pichot et al., 2014).

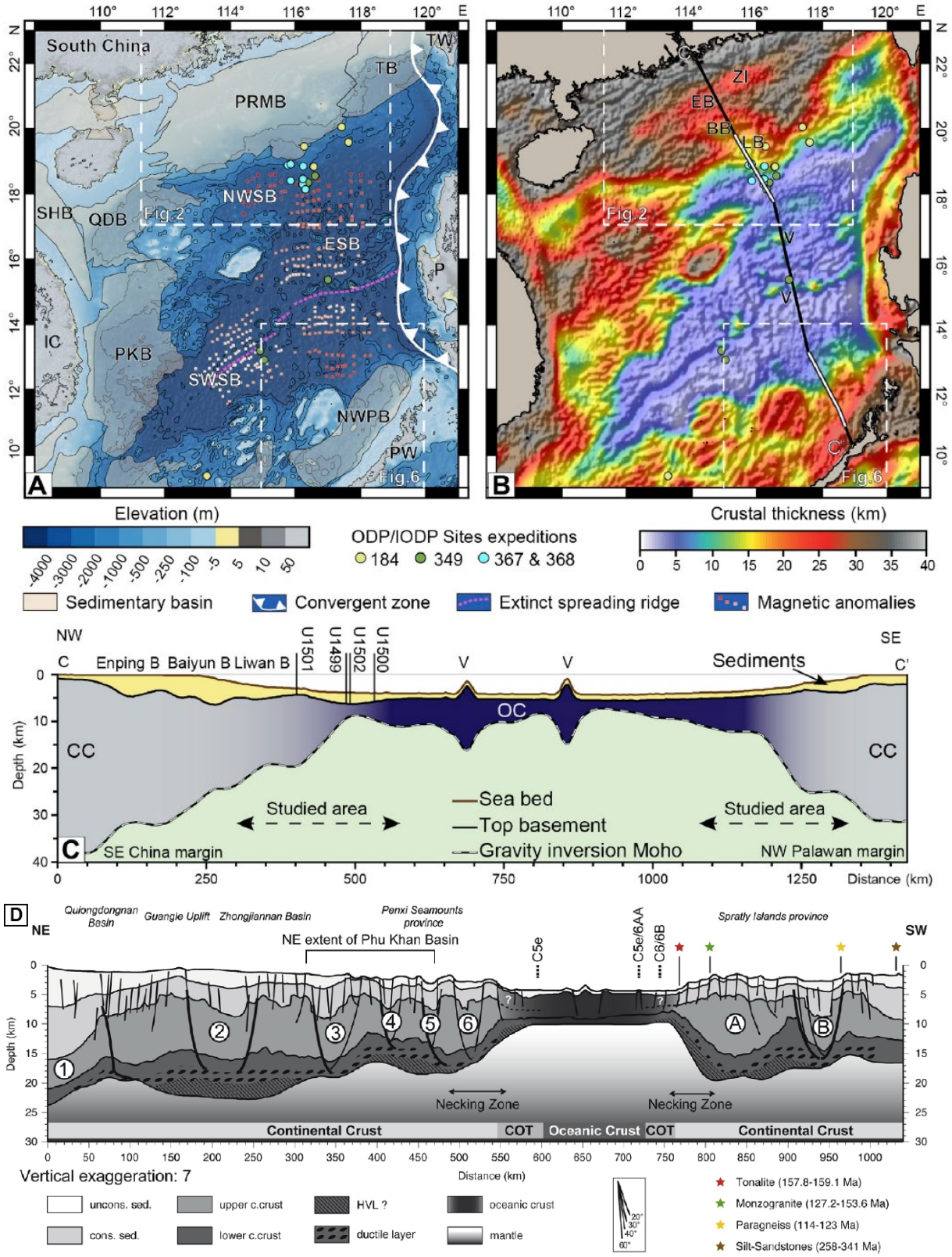

Among the marginal basin, the South China Sea has peculiar characteristics with wide stretched margins with many rifted basins surrounding the oceanic floor (Figure 2- 16A). The free-air gravity anomaly displays extensive rifted basins in the SCS margin where the crust thinned, especially in the western SCS margin (Figure 2- 16B).

The crust thickness thins seaward and the fault angle decreases to become a detachment fault on the distal margin (Lei and Ren, 2016; Liang et al., 2019; Xie et al., 2019)(Figure 2- 17 and Figure 2- 18). The COT is reported as narrow but without the existence of exhumed mantle in Baiyun Sag. Seismic data and IODP drilling have evidenced a rapid embryonic magma on the proximal high whereas the continental distal high encountered an adjacent pillow basalt series (Larsen et al., 2018; Nirrengarten et al., 2020a). The conjugated margin between SE China-NW Palawan revealed an asymmetrical margin during the breakup which implies an unstable period of the interplay between faulting and magmatism and is followed by subsequent stable and symmetrical seafloor spreading (Figure 2- 18) (Nirrengarten et al., 2020a). A possible detachment fault probably played an important role in thinning the crust, exhuming the asthenosphere and initiating the oceanic spreading.

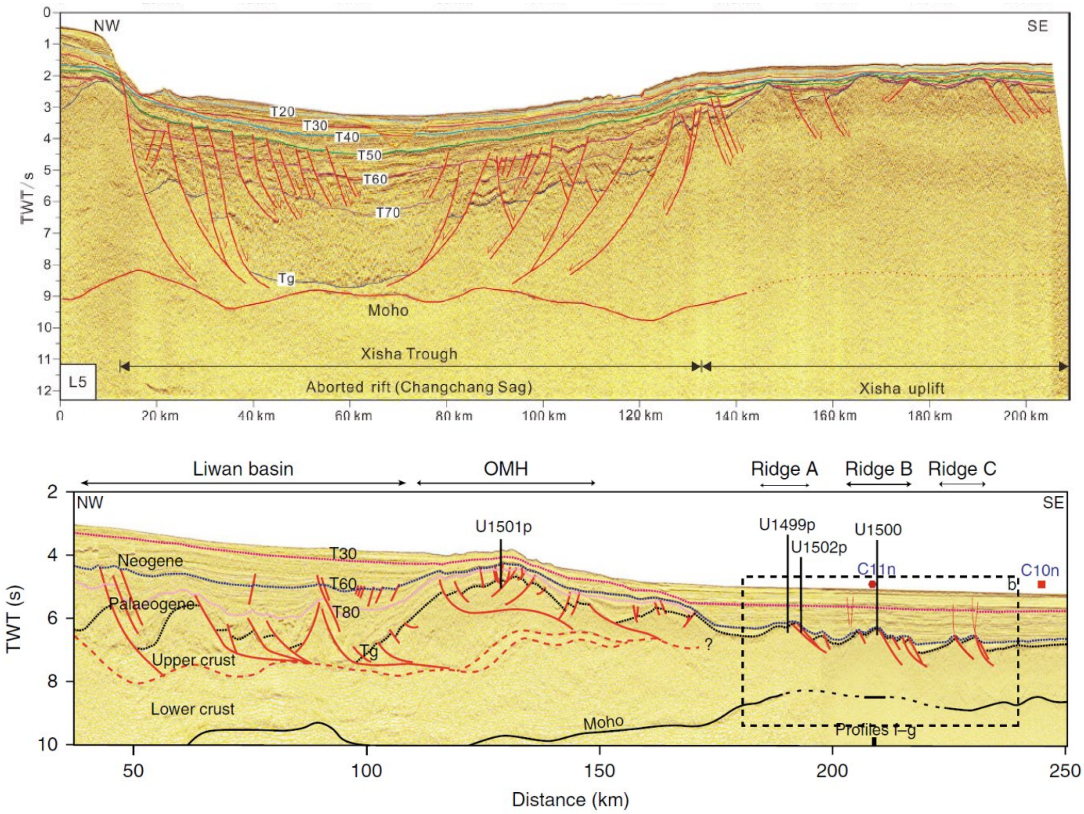

Figure 2- 17. (Upper) Crustal thinning occurs in the necking (Gao et al., 2016) and (lower) distal domain by the development of southward-dipping detachment fault in the northern margin of the SCS Margin (Larsen et al., 2018). The detachment fault thinned the continental crust mainly in the distal margin.

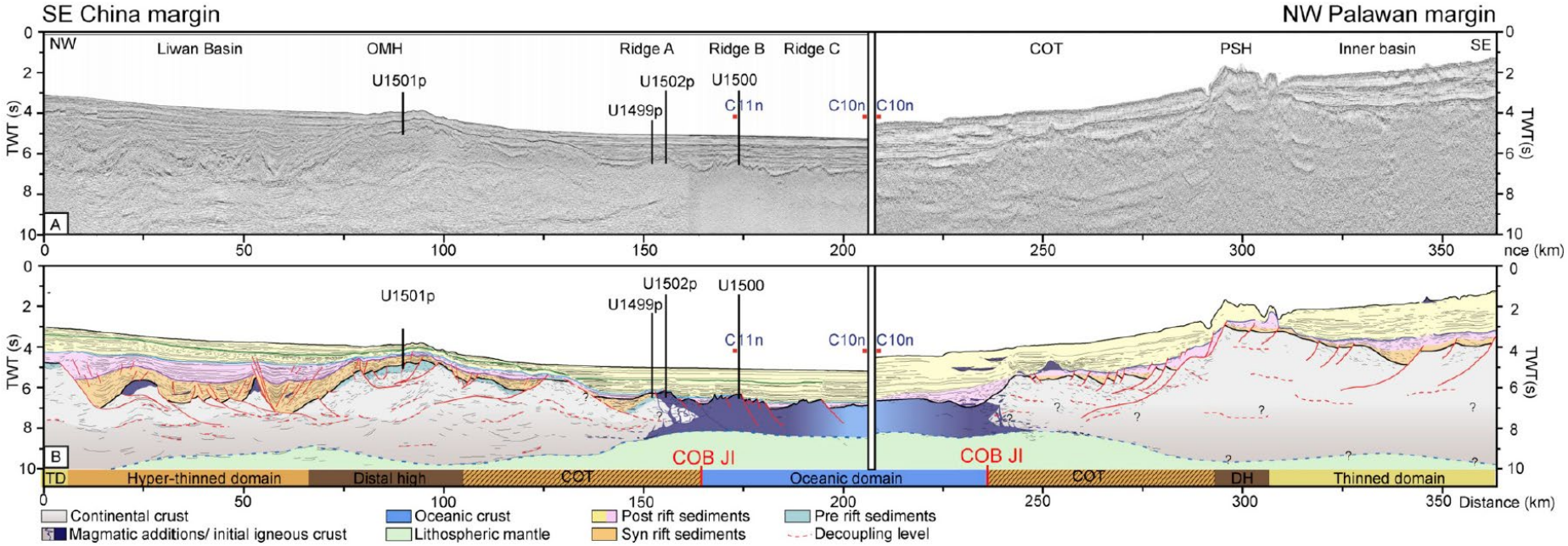

Figure 2- 18 Continent-ocean transition (COT) structure of conjugated margins of SE China-NW Palawan (Nirrengarten et al., 2020a).

Although there is no significant amount of the magmatism as SDRs, the syn-rift and post-spreading magmatism distribute extensively in the SCS margins (Figure 2- 20) (Yan et al., 2006; Zhao et al., 2016; Sun et al., 2019). The deep structure exposes a layer attached to the bottom of the crust having P-wave velocity higher than that of the crust (between 7.3-7.6 km/s, Franke (2013)). It is also well-known as the HVL in the SCS (red layer in Figure 2- 19) which constitutes one of the evidences to support a possibility of magmatic production, and this features has been linked to the abundant magmatic activity during syn-rift to recent time, such as the Dongsha Island and Hainan Plume (Lüdmann and Wong, 1999; Xie et al., 2017; Lei et al., 2019b).

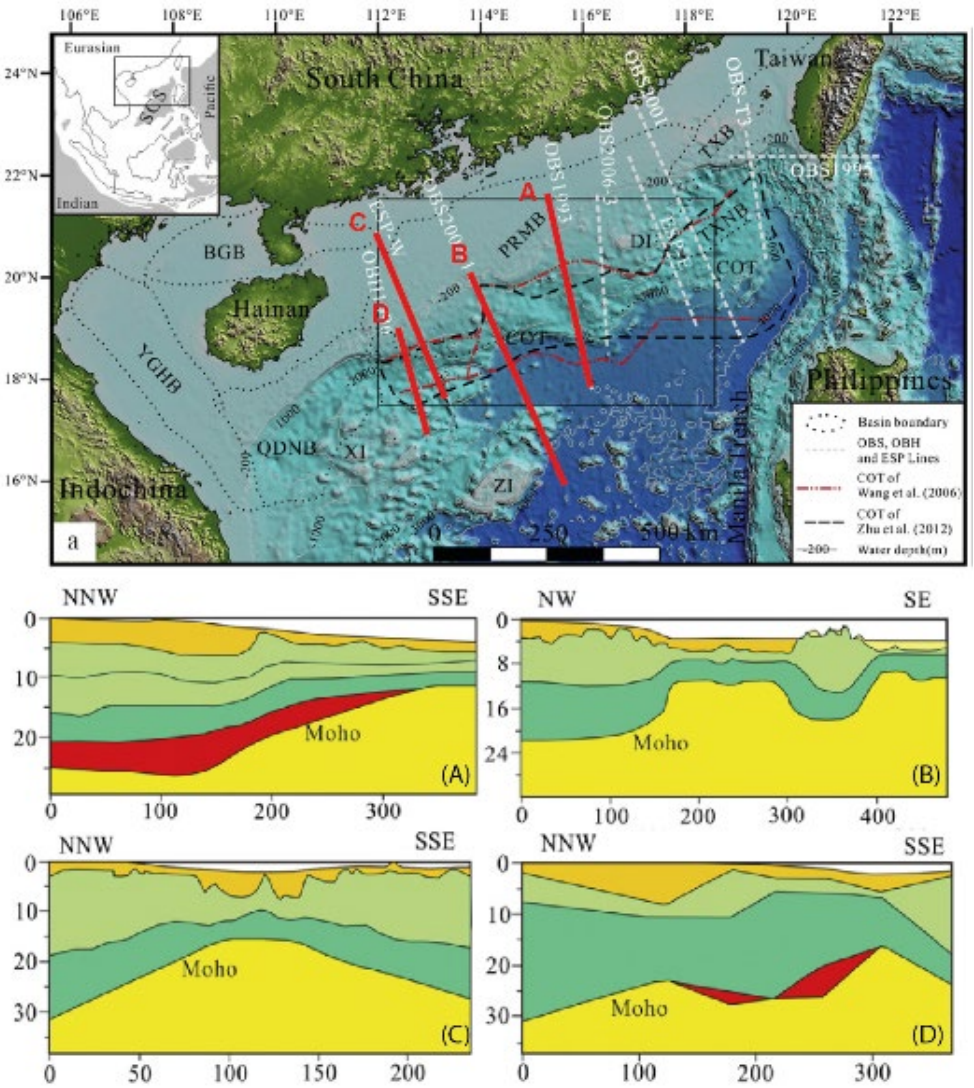

Figure 2- 19. The variation of crustal velocity structure along the northern SCS Margin, modified from (Gao et al., 2015). The red layer represents a high velocity layer (HVL) at the bottom of the crust, which is interpreted as magmatic underplating similar to that of the magma-rich margins.

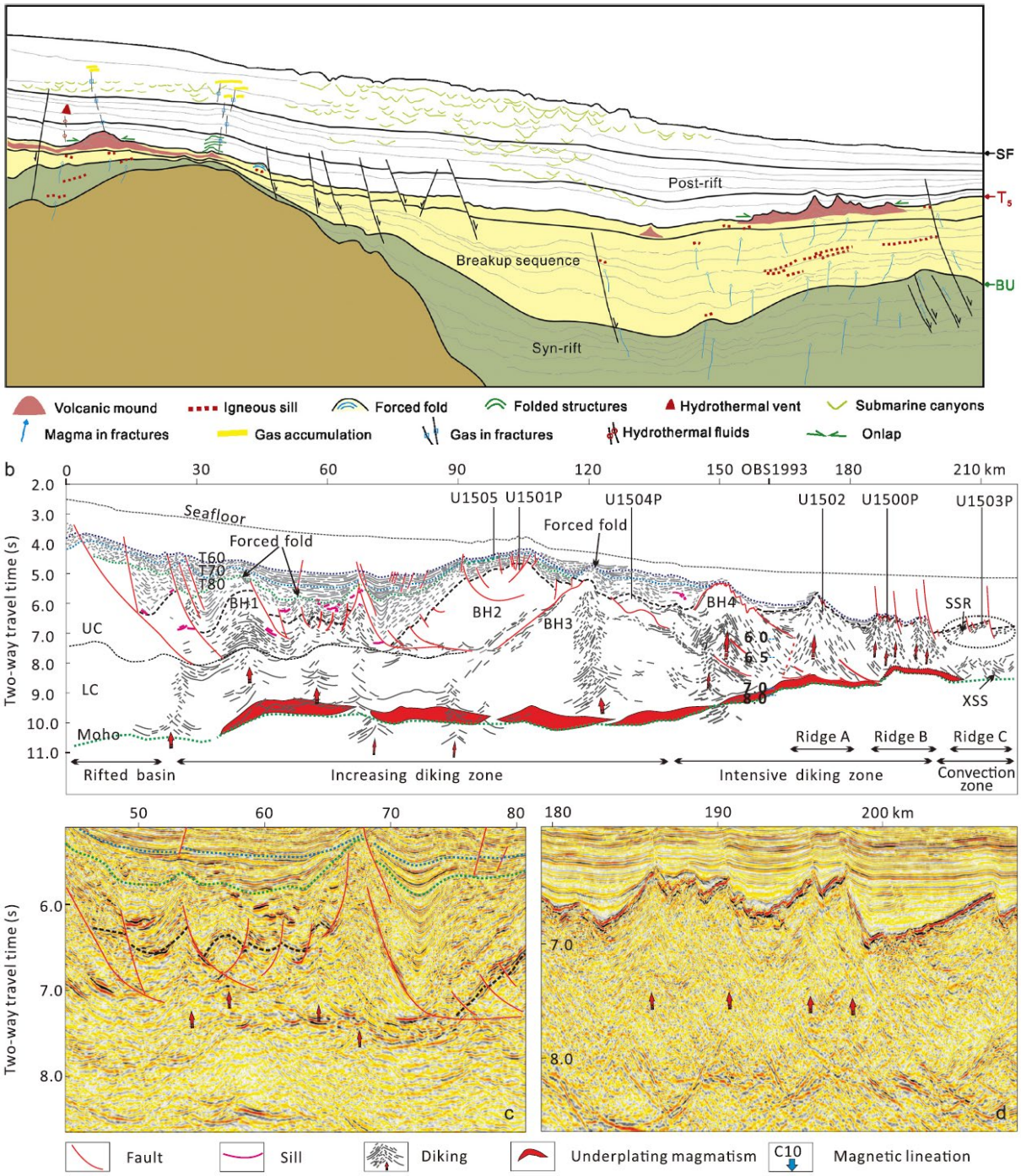

Figure 2- 20. The syn-rift magmatism in the SCS margin. Sills and volcanic mounds are illustrated and interpreted in the seismic profiles (Zhao et al., 2016; Sun et al., 2019). This may result from underplating at the base of the crust from which the volcanic laccolith originate.

The seafloor spreading period is identified mainly from the Oligocene to Early Miocene (Briais et al., 1993; Okubo et al., 1997; Barckhausen and Roeser, 2004). A significant V-shape reveal the propagator develop to the East and propagated westward (Figure 2- 21). During the spreading, the spreading center shifted twice; the second shift leading to the change of the opening direction N-S direction to NW-SE direction around 23 Ma, when a ridge jump occurred

and opened the SW sub-basin (upper on Figure 2- 22) (Li et al., 2014a; Qiu et al., 2016; Sibuet et al., 2016). The rifting of the SCS Margin resumed westward with clear diachronous rifting phenomena, with the breakup progressively migrating westward (Franke et al., 2014). The half-spreading rate from ca. 30 mm/yr decreased to ca. 15 mm/yr before the cessation of the seafloor spreading (lower on Figure 2- 22) (Briais et al., 1993).

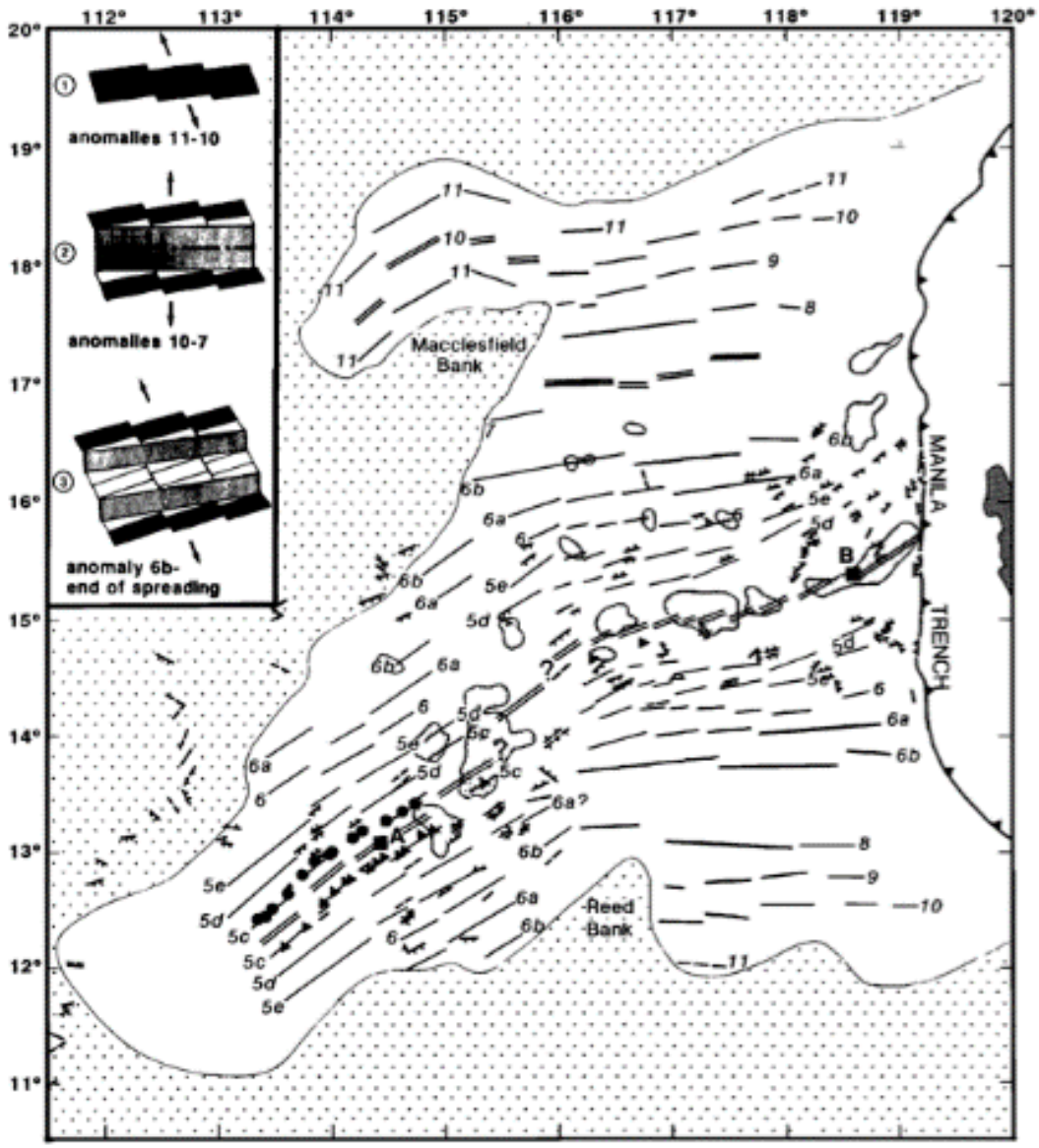

Figure 2- 21. The lineation of magmatic anomaly shows the seafloor spreading initiate in the east and propagated westward (Briais et al., 1993). Note the first shift in spreading center in the north of the NE sub-basin near anomaly 7.

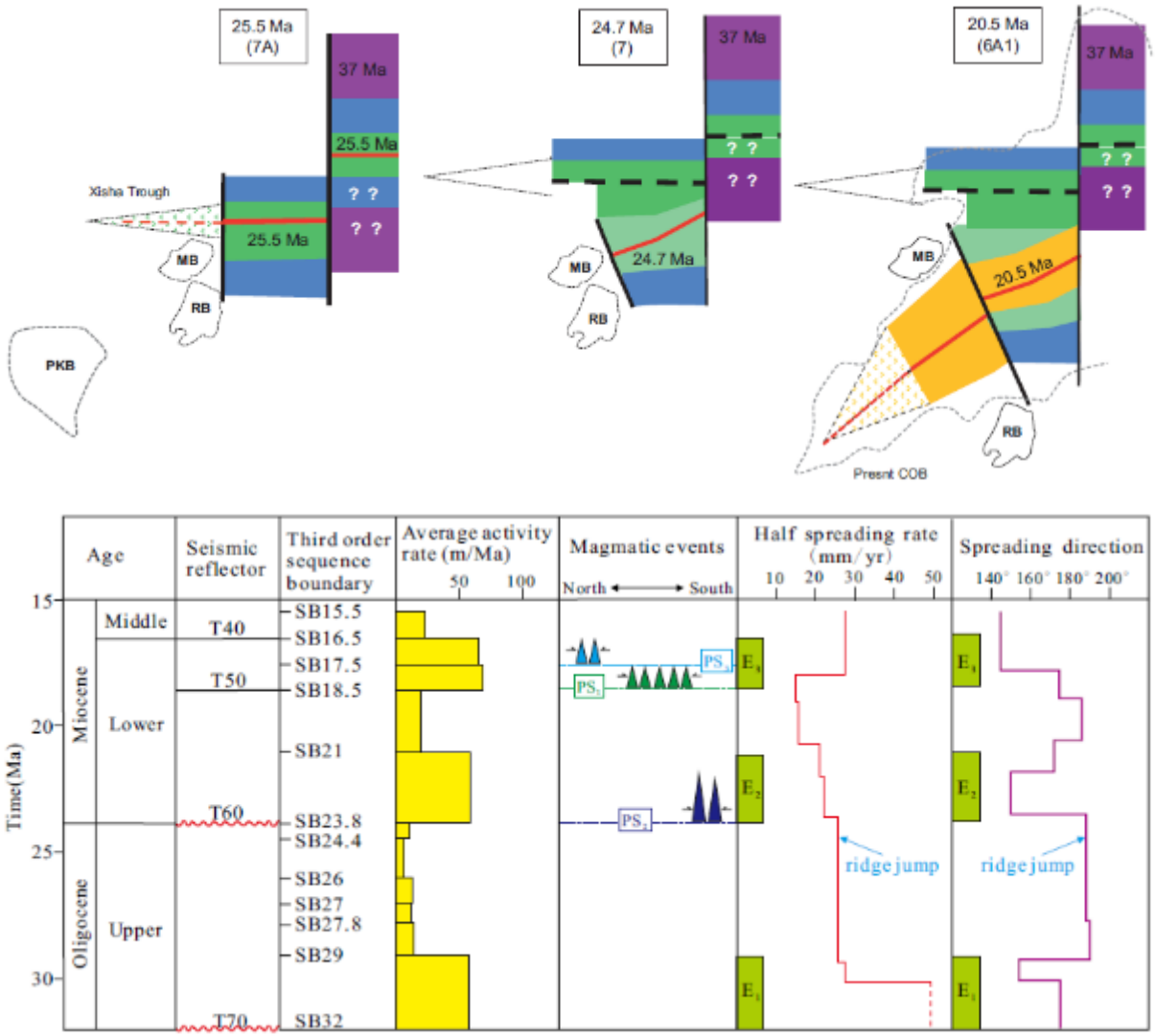

Figure 2- 22. (Upper) A progressive change of seafloor spreading direction from N-S to NW-SE (Cullen et al., 2010). According to magnetic anomaly, the counterclockwise change took place ca. 23-24 Ma. It went through a short stage during which anomalies were trending ENE, apparently trying to accommodate the shift of spreading directions. (Lower) Progressive change of seafloor spreading direction and correlation with the unconformities in the stratigraphy (Deng et al., 2018).

The change can be interpreted from the result of simulations by numerical modeling, which suggest that a far-field stress may control and halt a first phase of spreading propagation, and possibly trigger the development of a second phase of spreading propagation toward SW (Figure 2- 23), along a more suitable direction relative the regional constraints. Seafloor spreading since the Oligocene propagated globally westward and therefore the onset of the rifting and seafloor spreading transition (breakup) shows a diachronism along the rifting margin (Figure 2- 24) (Franke et al., 2014). It therefore reached a point where no oceanic crust is found, replaced by a series of coeval rifted basins distributed at the tip of the propagator whereas.

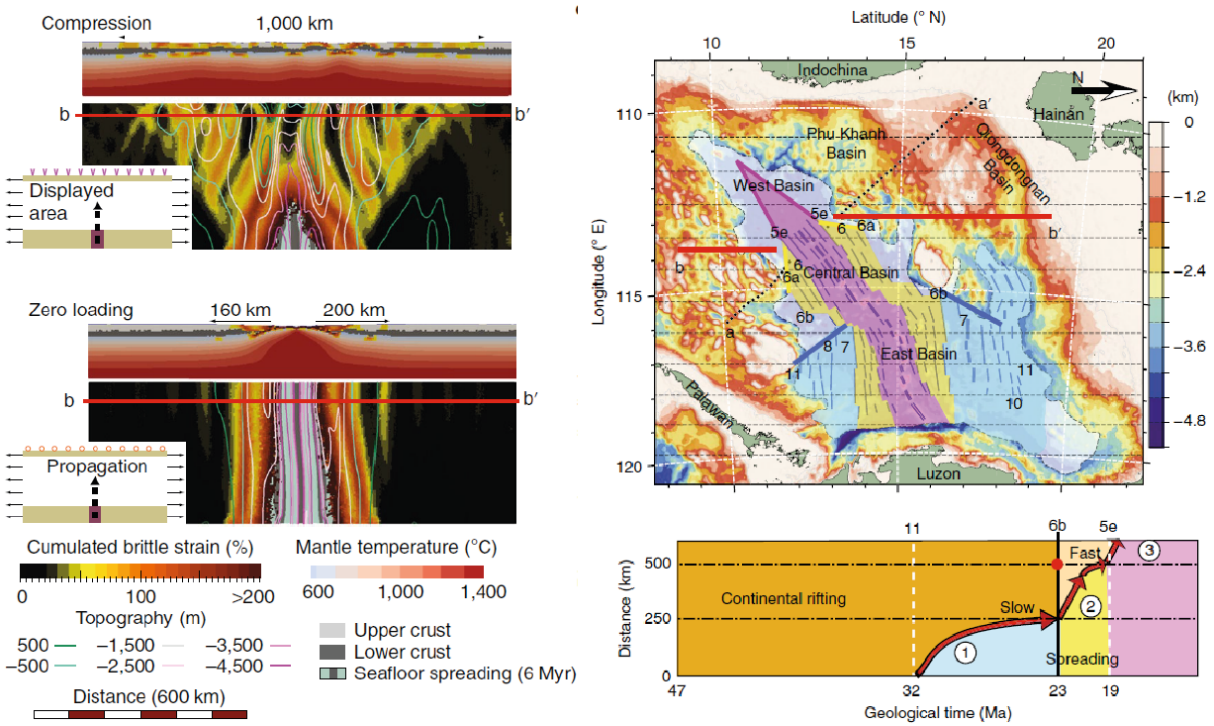

Figure 2- 23 Numerical simulation suggests extensive basins distributing adjacent to the tip of oceanic spreading and far-field stress determines the rifting history (Le Pourhiet et al., 2018). (A) Cylindrical rapid opening without along-axis compression (B) Model having along-axis compression. Only B is able to reproduce the V-shape opening and a wide continental rifted area. (C) V-shaped SCS margin modified from Sibuet et al., and rotated 90 degree to match the orientation of the model. (D) Extension rate through time speeded up around break-up (yellow).

The similar discrepancies in ages of unconformities can be traced in the stratigraphy. The breakup unconformity is shown at ~32 Ma, also well known as T7 or T70 (See correlation chart of stratigraphic references, Figure 2- 24), in the SE China-Palawan margins based on the IODP drilling across the ocean-continent boundary. The breakup unconformity shows a westward-younging diachronism along the margin. The main breakup unconformity in the western SCS, which is T6 (or T60 according to the terminology used in the literature) at 23 Ma, also appeared as a hiatus in the SE China margin (Larsen et al., 2018). Therefore, the unconformities named in T and numbers have added confusion in the understanding of geodynamic and tectonic evolutions in the South China Sea margin (Figure 2- 24) (Lin et al., 2003; Ding et al., 2008; Fyhn et al., 2009; Wu et al., 2009; Hu et al., 2013; Wang et al., 2013; Jin et al., 2014; Gao et al., 2015; Zhao et al., 2015; Zhou et al., 2015; Han et al., 2016; Zhao et al., 2016; Vu et al., 2017).

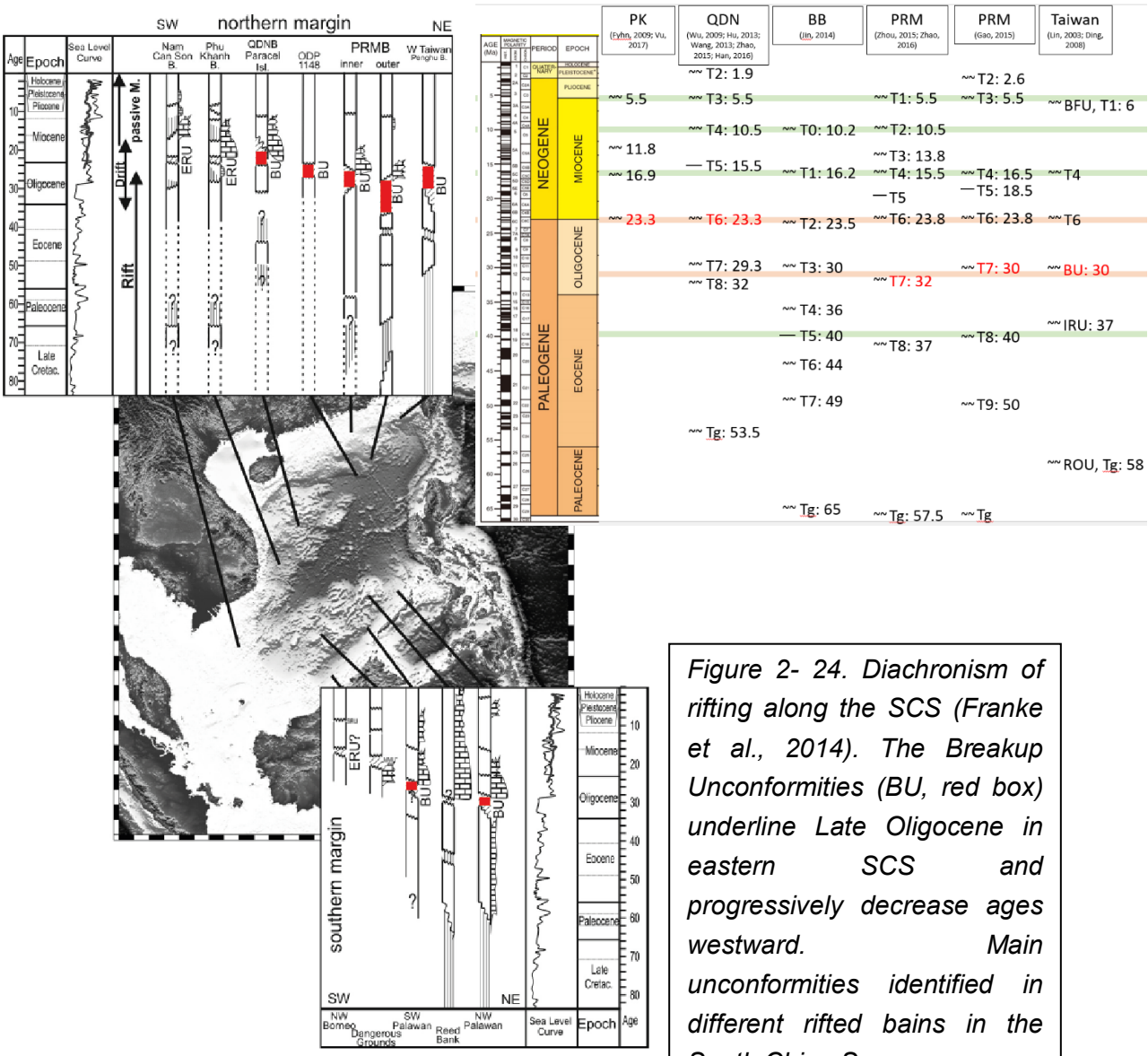

Figure 2- 24. Diachronism of rifting along the SCS (Franke et al., 2014). The Breakup Unconformities (BU, red box) underline Late Oligocene in eastern SCS and progressively decrease ages westward. Main unconformities identified in different rifted bains in the South China Sea.

2.3.2 Differences between N and S margin

The sedimentary basins also record the evolution in Cenozoic times. The depositional environment interestingly shares similarities during the pre- and syn-rift strata. Metamorphic rocks compose the basement of the pre-rift as known from early studies in the 1980s (Holloway, 1982). Some low metamorphic grade sediments have been collected by the later drilling and dredging (Kudrass et al., 1986). The syn-rift consisted of larger amount of coarse-grained sediments interfingering with fine-grained sediments. The environment became different only after the breakup. The post-rift successions yields fine-grained sediments representing the deep-sea environment in the northern margin, while the southern margin is characterized by carbonate or calcareous layers deposited at a relatively shallower water depth (Figure 2- 25).

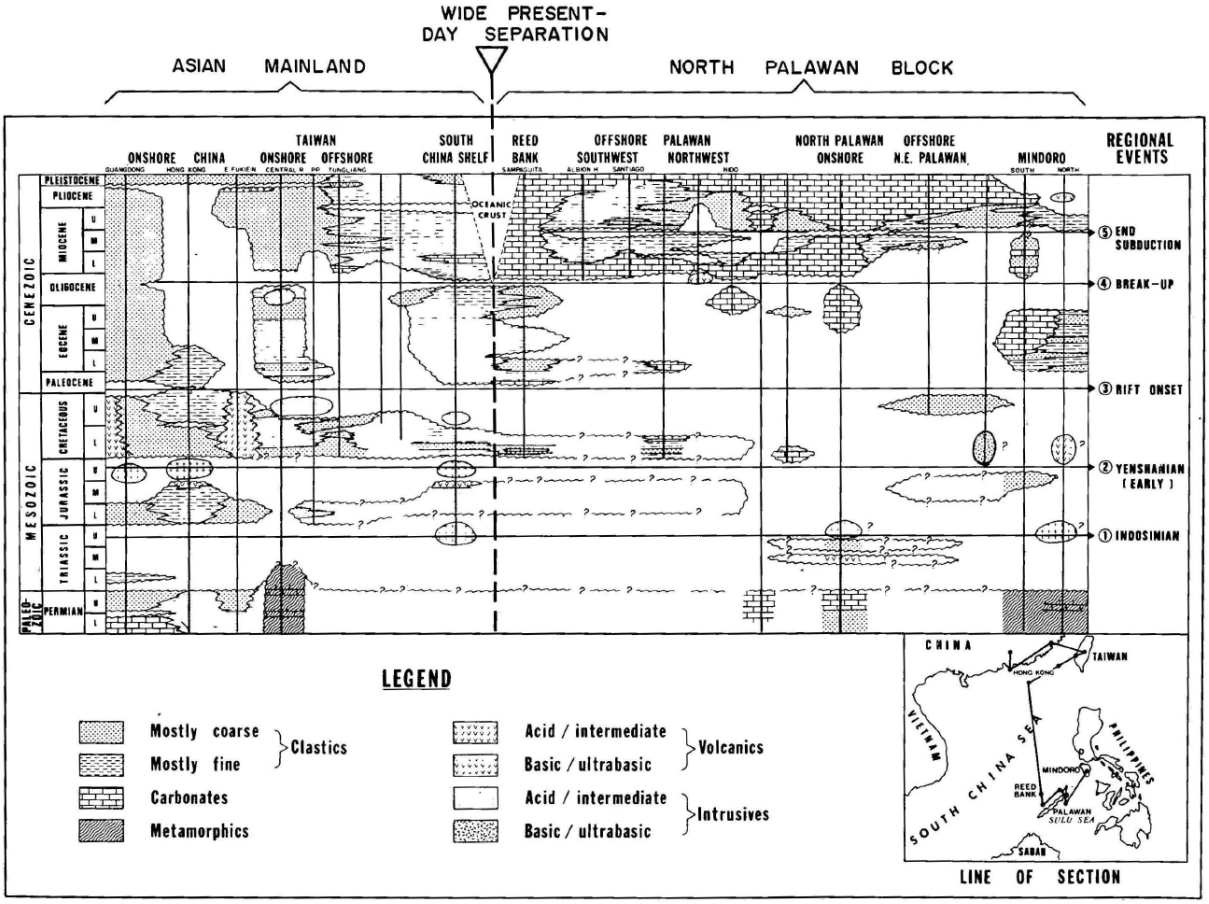

Figure 2- 25. Stratigraphic correlation across SE China-Palawan margin (Holloway, 1982). The depositional environment of post-rift strata has shown sharp difference between the Northern and the Southern margin.

The thickness of syn-rift unit also shows a significant variation from N to S (Figure 2- 26). The syn-rift layer pinches out in the NW Palawan offshore down to the 200 meters maximum thickness. Some wells find the Cretaceous basement underlain directly the Neogene Nido Limestone without the syn-rift sediments (Figure 2- 26). This hiatus can be identified from the seismic profiles to show an erosional surface to eliminate the syn-rift sediments (Franke et al., 2011; Steuer et al., 2014). Similar observations were done by Liang et al. (2019) in the Dangerous Grounds region.

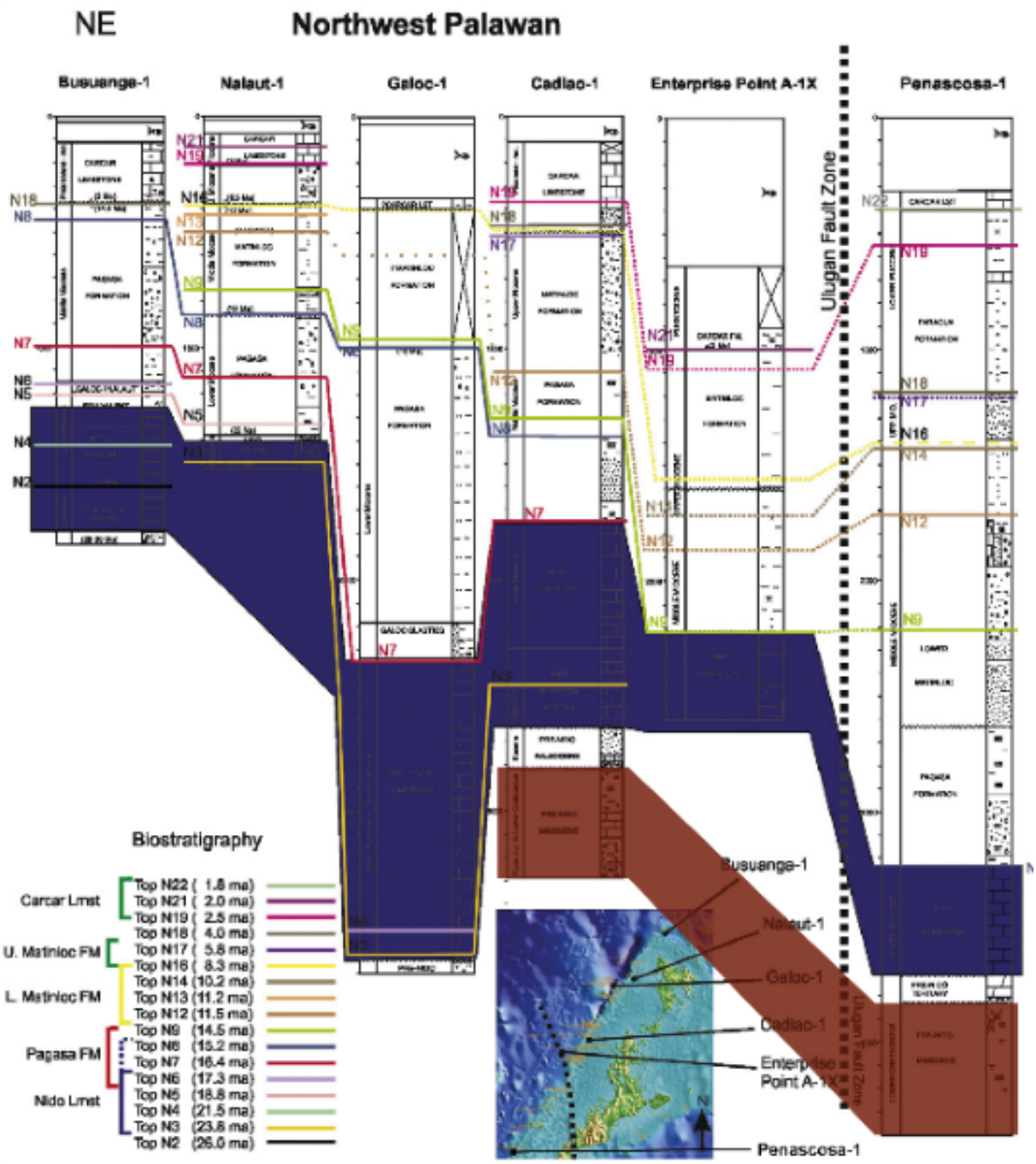

Figure 2- 26. Well correlation of Nido carbonate platform layer (dark purple color) within post-rift successions in the offshore Palawan, modified from (Steuer et al., 2013). The few-meters thin syn-rift layer superposed between the Nido and Mesozoic basement (brown color) imply the hiatus in the rifting history.

It has been widely accepted that southern margin of the SCS had penetrated deep underneath the Palawan and Borneo wedge (Figure 2- 27) (Franke et al., 2008; Sapin et al., 2011; Madon et al., 2013; Steuer et al., 2014; Tong et al., 2019). The influence of the developing wedge from the south to the north is illustrated by the growth of the carbonate platform in the Dangerous

Ground and Spratly Islands (Steuer et al., 2014; Chang et al., 2015). The carbonate platform mostly developed along the crest of the half-horst and drowned toward the Borneo Trough into deep-sea sediment again (Figure 2- 27) (Steuer et al., 2014; Jamaludin et al., 2017). The orientation of these spreading platform is similar with the distribution of Palawan-Borneo wedge; this having been interpreted by the wedge loading on an elastic crust creating a forebulge in the southern margin (Figure 2- 27) (Steuer et al., 2014).

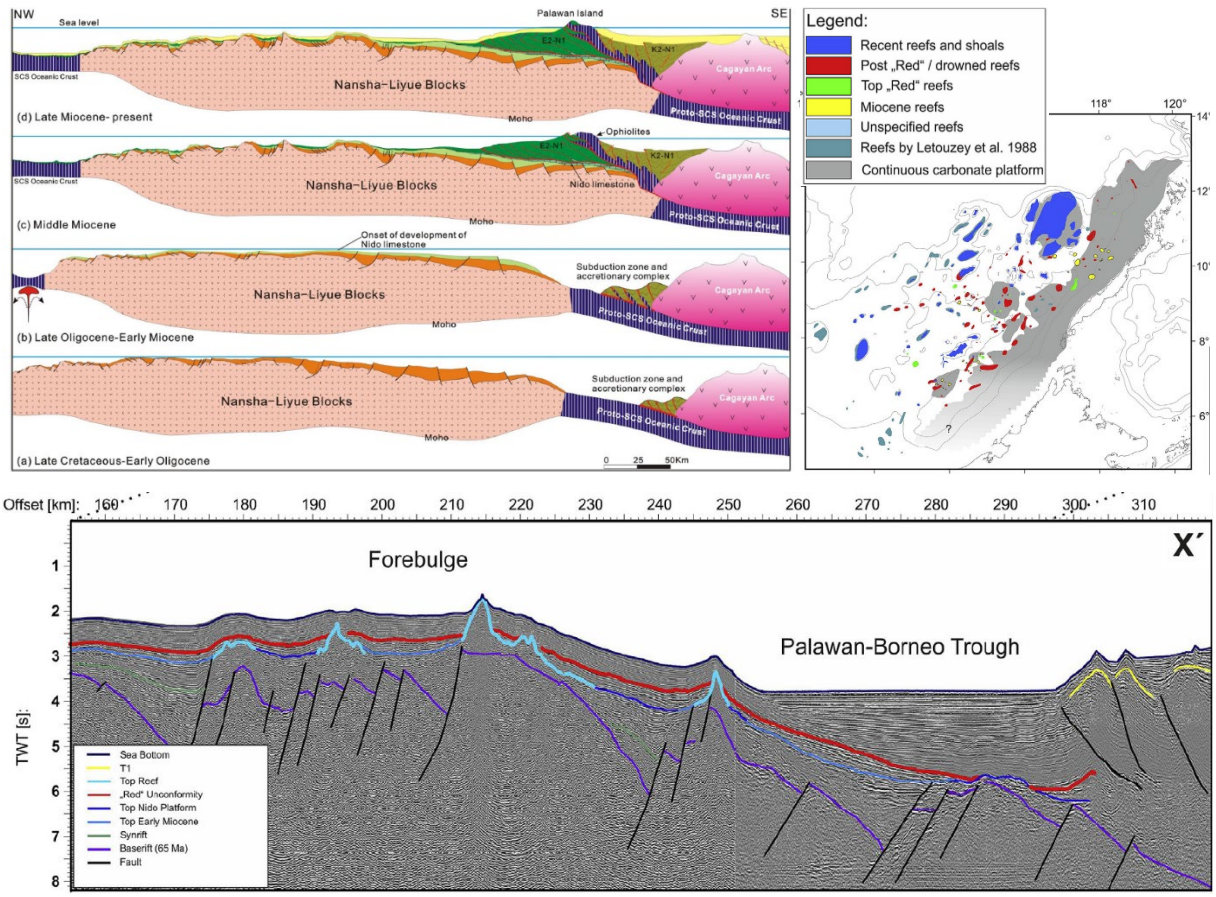

Figure 2- 27. (Top left) Cross section illustrating the basin evolution during the PSCS subduction (Tong et al., 2019). (Top right) Cenozoic carbonate distributes in the southern SCS margin next to the Palawan-Borneo Trough (Steuer et al., 2014). (Lower) the carbonate developed along the horst and sustain a shallower water depth at the forebuldge (Steuer et al., 2014).

This flexural feature has suggested the boundary forces are partly due to a larger loading in the south. The northern margin is relatively stable since Cretaceous times, whereas the southern margin has suffered from boundary forces from the subduction-related far-field stress. All the features and their differences between the N and the S could be crucial to understand and

illustrate the variation of far-field stress. This may not be sufficient though to explain the NW Borneo Trough which bears the characters of a graben.

2.4 Closure of PSCS: accretionary wedge, fold-and-thrust belt

2.4.1 Active subduction-collision boundary in the SCS

To the east side of the SCS, the active subduction-collision boundary between the SCS and Philippine Sea Plate composes the Philippine Mobile Belt (Figure 2- 28). This is a plate boundary amalgamated blocks and micro-plates in a narrow belt since Early Cenozoic (Pubellier et al., 2003; Aurelio et al., 2013). It follows a clockwise rotation of the plate motion; the Philippine Sea Plate moving northward along the east edge of Sundaland in SE Asia (Queano et al., 2007; Yamazaki et al., 2010; Richter and Ali, 2015; Wu et al., 2016).

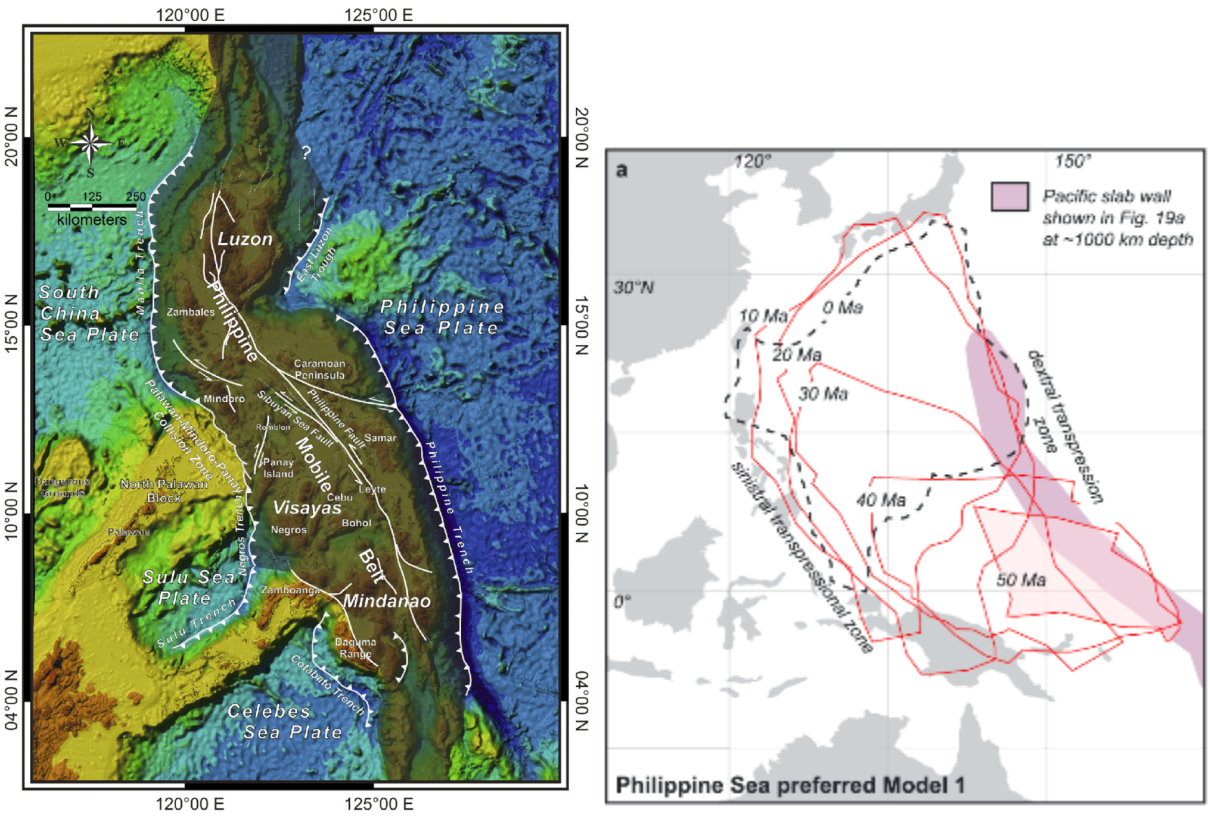

Figure 2- 28. (left) Philippine Mobile Belt is located at the eastern edge of the SCS (Aurelio et al., 2017), and (right) the plate reconstruction of Philippine Sea Plate to reveal the path of amalgamation of Philippine Mobile Belt (Wu et al., 2016).

While the SCS is subducting eastward beneath the Philippine Sea Plate, the various configuration of the lower plate from continent-arc collision in Taiwan and Mindoro still shows that the angle of the subducted plate varies (Figure 2- 29); deepening southward (Figure 2- 30).

The horizontal docking of the Philippine Mobile Belt (PMB) occurred when the continental bridge of Palawan (McCabe et al., 1982; Marchadier and Rangin, 1990) encroached the PMB and the subduction zone still proceeded in to the South China Sea, the Sulu and the Celebes seas.

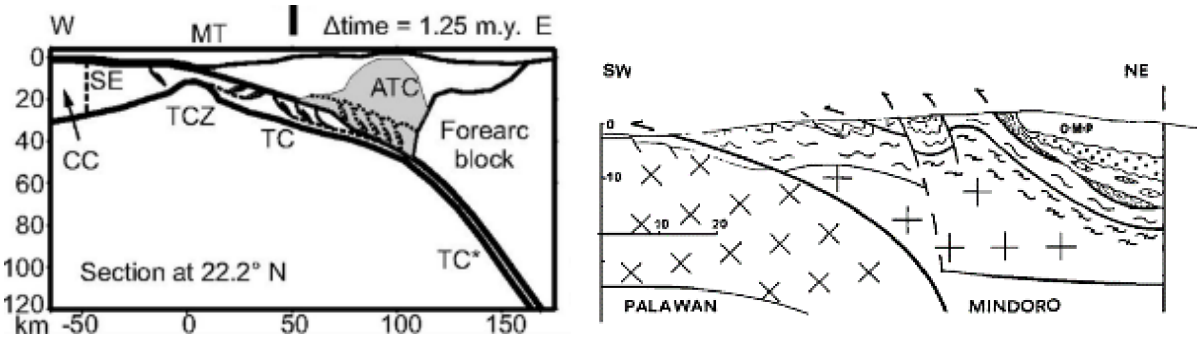

Figure 2- 29. Different styles of convergence along the SCS subduction-collision belt depending on the origin of the lower plate. Both are located at the edge of the Philippine Sea Plate as it encroaches the China margin. (Upper left) subducted continental crust causing the Taiwan Orogeny and, (upper right) a more complex continent-continent collision followed by an arc collision in Mindoro (McCabe et al., 1982; Faure and Ishida, 1990; Marchadier and Rangin, 1990; McIntosh et al., 2014).

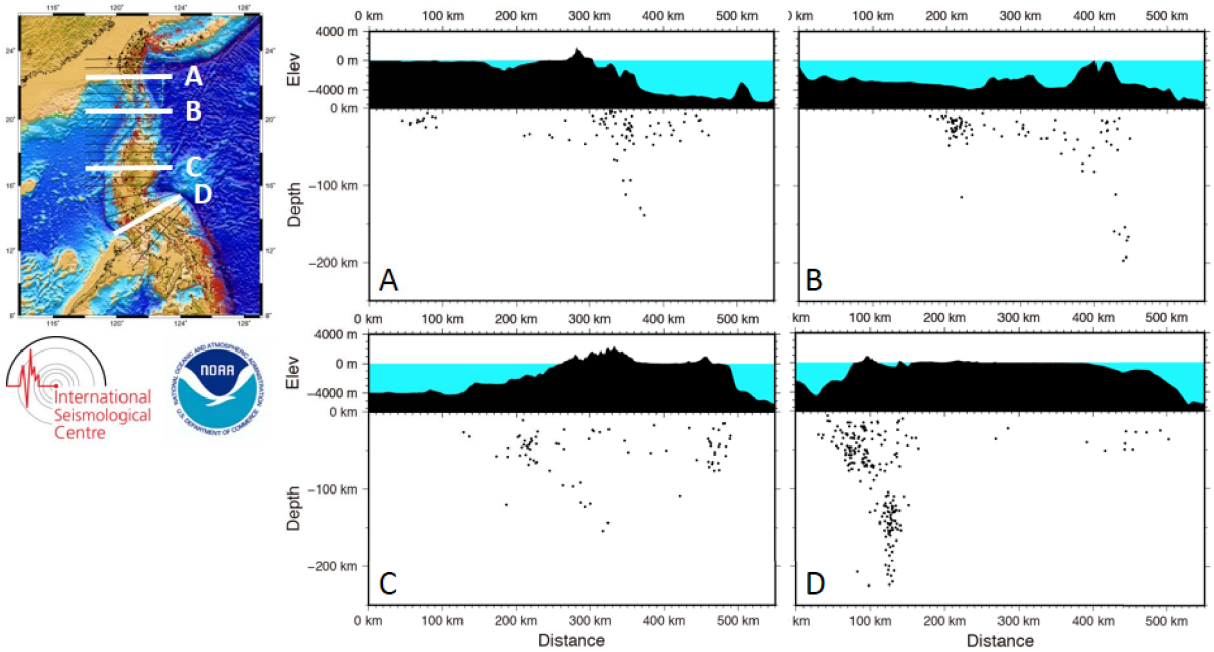

Figure 2- 30. Subduction occuring along Manila Trench and showing a variation of subducting angle of the lower plate.

The active accretionary wedge caused a loading to result in a flexural features along the Manila Trench, for instance, collision in the Taiwan area and oceanic subduction along the Manila Trench (Figure 2- 31) (Chang et al., 2013).

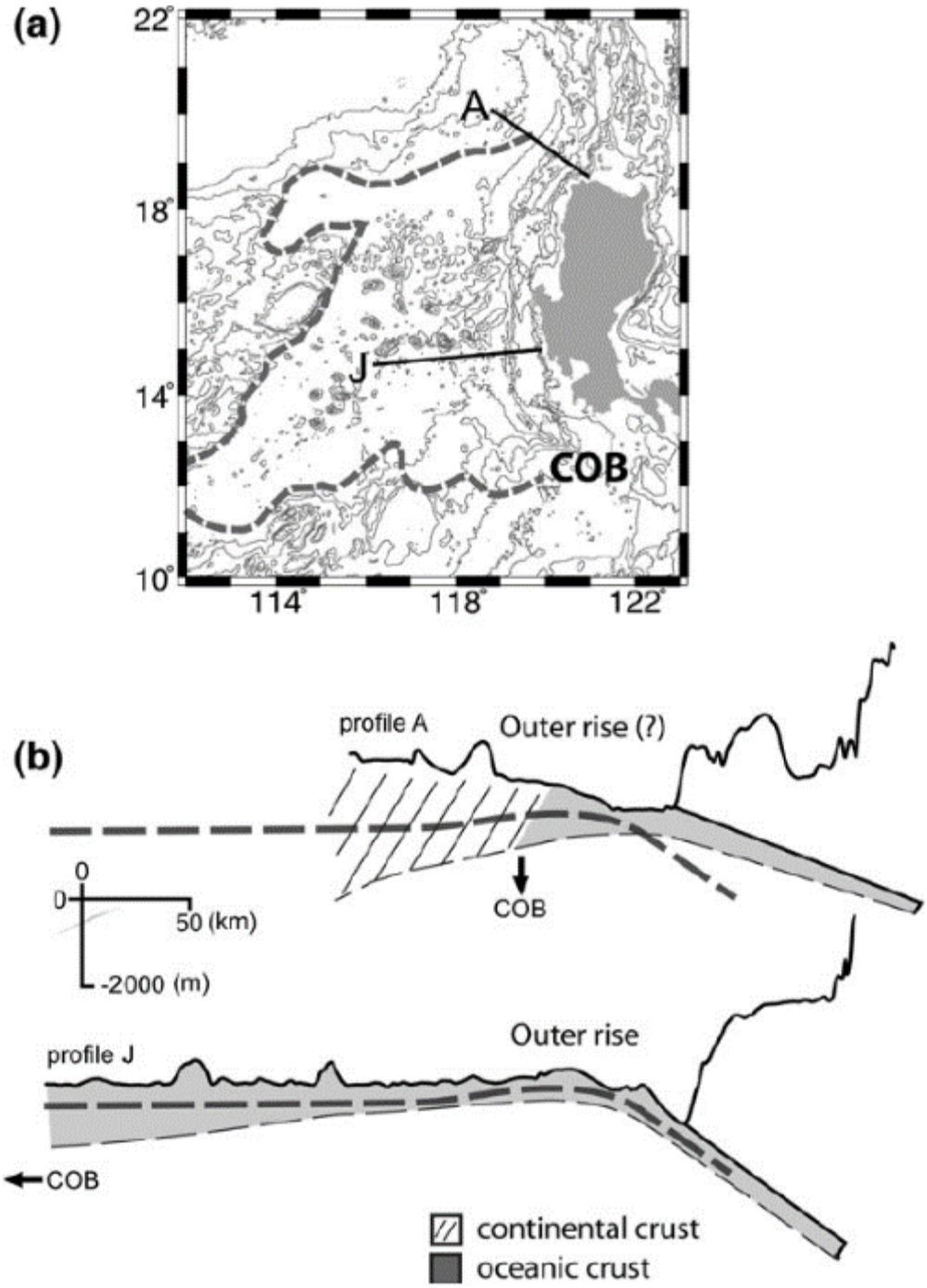

Figure 2- 31 Flexural features shown on the bathymetry along the Manila Trench (Chang et al., 2013).

2.4.2 The inactive subduction-collision zone of the PSCS

The closure of Proto-South China Sea, inactive since the Middle Miocene (McCabe et al., 1982; Fricaud, 1984; Marchadier and Rangin, 1990; Pubellier et al., 2001) is one of the most comprehensively documented inland and offshore, which accumulated accretionary complex and scattered ultramafic and mafic rocks in the Borneo and Palawan regions. Although the subduction has been debated in the last decade due to the different rotation results from paleomagnetism analyses (Figure 2- 32). The subduction initiated around 35 to 40 Ma, Late Eocene times having been dated in the metamorphic in Palawan and Eocene conglomerate formation engulfing ophiolite blocks in Sabah (Omang and Barber, 1996; Keenan et al., 2016). This closure can be recognized inland by ophiolite, volcanic arc, and the accretionary complex in various metamorphism.

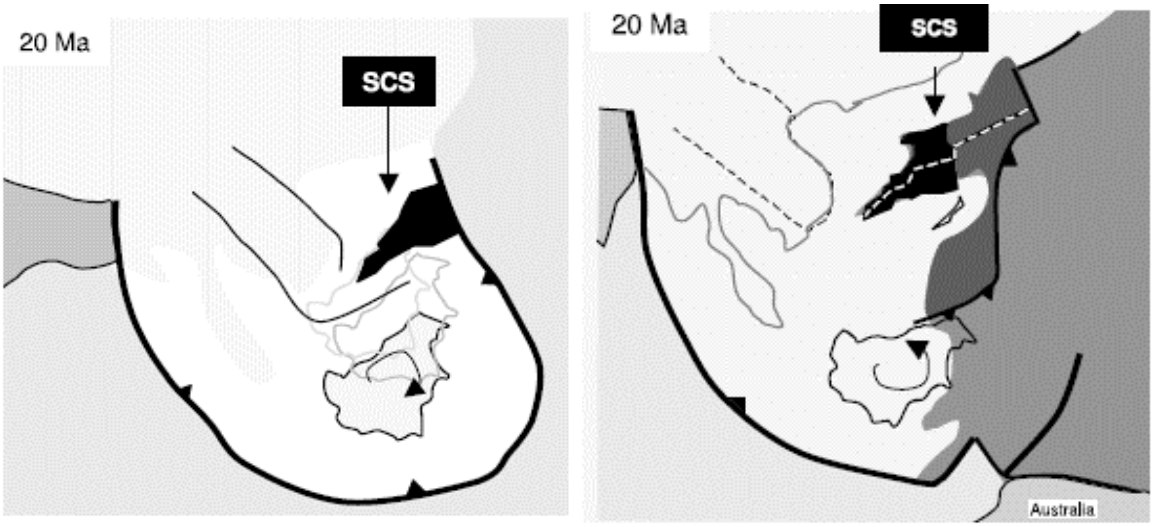

Figure 2- 32. Rotation during Miocene in Borneo and therefore two hypotheses whether the participation of PSCS subduction in the tectonic evolution (Fuller et al., 1991; McCabe et al., 1993; Fuller et al., 1999; Almasco et al., 2000; Cullen, 2010; Advokaat et al., 2018).

From the stratigraphic point of view, the Cenozoic strata distribute along mountain range in few hundred meters height, which are interpreted as the accretionary wedge seaward-younging associated to the PSCS subduction and collision. Few key widespread Cenozoic unconformities are documented onshore, Sarawak (Rajang) Unconformity and Deep Region (Nyalau) Unconformity (Figure 2- 33) (Cullen, 2010; Hennig-Breitfeld et al., 2019) and reference therein. These stratigraphic boundary separate the wedge into two stratigraphic groups; the Rajang Group and the Crocker Group (van Bemmelen, 1949; Hamilton, 1979; Tongkul, 2003). The two groups are usually recognized by the metamorphism with a higher degree in the Rajang

Group, as well as facies being generally more distal marine for the Rajang group. A lower metamorphism exists in the Crocker Group within the Oligocene to Lower Miocene strata.

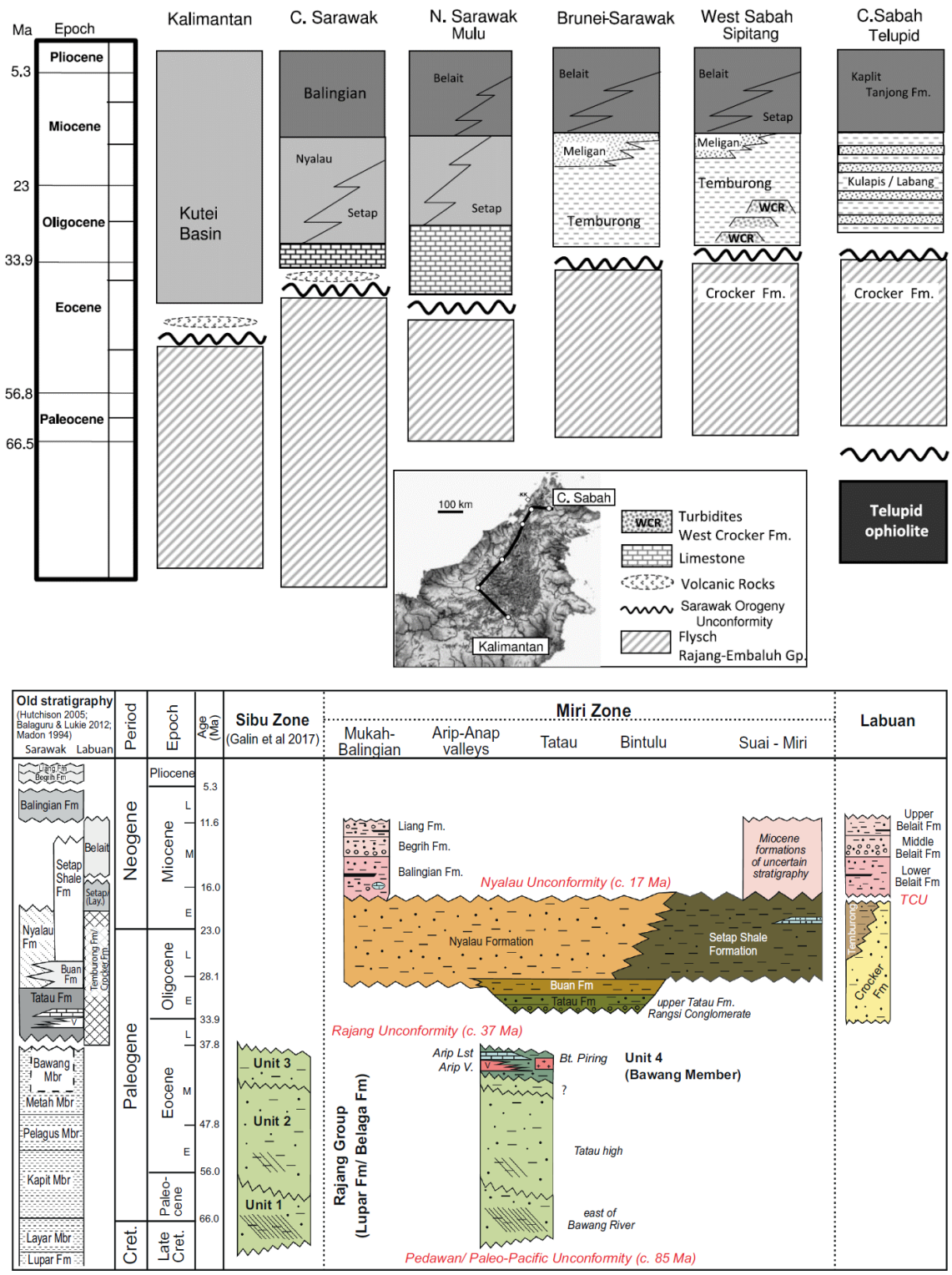

Figure 2- 33 Stratigraphic chart of northern and Southwest Borneo (Cullen, 2010; Hennig-Breitfeld et al., 2019), showing extensively distributed unconformity. Rajang and Sarawak Unconformity position around Late Eocene; Nyalau Unconformity and Deep-Regional Unconformity (DRU) around 16 Ma.

In the offshore, the fold-and-thrust belt shows various structures seaward to the Borneo-Palawan Trough (Cullen, 2010). In the offshore Sabah at the north, the Crocker Group appears in the proximal offshore (Figure 2- 34). The strata overlying upon the DRU-MMU delineating the termination of the orogeny (Cullen, 2010). The wedge structure varies southward to become wider and thicker delta deposition above the DRU. A large part of the Crocker Group (yellow and orange color on Figure 2- 34) or older stratigraphic units distributes onshore (blue and green color on Figure 2- 34).

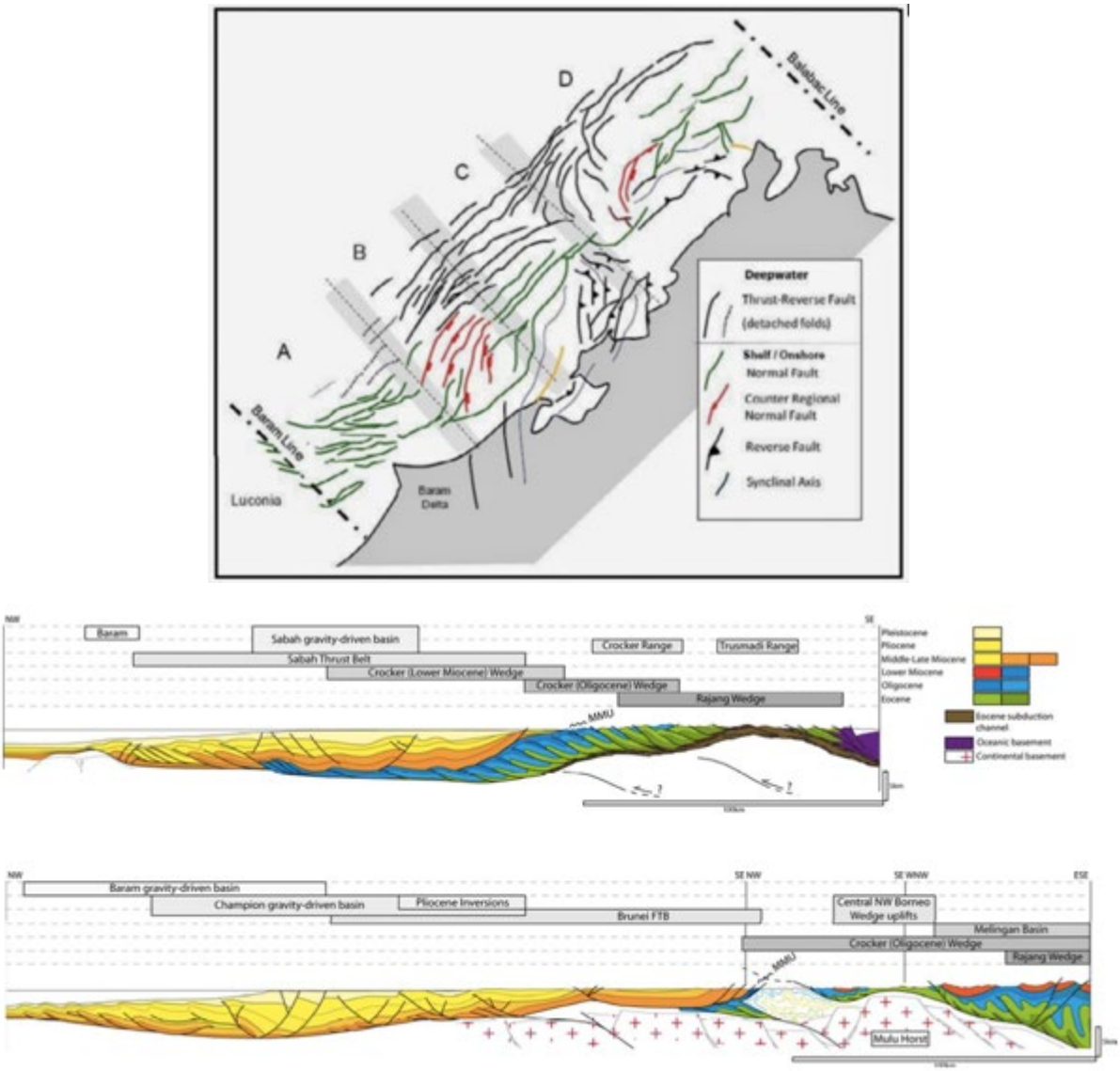

Figure 2- 34 (Top-left) The structural map of fold-and-thrust (FAT) belt in the offshore NW Borneo. (Middle) the cross-section of Sarawak and Brunei illustrates the FAT belt which older Eocene Rajang Group underlain by the younger and lower deformation Crocker Group (Sapin et al., 2011). (Lower) the cross-section of Sabah shows the younger Crocker Group which overlies the basement.

Although the collision was completed in the Middle Miocene, the thrusting has been demonstrated as active, and in fact reactivated in the recent time in the frontal wedge (Figure 2- 35) (Franke et al., 2008; Sapin et al., 2011). Many old studies therefore assumed that the convergence was sustained up to recent times and delineate a trench in the Borneo-Palawan Trough area (Hutchison, 2010). GPS studies have however suggested that the activity was simply the reactivation as a gravity collapse of the frontal part of the wedge into the Palawan Trough (Sapin et al., 2013), possibly owing to the Kinabalu uplift (Chang et al., 2019).

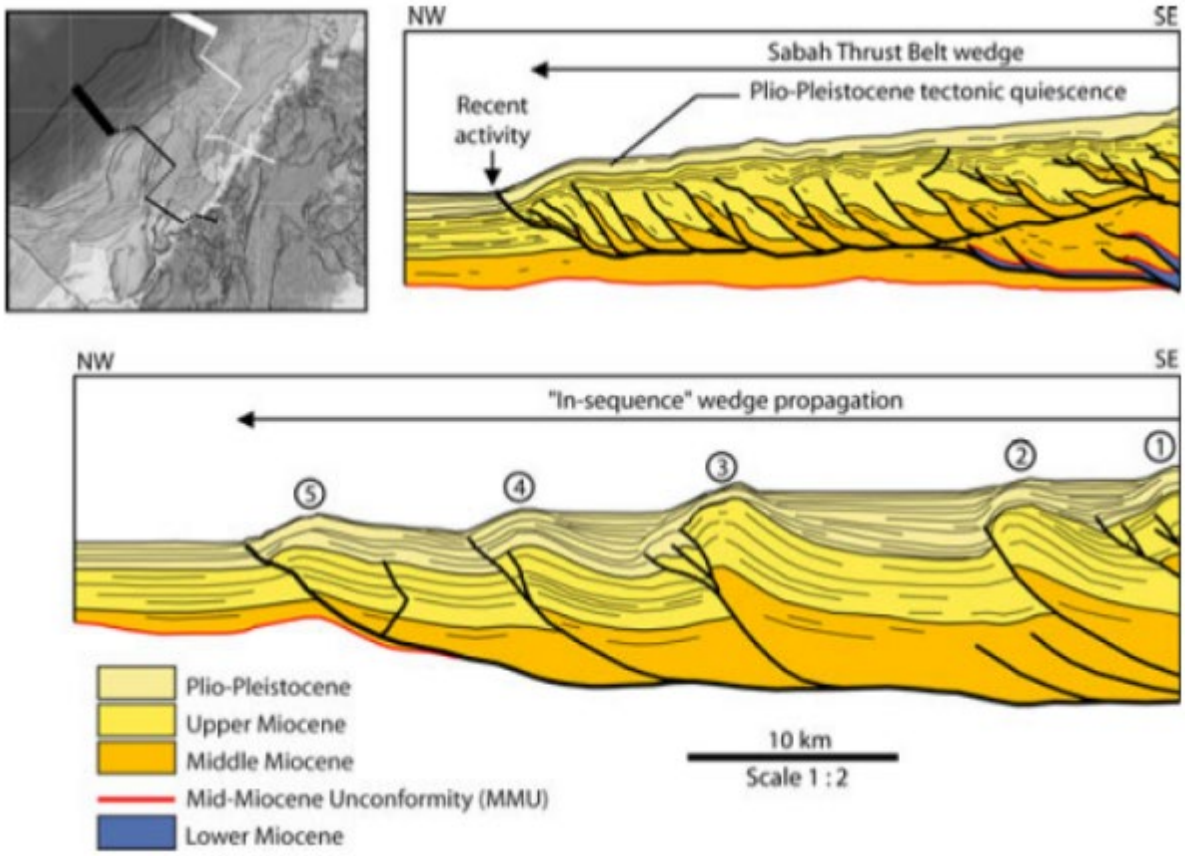

Figure 2- 35. The recently active stacking is observed, located at the frontal thrust in the offshore NW Borneo (Sapin et al., 2011).

Other observations indicate that shale tectonics occurred in the shallow part of the accretionary wedge coeval with the recent deformation, and the overlying Late Cenozoic strata, causing collapse of olistostrome or distal muddy layer. This layer is able to mobilize due to the over pressure and compensate the extensional motion landward therefore resulting in the compressional structures in the frontal wedge offshore Palawan (Figure 2- 37) or in the offshore Sabah and Brunei (Figure 2- 36) (Morley, 2007; Sapin et al., 2011). A similar mobilized layer

is underlain beneath the frontal wedge and characterizes a mass transport deposits in the offshore (Figure 2- 37) (Ilao et al., 2018).

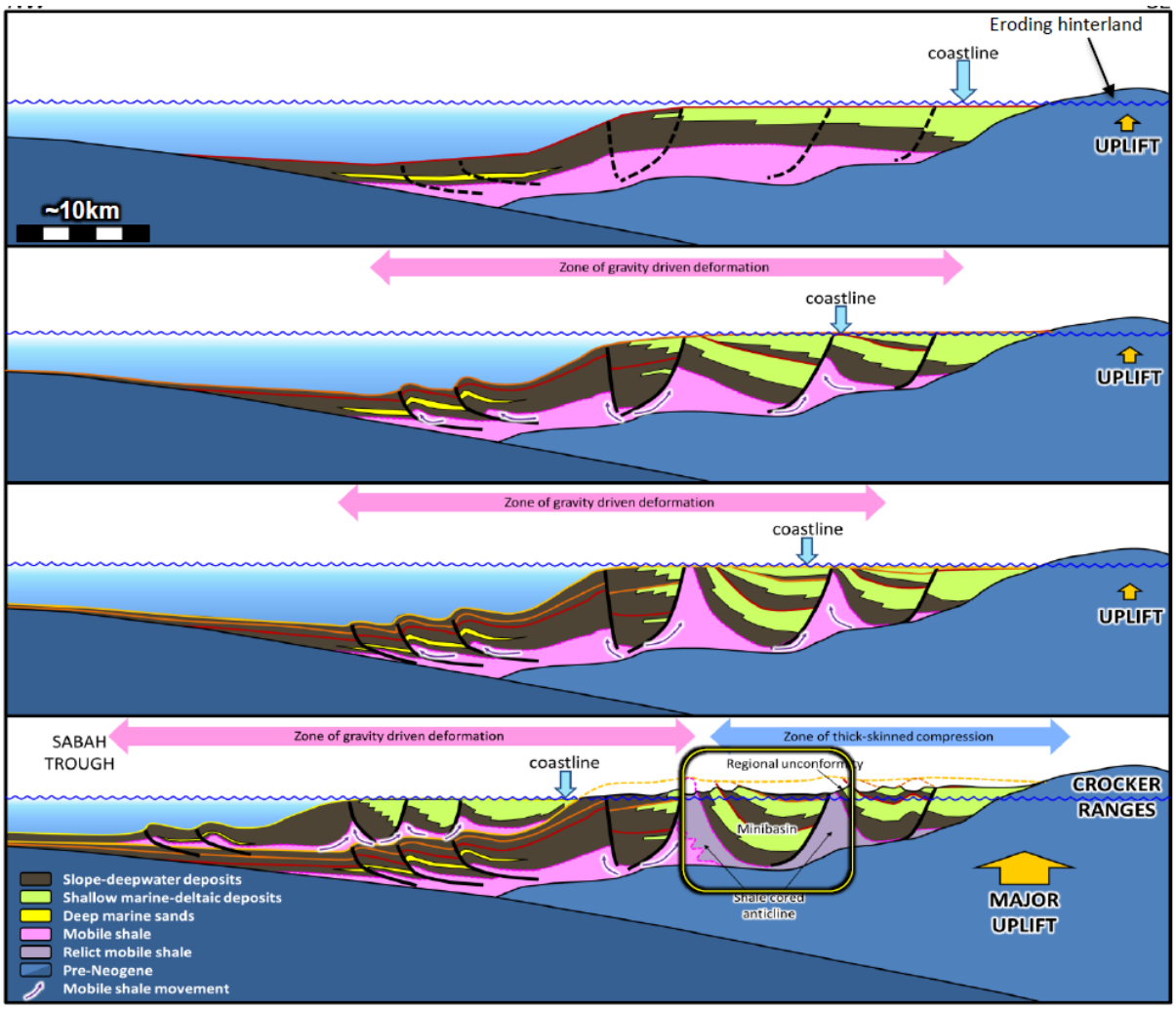

Figure 2- 36 Evolution of shale tectonics in the offshore Borneo (Clark, 2017). The shale (pink) behaviors the ductile deformation lead the overlying sediments deform as a gravity-driven while the basement continuous uplift.

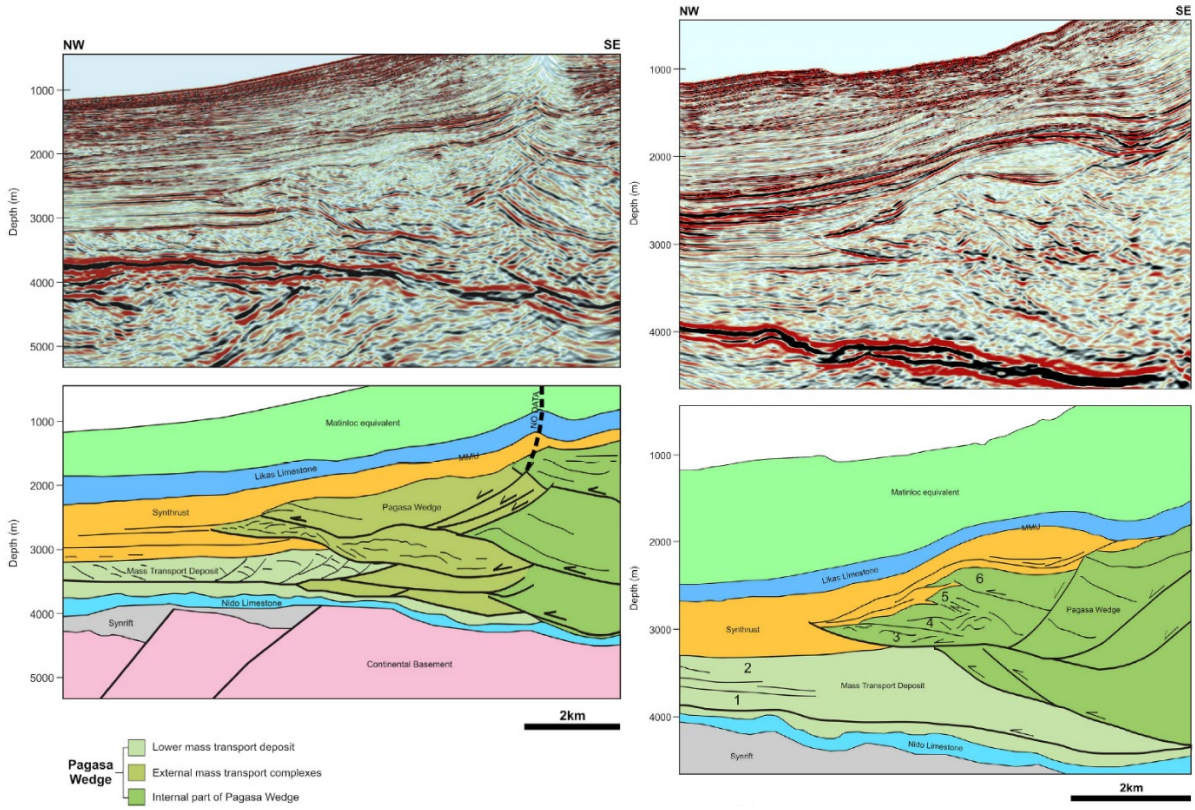

Figure 2- 37 The Pagasas wedge collapsed along the mass transport deposits in the offshore Palawan (Ilao et al., 2018).

Along the convergent margins, mélange composed of shale and/or serpentinite matrix, engulfing centimetric to metric exotic or native blocks, and their processes of formation and exhumation are debated since 1960's (Wilson, 1961; Hsü, 1968; Cowan and Page, 1975; Page, 1978; Tokuyama and Yoshida, 1984; Clennell, 1996; Festa et al., 2012; Festa et al., 2019). Although the terminology is mostly dedicated to accretionary prisms and referred to material formed either deep into a subduction channel or rocks crushed into crustal shears, it is also applied in ancient examples of heterogeneous mass transport complex (MTC), and upward rise of over-pressured material. Their origin is therefore tectonic, sedimentary (i.e. olistostrome), and diapiric (Festa et al., 2019). A conceptual model illustrates the theoretical occurrence of mélanges in different types and evolutionary stages of convergent margins (Figure 2- 39).

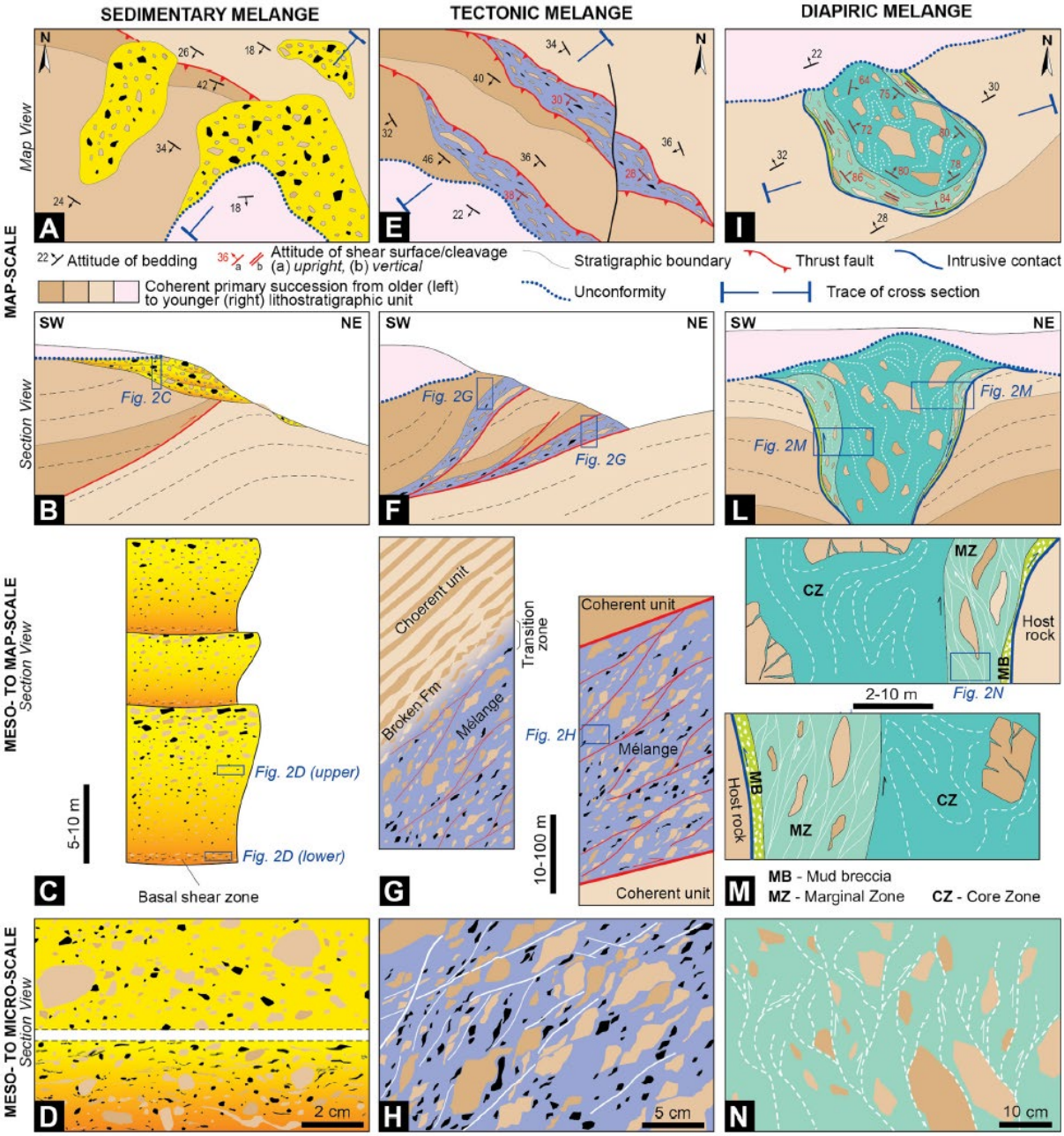

Figure 2- 38. Three main categories of mélange, (A-D) sedimentary, (E-H) tectonic and (I-N) diapiric mélange, in several scales (Festa et al., 2012; Festa et al., 2019).

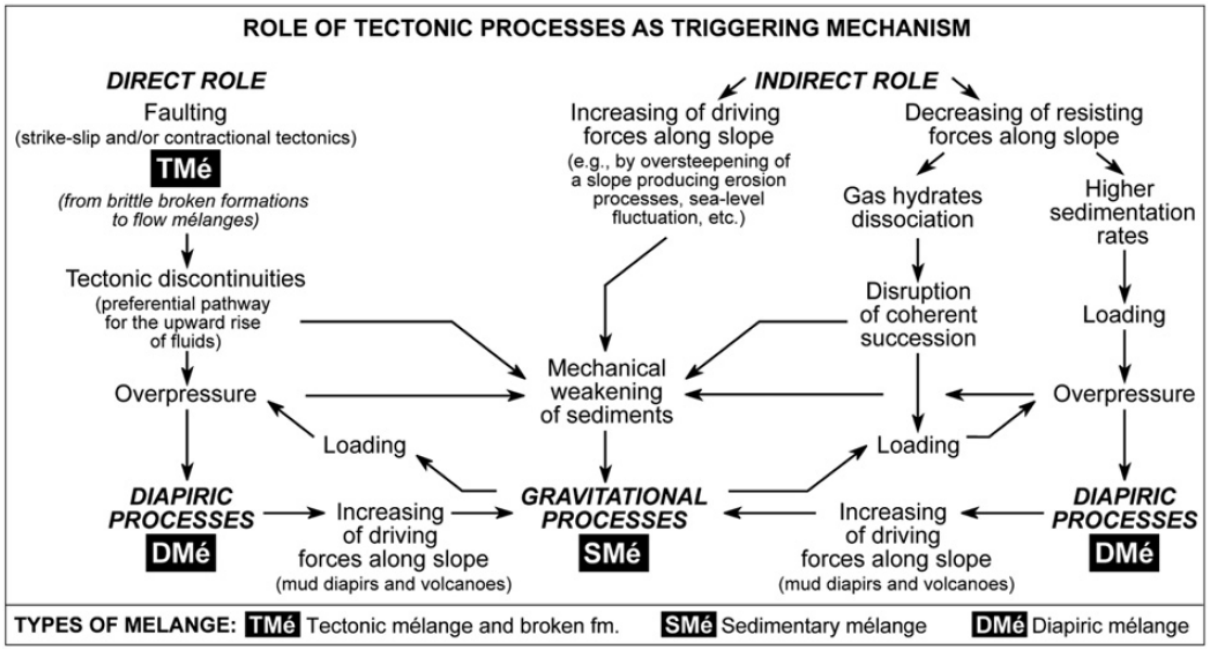

Figure 2- 39. The mélange distributes into three processes by faulting, gravity, and diapiric processes (Festa et al., 2012), and the production can be seen as tectonic (TMé), sedimentary (SMé), and diapiric (DMé) mélange respectively.

Many cases have been described where diapiric mélanges are associated with the evolution of subduction-accretionary complexes (Orange, 1990; Codegone et al., 2012; Barber, 2013; Festa et al., 2013)(and reference therein). The mud-prone characteristics of mélange is that they tend to rise up, such as described in the examples of shale tectonics. The mobile body is commonly triggered by overpressure condition caused by the weight of, for instance, the overlying shelf deposits (Figure 2- 41) (Mahanjane and Franke, 2014; Calvès et al., 2015; Cruciani and Barchi, 2016) or accretionary prisms (Figure 2- 40) (Duerto and McClay, 2011; Sapin et al., 2012; Ruh et al., 2018). Their occurrence may be misleading in fold-and-thrust belt, where they also seem to mark the end of compressional deformation (Duerto and McClay, 2011; Ruh et al., 2018). The involvement of tectonic processes in the formation of the mélange has not so far been clearly explained.

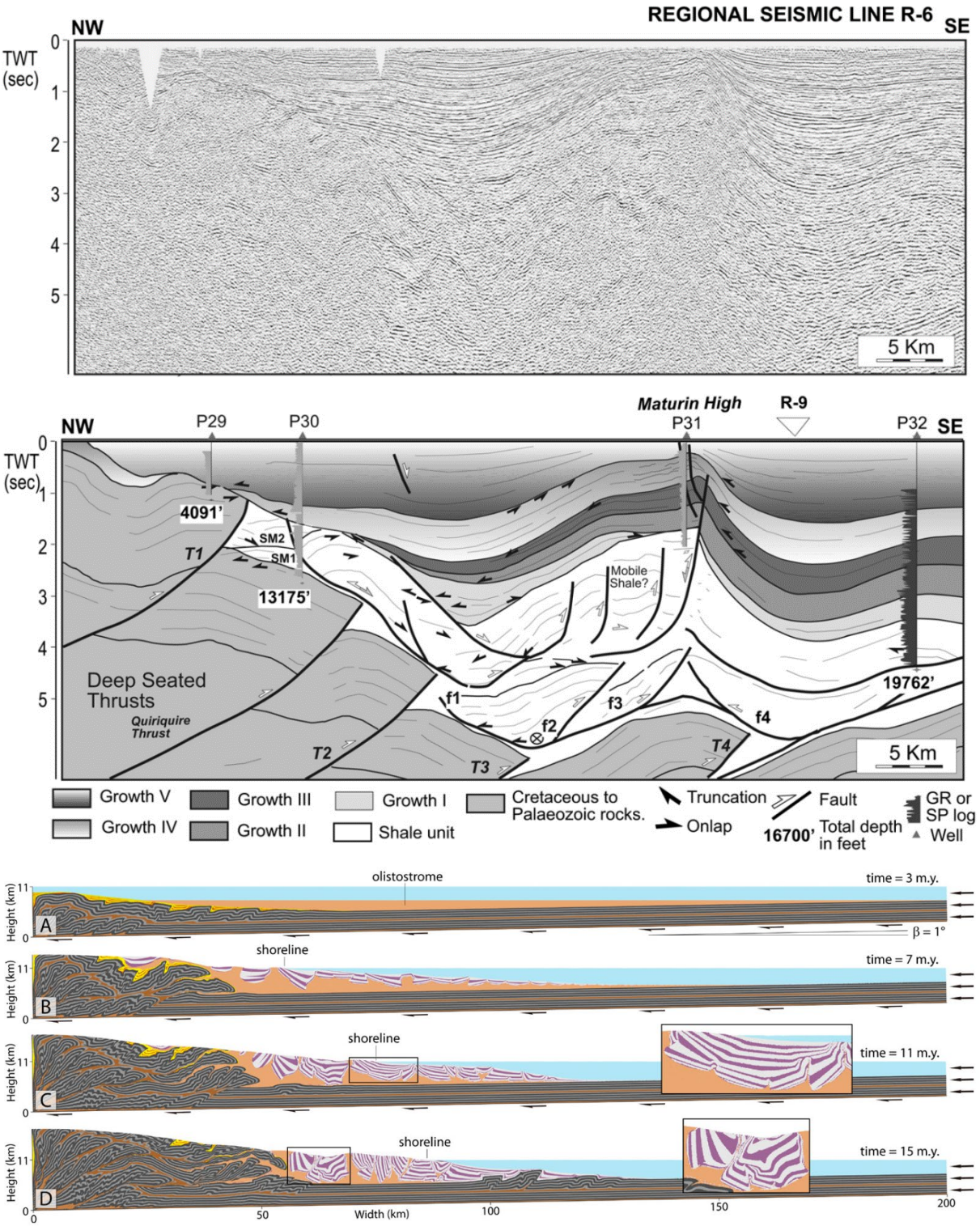

Figure 2- 40. mobile shale in active margins (from Duerto and McClay (2011); Ruh et al. (2018)). The mobile shale triggers the diapirism in the shallow accretionary wedge in the Venezuela and Makkran subduction wedges. Note that the mobile shale which postdate the compression is still slightly involved in the basement thrusts.

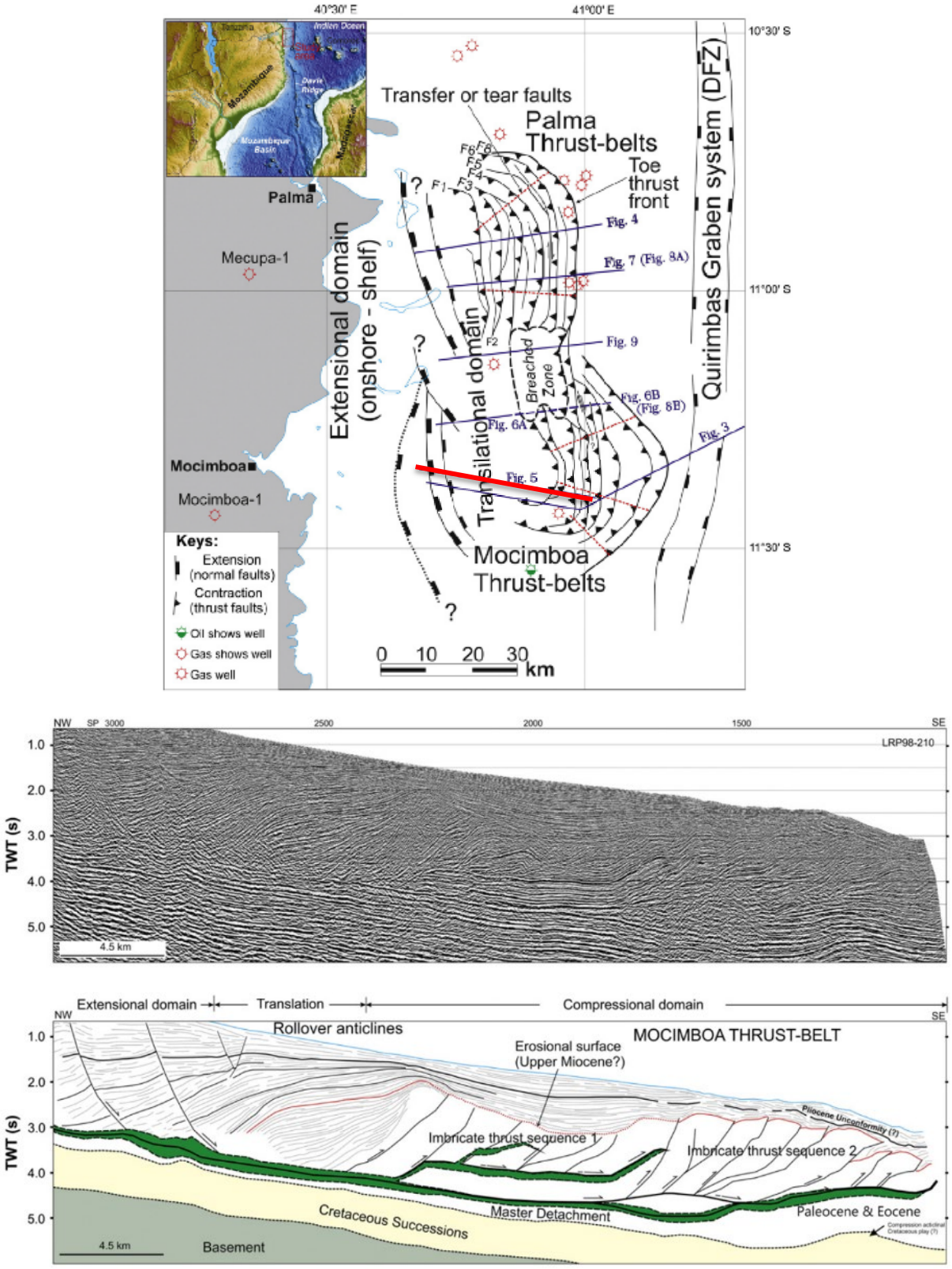

Figure 2- 41. Mobile shale in passive margins induced by delta loading (Mahanjane and Franke, 2014; Calvès et al., 2015; Cruciani and Barchi, 2016). The extension distributes landward and toe-thrust in the seaward along the seismic images (location on the red solid line).

Several mélange occurrences have been widely described in SE Asia, showing a close relationship between the process of their formation and the structural setting in which they are preserved. For example, Neogene to Recent and associated with well-known active subduction or recent collision zones, examples have been described in the Mentawai Islands and Sumatra (Wajzer et al., 1991; Pubellier et al., 1992; Samuel et al., 1997), in Laut Island offshore SE Borneo (Hamilton, 1979; Wakita et al., 1998) and in the center of Borneo (Lubok Antu Mélange of Tan (1975); Khan (2018)) units. It is often possible to establish links between the presence of these particular geological features and the geological framework. Borneo has been considered as a case study after the work of many authors Collenette (1958, 1965); Hamilton (1979); Tongkul (1990); Clennell (1996); Tongkul (2003); Sapin et al. (2012). In the northern Molucca Sea, Bader et al. (1999), had shown a progressive slivering of the oceanic crust, by which the conjugate set of fractures were created during the obduction or the late stages of the subduction, and isolated phacoid-shape blocks, which are found engulfed in a midst of the overlying mélanges. The mélange and mobile shale formation would be considered as key elements in both active and passive margin in order to correlate margins of the SCS and the PSCS in this work.

2.4.3 Relics of subduction: the igneous rocks in the PSCS

The Cretaceous and Eocene ophiolite are distinct indications of the vanished PSCS marginal sea. The ultramafic and mafic rocks crop out in Sabah and South Palawan (Jasin and Tongkul, 2013; Aurelio et al., 2014), and had been proposed as being the result of the obduction of the PSCS ocean floor (Figure 2- 42) (Aurelio et al., 2014). The ophiolitic lithologies in Early to Late Cretaceous are distributed from Palawan to the Sabah (purple color on Figure 2- 43) and are well correlated with a trend of high gravity anomaly (right on Figure 2- 43) (Cullen, 2010; Sapin, 2010). This trace is believed to reflect a distribution of the oceanic lithosphere offshore and obducted crust onshore. The obduction thrusts onto the Eocene strata in Palawan (Taguibao et al., 2012; Aurelio et al., 2014). The Sulu Sea opened behind this obduction belt (Rangin, 1989). In such a configuration, the volcanic arc would be located offshore, in the Cagayan Ridge and the Sulu Arc.

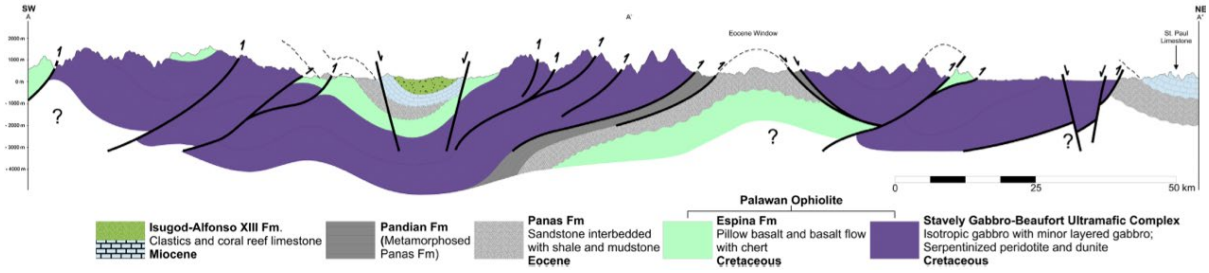

Figure 2- 42 The cross-section involving the ultramafic complex thrust on top of sedimentary rocks onshore Palawan (Aurelio et al., 2014).

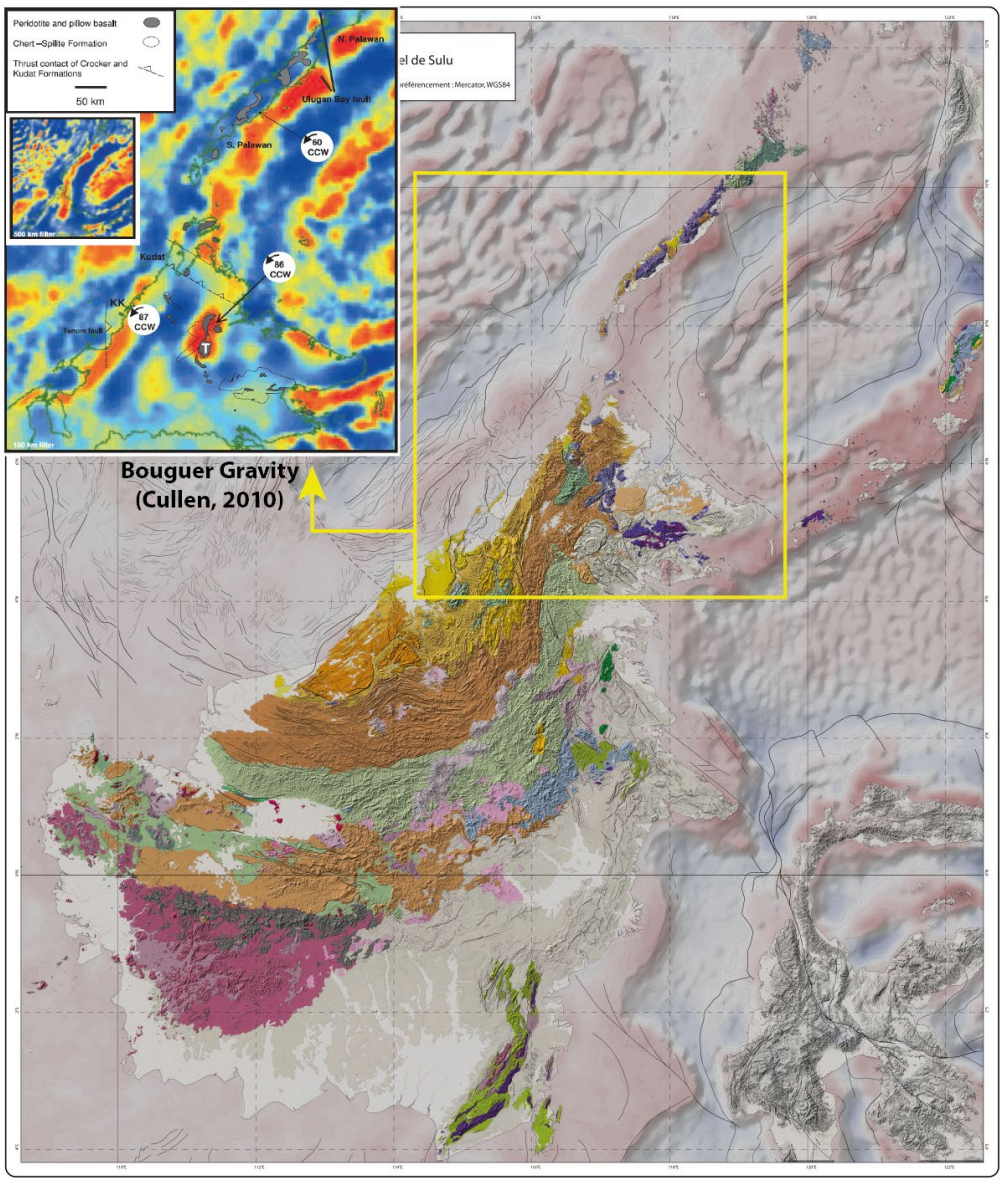

Figure 2- 43 (Left) Geological map of Borneo and Palawan (Sapin, 2010). The ophiolite terrain is marked as dark purple distribute mainly in Palawan and Sabah. The mountain range mostly in Sarawak, SW Borneo. (Right) The Bouguer gravity anomaly map with 150 km high-cut filter (Cullen, 2010). A high anomaly belt from Palawan to Sabah share the similar location with the ophiolite outcrop onshore.

In Borneo, Tertiary and Neogene volcanic bodies appear along strike the NW Borneo wedge. The volcanic rocks are mostly represented by the Sintang Suite, the Bau Suite, in the NE and E Kalimantan, and E Sabah (Figure 2- 44). The intrusive type consists of sills, stocks and dykes in Sintang Suite. Geochronological studies suggest three major groups of magmatic activity; Oligocene (30-23 Ma), Early Miocene, and Middle Miocene in Sarawak and Late Miocene to recent in Sabah (Prouteau et al., 1996; Prouteau et al., 2001; Cottam et al., 2013; Breitfeld et al., 2019) and references therein). A subduction-related origin was inferred due to the adakitic chemistry in Bau Suite and Sintang Suite by Hamilton (1979); Prouteau et al. (1996); (Soeria-Atmadja et al., 1999); Prouteau et al. (2001); (Hartono, 2006), although some studies argued the existence of the subduction slab and proposed post-collisional or post-subduction settings (Kirk, 1968; Williams and Harahap, 1987; Moss et al., 1998; Zaw et al., 2011; Hall and Breitfeld, 2017; Breitfeld et al., 2019).

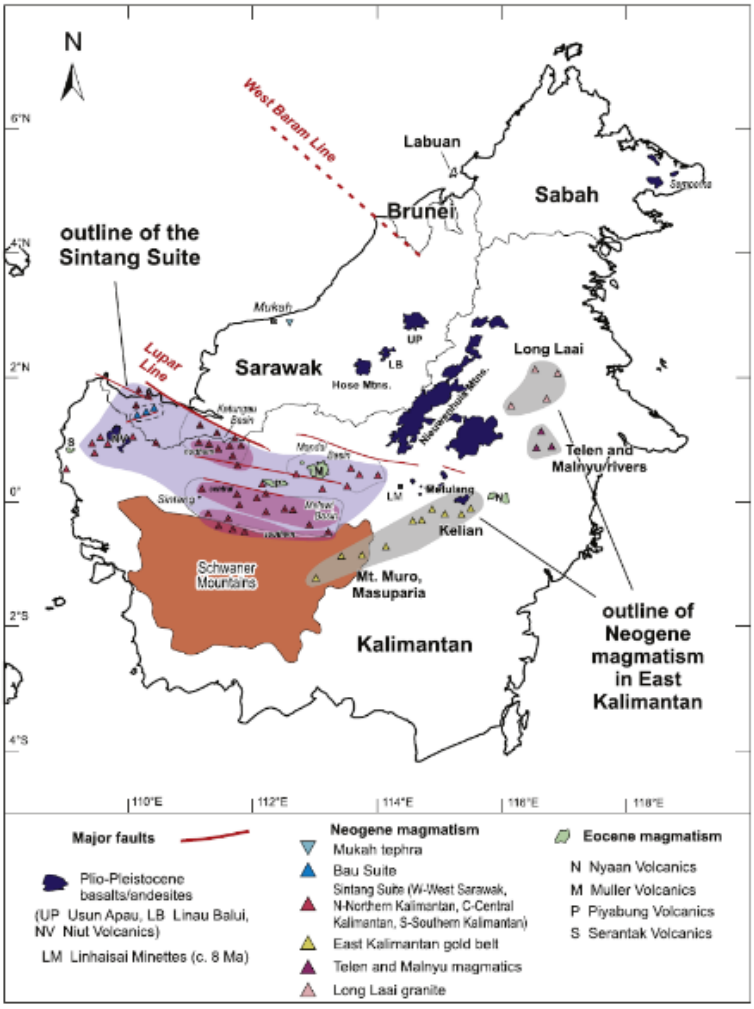

Figure 2- 44. The distribution of volcanic rocks in Borneo (Breitfeld et al., 2019).

In Sabah, a distinct Late Miocene granitic intrusion, the Mount Kinabalu, having been uplifted to 4000 meters height suggests an uplift rate reaching to 7 mm a^{-1} during the post-orogenic period (Hutchison et al., 2000; Swauger et al., 2000; Cottam et al., 2013). This intrusion may result from a slab detachment illustrating the termination of the slab pull of the PSCS (Figure 2- 45) (Hutchison et al., 2000; Swauger et al., 2000; Cottam et al., 2013; Hall, 2013).

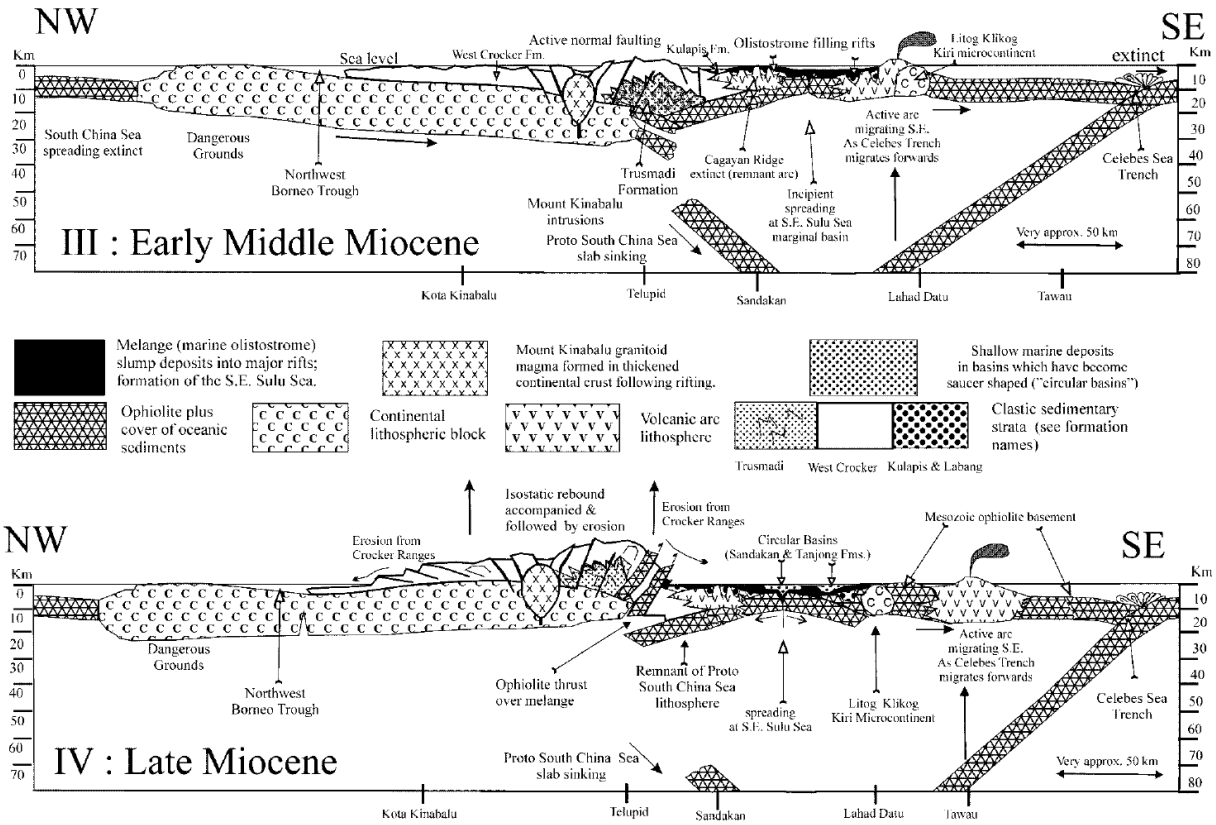

Figure 2- 45 The slab detachment of PSCS and the granitic intrusion of Mount Kinabalu (Hutchison et al., 2000).

2.4.4 The deep tomography image of the PSCS slab

If the slab detachment is still a matter of debate, the location of the detached slab of PSCS also raises some questions. Several studies underlined the absence of a significant slab beneath the subduction-collision zone with high P-wave velocity anomaly (upper on Figure 2- 46) (Rangin et al., 1999; Hall and Spakman, 2015). Recent work allowed to map a high velocity anomaly reservoir which could represent the possible location of the PSCS beneath the present-day SCS (middle on Figure 2- 46), and the subduction, therefore, the several possibilities may be considered such as a double-side subduction (Figure 2- 46) (Wu and Suppe, 2017), a former Tethys or Pacific slab (Figure 2- 47) (Sun et al., 2019), or a roll back of the PSCS slab.

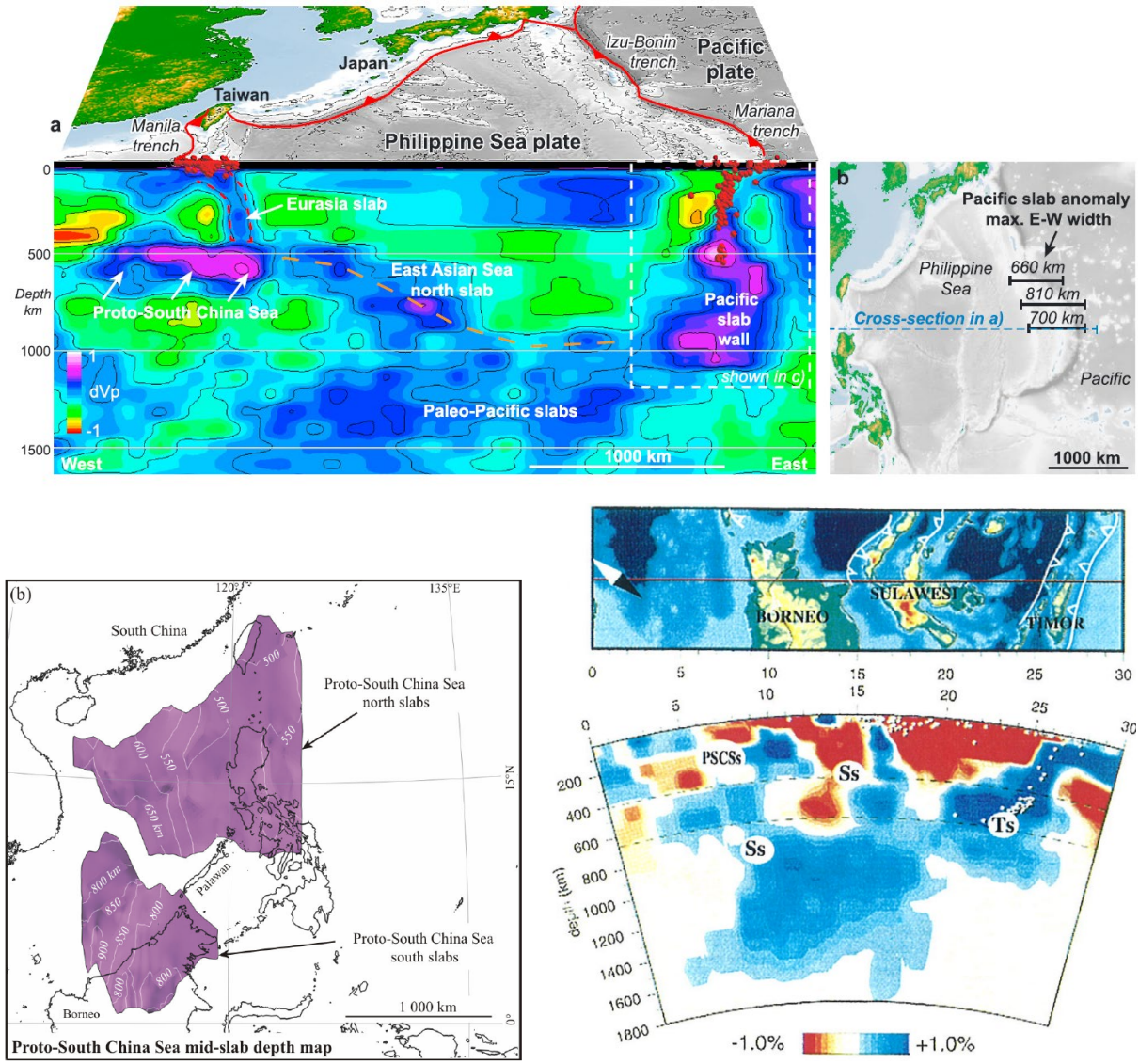

Figure 2- 46. The slab mapping of break-off PSCS from the tomography studies ((Rangin et al., 1999; Wu et al., 2016; Wu and Suppe, 2017)). The blue color on the upper panel and purple on the middle panel represent the infered slab. The PSCS is interpreted underneath the South China Sea margin as shown on the map on the lower panel.

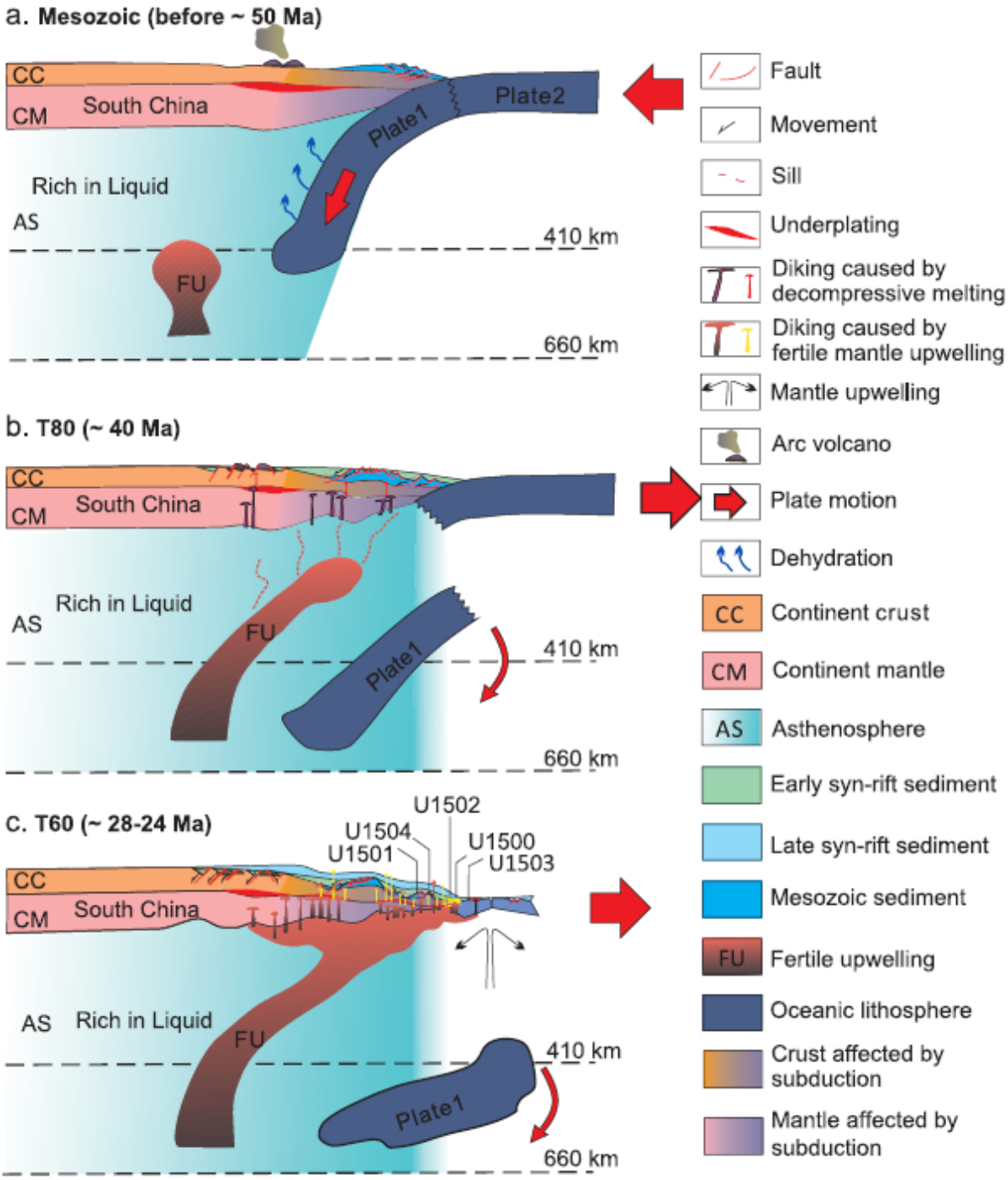

Figure 2- 47. Slab detachment accommodating the high velocity anomaly in the tomography introduces the syn-rift magmatism in the South China Sea margin (Sun et al., 2019).

2.5 Objectives: tectonic link between the SCS and the PSCS

Many studies had suggested a link between two marginal seas; the SCS and the PSCS (Figure 2- 48), although correlations of the tectonic events are still debated and hypothesis are sometimes conflicting in many aspects (Tapponnier et al., 1982; Hall, 2002; Pubellier et al., 2003; Morley, 2016; Wu and Suppe, 2017). Different boundary forces have been invoked, such

as the India-Eurasia collision induced extrusion of the Indo-China Block, a supra-subduction basin opened in the South China Sea, or a global gravity collapse of the margin after the Tibet/Himalayan thickening.

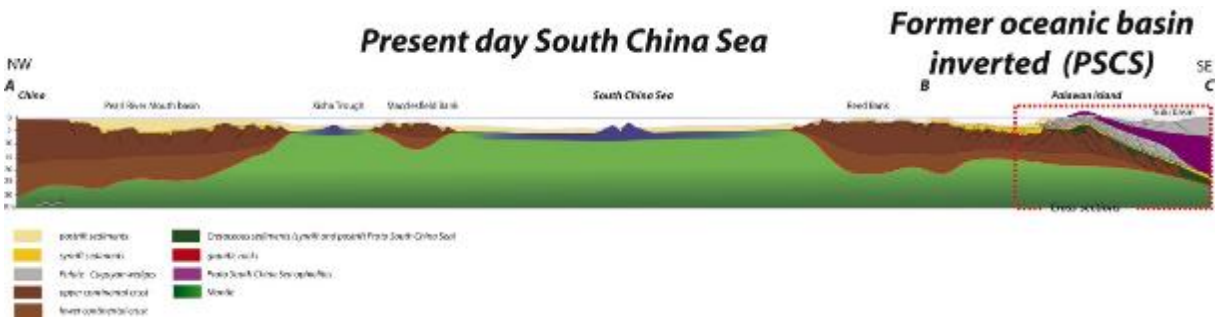

Figure 2- 48. Closure and opening of marginal seas between SCS and PSCS (Meresse et al., 2012).

However, the stratigraphic chart in the SCS and PSCS suggests some similar timing of tectonic events. For instance, the termination of the seafloor spreading of the SCS is contemporary with the Deep Rigional Unconformity (DRU), which implies the termination of the Sarawak Orogeny, around 16 Ma (Figure 2- 49). However, many ages of tectonic events are still in debate, especially that of the second orogeny in Sabah (Balaguru et al., 2003; Tongkul, 2003; Lunt, 2019).

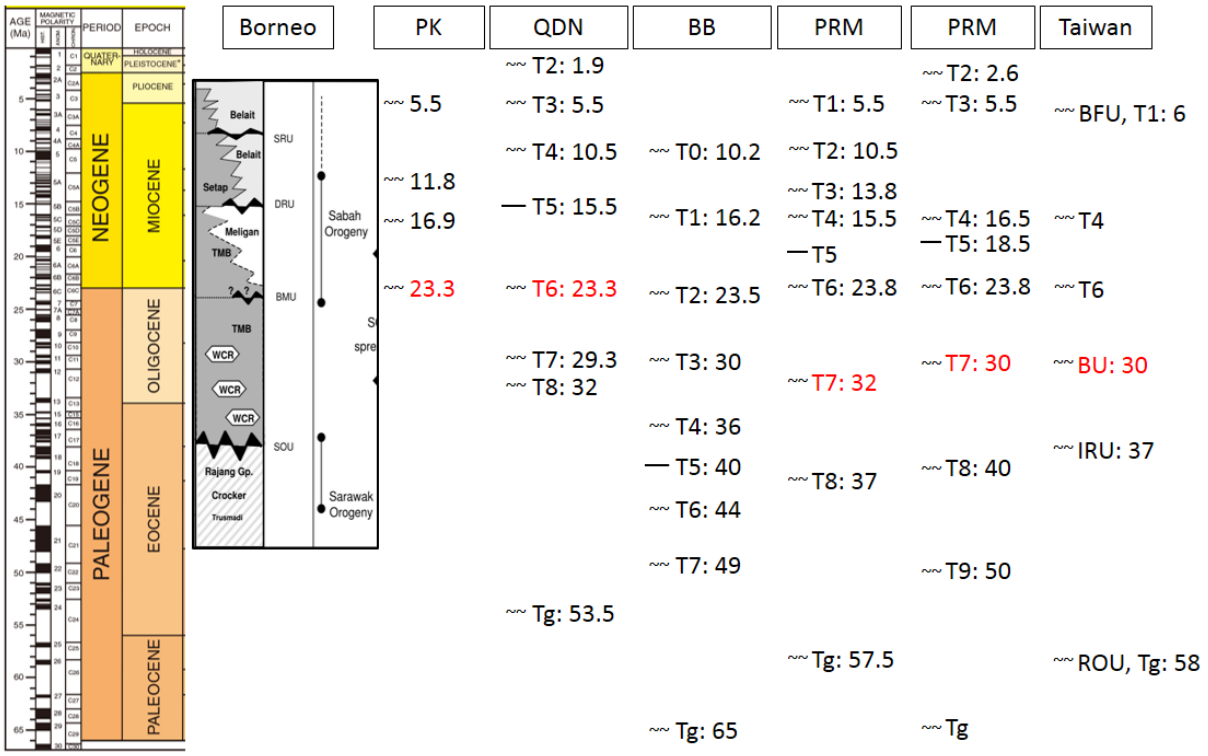

Figure 2- 49 Simplified stratigraphic charts for the SCS and the PSCS (Cullen, 2010; Ding et al., 2008; Fyhn et al., 2009; Gao et al., 2015; Han et al., 2016; Hu et al., 2013; Jin et al., 2014; Lin et al., 2003; Vu et al., 2017; Wang et al., 2013; Wu et al., 2009; Zhao et al., 2015; Zhao et al., 2016; Zhou et al., 2015). Several unconformities identified in the SCS annotated by T and numbers varying from basins that mislead the tectonic correlation. However, there are still several extensive unconformities widespread both offshore in the SCS and onshore in the Borneo area.

In map view, the particular mechanism is still unclear, and the main driving forces acting on the two margins (Figure 2- 50) still have to be explored in order to produce more convincing arguments.

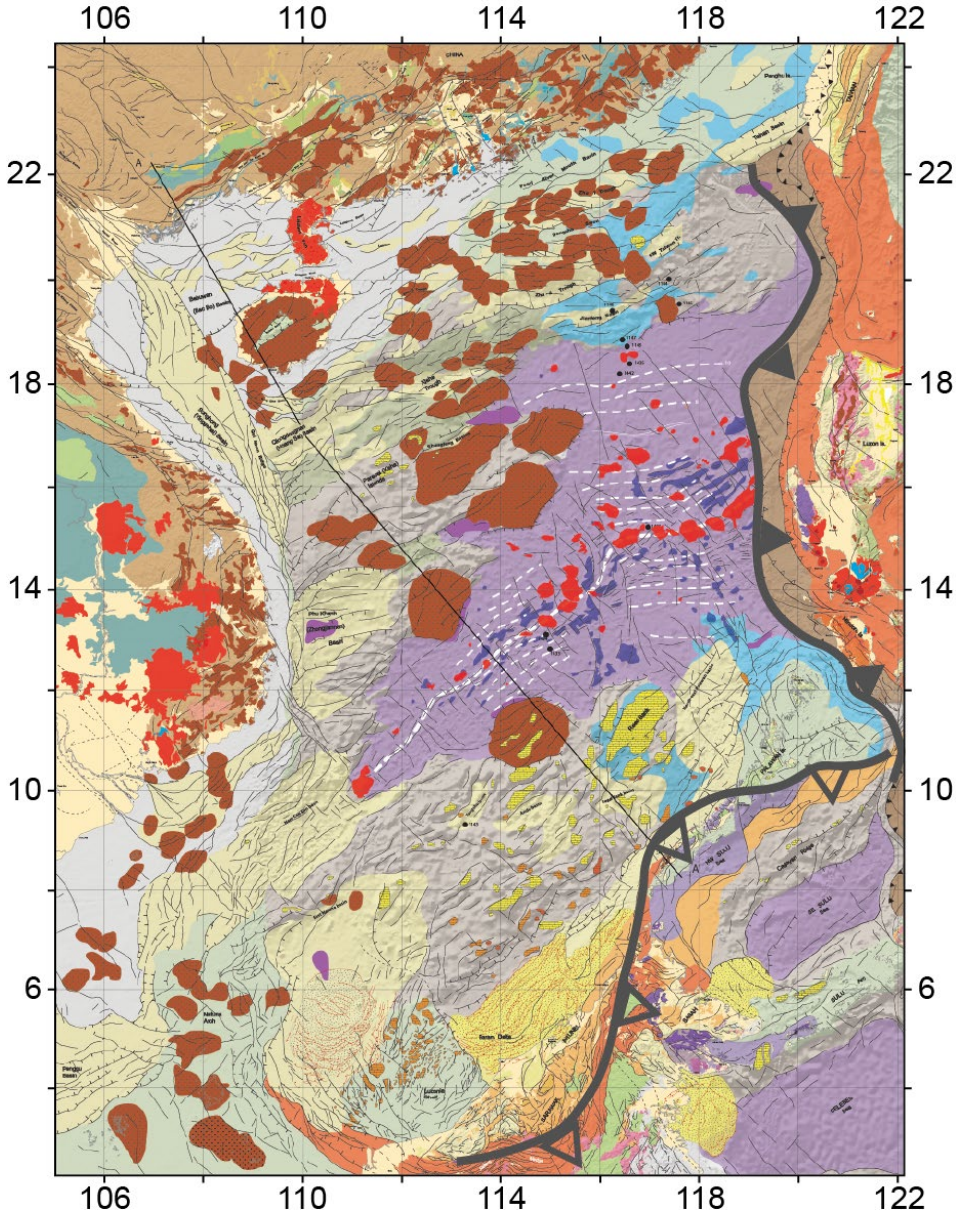

Figure 2- 50. Structural map underlining the extensional basin opening of the SCS (top purple) and the trace of the subducted basin (saw-teeth line) of the PSCS (Modified from (Pubellier et al., 2016).

To achieve the thesis goal, this study intends to address the following points:

- Illustrate the crustal structures and clarify the basin evolution along-strike the rifted margins in the SCS.
- Clarify the two orogenies which have been resulting from the PSCS closure in Sabah, and Borneo in general.
- Correlate the coeval tectonic events across both margins in order to propose a kinematic link between the tectonic processes.
- Explore the possible driving forces in the geodynamic context.

CHAPTER 3. The crustal architecture of the southwestern South China Sea: implications on breakup setting

3.1 Introduction

Many parameters control the crustal thinning and the breakup mechanism of rifted margin like the heterogeneities of the lithosphere, the rheology, and the thermal conditions (Clift and Lin, 2001; Lavier and Manatschal, 2006; Péron-Pinvidic et al., 2013; Gillard et al., 2015; Hart et al., 2017; Tetreault and Buiter, 2018; Lavier et al., 2019; Petri et al., 2019; Nirrengarten et al., 2020b). The effect of such parameters can be simulated and tested via numerical models (Lavier and Manatschal, 2006; Huismans and Beaumont, 2011; Svartman Dias et al., 2015; Duretz et al., 2016; Brune et al., 2017; Ros et al., 2017). In a multilayered material such as the lithosphere and more specifically the crust, strain localization is sensitive to local internal heterogeneities such as strong lithologic contrasts (Duretz et al., 2016; Petri et al., 2019). For example, batholiths intruded in the continental crust (Savva et al., 2013; Savva et al., 2014; Ding and Li, 2016a, b; Duretz et al., 2016; Petri et al., 2019), ductile layers (Clift and Lin, 2001; Morley and Westaway, 2006; Li et al., 2019), detachment shear zones (Masini et al., 2011; Masini et al., 2012; Lymer et al., 2019) or exhumed mantle (Whitmarsh et al., 2001; Lavier and Manatschal, 2006; Péron-Pinvidic et al., 2007; Franke et al., 2011; McIntosh et al., 2014; Tugend et al., 2014). In each case, a different behavior in response to extension will create a variety of crustal structures along the margins. Rigid layers could easily localize the strain at boundaries of morphostructures or in the vicinity of low-viscosity layer such as the ductile layer (Huismans and Beaumont, 2011; Clift, 2015; Brune et al., 2017; Li et al., 2019). However, these parameters still need to be studied further in the marginal seas, where multiple tectonic processes occurred.

The evolution of marginal seas, whether floored with oceanic crust or not, is usually related to the adjacent trench-arc system at the outskirt of continental margins, and is therefore influenced by the regional tectonics which shaped the crustal structure (Zhou, 2014; Chenin et al., 2017). Their thermal condition and heterogeneous lithospheric structures may dominate the rifting architecture during short-lived processes which may be different from the one observed at larger ocean margins (Li et al., 2014b; Chenin et al., 2017; Shi et al., 2017).

The South China Sea (SCS) is one of the marginal seas developed around the southeast rim of the Eurasian Plate (Zhou et al., 1995; Teng and Lin, 2004; Guan et al., 2016; Wu et al., 2016). This marginal sea presents a spectacular extended margin with 1000 kilometers of thinned continental crust and a 1200-kilometers long spreading ridge (Figure 3- 1). The rifted margins of the SCS are wide in contrast to classic stretched continental margins like magma-poor margins (Cullen et al., 2010; Savva et al., 2013; Franke et al., 2014; Savva et al., 2014; Brune et al., 2017). Initial conditions leading to deep sedimentary basin controlled by middle crust shear zones and to highly-extended continental crust may include higher heat flow (Mitchell et al., 1986; Brune et al., 2017; Shi et al., 2017). The V-shaped formation of oceanic crust results from a general propagation toward the southwest from the Early Oligocene to the Middle Miocene, including a change of the spreading direction with a "ridge jump" around 23 Ma (Briais et al., 1993; Lee and Lawver, 1995; Li et al., 2014a; Qiu et al., 2016; Sibuet et al., 2016; Ding et al., 2020). The conjugated margins have been investigated by oil and gas companies, as well as by academic institutions from proximal to distal areas in the past decades. Due to the lack of comprehensive stratigraphy along the E Vietnam/S Hainan-NW Borneo conjugated margins, a tectono-stratigraphy study is needed to precise the rifting structure and evolution of the passive margins.

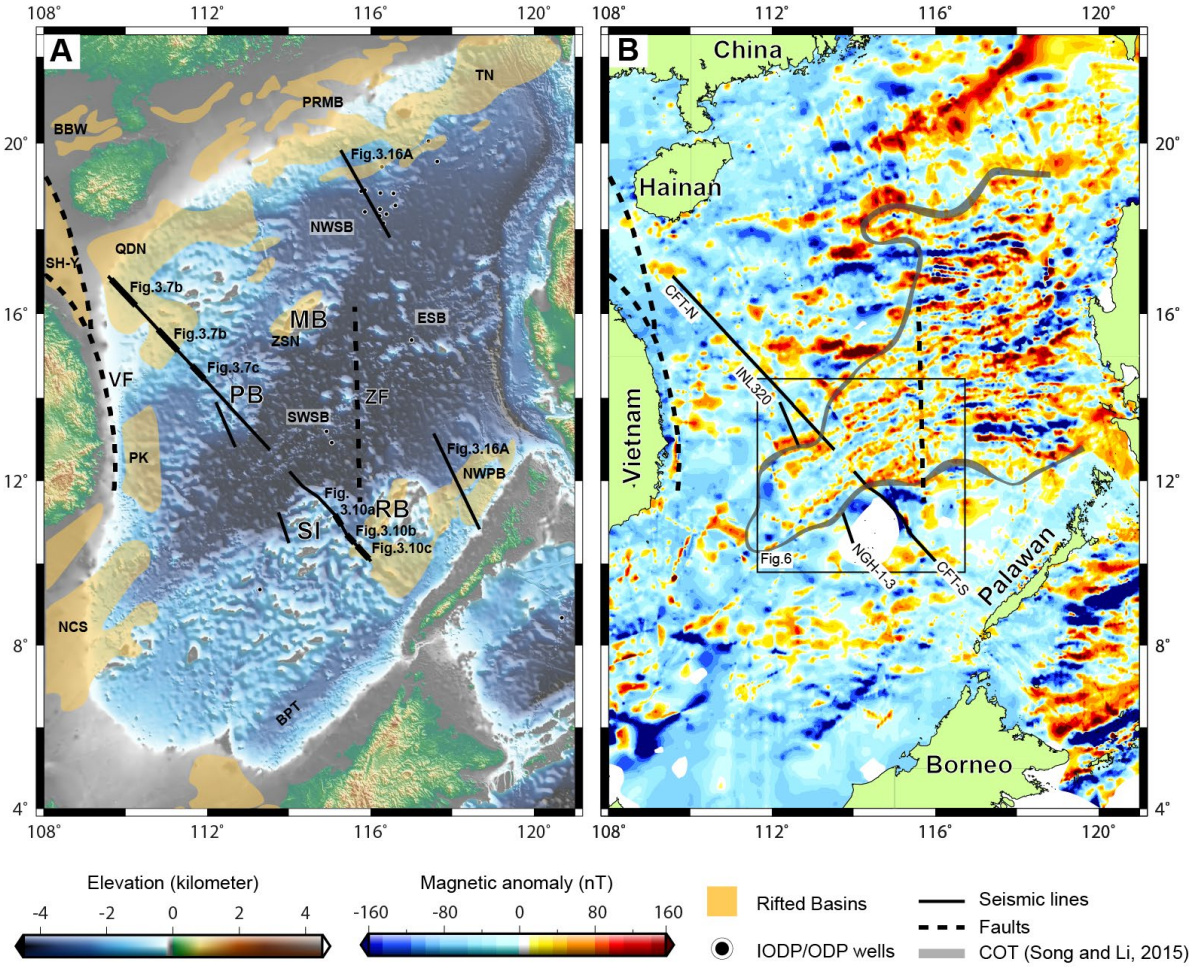

Figure 3- 1. (A) Elevation with rifted basins including BBW: Beibuwan Basin, NCS: Nam Con Son Basin, NWPB: NW Palawan Basin, PK: Phu Khanh Basin, PRMB: Pearl River Mouth Basin, QDN: Quiondongnan Basin, SH-Y: Song Hong-Yinggehai Basin, TN: Tainan Basins, ZSN: Zhongshanan Basin. The bathymetric map has a non-linear colour bar to assist in highlighting certain features. The black solid lines represent the location of seismic profiles and the black dash line are Vietnam Fault (VF) and Zhongnan Fault (ZF) respectively. (B) Marine magnetic anomaly map. The white area represents zones devoid of data. The COT distribution shown in the grey band (Song and Li, 2015). MB: Macclesfield Bank (Zhongsha Islands), SI: Spratly (Nansha) Islands, PB: Penxi Bank, RB: Reed (Liyue) Bank. ESB: East Sub-Basin, NWSB: Northwest Sub-Basin, SWSB: Southwest Sub-Basin, BPT: Borneo-Palawan Trough.

The aim of this study is to explore the architecture and extensional processes along a 1000 km long seismic profile (line CFT) crossing the conjugated continental margins of the SW sub-basin. To highlight the lateral variations of the margins, we describe two other seismic lines, (line INL320 and NGH-1-3 on Figure 3- 1, supplied by GMGS), crossing continent-ocean transition (COT) segment with different orientations to show the lateral variability of the structures and their relation to the direction of extension. This structural analysis is integrated

with the tectono-stratigraphic framework of the margin near the COT and along other areas of extremely stretched crust.

3.2 Geological Background

The extension in the southeast of the South China Block initiated in the Early Cretaceous in the context of convergence between the Pacific Plate and Eastern Eurasia (Zhou et al., 1995; Teng and Lin, 2004; Li et al., 2007). This event marked the end of a magmatic period illustrated by granite intrusions (Khanchuk et al., 2019; Xiao et al., 2019; Zhang et al., 2019a), which have been sampled in the offshore by drilling and dredges (Kudrass et al., 1986; Yan et al., 2010; Xiao et al., 2019). The first cycle of extension took place from Late Cretaceous to Paleocene with the development of narrow coarse-clastic basins (Yan et al., 2001; Morley, 2016), and evolved to a widely distributed rifting event in the proximal margins (Lin et al., 2003; Xie et al., 2006; Yao et al., 2012; Jin et al., 2014; Steuer et al., 2014). This event reflects the initial stretching of the continental lithosphere and is observable onshore (Schlüter et al., 1996; Chan et al., 2010; Nanni et al., 2017). The second extensional event took place during Eocene and Oligocene and corresponds to the main thinning event (Yan et al., 2001; Ding et al., 2013a; Franke et al., 2014; Cameselle et al., 2015; Li et al., 2015; Nirrengarten et al., 2020a) leading to the propagating continental breakup from Early Oligocene to Middle Miocene (Briais et al., 1993; Li et al., 2014a). This main extension shaped most of the crustal structure in the north of the SCS on Figure 3- 2 (Savva et al., 2013; McIntosh et al., 2014; Gao et al., 2015; Li et al., 2015; Lei and Ren, 2016; Larsen et al., 2018; Gong et al., 2019; Nirrengarten et al., 2020a) and south of SCS (Franke et al., 2011; Ding et al., 2013a; Madon et al., 2013; Franke et al., 2014; Li et al., 2014b; Clerc et al., 2018; Peng et al., 2018; Liang et al., 2019; Nirrengarten et al., 2020a).

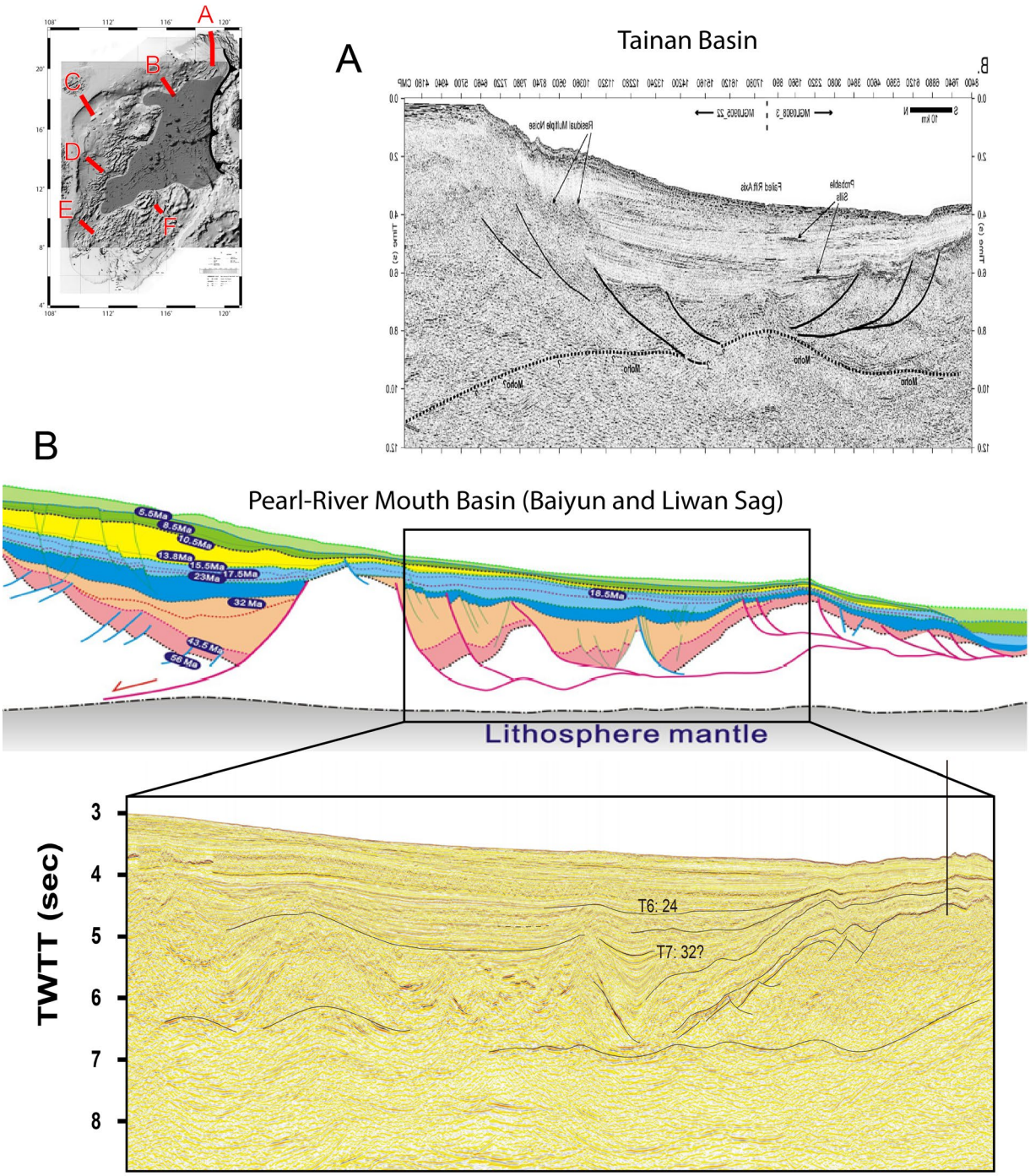

Figure 3- 2. Hyperextension Basins around the South China Sea margins (Savva et al., 2013; McIntosh et al., 2014; Ren et al., 2014; Clerc et al., 2018; Liang et al., 2019; Xie et al., 2019). (A) Tainan Basin interpreted mantle exhumation beneath the thickest sediment. (B) clear detachment faults along the top of lower crust in the PRMB, and two syn-rift sub-unit are recognized (dark and light pink). Upper one (light pink) has larger thickness variation of thickening toward detachment faults. (C) Detachment fault roots in the Moho at the QDN Basin. Lower syn-rift (orange) have typical wedge geometry, and upper syn-rift (pink) characterizes thickening toward where the crust is thinnest.

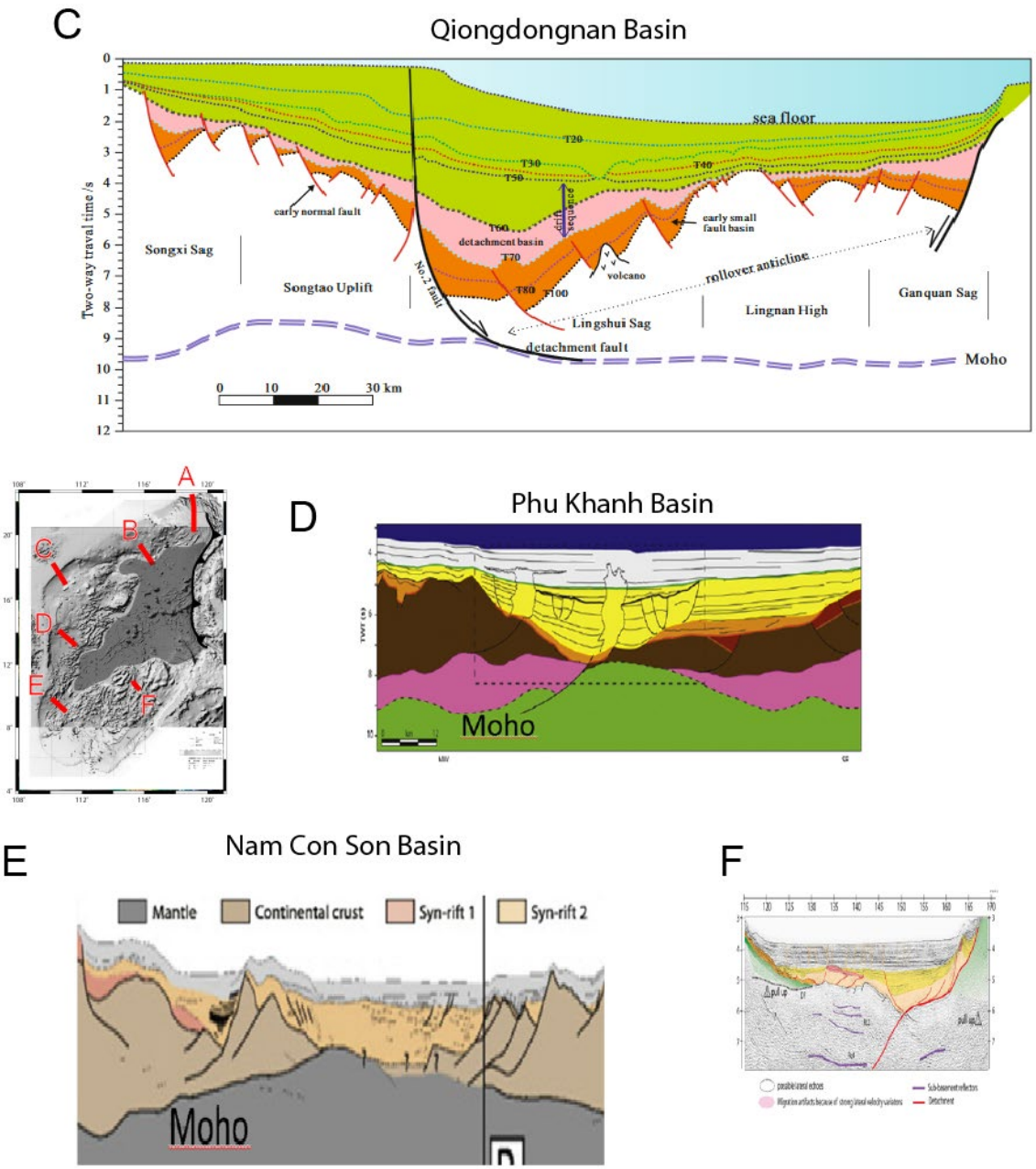

Figure 3.2 (continued) Hyperextension Basins around the South China Sea margins (Savva et al., 2013; McIntosh et al., 2014; Ren et al., 2014; Clerc et al., 2018; Liang et al., 2019; Xie et al., 2019). No significant detachment fault is interpreted but similar two-unit syn-rift is illustrated in (D) the PK Basin, (E) the NCS Basin, and (F) a basin in the East Spratly Islands.

Many Cenozoic unconformities have been identified on the conjugate margins of the SCS (Franke et al., 2014; Morley, 2016; Lunt, 2019). For the sake of clarification, we have distinguished an eastern margin which encompasses the SE China- NW Palawan conjugated margins, and a southwest set composed of the E Vietnam/S Hainan-NW Borneo conjugated margins. In the SE China margin, the unconformities underline and post-date a series of high-

angle normal faults and highly stretching by detachment faults localized thinning in the upper crust (Lei et al., 2019a; Xie et al., 2019). The detachment faults rooted either at the top of ductile layer (lower crust) or at the Moho. Two syn-rift units are commonly recognized along the margin (Figure 3- 2). While the lower syn-rift shows a typical geometry of wedge strata, the upper syn-rift usually varies thickness dramatically as U-shaped facies (Figure 3- 2B) or relatively thick sediment and thickening toward where the crust is thinnest (Figure 3- 2C, D and E).

Recently IODP drillings discovered oceanic and continental basement lithologies and disclosed precisely the breakup mechanism and the architecture of conjugated margins (Larsen et al., 2018; Nirrengarten et al., 2020a) along the Eastern oceanic sub-basin. There, a rapid transition from continental rifting to oceanic spreading is evidenced which shows a sharp thinning of the continental crust within a 10 Myr interval (Larsen et al., 2018). Some authors proposed an asymmetrical breakup in the early times followed by a more symmetrical and stable spreading after 28 Ma (Nirrengarten et al., 2020a).

The southwestern SCS is less known because of the existence of a thick cover of Mesozoic clastics and Eocene to Late Miocene carbonates present both on the NW Borneo margin on Figure 3- 3 (Franke et al., 2011; Madon et al., 2013; Steuer et al., 2014; Chang et al., 2015; Jamaludin et al., 2017) and the E Vietnam/S Hainan margin (Fyhn et al., 2013; Vu et al., 2017). The continental crust of a wide rifted margin is characterized by a flat and shallow Moho (depth 20 km), and interpreted as underlying a weak lower crust (Hayes and Nissen, 2005; Pichot et al., 2014; Lü et al., 2016; Dong et al., 2018a; Yu et al., 2018; Huang et al., 2019; Li et al., 2019). The extensional features include tilted basins and recently, large detachments have been found (Savva et al., 2013; Lei and Ren, 2016; Peng et al., 2018; Liang et al., 2019).

Based on bathymetry and magmatic anomalies, a change in the spreading direction linked with a ridge jump around 23 Ma has been suggested (Briais et al., 1993; Lee and Lawver, 1995; Barckhausen et al., 2014; Li et al., 2014a; Qiu et al., 2016; Sibuet et al., 2016). Sibuet et al. (2016) and Lei and Ren (2016) proposed the existence of an intermediate spreading event between the two stages, around 23Ma (Figure 3- 4). The root cause of the rotation is unclear, however, numerical modelling suggested that tectonic loading may have resulted in a stalling phase of the E-W propagation from 32 to 23 Ma, and was later followed by a NE-SW propagation across the whole region between 23 to 16 Ma (Le Pourhiet et al., 2018).

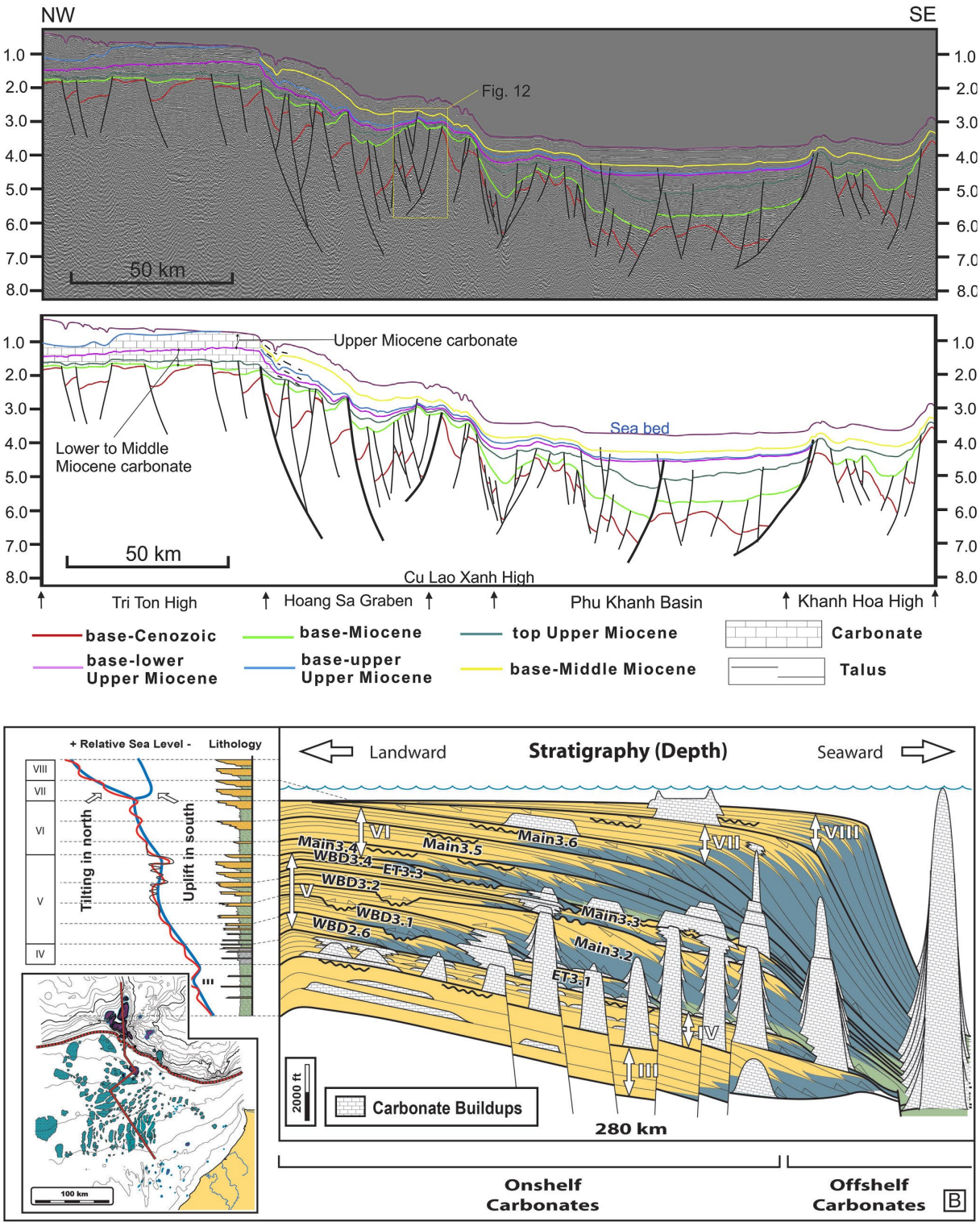

Figure 3- 3. Carbonate in the southwestern margin (Kosa et al., 2015; Vu et al., 2017). Extensive distribution of carbonate indicate a shallow water depth during the Early to Late Miocene, which is the latest rifting history in the SCS margin.

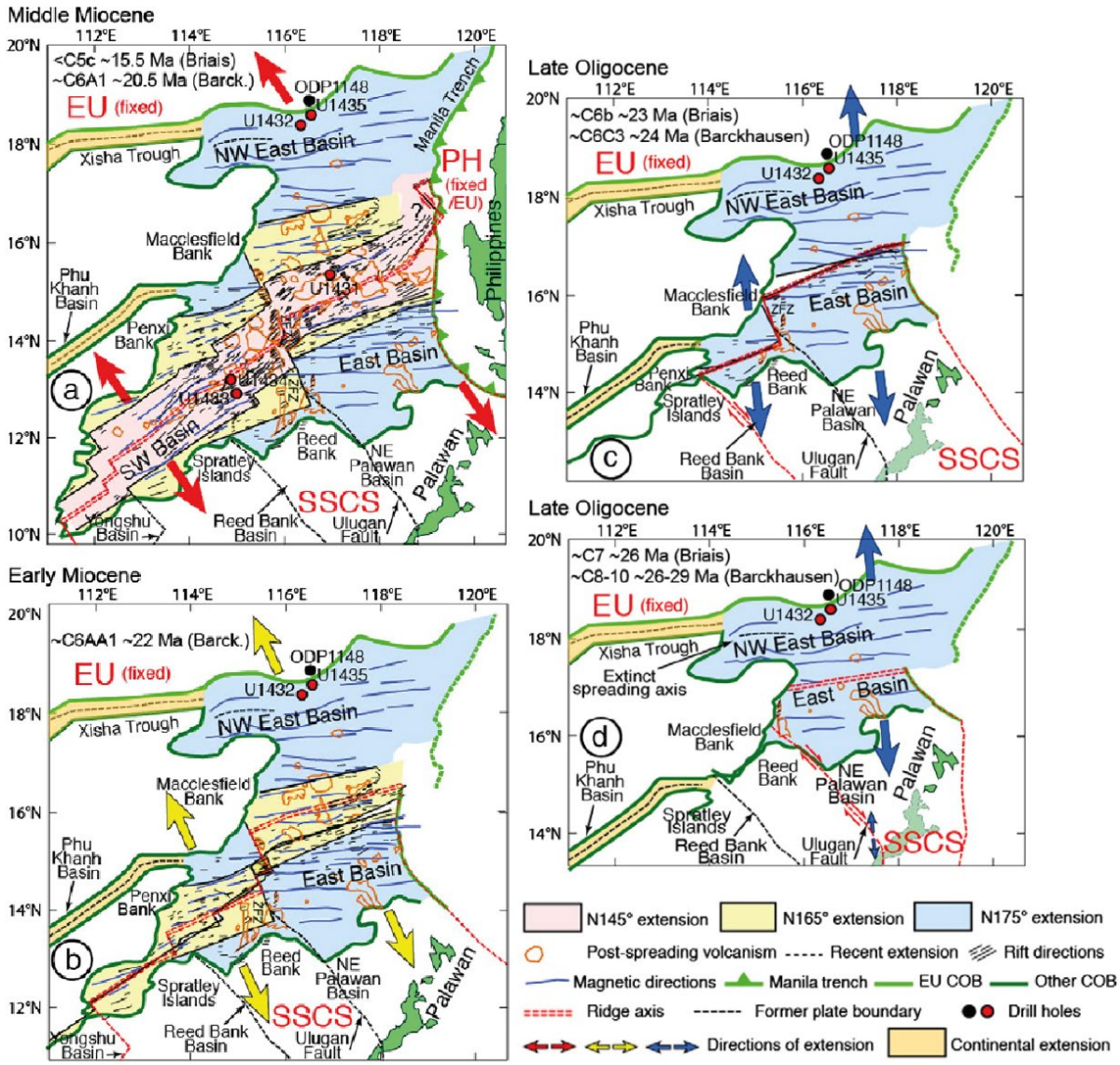

Figure 3- 4. Integration of the magnetic anomaly and bathymetry to identify the mechanics of the change of extension direction (Sibuet et al., 2016), via an intermediate stage (yellow) at 23Ma.

3.3 Data acquisition and processing

We made use of large cross sections along one profile in the vicinity of Penxi Bank and Spratly Islands (Nansha Islands) (Figure 3- 7 and Figure 3-10). This 1000-km-long multichannel seismic (MCS) data was collected by a project conducted by ENS-CNRS (France) and GMGS P.R of China, from 2011 to 2013 (Figure 3- 5). The vessels, R/V DongFang KanTan and R/V Tan Bao, shot at 50 m interval for reflection profiles after collecting refraction profile along the same navigation. The volume of the airgun array was roughly 7,000 cubic inch, and the streamer was 8 kilometers (640 channels) long in the Qiongdongnan adjacent and 6 km (480 channels)

long for other area. Both streamers have a 12.5 meters receiver interval. The record length is 16 sec TWT (seconds two-way travel time) with a 2 ms sampling rate.

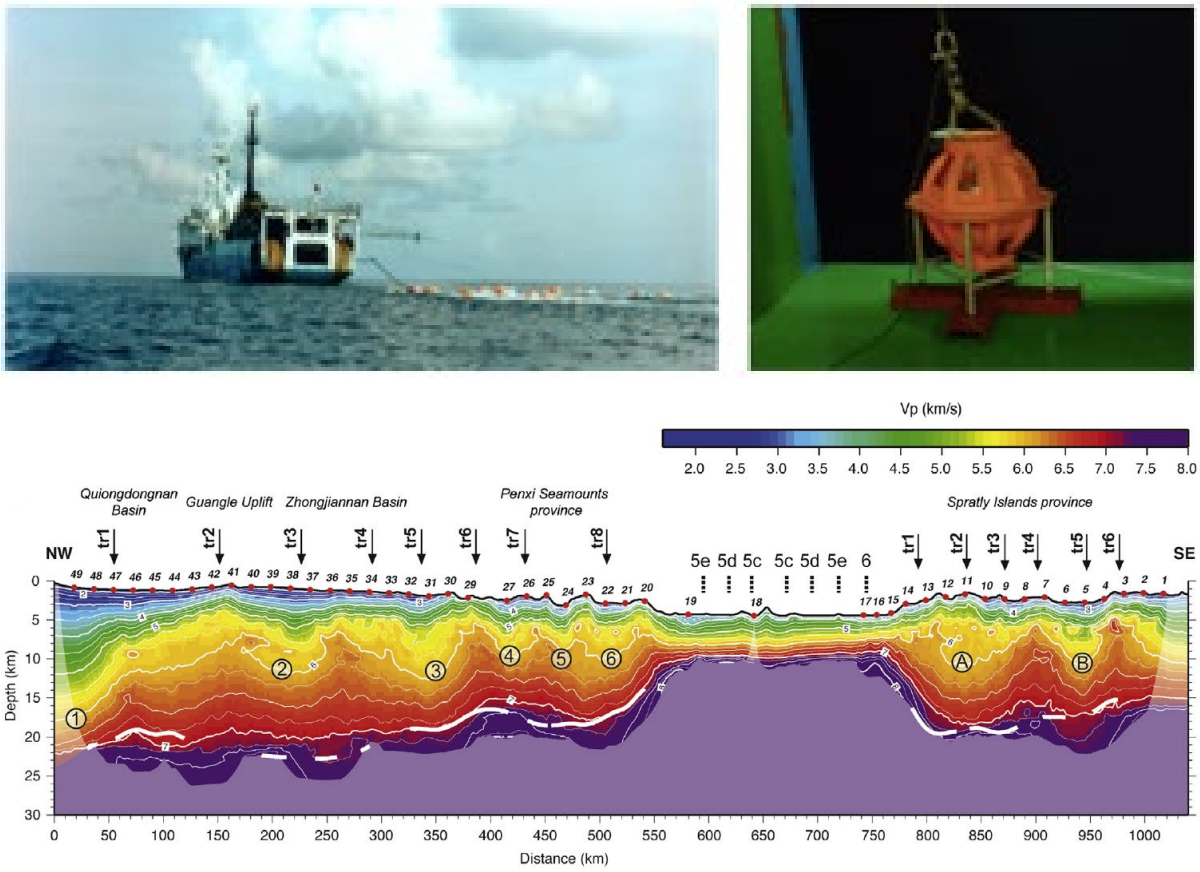

Figure 3- 5. Acquisition of MCS and OBS on the sea in 2011 and 2013. The velocity structure published in (Pichot et al., 2014).

This study supplies results on the whole China-France Transect MCS profile (CFT), for the first time, across the conjugated margin of SW the South China Sea. The processing was completed at Ecole Normale Supérieure and was designed to enhance the deep crustal structure by several procedures of multiple attenuation (Figure 3- 6). The workflow included geometry, filter, noise attenuation, trace editing, amplitude scaling, bin centering, offset regularization, predictive deconvolution, multiple attenuation (SRME, Radon, and F-K filter), high density velocity analysis by the CGG Geovation 2013 software. The migration was achieved by pre-stack Kirchhoff time migration, and AGC amplitude recovery in the final output image.

The efficiency of the anti-multiple procedure varies along the line because of the changes in impedance contrasts of the seafloor and basement. In many areas where sedimentation is limited,

the basement scatters back a lot of energy that is difficult to attenuate (from km 450 to 550 on the CFT-N, and km 150 to 270 on the CFT-S). More details can be found in Liang et al. (2019).

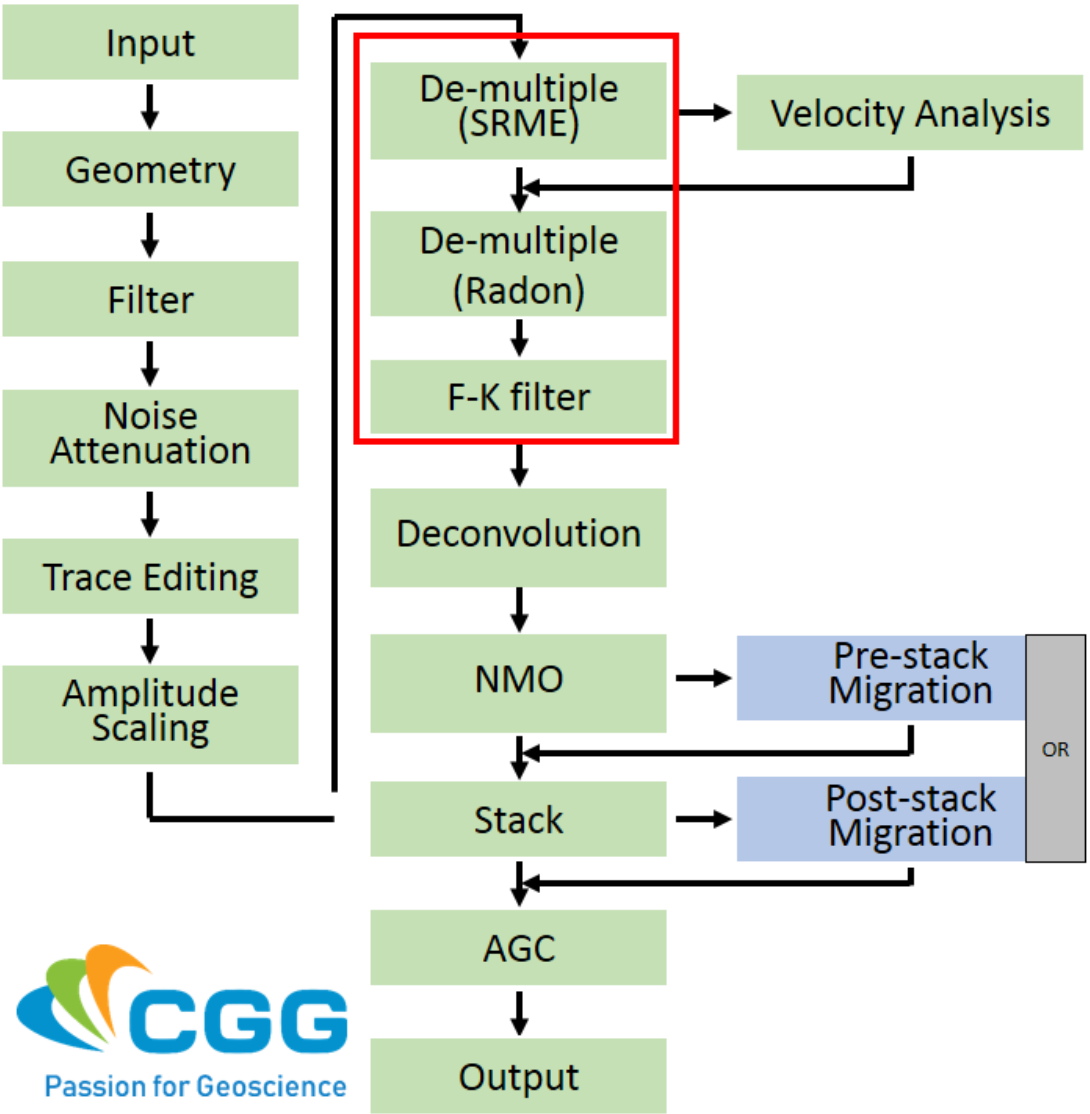

Figure 3- 6. Process flow chart and the examples for the improvement on the seismic images. Significant attenuation of multiple improves the deeper reflectors on the seismic images.

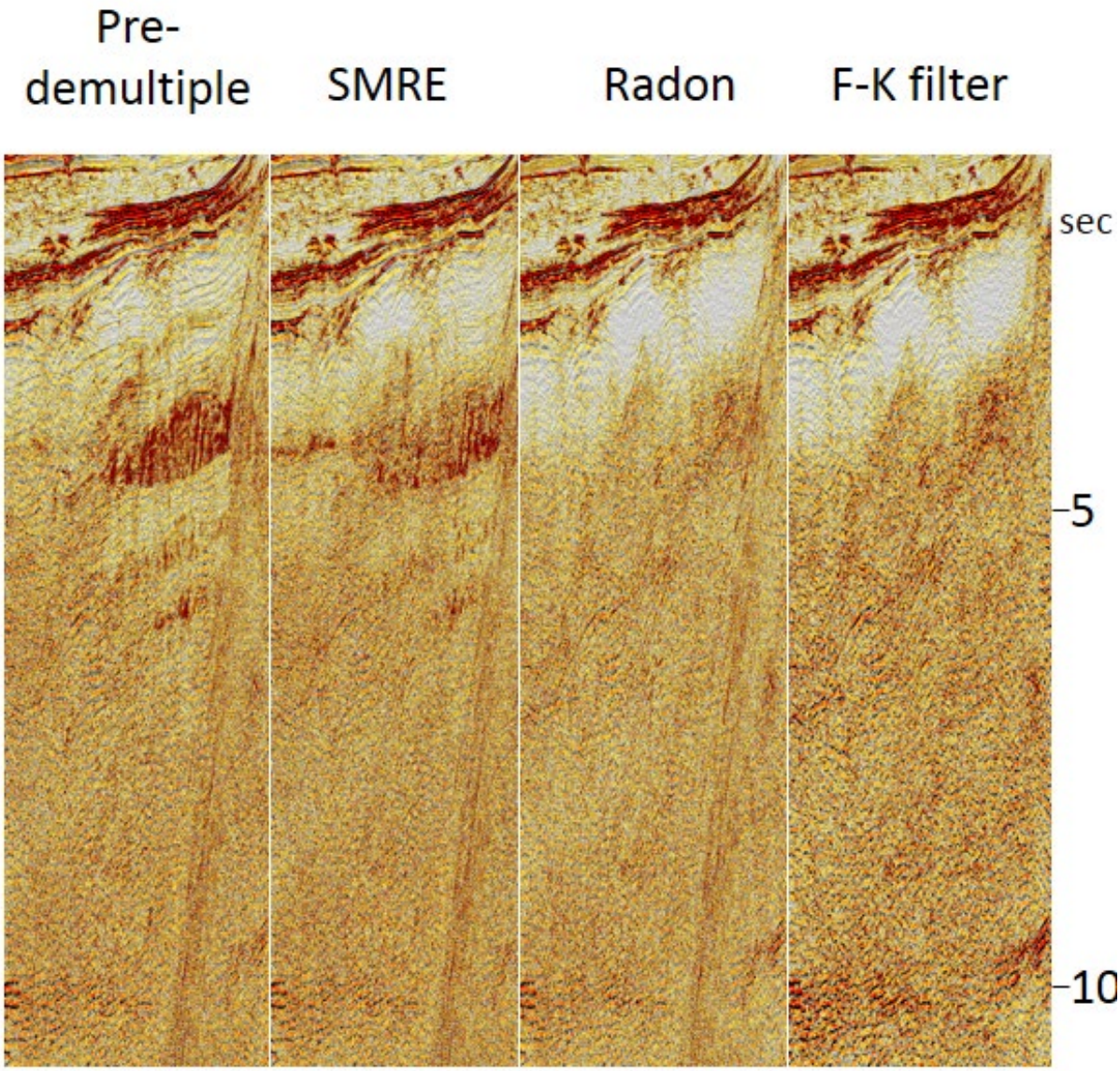

Figure 3-6 (continued). Process flow chart and the examples for the improvement on the seismic images. Significant attenuation of multiple improves the deeper reflectors on the seismic images.

3.4 Rifting architecture in the SW South China Sea

The architecture and extensional processes of the conjugate margins of the SW sub-basin offered by the CFT long transect, is exposed hereafter by extracting two parts of the profile, to the north (CFT-N) and to the south (CFT-S).

3.4.1 East Vietnam-South Hainan Margin of the SW sub-basin

The CFT-N profile extends over a 600-kilometers length of thinned crust (from the shelf break to the COT) along the E Vietnam/S Hainan margin, and shows a crustal thickness varying from

2 to 8 sec TWT. Most of the area belongs to the thinned and hyper-thinned domain similar to the domain described in the North by Nirrengarten et al. (2020a) (locate across East SCS margin on Figure 3- 1). The Moho shallows gently in a few hundreds of kilometers seaward with local fluctuation in less than 1 sec TWT. These Moho Depth undulations are due either to a pull-up effect or to more localized hyper-extension (distance 90 and 430 km on *Figure 3- 7*). Normal faults dip either seaward or landward and bound the edges of the basins with varying basement offsets. Several normal faults offset basement with little accommodation space (distance 70 and 250 km on *Figure 3- 7*), but these mostly affect the lower syn-rift unit, syn-rift I, showing they were active during the early stages of rifting. Another set of faults develops downward to roughly 7-8 sec TWT depth rooting into the deep lower crust and rotates the continental block above the lower crust where some horizontal reflectors may be traced (70, 220, and 330km on *Figure 3- 7*), thus suggesting the existence of a low viscosity layer as interpreted previously in adjacent basins (Pichot et al., 2014; Lei and Ren, 2016; Lei et al., 2019a; Xie et al., 2019). This deformation contrast is not obvious in the distal margin due to the strong artefact noise. According to the geometry of the Zhongshanan sedimentary basin (projected to the west, see location Figure 3- 1), the detachment fault (reflector D on *Figure 3- 7*A to C) created accommodation space through most of the syn-rift period and continued thinning the crust during the late extensional stages (Distance 220 km).

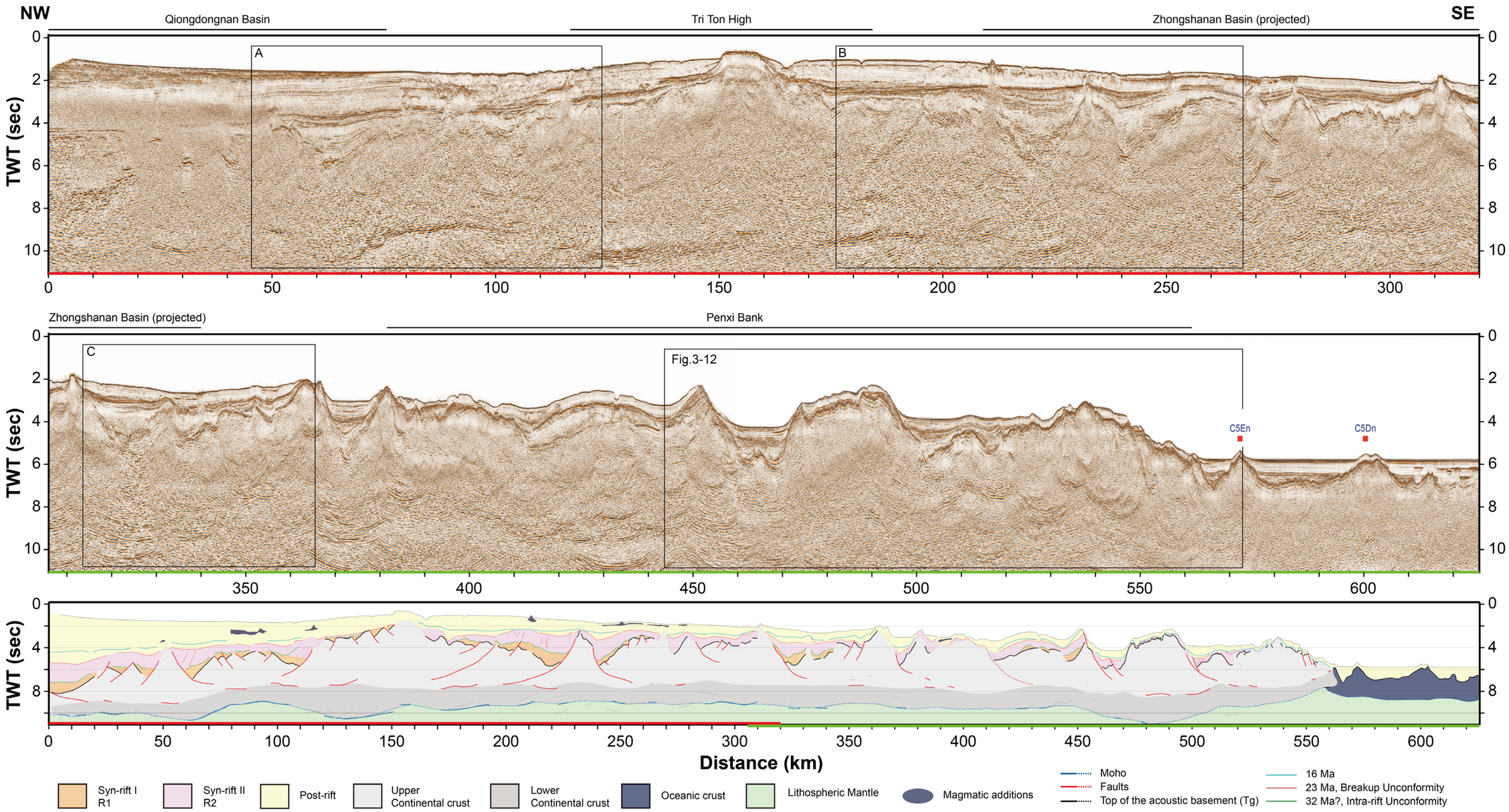

Figure 3- 7. Original and interpreted seismic profiles of line CFT-N across the E Vietnam/S Hainan Margin. The wide rifted margin characterizes distributed basins with two phases of syn-rift units, which bounded by detachment faults. The location shown on the Figure 3- 1.

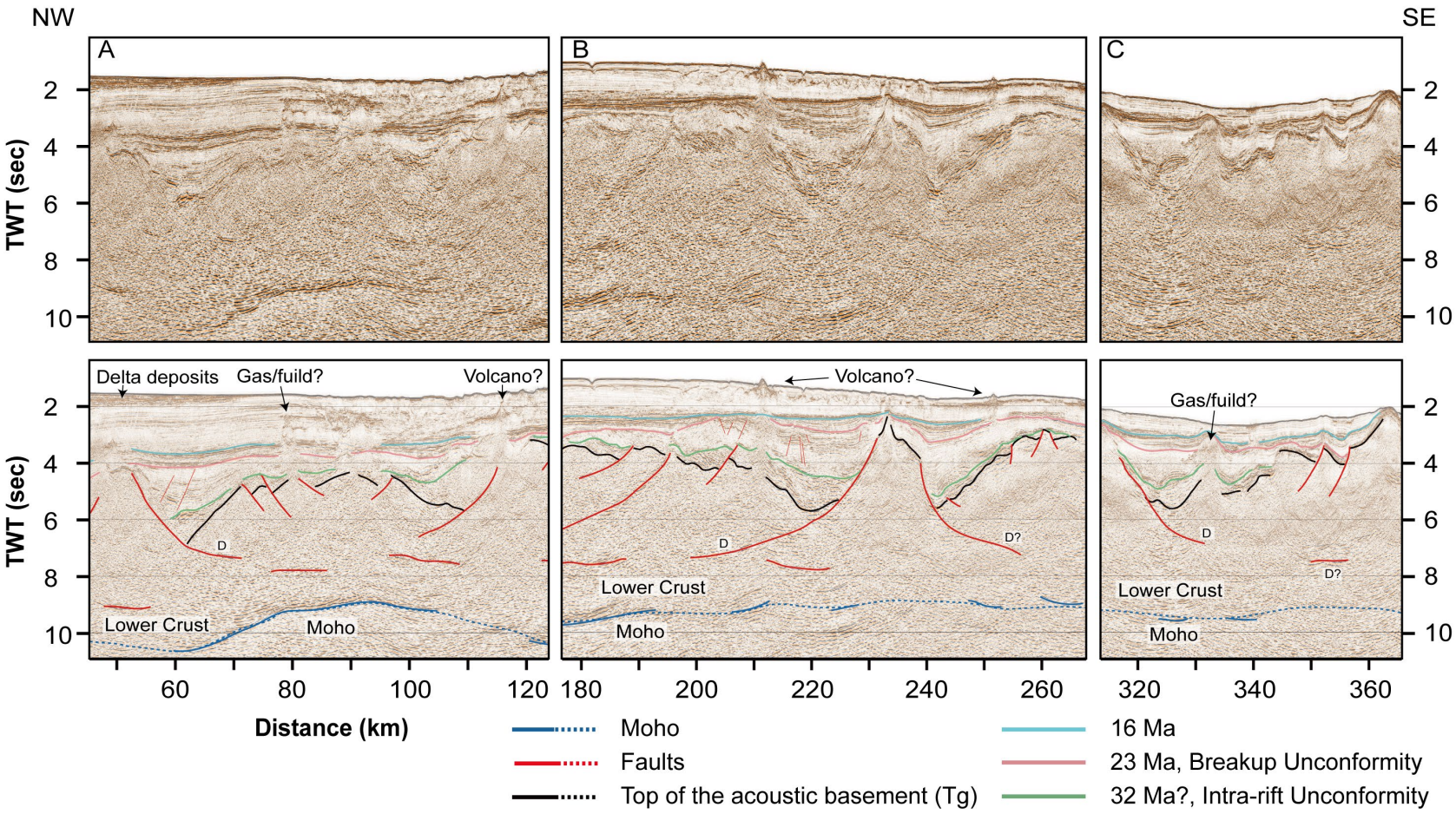

Figure 3-7 (continued). (A-C) Hyper-extented crust in the Qiongdongnan Basin and Zhongshanan Basin (projected). The syn-rift II (between green to red horizons) thickens toward the detachment faults (D), which normal faulting roots into the top of the lower crust and thins crust mainly. The locations are shown in the Figure 3- 1a.

The rifting basins extend far to the distal margin and their location corresponds to low velocities in the refraction section (Basin 1 to 6 in Pichot et al. (2014)). Strong amplitude reflectors are traced at the bottom of the Qiondongnan Basin and Zhongshanan Basins (projected) within 2 sec TWT thickness in the distance 0 to 20 km (*Figure 3- 7*) and 200 to 220 km (*Figure 3- 7*B) respectively. These strong amplitude reflectors are recognized as the syn-rift I in this study, showing a wedge-shaped unit in the lower syn-rift, but restricted to the proximal margin. This is not observed near the granitoid basement of the distal margin. One unconformity within the syn-rift succession is related to later stages of the evolution of the detachment faults interpreted from the thickening of the syn-rift II toward detachment faults, and has been recognized in other basins in the SCS as the detachment-related unconformity (Figure 3- 8) (Xie et al., 2019). Several faults offset syn-rift II and dip toward the depocenter (*Figure 3- 7*B and C), and seems to terminate at a similar time as the detachment faults. The breakup unconformity (BU) overlies the top of syn-rift II (*Figure 3- 7*), which is identified at 23 Ma (T6) along the E Vietnam/S Hainan margin based on correlation from seismic profiles tied to wells in adjacent basins (Savva et al., 2013; Lei and Ren, 2016; Vu et al., 2017).

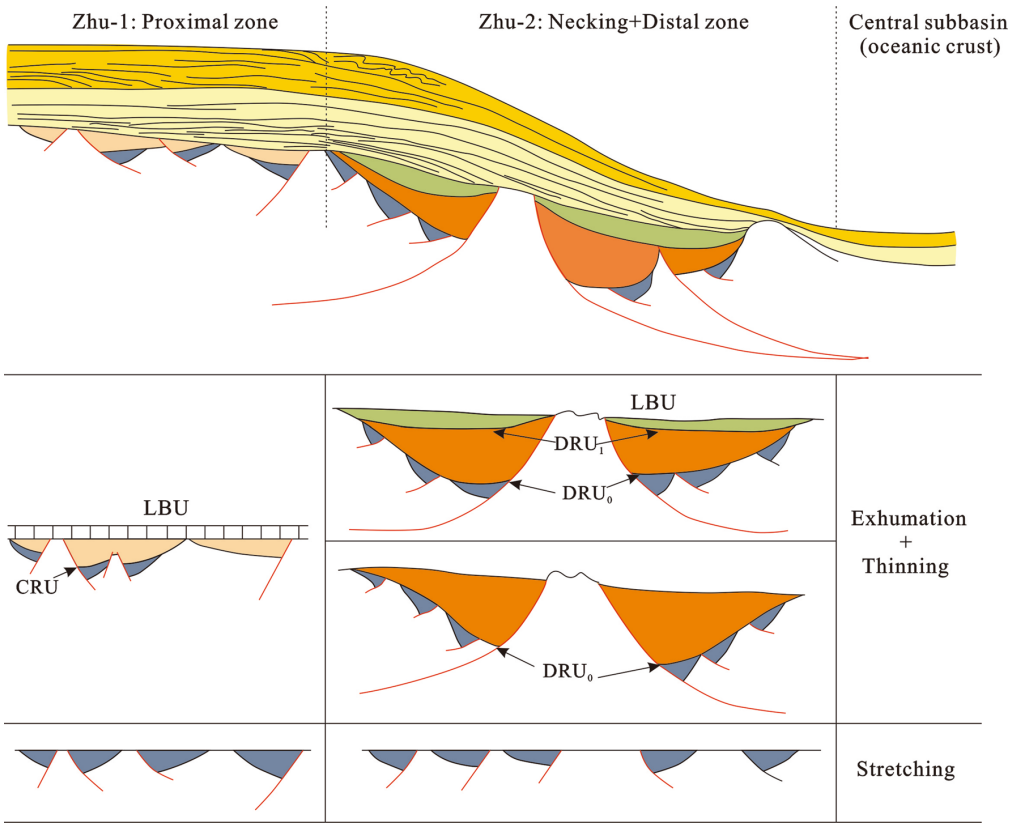

Figure 3- 8. Synthesitic model for the formation of unconformities in the rifted margin related the basin evolution (Xie et al., 2019). DRU refers to detachment-related unconformity in this figure; CRU for crack-related unconformity; LBU for lithosphere breakup unconformity.

A significant unconformity within post-rift succession is marked around Middle Miocene (blue on *Figure 3- 7*a-c), and is widely spread in the southwestern SCS margins (Savva et al., 2013; Li et al., 2014b; Vu et al., 2017). The post-rift sedimentation composes the deep sea blanket. It is associated with the thermal subsidence and closely followed by sediments shed by the large delta deposits from Vietnam coast, although these may in turn be affected by moderate tectonic movements during the post-rift period on Figure 3- 9 (Wang et al., 2013). Fluid/gas migration and volcanic bodies can be sporadically found in the post-rift succession shallower than 2 sec TWT. This is observed on the CFT-N profile (*Figure 3- 7*a-c) as well as on other adjacent seismic data (Wang et al., 2013; Gao et al., 2019).

3.4.2 Northwest Borneo margin of the SW Sub-basin

The NW Borneo margin extends over 600-kilometers southward to the Sabah as seen on seismic and gravity data (Cullen et al., 2010), and shares similar rifting history with that of the northern margin during the Paleogene (Holloway, 1982). A large part of it is nowadays subducted and covered by the Mid-Miocene deltas of Baram and Champion. The 250 km long seismic profile CFT-S across the NW Borneo Margin, illustrates only a part of the configuration of the southern margin, which has the presence of granitic bodies restricted to the distal margin. However, similarities with the northern margin are noticeable in terms of crustal thickness as well as style of faults. Detachment faults have been identified underlying a deep basin and several shorter period normal faults, appear between these detachments (Distance 70 and 20 km on Figure 3-10) (Peng et al., 2018; Liang et al., 2019).

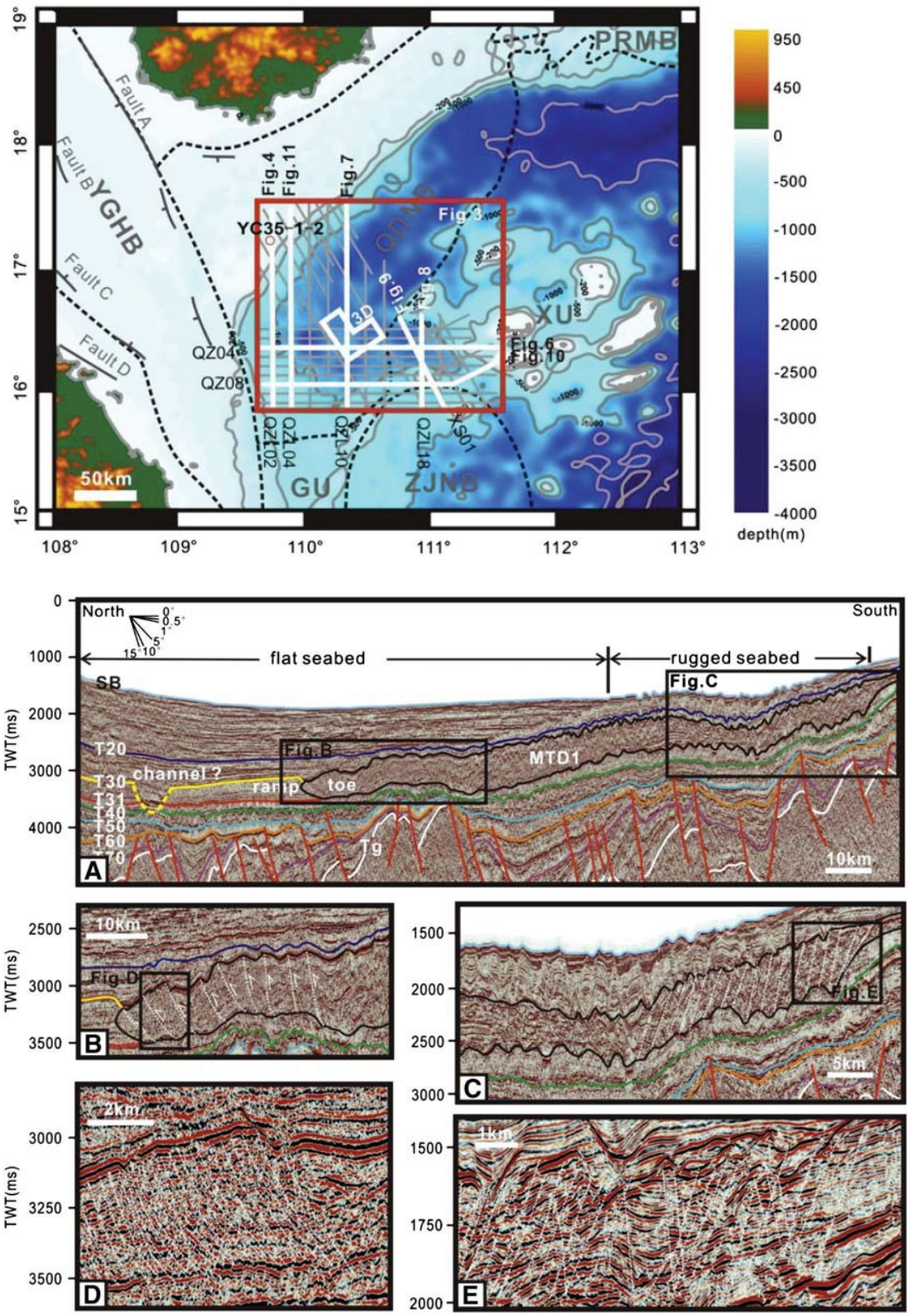

Figure 3- 9. Mass Transport deposits (MTDs) appear in the post-rift period (Wang et al., 2013), the location is at the "Fig.7" on the upper panel.

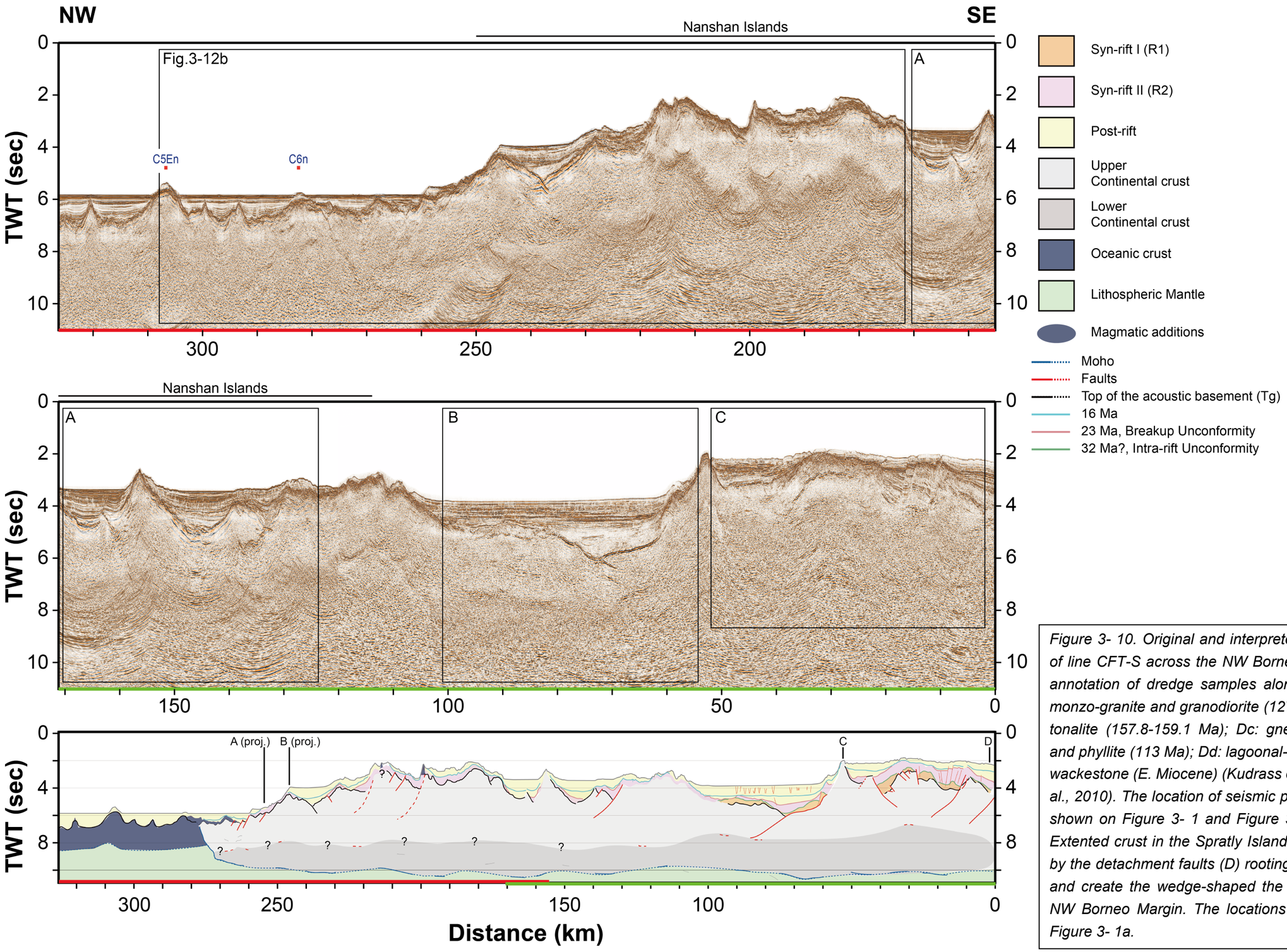

Figure 3- 10. Original and interpreted seismic profiles of line CFT-S across the NW Borneo Margin with the annotation of dredge samples along the profile. Da: monzo-granite and granodiorite (127.2-153.6 Ma); Db: tonalite (157.8-159.1 Ma); Dc: gneiss (115-123 Ma) and phyllite (113 Ma); Dd: lagoonal-reefoid packstone-wackestone (E. Miocene) (Kudrass et al., 1986; Yan et al., 2010). The location of seismic profile and samples shown on Figure 3- 1 and Figure 3- 11 respectively. Extented crust in the Spratly Islands accommondated by the detachment faults (D) rooting to the lower crust and create the wedge-shaped the syn-rift unit in the NW Borneo Margin. The locations are shown in the Figure 3- 1a.

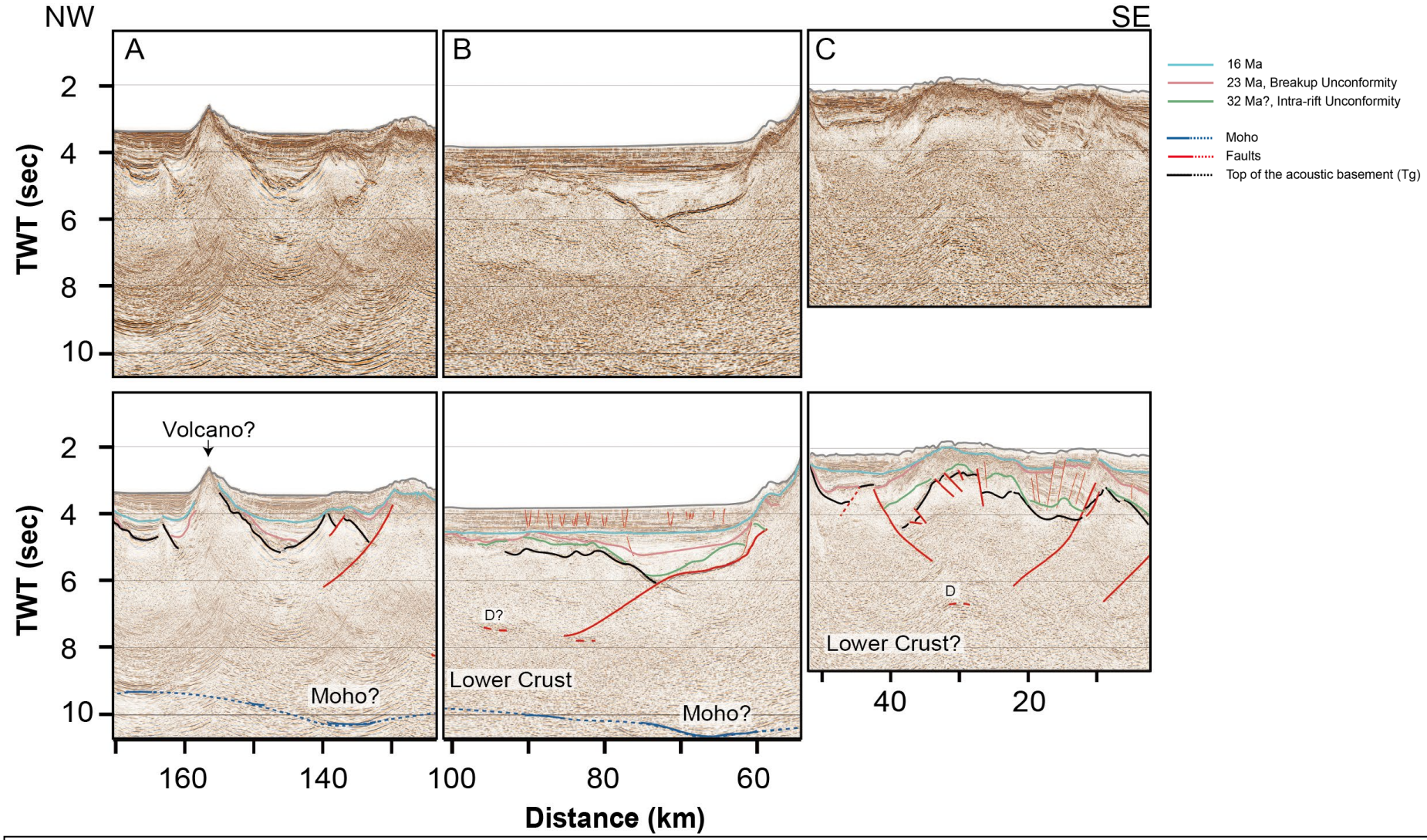

Figure 3- 10 (continued). Original and interpreted seismic profiles of line CFT-S across the NW Borneo Margin. The location of seismic profile and samples shown on Figure 3- 1 and Figure 3- 11 respectively. Extented crust in the Spratly Islands accommondated by the detachment faults (D) rooting to the lower crust and create the wedge-shaped the syn-rift unit in the NW Borneo Margin. The locations are shown in the Figure 3- 1a.

The best age constraint is established on the base of the well Sampaguita-1 (location S-1 on Figure 3- 11), which penetrated most Cenozoic strata until the Mesozoic (Taylor and Hayes, 1980; Yao et al., 2012; Steuer et al., 2014), although it is distant from our line by 80-kilometers. A seismic facies characterized by strong reflectors at the bottom of the sedimentary pile could correlate with similar early syn-rift I sediments of the northern margin (Figure 3- 10B and C) in the proximal margin. The syn-rift II does not appear as a wedge-shaped unit although detachment faults have also developed. An erosional surface exists atop the syn-rift succession (blue horizon on Figure 3- 10) and induced significant P-wave velocity contrast (Wang et al., 2016). More syn-rift strata were eroded and covered by the Late Miocene deposits, which suggests a post-rift tectonic movement in the NW Borneo margin. The erosion distributes southward until the Palawan-Borneo Trough (Ding et al., 2014; Steuer et al., 2014; Tong et al., 2019).

3.5 COT configuration prior to the break-up

The rifted margin displays lateral variations along the COT of Southwest SCS. An abrupt bathymetric jump marks an N-S contrast at the eastern edge of the Penxi Bank and the western edge of the Spratly Islands crustal morpho-structures (Figure 3- 11), whereas a gradual slope characterizes an E-W morpho-structure at the south of the Penxi Bank (Figure 3- 11a). Therefore, two distinct segments of N-S and E-W orientation appear as bathymetric feature. WE used two extracted profiles from line CFT to illustrate the N-S segment (Figure 3- 12a and Figure 3- 12b). The interpretation of E-W segments is supported by the analysis of two other pieces of seismic profiles, INL320 and NGH-1-3, acquired and processed by GMGS (Figure 3- 14a and Figure 3- 14b). It is worthy to examine the heterogeneous resulting lithosphere in view of the spatial diversity of the COT.

We reconstruct the conjugated margin on a cross-section by removing the oceanic crust following the magnetic anomaly identified by Briais et al. (1993) (Figure 3- 11b). Modelling along magnetic profile permit to define several chrons with an absolute age (Gee and Kent, 2007), indicated the earliest anomaly at C6n (20.1 Ma) and C5En (18.8 Ma) on southern and northern profiles respectively (Figure 3- 11b). Although the magnetic anomalies in the oceanic domain are progressively blurred toward southwest, this study prolongs the magnetic anomaly along the bathymetric features and allows to propose ages of the crust formation (Figure 3- 11b).

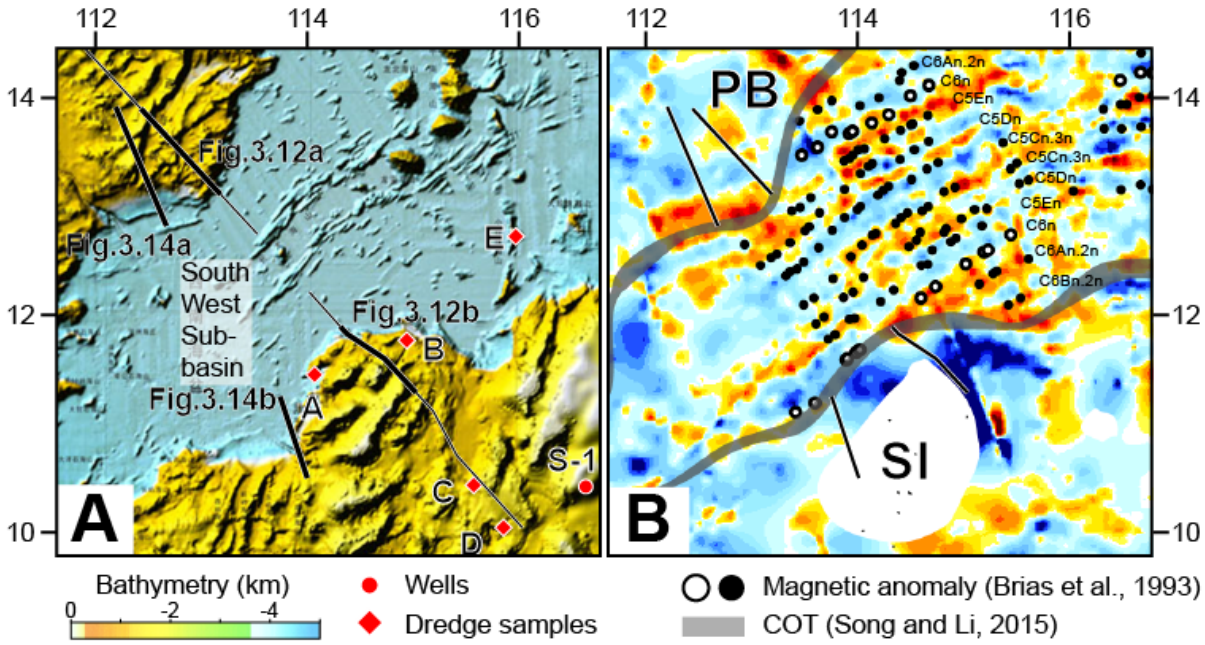

Figure 3- 11. (a) The morpho-structure shown by bathymetry separates two segments in N-S and E-W orientation near the continent-ocean transition of Penxi Bank (PB) and Spratly Islands (SI) in the southwestern SCS. Two cross-sections present the crustal architecture of conjugated margin by juxtaposing the E Vietnam/S Hainan Margin and NW Borneo Margin along two segment individually. S-1: Well Sampaguita-1. (b) The magnetic anomaly map is identified the ages by Briais et al. (1993). The open circle represents the C6n, which is the first anomaly along the seismic profiles. The reconstruction of the conjugated margins are established based on the C6n in this study.

3.5.1 N-S trending segments of the margin

The thickness of the crust, tracked by intermittent Moho reflectors, thins oceanward from 10 sec to 8 sec TWT (Figure 3- 12). This reflector runs beneath the continental basement around 10 sec in the NW Borneo margin, and ascends seaward until the oceanic crust near the magnetic anomaly C6n. The extension at the edge of the basin (boundary fault) may reach a possible level of detachment (Figure 3- 12a), although the base reflector is not as clear as the detachment level seen in the basins landward. The overlying sediments are restricted to small depressions landward of the COT, which displays a relatively thin sedimentary infill. They may record a hiatus induced by a tectonic uplift, indicated by significant erosional surfaces from basin to basement on both margins (red horizon on Figure 3- 13). This indicates the crust did not suffer hyper-thinning during the rifting and was sustained above the sea level before it subsided.

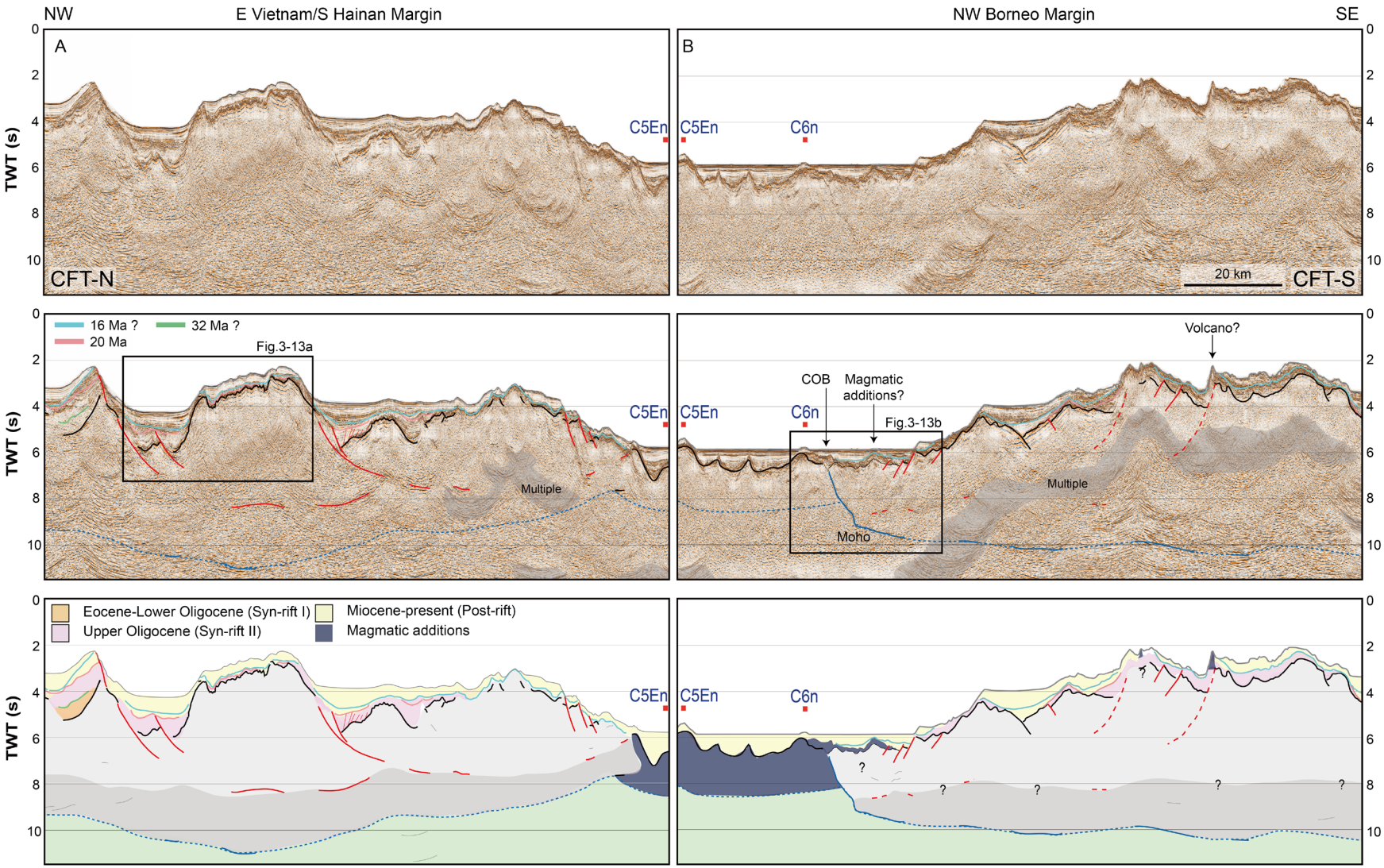

Figure 3- 12. Conjugated cross-section along the N-S segment presents the thinned crust covered by thin syn-rift sediment at the time of breakup (C6n, 20.1 Ma). The location of profiles is shown in Figure 3- 11a.

In the basin next to the first magnetic anomaly, the basement slope is slightly steeper along the E Vietnam/S Hainan margin showing less stretching than that of the NW Borneo COT area, displaying an asymmetric structure (Figure 3- 12). Some chaotic facies in the bottom sedimentary succession results from mass transport deposits along the abrupt slope adjacent the COT.

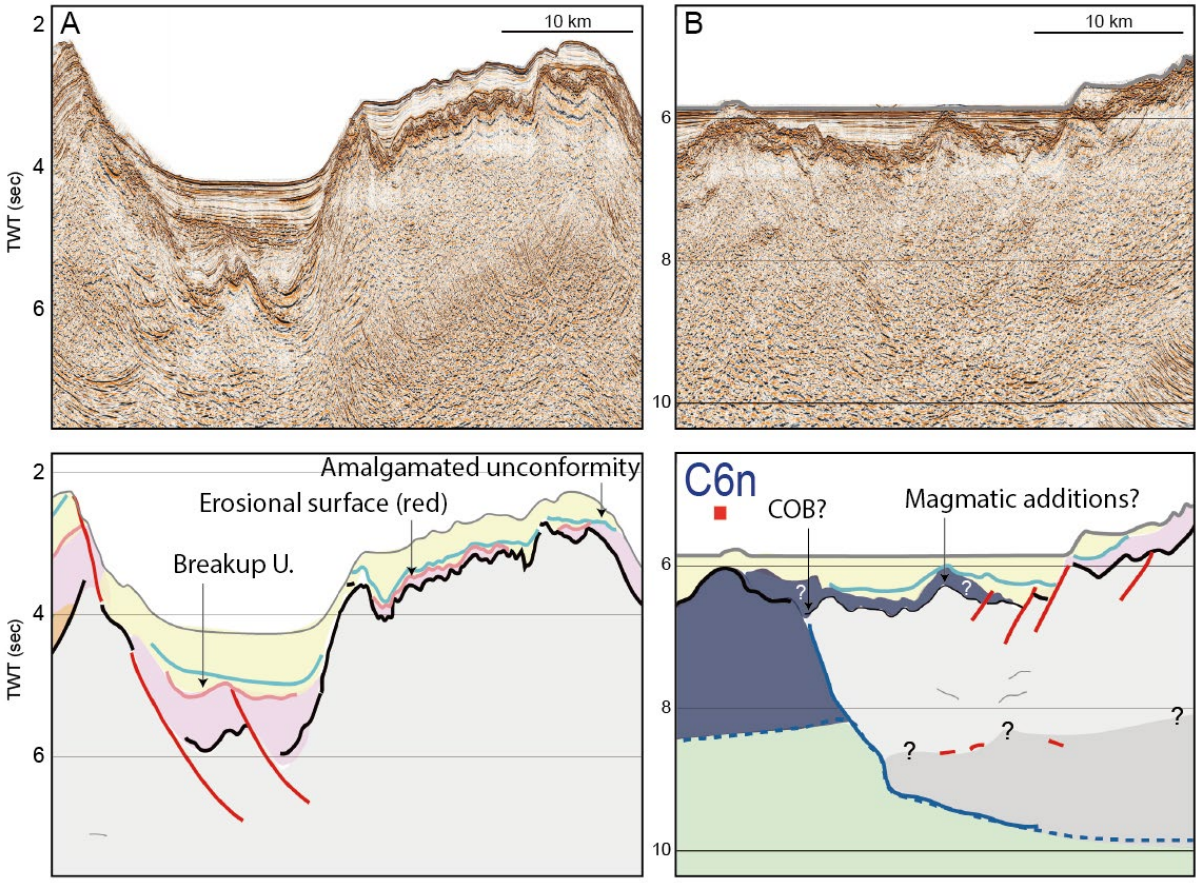

Figure 3- 13. The rifted basin illustrates thin syn-rift succession with an erosional surface distributing along the rifted basins and basement high in the N-S segment.

3.5.2 E-W trending segments of the margins

By contrast, the E-W trending segments of the margins display a thinner crust with a large amount of sediments near the COT (Figure 3- 14). A series of dense normal faults mildly offset most the syn-rift succession and dip seaward in both conjugated margins. The sediments appear collapsed where they are the thickest and rest on top of hyper-stretched continental material (Figure 3- 15). The mild offsets of the sedimentary package under the red horizon (20Ma, Early Miocene) can be confidently traced with similar seismic facies on both margins, and the unconformity from the top of the syn-rift correlates to the bottom of strata at the oceanic domain

as a breakup unconformity (Figure 3- 15). The upper syn-rift unit is characterized by a homogenous thickness. It is slightly thicker toward ocean, and the total width across both margins reaches to 75 km length. This syn-rift unit has abrupt concave-up disturbance and truncation atop at the seaward boundary close to the oceanic domain and are unconformably overlain by post-rift strata. The correlation of the syn-rift unit may be extended landward, prior to a breakup unconformity (red horizon on Figure 3- 14). The syn-rift shows tilted lower syn-rift strata with homogenous thickness of syn-rift II, highlighting the development of detachment faults necessary for upper syn-rift sediment deposition.

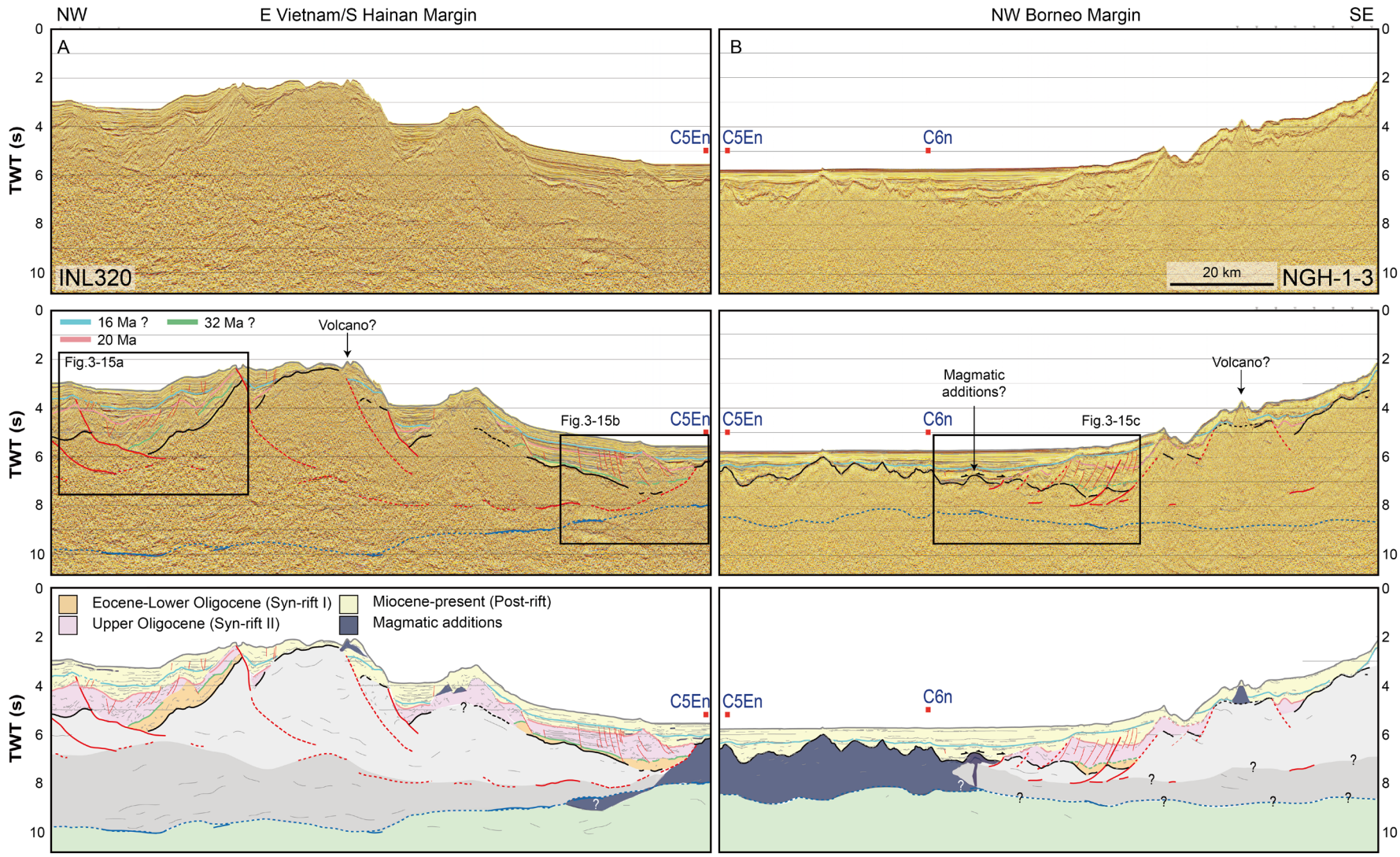

Figure 3- 14. Conjugated cross-section along the E-W segment presents the thick syn-rift sediment at the time of breakup (C6n, 20.1 Ma). The location of profiles is shown in Figure 3- 11a.

The tectono-stratigraphy of line NGH-1-3 has been discussed in several papers with varying interpretations for pre-rift, syn-rift and post-rift, of the COT area, due to a lack of well-established bio-stratigraphy studies (Ding et al., 2013a; Song and Li, 2015; Ding et al., 2016; Wang et al., 2016). This study uses a stratigraphic chart based on the correlation with the oceanic floor and IODP biostratigraphy (Li et al., 2015; Ding et al., 2016). The significant unconformity (blue), which tops the unit offset by the small normal fault, is not considered as breakup unconformity in this study, and we favor a more consistent syn-rift thickness in different units along the COT of both conjugated margins (Figure 3- 15).

The asymmetrical architecture of crust is shown by thinner crust and lower basement slope in the south. While the Moho ascends, part of basement exposed without overlying syn-rift succession before forming the first magnetic anomaly (C6n) in the NW Borneo Margin (Figure 3- 14 and Figure 3- 15), where perhaps is an exhumation of sub-continental lithospheric mantle (Ding et al., 2016) or part of the continental crust. An intrusive body penetrated through this exhumed material.

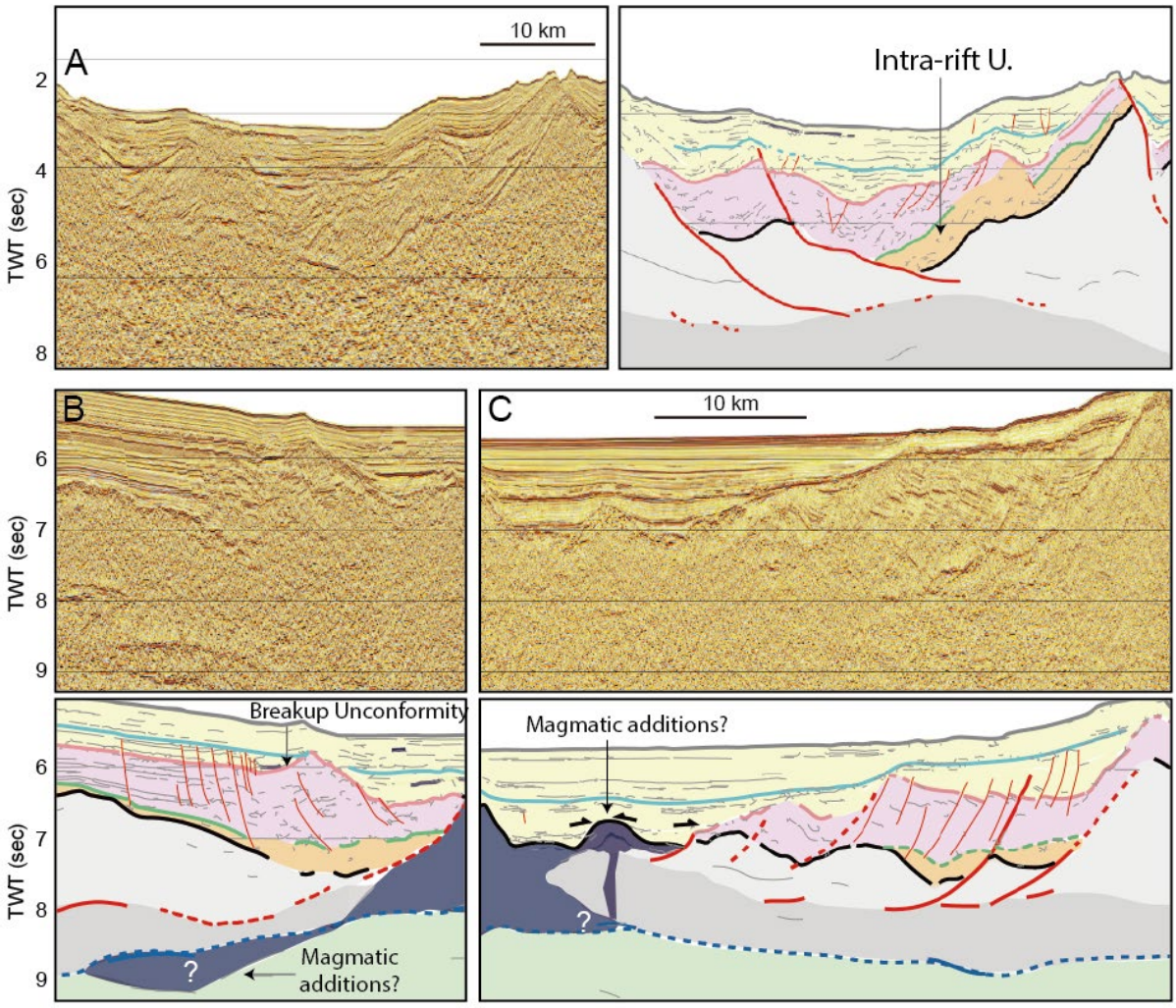

Figure 3- 15. A thicker sedimentary basin covers the COT of E-W segment with a regular thickness. The syn-rift unit next to the oceanic crust was disturbed and truncated to form the breakup unconformity. It is suspected that the green horizons (32 Ma) accommodates the slide motion at the base of the rotated package of sediments.

3.5.3 Lateral variation of COT structures

The crustal architecture appears to differ depending on the orientation of the COT. We observe significant variation of sediment thickness and a sharp difference between the N-S segment and the E-W segment. At the COT, the E-W segment illustrates an even more stretched crust and more sediment infill. Instead, segments connected by N-S abrupt relays, exhibit a sharp COT with thin overlying sediments. The lateral change of the crustal structure is also consistent in the bathymetry and an E-W trend of magnetic anomaly (Figure 3- 11). The pre- and syn-rift strata are mainly distributed in the areas which are oriented E-W, suggesting a thinning in agreement with N-S extension. The N-S segments on the contrary would have suffered a strong

wrench component (Figure 3- 16), thus making the early COT system compatible with pull-apart basins (Figure 3- 19).

The observation of the two sections in the southwest of the SCS allows us to highlight a similarity in the extensional process with the margins of the eastern SCS. When juxtaposed, the margins with thicker sediments show a similar hyper-extensional feature with thicker sediments in the western SCS with a discrepancy in breakup ages (Figure 3- 16). Therefore, the evolution of rifting architecture seems to involve similarly in the East SCS (section A on Figure 3- 16) and in the southwest (section B and C on Figure 3- 16) with time lag of 20 Myr. The margins of the Southwest Sub-Basin experienced a longer period of extension and resulted in extremely thin crust in several basins, for which the crustal thickness reaches values lower than 1.5 sec TWT, for instance, the Qiongdongnan Basin and basins near the COT (*Figure 3- 7* and Figure 3- 14). In several adjacent basins, we can even barely observe the crust between syn-rift sediment and lithospheric mantle with a constant thickness of syn-rift sediment as illustrated in this study (Savva et al., 2013; Lei and Ren, 2016; Clerc et al., 2018).

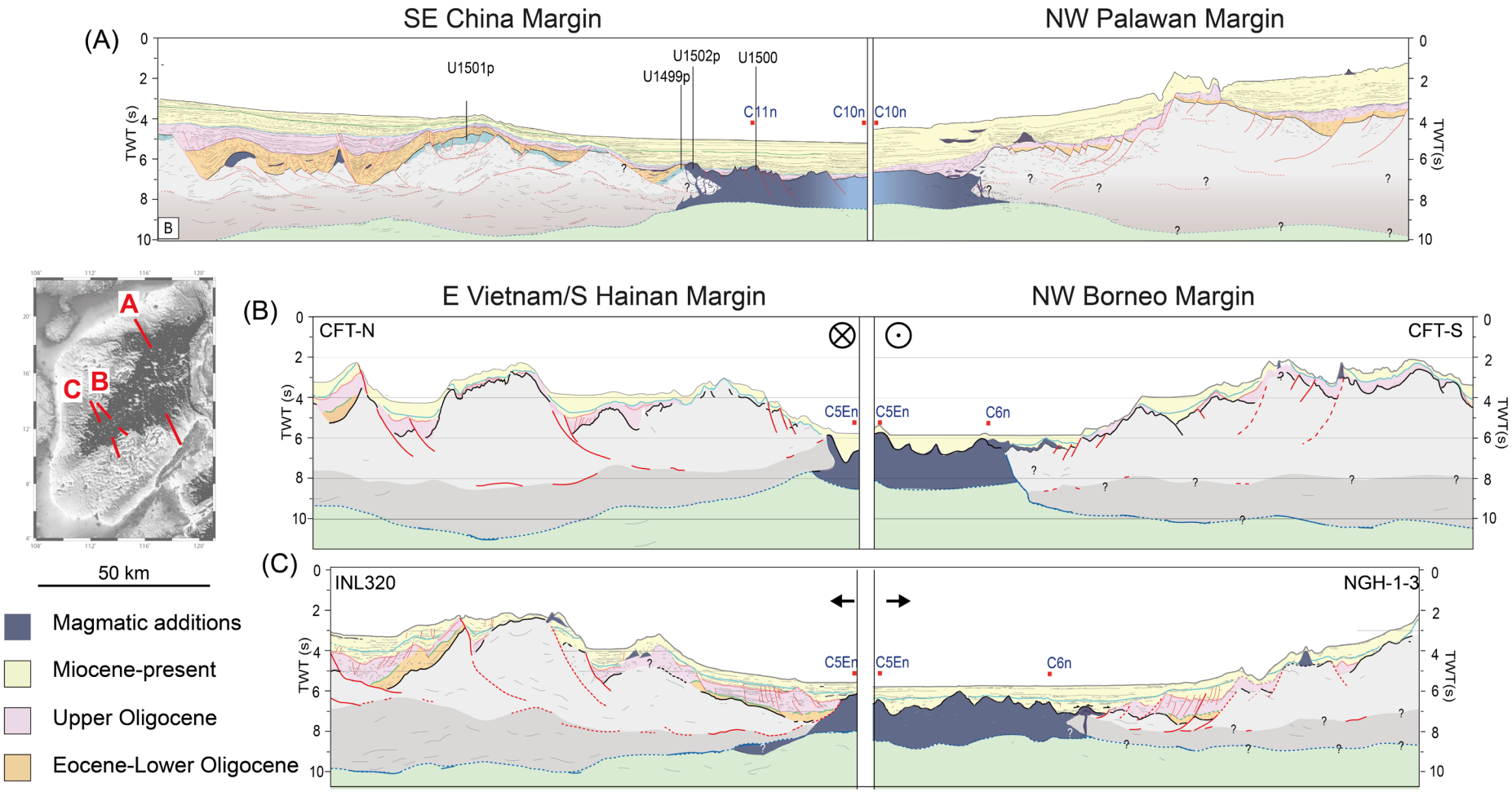

Figure 3- 16. The comparison of crustal configuration between East and Southwest SCS. The wrench component lead the N-S segment (section B) prior to the breakup. The pull-apart basin along the E-W segment (section C) with thicker syn-rift sediment. Different ages of breakup and breakup unconformity are presented between E Vietnam/S Hainan-NW Borneo Margin and SE China-NW Palawan Margin modified from Nirrengarten et al. (2020a). The similarity of asymmetrical structure appears near the COT.

3.6. Discussion

3.6.1 Breakup process in the SW margin

The tectono-stratigraphic analysis offers a scenario to understand the breakup evolution in the Southwest SCS. The observation of seaward dipping normal faults with limited offset dominate the latest stage of the crustal stretching (Figure 3- 15). A ductile layer is needed underneath the detachment fault for the decoupling as suggested in several simulations (Clift and Lin, 2001; Huismans and Beaumont, 2011; Brune et al., 2017; Ros et al., 2017). The lower crust was stretched in ductile condition and exhumed sub-continental mantle or lower crust. The exhumed material juxtapose the oceanic crust, showing the continental lithosphere was finally broken up by the ascending asthenosphere which produced locally intrusive bodies (Figure 3- 17).

This breakup process also interrupts the overlying syn-rift succession with concave-up features (Figure 3- 17b). It ultimately formed a first magnetic anomaly C6n in the south. This gives a hint that the propagator may have a strong impact on the breakup process. Rapid magmatism along the COT suggests hot crustal condition influencing the thinning and breakup processes leading to wide rifted margin (Brune et al., 2017; Le Pourhiet et al., 2018).

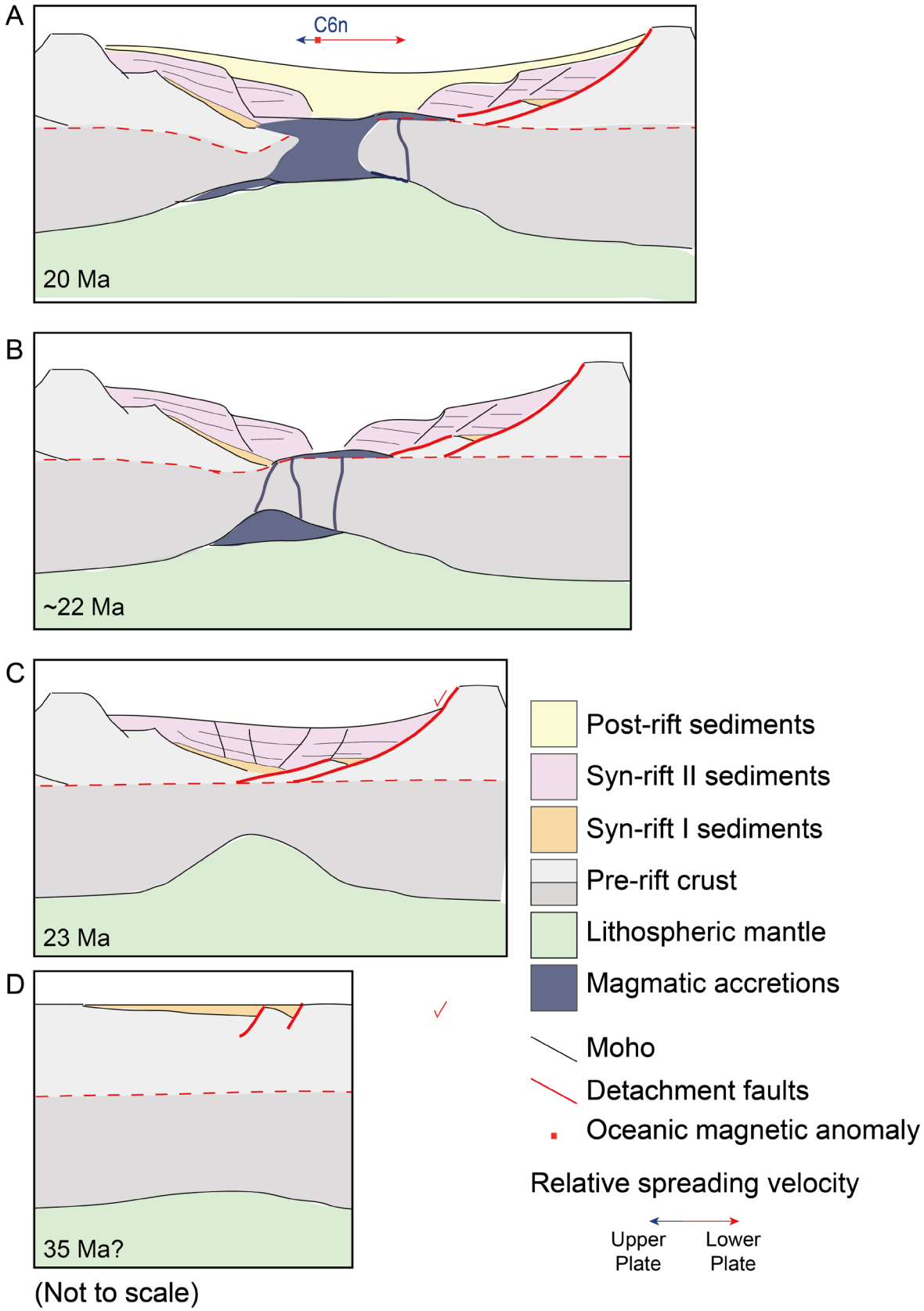

Figure 3- 17. Conceptual model of breakup in the southwestern SCS. The lower crust as ductile layer during the latest rifting to decouple the upper crust and the mantle, even the lithospheric mantle breakup prior to the continental crust.

3.6.2 Implication for the margin configuration just before breakup

This study, based on seismic profiles, allows us to highlight some aspects of the regional crustal architecture of the southwestern South China Sea also on a map view. When putting together the Spratly Islands (Nansha Islands) and Penxi Bank basing on the magnetic anomaly (Briais et al., 1993; Barckhausen et al., 2014), we obtain rhomboid basinal shape near the COT, which compose a chain of "en echelon" basins stretching in an N-S direction (Figure 3- 19). The lithosphere thinning factor inverted from the free-air gravity display the distribtution of the E-W orientation in the northern margin (Figure 3- 18). Their geometry is controlled by E-W hyper-stretched crust and N-S abrupt strike-slip COT. These are compatible with a right-lateral motion along a series of pull-apart basins. We may actually go further and propose that the change went through a stage where deep narrow troughs developed "en echelon" within a strike-slip framework between the Vietnam Fault (Maraquis et al., 1997; Roques et al., 1997; Fyhn et al., 2009) and Zhongnan Fault (Li et al., 2015). Shortly afterwards and as soon as the rhomb basins connected, the stress was released and the boundary conditions allowed a rapid propagation into the continental margin toward the SW (Savva et al., 2013; Ding et al., 2016). This is also seen in the nucleation of breakup in Red Sea (Augustin et al., 2014; Ligi et al., 2018).

Indeed, the late seafloor spreading in NW-SE direction remains around 30° angle with these pull-apart basins. It has been accepted that seafloor spreading changed progressively into NW-SE direction based on the magmatic and bathymetry analysis (Briais et al., 1993; Lee and Lawver, 1995; Sibuet et al., 2016). Therefore, not only the seafloor recorded the shift; the adjacent rifted basins also display changes in the direction of opening and the amount of sediments deposited. We suggest that the final rifting in the southwestern SCS during the coeval of seafloor spreading in the East SCS was compatible in orientation with that of the first phase of seafloor spreading in N-S direction from 32 to 23 Ma (Briais et al., 1993; Barckhausen et al., 2014), and this « intermediate « event around the ridge jump corresponds to the N165 "yellow" set of oceanic crust proposed by Sibuet et al. (2016). The gross distribution of the sedimentary accumulation indicates the stretching was in a N-S direction (Savva et al., 2013; Lei and Ren, 2016), and involved the orientation of normal fault developed in the NW-SE direction, for instance, the mapping of structures of the Phu Khanh Basin shows such change after the Middle Miocene (Savva et al., 2013). Numerical simulation suggests that oceanic propagation was stalled at the boundary between the eastern and SW basins because of compression in the EW

direction. This far-field stress direction necessarily had to change to shift propagation toward the southwest (Le Pourhiet et al., 2018).

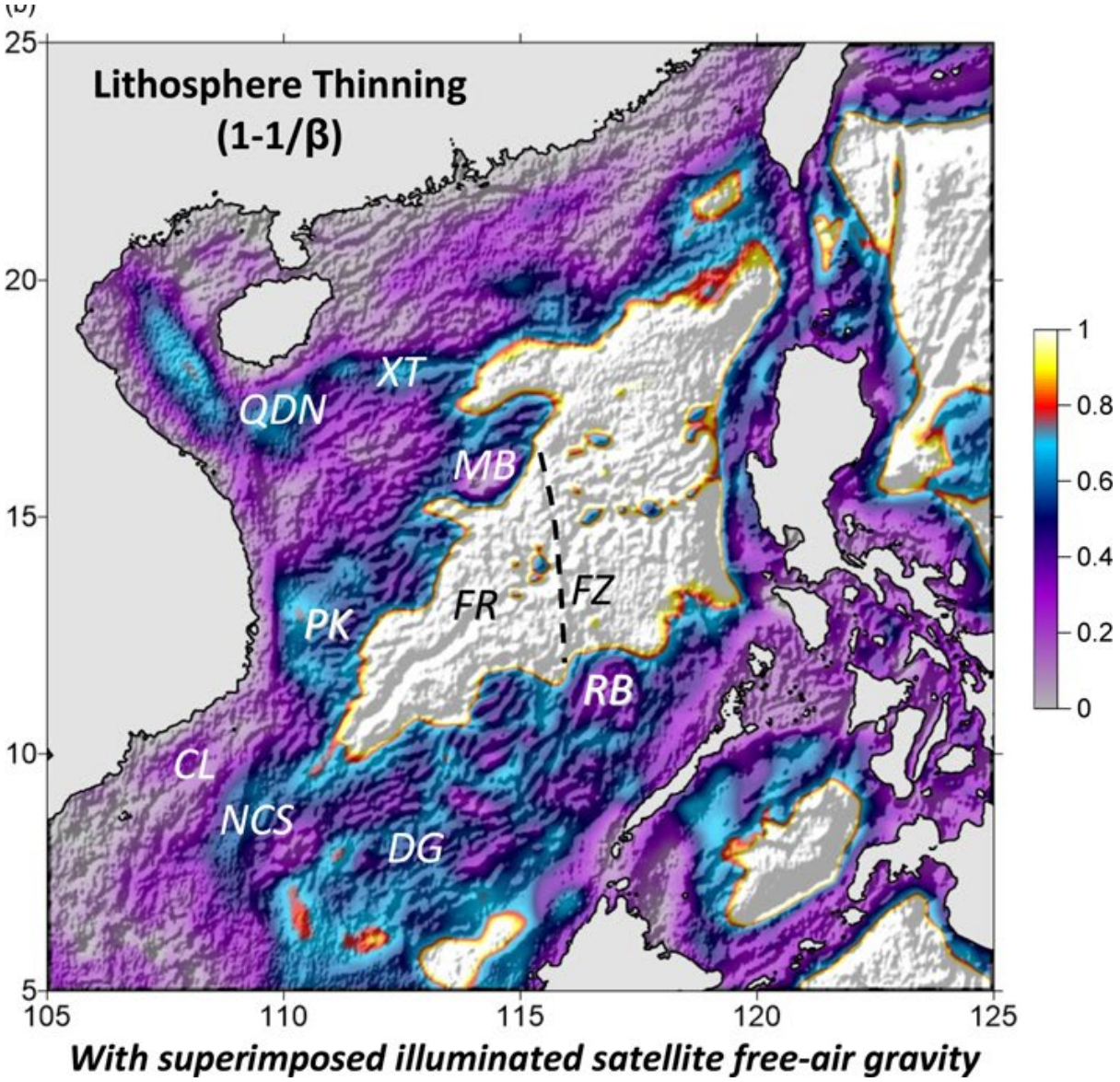

Figure 3- 18. Lithosphere thinning in the South China Sea (Gozzard et al., 2018). The hyperextension basins located at where the thinning value smaller than 0.6 (blue on the map), illustrating basins in an E-W orientation in the northern margin. The second stage of rifting is mostly marked by the blue areas (SW central sub basin and near-COT region in the NE sub-basin. However, this does not directly represent a discrimination between the 2 stages of rifting; it only marks the sum of the extension.

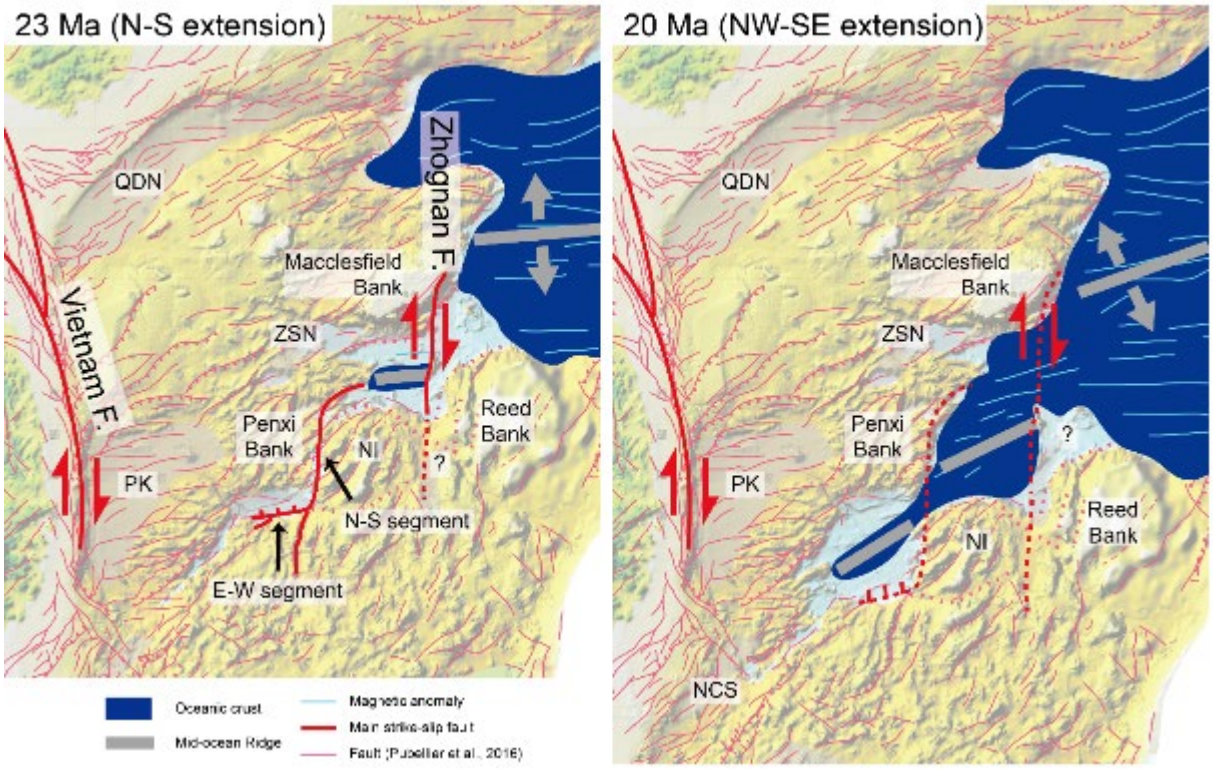

Figure 3- 19. Kinematic evolution in the SCS showing that the first phase of seafloor spreading induced a series of pull-apart basins in the southwestern SCS in a N-S extension and that the second phase changed the direction of seafloor spreading and initiate breakup and subsequent NW-SE spreading.

3.7 Synthetic rifting evolution in the South China Sea

The detachment fault plays an important role to thinning the SCS continental crust, illustrating the general configuration in East and Southwest SCS (Figure 3- 20 and Figure 3- 21). The similar crustal configurations could apply to the entire rifted margins such as the Phu Khank Basin and Nam Con Son Basin (modified from (Savva et al., 2013) and (Clerc et al., 2018) in the Appendix A.1). Proximal margin rifted by high-angle normal faults in the result of half-graben (Figure 3- 20). The syn-rift II is characterized by coherent thickness and is slightly thicker toward depocenter and the presence of later new normal faults having small offsets and dipping toward the depocenter (Figure 3- 20 and Figure 3- 21). Therefore, the syn-rift II units have less thickness variation within the rifted basins. This could suggest a possible thinning period marked by more lateral accommodation space instead of vertical subsidence. During this period, the crust thinning with the basin subsidence as well as the exhumation of mantle and lower crust to the seafloor.

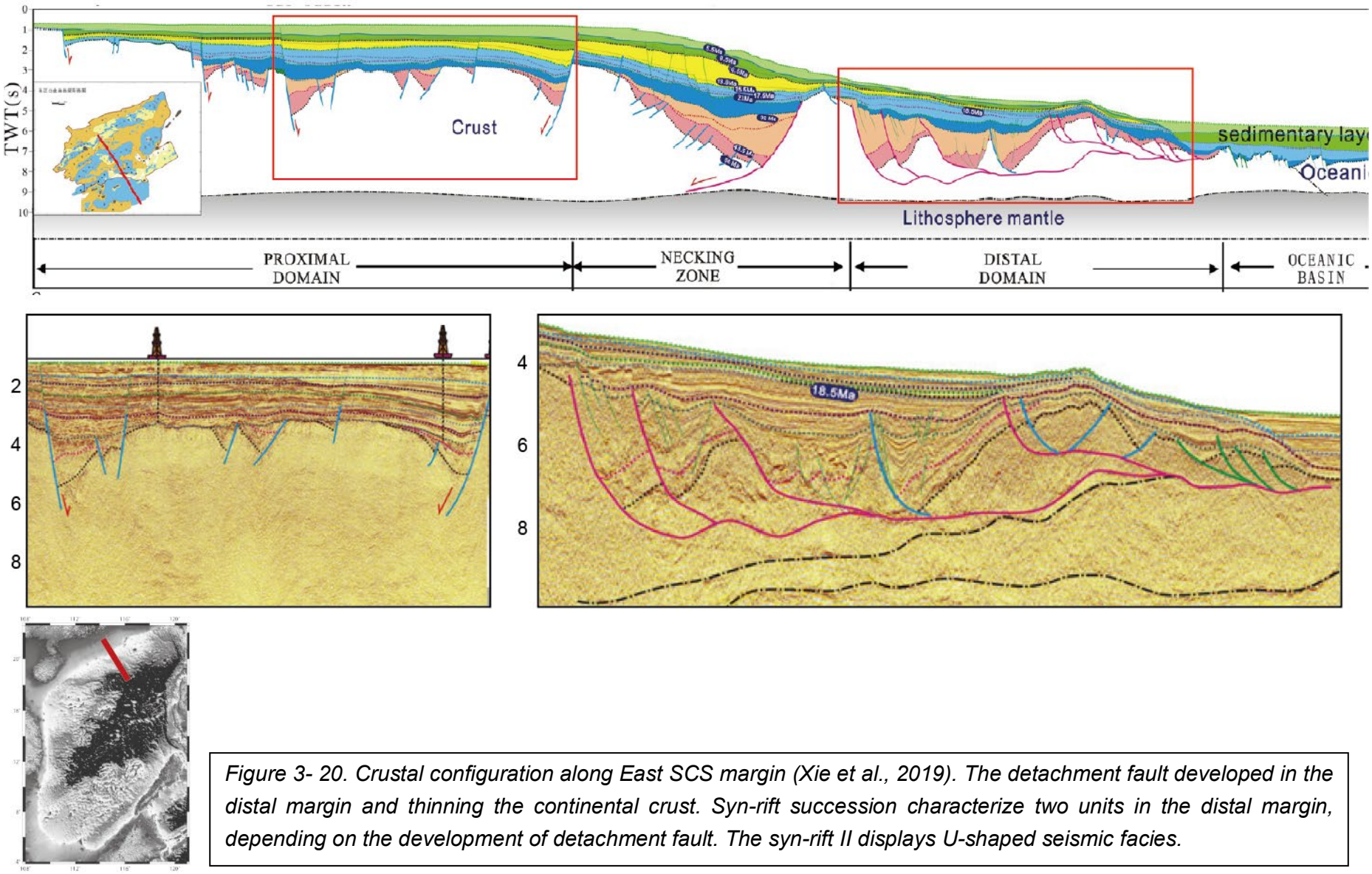

Figure 3- 20. Crustal configuration along East SCS margin (Xie et al., 2019). The detachment fault developed in the distal margin and thinning the continental crust. Syn-rift succession characterize two units in the distal margin, depending on the development of detachment fault. The syn-rift II displays U-shaped seismic facies.

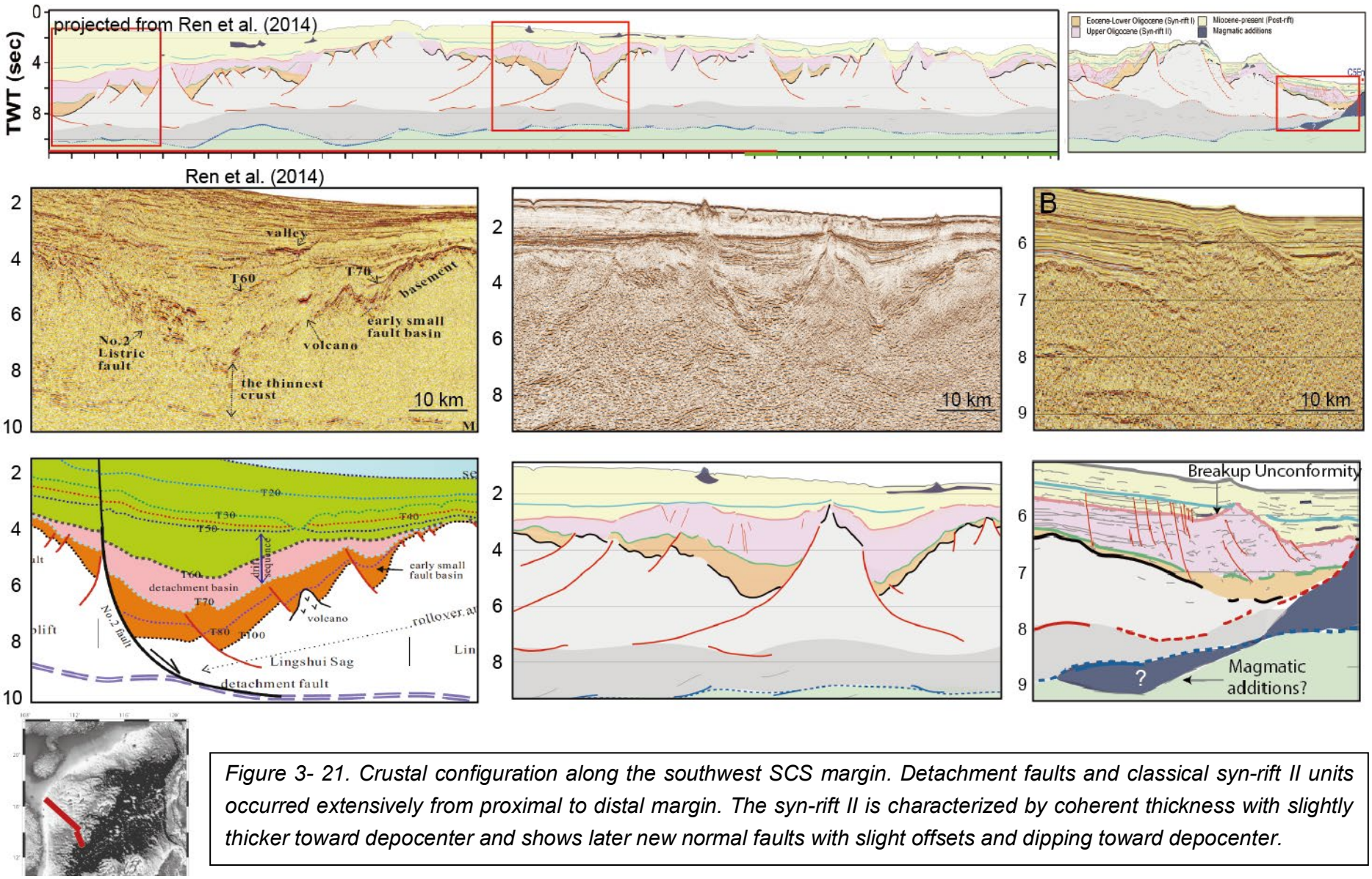

Figure 3- 21. Crustal configuration along the southwest SCS margin. Detachment faults and classical syn-rift II units occurred extensively from proximal to distal margin. The syn-rift II is characterized by coherent thickness with slightly thicker toward depocenter and shows later new normal faults with slight offsets and dipping toward depocenter.

In view of the complexity of the different extensional features on the entire margin in the South China Sea, we try to unravel the main criteria in a simplistic manner; remembering that this pattern of evolution migrates with time to the SW. The syn-rift I (R1) was deposited in a basement offset by the high-angle normal faults (orange on Figure 3- 22). Syn-rift II followed the top of the R1, Intra-rift unconformity (IRU), and characterize U-shaped seismic facies in the lower R2 (pink on Figure 3- 22) or the edge of the basin. The horizon of upper R2 flattening and become homogenous thickness in several basins (PK, NCS, and the COT of Nanshan Islands), offset by the slightly normal faults. This stage illustrates the accommodation space which develops preferably horizontally rather than vertically.

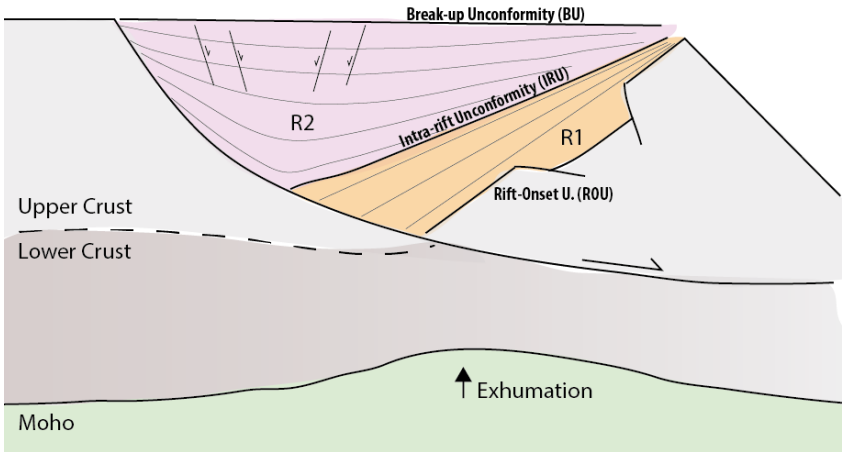

Figure 3- 22. Simplified rifting evolution in the South China Sea. Note that the block rotation occurs with a large amplitude during the first stage. Reactivation occurs during the subsequent stage and, if moderate, creates only a U-shape basin

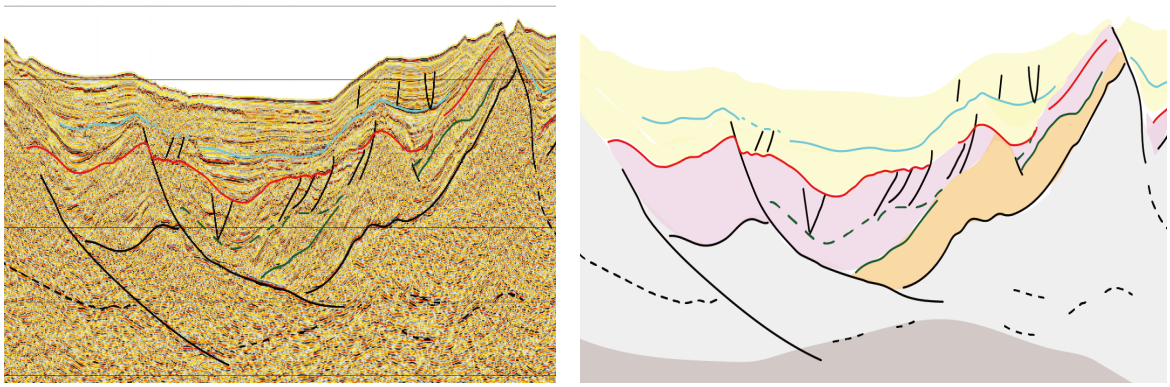

Figure 3- 23. Rifting stages, R1 and R2, may be more complex on concrete example. Extract from our line GMGS (Figure 3- 14).

The basin evolution would follow the crustal thinning and stretching history. The proximal margin scarcely develop detachment faults (except the LANF described by Savva in the very

early Eocene stage) whereas the distal margin has significantly developed detachment faults which efficiently thinned the crust up to breakup. Meanwhile, the southwestern margin developed extensive basins with detachment faults resulting ultimately in a thinner crust (Figure 3- 24).

The timing of breakup and rifting has been interpreted as a diachronous event from east to southwest (Franke et al., 2014). Although the onset of rifting has been long debated due to lack of numerous drilling, the age of the detachment fault, as well as the age of the breakup show a diachronous evolution on Figure 3- 25. The evolution of rifted basins stopped at ca. 16 Ma around the cessation of the spreading. It looks like most of the classical stages of evolution of a margin offers specificities in the South China Sea. The evolutionary ages of most rifted basins surrounding the SCS have been compiled in Figure 3- 25 to illustrate the temporal and spatial discrepancy.

3.8. Conclusion

This study explores the crustal architecture and evolution of the southwestern South China Sea. The kilometer-length profile illustrates distributed rifted basins, which thinned thanks to low-angle detachment fault rooted into the top of ductile layer in the lower crust. The continental lithosphere stretching and thinning were dominated by ubiquitous large detachments in the E Vietnam/S Hainan-NW Borneo margins. Tectono-stratigraphy analysis in the vicinity of the COT suggests that hyper-extension is restricted to the E-W segments of the distal margin (mostly composed of crystalline basement), whereas the N-S segments are abrupt and covered by a thin blanket of sediments overlying on the basement. These COT boundaries delineate small en-echelon rifted basins whose distribution is indicative of right-lateral motion prior 23 Ma, during the first phase of seafloor spreading in the East SCS. Most of the extension developed in N-S direction prior to breakup, and then started to change progressively to the NW-SE during the second phase of spreading. The small rifted basins would thus underline the transitional period. The succession of events is strikingly able to correlate the far-field stress change induced from the adjacent subduction and closure of the PSCS in Palawan-Borneo.

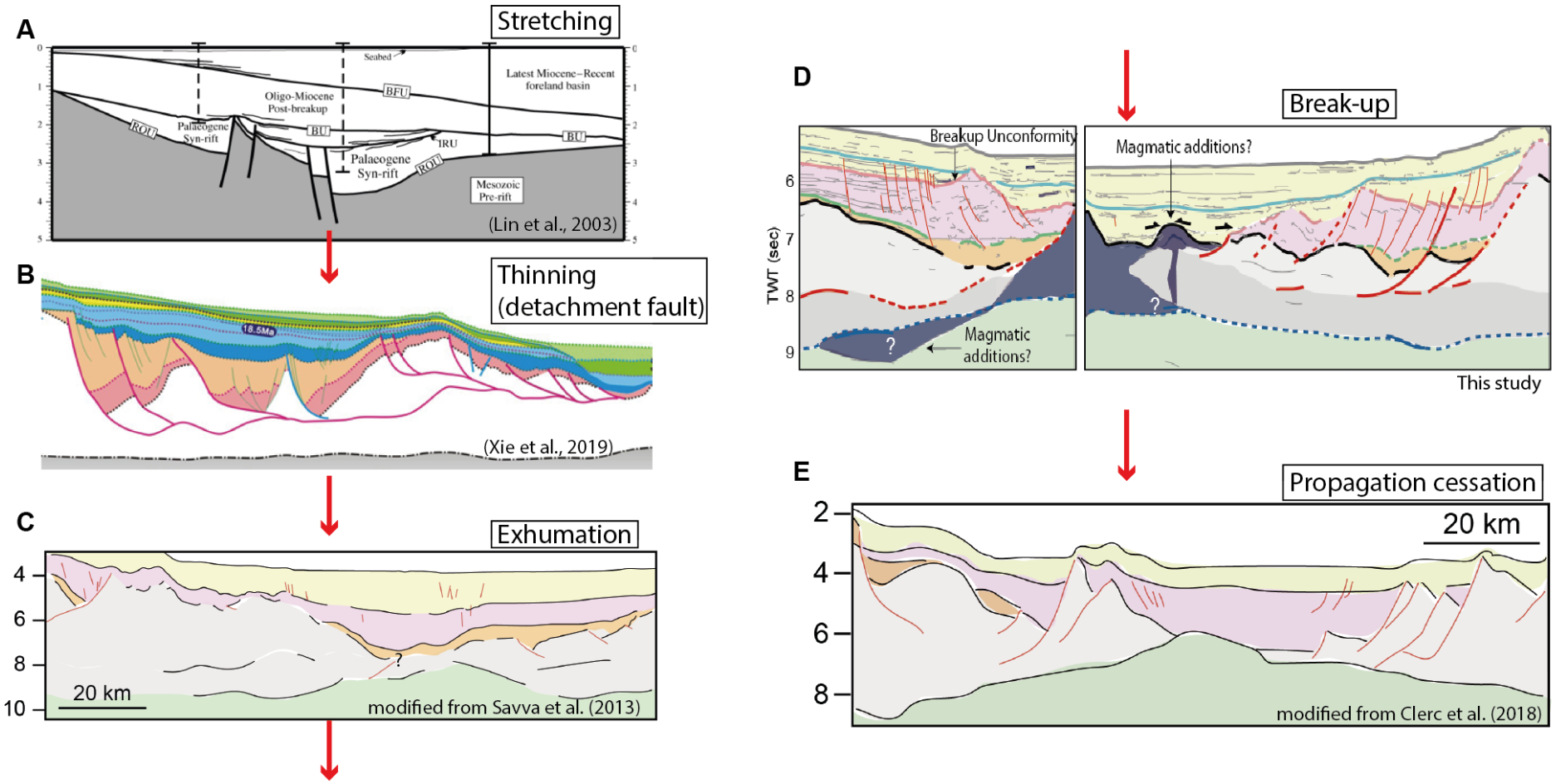

Figure 3- 24. Recapitulation of the rifting structure of the South China Sea. Selected seismic images illustrate the high-angle normal faulting (A, Lin et al., 2003) and subsequent development of detachment faults (B, Xie et al., 2019), dramatically thinning the continental crust into boundinage feature (C, modified from Savva et al, 2013). The exhumation (C and D) finally made the asymmetrical structures of breakup (D, this study) and thermal subsidence in post-rift unit, or without the formation of oceanic and with directly the effect of subsidence at the tip of propagation (E, modified from Clerc et al., 2018).

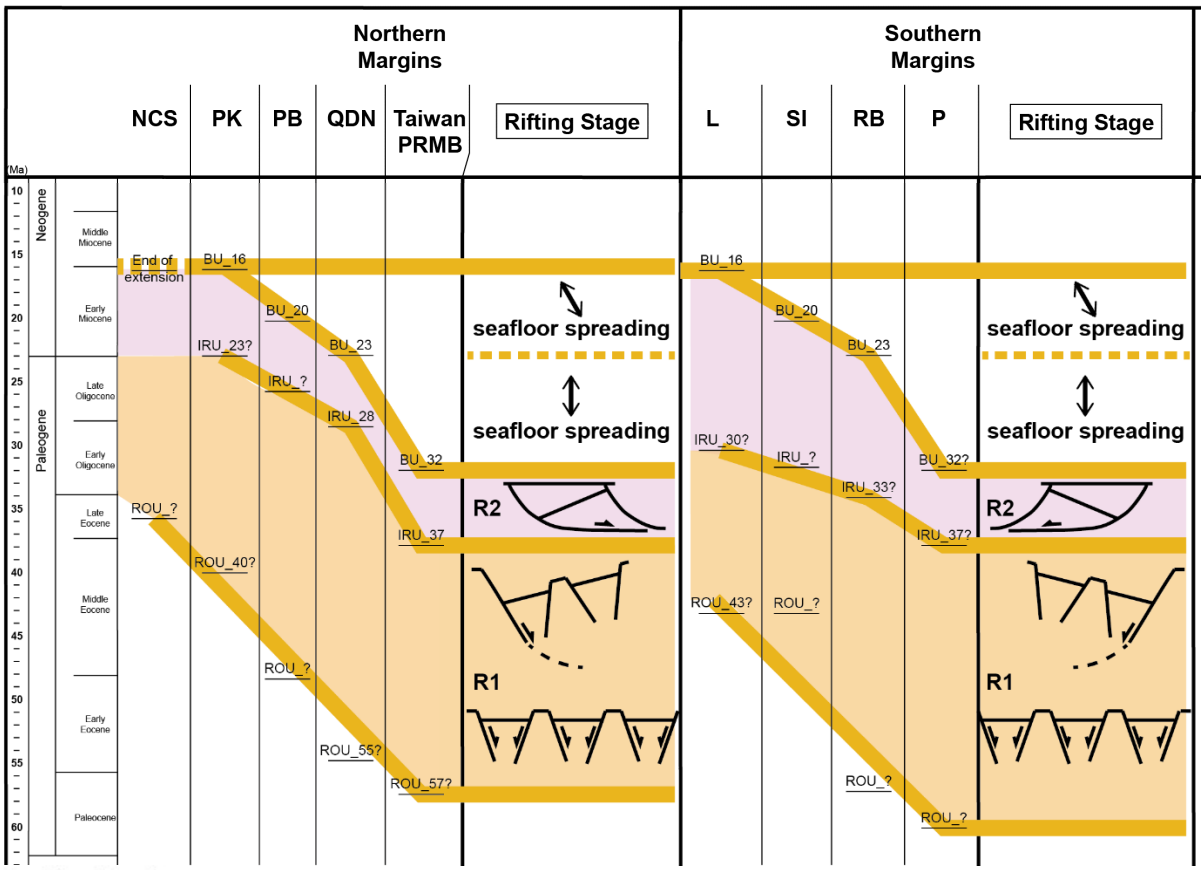

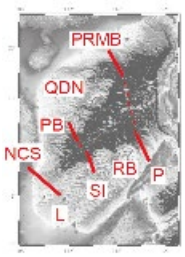

Figure 3- 25. Tectono-stratigraphy chart in diachronism along the SCS margins. The development of detachment faults and breakup result from the two stages of structural evolution in R1 and R2, and show the various timing along the margin.

CHAPTER 4. Collision, mélange and circular basins in north Borneo: a genetic link?

4.1 Introduction

In the southernmost of the South China Sea, Tertiary convergence resulted in a fold-and-thrust belt in the Borneo and Palawan area. This concomitant shortening process and the rifting in the SCS has been debated in terms of chronology and mechanical evolution. Several occurrences of mélange appear in this subduction-related wedge. The mélanges are classically characterized by the process of genesis: tectonic, sedimentary, and diapiric. Mélanges were deformed and also played an important role in the deformation of the overlying strata from syn-orogenic to post-orogenic stages.

The circular basins are one of the common features in Sabah (Figure 4- 1). This morphologic term has been used in under-compacted shale such as in Papua New Guinea, Makran and Venezuela (Granath and Argakoesoemah, 1989; Duerto and McClay, 2011; Oil Search, 2016; Ruh et al., 2018), or salt and shale tectonics domains (Morley and Guerin, 1996; McClay et al., 1998; Mourgues et al., 2009). Their morphologies show several isolated anticline or syncline topographic features (Rangin et al., 1990; Balaguru et al., 2003), and the strata have sag-like characteristic (Clennell, 1996). The similar feature can also appear in different places of Borneo, for instance, the Kudat Peninsula (Tongkul, 2003; Rahim et al., 2017) and Brunei (Morley et al., 2003; Cullen, 2010; Sapin et al., 2011; Sapin et al., 2012; van Hattum et al., 2013; Berthelon et al., 2018).

This chapter aims to propose a genetic link between the occurrence of different mélange types in northern Sabah (North Borneo), their processes of formation and the tectonic setting of their occurrence through a field, satellite and seismic study. We propose that these sedimentary mélanges formed by the downslope emplacement of heterogeneous unconsolidated material and become source for the extrusion of diapirs. Episodic diapiric processes during the post-collision period are also responsible for the deformation of the overlying strata into “circular basins” and broad rounded anticlines, which rest on both the oceanic crustal sequence of the

upper plate, and the former accretionary wedge of the lower plate (Figure 4- 2) (Clennell, 1991; Oil Search, 2016; Clark, 2017).

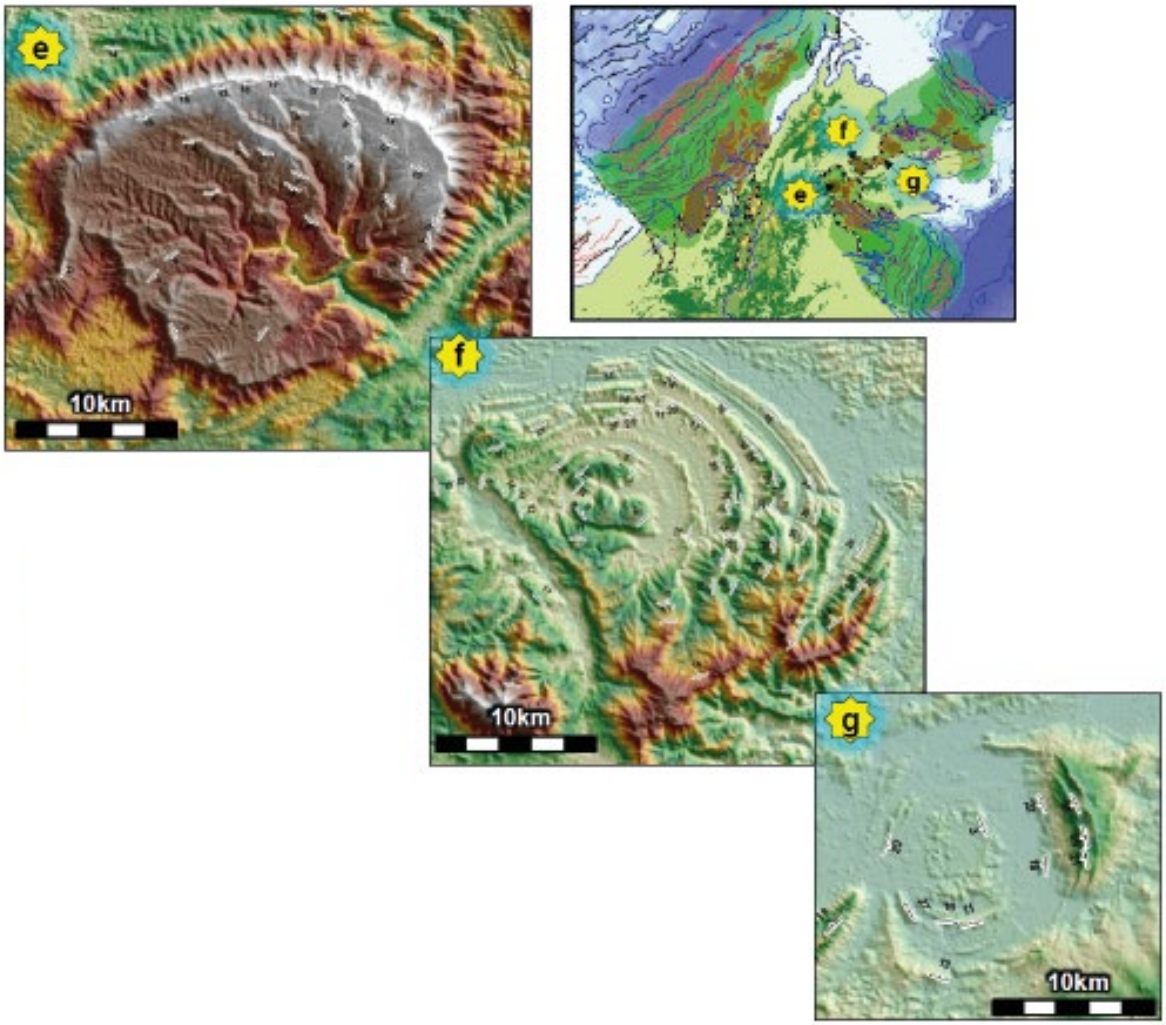

Figure 4- 1. Circular basins distribute in East Sabah (Clark, 2017). The bedding measurements correspond to the circular features on the topography.

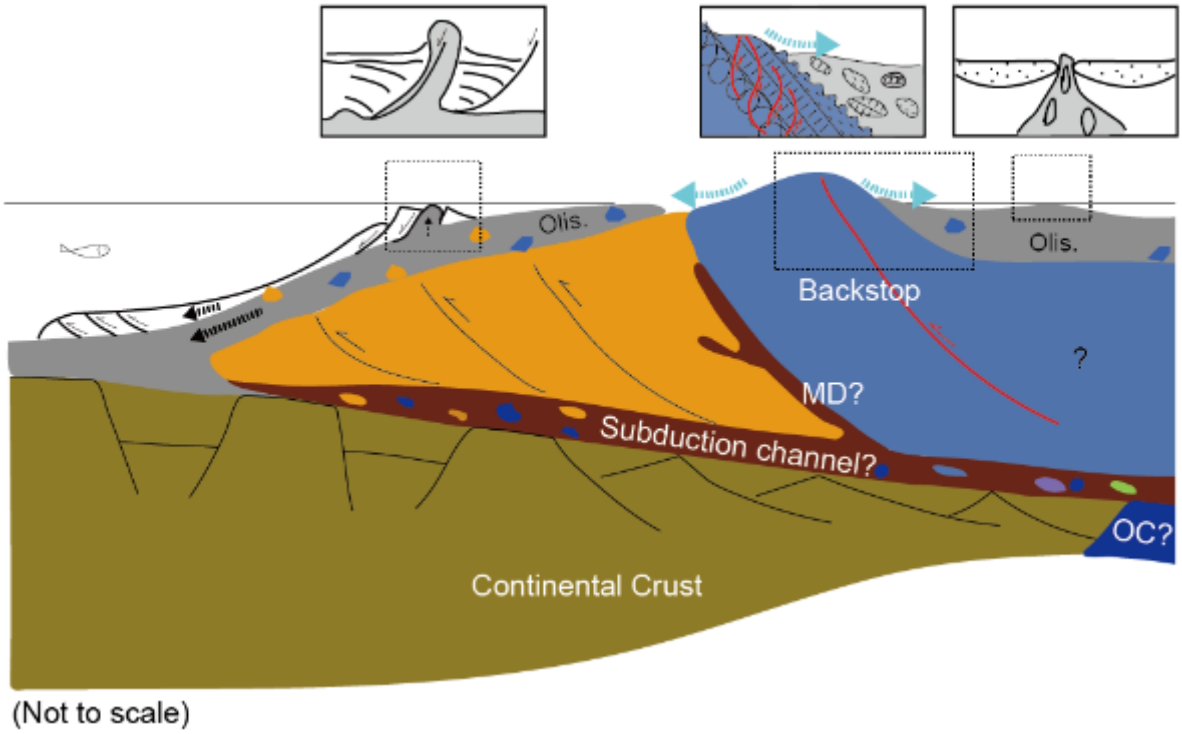

Figure 4- 2. Schematic cartoon of some key hypotheses for the formation of mélanges and subsequent diapirs related to active margins (modified from Festa et al. (2012). Olis.: olistostrome, MD: mélange dike.

4.2 Geological Background

Northern Borneo is adjacent to three marginal seas; the South China Sea, Sulu Sea and Celebes Sea (Figure 4- 3). Regarding plate configuration, the Sabah province of Malaysia is located above a former subduction and collision zone in which the southern margin of the South China Sea is composed of stretched continental crust, under-thrust beneath a large accretionary belt (Figure 4- 5). Below the base of the accretionary wedge is the Oligocene to Early Miocene Nido Carbonate, and seismic lines show that it is also offset by thrusts within the fold-and-thrust belt. The seismic images show the imbrication of the wedge and covered by the well-stratified seismic facies representing the post-orogeny succession, although the frontal wedge still shows deformation which also uplift this basically post-orogeny unit.

Scattered Cretaceous ophiolites (Omang and Barber, 1996; Balaguru et al., 2003; Cullen, 2010; Jasin and Tongkul, 2013; Kessler and Jong, 2016) are also believed to be a part of the upper plate that were emplaced during the obduction of the Proto-South China Sea in Northern Borneo (Figure 4- 5). The correlation of the ophiolite belt with those of Palawan is solid and presumably based on the continuity of the gravity anomaly (Figure 4- 3b).

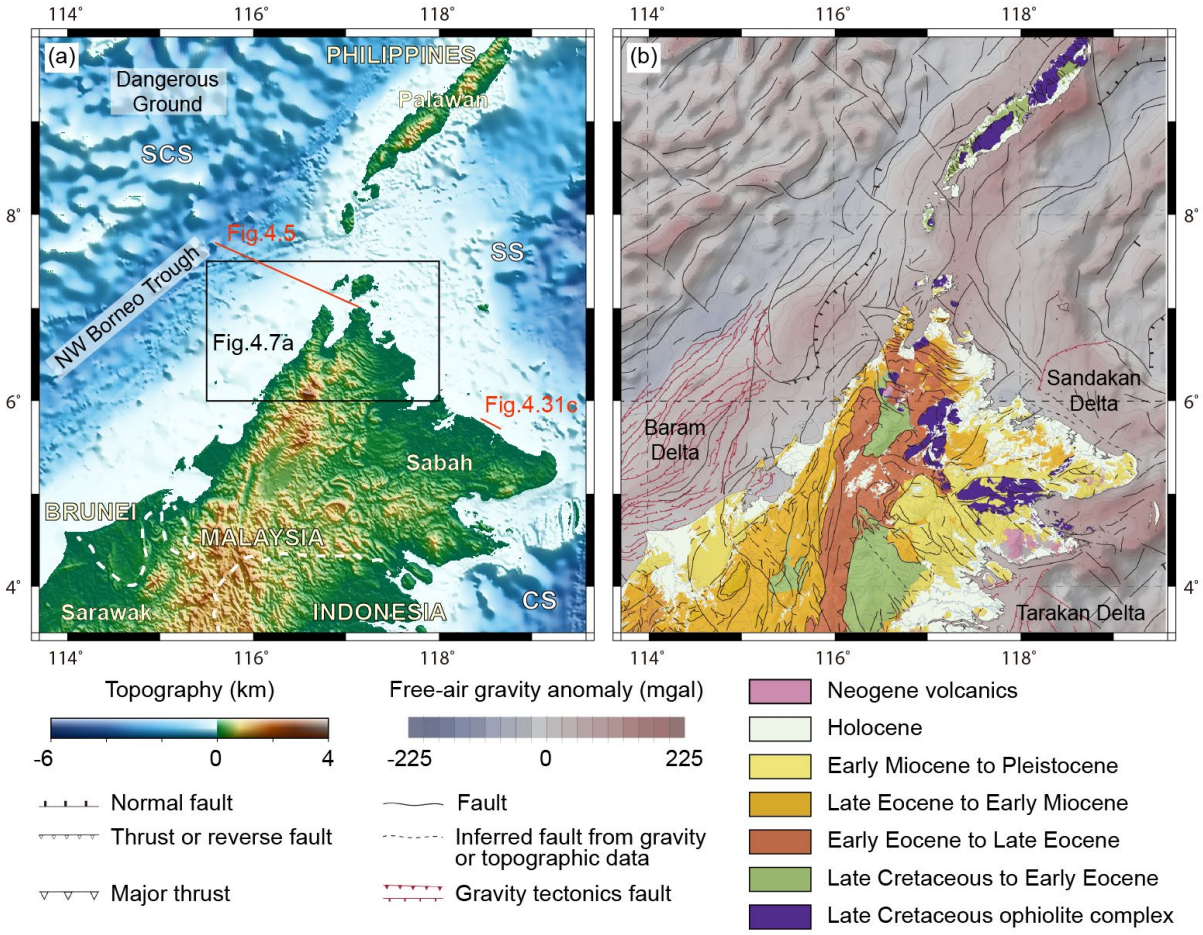

Figure 4- 3. (a) Topography in northern Borneo and southern Palawan. The topography is from GMRT (Global Multi-Resolution Topography). (b) Geological map of northern Borneo and distribution of ophiolite (purple) and volcanic intrusion (pink) modified from Pubellier et al. (2016). SCS: South China Sea, SS: Sulu Sea, CS: Celebes Sea. (For interpretation of the references to colour in this figure legend, the reader is referred to the web version of this article.)

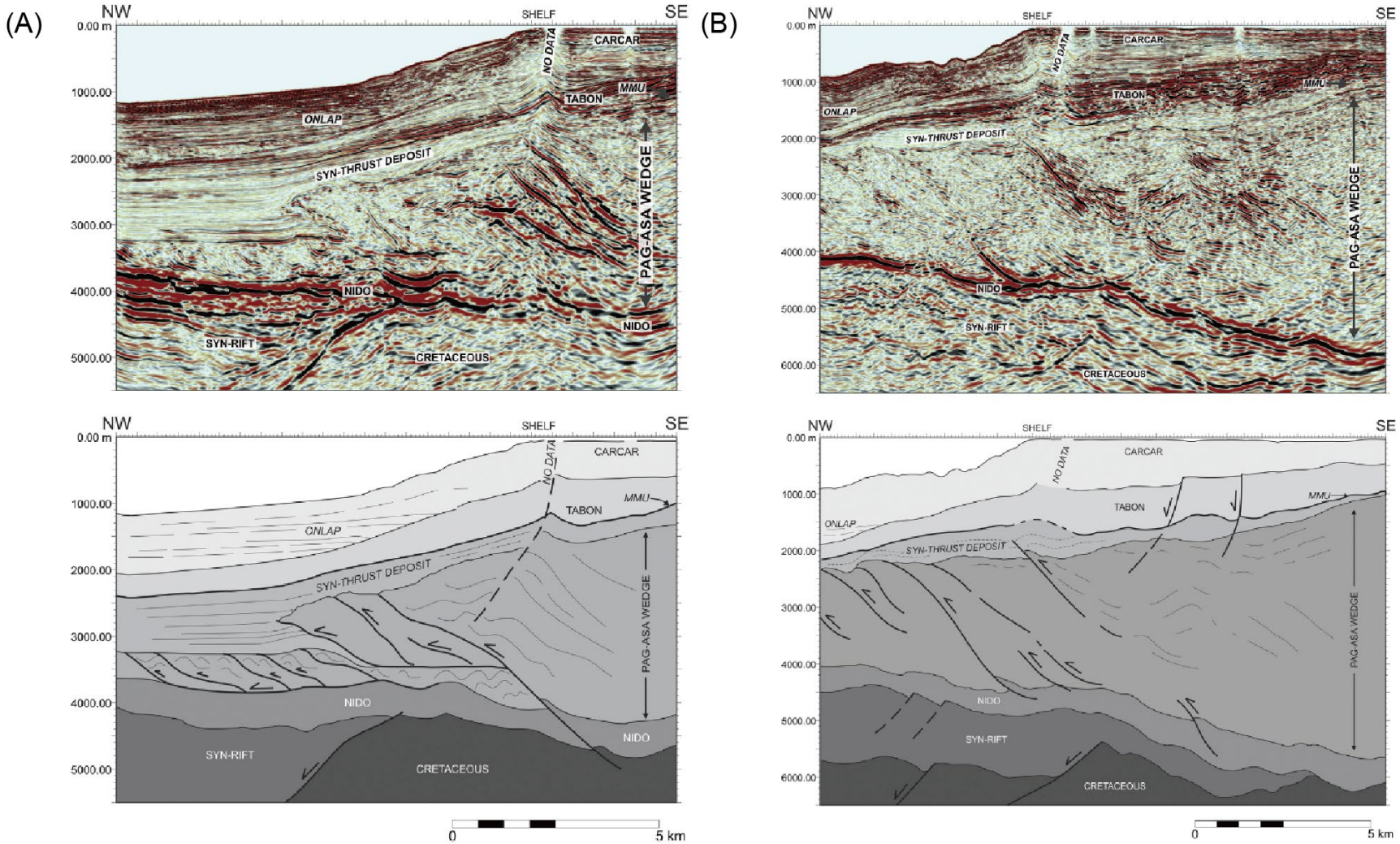

Figure 4- 4. Stacking of Nido at the base of wedge in the offshore Palawan (Aurelio et al., 2014). Imbricated wedge and syn-thrust deposits interfingerred at the frontal wedge overlying the Nido carbonate.

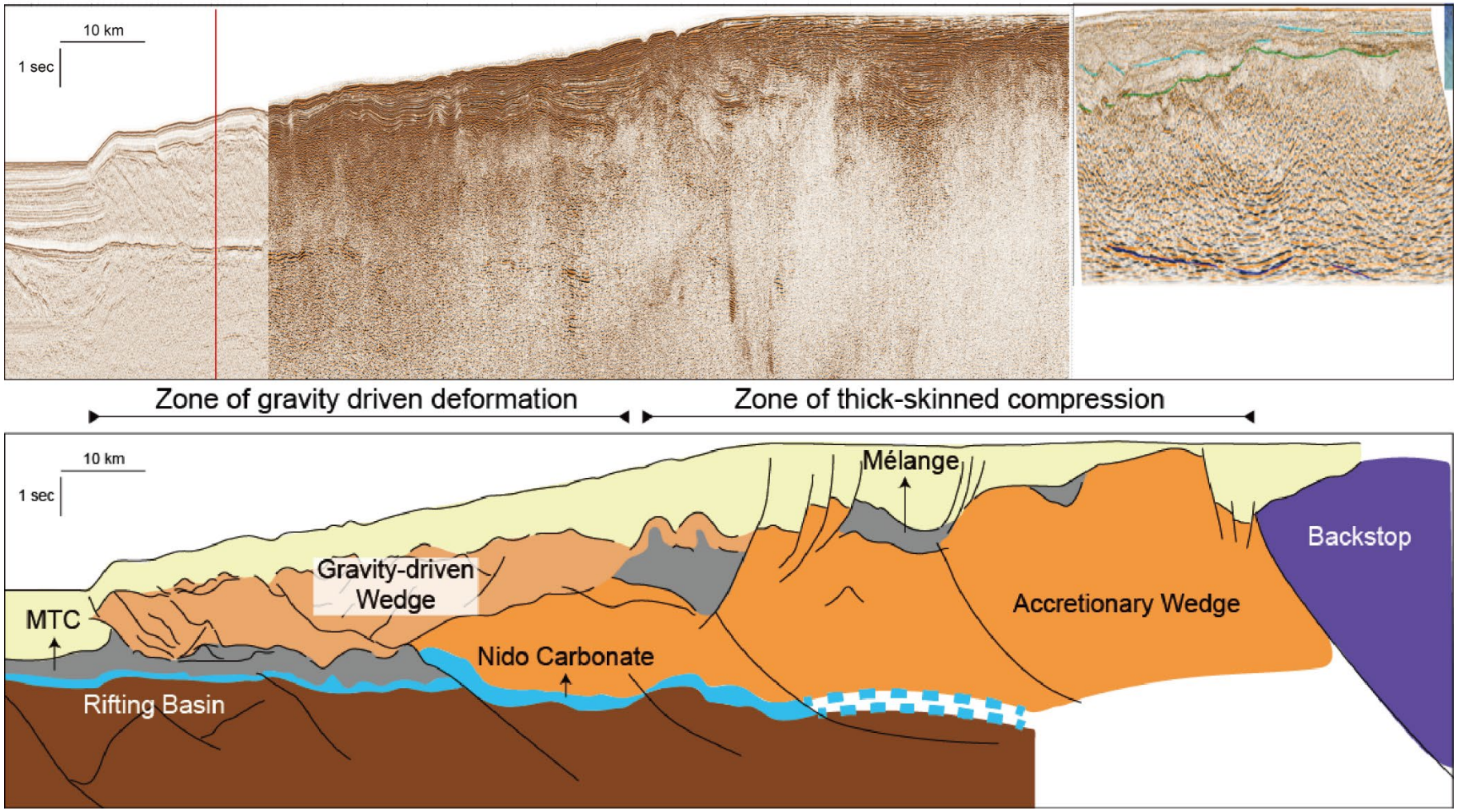

Figure 4- 5. Integrated interpretation of the accretionary and the gravity-driven wedge. The cross section is compiled from various MCS lines BGR and PETRONAS (Leong, 1999; Franke et al., 2008). Location shown in Figure 4- 3a. The dark blue delineates the extent of the Nido Carbonate and the accretionary wedge represent between dark blue and green contained several strong reflectors to infer the imbrication structures in the wedge.

The subduction forming the accretionary wedge began in the Eocene (Omang and Barber, 1996), and it was not a simple continuous deformation process. The Rajang and Crocker Belt represent the different metamorphosed and depositional environments through subduction history which began after the Sarawak Orogeny and was followed in the Miocene by the Sabah Orogeny as seen in the seismic profiles of offshore Sabah and Sarawak (Franke et al., 2008) (Cullen, 2010; Hutchison, 2010). The Sabah Orogeny has been well documented through field observation, multichannel seismic (MCS) profiles (Figure 4- 6) and via GPS data (Hesse et al., 2009; Sapin et al., 2013) but remains conflicting. Moreover, it may either represent the collision process, the wedge formation, or it may be due to gravity tectonics. Therefore, the termination of the Sabah Orogeny varied from the Middle Miocene, marked by Deep Regional Unconformity (DRU) or Middle Miocene Unconformity (MMU) (Figure 4- 6) (Hamilton, 1979; Hutchison et al., 2000; Hutchison, 2005; Hall et al., 2008) to the recent period (Sapin et al., 2013; Lunt and Madon, 2017).

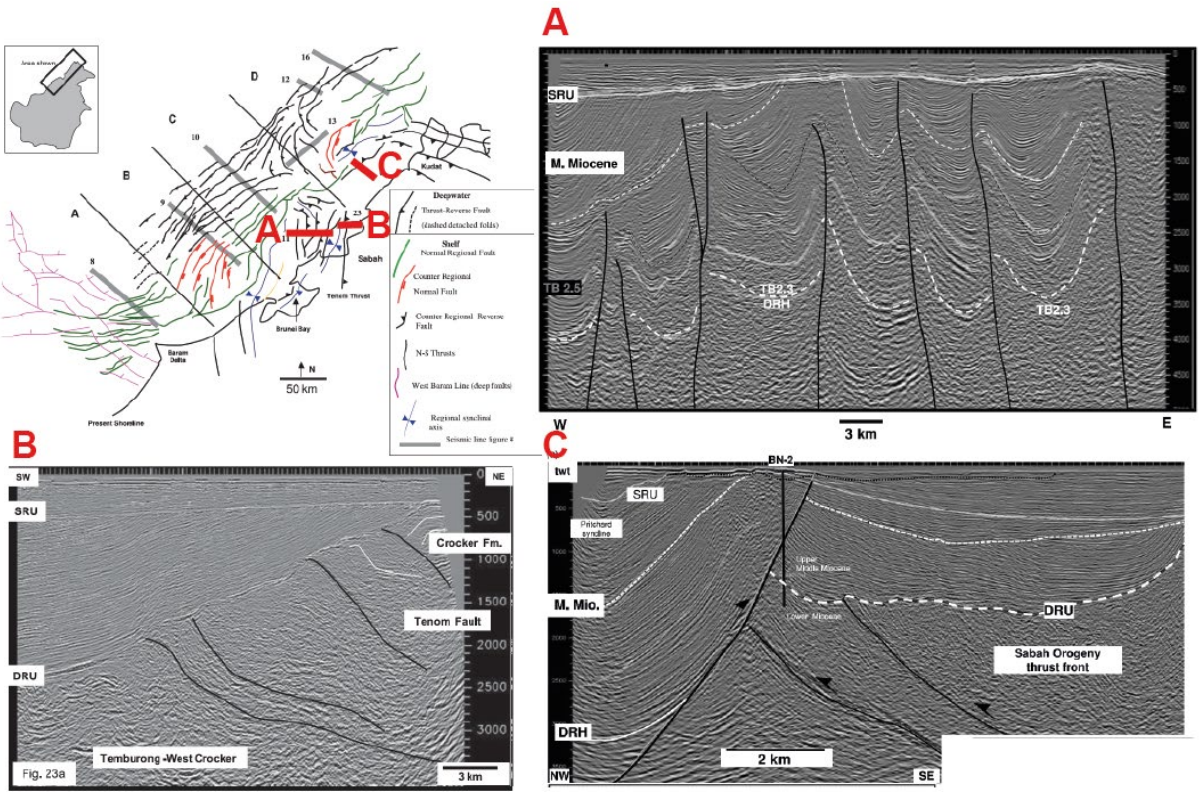

Figure 4- 6. DRU in previous studies in the offshore Sabah. The seismic images show that the post-orogeny succession overlies the DRU (Cullen, 2010).

Nevertheless, the presence of discontinuous rounded structures marks the morphological features of North Sabah (Figure 4- 7b). Although some of them are poorly steeping anticlines, and most are anticlines and synclines referred to as “circular basins”. Balaguru et al. (2003) led a comprehensive investigation and interpreted the basins as a result of left-lateral wrench faulting during the syn-orogenic period. In North Sabah, a similar mechanism of shortening between the Palawan and Borneo collision is attributed to the E-W topographic orientation (Figure 4- 8) (Tongkul, 2003; Lunt and Madon, 2017; Rahim et al., 2017). An alternative interpretation associated with collapse tectonics is also found in the literature (Clark, 2017). It is thought that these circular basins were initially created from the Middle Miocene to the Upper Miocene period where several mélanges were adjacent to circular basins in East Sabah, along with many diapirs appearing in western offshore Sabah. Some authors sporadically relate the influence of gravity tectonics related to the tremendous uplift of Mt. Kinabalu on the Neogene stratigraphy (Hall, 2013).

The Kudat Peninsula is located at the junction of the fold-and-thrust-belt, circular basins and ophiolite. Even though the detailed stratigraphy is debated, most authors tend to agree to the following general succession (Figure 4- 7c). Cretaceous ophiolite rests on the northern peninsula and Pitas, with structural contact with the Eocene to Oligocene Crocker Formation in the deep-sea depositional environment (Zakaria et al., 2013). The Wariu Mélange or similar shale material overlying, overlies atop with varied thickness (van Hattum et al., 2013) and the Kudat Formation overall is composed of coarser shallow-marine sediments, although, its biostratigraphy is in contention (Tongkul, 2003; van Hattum et al., 2013; Lunt and Madon, 2017; Rahim et al., 2017). The Middle and Upper Miocene of Bongaya Formation rests unconformably following the DRU in the shallow marine environment. According to the industrial wells in offshore Sabah, the stratigraphy of the onshore and offshore regions can be revised based on cross-cutting relationships of basement deformation, unconformities and diapir injection. Therefore, this presents an excellent opportunity to investigate the genetic link during the late orogeny in Sabah.

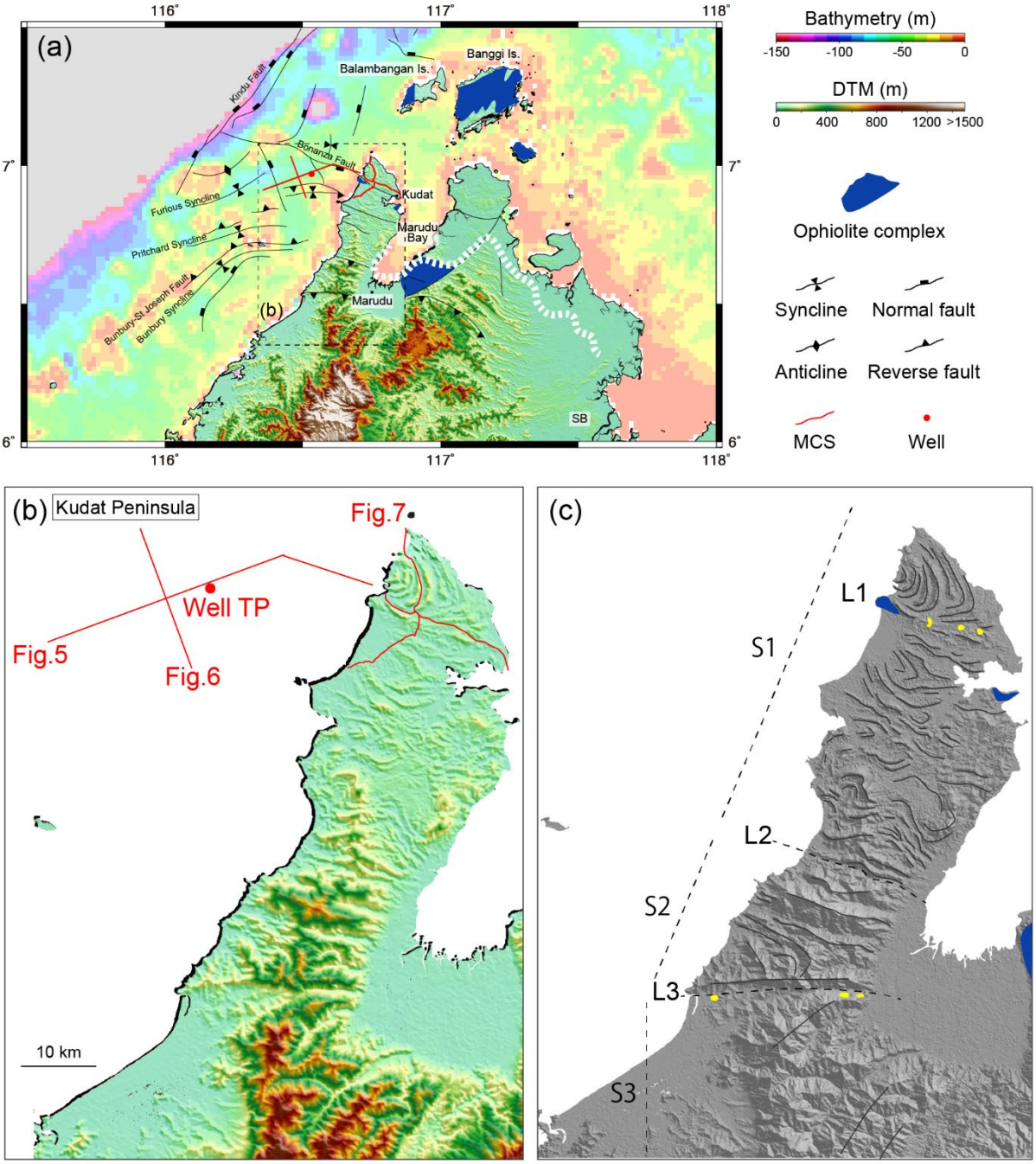

Figure 4- 7. (a) Bathymetry and DEM covering the Kudat Peninsula, the Marudu Bay and the NW of the Sandakan basin. Bathymetry data from GEBCO retrieved from GeoMapApp (http://www.geomapapp.org) and DEM from SRTM 1 arc-second. Stratigraphic boundaries and structures based on the DTM and Tongkul (2003). The white dash line delineates the Deep Regional Unconformity (DRU) and dark blue area represents the distribution of ophiolite in northern Borneo. SB: Sandakan Basin. (b) DEM of the northern Borneo covering the Kudat Peninsula, and location of MCS lines and wells. The interpretation map illustrates the lineaments and the textural distinction along the topography. (c) The stratigraphic chart of Kudat Peninsula, modified from Leong (1999), Tongkul (2003), van Hattum et al. (2013), and Rahim et al. (2017).

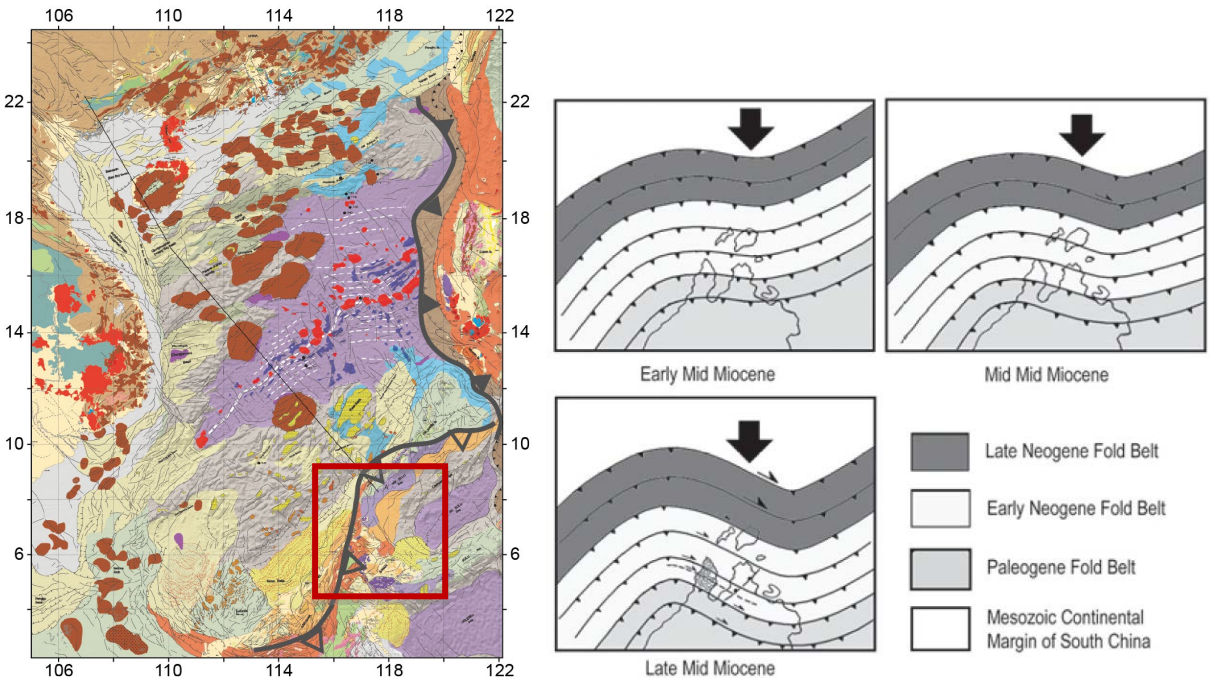

Figure 4- 8. N-S shortening (red rectangular) during the Sabah Orogeny (modified from Pubellier et al., 2016). The tectonic event explains the collision between the Palawan and Borneo collision is attributed to the E-W topographic orientation (Tongkul, 2003).

4.3 Geological observations

Digital Terrance Model (DTM) observations allowed us to reassess the good quality geological mapping proposed by Tongkul (2003), and we had performed ground-truthing. Small-wavelength folds and round-shaped folds in topography (S1 on Figure 4- 7b) are observed, and the circular basins region (anticline) is cross-cut by one onshore profile at northern peninsula and several offshore profiles (Figure 4- 7b). One well TP allows us to tie with the E-W offshore profile. The seismic profiles and well reports are kindly provided by Malaysian Petroleum Management (MPM), PETRONAS (Petroliam Nasional Berhad) for the purpose of study conducted at Universiti Teknologi PETRONAS (UTP) and its collaborators.

4.3.1 Integration of offshore and onshore multichannel seismic profiles

We recognize several units in the MCS profiles (Figure 4- 9, Figure 4- 10 and Figure 4- 11), basing on the sequences limited by unconformities or boundaries between two different seismic facies. At the base of these profiles, Unit 1 has a massive facies. A discrete strong-reflector apparently separates the overlying strata in the offshore profiles, but is unfortunately not as clearly marked on the onshore one. This boundary fluctuates slightly around 4 sec TWTT due to the occasional reflectors in the offshore, and ascends eastward and seems to be exposed in

western coast of the peninsula (Figure 4- 9). This depth can be correlated to that of the onshore profile and compared to the stratigraphic descriptions. The massive facies is frequently interpreted as subduction complex with severely distorted strata because of the lack of clear stratigraphic horizons within the sequence. This study favors the interpretation of the fluctuating reflectors as representing thrust faults within an imbricated wedge, which shown clearer in Figure 4- 5 and Figure 4- 6. It may represent the Crocker and Rajang Belt during the subduction to the following collision.

Unit 2 presents a chaotic facies and rests on a roughly continuous reflector (Figure 4- 9b and Figure 4- 10). This is different from the overlying strata (Unit 3 and 4), which appears as a well stratified seismic facies. The geometry of this layer shows an undulate thickness variation along the profiles, connects to mushroom-shaped diapirs which pierce the overlying strata (Figure 4- 10). We interpret this chaotic facies as a plastic material capable of being remobilized and extruded from an overpressured zone. The mobile material resulted in the deformation the whole overlying strata.

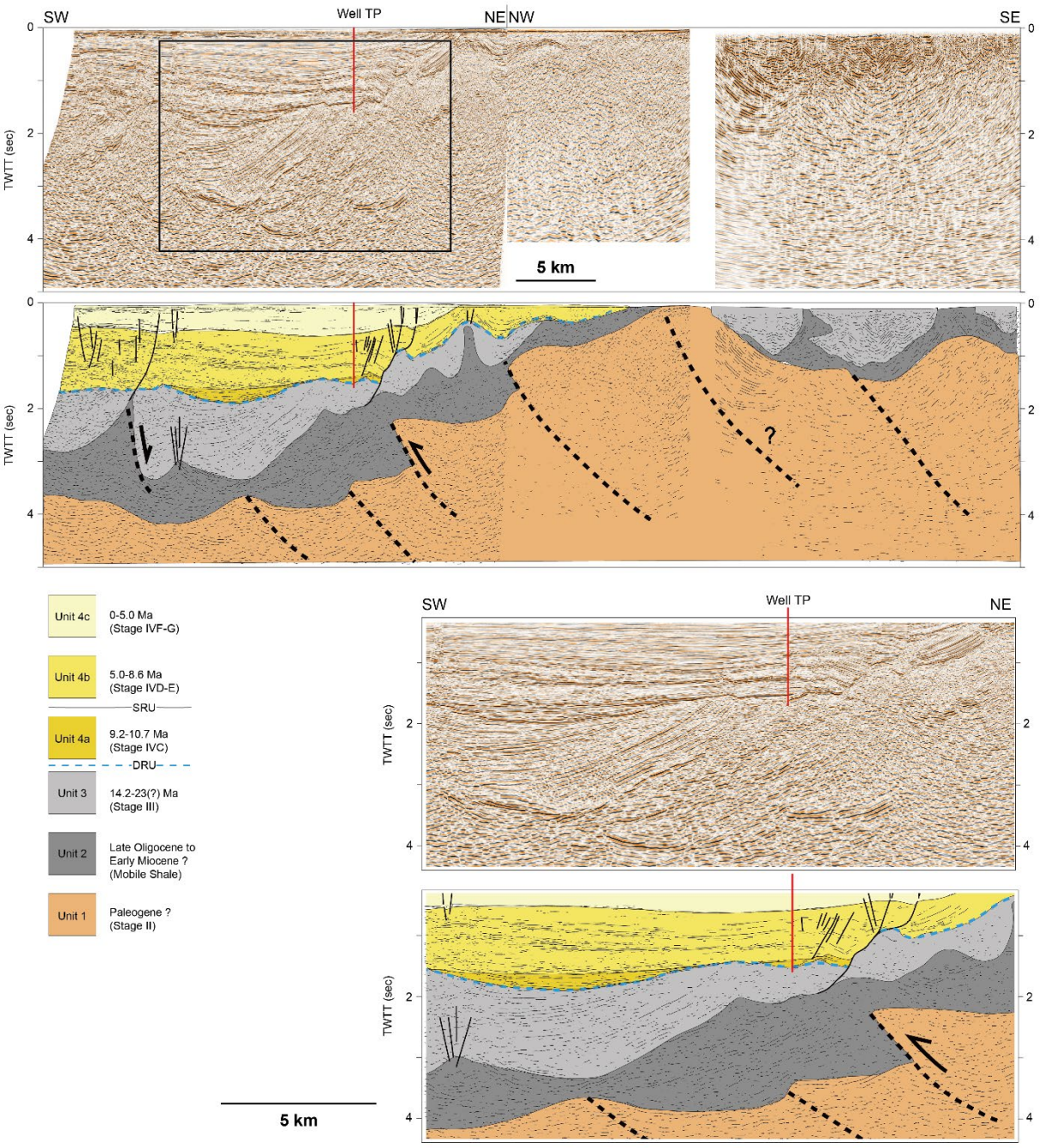

Figure 4- 9. Integrated offshore and onshore seismic profile across Kudat Peninsula. Note that the sag basins in Unit 3 are interpreted as representing the successor "circular basins" resting on unstable layer (mélange) and affected by gravity extensional tectonics and diapiric intrusions of the mélange. The blue dash line represents the DRU, which dated by the Well TP. For location see Figure 4- 7. Data kindly provided by Malaysian Petroleum Management (MPM), PETRONAS for the UTP study. (For interpretation of the references to colour in this figure legend, the reader is referred to the web version of this article.)

Unit 3 is characterized by well-stratified and oblique facies. An angular unconformity separates this units from the underlying Unit 4. The oblique facies of this unit is dragged close to the margins of the diapiric structure both onshore (Figure 4- 11) and offshore (Figure 4- 9 and Figure 4- 10), which explaining the onshore anticline in the northern Kudat seems affected by the normal fault (Figure 4- 11). This structure has been interpreted as a "break-through normal faulting" in Venezuela due to the high sedimentary load (Duerto and McClay, 2011). The top of Unit 3 is dated 14.2 Ma as the DRU (blue dash line in Figure 4- 9 and Figure 4- 10) from Well TP (Noon, 2011), and it represents the Stage III of Sabah stratigraphy in Lower Miocene to Middle Miocene. This unconformity, DRU, marks the end of orogeny in the Borneo according to Cullen (2010). This unit is interpreted as the top of the accretionary wedge during the last stage of subduction story.

Unit 4 has characteristics of well-stratified and horizontal to sub-horizontal facies. The bottom of the whole Unit 4 is 10.7 Ma so that a 3.5 m.y. hiatus exists for the DRU (Noon, 2011). Two unconformities within this unit allows us to separate it into three different sub-units (Unit 4a to Unit 4c). A 0.5 m.y. hiatus between Unit 4a and 4b, and a boundary, which is estimated at around 5 Ma according to the deposition rate, seals a former roll-over (adjacent to Well TP in Figure 4- 9b) to distinguish the Unit 4b and Unit 4c. The Unit 4a, 4b and 4c are equivalent as Stage IVC, IVD-E, and IVF-G respectively in the stratigraphic chart of Sabah(Leong, 1999). This mobile body was emplaced after the deposition of Unit 4 as shown by the cross-cut and tilted strata in its flanks, and continues to 5 Ma. The overlying strata tend to either sag forming many mini-basins (circular basins), or create shale-cored anticlines in the offshore.

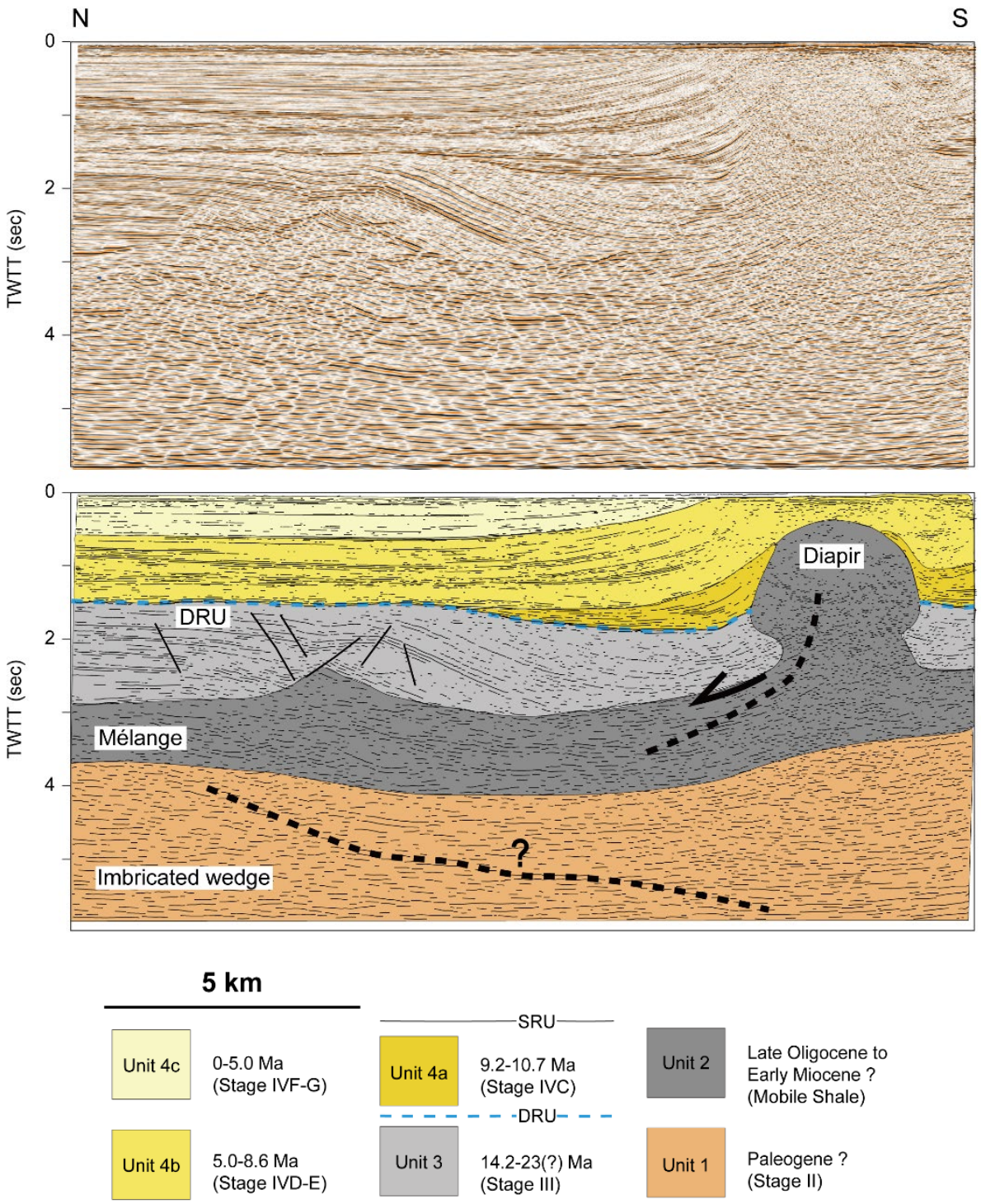

Figure 4- 10. The N-S seismic profiles in offshore Kudat, showing the diapiric mélange remobilized after DRU. For location see Figure 4- 7.

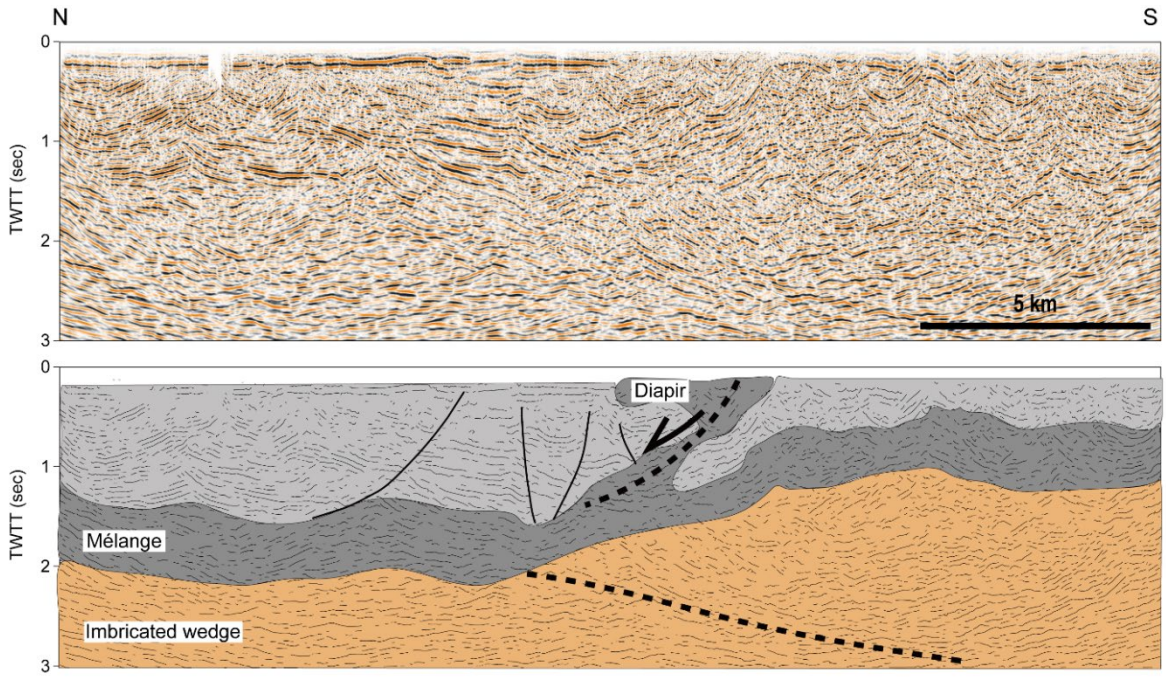

Figure 4- 11. The N-S seismic profiles onshore Kudat Peninsula, showing the anticline feature located at the northern peninsula deformed along the diapiric mélange. The legend follows the Fig. 4.5, and for location see Figure 4- 7.

The distribution of the diapirism can be seen in a map-view from 3D seismic block (Figure 4-12). Dispirism (mélange, Unit 2) represent in the east and south where adjacent to the Kudat Peninsula, surrounding the overlying strata (Unit 3 and 4) showing strata in an E-W orientation with the circular features in map-view.

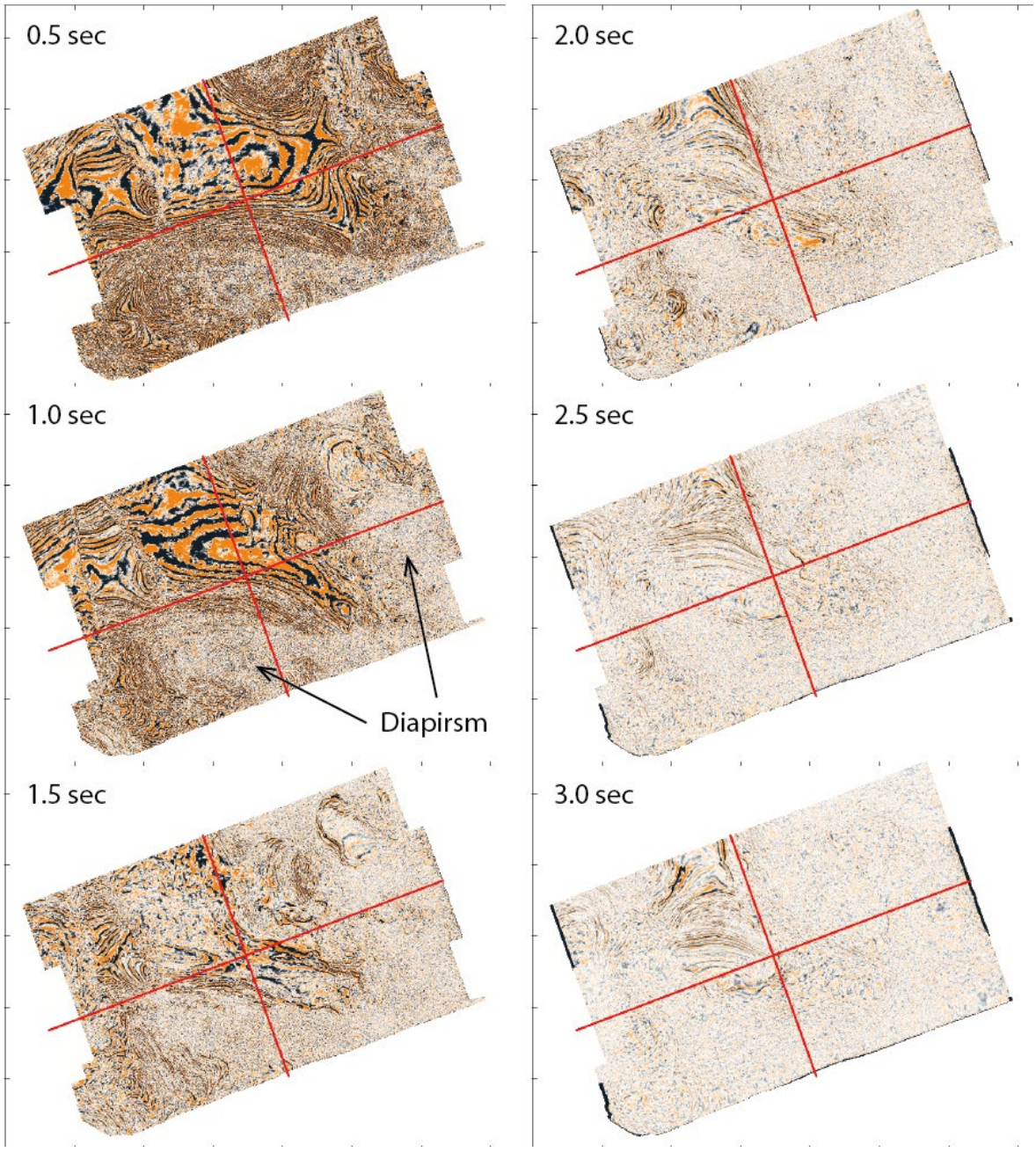

Figure 4- 12. 3D slices images in depth from 0.5 sec to 3.0 sec TWT. Dispirism (mélange, Unit 2) represent in the east and south surrounding the mini-basin (circular basins) of younger Unit 3 and 4. The map-view pattern shows the deformation in an E-W orientation, which is oblique with the regional orientation to form the accretionary wedge in NE-SW.

4.3.2 Onshore subsurface field observations

In Kudat, Pitas and the islands of Banggi and Balambangan (Figure 4- 7), our field observations had distinguished three different occurrences of mélanges, tectonic, sedimentary, and diapiric mélange, and these are corresponding to the onshore emerging sector of the diapiric structure shown in the seismic line (Figure 4- 11). We follow the stratigraphic formation based on previous geological mapping proposed by Tongkul (2003) and distinguished the lithology and structures between sedimentary rock and mélange. The geological mapping of the ophiolite outcrops displays on Figure 4- 13.

The relatively autochthonous basement is a massive and dismembered ophiolite sequence for which the peridotite sequence, is not clearly exposed in Kudat (Figure 4- 14A and B), except as serpentinite (light blue on Figure 4- 13; and Figure 4- 16) and extensive basalt and radiolarite (purple in Figure 4- 13). The igneous sequence is abundant and well exposed in Banggi Island, with a remarkable pillow lava series (Figure 4- 14E) associated with abundant radiolarite (Figure 4- 14C and D); composing large cliffs cut by the river Air Terjun Bunga near Kalangkaman Village.

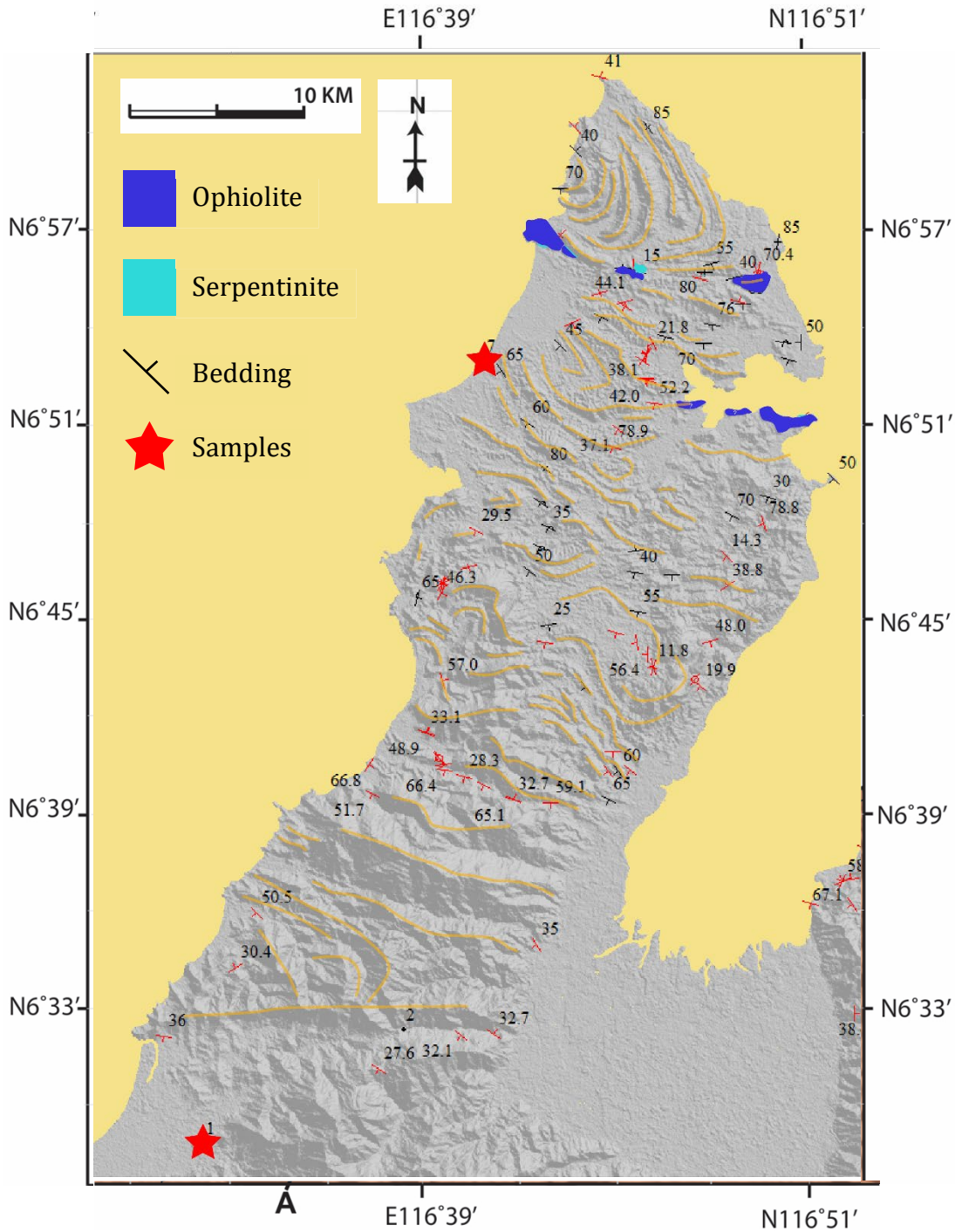

Figure 4- 13. Bedding measurements in Kudat Peninsula and geological mapping for the distribution of basalt and radiolarite in the Kudat Peninsula. The purple color represents the basalt and radiolarite and light blue color is serpentinite.

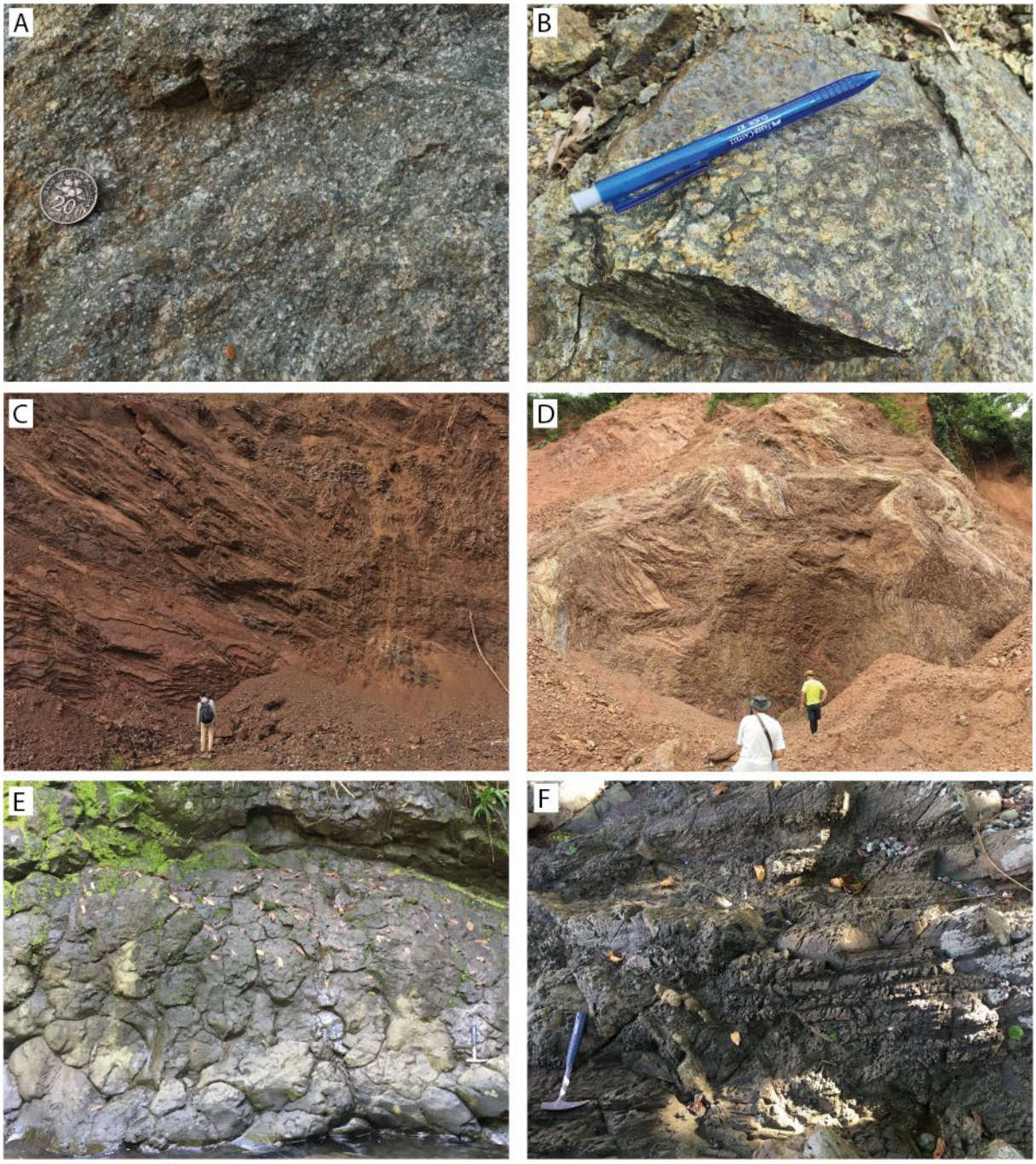

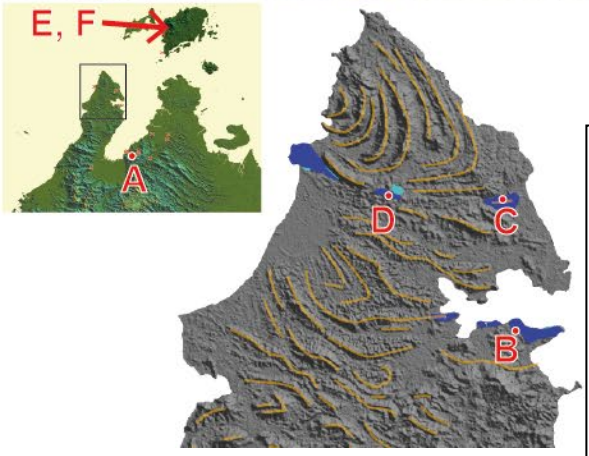

Figure 4- 14. The backstop of the Borneo wedge in the Kudat Peninsula: the oceanic series of the Proto-South China Sea. (A and B) ultra-mafic rocks and (C) relatively undeformed and (D) distorted radiolarite, (E) Pillow-lava basalt from the Pulau Banggi, and (F) Overlying fine-grained and thinly-bedded sediments.

The ophiolitic series composed of mantle and crustal sequences were thrust to the surface probably as a result of the obduction. On the west coast of Kudat Peninsula and some zone in Marudu area, we observed highly sheared outcrops (Figure 4- 15, Figure 4- 16 and Figure 4- 17), particularly at the contact between the pillow-basalts and the deep marine radiolarite sequence. The phacoid cohesive blocks are still in place and deformed in situ along a 20m thick contact (Figure 4- 15A to D) in western coast of the Kudat Peninsula where they are exposed as a result of basement uplift due to wedge formation, and in the Pitas Peninsula (Figure 4- 17A to C). The serpentinite, which records structural similarity (phacoid-shaped blocks) is seen in both peninsulas (Figure 4- 16). The MCS profiles also illustrate uplift resulting in the shallowing of Stage II, and the exposure the dismembered ophiolite along the western coast (Figure 4- 9). The sequence of thick hemipelagic clay which is expected in the basin, including all the marginal basins of SE Asia (Rangin et al., 1989).

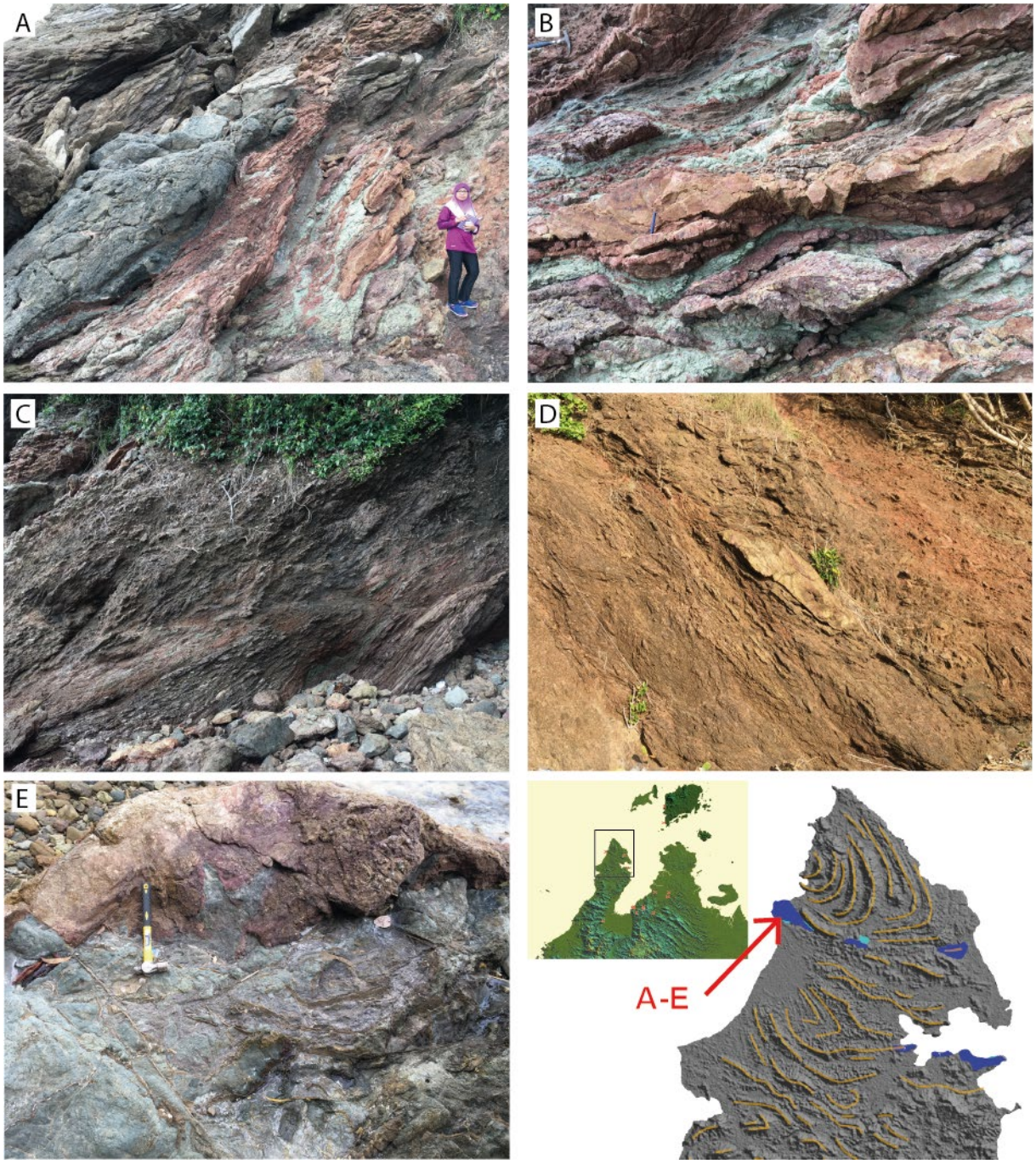

Figure 4- 15. Highly-sheared and fractured outcrops in Kudat Peninsula. (A and B) shear zone affecting radiolarite (red), hemipelagic sediments (green) basalt (dark grey) note the phacoid-shaped blocks of radiolarite and basalts. We interpret some blocks of the mélange as originated from these tectonic shears. (C and D) similar occurrence of sheared matrix and engulfing smaller blocks. (E) Zoom of the contact of the hemipelagic clay and phacoid shape radiolarite.

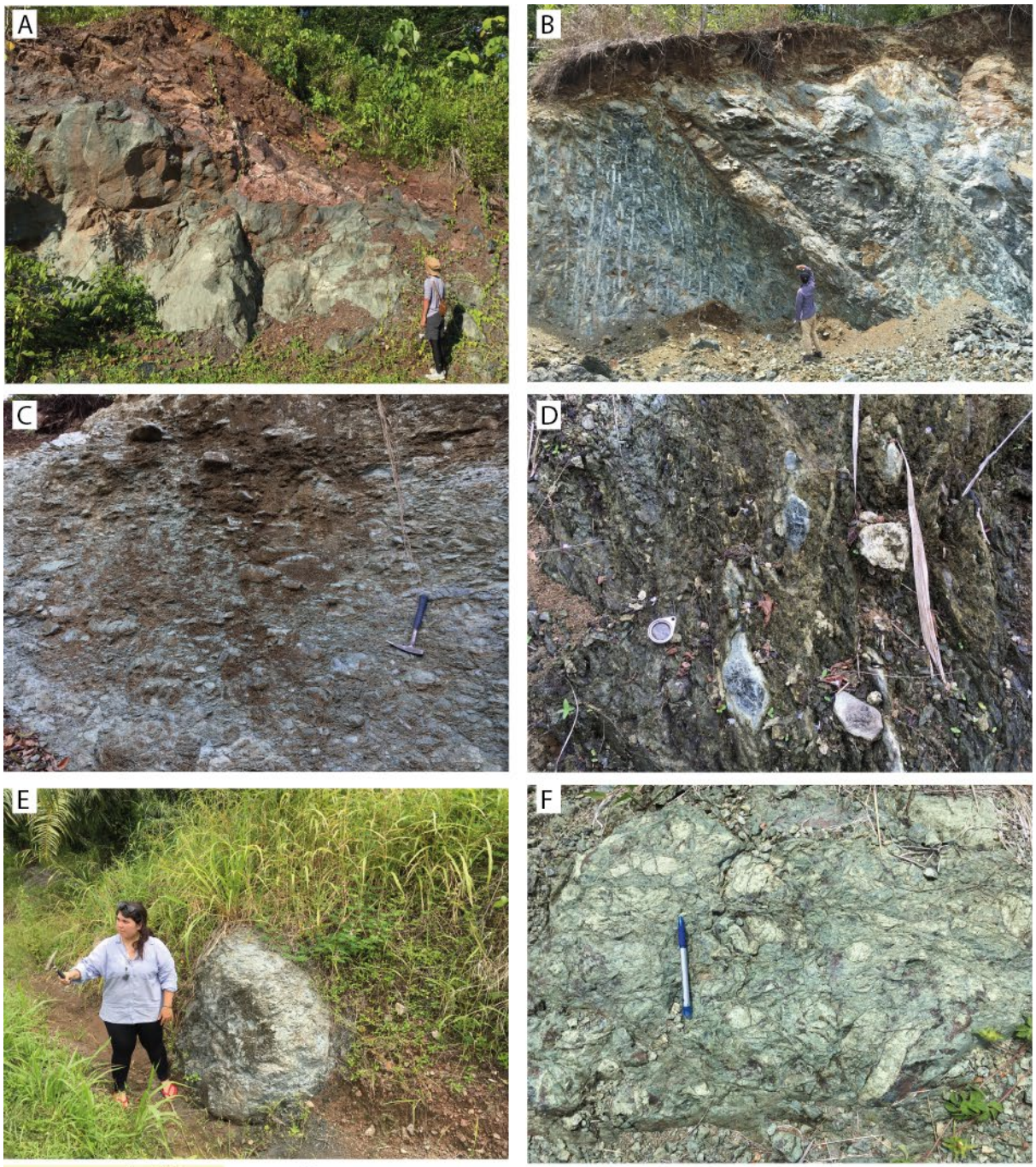

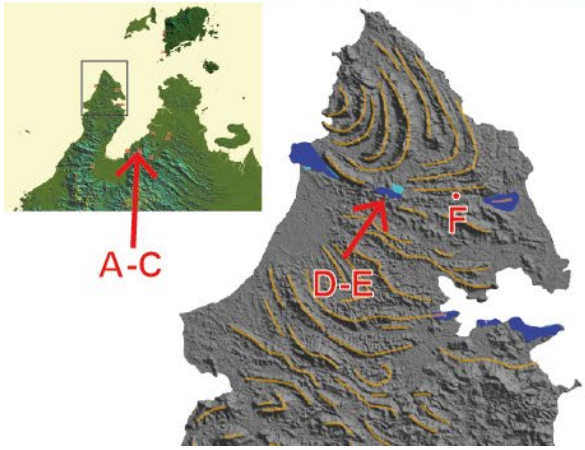

Figure 4- 16. Typical tectonic mélange in the Kudat and Pitas Peninsula. (A and B) ten centimeters to two meters knockers; and (C to F) Centimetric size of phacoid pebbles. Locally we still observe the contact between radiolarite and serpentinite within the meters-sized block (A).

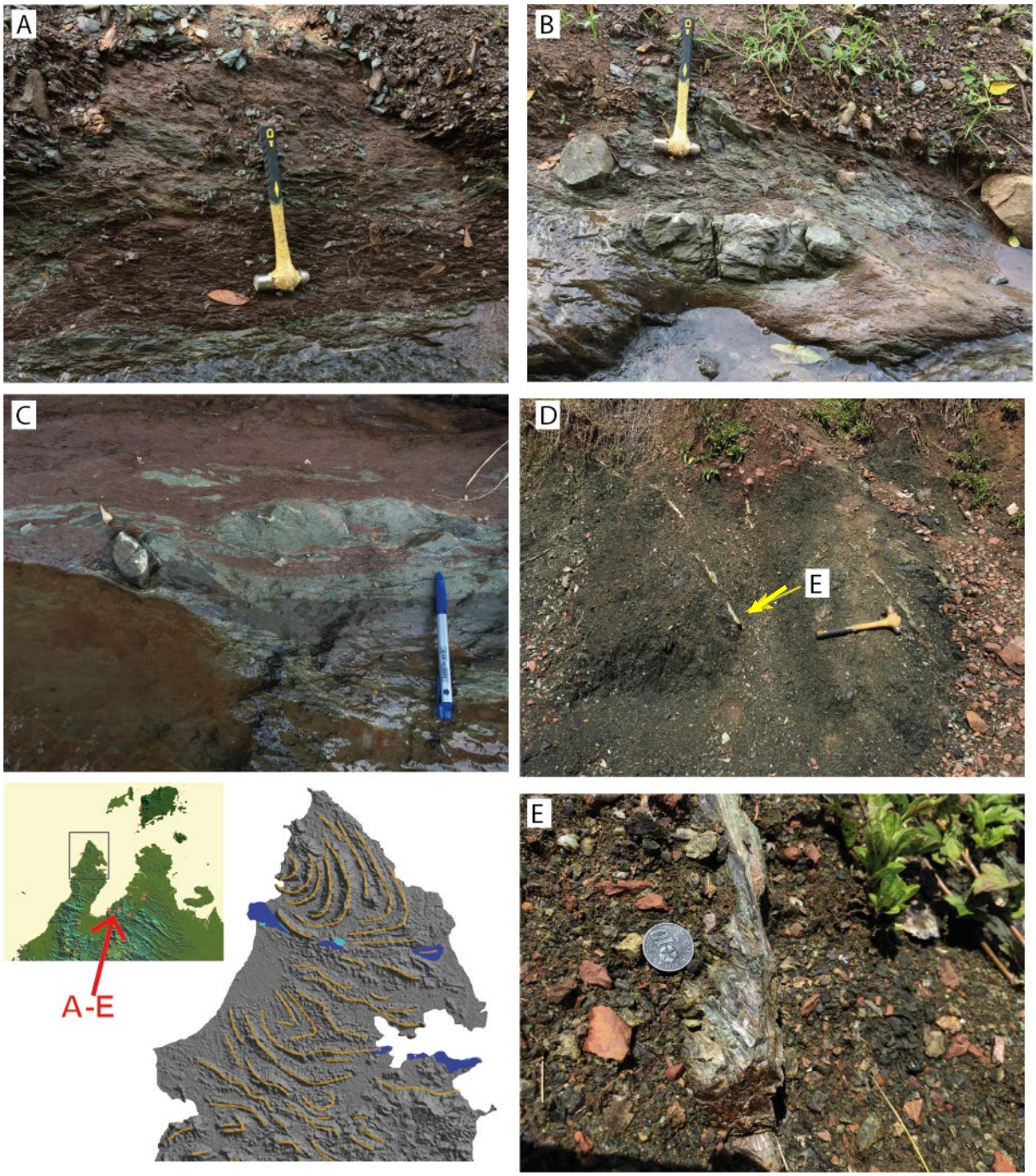

Figure 4- 17. Highly-sheared and fractured mélange in the Pitas Peninsula. (A) Fine-grained matrix composed by hemipelagic clay and radiolarite, and with (B and C) basalt blocks. (D and E) polished serpentinite (yellow arrow for location on D) aligned in the fine-grained matrix.

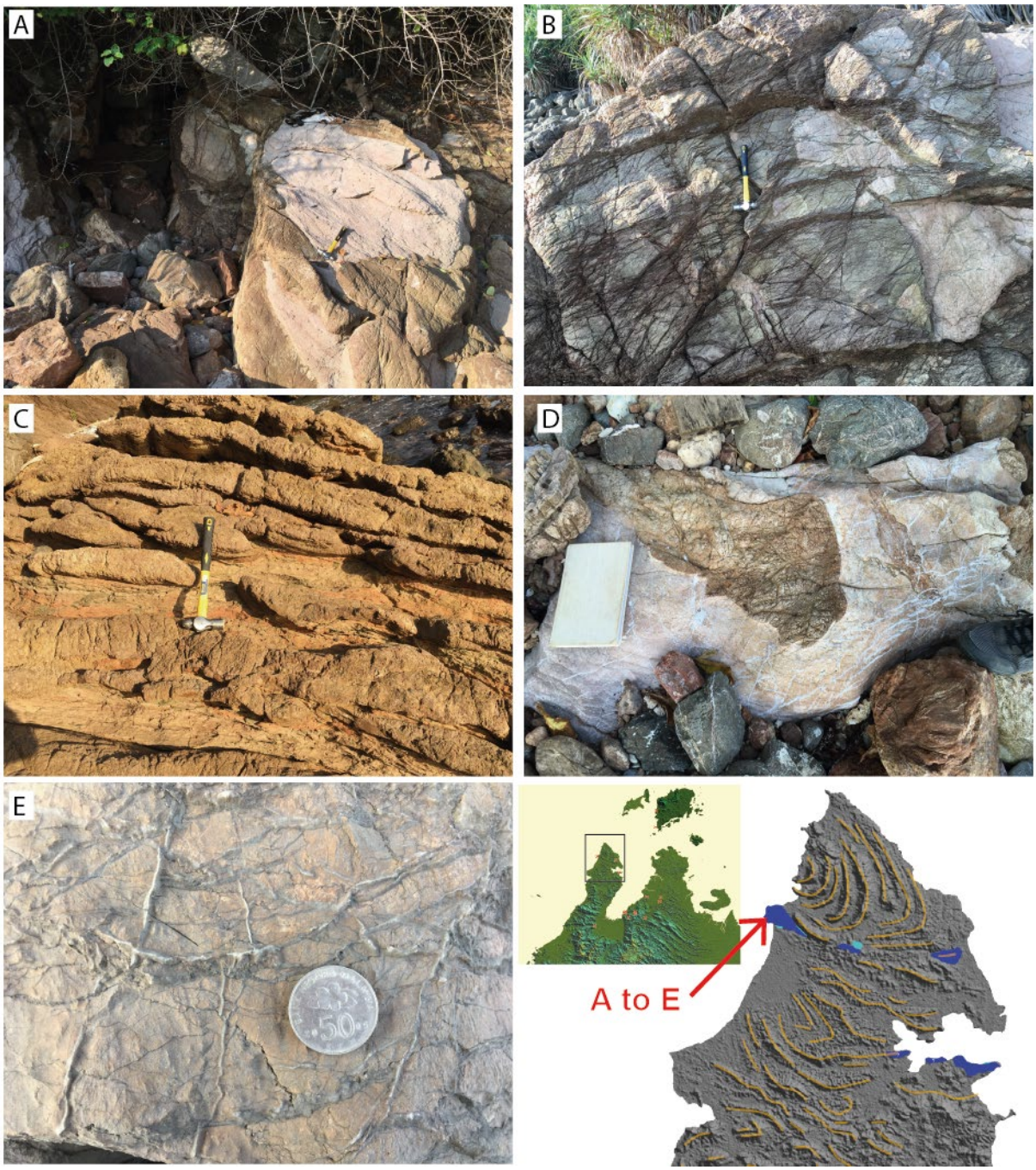

Figure 4- 18. Lithologies around the mélange: mostly sandstone with thin veins of calcite (A, C, and E) fine calcite veins or fractures underlying the variation of competence. (B and D) larger calcite veins postdating the fractures of the blocks (B and D).

The chaotic rock unit sits adjacent to the syncline, and distributed in an E-W belt (Tongkul, 2003; Rahim et al., 2017), yellow in Figure 4- 7b). The blocks expose all the lithologies of the subduction wedge, for instance, serpentinite and metamorphic, and siliceous clay and radiolarite blocks (Figure 4- 19). They vary in size from 20cm to several meters and generally have internal phacoid shape when not broken. We often observe the high-angle dipping cleavage and disturbance in the host rocks to suggest a deformation result from a vertical movement (Figure

4- 16D). The matrix of scaly clay (Figure 4- 19C) and has been previously interpreted as the result of either shearing or submarine slumping (Rahim et al., 2017) (Hamilton (1979) and references therein), and preliminary physical analyses including SEM, XRD and XRF in the Appendix (A.3). The similar blocks have also been found in Sandakan area. The blocks acquired their phacoidal shape and the striation within the thrust of the ophiolite and radiolarite probably inherited the previous structure resulting from crushing in the faults. Some blocks are distributed along the coast where the matrix has been washed away and, and thus exposes them in good condition.

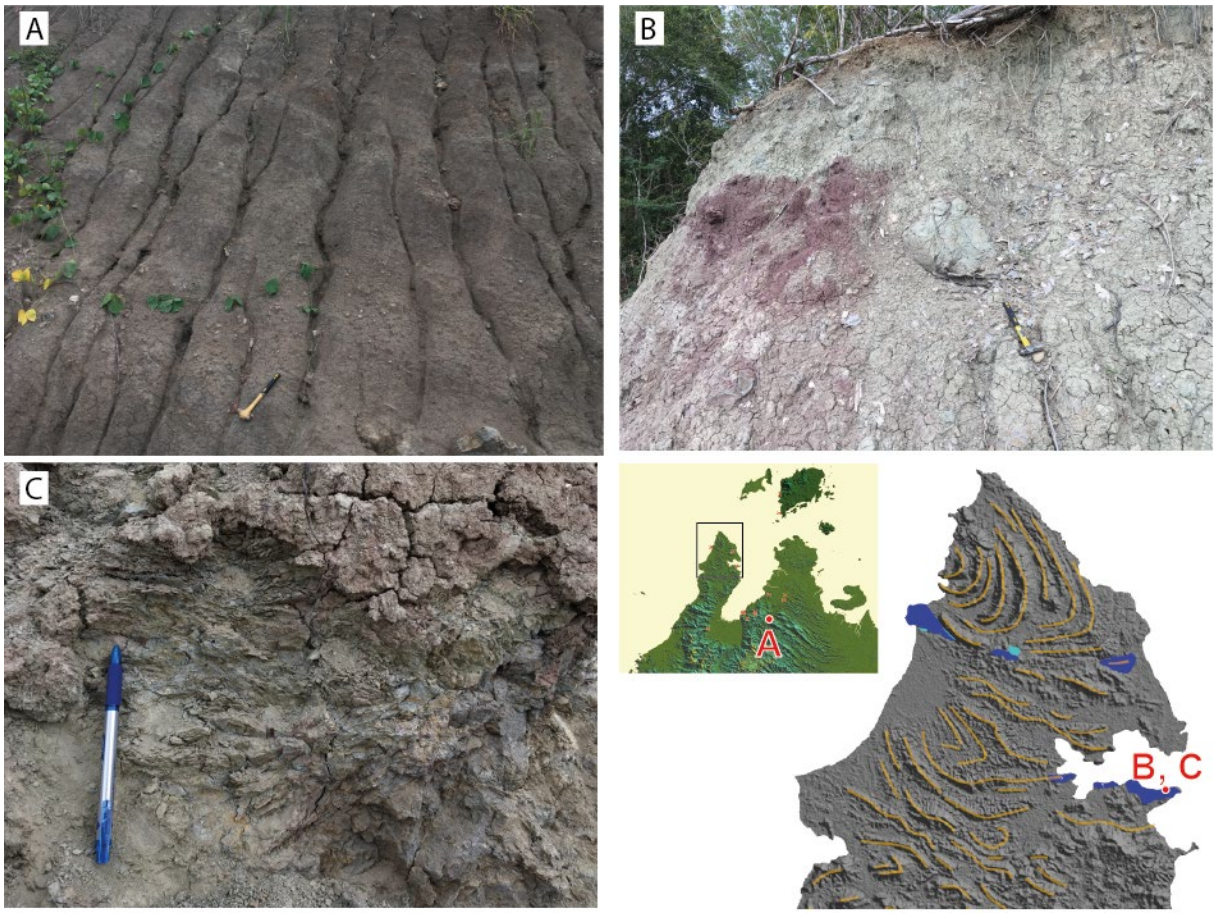

Figure 4- 19. Sedimentary mélange in Sabah. The matrix-supported blocks represent in laminated arrangement in the mélange.

These blocks could occur if the transported tectonic mélange was later affected by diapirism (Figure 4- 20 and Figure 4- 21), or else at the base of the gravitational body due to emplacement related shearing (Figure 4- 19) (Festa et al., 2019). Because the underlying succession is the basement, it is most likely that it is the clayey fraction of the basement sediments which have been reworked into the mélange matrix.

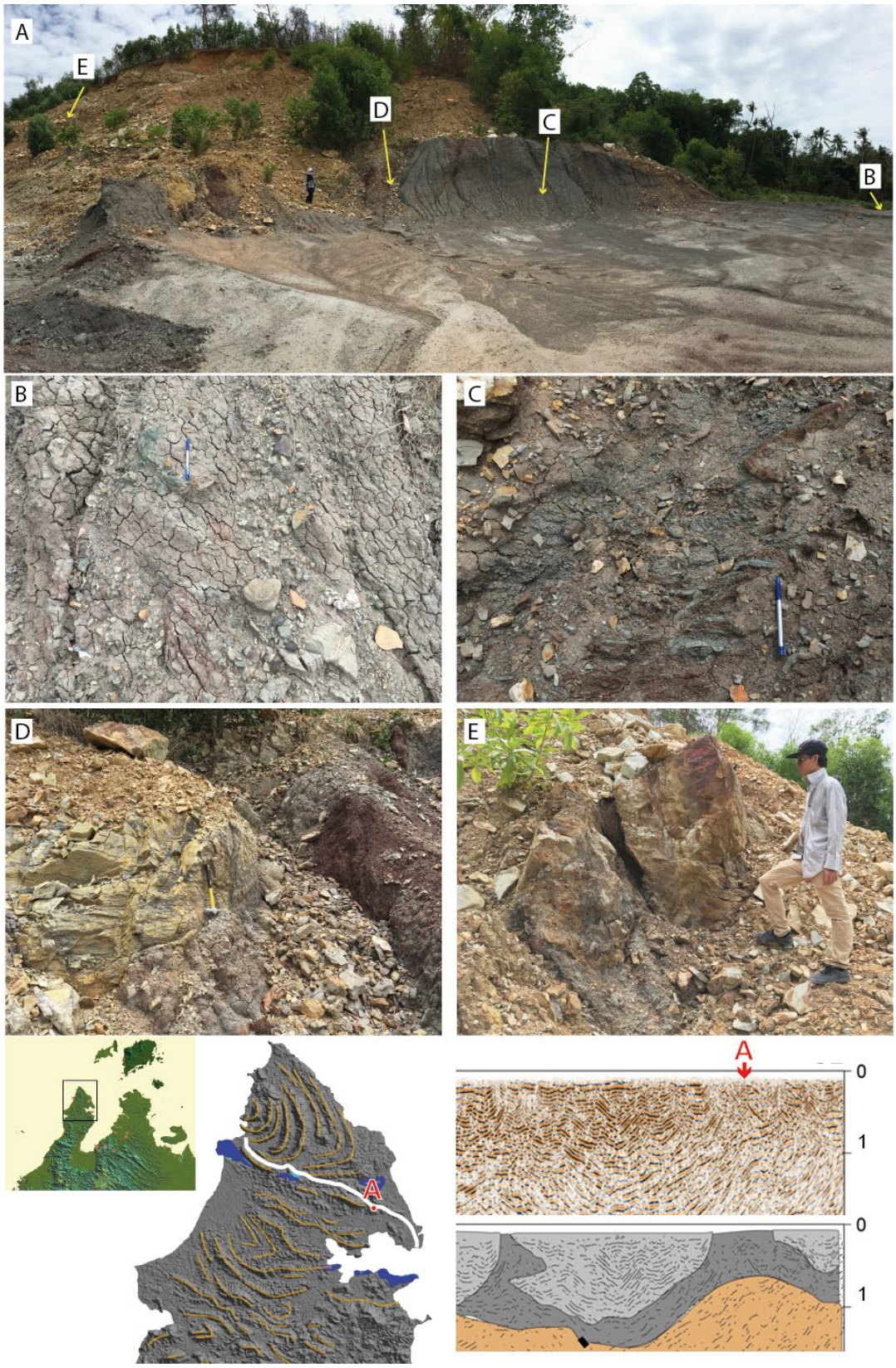

Figure 4- 20. Diapiric mélange (location A-E) outcropped close to the exposure of the Unit 2 from seismic profiles (location F) in Kudat Peninsula. (B and C) The stratigraphic relatively low position composed of fine-grained matrix with serpentinite blocks (B), adjacent to the broken formation of overlying thin-bedded strata (C). (D) The contact with the stratigraphic high position of coarse-grained sandstone, and (E) the sandstone broken by the shale bodies.

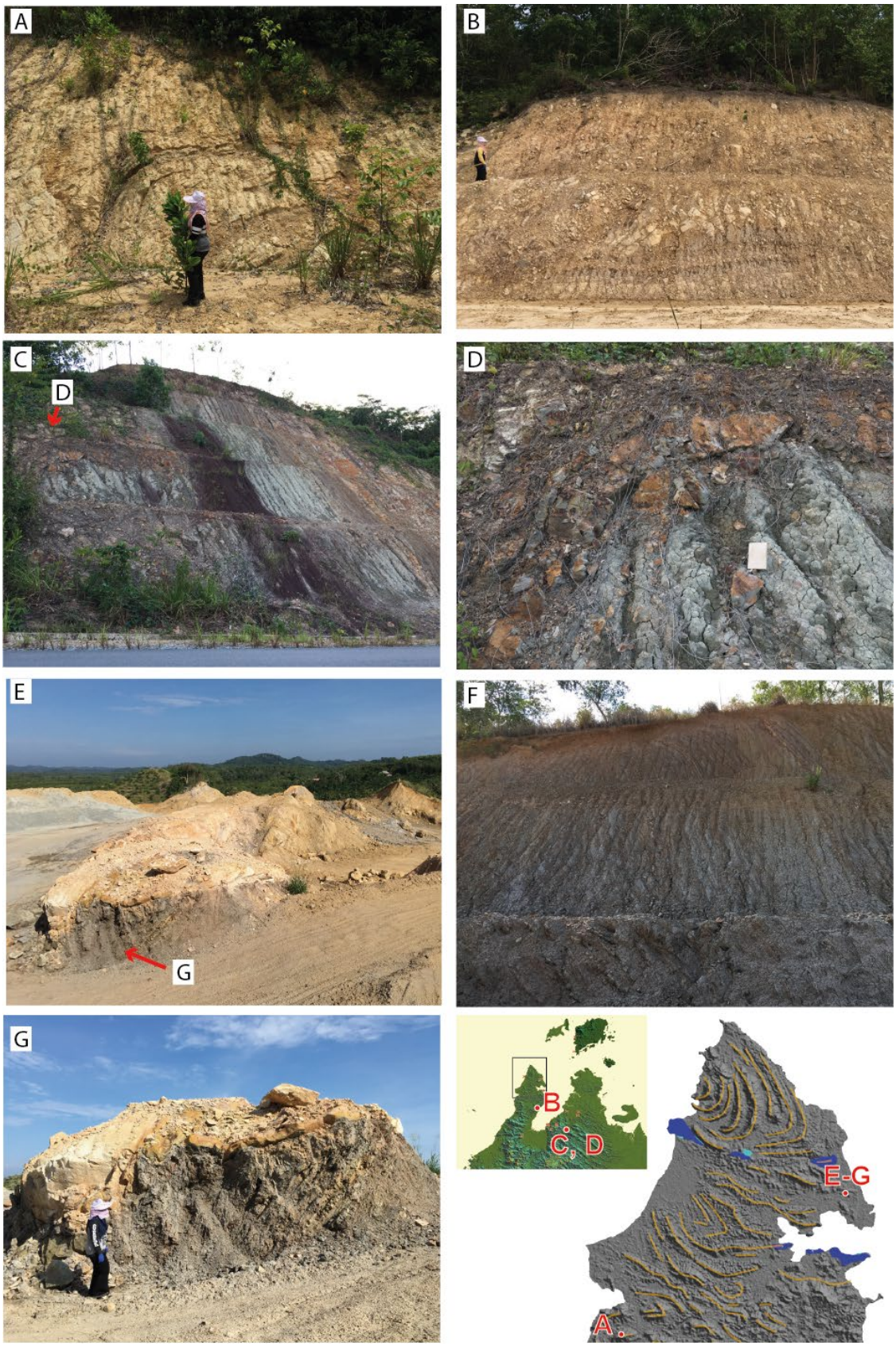

Figure 4- 21. Diapiric mélange and mobile shale in the Kudat Peninsula and the Pitas Peninsula. Several folding exposure in recent quarries showing ductile deformation underlain by massive shale. (E and G) Sandstone remobilized by shale underneath. (F) the strata overlying the mobile shale show folding with high dipping bedding next to the outcrop E.

Interestingly, the overlying units (Units 3 and 4) are above the mélange and are composed of clastic sediments deformed by metric folds which are also clastic in nature (Figure 4- 23). The bedding is also gently dipping (less than 40º, Figure 4- 23D), and is only affected by widely-spaced joints. Moreover, it is mainly composed of slightly to very indurated white to brownish metric to pluri-metric beds of sandstone, siltstone, and some conglomerates, separated by thinner layers (20 to 50 cm) of dark grey clay (Figure 4- 22). The axis of the large northern anticline plunges to the east in northern peninsula and there, this unit is dismantled in places and is locally steep and appears deformed at the boundary with an E-W fold injected with mélange (Figure 4- 23E). Strata are also offset by the later normal faulting (Figure 4- 23C to G). They are as well affected by some slumping figures (Figure 4- 23A and B).

Although the age revision highlights the existence of Late Oligocene (Lunt and Madon, 2017), some samples yielding a bio-stratigraphic Letter Stage Te5 in this study. This stage usually covers *pro parte* the Early Miocene (see the bio-stratigraphic results in the Appendix A.2), and remains present in the northern peninsula. Older Letter Stage Te1-4 are distributed to the west(van Hattum et al., 2013; Lunt and Madon, 2017), representing this younging-eastward succession, possibly due to the formation of the accretionary wedge.

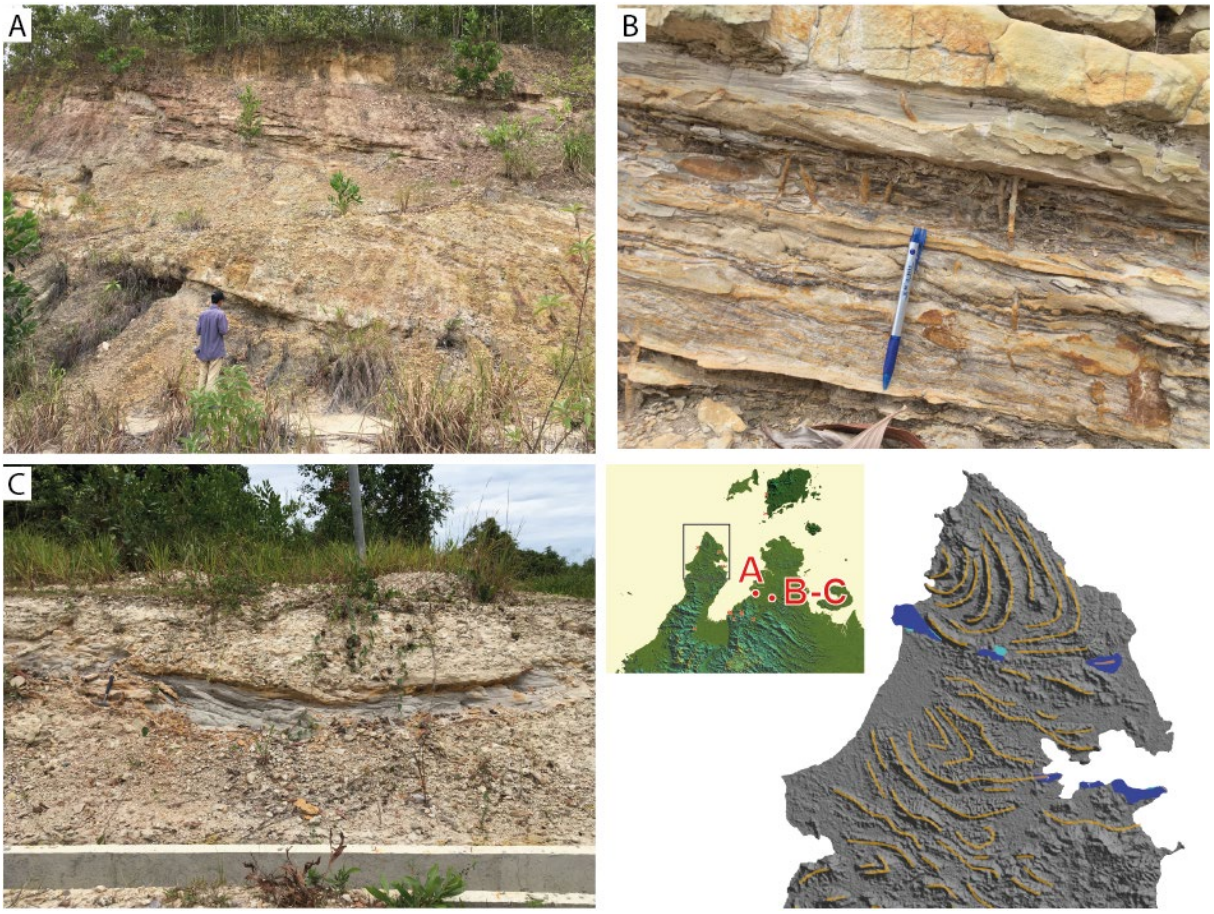

Figure 4- 22. Post-orogenic sediments showing shallow-water environment. They yield conglomerates and shallow marine with trace fossils.

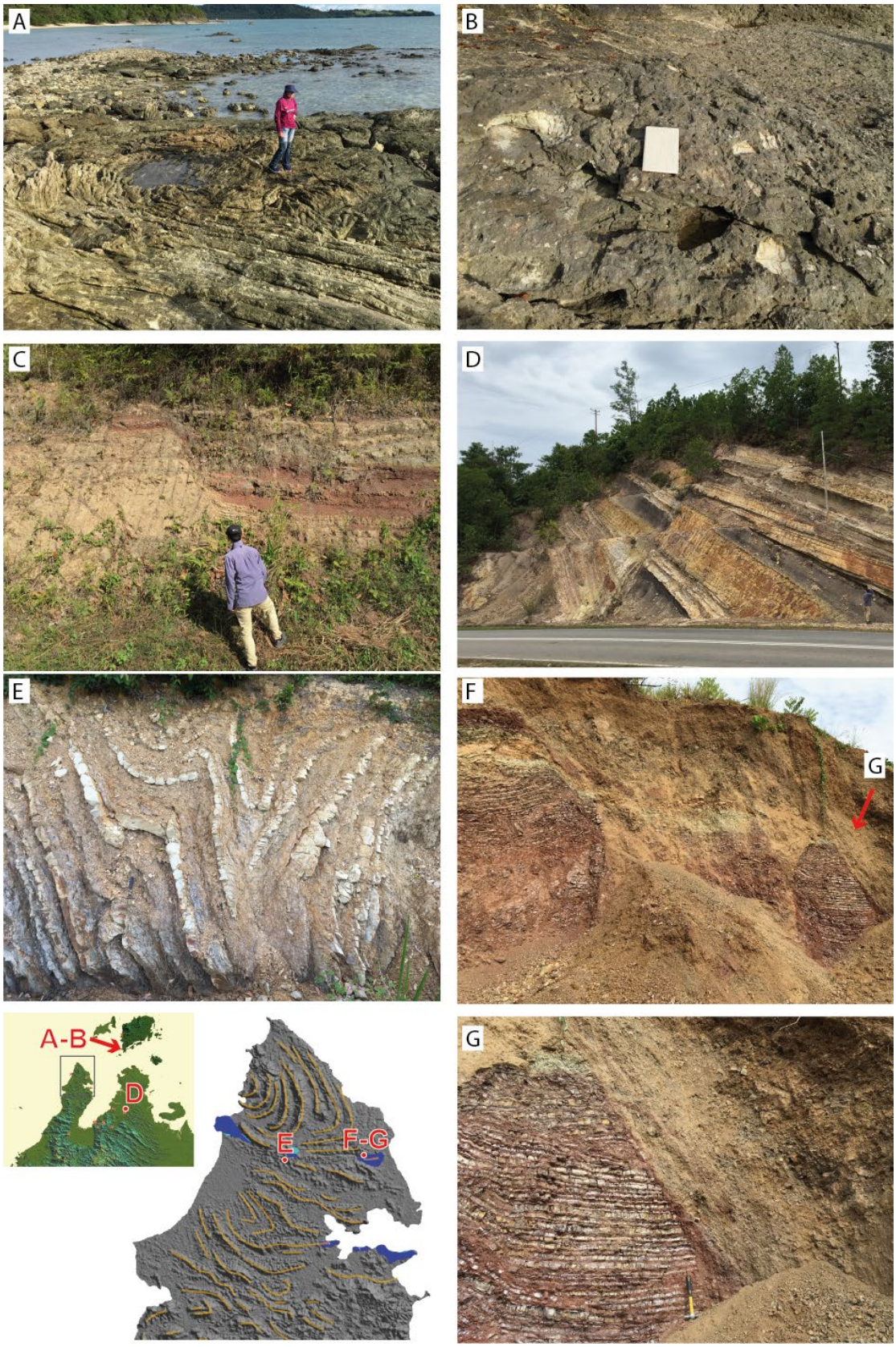

Figure 4- 23. Series deformed structurally above the mélange. (A and B) Slump of Miocene sediments and (C and D) normal faulting in the late Neogene sediments. (F) Fault contact between the radiolarite and late Neogene sediments (zoom on G). These are inferred to be the collapse features in North Sabah.

4.3.3 Morphological expression of the deformation

The topographic texture based on the DTM, allows to distinguish different regions, which are annotated as two main features, circular basins and ophiolite (Figure 4- 24), as well as S1, S2 and S3, corresponding to specific structural styles (Figure 4- 7b). The northern part of Northern Sabah (the Kudat Peninsula) (S1 on Figure 4- 7b) is mainly dominated by the Kudat Formation and characterized by plains or small hills (Tongkul, 2003). Structures are small-wavelength folds and round-shaped folds. The features are similar in shape to the known examples in Sandakan Basin (Tongkul, 1990), Brunei (Morley et al., 2003; Sapin et al., 2013; van Hattum et al., 2013) or further to the front of the foothills of the Central Range of Papua New Guinea (Granath and Argakoesoemah, 1989). The rounded shape implies that the maximum principal ($\sigma 1$) is vertical and that the horizontal stresses ($\sigma 2$ and $\sigma 3$) have close values on the Mohr's Circle, which indicates that the morphology is gravity controlled and suggests that a low viscosity layer sits underneath. Faults are not well expressed because of the incompetence of the rocks, except for an E-W structure (L1 on Figure 4- 7b) passing north of Kudat Town, which is of the same direction as the one which showed the serpentinite block-bearing mélange.

A topographic and textural contrast is observed at the boundary (L2 on Figure 4- 7b) with the middle region in the Kudat Peninsula (S2). This region corresponds to sandstone layers and interbedded sandstone and siltstone of the Crocker Formation. This area is marked by E-W orientated bedding traces (N100-N110), which runs across both the Kudat Peninsula and the Marudu Bay (Figure 4- 7), except for existing round-shaped folds in the SW corner (Figure 4- 7b). This fold trends probably connects to the western Sandakan Basin (Figure 4- 7a).

The southernmost region of the Crocker Formation (S3) is located at the south of the peninsula (Figure 4- 7b). This region shows a boundary with S2, based on the different orientation of the hills which are mainly trending NE-SW (N30-N45), in accordance with the orientation of the NW Borneo wedge. The boundary, L3, appears in few outcrops which expose mélange bearing serpentinite blocks. This boundary represents the southern limit of the gravity tectonics province (L3 in Figure 4- 7b). A small area on the opposite eastern side of the Marudu Bay is unconformable on the ophiolite. This major unconformity is therefore attributed to the DRU (white dash line in Figure 4- 7a), which is also a major unconformity in the offshore profiles. The unconformity can easily be drawn to the west at the edge of the Sandakan basin via DTM data.

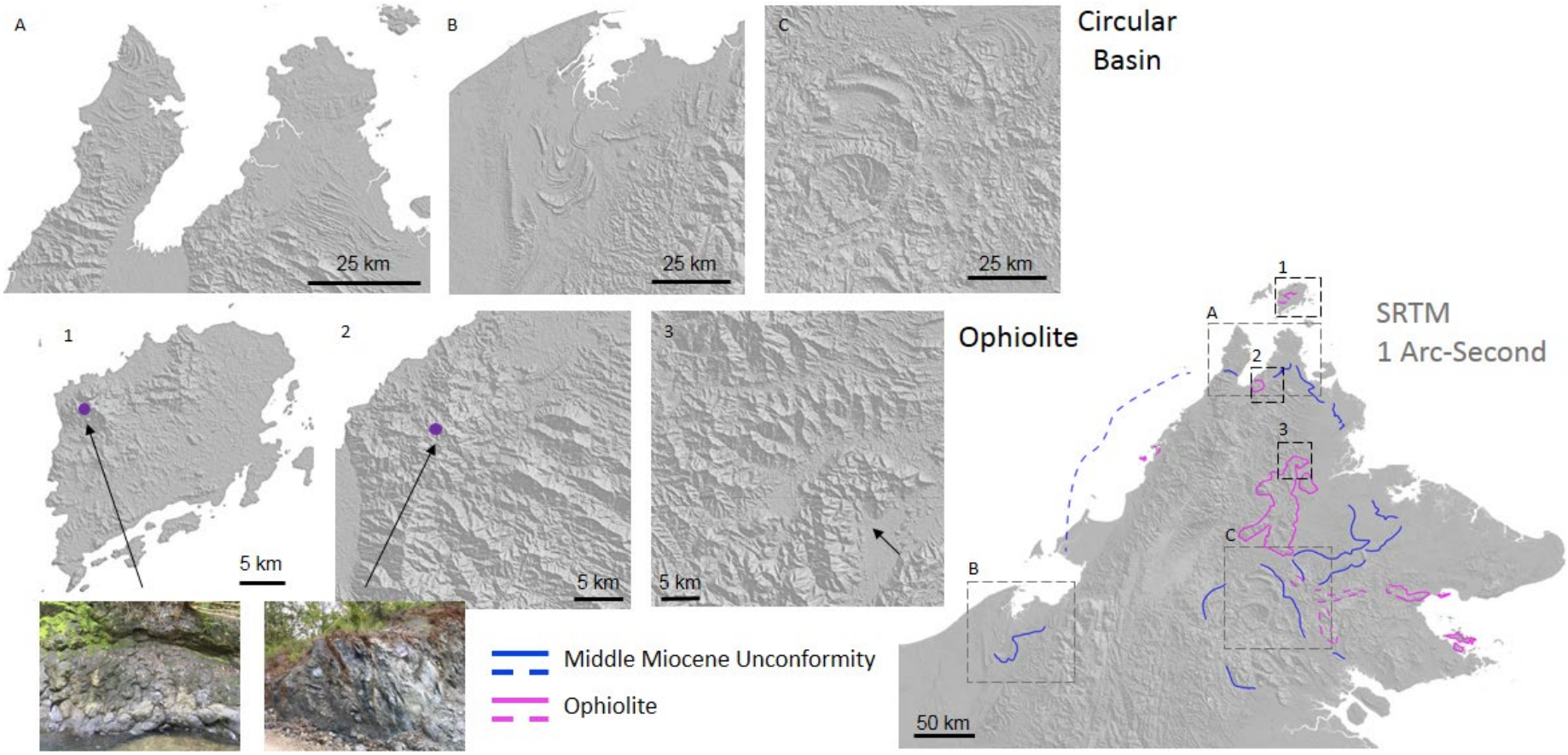

Figure 4- 24. SRTM topography in the Sabah area (Chang et al., 2018). Two main features are identified as circular basins with synclinal and anticlinal shapes and ophiolite in massive texture. These two features are represented in pink color for ophiolite and blue color for the edges of the circular basins on the map.

4.4 Different significances of the mélange of Kudat Peninsula

As observed in many examples of late stages of convergence, mélanges have both sedimentary and tectonic significance (Duerto and McClay, 2011; Festa et al., 2012; Ruh et al., 2018). They may represent olistostromic sedimentary deposits, and play a role in the late stage of the tectonic deformation particularly in post-tectonic gravity movements. As described for the evolution of different convergent margins worldwide, both tectonics and slope instability are significant processes in forming mélanges (Raymond, 1984; Cowan, 1985; Duerto and McClay, 2011; Festa et al., 2012; Festa et al., 2014; Ruh et al., 2018). Particularly, sedimentary mélanges or olistostromes represent useful markers for the timing of tectonic events using cross-cutting relationship (Festa et al., 2016).

In northern Sabah, the backstop of the wedge (Rajang wedge) is composed of Cretaceous ophiolite thrusted onto highly metamorphosed strata. We observe in the fields shear zones with frequent phacoid-shaped blocks, composed mostly of pillow basalt, radiolarite and clay, separated by thrusts. These blocks are found within the mélanges of Kudat Peninsula and the base of the Sandakan Basin. This stage of formation of the mélange is represented in Figure 4-25b, and took place during Oligocene (Lunt and Madon, 2017) and probably Early Miocene (Lunt, personal com., Figure 4- 30). This section was still depositing during the late motion of the wedge, which is responsible for the formation of N-S structures (Figure 4- 25a). The diapir started before the DRU (16 Ma), and the normal faults root inside the sedimentary mélange and offset the Early Miocene strata (light gray on Figure 4- 9a and Figure 4- 10). It is likely that the presence of this fault triggered the location of the diapir rise. The DRU is a significant unconformity marking the top of the wedge. The maximum age is around 14 Ma as dated in the industry wells (Noon, 2011). We interpret this age as being the end of the compressional deformation.

The unstable shale material seems to have been mobile episodically until the Early Pliocene (Unit 4a and 4b). The mobile body penetrated and dragged upward the overlying strata of Upper Miocene and Pliocene age. Diapiric evolution resumed to activate newly formed normal faults, and generated roll-over structure prior to 5 Ma (Figure 4- 9b). This triggered the formation of circular basins and E-W orientation topographic features locally in Northern Sabah. This deformation could be linked to the coeval magmatic intrusion of Mt. Kinabalu (Figure 4- 26), which dominant the collapsing tectonic in adjacent sedimentary stratigraphy (Hall, 2013). This

intrusion may have resulted from the break-off of Proto South China Sea subducting slab at 7-8 Ma (Hutchison et al., 2000; Swauger et al., 2000; Sapin et al., 2013).

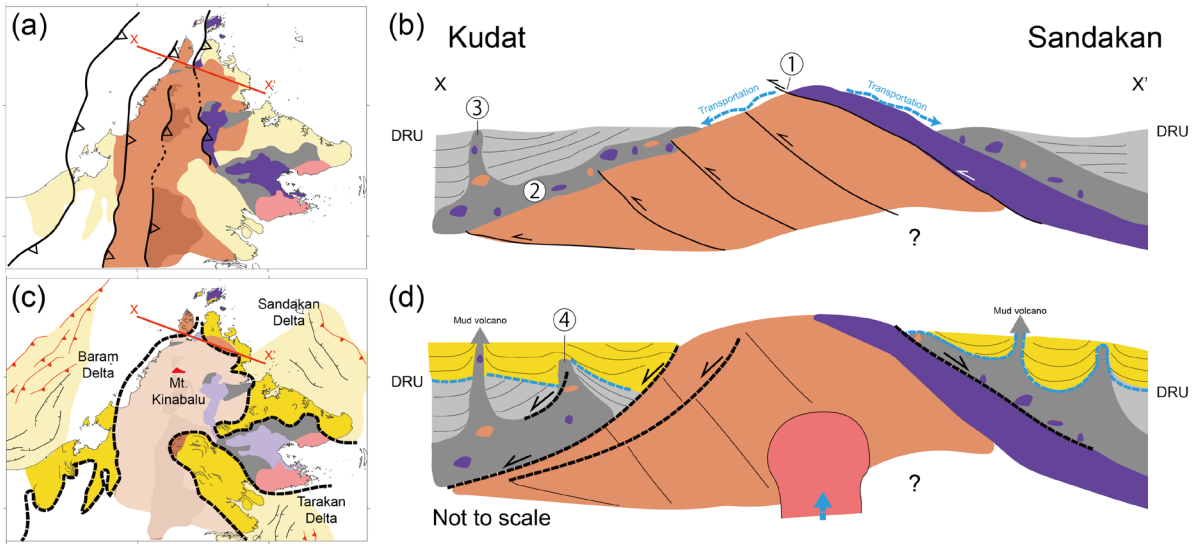

Figure 4- 25. Tectonic evolution and schematic cross-sections during the end of orogeny in Sabah. (c) Modified from Clark (2017). (1) the tectonic mélange (sheared and crushed blocks in the matrix), (2) sedimentary mélange, (3) diapiric mélange formed by overpressure on the sedimentary mélange, and (4) up-rise diapiric mélange induced by gravity tectonics.

Figure 4- 26. View from the peak of Mount Kinabalu. Photo credit: Manuel Pubellier and François Sapin.

4.5 Discussion

4.5.1 Mélange and the termination of the orogeny

The occurrence of mélange may be misleading within the formation of the fold-and-thrust belt. The observations presented in this study offer a scenario by which the mélange of northern Borneo somehow links the latest stage of the subduction/collision and the gravity tectonics. The gravity tectonics induced by shale or mélange started although the wedge was still active in the west offshore Sabah (Sapin et al., 2012). This scenario leads to a misunderstanding of what actually happened during the Late Paleogene and Early Neogene "Sabah Orogeny". The cross sections of offshore Sabah display extensional features developed within series deposited on top of the wedge. Similar normal faults distribute extensively in offshore Brunei and Palawan (Figure 4- 27) (Cullen, 2010; Ilao et al., 2018).

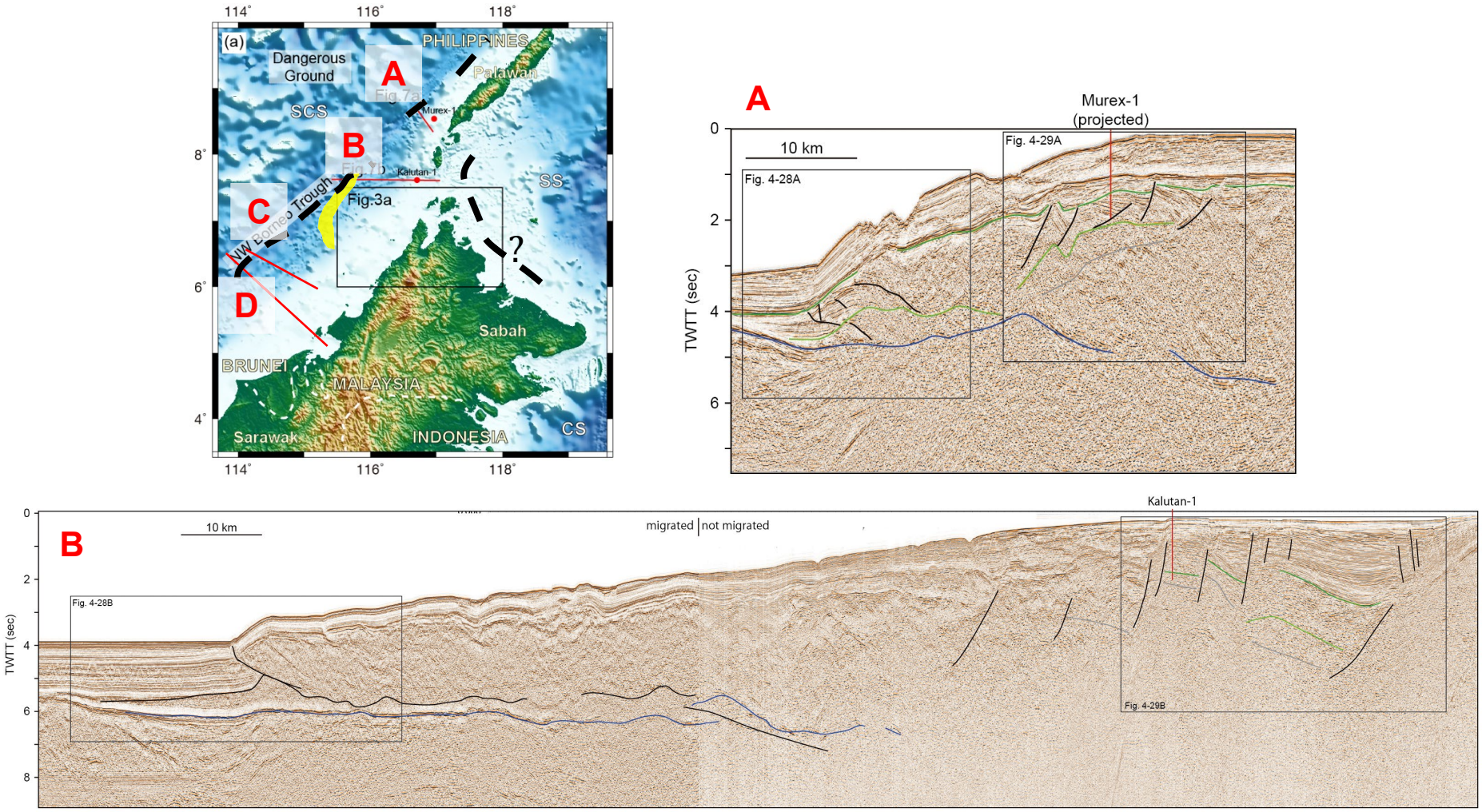

Figure 4- 27. Lateral variation along the fold-and-thrust belt among Sarawak, Sabah and Palawan, showing the gravity tectonics induced by the present mobile shale. Detail of toe-thrust segments on the Figure 4- 28, and detail of the upper wedge of the circular basins on the Figure 4- 29. The Palawan profile refers to Figure 2- 37 which is the interpretation of gravity tectonics from Ilao et al. (2018). Yellow: high velocity body identified from OBS velocity structure (Franke et al., 2008).

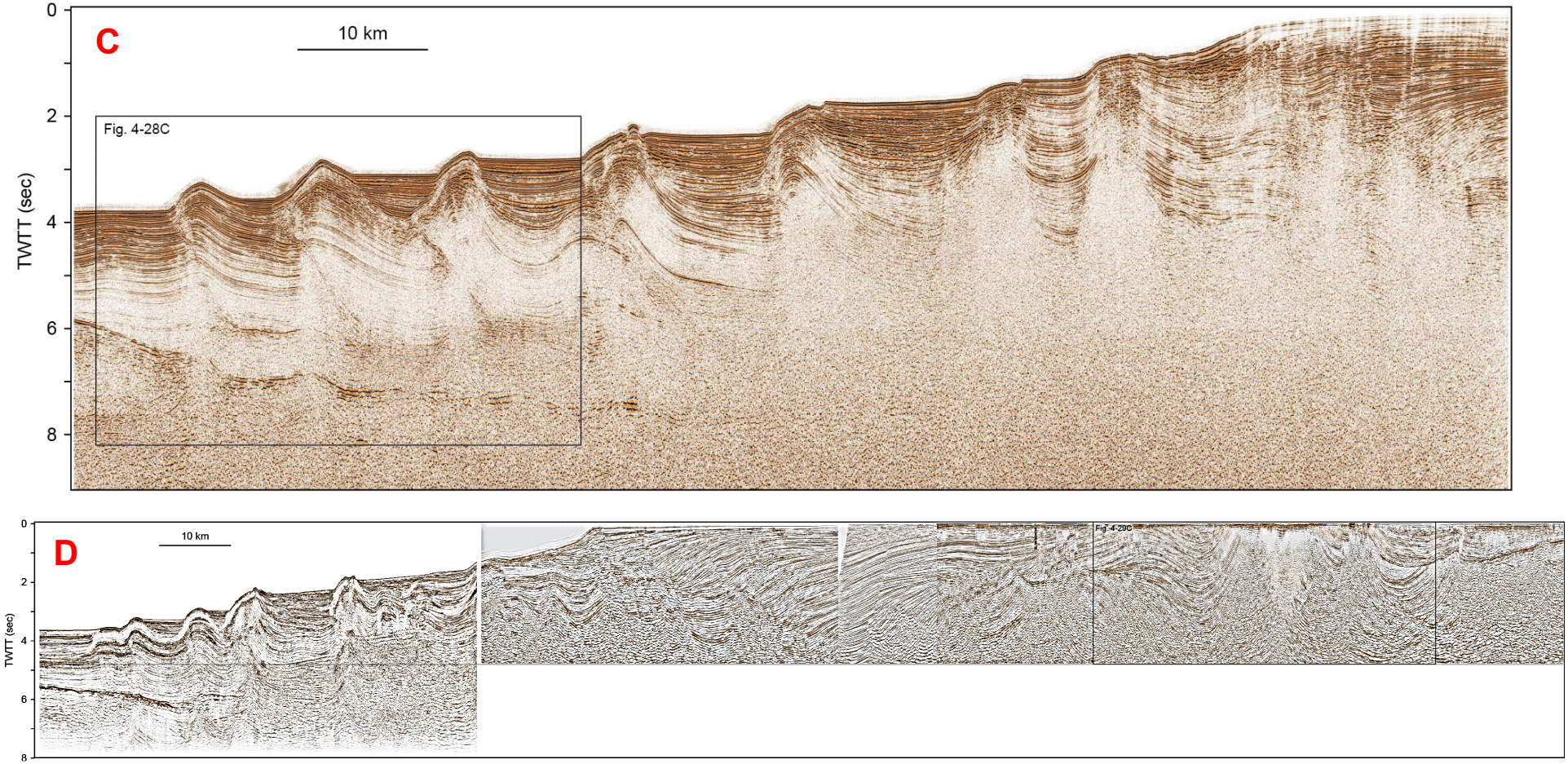

Figure 4-27 (continued). Lateral variation along the fold-and-thrust belt among Sarawak, Sabah and Palawan, showing the gravity tectonics induced by the present mobile shale. Detail of toe-thrust segments on the Figure 4- 28, and detail of the upper wedge of the circular basins on the Figure 4- 29. The Palawan profile refers to Figure 2- 37 which is the interpretation of gravity tectonics from Ilao et al. (2018).

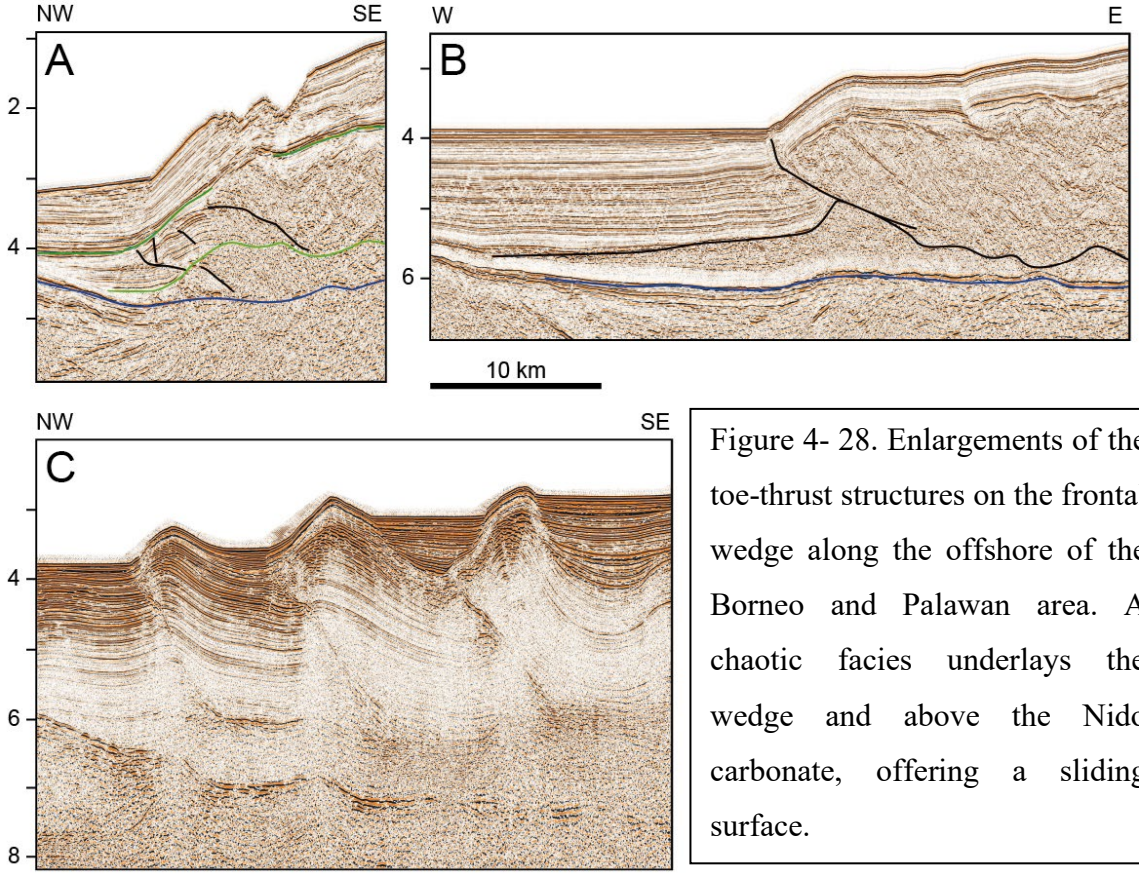

Figure 4- 28. Enlargements of the toe-thrust structures on the frontal wedge along the offshore of the Borneo and Palawan area. A chaotic facies underlays the wedge and above the Nido carbonate, offering a sliding surface.

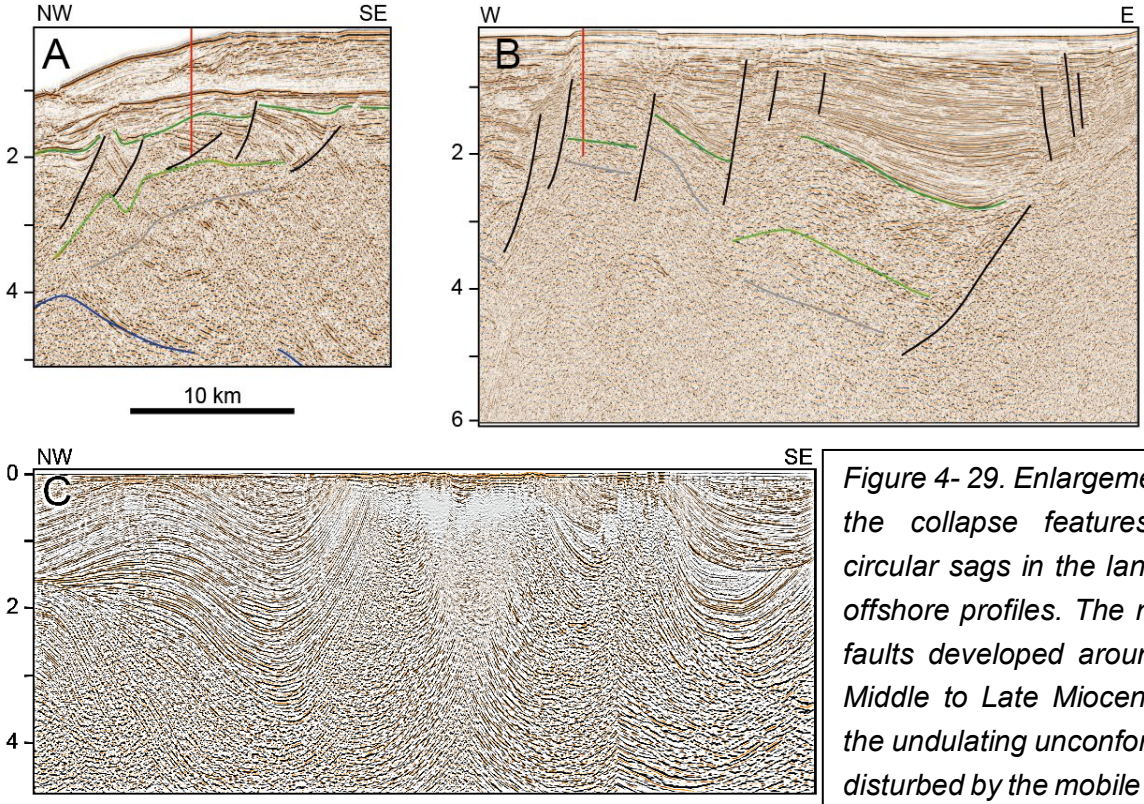

Figure 4- 29. Enlargements of the collapse features and circular sags in the landward offshore profiles. The normal faults developed around the Middle to Late Miocene and the undulating unconformities disturbed by the mobile shale.

This study reveals that this series are mainly poorly-viscous sedimentary mélanges which are easily remobilized into diapir and deformed the overlying sediment as circular anticlines and synclines. We think that the mud-prone low viscosity material near the frontal wedge accommodated most of the gravity slides. The style of deformation is therefore different from that of the actual shortening of the orogenic wedge. The shift from the wedge construction to the wedge collapse is bracketed between the beginning of sedimentary mélange (Unit 2) and the faults affecting Unit 3 before the DRU.

The correlation with the offshore in Palawan and Sabah is presented in Figure 4- 27 and Figure 4- 30. Paleogene sedimentation of the wedge; Crocker Formation in Brunei, Stage II in Kudat and pre-Ransang Limestone including Panas/Pandian Formation in Palawan. They stop at the TCU (Top Crocker Unconformity) or the boundary between Oligocene and Miocene around 23 Ma. Above this unconformity, we recognize predominantly shale and mélange which include the Setap Formation in Sarawak and Brunei, chaotic facies of mélange in Kudat, and Pagasa Formation. The sedimentation of the above units (Meligan Formation, Kudat Formation or Stage III, and Isugod Formation/Pagasa wedge) vary in age in these three columns but it is often as a response to the behavior of the low-viscosity material below. The circular basins are also observed in the unconformable Meligan Formation (Sapin et al., 2011), synclines and anticlines of the Kudat Formation, and the collapsed Pagasa Wedge in the offshore of Palawan (Ilao et al., 2018). However, it seems to be slightly diachronous among the DRU (16 Ma in Brunei and 14.2 Ma in Kudat), and the Red Unconformity/MMU in Palawan (~12 Ma, Ilao et al. (2018)). An alternative explanation is that the DRU is not recognized in Palawan or that the Red U/MMU is not properly identified in Brunei or Kudat. We suspect that the TCU at 23 Ma represents the latest stage of the orogeny (Lunt and Madon, 2017) and that were still small motion of the wedge associated with the uplift until the DRU and the Red U/MMU in Sabah and Palawan respectively.

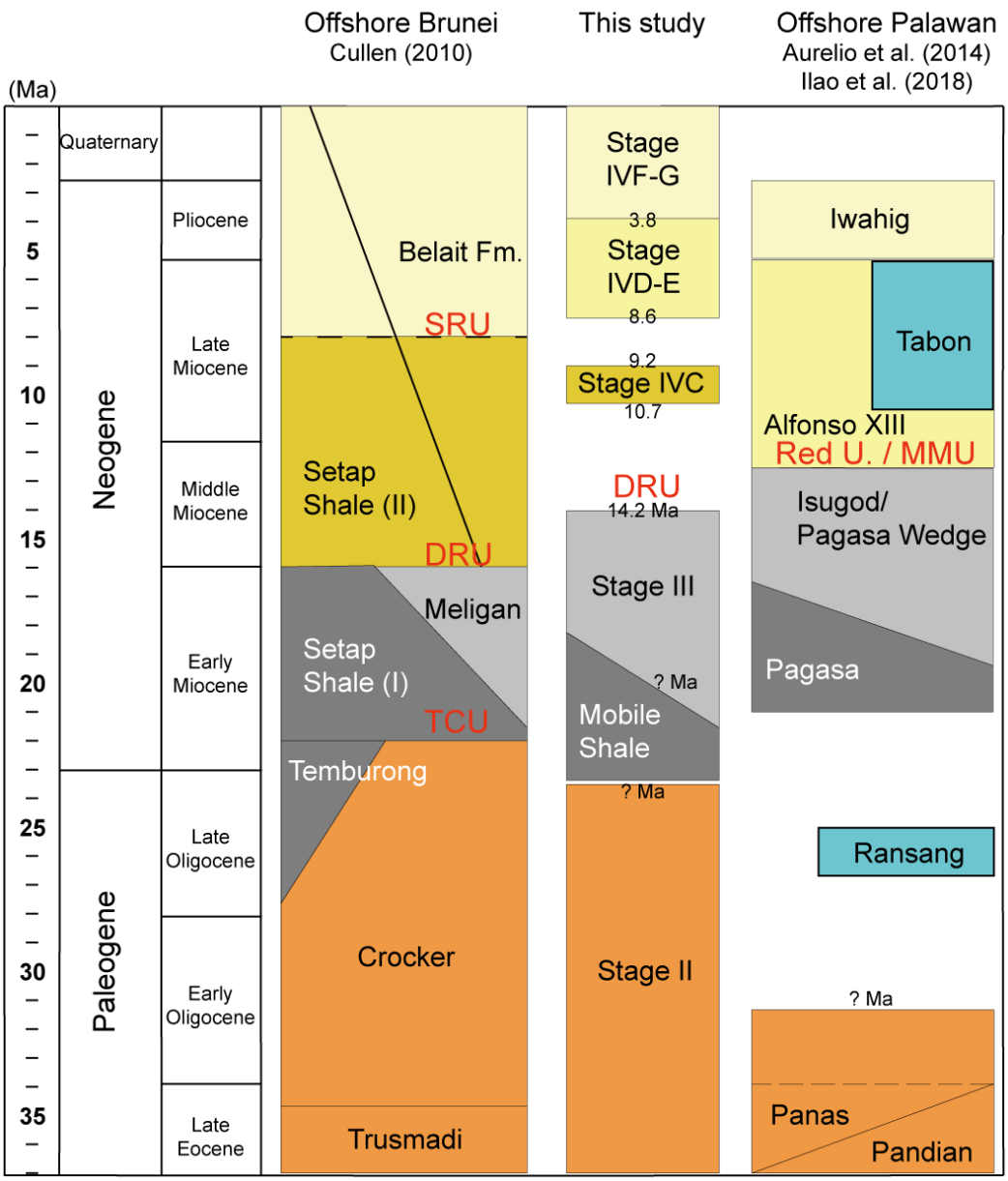

Figure 4- 30. The stratigraphic correlation of Sabah, the offshore Palawan and Borneo. The column of this study based on Well TP (Noon, 2011), and others are modified from Cullen (2010), Aurelio et al. (2014), and Ilao et al. (2018). Most Lower Eocene formations are composed by mélange or fine-grained strata and overlain by the DRU and MMU from 16 Ma in Sarawak to 12 Ma in Palawan.

4.5.2 A review of the mélange in Sabah

The genetic link between subduction and mélanges is not specific to Kudat Peninsula, and has to be compared to the other places around East Sabah. Other mélanges (Ayer, Kuamut and Garinono Formation) have been extensively documented (Clennell (1991) and references therein). According to the limited biostratigraphy analysis, the chaotic rock units were generated in Early Miocene to Middle Miocene (Clennell, 1991; Balaguru et al., 2003; Lunt

and Madon, 2017). In the vicinity of mélanges (grey color in Figure 4- 25), mud volcanoes were present (Leong and Anuar, 1999; Tongkul, 2017) and small patches present circular basins topographic features (Meliau, MaIibau, Tidung, Bangan and Bukit Garam sub-basins). The circular basins are composed of Middle to Upper Miocene formations (Balaguru et al., 2003), and a comprehensive measurement shown perfect circular synclines in East Sabah (Clark, 2017). It appears that gravity tectonic processes became dominant after the termination of the orogeny in Sabah.

In addition, chimneys and mobile shale structures are also observed in the offshore Sandakan (Clennell, 1996). The Lower Miocene mobile body (Ayer Formation?) penetrates the overlying formation, which was interpreted previously flower structures. In this study, the similar feature is able to be reinterpreted as a diapirism in the offshore seismic profile (Figure 4- 31). Those mini-basins are usually like a syncline or anticline from the top view, which could connect to those circular basins onshore.

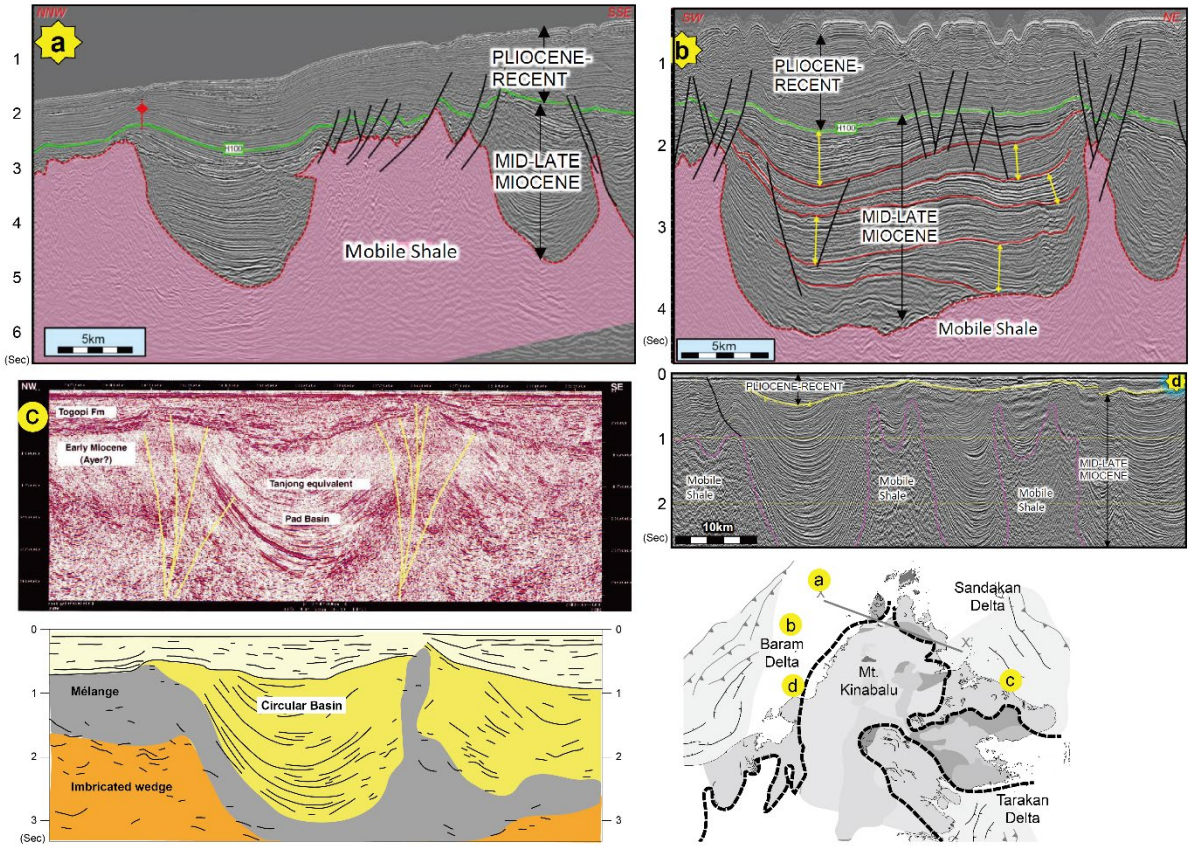

Figure 4- 31. The reinterpretation of diapiric mélange in eastern offshore Sabah. The original profile is from Leong and Anuar (1999), Clark (2017) and Chang et al. (2019). The location shown in the Figure 4- 3a.

Note that Baram, Sandakan and Tarakan Deltas also suffer from gravity tectonics with normal faults landward and toe-thrust in the frontal delta (Clennell, 1996; Leong and Anuar, 1999; Clark, 2017). The Baram Delta presents a remarkable fold-and-thrust belt in Brunei offshore (Morley and Guerin, 1996; Cullen, 2010; Sapin et al., 2011). Massive structure of gravity tectonics is widely distributed in the offshore NW Sabah and Brunei, and distribute around shelf break. In west Sabah and Palawan, diapiric features are widely distributed with mélange or mud-prone stratigraphy (Clennell, 1991; Morley et al., 2003; Hall, 2013; Ilao et al., 2018), although some of the structures maybe only reactivated normal faults under the differential loading due to the sediment accumulation (Sapin et al., 2012). However, the distribution of deltas and diapiric mélanges are surrounding the northern Sabah (Figure 4- 25c and Figure 4-26) with Mt. Kinabalu being the center.

Previous low-temperature thermochronology studies crossed the Sabah area to illustrate the exhumation history. The results show that the samples from Late Miocene granites display a similar ages in AFT/ZFT (apatite and zircon fission-tracks, Group 1 on Figure 4- 32). However, the samples collected from sedimentary rocks in detritus minerals revealing the Group 2 have Miocene age in AFT whereas Mesozoic ages in ZFT, and the Group 3 have old ages in both AFT and ZFT (Figure 4- 32). This may indicate the Group 2 had been exhumed from shallow depth, which can reset the apatite fission tracks but not the zircon minerals, whereas the Group 3 has remained the surface for a long geological time. In the cross-section plot, this Group 2 surrounding the Mount Kinabalu (red rectangular on Figure 4- 33). Therefore, we suspect the gravity tectonics could be also induced by this magma intrusion in Late Miocene (Hall, 2013). Because the low-viscosity material is extensively distributed around the intrusion of magma, hence contorting the overlying strata, which are also widespread in Sabah (Figure 4- 25d).

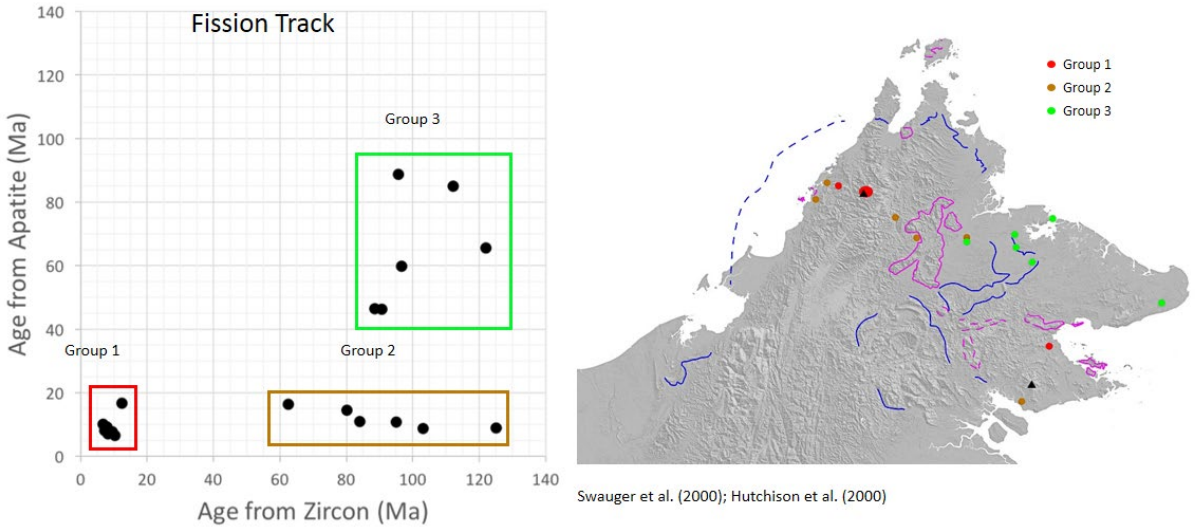

Figure 4- 32. Three groups characterize the different thermal and exhumed history (Chang et al., 2018). The Group 1 represents the igneous rocks reflecting the origin ages in Late Miocene. The Group 2 and 3 collected from sedimentary rocks, and the apatite fission-tracks show reset in group 2 whereas it is unreset in group 3. Both groups 2 and 3 show unreset fission-track ages in zircons. Data compiled from (Hutchison et al., 2000; Swauger et al., 2000; Cottam et al., 2013).

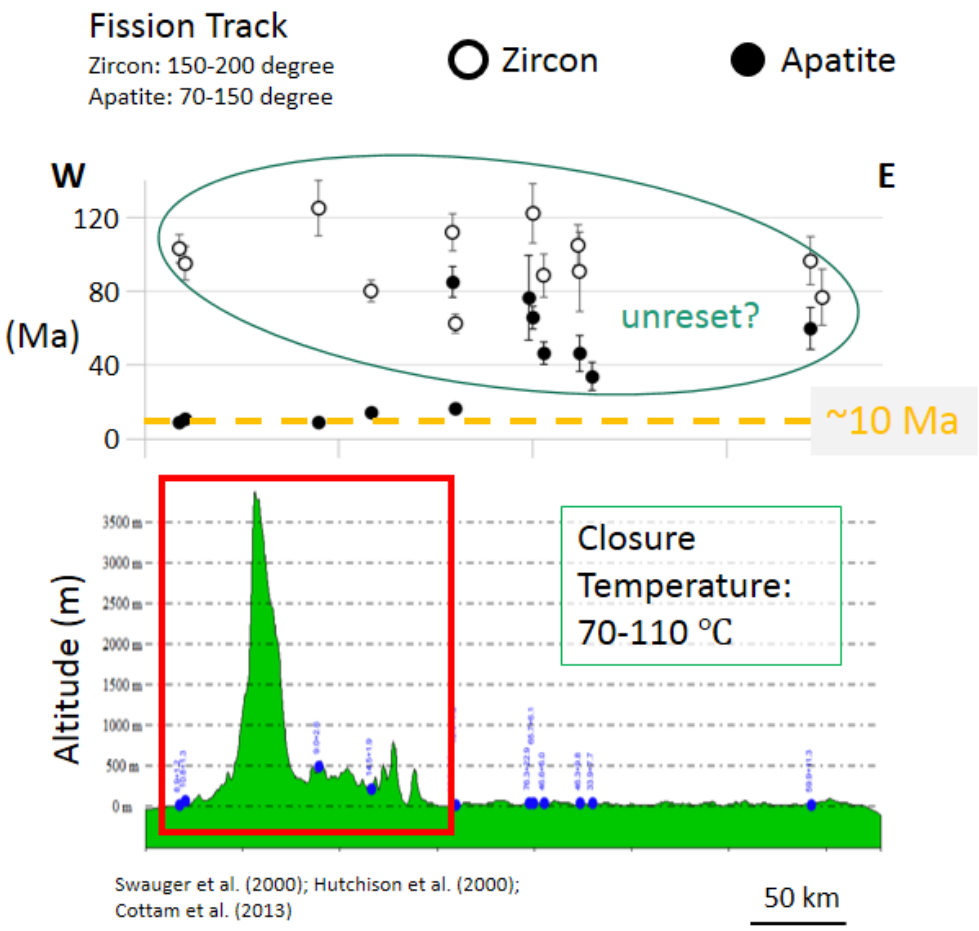

Figure 4- 33. AFT and ZFT data from the detrital minerals in the Group 2 and 3.

4.6 Conclusion

Mountain ranges were formed by the shortening process during plate convergence. They later are subjected to erosion and collapse. Sedimentary mélanges, which are actually olistostromes with unmetamorphosed matrix, have been often associated with the termination of the mountain building. The observations presented in this study offer a scenario in which the sedimentary mélange of the Northern Borneo somehow links the latest stage of the subduction/collision and the gravity tectonics. This allows us to discuss the rheology of the mélange and its sedimentary cover. The ophiolitic series composed of mantle and crustal sequences mostly represented by pillow lavas and radiolarite were thrust and uplifted to the surface during the obduction. Good outcrops show massive pillow deformed by thrusts and the thick radiolarite cover appears detached and sheared on top of it. The unconformable overlying units of either sedimentary mélanges (olistostrome) or Neogene sandstones indicates that this basement has undergone severe erosion and uplift events. In the field, the geometry and the nature of the blocks are strikingly similar to that of the shear zones. The matrix of the mélange cannot be observed in detail but is largely clayey and locally serpentinized as observed by previous authors. Many isolated blocks of serpentinite, gabbro and peridotite are involved in this unit. We think that the blocks of the mélange are olistoliths which are likely to come directly from the ophiolitic rocks. The diapiric mélange including the serpentinite blocks appear to have a source tapped from the sedimentary mélange exhumed as chaotic rock unit adjacent folds of late Neogene sandstones. We interpret the presence of the mélange as a diapiric injection facilitated by faults affecting the sandstone cover. This suggests that the injected material is poorly plastic and can be easily remobilized, triggering the activation of normal faults, where the mélange become unstable and interrupt the overlying strata to the surface. Some of the strata deformed in rounded folds, and shaped the so-called “circular basins”. Muddy mélange and Circular features also appear in other places like the Sandakan Basin in East Sabah and Brunei. Deformation process of the overlying strata may be similar to the one which creates the circular feature of Kudat Peninsula. Therefore, we suspect that the gravity tectonics is dominant in northern Borneo during late Miocene and Pliocene, surrounding the Mount Kinabalu which is a magmatic intrusion during Late Miocene, well within the post-rift period of the South China Sea.

CHAPTER 5. Late Miocene vertical movements; Slab detachment and plumes consequence

We have seen that the extension in the SCS margin was prolonged until the end of the Middle Miocene, possibly due to the propagator effect and the delay between mantle and crust breakup. Starting from this time (circa 16Ma), the SCS terminated mostly the significant extension and underwent thermal subsidence with vertical motion showing typically draping strata covering the syn-rift successions. At the same time an important magmatism took place in the oceanic crust as well as on the stretched continental crust, which post-date the rifting and the spreading. The magmatism caused opposite vertical movement uplift and pierced the basement as well as the draping strata. This is specific to the SCS and has to be discussed on the grounds of maps distribution, assisted by seismic lines in order to highlight the relationship between tectonic processes during the post-spreading period.

5.1 Post-rift thermal subsidence

During seafloor spreading, the thermal cooling results in the oceanic lithosphere to subside in order to reach isostatic equilibrium through time. Since the 1970s, theoretical cooling models of the ocean floor have been proposed in theoretical and empirical equations in the relationship between the age, the depth or the heat flow of oceanic floor (Parsons and Sclater, 1977; Stein and Stein, 1992, 1993; Hillier and Watts, 2005; Crosby et al., 2006; Korenaga and Korenaga, 2008; Crosby and McKenzie, 2009; Hasterok, 2013). Therefore the water depth tends to deepen toward the older crust due to the longer period for cooling.

The extended lithosphere also subsides during the post-rifting period. The amount of thermal subsidence can be estimated by a widely-used uniform lithosphere-stretching models to calculate the theoretical water depth (McKenzie, 1978; Jarvis and McKenzie, 1980). However, several marginal seas are ill-constrained influenced by the neighboring tectonic processes, for instance, subduction or collision-related deformation and therefore, the indicators are not adequate for seas influenced by the adjacent tectonic stress such as marginal seas.

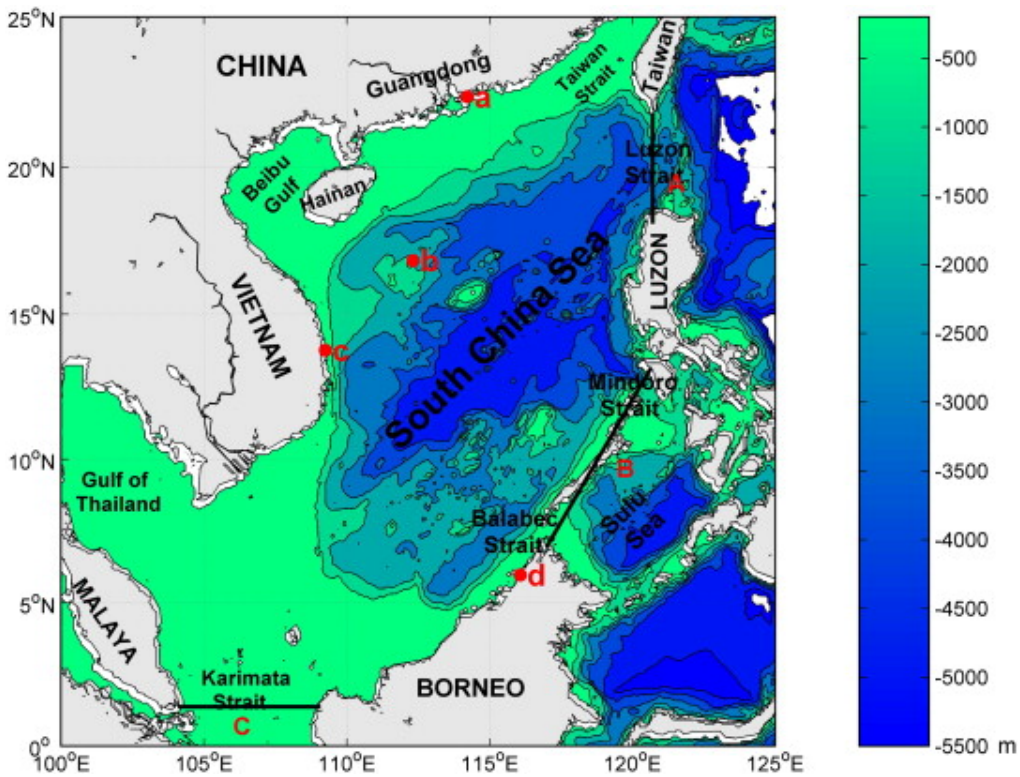

Figure 5- 1. Bathymetry of the South China Sea (Cheng and Qi, 2007). The deepest water depth appears localized on the southwest margin, where the oceanic crust is youngest. This is not a usual trend for the lithospheric cooling on the oceanic domain, suggesting the SCS experienced other tectonic factors impacting the subsidence history.

In the South China Sea, bathymetry shows deeper water depth delineated by the contour of 4000-meter water depth at the center toward the ancient mid-ocean ridge, especially in the Southwest Sub-Basin (dark blue on Figure 5- 1). Therefore, a colder oceanic crust has been suggested in the thermal history with brittle faulting on the oceanic formation (Ding et al., 2016; Yu et al., 2018a). Yet, the geothermal measurements in the South China Sea commonly indicate that this marginal sea has warmer flow, possibly due to the thermal structure inherited from the back-arc extension (Li et al., 2015; Hu et al., 2019).

The rifted basins on the continental crust also underwent abnormal thermal subsidence during post-rift period. During the cooling period, the depositional environment followed strong subsidence in the deep-sea ocean as well as in the rifted basins. The peculiar rapid subsidence is revealed by back-strip techniques in several basins, suggesting rapid subsidence related to tectonic events during post-rift time (Figure 5- 2) (Lin et al., 2003; Clift and Sun, 2006; Xie et al., 2006; Ding et al., 2014; Li et al., 2014b; Xie et al., 2014; Clift et al., 2015; Cao et al., 2017;

Shi et al., 2017; Tang et al., 2017; Zhao et al., 2018b), and appears to be actually delayed by a few million years after breakup, around 10 to 5 Ma (Li et al. (2014b) and reference therein).

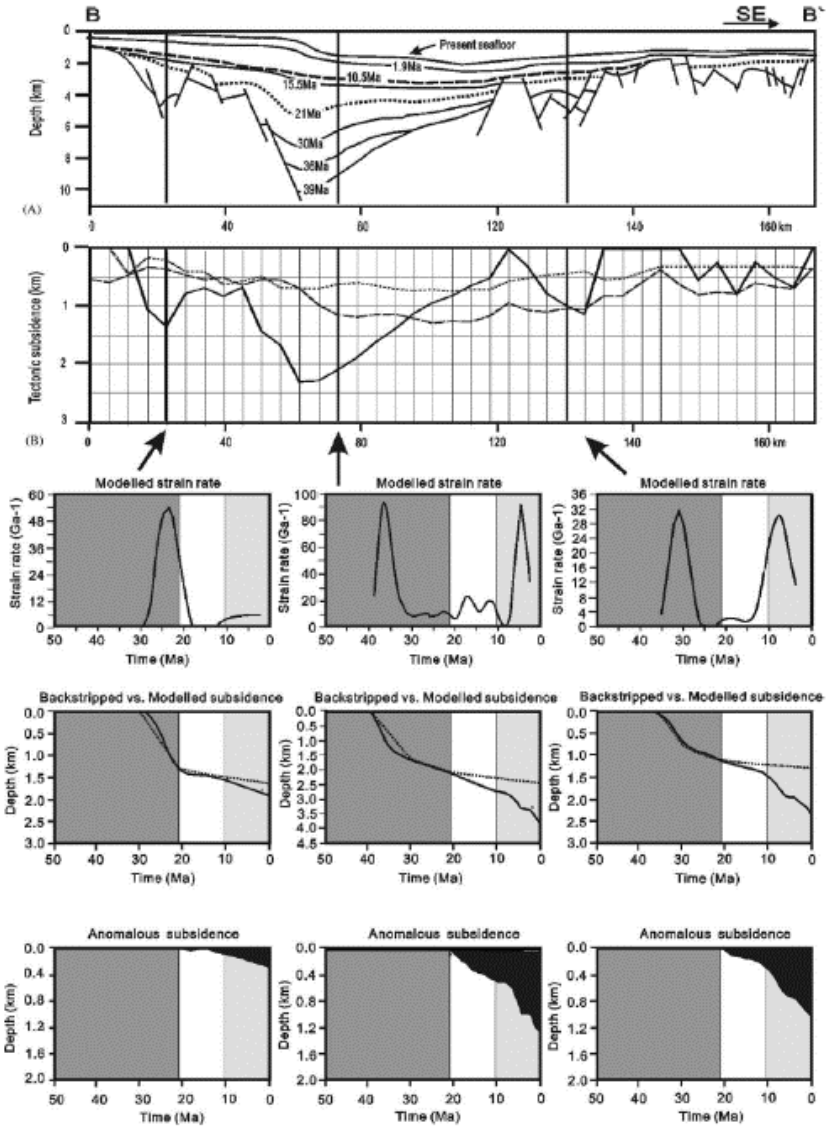

Figure 5- 2. Qiongdongnan Basin subsidence history through the syn- to post-rift period (Xie et al., 2006). The difference between backstripped and modelled subsidence demonstrates the abnormal subsidence in the South China Sea, particularly during the post-rift period initiating between 18Ma and 10Ma and becoming very strong after 10Ma (see bottom examples). Dark grey is the rift stage, and light grey is the regional subsidence stage.

5.2 Post-spreading magmatism in the SCS

At the same time, an extensive and widespread post-spreading magmatism has been mentioned in literature of the past decade in the Pearl River Mouth Basin (Yan et al., 2006; Zhao et al.,

2016; Fan et al., 2017a; Xia et al., 2018), the Qiongdongnan Basin (Gao et al., 2019), the Phu Khanh Basin (Savva et al., 2013; Vu et al., 2017), the Xisha Trough (Lei and Ren, 2016; Gao et al., 2019), the Nam Con Son Basin (Li et al., 2014b), the central basins (Jiang et al., 2018; Zhao et al., 2018a; Yang et al., 2019; Zheng et al., 2019), the Dangerous Grounds (Chang et al., 2017), the offshore Palawan (Franke et al., 2011), and the Borneo-Palawan Trough (Franke et al., 2008). The seismic images illustrate extrusive features; either buried volcanic bodies with thin sediment layer or conical shape situated at the seafloor (Chang et al. (2017); Figure 5- 3). Intrusive bodies also appear as sills within the sedimentary basins with fluid or gas escape features occurred upon the intrusion (Figure 5- 3) (Gao et al., 2019).

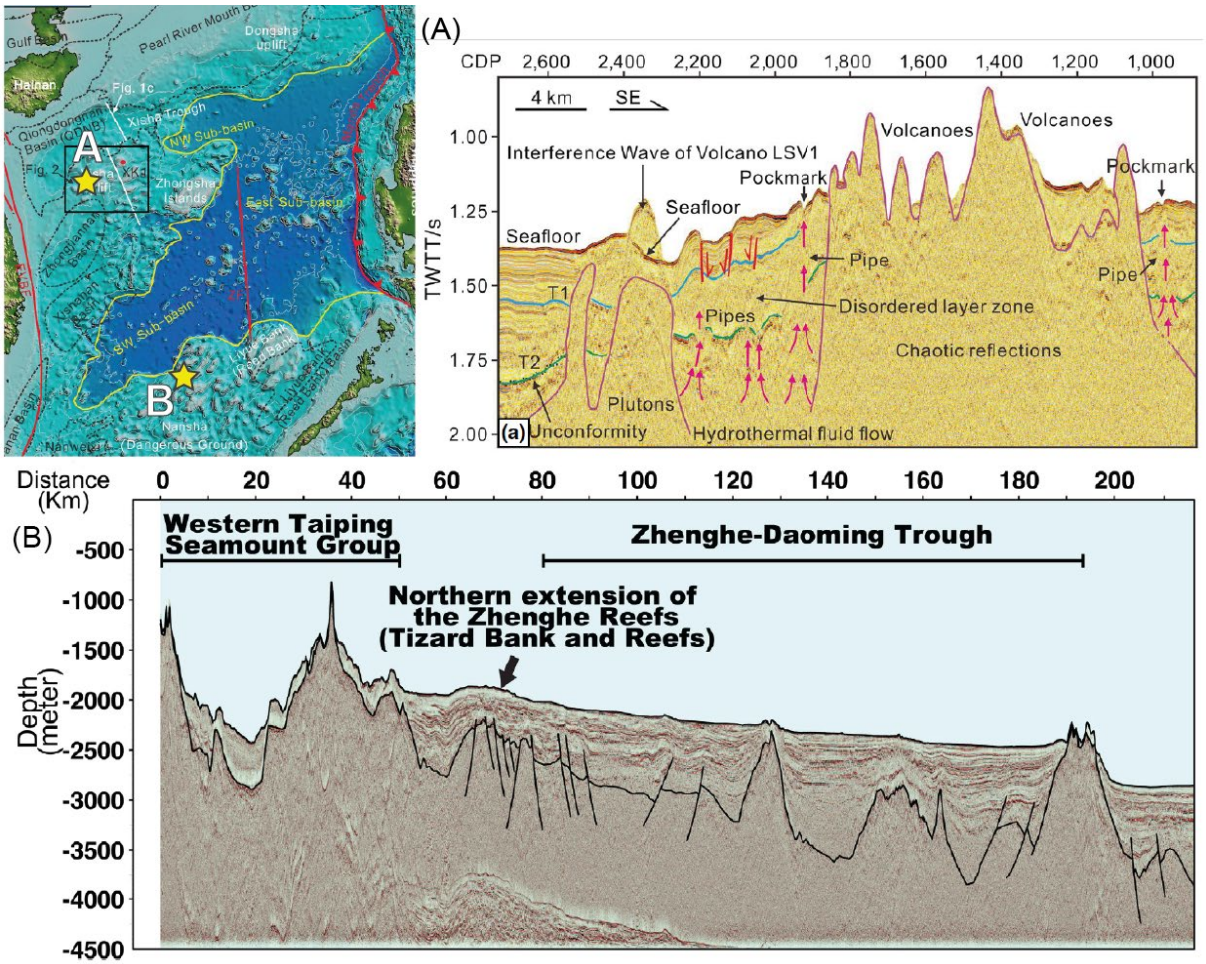

Figure 5- 3. Extrusive volcanic and intrusive features in the seismic images in Xisha Islands and Dangerous Ground (Chang et al., 2017; Gao et al., 2019). The geometry of extrusive bodies protrudes to the seafloor overlain by thin sediment carpet around the apron or without sediment around the center.

Geochronological studies on volcanic and intrusive samples were performed on the scattered ages in the South China Sea from Late Miocene to less than 1 Ma, indicating magmatic activity occurred mainly during the post-spreading period (Hui et al. (2016) and reference therein). Geochemistry shows that the whole rock composition displays a higher K2O-Na2O (likely the OIB-type basalt; alkali basalt) than normal MORB-type basalt (Jiang et al., 2018; Yang et al., 2019; Zheng et al., 2019). The Sr–Nd–Pb–Hf isotopic compositions indicate a magma source derived from the upper mantle, and later mixed with three components through the magma path, namely MORBs, lower continental crust, and oceanic island basalts (Zheng et al., 2019). The crystallization temperature reaches to ca. 1300 degree, which is considerably higher than the normal mid-ocean ridge origin but comparable to the OIB (Oceanic Island Basalt) basalts (Yang et al., 2019).

However, the relationship between the subsidence in post-rift succession and the coeval uplifts from magmatic intrusions during post-spreading time in terms of opposite vertical movement is still unclear. In addition, the thermal state during the formation of the oceanic crust has also been a matter of conflicts in the literature. This chapter focuses on the tectono-stratigraphic point of view to illustrate a layer deposited mainly hemipelagic sediments during the thermal subsidence stage and intrusive bodies to identify the relation in the southwestern SCS margin (Figure 5- 4).

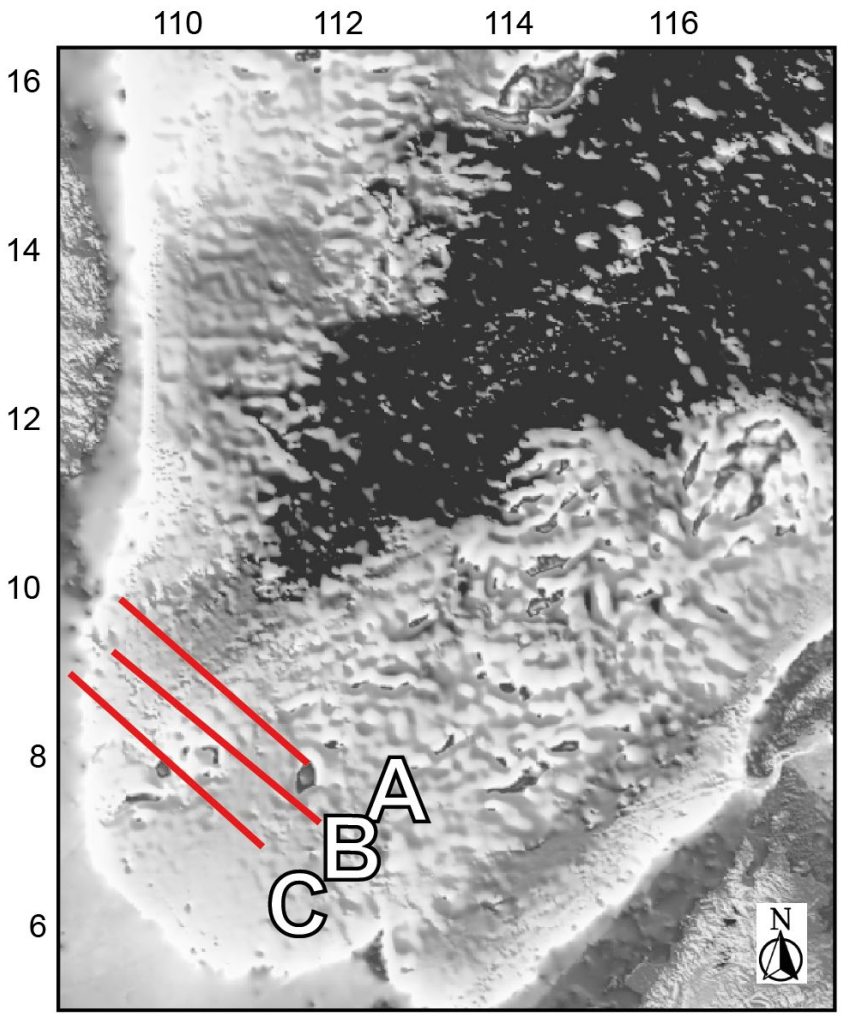

Figure 5- 4. Location map of MCS data, near the tip of the oceanic propagator in the area where subsidence is strong and reflected by a highly sedimented graben. Red dots are for the ODP/IODP locations. Profiles are modified from the GRI report (Pubellier et al., 2014, unpublished) and literature (Franke et al., 2014; Savva et al., 2014; Clerc et al., 2018).

5.3 Thermal subsidence post-rift succession

Thermal subsidence is characterized classically by coherent seismic facies in the homogenous thickness without significant faulting (Figure 5- 5 and Figure 5- 6). In the SCS, the post-rift subsidence layer covers the syn-rift I and II as well as the rifting features near the center of ancient mid-ocean ridge (Figure 5- 6 and Figure 5- 7). Bio-stratigraphic results suggest the base of the thermal subsidence is around 16 Ma based on the industrial wells (Figure 5- 6). Therefore, subsidence initiated just after the termination of the seafloor spreading, consistent with the fading of normal faulting in Southwest SCS (Li et al., 2014b; Vu et al., 2017). The deposition draped the morphology and displays parallel-deposits on the surface. This is recognized along most seismic profiles (Figure 5- 5).

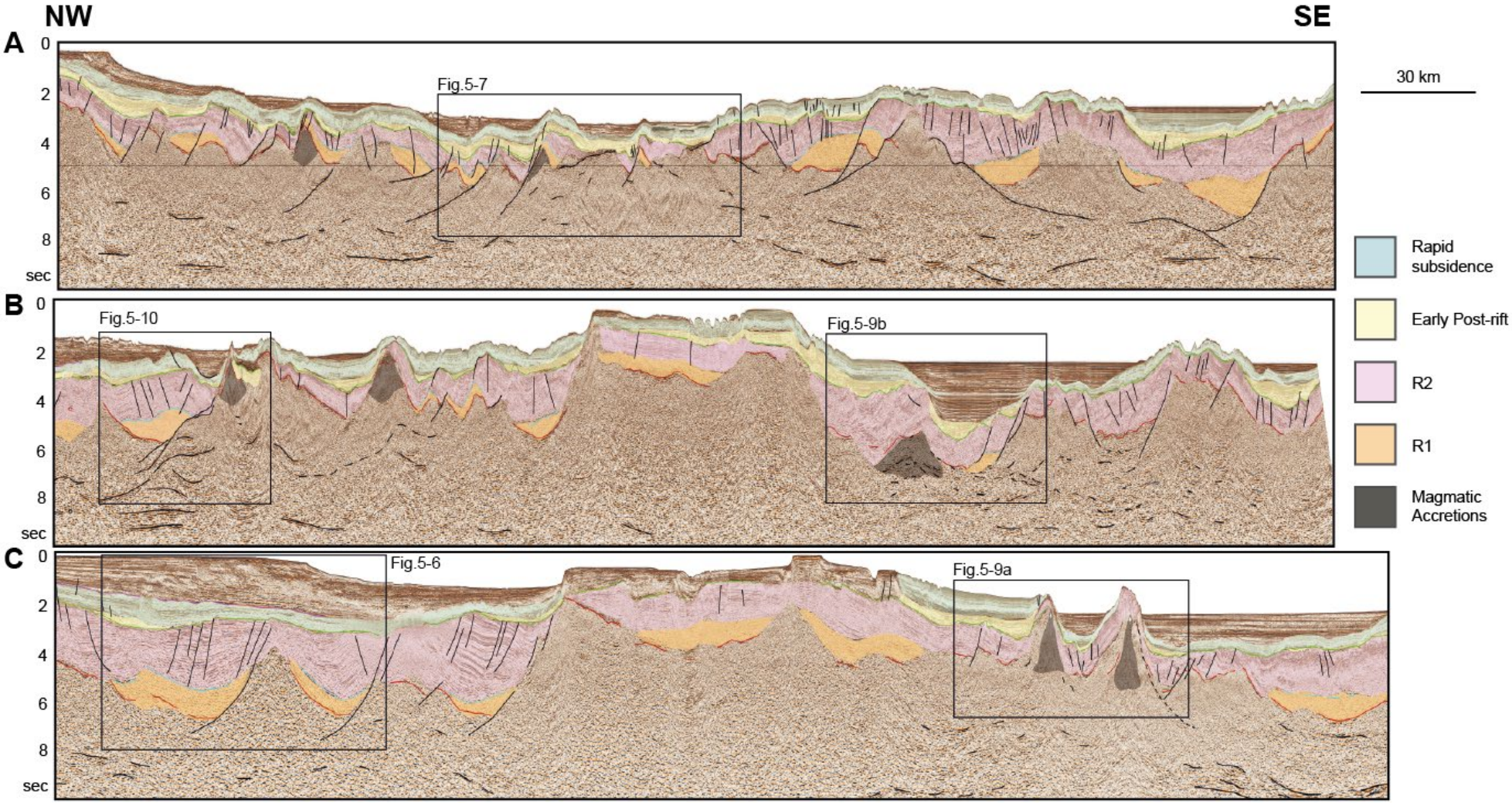

Figure 5- 5. Interpretation of seismic profiles in the Southwest SCS margin. The post-rift subsidence layer (white shade) may be traced in the entire region.

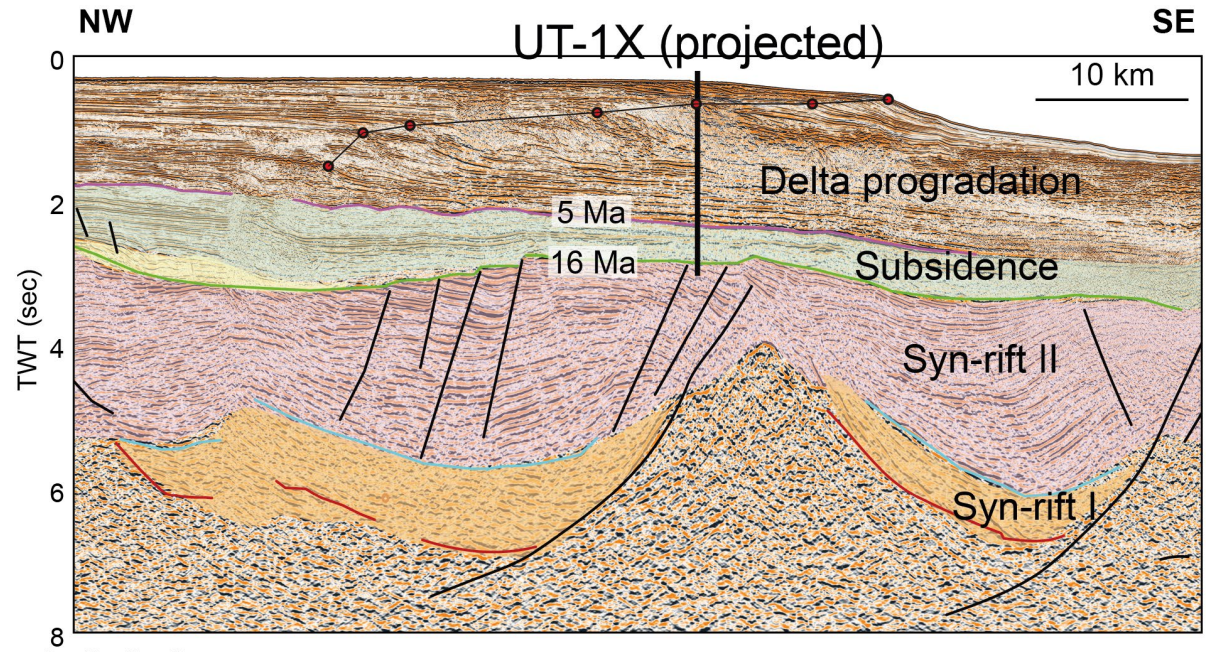

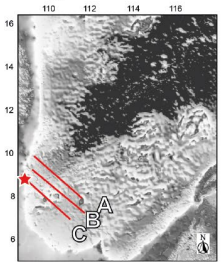

Figure 5- 6. The seismic stratigraphy interpretation of Nam Con Son Basin in the Southwest SCS margin with one industrial well offering bio-stratigraphic ages. The main horizons are represented with the major sedimentary periods of time. Note the delta progradation showing the adaptation of the shelf to the subdsidence.

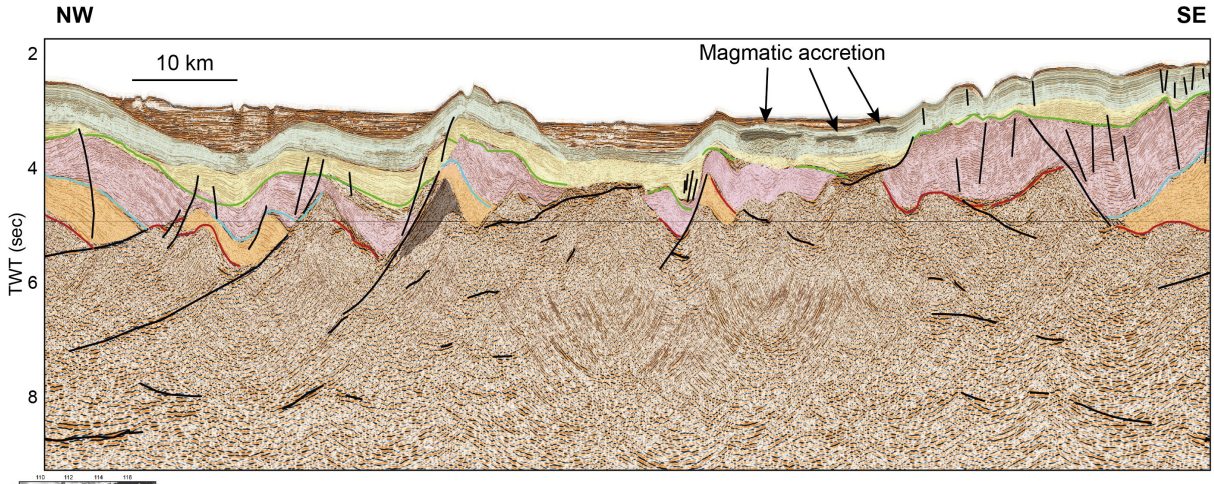

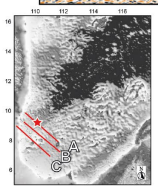

Figure 5- 7. Post-rift subsidence layer overlays the ancient mid-ocean ridge extending from the tip of the oceanic crust.

The depositional environment from the well records shows facies deepening-upward sequences until the hemipelagic environment above (Madon et al. (2013); Figure 5- 8). The unconformity, named EMU in Madon et al. (2013), exhibits hiatus by erosion since Early Miocene and is overlain by deep-sea deposits along a traceable horizon at ca. 10Ma (Madon et al., 2013). It is comparable to the unconformity recorded in the ODP wells (Nathan and Leckie, 2003), with show that subsidence resumed to reach the present water depth during post-spreading time.

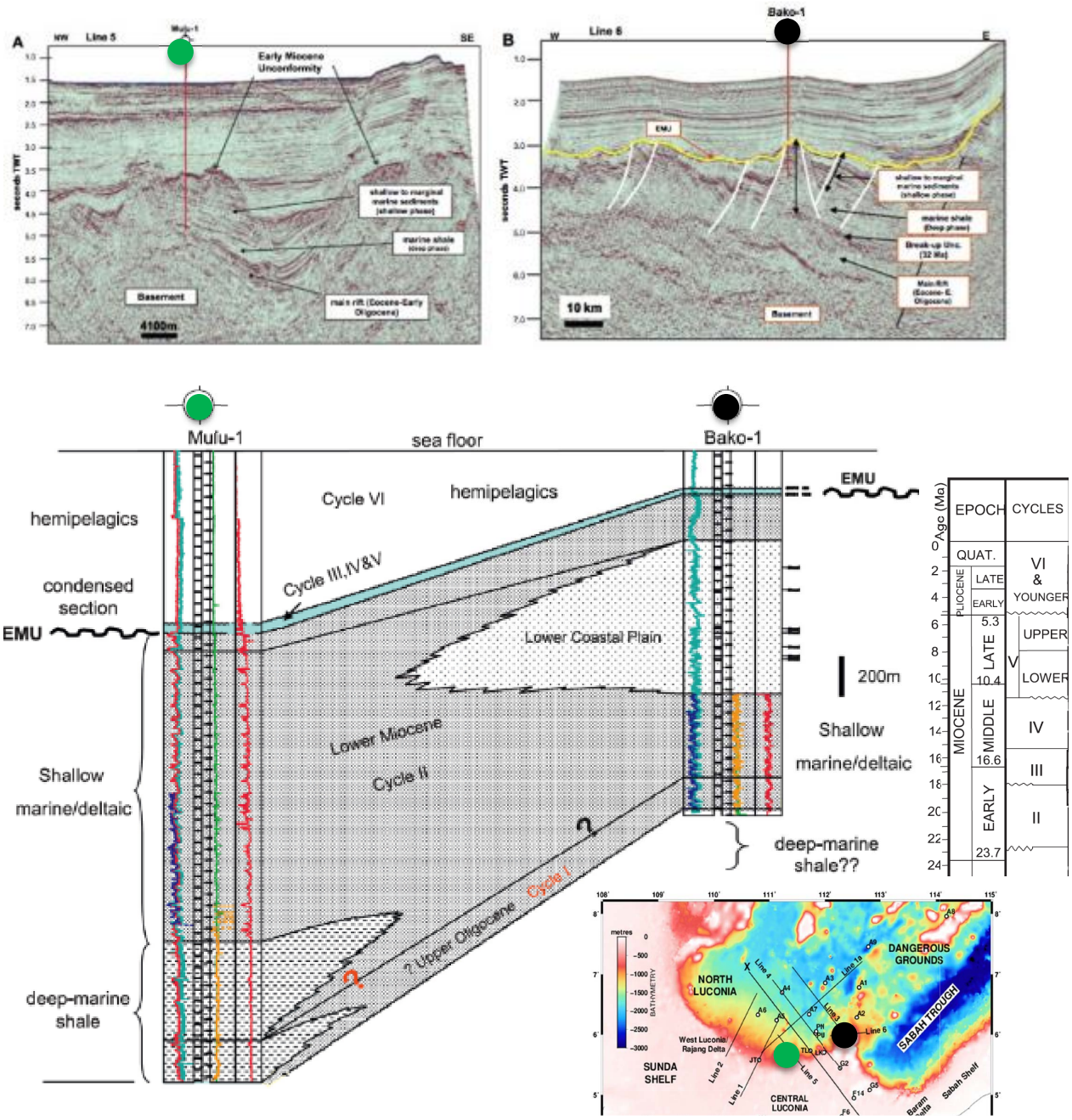

Figure 5- 8. Bio-stratigraphy results in the southern SCS margin (Madon et al., 2013) showing the thickening of the series toward the West and in the Miocene section.

In the Dangerous Grounds, the termination of the subsidence is not straightforward; being indicated by thin cover of sediments with a slow depositional rate. The deep sea basins fringing the coast received considerable amount of sediments from the Vietnam landmass. The subsequent propagating delta sedimentation overlaid the subsidence sequence, indicating a decrease of the thermal subsidence (Figure 5- 6). Delta deposits initiated at ca. 5 Ma as dated from the well, in the Nam Con Son basin. The shelf edge trajectory within the delta sedimentation shows the shelf edge aggraded by the beginning of the delta deposition, keeping in mind the onset of sea-level drop which is of minor important (Figure 5- 6). This may represent the accommodation space created persistently by the subsidence. The subsequent progradation delta package appeared after a few million years, as suggested by the similar sea level fluctuation in other rifted basins (Zhuo et al., 2018).

5.4 Post-spreading uplifts and intrusions

I observe uplift features occasionally interrupting the continuity of the post-rift subsidence layer on seismic images in Southwest SCS. Basement high protrude above the seafloor (Figure 5- 9 and Figure 5- 10). The uplifts accompany occasionally magmatism illustrated by strong reflectors (Figure 5- 10). The intrusions distribute generally on Figure 5- 10 kilometers-width intervals, and there, intra-crust reflectors appear within the crust. The intrusions underlay sedimentary strata which tilt toward the adjacent basins (Figure 5- 9). They may slide along the interface between basement and sediments (Figure 5- 10). These layers include the former pre- and syn-rift sedimentation and the lower part of the post-rift successions (green on Figure 5- 9 and Figure 5- 10). The subsequent sedimentation onlaps the tilted strata and the top of the uplifted center with an angular unconformity.

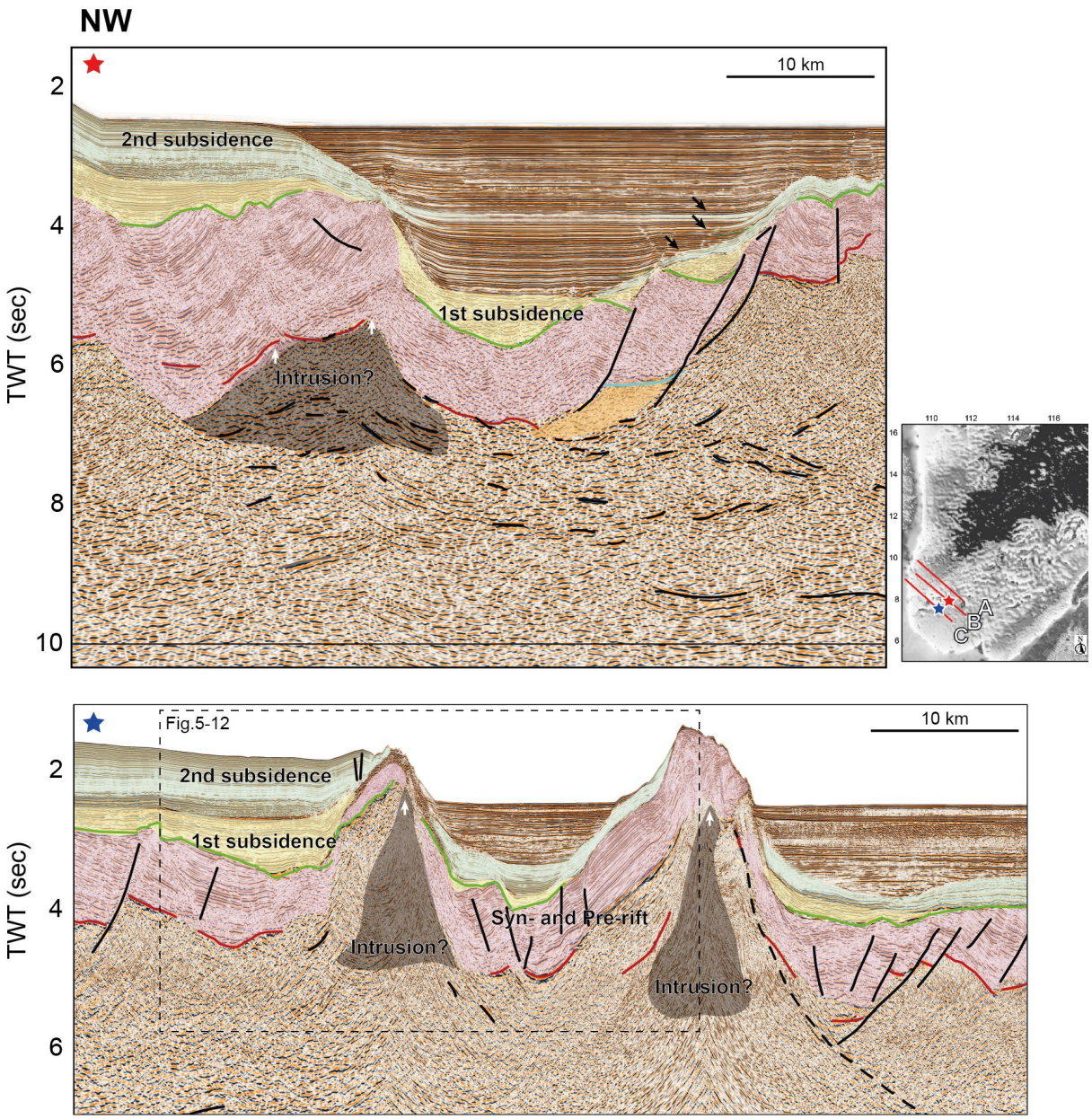

Figure 5- 9. Magmatic intrusions pierced the overlying strata interrupting the 1st subsidence. The 2nd subsidence continued after the intrusive events.

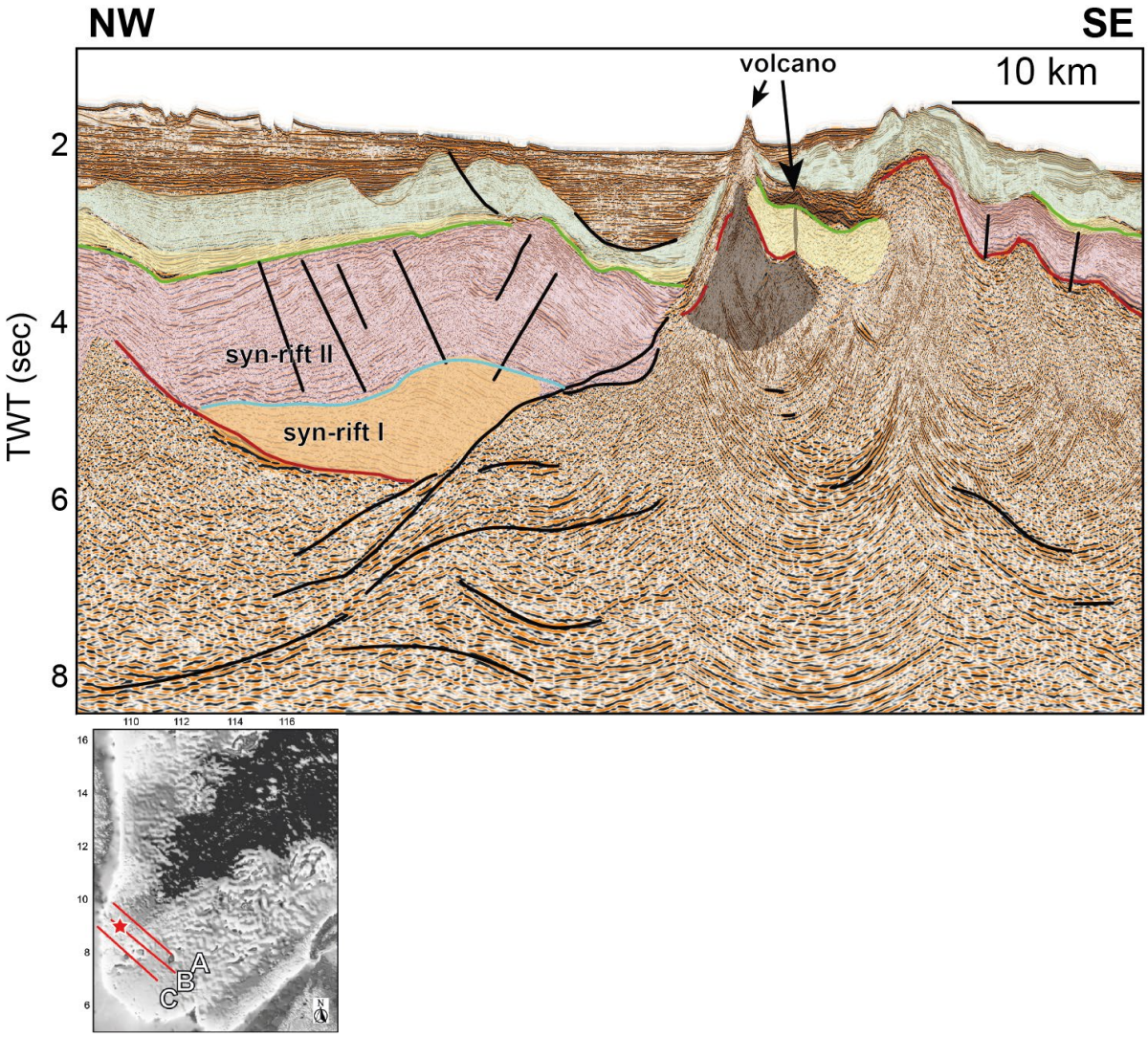

Figure 5- 10. Magmatic intrusions pierced the overlying strata and preexisting syn-rift I and II slide along the intrusion.

Although same profiles have been interpreted by other authors as witnessing the rifting process with offset of the basement (Franke et al., 2014; Savva et al., 2014; Clerc et al., 2018); it seems difficult to rise in excess the seafloor basement via normal faulting in rifting context (Figure 5-9). Instead, normal offset may happen along the sliding surface due to the intrusions uplifts (Figure 5- 10). Therefore, I re-interpreted the profiles from Franke et al. (2014), Savva et al. (2014) and Clerc et al. (2018) under the angle of post-spreading magmatism. This similar post-rift features can also apply to the adjacent rifted basins (Figure 5- 11).

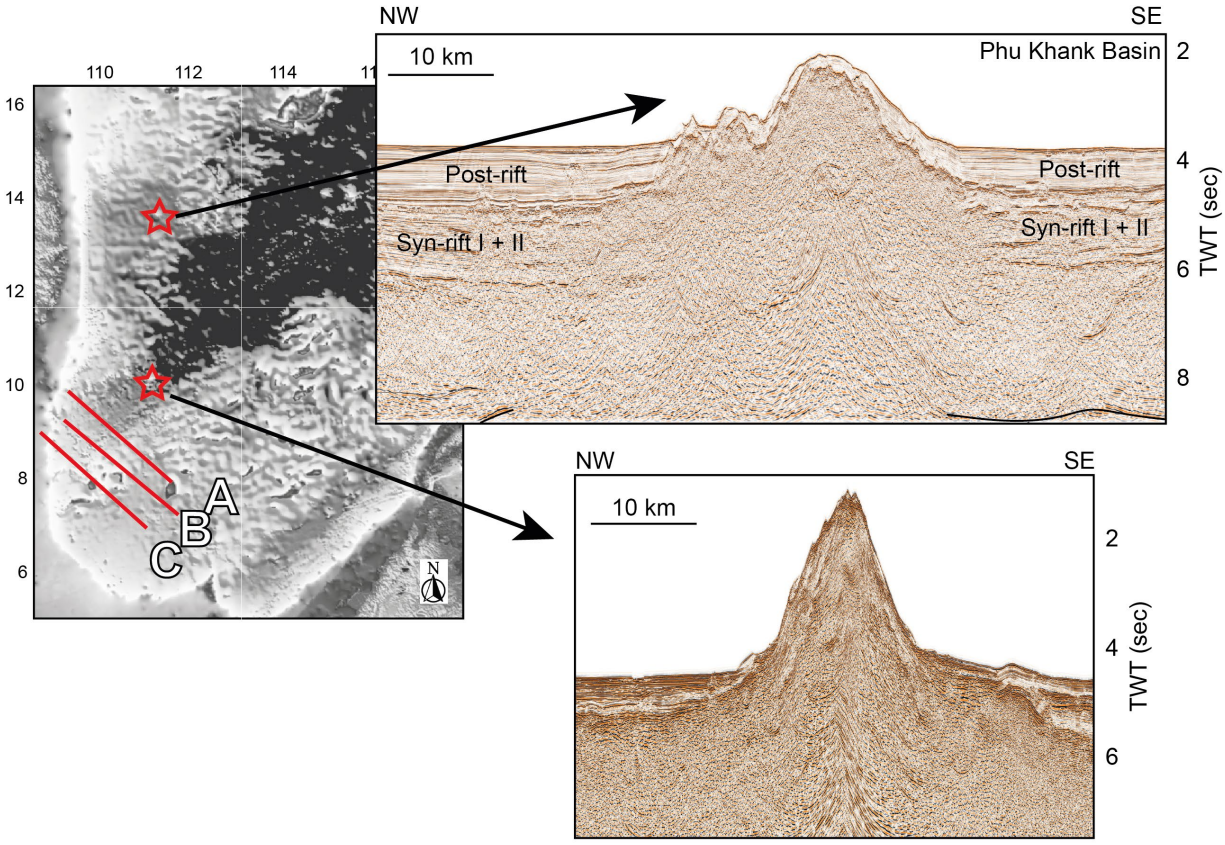

Figure 5- 11. Other magmatic events in the South China Sea, showing the distinct basement high protruding to the seafloor and recognizable from the bathymetry in few tens kilometer diameter.

The time span covered by the intrusions is determined approximately using the unconformity between the tilted strata and the overlying strata. Due to a moderate erosion restricted to the top of the uplifted center, sediment packages related to this uplift deposited along the side of the intrusive bodies (Figure 5- 12). The seismic facies display a chaotic texture linked to mass transport deposits (MTD on Figure 5- 12). Although no bio-stratigraphy data is available to assign a precise age, the approximate period of deposition is estimated by post-spreading time, maybe related to the distinct unconformity marking the base of the deep-sea deposits of the neighboring basins. The unconformity is composed of a condensed section and followed by hemiplegic deposits around 10 Ma from well records (Figure 5- 8) (Nathan and Leckie, 2003; Madon et al., 2013).

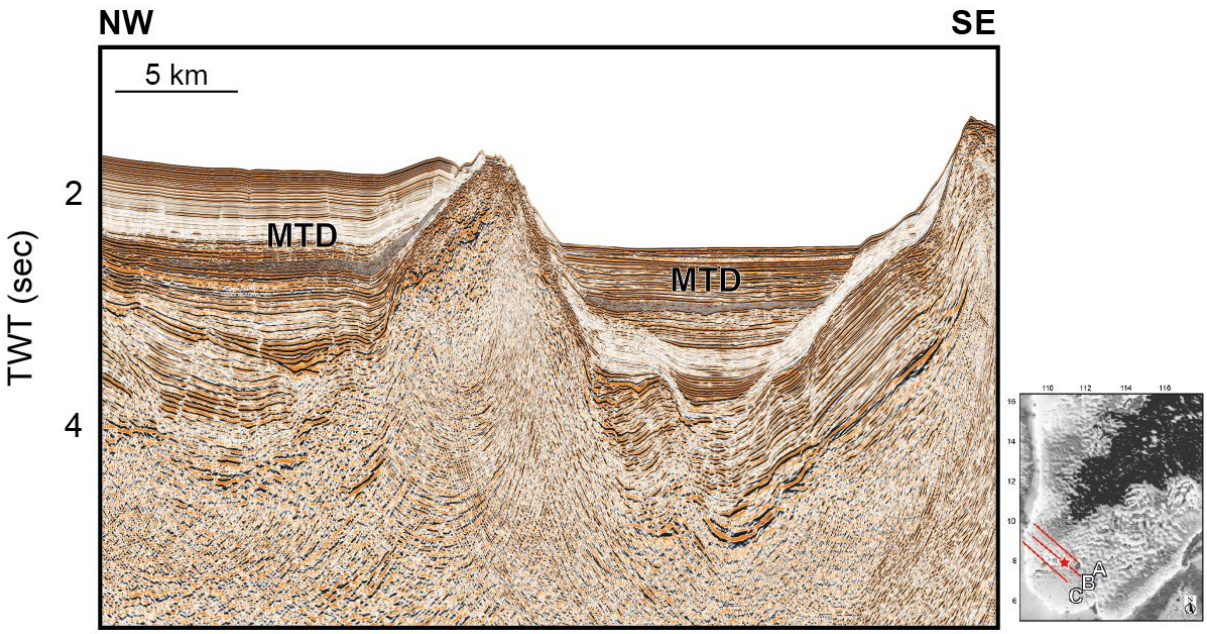

Figure 5- 12. Mass transport deposits (MTD) appear in the adjacent low place of intrusions. This suggests the timing of intrusions and the material from the eroded basement high.

Interestingly, deep seismic images commonly evidence several reflectors situated beneath the Moho in the southwestern margins. These usually accompany magmatic intrusions characterized by their strong amplitude at shallow depth (Figure 5- 13). These intrusions show that the magma tends to follow the inherited faults as conduits in the rifting basins, and fractured cracks offered the pathway for the volcanic material. Intrusions are therefore of relatively small size (10 km). Gas/fluid signatures appear in the vicinity of magmatic signature (Lei and Ren, 2016; Fan et al., 2017a). This supplies a possible scenario of intrusions including the source, the pathways, and the final magmatic production, although more detailed geophysical analyses are further needed (velocity, rheology, etc.) to validate this conclusion.

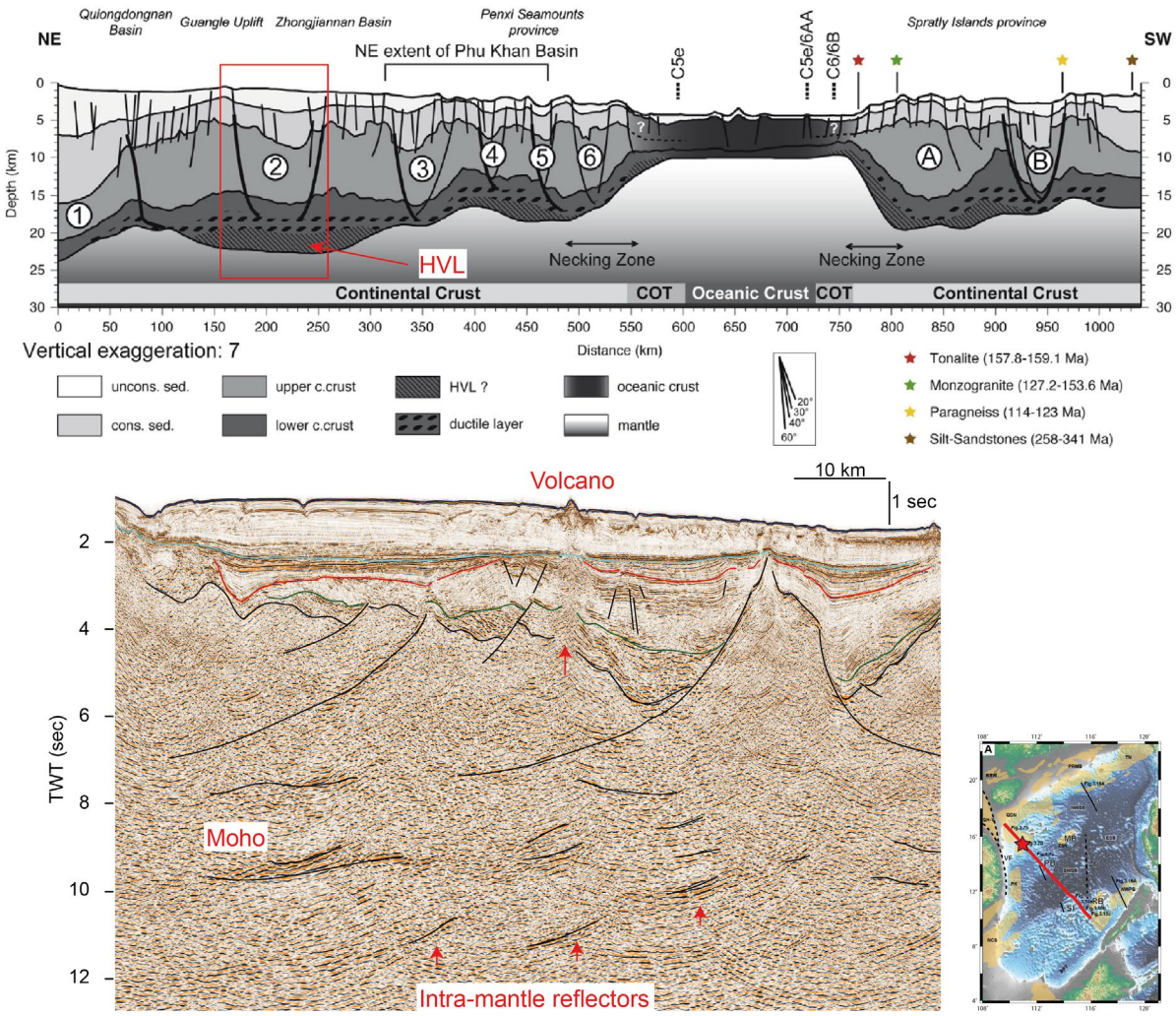

Figure 5- 13. High Velocity Layer (HVL) along the southwest SCS margins modified from Pichot et al. (2014). The location is shown by the red solid line. The same depth appears strong amplitude reflectors beneath Moho reflectors on the MCS profile. The volcanic magmatism is located above the intra-mantle reflectors and also near the thinnest continental crust.

5.5 Discussion and conclusion

To conclude, coeval regional thermal-subsidence and magmatic intrusions prevailed on proper tectonic processes during the post-spreading period. Their relationship however shows that the intrusions were actually local incursions within a continuous subsidence sporadically in 10-km diameter, thus illustrating an episodic subsidence in the southwestern SCS. This suggests that the subsidence was influenced by others tectonic events rather than being dominated by a single event of thermal subsidence during the post-spreading period.

The geochemical analysis suggests a magma sources mixed among the upper mantle, the lower continental crust, and OIB-oriented signature. The seismic reflection images also suggest a magma-fed pathway from beneath the continental crust and through the existed faulting fracture to the surface. The intrusions may originate from the deep mantle. Furthermore, many papers have mentioned and reviewed the observation of a High-Velocity Layer (HVL or HVDLC, (Wei et al., 2011; McIntosh et al., 2014; Chang et al., 2017)) in the northern margin, and a few in the southern margin (Figure 5- 13) (Pichot et al., 2014; Gao et al., 2015; Chang et al., 2017; Lei et al., 2019b).

The source is probably located in the deep mantle and offers ages around 10 Ma (consistent with the tectono-stratigraphy studies), which are represented by OIB-liked basalts. However, at the same time, volcanic series in Borneo and Palawan are produced (Cottam et al., 2010; Padrones et al., 2017; Breitfeld et al., 2019) in the Neogene. The further discussion attempts to propose the possibility of a genetic mechanism, associated with the geodynamic evolution of subduction and is presented the next chapter (Chapter 6).

Chapter 6. Discussion

In the past three chapters, I have described the structures and attempted to establish a correlation of the tectonic events reflecting specific particular geological processes in the respective passive and active margins of the SCS basin, and also in the islands of Borneo and Palawan during the Neogene and part of the Paleogene. This chapter will firstly recall the main observations of this study and discriminate the tectonic evolution into three stages. In addition, this compilation also integrates other geological observations of diverse aspects in order to explore the relevance of the main tectonic processes which occurred in this area during Cenozoic times. This tentative approach offers further opportunity to establish a universal framework of divergent margins induced by the boundary force of an adjacent subduction.

6.1 Introduction: recalling the main relevant observations in the SCS and Borneo

Chapter 3 described the structure of the SCS Margin in terms of crustal structures, faults geometry, and basin evolution. One of the striking results is around the importance of detachment faults. These features played an important role in thinning the upper continental crust, and they merged at depth to the top of the ductile lower crust in most places. They also created an accommodation space sufficient to allow the deposition of a relatively homogenous thickness of upper syn-rift (syn-rift II, R2) succession, and emphasize the horizontal faulting movement compared to the vertical one. The basins formed a series of pull-apart basins with a rhombic-shape located at the COT of the southwestern margins. Finally, with the breakup starts a period marked by magmatic intrusions and rapid formation of the oceanic floor. Although a development through the now classical stretching, thinning, and breakup stages appears to rule the SCS margin formation, we concluded to a diachronous evolution in space and time along the different basins. This study identifies three main unconformities, namely the rift-onset unconformity (ROU), the intra-rift unconformity (IRU), and the breakup unconformity (BU), which illustrate the diachronism among each southwestward-younging unconformities. Interestingly, the breakup period in the southwest margin exhibits a change of extensional direction from an E-W orientation of the COT alignment to a NE-SW orientation of magnetic anomalies in the oceanic crust. This counterclockwise modification appeared progressively since c. 23 Ma based on the magnetic anomaly and bathymetry studies, and is described in the evolution of the COT configuration in this study.

In the Chapter 4, the striking point focuses on the importance of the behavior of the mobile shale at the shallower level of the accretionary wedge, both in the offshore and the onshore of Sabah (NW Borneo). It is suggested that the onset of the mobile shale initiated due to the loading of the wedge in the latest stage of orogeny. The existing mobile shale inherited from the chaotic sedimentary mélange and was remobilized during the post-orogenic period. This study identifies an unconformity bracketed between these two periods circa 16 Ma according to the offshore seismic data. The geological field survey showed that the material responsible from the origin of the diapirism is actually a fine-grained sedimentary mélange, which later underwent overpressure conditions providing ductile characteristics. The mélange would lead the deformation during the latest stage of orogeny as well as the post-orogenic period. The rheology of the mobile shale also resulted in the overlying strata forming mini-basins or circular basins appearing onshore and offshore. The mapped area covered by these features surround the Mount Kinabalu, suggesting that the magmatic intrusion was caused by a large event; probably the breakoff of subducting slab, and that the subsequent uplift impacted the slope stability to trigger the deformation of the sedimentary mélange.

Chapter 5 compiles the considerable magmatic activities in the SCS margins during the post-spreading period. Several key seismic images show that the uplift goes with important magma production, interestingly within a regional subsidence period. This large global subsidence is anomalous compared to the theoretical thermal subsidence of post-rifting basins. The subsidence after intrusion, hence, occurred as episodic subsiding features. We also discussed an integrated scenario of magma production embedded by subsidence layers in rifted basins and oceanic basins. Therefore, this study proposes tentatively that the opposite vertical movements resulted from a sinking break-off slab, explain the regionally enormous subsidence, and locally initiate magmatic intrusions originated from the deep mantle after slab detachment.

6.2 Correlation of SCS and PSCS

These two margins certainly underwent a contrasting dynamic evolution, however some of key tectonic events are similar in ages, with key periods at 23 Ma and 16 Ma (Figure 6- 1). This study, hence, attempts to correlate these events and establishes an evolution in three stages fitting both margins.

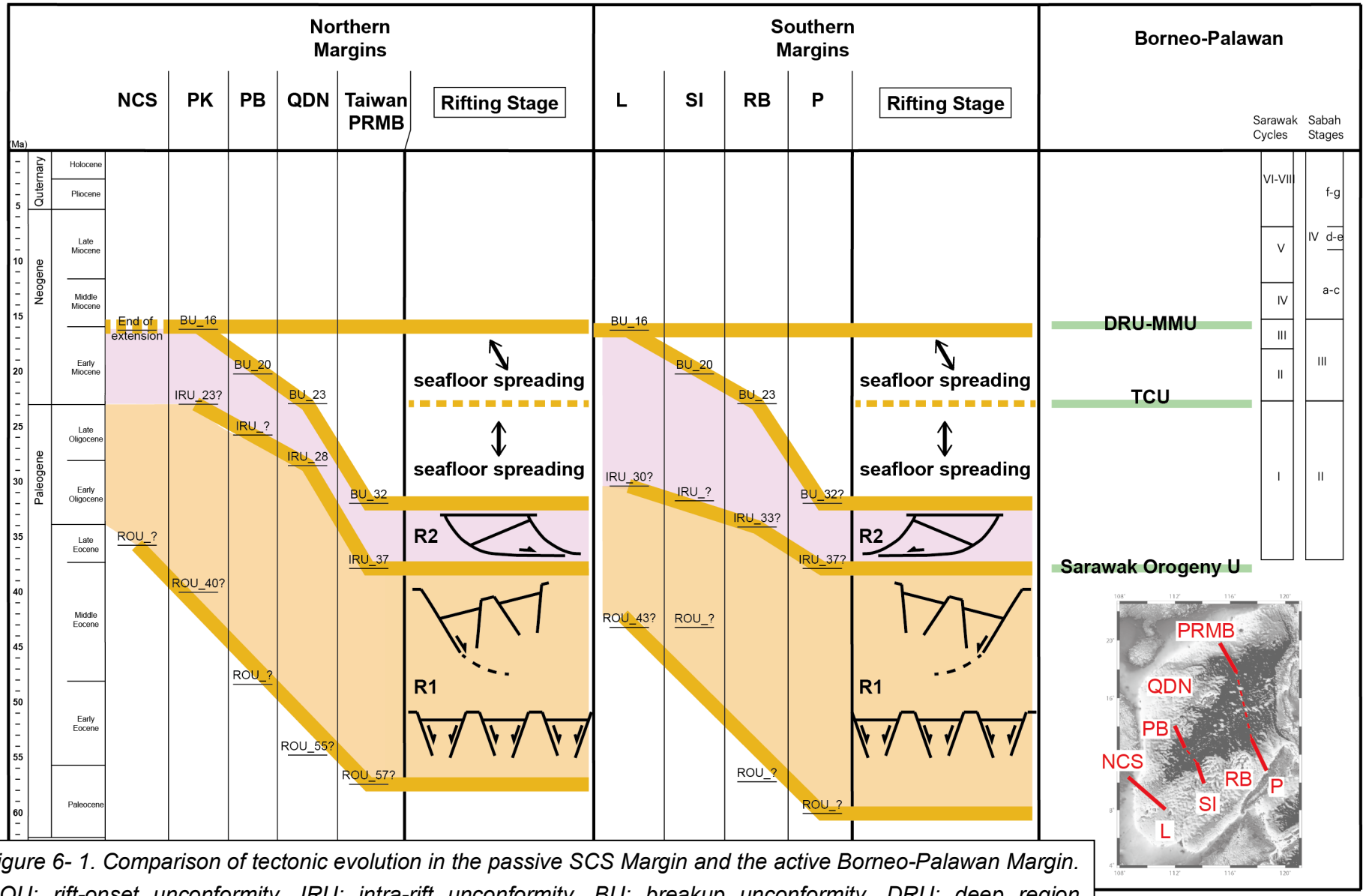

Figure 6- 1. Comparison of tectonic evolution in the passive SCS Margin and the active Borneo-Palawan Margin. ROU: rift-onset unconformity, IRU: intra-rift unconformity, BU: breakup unconformity, DRU: deep region unconformity, MMU: Middle Miocene unconformity, and TCU: top Croker unconformity. See text for more details.

The evolution can be expressed by unconformities on the two margins. In the South China Sea, three main unconformities including the rift-onset unconformity (ROU), the intra-rift unconformity (IRU), and the breakup unconformity (BU) may illustrate simply the diachronism of the rifting process from east to southwest (Figure 6- 1). Rifted basin examples are listed in a chart that includes Taiwan-PRMB (Pearl River Mouth), QDN (Qiongdongnan), PK (Phu Khanh), and NCS (Nam Con Son) from east to west on the northern margin, as well as in the southern margin for the offshore Palawan, Reed Bank, Spratly Islands, and Luconia (Figure 6- 1). Two stages of rifting period (R1 and R2) have been recognized, separated by the IRU. Eventually, both the rifting at the tip of the propagator and the seafloor spreading terminated at 16 Ma.

Similarly, the convergent margin history in Borneo is also marked by some key unconformities which represent different stages of subduction and subsequent collision. The Sarawak Orogeny Unconformity may represent the initiation of subduction, and the top Crocker unconformity (TCU) expressed the transition from subduction to collision (Figure 6- 1). The termination of orogeny is also marked at 16 Ma and slightly diachronous along the subduction zone.

6.2.1 Paleogene: N-S extension and N-S Subduction

Paleocene to Eocene (prior to 37 Ma)

The first stage is known by drilling although poorly dated since Paleocene. This period is actually based on compilation of other observations in the SCS and the Borneo-Palawan area. The context may still be reconstructed in a southward subduction scenario (Figure 6- 2). The initiation of subduction is Paleocene and it developed during Eocene times based on geochronologic and stratigraphic studies although the precise age is still in debate (Tan, 1979; Pieters et al., 1987; Bladon and Supriatna, 1989; Omang and Barber, 1996; Keenan et al., 2016; Hennig-Breitfeld et al., 2019). We have some information from literature concerning the age that a cluster of Paleocene and Eocene volcanism with arc-like magmatic characteristics is located in the Sarawak and Kalimantan (NE Indonesian Borneo) regions (Figure 6- 2). A few samples of metamorphic sole dated at 34 Ma underlay the ophiolite in Palawan, possibly indicating the incipient subduction at a mid-ocean ridge (Keenan et al., 2016). On the stratigraphic aspect, an extensive hiatus reflects the Sarawak Orogeny (or Rajang) Unconformity and is distributed extensively onshore Borneo at c. 37 Ma (Cullen, 2010; Hennig-Breitfeld et al., 2019). An Eocene conglomerate composed by ophiolitic pebbles is also known

in Sabah (Omang and Barber, 1996). This has been interpreted to represent the initiation of subduction.

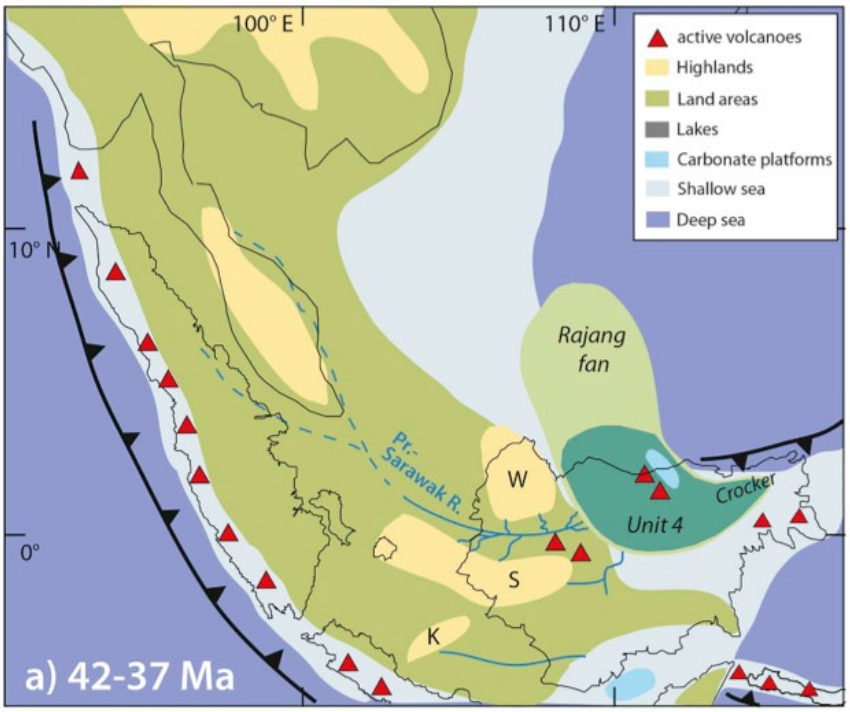

Figure 6- 2. Reconstruction of the Borneo region from Paleocene to Eocene times (Hennig-Breitfeld et al., 2019). Active volcanoes (red triangle) distribute along the Sumatra subduction zone and in Borneo where possibly corresponding to the volcanic arcs above the subduction of PSCS.

Few ages for the magmatism reach down to the Paleocene, which may indicate the beginning of the subduction. Volcanism initiated before 37 Ma and, estimating a slow subduction rate of 1 cm/yr, it may reach around 50 Ma for the slab to reach the adequate P-T conditions around 100 km depth. However, this remains extremely speculative. A diachronism along subduction zone from south toward north may also be responsible for the scattered ages, and it is therefore hazardous to pin point an exact age for the initiation of the subduction.

The post-Yenshanian extensional context of the South China Sea dates back from the late Cretaceous time (Yan et al., 2001a; Lin et al., 2003; Jin et al., 2014) and regionally encompasses the stretched crust inland SE China and the extensional basins in the offshore. The latter basins include, for instance the Penhu Basin in the offshore Taiwan, the Zhu I depression in the PRMB, and the Beibuwan Basin in the south of Hainan Island. These basins allowed us to document the extension period from Upper Cretaceous to Lower Paleocene (Lin et al., 2003; Jin et al.,

2014). This early extension could also be somehow related to the subduction of the PSCS in the south. It is marked by E-W and NE-SW faults (Figure 6- 3), some of which are low angle normal faults (Savva et al., 2014). A relatively similar pattern has been proposed by Ye et al. (2020).

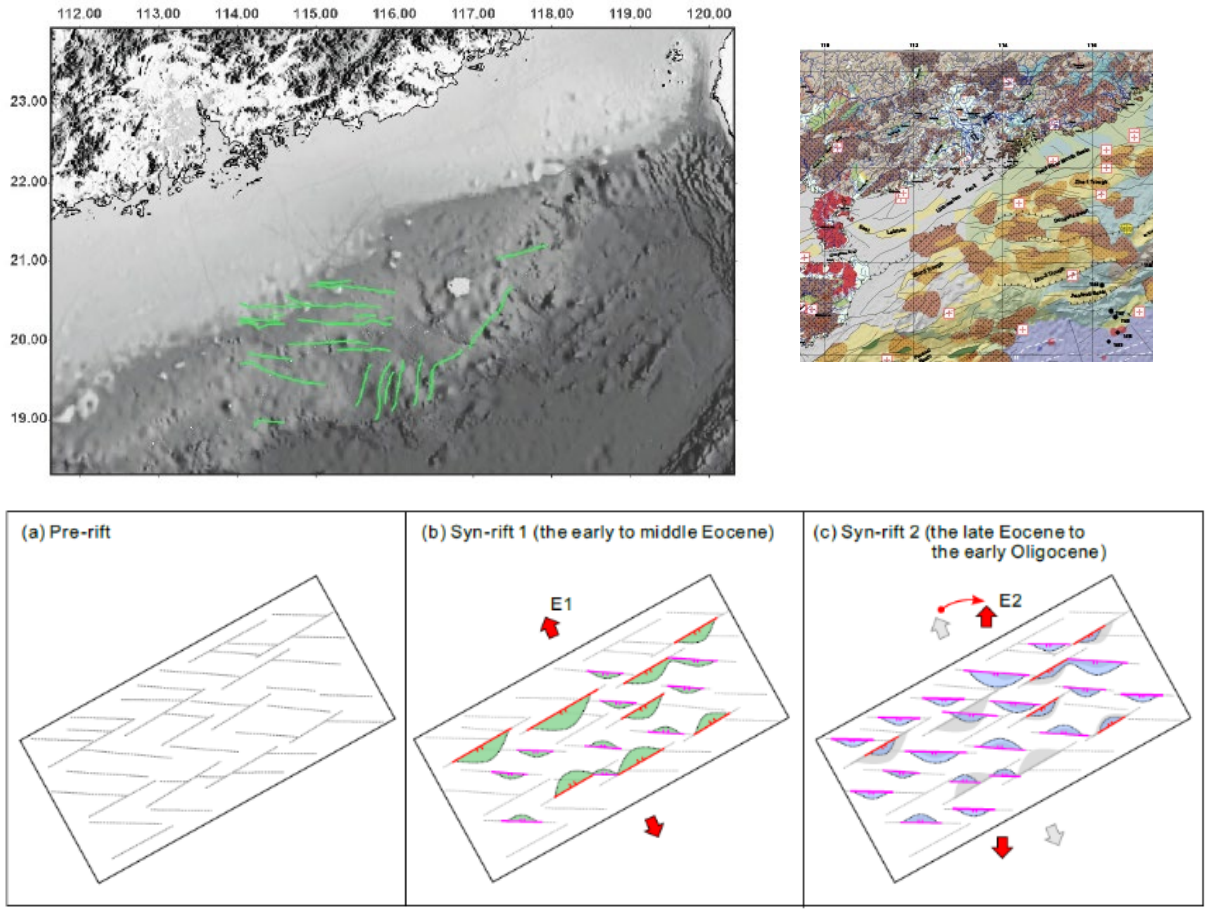

Figure 6- 3. (Upper) Structural map of the northern SCS margin in Late Cretaceous to Paleocene, showing no specific orientation before Early Miocene (Savva, 2013). (Lower) A change of extensional direction between Middle and Late Eocene (Ye et al., 2020).

Therefore, the evolution before 37 Ma is still unclear in the Borneo and Palawan although most literature interpreted it as the result of the evolution of a subduction accretionary wedge. Comprehensive stratigraphy and structural studies are lacking due to the limited outcrops of the tropical rain forests, although a lot of information is available offshore on the shelf from oil-and-gas exploration. On the other hand, the post-Yanshanian orogenic setting involving the Proto South China Sea margins may also have triggered tectonic collapse and the resulting extension may have led to the subsequent rifting and formation of oceanic floor of the SCS in the Tertiary. The PSCS is however relatively old, including Albian bio-stratigraphic ages as

well as Early Cretaceous ages (Tan, 1979; Tan, 1982; Jasin and Geologi, 1992; Jasin and S, 1993; Asis and Jasin, 2012; Jasin and Tongkul, 2013). The transition between the opposite subducting slabs, from west verging during the Cretaceous to East verging in the Tertiary (subduction reversal) is however too long compared to places where such reversal has been documented (Mindanao, Java, or Sumba) where they have proven to happen within a few million years. Therefore, the relation between the two margins of the PSCS and the SCS is still unclear.

Late Eocene (Priabonien) to Late Oligocene (37-23 Ma)

The first stage is characterized by features resulting from concomitant N-S movement in both the convergent and the divergent margins. A series of Eocene rifted basins illustrate an E-W distribution. They include the Zhu II half graben of the Pearl River Mouth Basin and the Qiangdongnan Basin on the northern margin (Lei and Ren, 2016; Zhuo et al., 2018). The outline of the depocenter, which is roughly corresponds to the location of the hyper-extended basins, can be traced along the E-W orientation indicating an N-S extensional direction (Figure 6- 4 and Figure 6- 5). Meanwhile, a coeval age confirmed by the bio-stratigraphy studies (Xie et al., 2019), is also recognized as the initiation of developing detachment faults in the SCS margins. It is worthy noticing that the N-S divergent direction of the rifting is also that of the first stage of the development of oceanic crust in the East Sub-Basin until 23 Ma, based on E-W magnetic anomaly between C11n to C6n (Briais et al., 1993). There is no significant change of direction for the divergence through the rapid breakup process (Larsen et al., 2018; Nirrengarten et al., 2020a).

One of the striking and peculiar aspect of the extension in the SCS, is that during the formation of oceanic floor in the east, several rifted basins developed in the southwestern margin concurrently. Several strike-slip faults aligned sub-parallel or parallel to N-S with horse-tailed features in the end (Figure 6- 6). The extensional stress resulted in a series of E-W pull-apart basins contained laterally by strike-slip faults. For instance, the basin adjacent of Pengxi Bank and Spratly Islands (see the Chapter 3). This scenario has been modelled in numerical simulations suggesting the simultaneous extension contributed a similar orientation in both regions from the tip of spreading (Le Pourhiet et al., 2018).

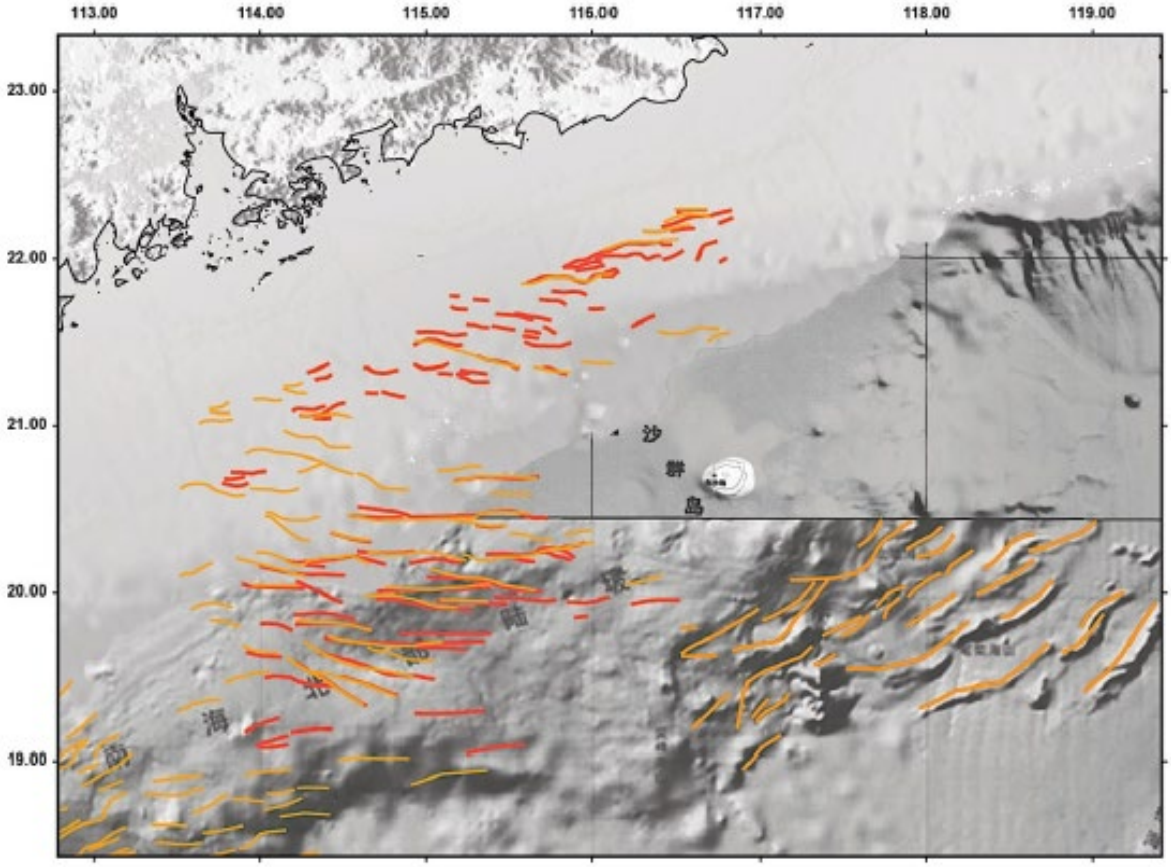

Figure 6- 4. Structural map of the northern SCS margin in Eocene to Oligocene (Savva, 2013). Note the abundance of E-W faults in the Eocene mostly along a strip in the shelf, often reactivated in the Oligocene, and the NE-SW direction in the distal domain

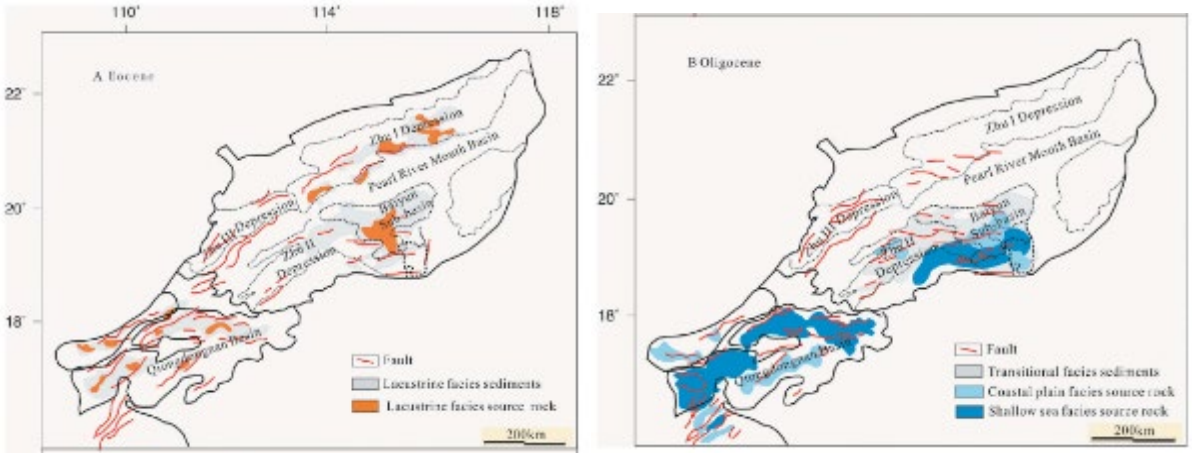

Figure 6- 5. Structural map of the northern SCS margin in Eocene to Oligocene (Zhang et al., 2019c). The Eocene and the Oligocene maps may be segmented into 3 areas dominated by E-W faults.

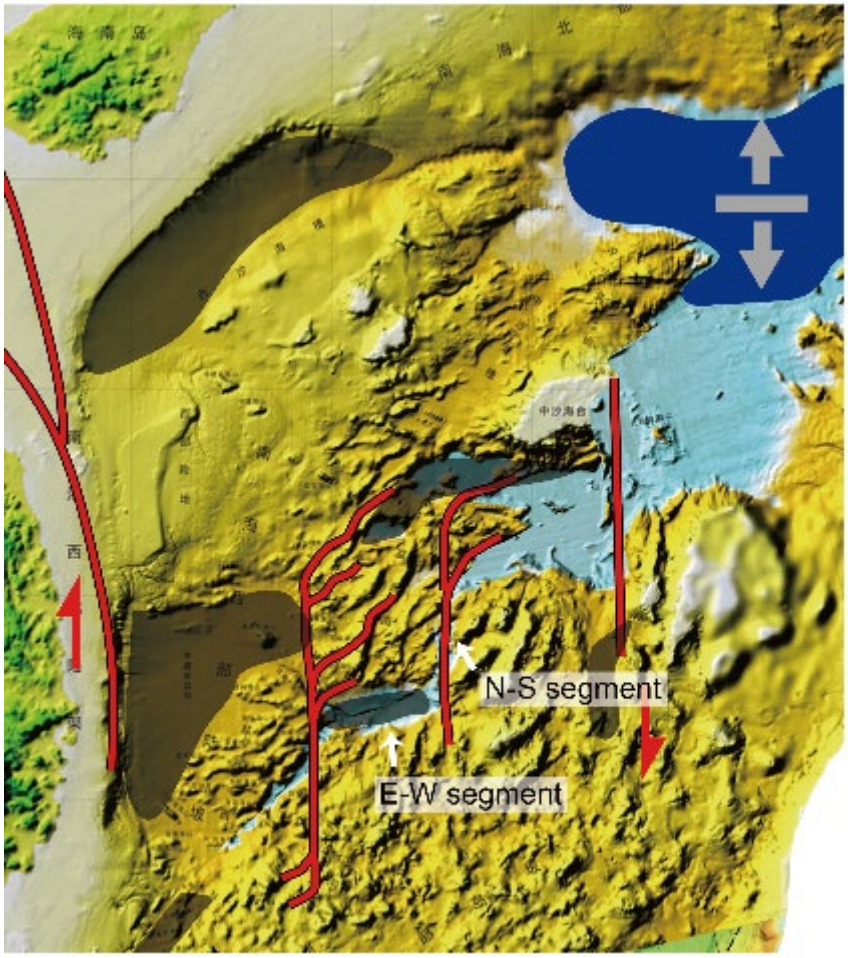

30 Ma (N-S extension)

Figure 6- 6. Reconstruction map of the SCS margin prior to the breakup of southwestern margin.

In order to discuss the postulated correlation between the convergence in the south of the SCS and its extension, the gross lines of the convergence history must be reviewed. In Borneo and South and Central Palawan, the distribution of the volcanic arc delineates a roughly E-W alignment in the south (Figure 6- 7), with an orientation similar to that of the backbone of the mountain range in Sarawak and Kalimantan. Some studies also extend the volcanic arc eastward to the eastern Sabah and Sulu Arc (Figure 6- 2).

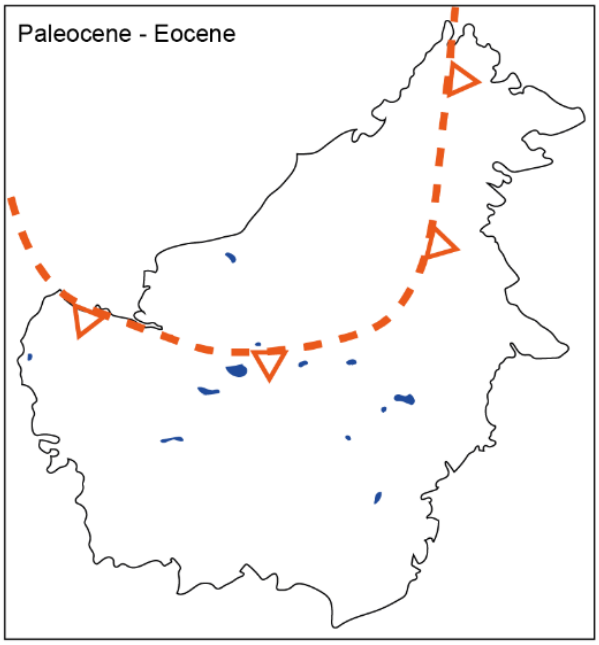

Figure 6- 7. Distribution of the Eocene magmatic rocks in Borneo and indication of the paleo-suture zone (modified from (Hamilton, 1979; Moss et al., 1998; Sapin, 2010; Breitfeld et al., 2019).

The main rifting period and incipient subduction in the Eocene appears as a parallel-driven N-S movement in both SCS margin and PSCS margin. I demonstrated the dynamic condition driven by specific tectonic processes, which imply a southward pull due to the convergence in the Borneo and Palawan and a coeval divergence behind in the South China Sea (Figure 6- 6). The advancing development from stretching to thinning stage is distinguished by the presence of detachment faults. These may indicate an increase of extensional stress induced by pulling forces from the initiation of subduction in the south. This configuration recalls the type B in divergent (Figure 1- 1) settings led by boundary force from subduction, for which the slab-pull is considered as one of the main driving forces in the formation of basins.

6.2.2 Early Miocene (23-16 Ma): collision-induced counterclockwise change of direction

The southward subduction was sustained until the late Late Oligocene when the margin of the PSCS entered the subduction and triggered the formation of NW Borneo orogeny. This event caused a change of the block motion from N-S to NW-SE orientation expressed in the SCS and the Borneo-Palawan area. This change is argued based on stratigraphy and others geological evidence.

Subducted thinned continental crust and flexural forebulge

The tectono-stratigraphic observation allows us to correlate, based on coeval unconformities among the rifting-drifting history in the South China Sea, and the orogeny in the Borneo-

Palawan area. The latest Oligocene (23 Ma) highlights the initiation of shifting the extensional direction in the SCS, and the related unconformity (Top Croker Unconformity - TCU) can be traced widespread c. 23 Ma ((Briais et al., 1993; Sibuet et al., 2016; Lunt, 2019) and reference herein; Figure 6- 1). In addition, the spreading propagator continued operating southwestward and the spreading rate decreased from 25 to 15 mm yr-1 in half spreading rate until it stopped at 16 Ma (Briais et al., 1993). Another unconformity, known as the deep-regional unconformity (DRU) or Middle-Miocene Unconformity (MMU), marks the termination of orogeny in Borneo and Palawan (Ilao et al., 2018; Chang et al., 2019). Chang et al. (2019) suggested that this unconformity is diachronous along the collision zone, which is dated at 16 Ma in Sarawak and becomes younger northward toward Palawan at c. 12 Ma (Steuer et al., 2014).

This observation may reflects a deceleration on both margins of the subduction-driven process, and therefore a reasonable speculation imply that a continental crust - an attenuated crust is probably more realistic - derived from the north initiated the collision. The continental crust may come from a drifted block from the southern SCS Margin, similar to those of Dangerous Ground, Reed Bank, Spratly Islands, North Palawan, and Mindoro etc. The continental crust depicts more positive buoyancy than the underthrust oceanic crust, which had been the main crustal type of lower plate during previous subduction stage.

The influence of subduction-collision is commonly underlined by a flexure-forebulge due to the loading of accretionary wedge or the forming mountain belt. For example, (Chang et al., 2013) observed a flexured oceanic crust along the Manila Trench as well as in the along-strike foreland basins of the Taiwan Orogeny (Figure 2- 31) (Lin and Watts, 2002; Chang et al., 2012). Steuer et al. (2014) have described a similar flexural feature in the southern SCS Margin that would result from the collision stage by subducting thinned continental crust in the Borneo-Palawan area. The forebulge region also resulted in a widespread area of shallow-water depositional environment, which developed a significant carbonate layer (Nido carbonates) deepening toward the Borneo-Palawan Trough, as well as a built-up reef along the crest of the horst in Dangerous Ground (Jamaludin et al., 2017). The carbonates of the Nido platform would therefore help placing the Middle Miocene Unconformity during 15-20 Ma, Oligocene to Early Miocene (Cullen et al., 2010; Steuer et al., 2014; Kessler and Jong, 2016), thus indicating that the collision completed approximately before the Middle Miocene.

The marine free-air gravity illustrates the regional crustal structure influenced by crustal flexure. The raw-data profile displays generally 0 mGal of average in the E Vietnam/S Hainan Margin. However, the increase of the free-air gravity in southern margin and drops to around -50 mGal in the vicinity of the Borneo-Palawan Trough (red curve on Figure 6- 8). A similar tendency appears at the seafloor and basement of oceanic floor which crook southward as seen on the bathymetry and seismic images (Li et al. (2015) (Figure 6- 9). These indicators illustrate roughly that the flexure-dominated effect was localized to the south, where it is adjacent to the subduction-collision zone of the PSCS proposed.

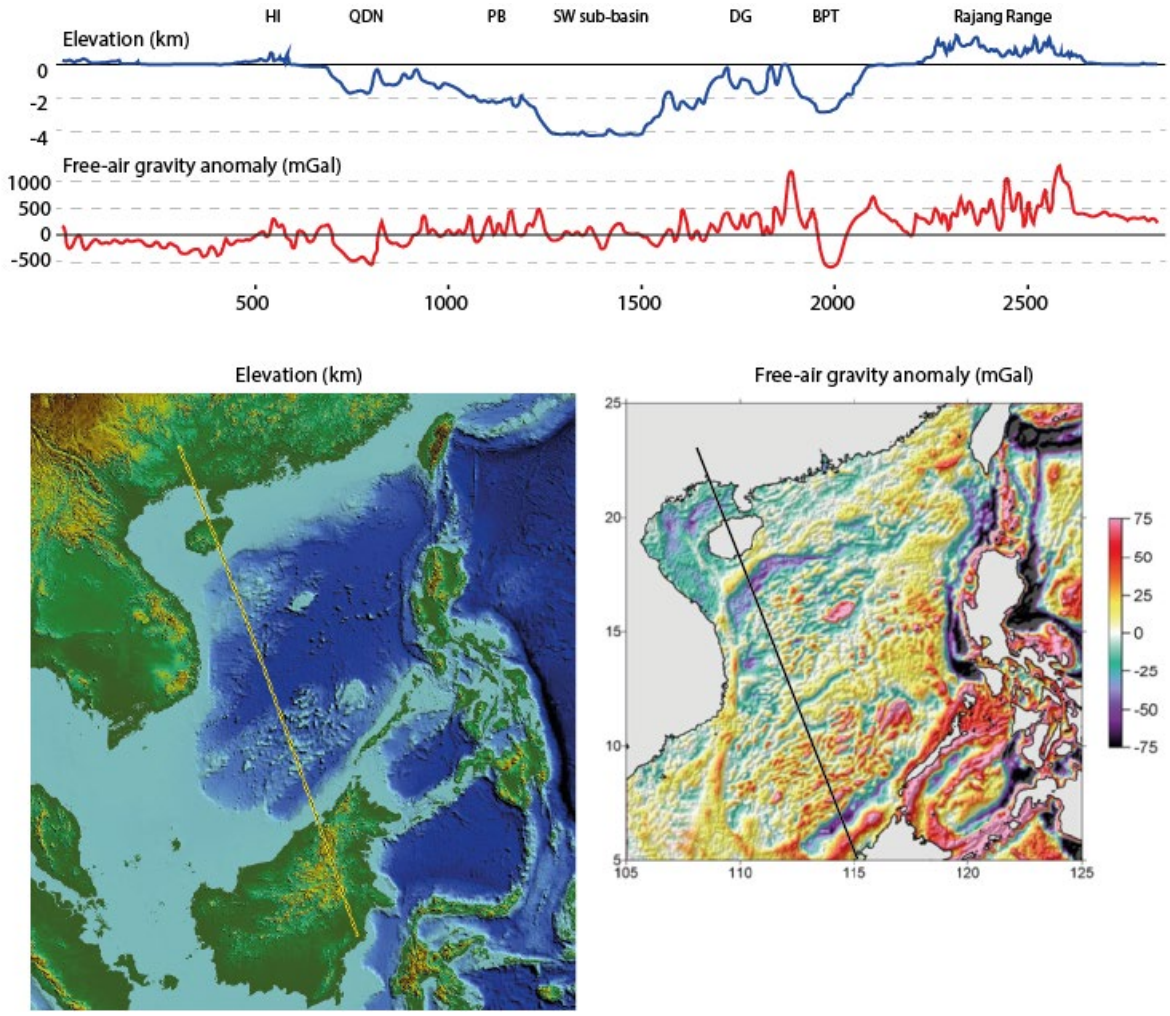

Figure 6- 8. Cross profile of elevation and free-air gravity illustrating the increase of gravity anomaly toward the Borneo-Palawan collision zone. Free-air grvity map from Gozzard et al. (2018). A pair of peak and trough in the vicinity of Dangerous Grounds and Borneo-Palawan Trough indicate the forebulge feature. HI: Hainan Island, QDN: Qiongdongnan Basin, PB: Pengxi Bank, DG: Dangerous Grounds, BPT: Borneo-Palawan Trough.

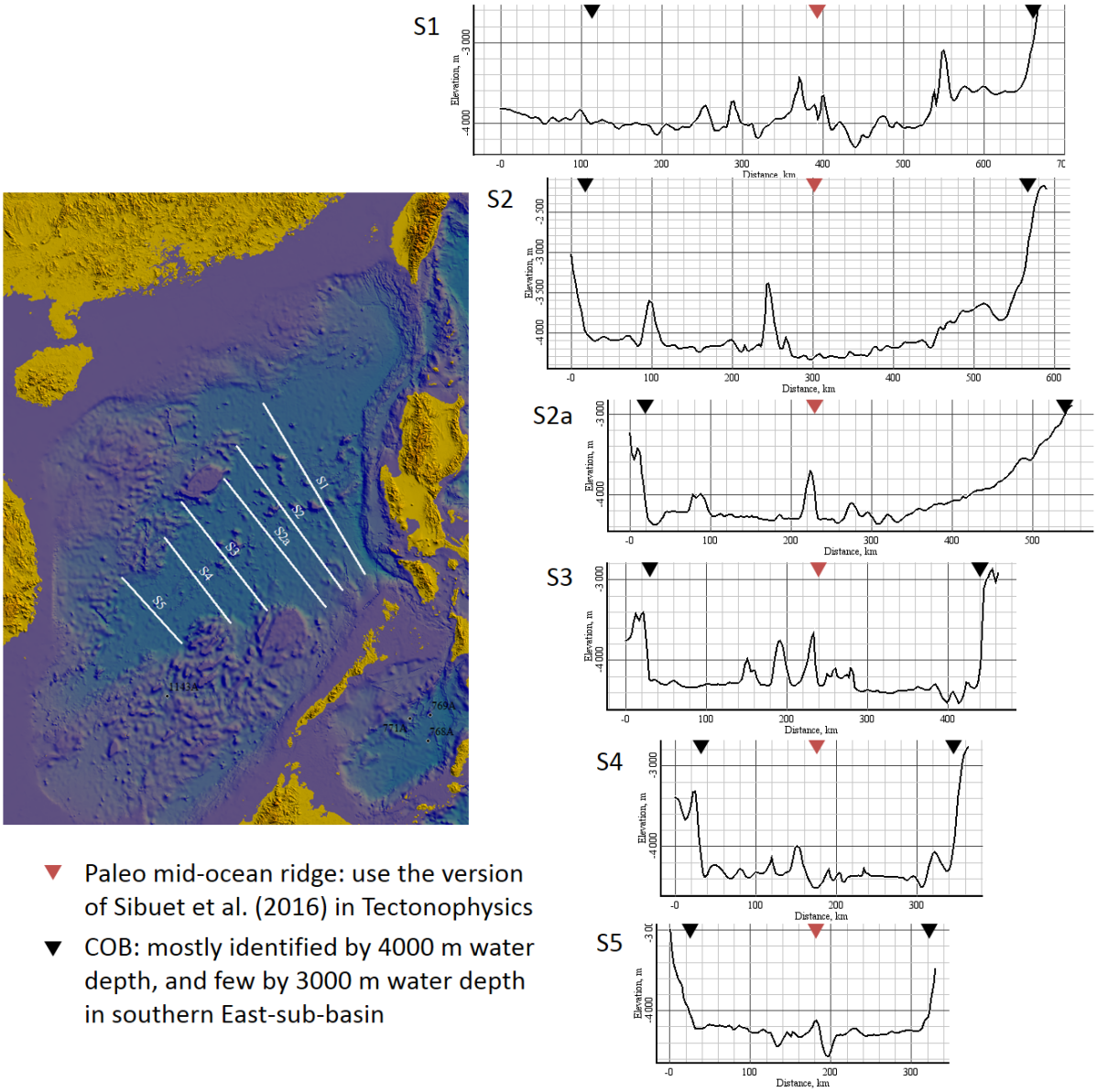

Figure 6- 9. Bathymetric profiles of oceanic domain display the southward deepening toward the subduction zone of PSCS.

The flexural influence is also witnessed in the stratigraphy of the southern SCS margin. Although it underwent a similar rifting history, the southern margin experienced more rigorous erosion than the northern margin (Figure 6- 10) (Steuer et al., 2013; Liang et al., 2019). According to industrial wells on the shelf of the offshore Palawan, at least seven wells show that the Nido carbonates overlay the Eocene syn-rift succession or directly cover the Cretaceous basement without syn-rift unit (Cadlao-1, Catalat-1, Destacador-A-1x, Galoc-1, Guntao-1, Maiajon-1, Penascosa-1; (Holloway, 1982; Steuer et al., 2013; Steuer et al., 2014)). The well Sampaguita-1 is one of the most comprehensive records in the southern margins covering the stratigraphy of Late Cretaceous and Cenozoic (Figure 6- 10). The depositional environment of

southern margin characterizes of delta-littoral sea in Paleocene, deep-sea in Lower to Middle Eocene, and a marginal sea in Upper Eocene to Lower Oligocene (Taylor and Hayes, 1980; Yao et al., 2012; Steuer et al., 2014), therefore showing it experienced a different history (Figure 6- 10). The significant hiatus is also displayed on the seismic profiles in the offshore Palawan, on which the strata beneath the Nido are much thicker in the distal margin (Franke et al., 2011).

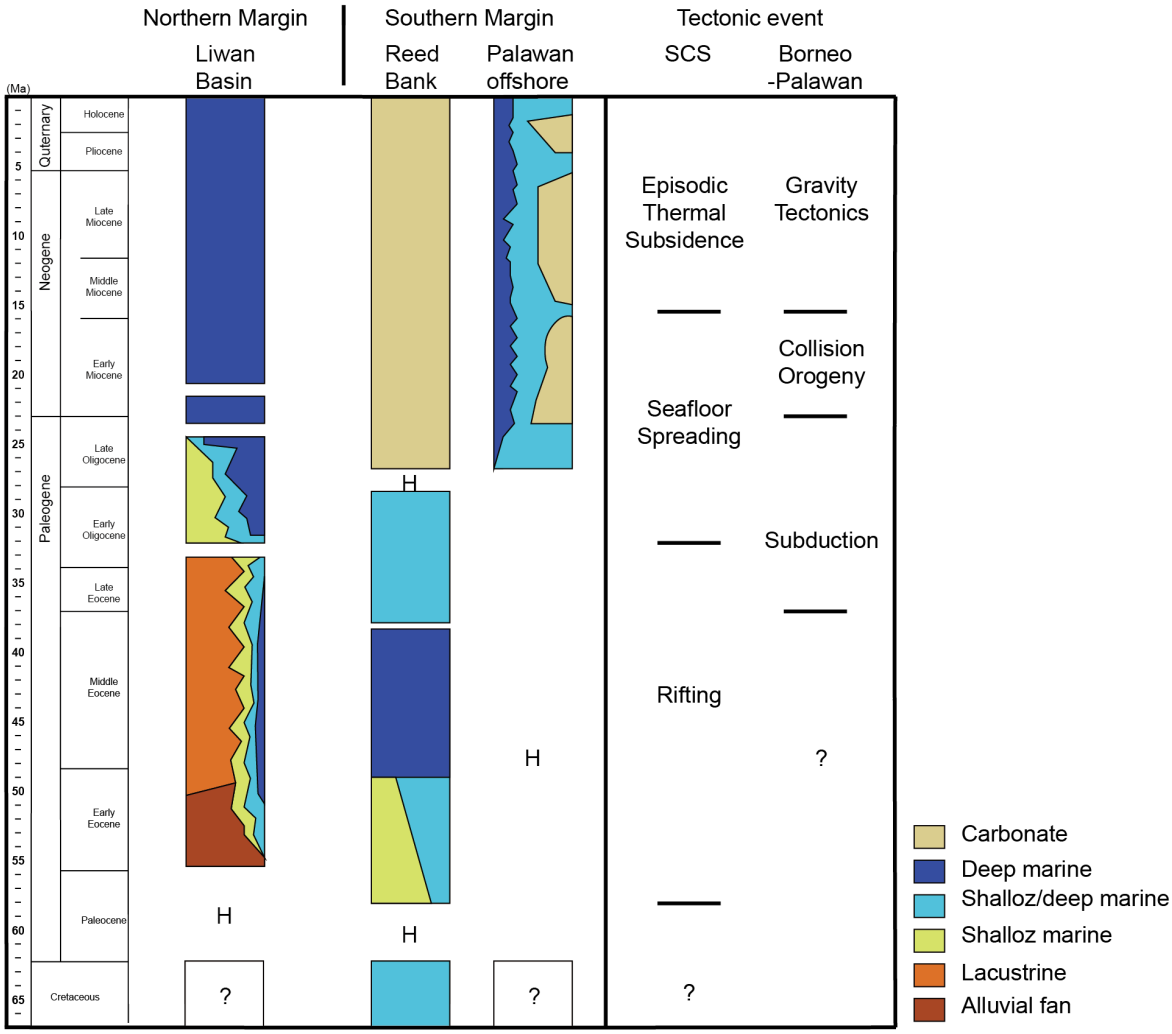

Figure 6- 10. Stratigraphy from the northern to the southern margins (modified from Yao et al. (2012), Steuer et al. (2013), and Nirrengarten et al. (2020a)). The southern margin experienced deeper depositional environment in the Paleogene time, and a long-lived hiatus in the proximal offshore, equivalent syn-rift period in the SCS margin. It may suggest the erosion accompany the flexure from the subduction loading. H for hiatus.

This study therefore suggests that the southern SCS margin was sensitive to the transition of subduction to collision of the PSCS and resulted in a flexural feature due to the loading of the

accretionary wedge, which is not clearly expressed in the structure and stratigraphy of the northern margin.

In Borneo, although the onshore stratigraphy study was not the main target in this work, a literature review shows several indications. Paleo-drainage reconstructions based on the age population of detrital zircon according to the sediment source suggest the NE-SW backbone in Borneo was extensively uplifted since Miocene (Menier et al., 2017; Hennig-Breitfeld et al., 2019). Few thermo-chronological studies in the East Kalimantan reveal the apatite fission track data from the Cretaceous sandstones, indicating a period of rapid cooling in the late Oligocene (c. 25 Ma) (Moss et al., 1998). This resulted in the change of the paleo-coastline from NW-SE to NE-SW (Figure 6- 11) (Hennig-Breitfeld et al., 2019). The depositional environment also changed from deep-sea to marginal marine or shallow marine in Croker Formation in Sabah as well as Nyalau Formation in Sarawak (Hennig-Breitfeld et al., 2019).

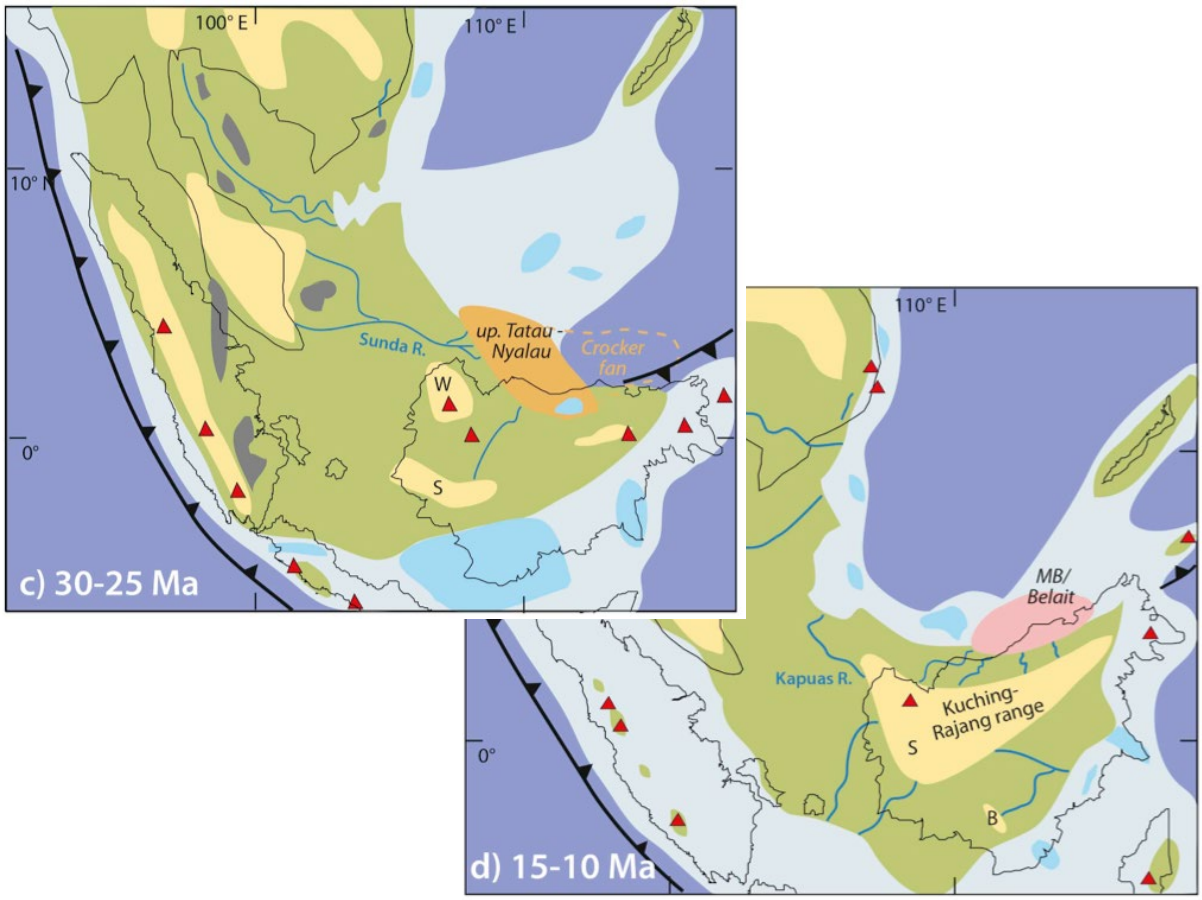

Figure 6- 11. Reconstruction of the Borneo area in Oligocene to Miocene time (the figure from Hennig-Breitfeld et al. (2019)). The paleo-drainage result indicates new sediment source from Kuching-Rajang Range (right), indicating the timing of collision between 25-15 Ma.

In Sabah, an increase of ophiolitic deposits above the TCU in Meligan-Setap Formation and Kudat Formation, is noticed compared to those from the Crocker Formation in Sabah. The different sources of sediments classified into five categories, showing ophiolitic deposits increased around Late Oligocene (Figure 6- 12) (van Hattum et al., 2013). This can imply the obduction initiated and exposed the ophiolite complexes to the surface and input the mafic sediments by the erosion and transportation.

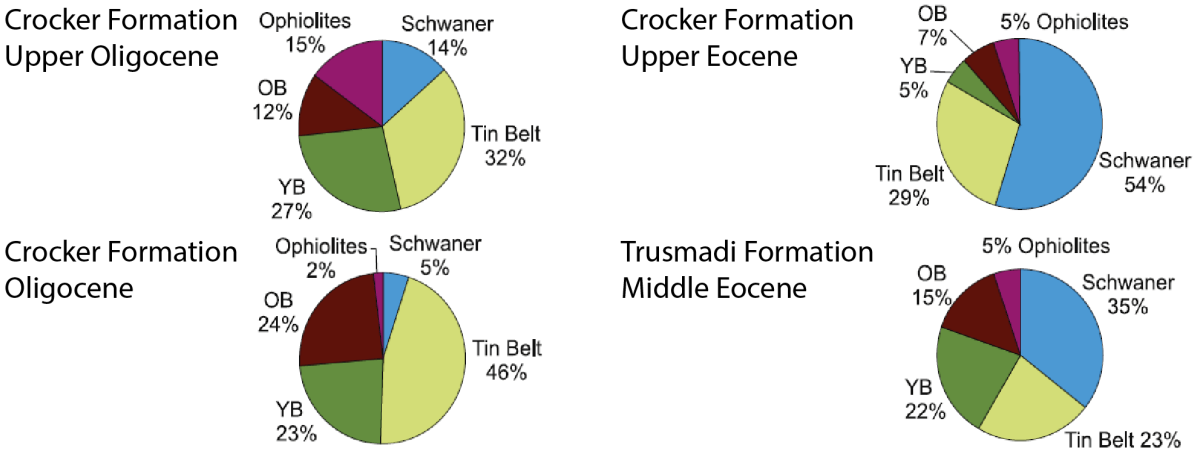

Figure 6- 12. Detritus zircon spectrum from Eocene to Oligocene in Borneo (van Hattum et al., 2013). Since Middle Miocene, the ophiolite supplied minor percentage until the sample from Upper Oligocene, Crocker Formation, implying the exhumation of ophiolite exhumed to the surface. Provenance categories are Schwanner: Cretaceous granites of Schwanner Mountains; Tin Belt: Permian–Triassic granites of Malay-Thai Tin Belt; YB: Young basement; OB: Old Basement; Ophiolites: ophiolitic basement.

Change of extensional direction and rotation of Borneo

In the SCS, N-S extension in rifting and seafloor spreading lasted until 23 Ma and commenced changing progressively to a NW-SE extensional direction. Precisions for the shift is luckily recorded by a total of 30 degree between the final rifting in N-S direction and the oceanic formation in NW-SE direction (Figure 6- 1), and is seen in the magnetic anomalies and the bathymetry on oceanic crust (Briais et al., 1993; Lee and Lawver, 1995; Sibuet et al., 2016). It is also seen in the structural mapping of the Phu Khank Basin (Savva et al., 2013). This modification was interpreted as a ridge jump in the oceanic formation. The counterclockwise change is however relatively less obvious in the East Sub-Basin.

A counter-clockwise (CCW) rotation in Borneo and Palawan happened in the same period of time (McCabe et al., 1993; Fuller et al., 1999; Almasco et al., 2000; Cullen, 2010; Wu and

Suppe, 2017; Advokaat et al., 2018). Paleomagnetism analysis displays the CCW rotation during Early Miocene, although some CW results are also documented (Fuller et al., 1999). A strict paleomagnetism test excludes most CW rotation due to later deformation overprinting the inclination and declination direction. Hence, the well-analyzed results and other recent data have confirmed a continuous CCW rotation in Borneo since Late Mesozoic (Figure 6- 13) (Advokaat et al., 2018).

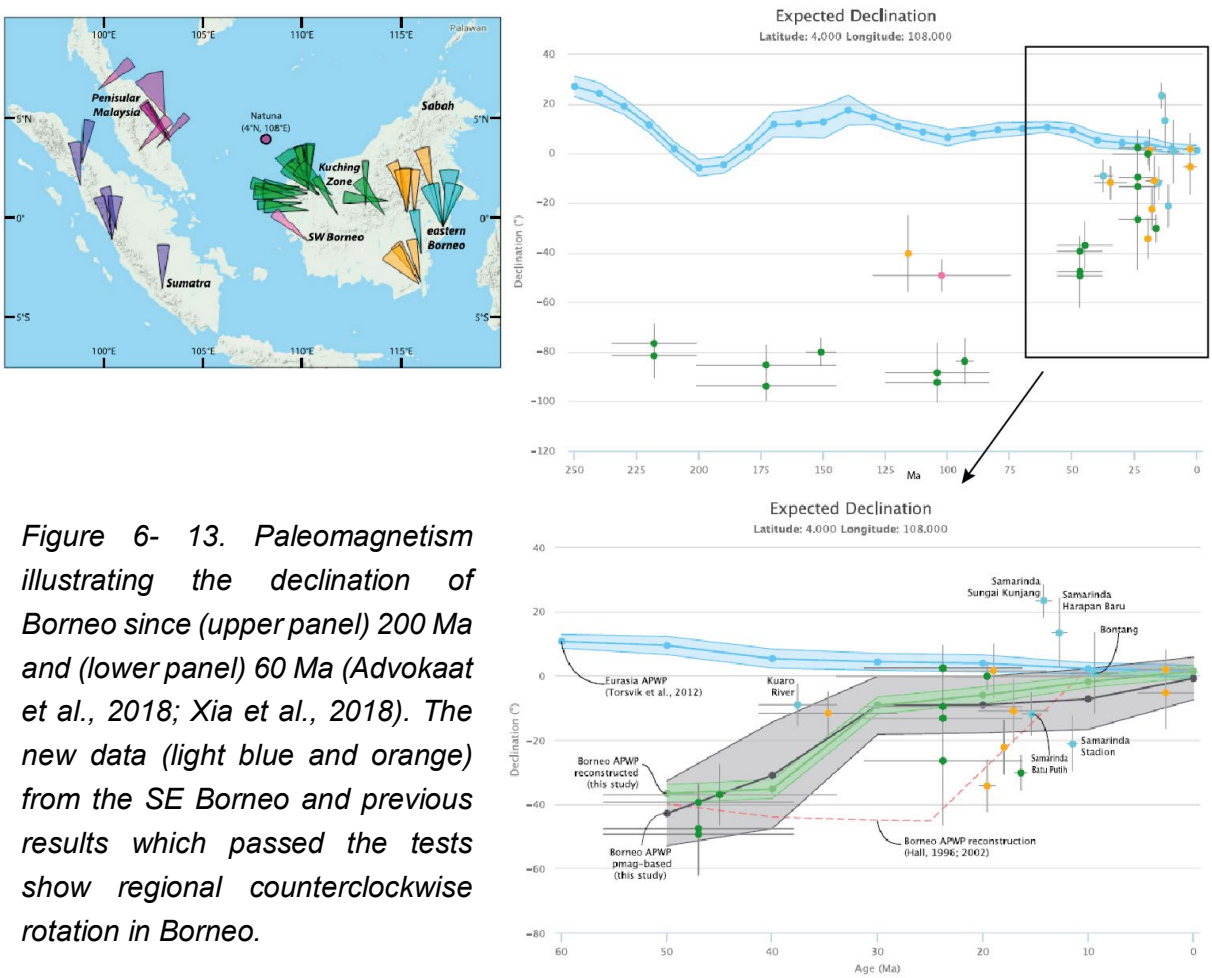

Figure 6- 13. Paleomagnetism illustrating the declination of Borneo since (upper panel) 200 Ma and (lower panel) 60 Ma (Advokaat et al., 2018; Xia et al., 2018). The new data (light blue and orange) from the SE Borneo and previous results which passed the tests show regional counterclockwise rotation in Borneo.

The Oligocene and younger magmatism distribution shows a change of orientation from E-W to NE-SW (Figure 6- 14). The pattern illustrates that the magmatism evolvement followed the regional counterclockwise modification, and the younger magma source is different from the arc-liked magmatism in Eocene. The Sintang and Bau Suite were further involved to adakites or granitoid intrusions (Prouteau et al., 1996; Prouteau et al., 2001; Breitfeld et al., 2019).

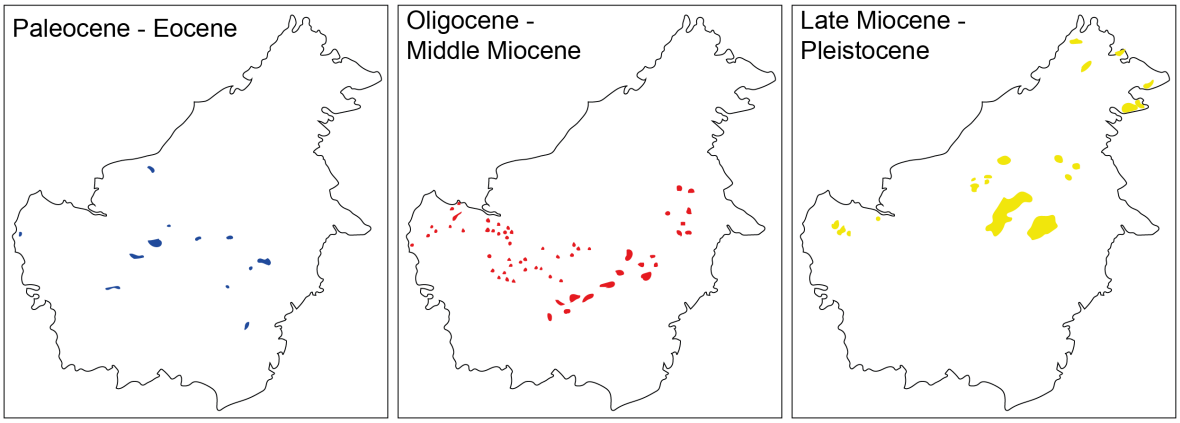

Figure 6- 14. The magmatism distribution in Borneo. Modified from Moss et al. (1998), Sapin (2010) and Breitfeld et al. (2019).

The Sulu Sea, in the southeast sector of the study area, extends 150 km in width and 350 km in length. It opened behind the collision zone in Palawan and is also coeval to this period, being opened around 18 to 12 Ma (Rangin, 1989; Balaguru et al., 2003). According to the tectonic setting of collision, the Sulu Sea has been recognized as back-arc extension (Weissel, 1980; Rangin, 1989; Silver and Rangin, 1991), which is type-A extensional basin induced by the subduction system in this study (see Chapter 1). This also gives a hint for the frontal wedge proceeding NW direction in Palawan and the northern Borneo while opening, whereas collision was relatively stable in S Borneo. This illustrates a differentiated evolution of the two regions. This scenario can fix the development of CCW rotation in time; the transition occurring between the back-arc development and collision region in Palawan and Sarawak respectively. Strike-slip motion has been evidenced in East Sabah such as along the Balabac Line (Balaguru et al., 2003; Sapin, 2010), which separates the two regions.

The mechanics of collision and rotation

Convergence between two plates likely brings together different crust types, thicknesses and rheologies along strike the collision, and therefore, the response of deformation is expected to vary. This will generate segments where the rotation of blocks is easier than others to accommodate these variations. Many examples involving the collision with a buoyant indentor have been proposed worldwide, such as in the East Mediterranean Sea (Armijo et al. (1996); Menant et al. (2016); Figure 6- 15), for the Himalaya-Tibet, for the marginal seas in the Pacific Ocean (Wallace et al. (2009); Figure 6- 15), the North arm of Sulawesi (Surmont et al., 1994). We observe in this context a simultaneous back-arc extension while the continental crust derives (Wallace et al., 2009). As a result, the lateral heterogeneity of the subducting plate

controls the block rotation (Menant et al., 2016; Magni et al., 2017). In numerical simulations, the different origin of the simulated lower plate drives the subduction zone, which results in variation of subduction and collision style along the suture. The collision zone remains relatively immobile and the subduction front proceed evolving and moving forward to the trench. The back-arc extension initiates behind the volcanic arc, as shows for the temporal and spatial variation in the Eastern Mediterranean Sea (Menant et al., 2016). In addition, this lateral variation along subduction zone also triggers rotational movement near the transition between the collision and subduction (Wallace et al., 2005; Menant et al., 2016; Magni et al., 2017); Figure 6- 16). A driving force in the asthenosphere has been suggested in many numerical simulations to propose that toroidal flows induced when the slab teared and asthenospheric flows when through the gaps within the lower plate, and flow counterclockwise on Figure 6-16 toward the subducting region.

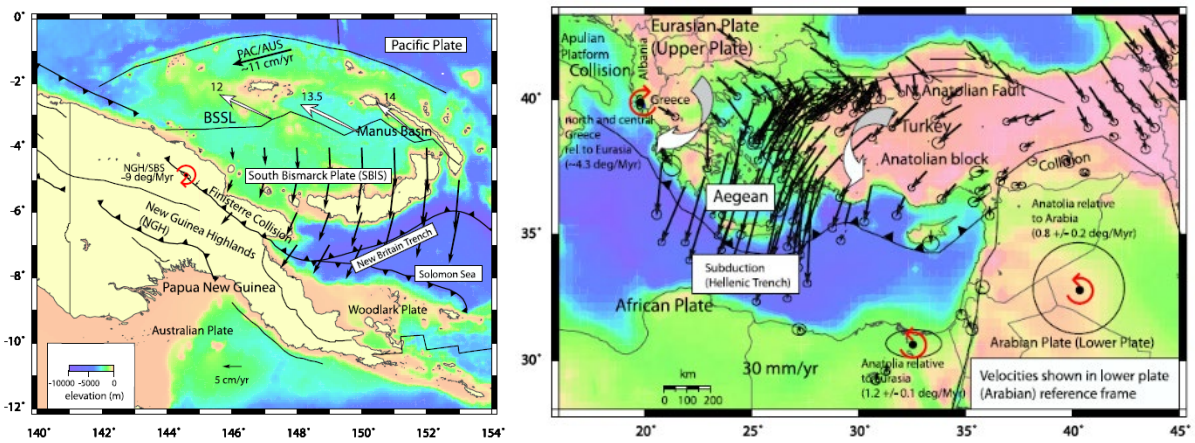

Figure 6- 15. Rotation shown by the GPS observation in Papua New Guinea and Eastern Mediterranean Sea (Wallace et al., 2009). These two examples demonstrate the subduction zone involved heterogenous lithosphere on the down-going plate, inducing significant rotation component on the overriding plate.

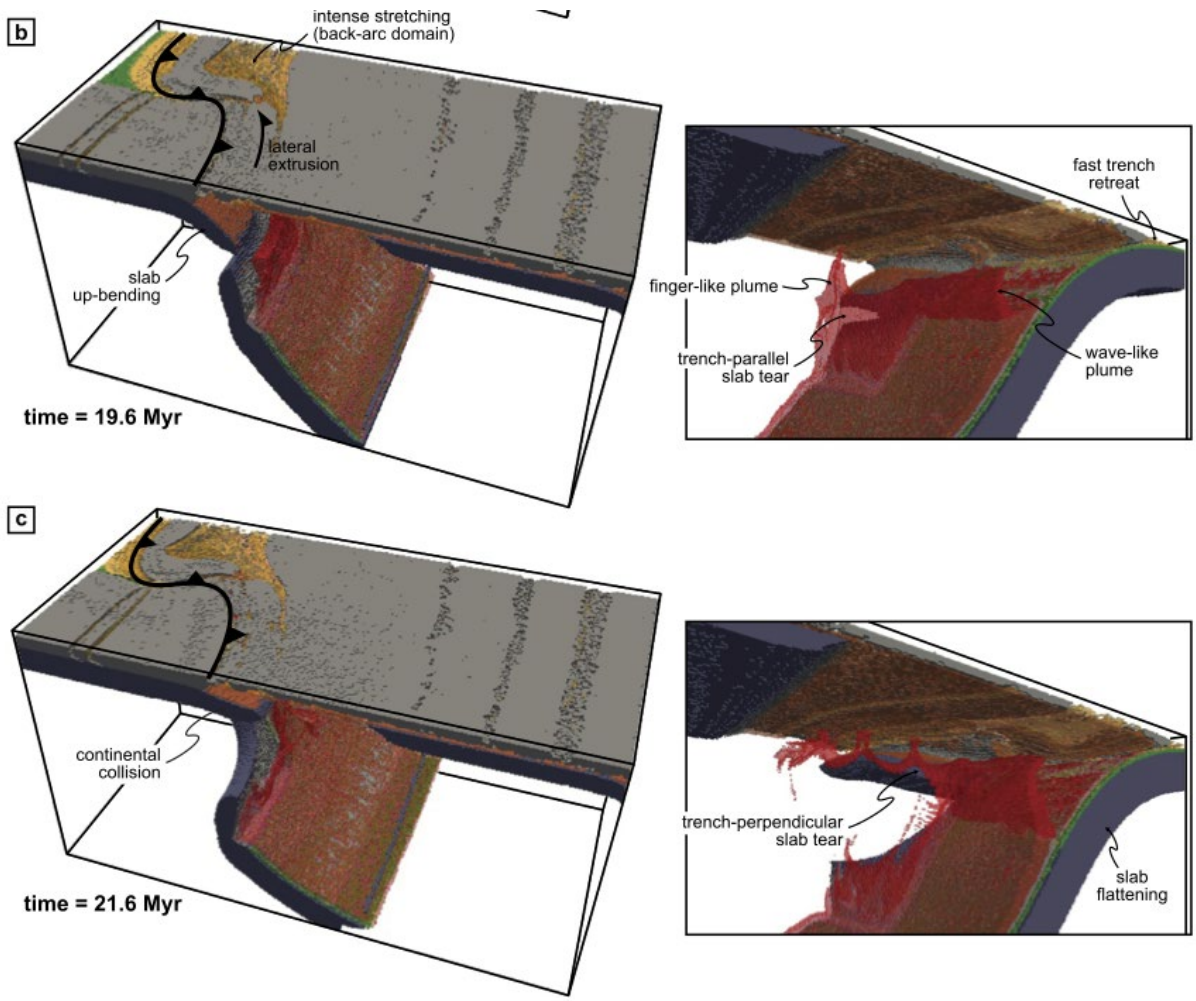

Figure 6- 16. Collision scenario results in rotation in simulation results (Menant et al., 2016). (b) beginning of the slab tear and plume and onset of extrusion. (c) continental collision at the surface resulting in slab break-off propagation

Such analogous configuration with heterogeneous converging plates applies to the subduction of the PSCS. While the continental block of Dangerous Grounds and North Palawan derived toward the subduction zone in the offshore Sarawak, it initiated the deformation by shortening, which drastically modified the topography of the NW Borneo Range (the present mountain range) as well as paleo-drainage. The collision and erosion initiated around 23 Ma in the central and southern Borneo, resulting in more ophiolitic fraction in the sediment shed into the neighboring basins around this time. Meanwhile the subduction continued in the Palawan-northern Borneo (Figure 6- 17). This discrepancy resulted also in a migration of the volcanic arc (such as Cagayan Ridge) toward the lower plate. The trench moved forward and changed the direction into NW-SE in South China Sea probably due to the slab retreat associated with the counterclockwise rotation. It is interesting and important to note that it also opened the back-arc basin of the Sulu Sea (Rangin, 1989).

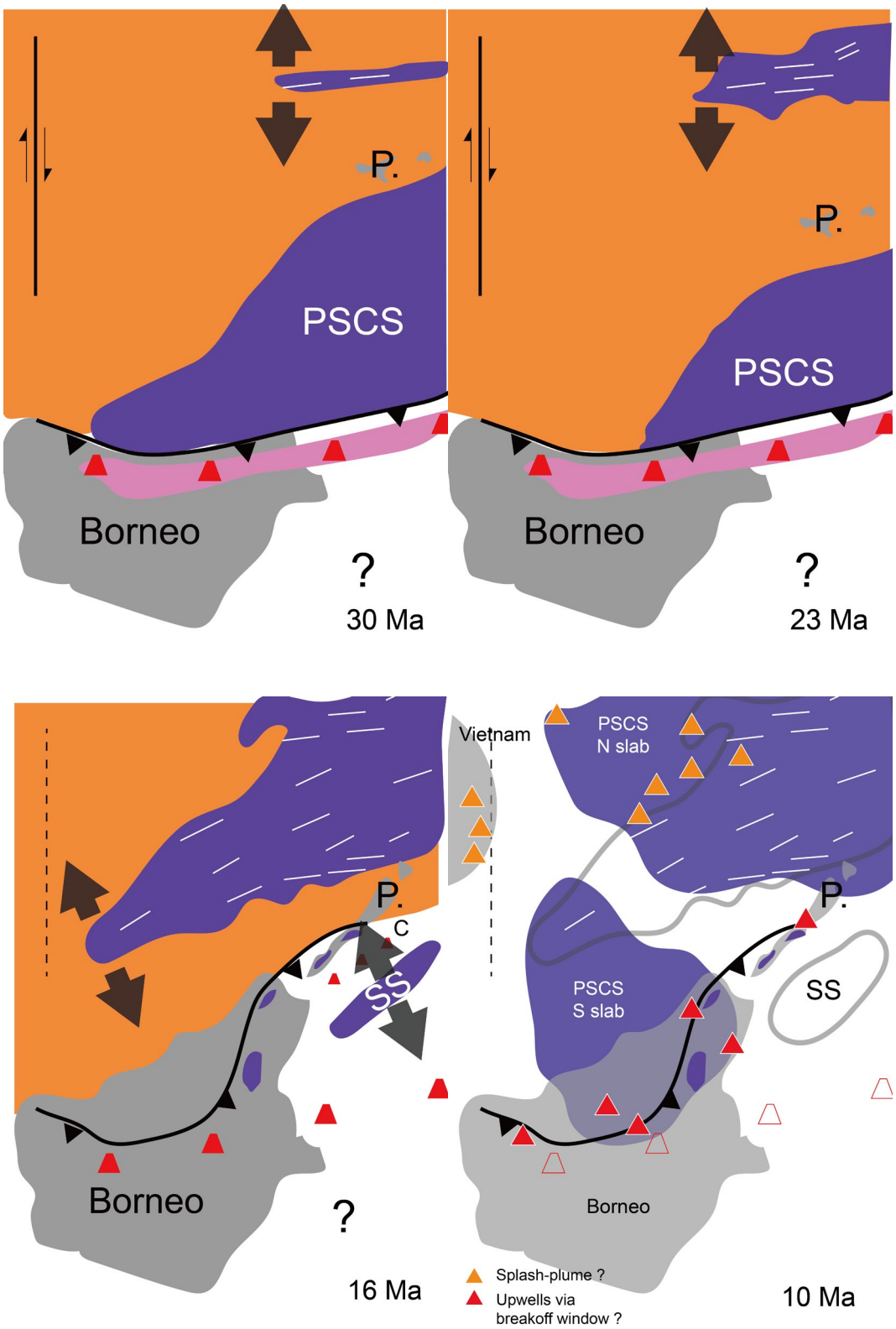

Figure 6- 17. The tentative model for the tectonic evolution in the SCS and the Borneo-Palawan area. Paleogene N-S extension is coeval with the subduction of the PSCS (ca. 30 Ma). The cessation of the subduction would coincide with the Miocene collision, and the free edge of the collision (Palawan) would induce a counterclockwise rotation (ca. 16 Ma). P for the Palawan Island; C for the Cagayan Ridge.

I therefore propose that the lateral crust heterogeneity along the subduction zone led the rotation and changed the convergent direction of the upper plate, as well the spreading direction at the lower plate -the SCS -. The rotation happened at the transition of these two regions to adjust the stress in between. In other words, there is a link between the beginning of the orogeny in the N of Borneo changed the far-field stress in the South China Sea, and the modified the spreading direction from N-S to NE-SW. The bathymetric and magnetic anomalies reflect the lateral change along the trench. As for the global evolution of the SCS, it may be viewed as a first propagator migrating from East to West, stalling near the edge of the former granitic arc, with a slight E-W compression (Le Pourhiet et al., 2018). Then, a change for a southwestward propagator, escaping the volcanic arc and escaping the margin of the Indochina Peninsula. The change is concomitant to the collision described in Borneo at 23Ma.

6.2.3 Middle Miocene to present day (16-0 Ma): regional subsidence and local vertical intrusion

The Middle Miocene marks a drastic change in the life of the SCS basin and margins. The processes described earlier; namely the seafloor spreading and the orogeny, terminated around 16 Ma in the SCS and the Borneo area. Although Chang et al. (2019) proposed that the end of the orogeny demonstrates a younging-northward diachronism, the earliest termination of orogeny in the Borneo may be correlated with the termination of the seafloor spreading all along the ridge axis in the SCS. The following event that occurred was a thermal subsidence which became ubiquitous in the South China Sea and is marked by a remarkable draping of all the rifting structures by a blanket of pelagic sediments (Figure 6- 18).

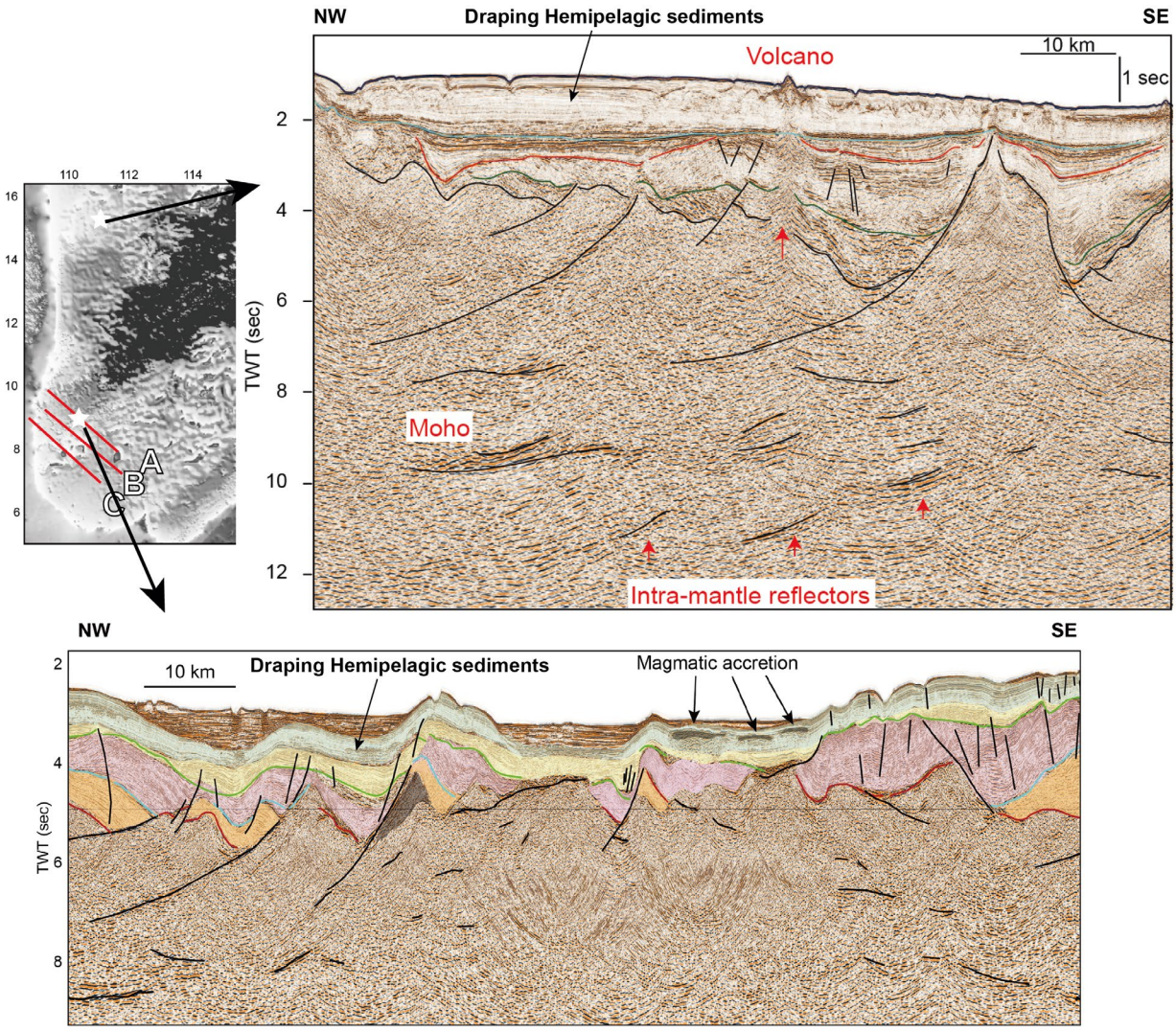

Figure 6- 18. Draping of hemipelagic sediments cover syn-rift and basement high after the concomitant end of contraction in Borneo and cessation of spreading at the tip of the propagator in SCS.

At the same time, a magmatic impulse induced extensive uplifts locally and sporadically in both onshore and offshore. One of the granitoid intrusions, Mount Kinabalu, has an adakitic composition (Prouteau et al., 2001; Cottam et al., 2010) and it had been suggested that it was related to a slab detachment c. 7-8 Ma in Sabah (Sapin et al., 2011). However, the relationship of these coeval events between the onshore intrusions and extensive post-spreading magmatism still remains speculative.

Granite intrusions induced by the slab detachment (break-off)

Neogene magmatism is composed of granitoid rocks during this period (Cottam et al. (2010); Cottam et al. (2013); Breitfeld et al. (2019); Figure 6- 19). Few area has been comprehensively

investigated by geochemistry and geochronology. The largest and highest of the batholiths is the Mount Kinabalu (highest elevation in Borneo, with c. 4100 meters) situated in the Malaysian state of Sabah. The pluton was emplaced with a series of dyke-fed granite sheets within 0.8 Myr bracket between 7 to 8 Ma, and is composed of three main lithologic layers; biotite granodiorite, hornblende granite, and porphyritic facies (Figure 6- 19) (Cottam et al., 2010). Based on petrologic studies, the intrusive plutons crystallized at depths between 3 and 8 km (Vogt and Flower, 1989). Taking into account the current elevation, the uplift associated to the rebound could reach up 10 km after the slab detachment ignoring other effects such as elastic flexure, erosion or sedimentation. The uplift rate induced by the lithospheric delamination or break-off of a subducted slab beneath Sabah (Hutchison et al., 2000; Cottam et al., 2013) would exceed 7 mm/yr during Late Miocene and Early Pliocene (Cottam et al., 2013).

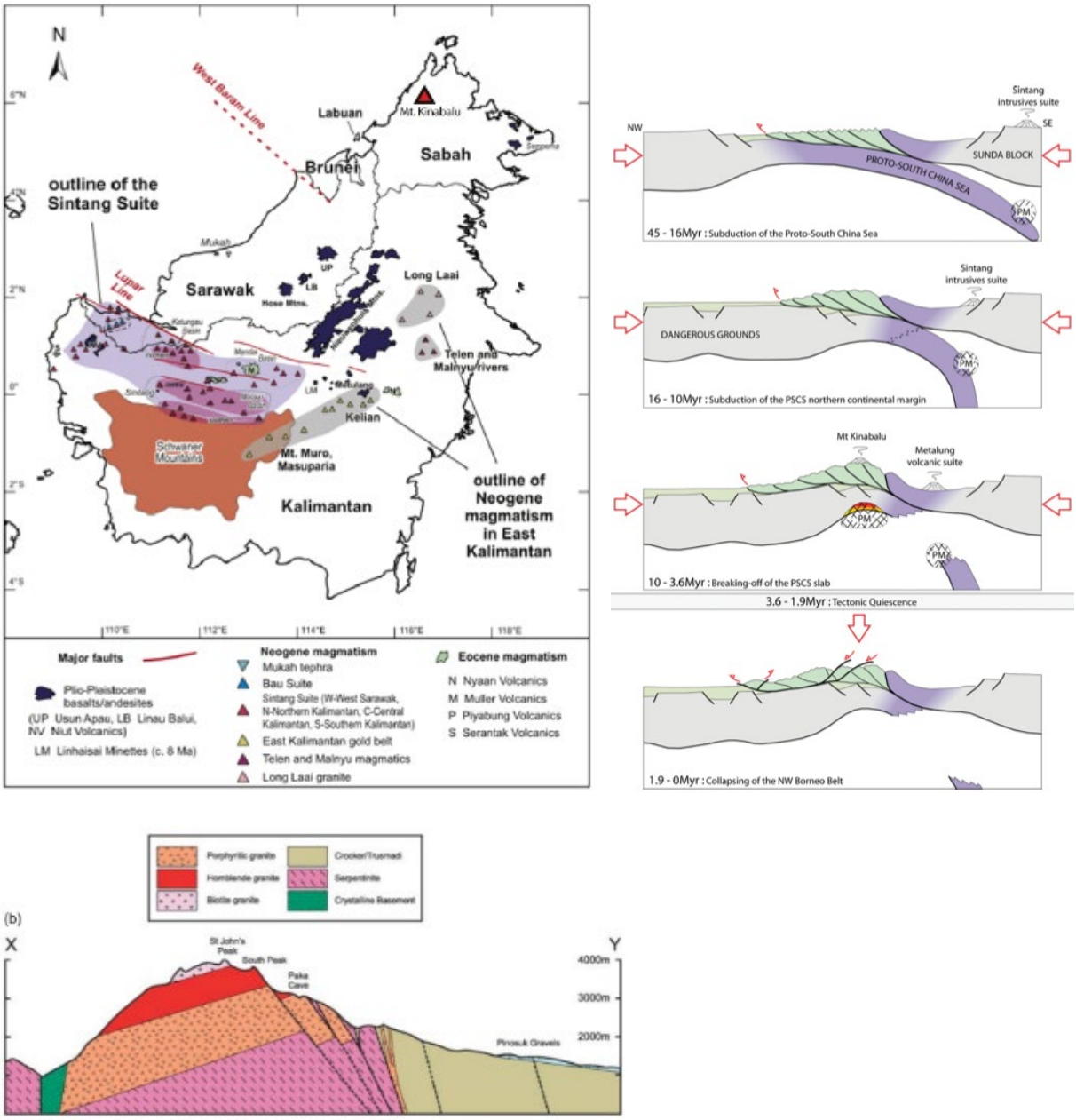

Figure 6- 19. (Up) Distribution of Cenozoic magmatism in Borneo from Breitfeld et al. (2019). (Below) Dyke-fed intrusion of Mount Kinabalu, composed by three-layer granitoid rocks, in the northern Borneo (Cottam et al., 2010). Scenario of slab breakoff and and magmatism (Sapin et al., 2013). See text for more details

In the south, sporadically intrusive bodies are documented in the central or southwestern Borneo. Adakites present in the so-called Sintang Suite, have been found coeval with the termination of seafloor spreading in 16-17 Ma, and would indicate also an asthenosphere upwelling due to slab detachment (Prouteau et al., 1996; Prouteau et al., 2001) or possibly even without a slab (Figure 6- 20) (Breitfeld et al., 2019). Most intrusions from the mantle appear to follow the period which brackets the end of collision since Early Miocene in Borneo.

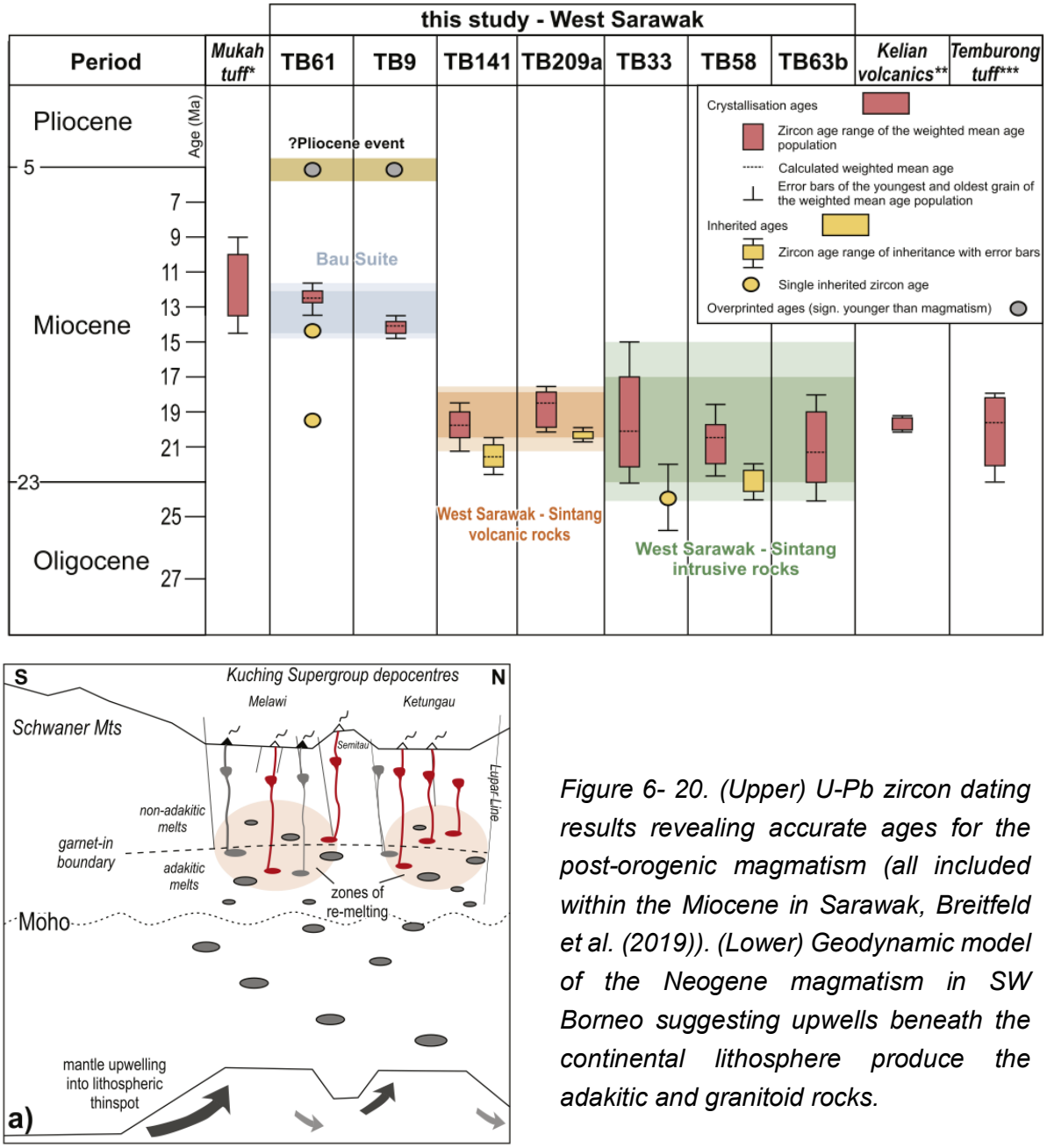

Figure 6- 20. (Upper) U-Pb zircon dating results revealing accurate ages for the post-orogenic magmatism (all included within the Miocene in Sarawak, Breitfeld et al. (2019)). (Lower) Geodynamic model of the Neogene magmatism in SW Borneo suggesting upwells beneath the continental lithosphere produce the adakitic and granitoid rocks.

These intrusions impacted strongly overlying strata during the exhumation up to the surface (see Chapter 4). Deformation affects mostly an Oligocene-Early Miocene ductile layers with diapirs and intra-formational normal faults as the granitoids was piercing the overlying strata landward. The deformation propagated to the frontal wedge along the offshore Sabah, accompanied with toe-thrust stacking of slices (Franke et al., 2008; Cullen, 2010; Sapin et al., 2011; Clark, 2017; Chang et al., 2019). This tectonic event corresponds to an unconformity; the Shallow Regional Unconformity (SRU), known in the offshore around 8 Ma (Figure 6- 1). The deformation zone which can encompass the circular basins area is bounded approximately by

the former Deep Regional Unconformity (DRU) contour in the eastern Sabah and the eastern offshore Sabah, surrounding the Mount Kinabalu (Figure 6- 21) (Clennell, 1991, 1996; Chang et al., 2019), which marked the end of the compression. Therefore gravity tectonics including diapirism and shallow faults rooting in the mélange found along the coastline of Sarawak, Brunei, and the offshore Palawan (Morley, 2009; Berthelon et al., 2018; Ilao et al., 2018; Chang et al., 2019; Xu et al., 2019), is also expressed in the circular basin.

The fission track results record the thermochronological history from the sedimentary strata surrounding the Mount Kinabalu. The minerals collected mostly from the Neogene strata ages indicate that ages from the detrital minerals depend on when they were exhumed through the geotherm bracket (c. 70 to 150 °C). Two distinct regions are discriminated in the Sabah area. The first group shows apatite with inherited ages (with wider error bars), indicating un-reset minerals after deposition since Cretaceous to Early Paleogene. However, another set of younger ages around 15 Ma shows narrow errors bars (Figure 6- 21). This younger group exhibits concordant results and imply the minerals have been exhumed above the isotherm around the dating ages. In map view, the younger group distributes around the Mount Kinabalu, fixing the boundary of DRU and circular basins (Figure 6- 21).

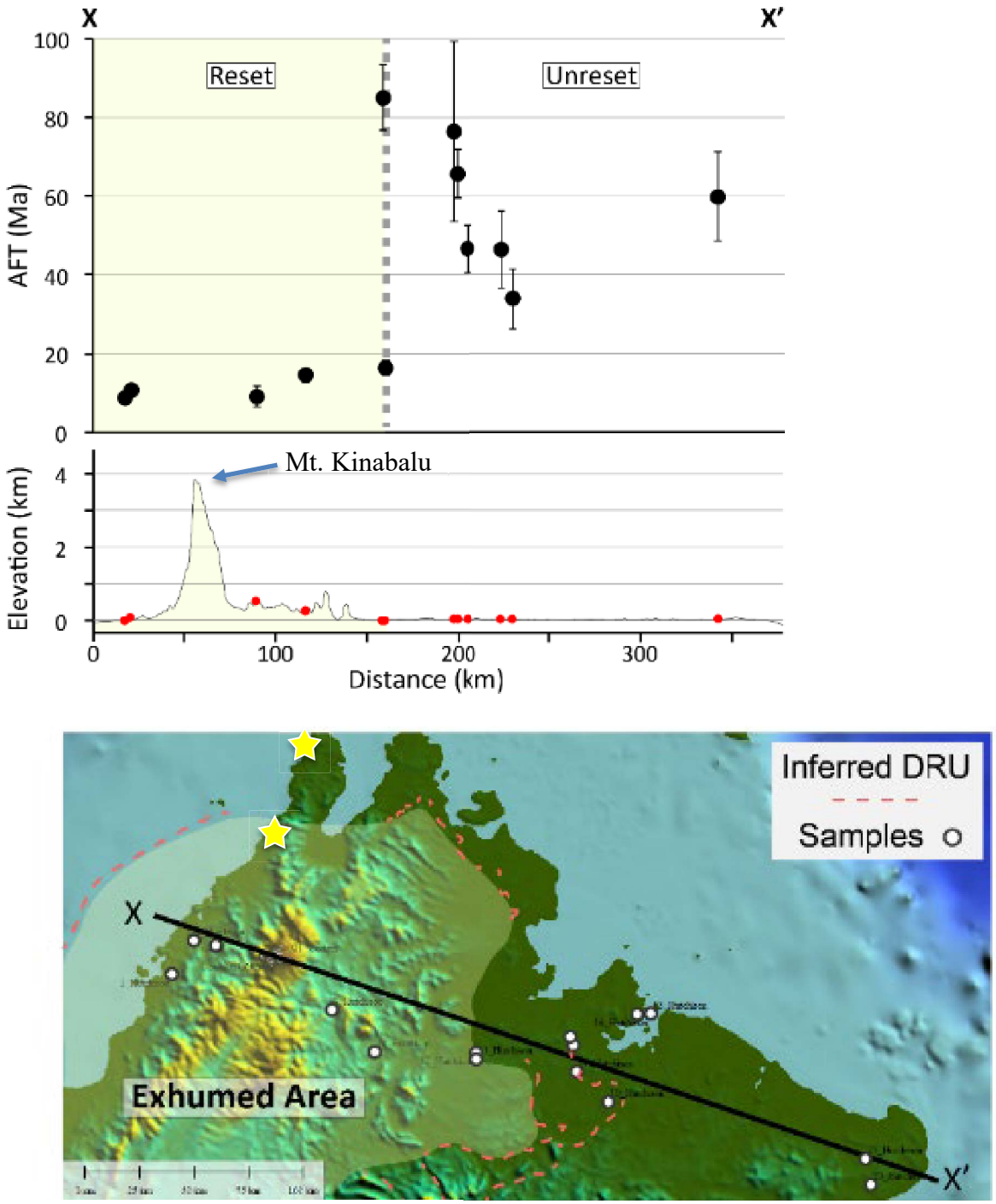

Figure 6- 21. Fission-track (AFT) results of detrital apatites in sedimentary rocks illustrating the Miocene exhumation around the Mount Kinabalu (compiled from Hutchison et al. (2000); Swauger et al. (2000)). The Neogene intrusion is illustrated c. 4000 meters height in topography along the cross-section X-X'. The dating shows a group of Miocene ages with narrow error bar adjacent the intrusion and another group of un-reset apatites with inherited ages in the eastern Sabah. Note the two samples in the northernmost part of Sabah indicating by the stars around the Kudat Peninsula.

Other intrusions similar in age were also documented in the northern Palawan, Sarawak and the eastern Sabah (Encarnacion and Mukasa, 1997; Padrones et al., 2017; Breitfeld et al., 2019), indicating that the post collision magmatism was more widespread. Fission tracks result from Palawan and East Sabah, although dating are less comprehensive, and suggest a similar process. The fission-track ages show a Late Miocene exhumation in the northern Palawan (Figure 6- 22) (Pubellier et al., 2014, unpublished; Padrones et al., 2017) with data showing similar pattern (AFT with the reset ages) in post-orogenic period.

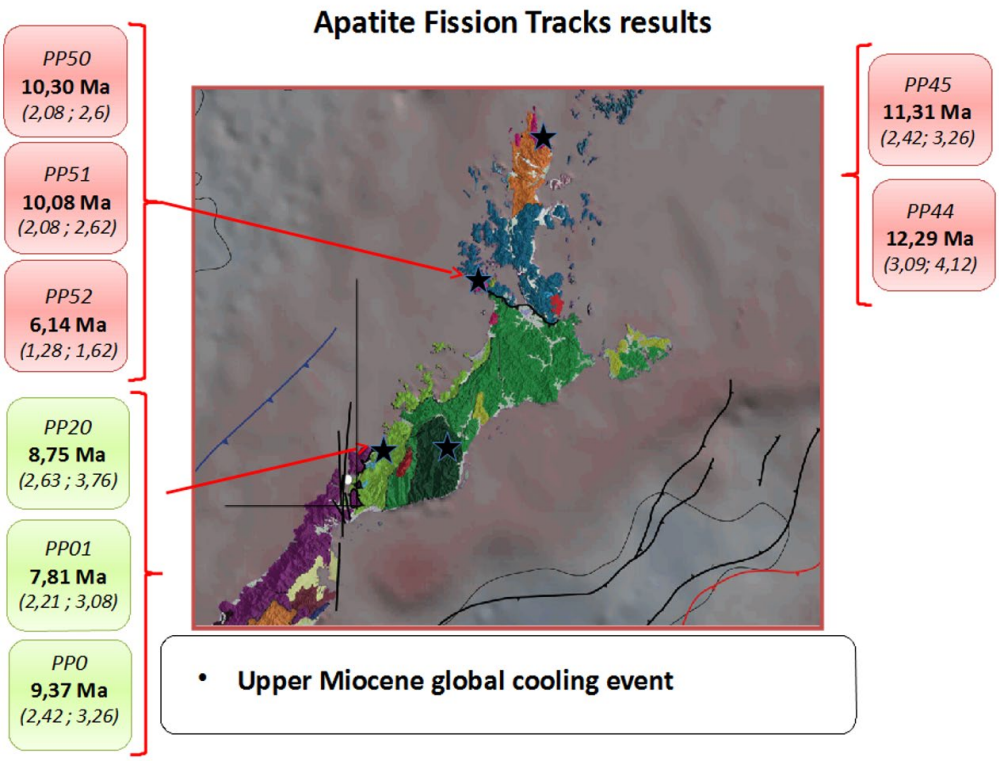

Figure 6- 22. Apatite fission track results in Palawan. The Capoas Granite dated in Late Miocene displays a similar exhumation history as Mt. Kinabalu (unpublished data, Pubellier et al. (2014)). Thermochronology results in fission tracks show that the magmatic and metamorphic rocks underwent exhumation in 12-6 Ma.

The current location of the PSCS slab is puzzling and has been the matter of debates in the past years. Ambiguous literatures dispute the existence of the PSCS slab as well as the subduction itself (Tapponnier et al., 1982). Tomography studies have been investigated for several decades. There is no significant wide P-wave velocity anomaly right beneath the Sabah area, but only patchy anomaly in depth of 700 km (Rangin et al., 1999; Wu and Suppe, 2017). However, there is a wide "reservoir" or "high P-wave anomaly" situated beneath the current South China Sea (Profile A, B and F on Figure 6- 23), which has been interpreted as the detached slab of the

Proto-South China Sea (Wu and Suppe, 2017; Sun et al., 2019). Fan et al. (2017b) also recognizes similar features but the slab distributes wider beneath the Philippine Sea Plate and at depth around 700 km (Profile D and E on Figure 6- 23). Further east, another slab was identified as Asian Sea Slab at the same depth and location in Wu et al. (2016), which may be interrupted by the PSP in Profile A on Figure 6- 23. The most consistent interpretation used in this study is that of a PSCS slab located beneath the current SCS (white shade on Figure 6- 23), with the southernmost edge located at the apex of the paleo-suture zone. This raises question about the whole geometry of the subducted slab (see discussion below)

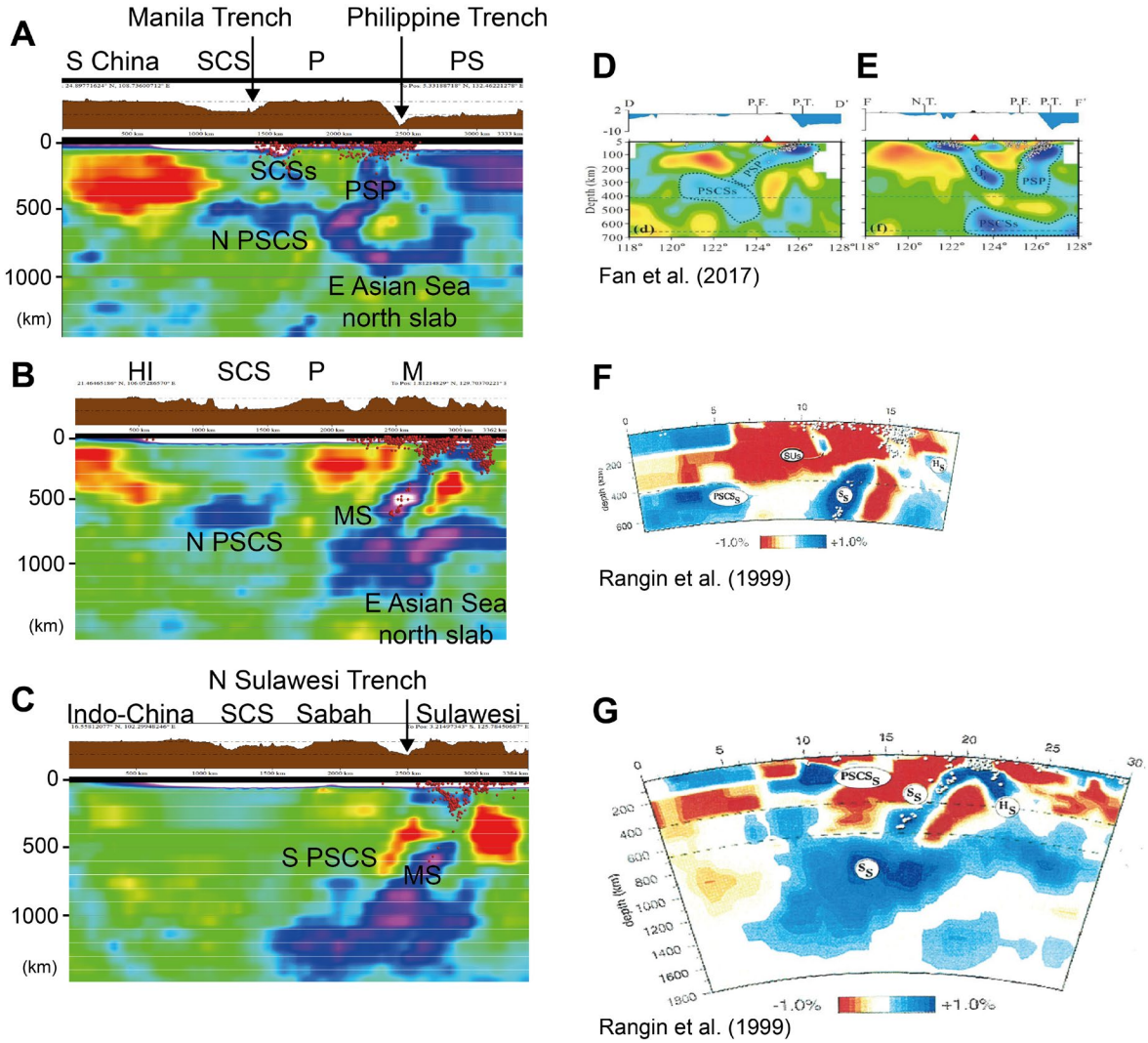

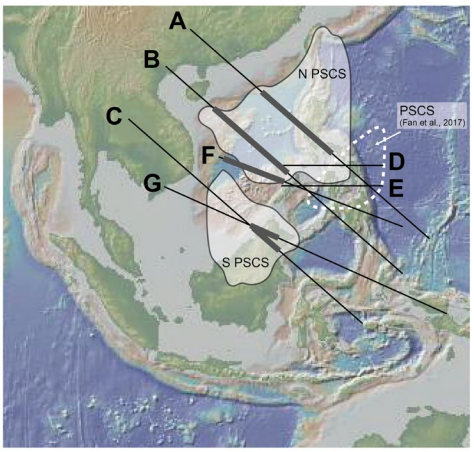

Figure 6- 23. Current location of the PSCS slab (white shades on the map) identified from tomography studies locates around 500-700 km depth (Rangin et al., 1999; Wu et al., 2016; Fan et al., 2017b). Three profiles (A, B and C) obtain in the collaboration with J. Wu and following the interpretation of Wu et al. (2016), and profiles D and E from Fan et al. (2017b) as well as profiles F and G from Rangin et al. (1999). Thick grey lines represent the location of the PSCS slab along the tomographic images, suggesting the North PSCS slab distributes beneath the present SCS and the Luzon area, and the South PSCS is narrower than the interpretation of Wu and Suppe (2017) beneath the Sabah area. Fan et al. (2017b) includes a high velocity layer (white dash line) beneath Philippine Sea Plate, which is interpreted the Asian Sea Slab in Wu et al. (2016).

Slab sinking and splash plumes

In the SCS, many magmatic intrusions protrude in the seafloor or are buried within sediments during the post-rift period after 16 Ma. These magmatic intrusions resulted in basement highs barely covered by thin sedimentation on top. The raise of some of these intrusive bodies deformed overlying strata and triggered mass transportation deposits (MTD) in the adjacent area (See Chapter 5). Xia et al. (2018) compiled the distribution of post-spreading and revealed that the intrusions in fact spread in the SCS, Hainan Island and Vietnam (Figure 6- 24). The geochemistry is that of OIB-liked basalts (Jiang et al., 2018; Yu et al., 2018b; Zhao et al., 2018a; Yang et al., 2019; Zheng et al., 2019), SE China (Huang et al., 2012) and Vietnam (Hoang et al., 2019). We note as well a high heat flow in rifted basins of the SCS suggesting the existence of post-rift thermal influence (Shi et al., 2017).

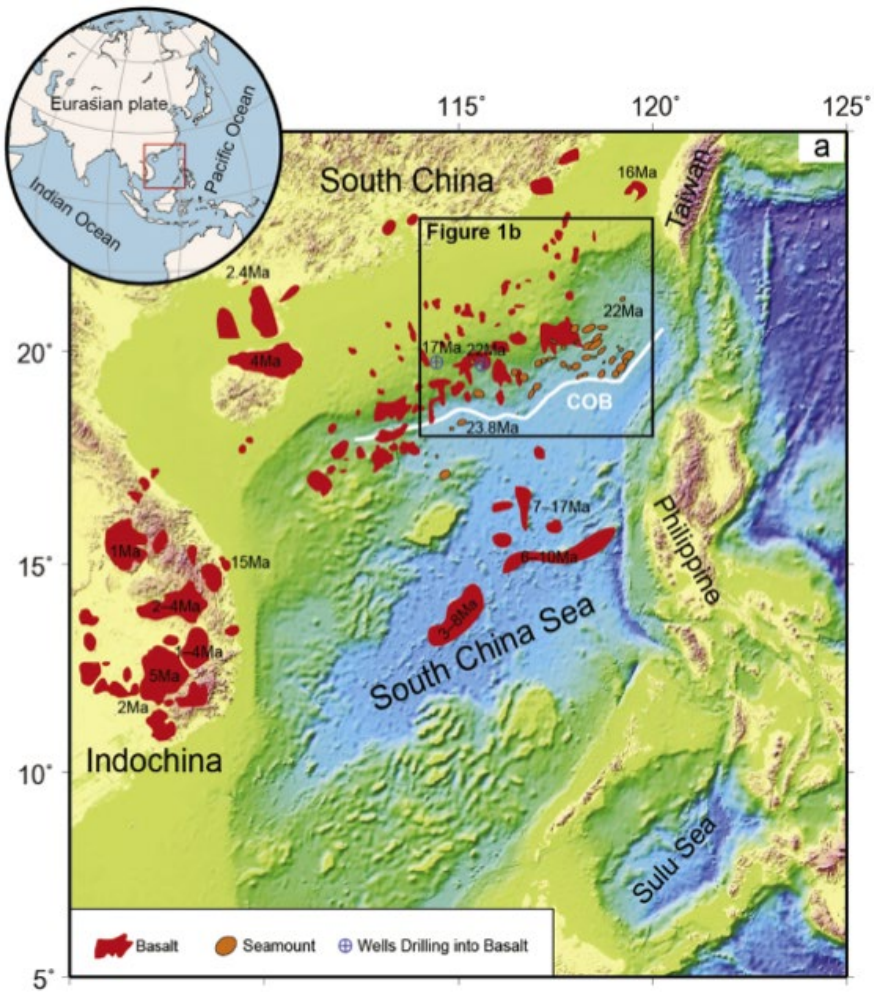

Figure 6- 24. Distribution and ages of post-spreading magmatism in the SCS (Xia et al., 2018). The magmatic intrusions are scattered around the fossil mid-ocean ridges and along the distal SCS margin in the offshore, as well as onshore in Indochina, Hainan Island and SE China.

The coeval thermal subsidence prevailed and is widespread in the region. It resulted in a deep-sea environment which still presents nowadays over the oceanic crust, with a seafloor abnormally deeper than that predicted theoretically through conventional models of thermal subsidence. A rapid subsidence has been proposed according to the paleo-water depth from industrial wells in rifted basins, for instance, NCS, PK, QDN, and Luconia (Xie et al., 2006; Madon et al., 2013; Li et al., 2014b; Xie et al., 2014; Clift, 2015; Shi et al., 2017; Zhao et al., 2018b), although some basins were influenced by compressional tectonics or strike-slip movement (Lin et al., 2003; Xie et al., 2006). The deep-sea sedimentation overlays the marginal sea deposits, suggesting a significant increase in water depth since Middle Miocene (Madon et al., 2013). In this study, I consider that subsidence was interrupted episodically by local uplifting in the vicinity of individual intrusions as shown on the seismic images during the post-spreading period (See Chapter 5).

However, globally, the regional subsidence and local uplifts are contrary during the Late Miocene to recent period. The relative vertical movement may result from differential subsidence and magmatic intrusions linked to a sinking break-off slab beneath the SCS. The distribution is compatible with the location of the two PSCS slabs identified by the tomographic analysis (Rangin et al., 1999; Wu et al., 2016; Fan et al., 2017b). Besides, the post-spreading age of the movement's clusters around the slab detachment (dated by the intrusion onshore Borneo, see above). This offers an opportunity to link and correlate these tectonic processes. Additionally, the distribution of the post-spreading magmatism is coincident above the trace of the PSCS slabs (Figure 6- 25).

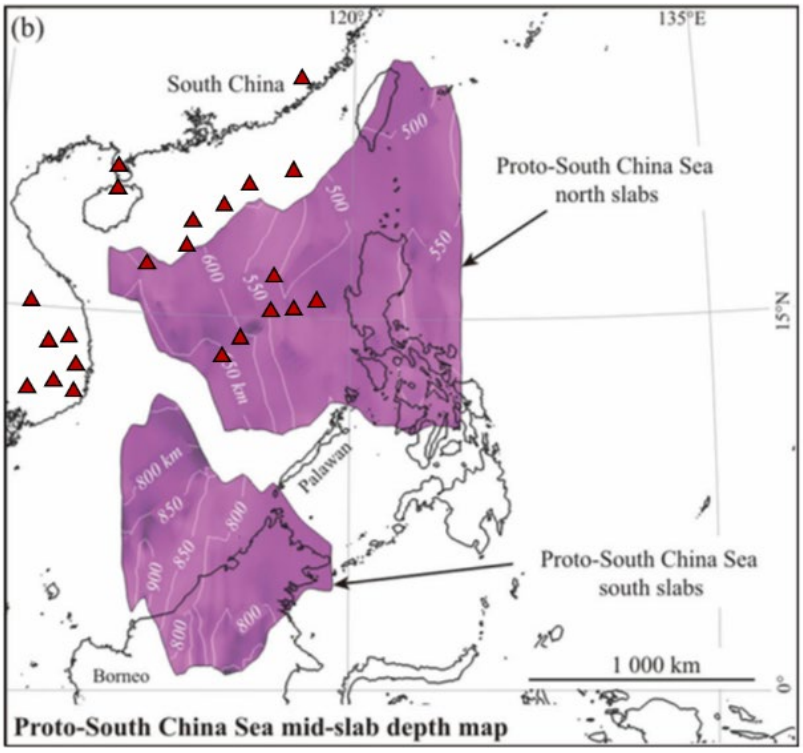

Figure 6- 25. Post-spreading magmatism and the PSCS slabs (Wu and Suppe, 2017). Occurrences of magmatism with OIB-liked geochemical characteristic inferred from deep mantle material, locating around the edge of the PSCS slabs.

Interestingly, deep seismic images commonly show reflectors beneath the Moho, and these are suspected to accompany magmatic intrusions (with strong amplitude) at shallow depth. Observation of a High-Velocity Layer (HVL or HVDLC, Gao et al. (2015); Chang et al. (2017) and reference therein) in the northern margin or few in southern margin (Figure 6- 26) have been mentioned in the literature and may illustrate features of intrusions tapping in the deep mantle. A post-rift uplift in the vicinity of Dongsha Island, located above the thickest HVL (Figure 6- 26) during Late Miocene has been debated (Xie et al., 2017). According to these authors, this would allow to visualize a complete image from the source, via the conduit, until the production of the post-rift magmatism, although detailed information such as the geophysical characteristics (velocity, rheology etc.) are lacking.

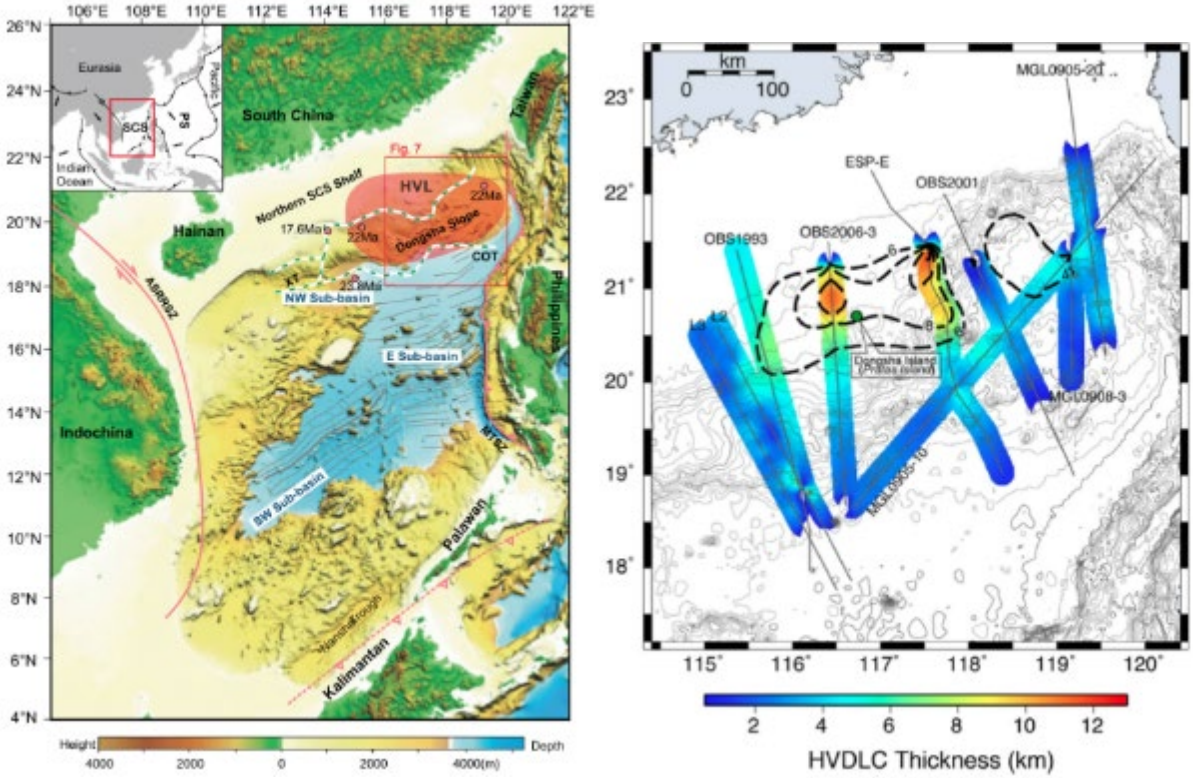

Figure 6- 26. Distribution of high-velocity layer (HVL) obtained from OBSs (Fan et al., 2017a) and estimated thickness (Chang et al., 2017). The thickest area is consistent with the location of Dongsha Island, which experienced uplift during Late Miocene.

A scheme to integrate Neogene magmatism on both margins

In the end of both the subduction-collision and the seafloor spreading, the break-off occurred by Middle to Late Miocene, resulting in the production of extensive magmatic intrusions in the SCS and the Borneo area. The detached subducting slab dominated the tectonic evolution. Several simulations suggest the consequence of a detachment slab upwelling the asthenosphere (Menant et al., 2016; Magni et al., 2017) (Figure 6- 27), as well as its sinking inducing deeper material traveling to the surface from the edge of slab as splash plumes (Davies and Bunge, 2006; Cullen et al., 2010) (Figure 6- 27). However, the subduction polarity seems to be controversial in the result of detached slab locating beneath the lower plate, and this issue is discussed details in the Section 6.3.2.

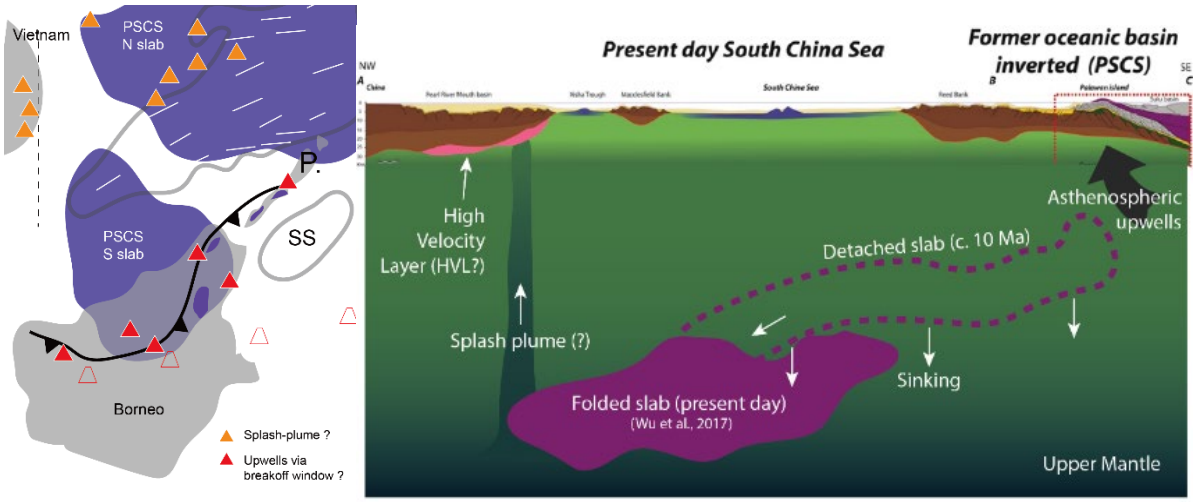

Figure 6- 27. A tentative model of the post-spreading and post-orogenic magmatism respectively in the SCS and PSCS margins (modified from Meresse et al. (2012)). The PSCS slab broke-off and sank into the mantle around 660 km, inducing magmatism from asthenospheric upwelling (passing through the newly formed asthenospheric window) in Palawan and Borneo. These may include also as splash plumes from deep mantle at the frontal edge in the SCS.

The correlation allows us to suggest that both cessation of spreading around 16Ma and termination of shortening in the SCS and the PSCS respectively resulted from a decrease of the slab pull. The onset of break-off marks the end of extensional stresses within the lower plate, and compressional stresses that sustained the compressional wedge in Borneo. This could imply a trade-off between subduction and the seafloor spreading in the SCS, the driving force being the subduction that becomes difficult from 23Ma before halting at 16Ma and the spreading in the SCS which was re-oriented at 23Ma and ceased at 16Ma. The evolution of this paired system is not fully resolved for the beginning of the rifting and the breakup, relative to the beginning of the subduction of the PSCS.

6.3 Geometry of PSCS Margin

The discussion above concerning the beginning of the subduction and the incipient shortening relies a lot on the geometry of the former margin of the PSCS, which is nowadays almost entirely disappeared. This study revisits the tectonics and the stratigraphy to finally show that the subduction-collision processes dominated both the opening and the closure of contiguous basins at the lower and the upper plate (Rangin et al., 1989; Lee and Lawver, 1995; Pubellier and Meresse, 2013). The formation of oceanic floor neighbors the rifted basins as discussed above, has a profound incidence on the behavior of the subduction, and eventually induces

rotations. This is observed all over SE Asia, from the South China Sea, the Celebes Sea formed in the Paleogene (Weissel, 1980; Silver and Rangin, 1991), to the back-arc opening of the Sulu Sea on the overriding plate (Rangin, 1989). This work is along the same line proposed early by (Holloway, 1982) in which as subduction-related extension on the PSCS lower plate in the SCS margin leads the evolutionary rifting and seafloor spreading in the SCS margin.

6.3.1 Shortening a V-shaped margin

On the other hand, the convergence of the PSCS margin ended with a period of collision along the subduction zone trench, and the geometry of the collision and the heterogeneity of subducting plate may have played a role. The collision-related rotation between Dangerous Ground and Borneo implies shorter-lived subduction of a narrower oceanic crust in the vicinity of Sarawak, whereas the proceeding subduction in Palawan and Sabah resulted from a wider oceanic crust on the lower plate. This offers a scenario, which implies that a lateral heterogeneity of the subducting plate drives the modalities of the subduction/collision process; and of course the above mentioned rotation.

Although we cannot have access to the precise geometry of the northern margin of the PSCS, we still observe that the presence of ophiolite in Borneo is restricted to the North Sabah and Palawan region. The distribution of outcrops and the gravity delineate faithfully the contour of the former obducted basin (Pubellier et al., 2004; Cullen, 2010; Sapin, 2010), considering the relatively autochtonous (intra-margin basin) ophiolites (Figure 6- 28).

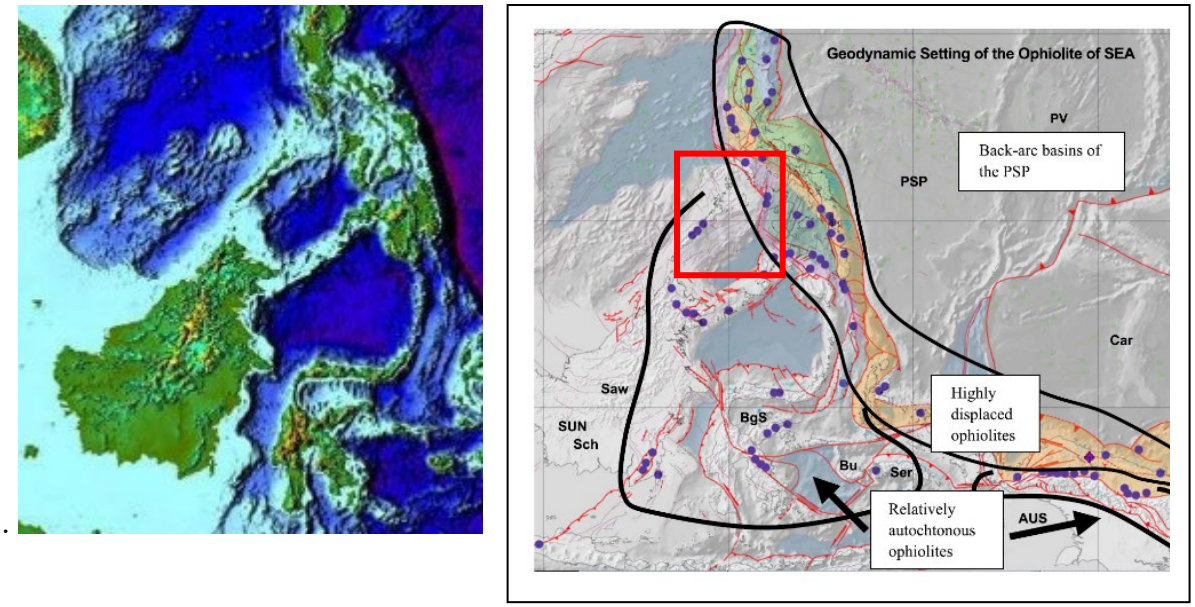

Figure 6- 28. Distribution of ophiolite complexes in the SE Asia (ref). The autochtonous ophiolites distribute in Sabah, Palawan and Sulawesi, and highly displaced ophiolites along the Philippine Mobile Belt (PMB). The obduction mentioned in this study is situated in the red rectangle.

Besides, the geochemical and structural studies shows that the subduction-related processes are obvious on Sabah and Palawan (Hall, 2013; Hall and Spakman, 2015; Hall and Breitfeld, 2017) and lacking slab in Sarawak (Breitfeld et al., 2019). Therefore, this spatial variation in the oceanic width gives the image of a configuration of the PSCS Margin as a series of basins narrowing toward the southwest, roughly in a V-shaped geometry (Figure 6- 29). A similar manner shows that the Celebes Sea passes to the N. Makassar Basin, and then to the S. Makassar Basins prior to the subduction. Therefore the configuration of the PSCS is probably rather similar to the present Celebes Sea/Makassar Basin, than a proper V-Shape like that of the SCS (Figure 6- 29).

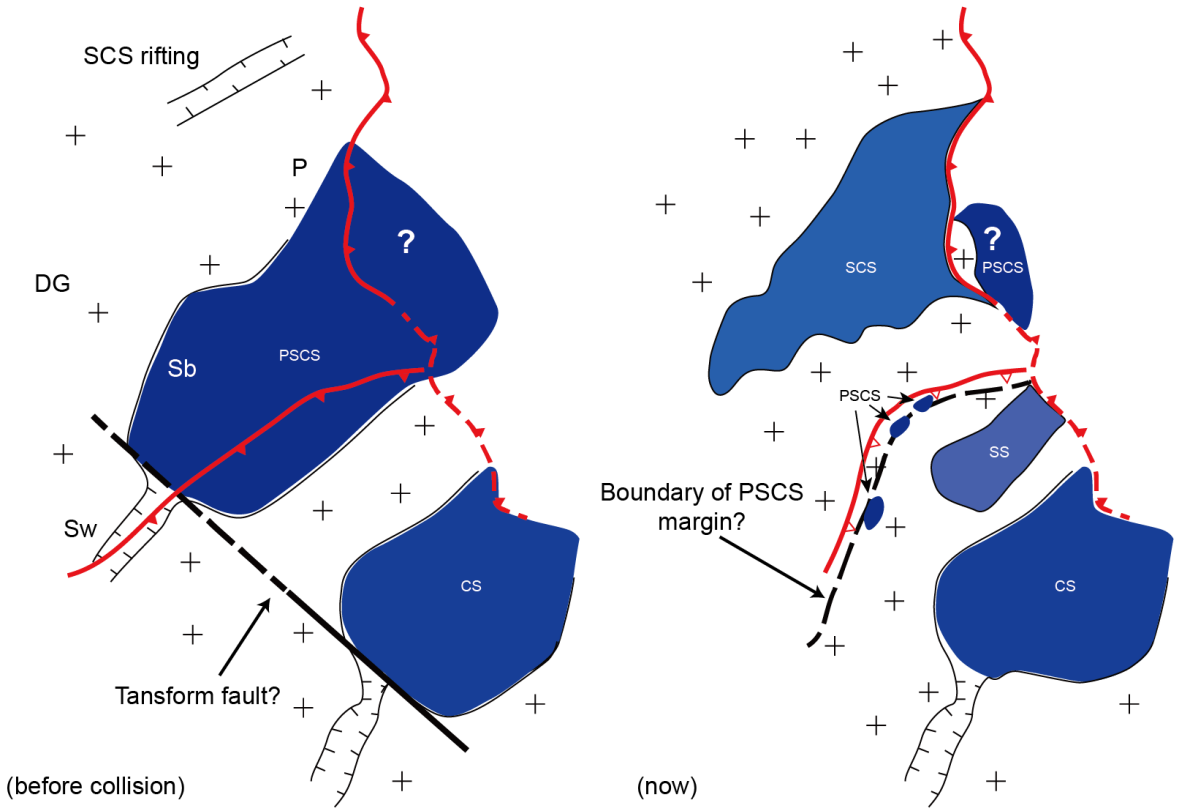

Figure 6- 29. Reconstruction of the PSCS margin. The rough V-shaped oceanic formation of the PSCS (is compared in the text to the Celebes Sea/Makassar Basin) dominated the geodynamic evolution during the subduction and collision processes. Note the different styles of narrowing toward the SW, with large transform faults or a proper V-shape in the South China Sea (SCS).

Furthermore, some ultramafic rocks in the Zambales Massif also dated Eocene and possibly Late Cretaceous (Bachman et al., 1983; Hawkins and Evans, 1983; Rossman et al., 1989) is an abnormally elevated massif (up to 1100m) next to the coast. The contrasting morpho-structures varies from S to N in terms of geometry and bathymetry shown on Figure 6- 30 (Lewis and Hayes, 1984). Unlike North of 17°N, the subduction zone is atypical and segmented with a southern part characterized by contrasted bathymetry including an extremely narrow wedge, a wide forearc basin showing morphological indicators of massive volcaniclastic deposits. This high-density package of rocks is unlikely to remain at such an elevation if thrust on accreted sediments, and thus a continental basement is suspected beneath the forearc by preliminary seismic data (Arfai et al., 2011). The origin of the micro-continent and the obducted ophiolite therefore and possibly derived from the PSCS in Palawan is illustrated on the tentative reconstruction on Figure 6- 29.

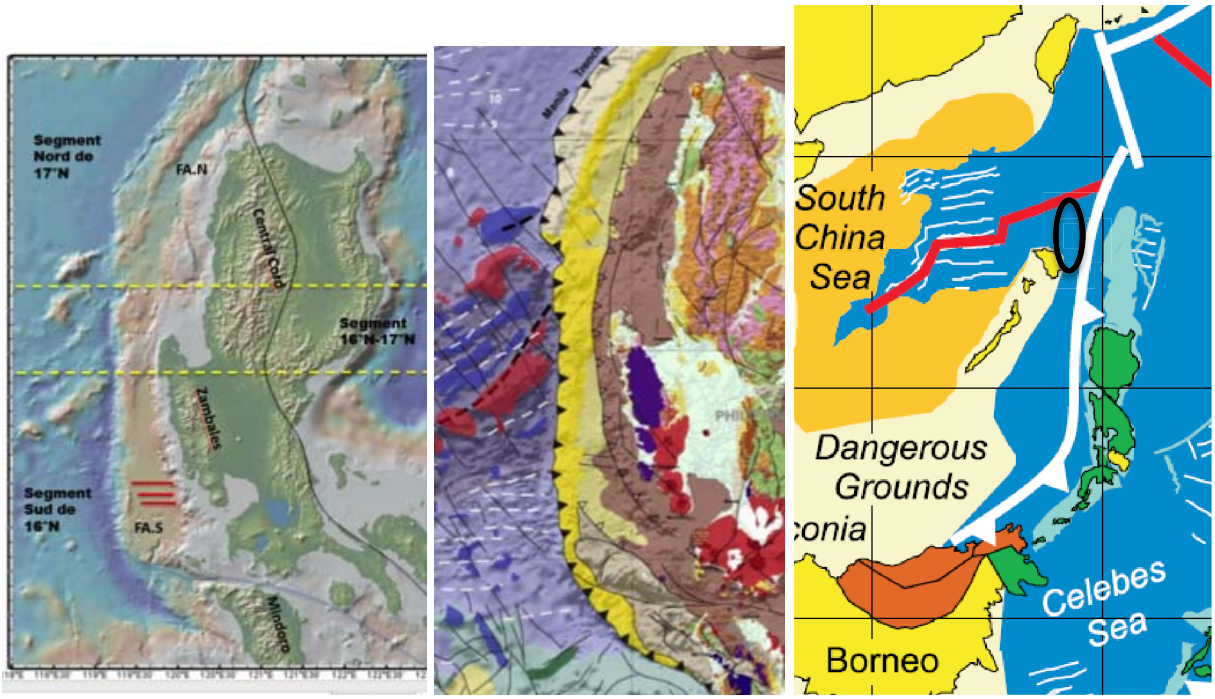

Figure 6- 30. Elevation, geological map and plate reconstruction in Luzon (Hall, 2012; Pubellier et al., 2016). The special of the Zambales Massif composed by ophiolite complex with 1000-meter elevation represents the possibility of an amalgamated block derived from the PSCS (black circle on the right figure) in Palawan. The massif of Zambales includes Cretaceous and Eocene ophiolites (just like the PSCS) and may have been thrust obliquely on a continental sliver.

6.3.2 Subduction polarity of the PSCS

The existence and subduction polarity of the PSCS slab has been a hot debate for several decades. We see in this study a consistent geodynamic framework and a scenario of evolution of a southward subduction which explain most geological features both offshore and onshore. It however has to face arguments from tomography that shows a possible location of the detached slab underneath the SCS identified by the high-velocity anomaly. The slab sinking causing subsidence and mantle intrusions also postdated the slab detachment in Borneo and Palawan, enabling us to interpret the detached PSCS Slab from the tomographic images.

However, one possible slab identified from the tomography underneath the SCS is actually in the north of the subduction trench, which interpreted the SCS as the upper plate and a back-arc opening. An alternative geological hypothesis proposes a double-sided subduction explaining the current location of the PSCS slab corresponding to a northward subduction (Wu et al., 2017; Scenario B on Figure 6- 31). However, less geological evidences support this scenario among the tectono-stratigraphy, forebulge feature, and volcanic arc to support the northern subduction.

An alternative manner, which I favor, to explain most geological observations is to keep a southward subduction (Scenario A and C on Figure 6- 31), and invoke the existence of an overturned subducted PSCS slab. It would accommodate the southward subduction and allow a detached slab in the north. The overturned feature is scarcely observed in the configuration in present day, however, shown in the simulation results in the condition of a fast subduction (van Hunen and Allen, 2011).

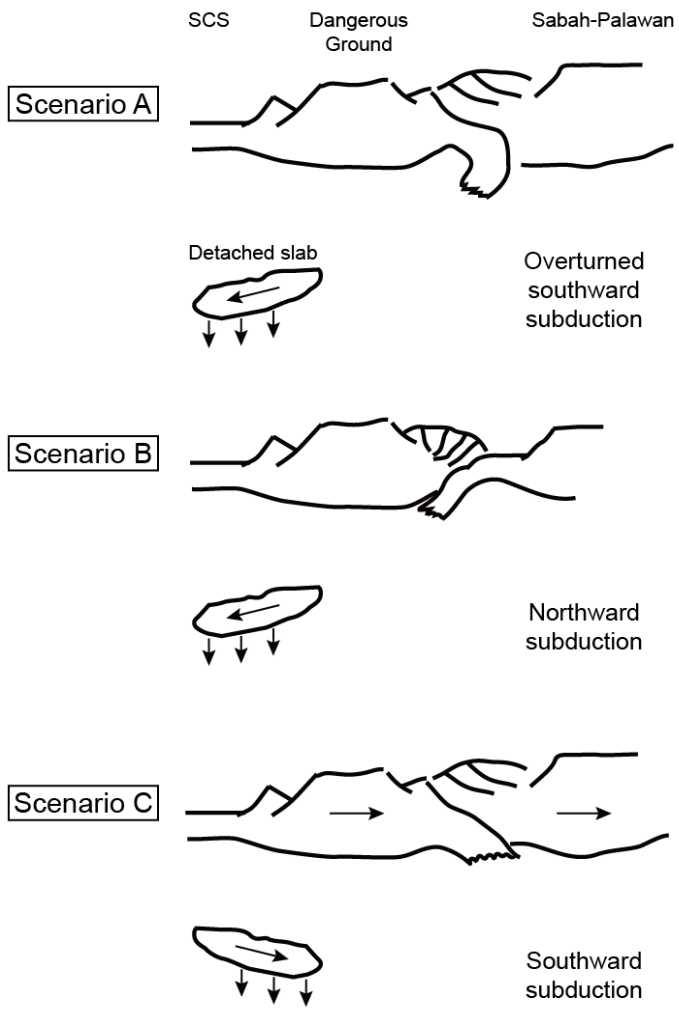

Figure 6- 31. Three scenarios of the PSCS slab detachment. (A) An overturned subducting slab and subsequent sinking after breakoff (this study). (B) a northward subduction (Wu and Suppe, 2017). (C) a southward subduction with relatively moving southward SCS margin.

In the scenario C, the SCS margin can resume its southward motion after break-off to adjust the southward subduction. The SCS seafloor spreading drove the southern SCS margins toward the subduction in the Borneo-Palawan which was a free edge prior to the slab breakoff. However, the slab detachment occurred concurrently or just after the termination of the seafloor spreading. Furthermore, the SE China Continent is relatively stable since the Late Cretaceous according to the paleomagnetism (Torsvik et al., 2012; Advokaat et al., 2018). This would hardly adapt the driving forces to southward movement after the slab detachment of the PSCS slab.

6.3.3 Mesozoic ophiolite in Borneo

A series of dating on the volcanic arc or metamorphic sole precise the timing of subduction (Keenan et al., 2016; Hennig-Breitfeld et al., 2019). Few ophiolites dated as Late Eocene (Keenan et al., 2016) suggest that the initiation of subduction may have taken place at the fossil mid-ocean ridge by Eocene times (Keenan et al., 2016). Taking into account the extensive distribution of PSCS from Early to Late Cretaceous age (Figure 6- 32) (Jasin and Geologi, 1992; Jasin and S, 1993; Asis and Jasin, 2012; Jasin and Tongkul, 2013), obliges us to consider a long period of spreading or a sporadic spreading in order to include these two ophiolitic complexes into the same scenario.

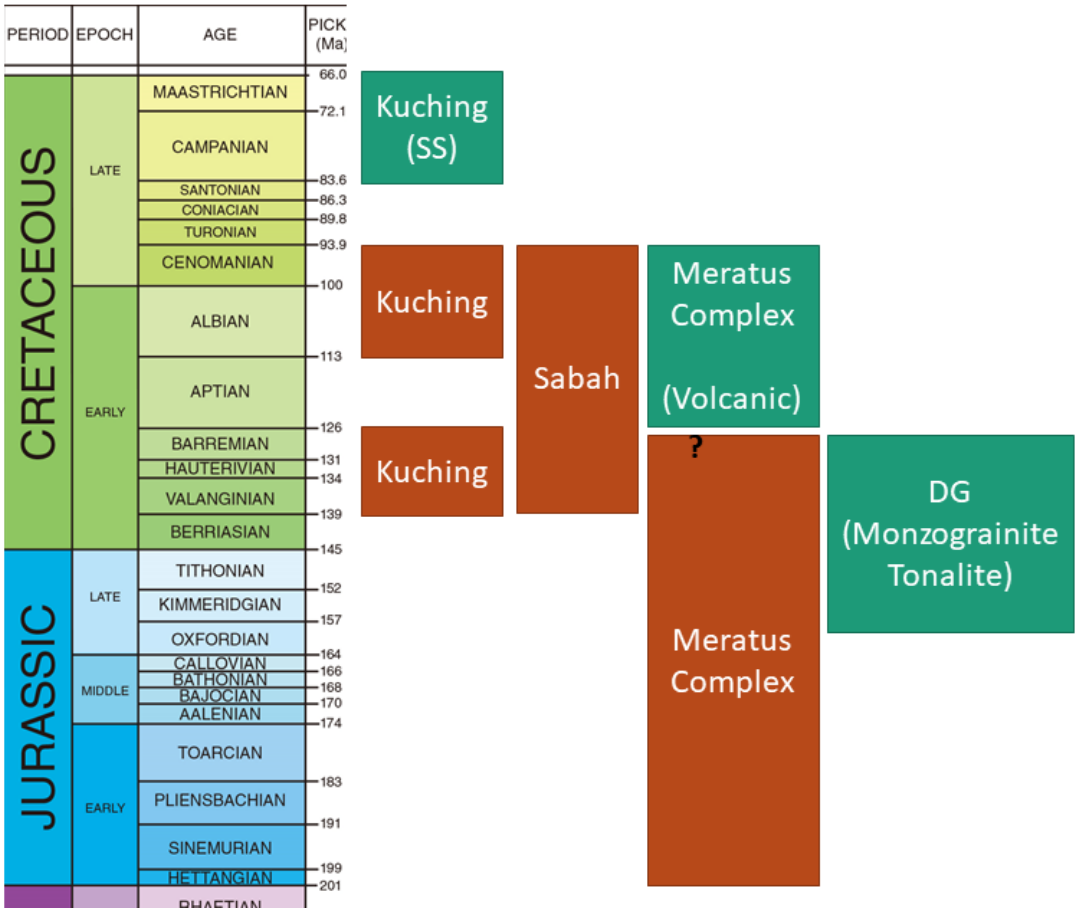

Figure 6- 32. Radiolarite bio-stratigraphy results from the ophiolite (brown) and mélange, granitoid ages (green) in Borneo.

In other words, if Eocene and Cretaceous ophiolites belong to the same oceanic formation, the long-lived oceanic crust should open for more than 70 million yrs. Yet, only part of the obducted oceanic crust (the weakest) is thrust. It may for instance, be the spreading center, transform faults, and the COT. Such long periods of seafloor accretion are common for large oceans; in

the Pacific, the Atlantic or the Indian Ocean. However, the distribution of the PSCS slab interpreted in the tomography displays a limited size for the long-lived oceanic formation.

An alternative setting is to invoke two separated periods of oceanic crust formation (Hutchison, 2010; Sapin, 2010; Keenan et al., 2016). In my work, the younger oceanic crust of the PSCS corresponds to the convergent period during the Cenozoic (Alpine Suture in Sapin (2010); Figure 6- 33). Other scattered ophiolite found along the southern Palawan and northern Borneo can extend further to Adio and Meratus ophiolite complexes, in East and Southeast Borneo (Tethys Suture of Sapin (2010); Figure 6- 33). This belt can splits on each side of the Sulu Sea after the back-arc opening. Their dating is mostly in Mesozoic times, which does not fit the Paleogene subduction-related evolution.

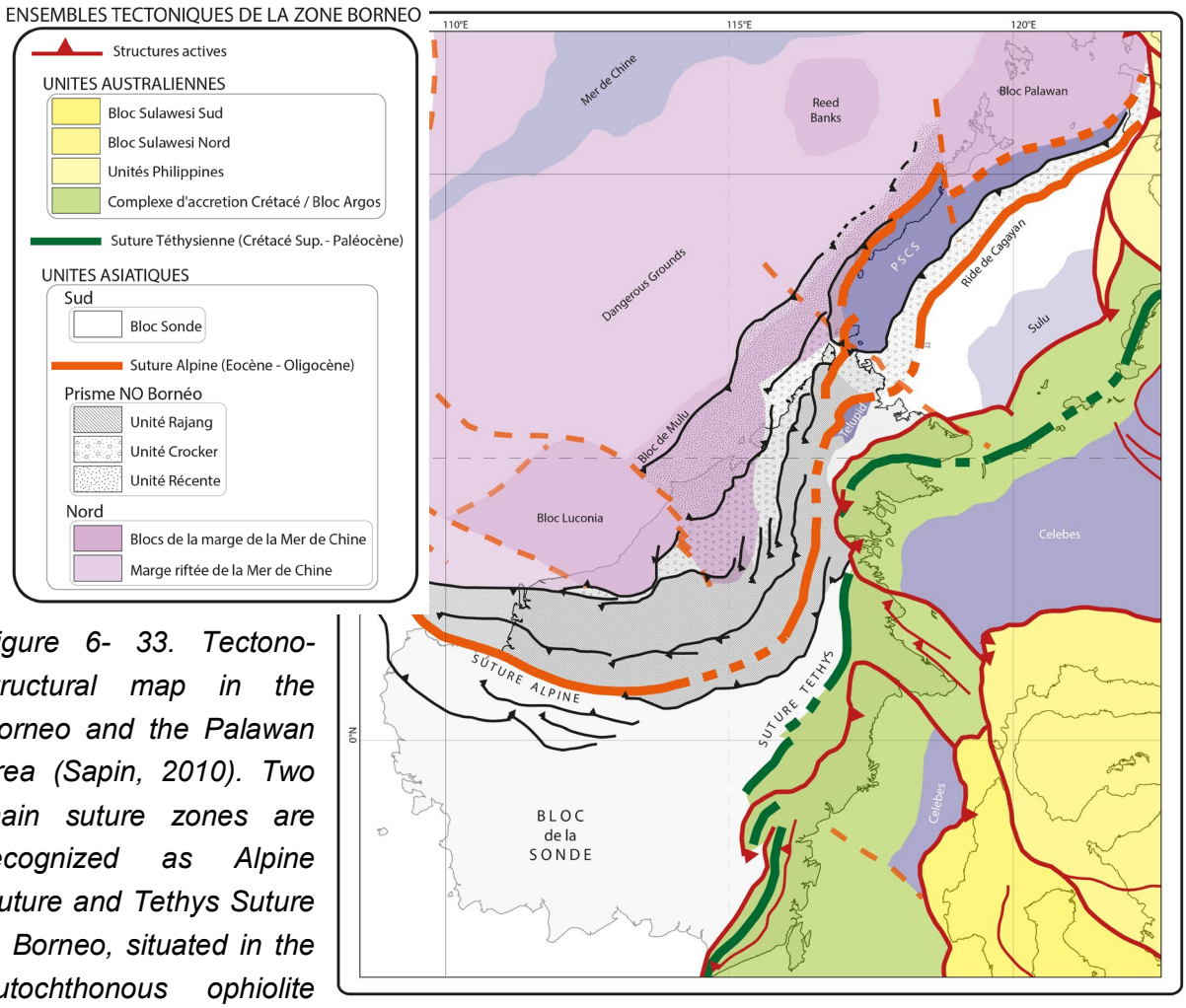

Figure 6- 33. Tectono-structural map in the Borneo and the Palawan area (Sapin, 2010). Two main suture zones are recognized as Alpine Suture and Tethys Suture in Borneo, situated in the autochthonous ophiolite group identified by (Pubellier et al., 2004) in the SE Asia.

If we consider the Mesozoic ophiolite as part of another period of oceanic formation, a speculative but new evolution of PSCS suggesting divergent and convergent periods during Mesozoic and Cenozoic times may be proposed (Figure 6- 34). The basement of the Cagayan Ridge (CR) and Sulu Arc documented Mesozoic metamorphic and igneous rocks, which can correlate with SE China (Liu et al., 2014), so that these area were juxtaposed if we close all the Cenozoic marginal seas in a simple reconstruction. The subsequent formation of the Tertiary PSCS (T PSCS) started, and the Mesozoic PSCS (K PSCS) drifted away from Eurasia Plate creating slivers of scattered micro-continents; each of them keeping bits and pieces of the Cretaceous ophiolite (Figure 6- 34). All the above-mentioned basins and oceanic floors were jamming by the time the SCS was opening (Figure 6- 31d).

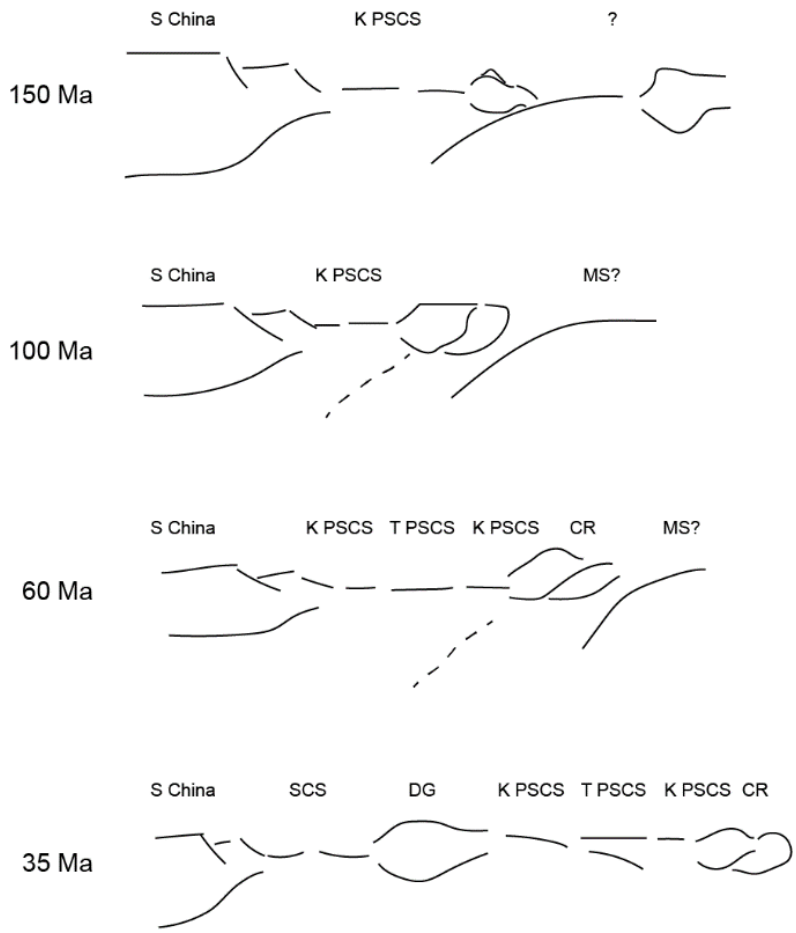

Figure 6- 34. Synthesis of the evolution of the PSCS slabs. The Albian ophiolite presents as the Cretaceous PSCS was formed during the older convergent setting, and was followed by a back-arc extension setting during the Early Paleocene time. CR: Cagayan Ridge. DG: Dangerous Ground. MS: Molucca Sea.

Conclusion

This study uses tectono-stratigraphy to argue that the opening in the South China Sea was strongly affected by the closure of the Proto-South China Sea in the Borneo and Palawan area during Cenozoic times. The South China Sea extended dramatically since Early Eocene by the means of a dense network of normal faults and detachment until a breakup, which propagated southwestward, creating a diachronous variation and migration of the tectonic styles along strike the margins. There was however, change the extensional spreading direction from N-S to NW-SE around latest Oligocene. This period is concomitant with a counter-clockwise rotation of Borneo, which is induced by the heterogeneous lithosphere of subducting plate that collision in the south as well as coeval subduction in the north. This was also followed by the Sulu Sea opening as a back-arc basin. Both the seafloor spreading and the closure terminated synchronously at 16 Ma. Interestingly, the subsequent slab detachment produced large amount of magmatism in the PSCS margin coeval to magmatic intrusions within the SCS margin, suggesting a common influence of the detached PSCS slab.

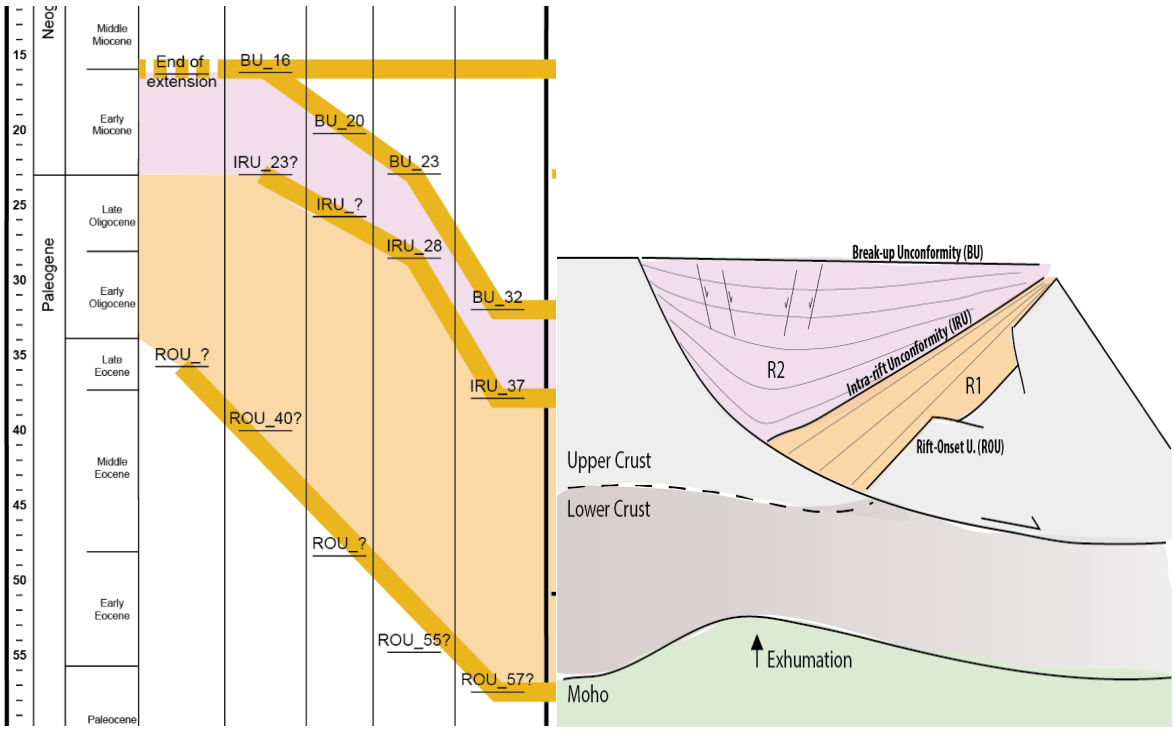

Reference

Abbott, L. D., Silver, E. A., and Galewsky, J., 1994, Structural evolution of a modern arc-continent collision in Papua New Guinea: Tectonics, v. 13, no. 5, p. 1007-1034.

Advokaat, E. L., Marshall, N. T., Li, S., Spakman, W., Krijgsman, W., and van Hinsbergen, D. J. J., 2018, Cenozoic Rotation History of Borneo and Sundaland, SE Asia Revealed by Paleomagnetism, Seismic Tomography, and Kinematic Reconstruction: Tectonics, v. 37, no. 8, p. 2486-2512.

Almasco, J. N., Rodolfo, K., Fuller, M., and Frost, G., 2000, Paleomagnetism of Palawan, Philippines: Journal of Asian Earth Sciences, v. 18, no. 3, p. 369-389.

Arfai, J., Franke, D., Gaedicke, C., Lutz, R., Schnabel, M., Ladage, S., Berglar, K., Aurelio, M., et al., 2011, Geological evolution of the West Luzon Basin (South China Sea, Philippines): Marine Geophysical Research, v. 32, no. 3, p. 349-362.

Armijo, R., Meyer, B., King, G. C. P., Rigo, A., and Papanastassiou, D., 1996, Quaternary evolution of the Corinth Rift and its implications for the Late Cenozoic evolution of the Aegean: Geophysical Journal International, v. 126, no. 1, p. 11-53.

Asis, J., and Jasin, B., 2012, Aptian to Turonian Radiolaria from the Darvel Bay Ophiolite Complex, Kunak, Sabah: Bulletin of the Geological Society of Malaysia, no. 58, p. 89-96.

Audley-Charles, M. G., Carter, D. J., Barber, A. J., Norvick, M. S., and Tjokrosapoetro, S., 1979, Reinterpretation of the geology of Seram: implications for the Banda Arcs and northern Australia: Journal of the Geological Society, v. 136, no. 5, p. 547.

Augustin, N., Devey, C. W., van der Zwan, F. M., Feldens, P., Tominaga, M., Bantan, R. A., and Kwasnitschka, T., 2014, The rifting to spreading transition in the Red Sea: Earth and Planetary Science Letters, v. 395, p. 217-230.

Aurelio, M. A., Dianala, J. D. B., Taguibao, K. J. L., Pastoriza, L. R., Reyes, K., Sarande, R., and Lucero, A., 2017, Seismotectonics of the 6 February 2012 Mw 6.7 Negros Earthquake, central Philippines: Journal of Asian Earth Sciences, v. 142, p. 93-108.

Aurelio, M. A., Forbes, M. T., Taguibao, K. J. L., Savella, R. B., Bacud, J. A., Franke, D., Pubellier, M., Savva, D., et al., 2014, Middle to Late Cenozoic tectonic events in south and central Palawan (Philippines) and their implications to the evolution of the south-eastern margin of South China Sea: Evidence from onshore structural and offshore seismic data: Marine and Petroleum Geology, v. 58, no. 0, p. 658-673.

Aurelio, M. A., Pena, R. E., and Taguibao, K. J. L., 2013, Sculpting the Philippine archipelago since the Cretaceous through rifting, oceanic spreading, subduction, obduction, collision and strike-slip faulting: Contribution to IGMA5000: Journal of Asian Earth Sciences, v. 72, p. 102-107.

Bachman, S. B., Lewis, S. D., and Schweller, W. J., 1983, Evolution of a forearc basin, Luzon central valley, Philippines: AAPG bulletin, v. 67, no. 7, p. 1143-1162.

Bader, A. G., Pubellier, M., Rangin, C., Deplus, C., and Louat, R., 1999, Active slivering of oceanic crust along the Molucca ridge (Indonesia-Philippine): Implication for ophiolite incorporation in a subduction wedge?: Tectonics, v. 18, no. 4, p. 606-620.

Balaguru, A., Nichols, G., and Hall, R., 2003, The origin of the 'circular basins' of Sabah, Malaysia: Bulletin of the Geological Society of Malaysia.

Barber, A. J., 2013, The origin of mélanges: Cautionary tales from Indonesia: Journal of Asian Earth Sciences, v. 76, p. 428-438.

Barber, A. J., Crow, M. J., and Milsom, J. S., 2005, Sumatra: Geology, Resources and Tectonic Evolution: Geological Society, London, Memoirs, v. 31, no. 1.

Barckhausen, U., Engels, M., Franke, D., Ladage, S., and Pubellier, M., 2014, Evolution of the South China Sea: Revised ages for breakup and seafloor spreading: Marine and Petroleum Geology, v. 58, Part B, no. 0, p. 599-611.

Barckhausen, U., and Roeser, H. A., 2004, Seafloor Spreading Anomalies in the South China Sea Revisited, Continent-Ocean Interactions Within East Asian Marginal Seas, American Geophysical Union, p. 121-125.

Berthelon, J., Yuan, X., Bouziat, A., Souloumiac, P., Pubellier, M., Cornu, T., and Maillot, B., 2018, Mechanical restoration of gravity instabilities in the Brunei margin, N.W. Borneo: Journal of Structural Geology, v. 117, p. 148-162.

Bladon, G. M., and Supriatna, S., 1989, Catalogue of Isotopic Ages Commisioned by the Indonesia-Australia Geological Mapping Project for Igneous and Metamorphic Rocks in Kalimantan: Preliminary Geological Report, Indonesia-Australia Geological Mapping Project, Geological Research and ….

Brakel, A. T., Totterdell, J. M., Wells, A. T., and Nicoll, M. G., 2009, Sequence stratigraphy and fill history of the Bowen Basin, Queensland: Australian Journal of Earth Sciences, v. 56, no. 3, p. 401-432.

Breitfeld, H. T., Macpherson, C., Hall, R., Thirlwall, M., Ottley, C. J., and Hennig-Breitfeld, J., 2019, Adakites without a slab: Remelting of hydrous basalt in the crust and shallow mantle of Borneo to produce the Miocene Sintang Suite and Bau Suite magmatism of West Sarawak: Lithos, v. 344-345, p. 100-121.

Briais, A., Patriat, P., and Tapponnier, P., 1993, Updated interpretation of magnetic anomalies and seafloor spreading stages in the south China Sea: Implications for the Tertiary tectonics of Southeast Asia: Journal of Geophysical Research: Solid Earth, v. 98, no. B4, p. 6299-6328.

Brune, S., 2018, Forces within continental and oceanic rifts: Numerical modeling elucidates the impact of asthenospheric flow on surface stress: Geology, v. 46, no. 2, p. 191-192.

Brune, S., Heine, C., Clift, P. D., and Pérez-Gussinyé, M., 2017, Rifted margin architecture and crustal rheology: Reviewing Iberia-Newfoundland, Central South Atlantic, and South China Sea: Marine and Petroleum Geology, v. 79, p. 257-281.

Calvès, G., Huuse, M., Clift, P. D., and Brusset, S., 2015, Giant fossil mass wasting off the coast of West India: The Nataraja submarine slide: Earth and Planetary Science Letters, v. 432, p. 265-272.

Cameselle, A. L., Ranero, C. R., Franke, D., and Barckhausen, U., 2015, The continent-ocean transition on the northwestern South China Sea: Basin Research.

Cao, Y., Li, C.-F., and Yao, Y., 2017, Thermal subsidence and sedimentary processes in the South China Sea Basin: Marine Geology, v. 394, p. 30-38.

Chan, L. S., Shen, W., and Pubellier, M., 2010, Polyphase rifting of greater Pearl River Delta region (South China): Evidence for possible rapid changes in regional stress configuration: Journal of Structural Geology, v. 32, no. 6, p. 746-754.

Chang, J.-H., Hsieh, H.-H., Mirza, A., Chang, S.-P., Hsu, H.-H., Liu, C.-S., Su, C.-C., Chiu, S.-D., et al., 2017, Crustal structure north of the Taiping Island (Itu Aba Island), southern margin of the South China Sea: Journal of Asian Earth Sciences, v. 142, p. 119-133.

Chang, J.-H., Hsu, H.-H., Liu, C.-S., Lee, T.-Y., Chiu, S.-D., Su, C.-C., Ma, Y.-F., Chiu, Y.-H., et al., 2015, Seismic sequence stratigraphic analysis of the carbonate platform, north offshore Taiping Island, Dangerous Grounds, South China Sea: Tectonophysics.

Chang, J.-H., Yu, H.-S., Hsu, H.-H., and Liu, C.-S., 2012, Forebulge migration in late Cenozoic Western Taiwan Foreland Basin: Tectonophysics, v. 578, p. 117-125.

Chang, J.-H., Yu, H.-S., Lee, T.-Y., Hsu, H.-H., Liu, C.-S., and Tsai, Y.-T., 2013, Characteristics of the outer rise seaward of the Manila Trench and implications in Taiwan–Luzon convergent belt, South China Sea: Marine Geophysical Research, v. 33, no. 4, p. 351-367.

Chang, S.-P., Fathiyah Jamaludin, S., and Pubellier, M., Can the Northern Borneo Mélange Help Us Understand the End of the Subduction?, in Proceedings EGU General Assembly Conference Abstracts2018, Volume 20, p. 16052.

Chang, S.-P., Jamaludin, S. N. F., Pubellier, M., M. Zainuddin, N., and Choong, C. M., 2019, Collision, mélange and circular basins in north Borneo: A genetic link?: Journal of Asian Earth Sciences, v. 181, p. 103895.

Cheng, X., and Qi, Y., 2007, Trends of sea level variations in the South China Sea from merged altimetry data: Global and Planetary Change, v. 57, no. 3, p. 371-382.

Chenin, P., Manatschal, G., Picazo, S., Müntener, O., Karner, G., Johnson, C., and Ulrich, M., 2017, Influence of the architecture of magma-poor hyperextended rifted margins on orogens produced by the closure of narrow versus wide oceans: Geosphere, v. 13, no. 2, p. 559-576.

Chu, M.-F., Chung, S.-L., Song, B., Liu, D., O'Reilly, S. Y., Pearson, N. J., Ji, J., and Wen, D.-J., 2006, Zircon U-Pb and Hf isotope constraints on the Mesozoic tectonics and crustal evolution of southern Tibet: Geology, v. 34, no. 9, p. 745.

Chung, S.-L., Chu, M.-F., Zhang, Y., Xie, Y., Lo, C.-H., Lee, T.-Y., Lan, C.-Y., Li, X., et al., 2005, Tibetan tectonic evolution inferred from spatial and temporal variations in post-collisional magmatism: Earth-Science Reviews, v. 68, no. 3-4, p. 173-196.

Clark, J., 2017, Malaysia: Neogene tectonics of northern Borneo: a simple model to explain complex structures within Miocene-Recent deltaic-deepwater sediments both onshore and offshore. , The Seapex Exploration Conference 2017.

Clements, B., and Hall, R., 2011, A record of continental collision and regional sediment flux for the Cretaceous and Palaeogene core of SE Asia: implications for early Cenozoic palaeogeography: Journal of the Geological Society, v. 168, no. 5, p. 1187-1200.

Clennell, B., 1991, The origin and tectonic significance of melanges in Eastern Sabah, Malaysia: Journal of Southeast Asia Earth Science, v. 6, no. 3/4, p. 407-429.

-, 1996, Far-field and gravity tectonics in Miocene basins of Sabah, Malaysia.

Clerc, C., Ringenbach, J.-C., Jolivet, L., and Ballard, J.-F., 2018, Rifted margins: Ductile deformation, boudinage, continentward-dipping normal faults and the role of the weak lower crust: Gondwana Research, v. 53, p. 20-40.

Clift, P., and Lin, J., 2001, Preferential mantle lithospheric extension under the South China margin: Marine and Petroleum Geology, v. 18, no. 8, p. 929-945.

Clift, P. D., 2015, Coupled onshore erosion and offshore sediment loading as causes of lower crust flow on the margins of South China Sea: Geoscience Letters, v. 2, no. 1.

Clift, P. D., Brune, S., and Quinteros, J., 2015, Climate changes control offshore crustal structure at South China Sea continental margin: Earth and Planetary Science Letters, v. 420, p. 66-72.

Clift, P. D., and Sun, Z., 2006, The sedimentary and tectonic evolution of the Yinggehai-Song Hong basin and the southern Hainan margin, South China Sea: Implications for Tibetan uplift and monsoon intensification: Journal of Geophysical Research: Solid Earth, v. 111, no. B6, p. n/a-n/a.

Codegone, G., Festa, A., Dilek, Y., and Pini, G. A., 2012, Small-scale polygenetic mélanges in the Ligurian accretionary complex, Northern Apennines, Italy, and the role of shale diapirism in superposed mélange evolution in orogenic belts: Tectonophysics, v. 568-569, p. 170-184.

Collenette, P., 1958, The geology and mineral resources of the Jesselton-Kinabalu area, North Borneo. : British Terr. Borneo Geol. Survey Dept. Mem., v. 6.

-, 1965, The geology and mineral resources of the Pensiangan and upper Kinabatangan area, Sabah, Malaysia: Borneo Region Malaysia Geol. Survey Mem. , v. 12.

Cooper, P., and Brian, T., 1989, Seismicity and focal mechanisms at the New Britain Trench related to deformation of the lithosphere: Tectonophysics, v. 164, no. 1, p. 25-40.

Cottam, M., Hall, R., Sperber, C., and Armstrong, R., 2010, Pulsed emplacement of the Mount Kinabalu granite, northern Borneo: Journal of the Geological Society, v. 167, no. 1, p. 49-60.

Cottam, M. A., Hall, R., Sperber, C., Kohn, B. P., Forster, M. A., and Batt, G. E., 2013, Neogene rock uplift and erosion in northern Borneo: evidence from the Kinabalu granite, Mount Kinabalu: Journal of the Geological Society, v. 170, no. 5, p. 805-816.

Cowan, D. S., 1985, Structural styles in Mesozoic and Cenozoic mélanges in the western Cordillera of North America: Geological Society of America Bulletin, v. 96, no. 4, p. 451.

Cowan, D. S., and Page, B. M., 1975, Recycled Franciscan Material in Franciscan Mélange West of Paso Robles, California: Geological Society of America Bulletin, v. 86, no. 8, p. 1089.

Crosby, A., and McKenzie, D., 2009, An analysis of young ocean depth, gravity and global residual topography: Geophysical Journal International, v. 178, no. 3, p. 1198-1219.

Crosby, A., McKenzie, D., and Sclater, J., 2006, The relationship between depth, age and gravity in the oceans: Geophysical Journal International, v. 166, no. 2, p. 553-573.

Cruciani, F., and Barchi, M. R., 2016, The Lamu Basin deepwater fold-and-thrust belt: An example of a margin-scale, gravity-driven thrust belt along the continental passive margin of East Africa: Tectonics, v. 35, no. 3, p. 491-510.

Cullen, A., Reemst, P., Henstra, G., Gozzard, S., and Ray, A., 2010, Rifting of the South China Sea: new perspectives: Petroleum Geoscience, v. 16, no. 3, p. 273-282.

Cullen, A. B., 2010, Transverse segmentation of the Baram-Balabac Basin, NW Borneo: refining the model of Borneo's tectonic evolution: Petroleum Geoscience, v. 16, no. 1, p. 3-29.
Davies, J. H., and Bunge, H. P., 2006, Are splash plumes the origin of minor hotspots?: Geology, v. 34, no. 5.
Deng, P., Mei, L., Liu, J., Zheng, J., Liu, M., Cheng, Z., and Guo, F., 2018, Episodic normal faulting and magmatism during the syn-spreading stage of the Baiyun sag in Pearl River Mouth Basin: response to the multi-phase seafloor spreading of the South China Sea: Marine Geophysical Research, v. 40, no. 1, p. 33-50.
Ding, W.-w., Li, J.-b., Li, M.-b., Qiu, X.-l., Fang, Y.-x., and Tang, Y., 2008, A Cenozoic tectono-sedimentary model of the Tainan Basin, the South China Sea: evidence from a multi-channel seismic profile: Journal of Zhejiang University SCIENCE A, v. 9, no. 5, p. 702-713.
Ding, W., Franke, D., Li, J., and Steuer, S., 2013a, Seismic stratigraphy and tectonic structure from a composite multi-channel seismic profile across the entire Dangerous Grounds, South China Sea: Tectonophysics, v. 582, p. 162-176.
Ding, W., and Li, J., 2016a, Conjugate margin pattern of the Southwest Sub-basin, South China Sea: insights from deformation structures in the continent-ocean transition zone: Geological Journal, v. 51, p. 524-534.
-, 2016b, Propagated rifting in the Southwest Sub-basin, South China Sea: Insights from analogue modelling: Journal of Geodynamics, v. 100, p. 71-86.
Ding, W., Li, J., and Clift, P. D., 2016, Spreading dynamics and sedimentary process of the Southwest Sub-basin, South China Sea: Constraints from multi-channel seismic data and IODP Expedition 349: Journal of Asian Earth Sciences, v. 115, p. 97-113.
Ding, W., Li, J., Dong, C., and Fang, Y., 2014, Oligocene–Miocene carbonates in the Reed Bank area, South China Sea, and their tectono-sedimentary evolution: Marine Geophysical Research, v. 36, no. 2-3, p. 149-165.
Ding, W., Li, J., Li, J., Fang, Y., and Tang, Y., 2013b, Morphotectonics and evolutionary controls on the Pearl River Canyon system, South China Sea: Marine Geophysical Research, v. 34, no. 3-4, p. 221-238.
Ding, W., Sun, Z., Mohn, G., Nirrengarten, M., Tugend, J., Manatschal, G., and Li, J., 2019, Lateral evolution of the rift-to-drift transition in the South China Sea: Evidence from multi-channel seismic data and IODP Expeditions 367&368 drilling results: Earth and Planetary Science Letters, p. 115932.
Doig, A., and Stanmore, P., 2012, The Clarence-Moreton Basin in New South Wales; geology, stratigraphy and coal seam gas characteristics: Eastern Australasian Basins Symposium IV.
Dong, M., Wu, S., Zhang, J., Xu, X., Gao, J., and Song, T., 2018a, Lithospheric structure of the Southwest South China Sea: implications for rifting and extension: International Geology Review, p. 1-14.
Dong, S., Zhang, Y., Li, H., Shi, W., Xue, H., Li, J., Huang, S., and Wang, Y., 2018b, The Yanshan orogeny and late Mesozoic multi-plate convergence in East Asia—Commemorating 90th years of the "Yanshan Orogeny": SCIENCE CHINA Earth Sciences, v. 61, no. 12, p. 1888-1909.
Duerto, L., and McClay, K., 2011, Role of the shale tectonics on the evolution of the Eastern Venezuelan Cenozoic thrust and fold belt: Marine and Petroleum Geology, v. 28, no. 1, p. 81-108.
Duretz, T., Gerya, T. V., and Spakman, W., 2014, Slab detachment in laterally varying subduction zones: 3-D numerical modeling: Geophysical Research Letters, v. 41, no. 6, p. 1951-1956.
Duretz, T., Petri, B., Mohn, G., Schmalholz, S. M., Schenker, F. L., and Muntener, O., 2016, The importance of structural softening for the evolution and architecture of passive margins: Sci Rep, v. 6, p. 38704.
Encarnacion, J., and Mukasa, S. B., 1997, Age and geochemistry of an 'anorogenic' crustal melt and implications for I-type granite petrogenesis: Lithos, v. 42, no. 1-2, p. 1-13.
Eyles, C., Mory, A., and Eyles, N., 2003, Carboniferous-Permian facies and tectono-stratigraphic successions of the glacially influenced and rifted Carnarvon Basin, Western Austalia: Sedimentary Geology, v. 155, p. 63-86.
Fan, C., Xia, S., Zhao, F., Sun, J., Cao, J., Xu, H., and Wan, K., 2017a, New insights into the magmatism in the northern margin of the South China Sea: Spatial features and volume of intraplate seamounts: Geochemistry, Geophysics, Geosystems, v. 18, no. 6, p. 2216-2239.

Fan, J., Zhao, D., Dong, D., and Zhang, G., 2017b, P-wave tomography of subduction zones around the central Philippines and its geodynamic implications: Journal of Asian Earth Sciences, v. 146, p. 76-89.

Faure, M., and Ishida, K., 1990, The Mid-Upper Jurassic olistostrome of the west Philippines: a distinctive key-marker for the North Palawan block: Journal of Southeast Asian Earth Sciences, v. 4, no. 1, p. 61-67.

Faure, M., Vuong, N., Hoai, L., and Lepvrier, C., 2018, Early Paleozoic or Early-Middle Triassic collision between the South China and Indochina Blocks: The controversy resolved? Structural insights from the Kon Tum massif (Central Vietnam): Journal of Asian Earth Sciences, v. 166.

Festa, A., Dilek, Y., Codegone, G., Cavagna, S., and Pini, G. A., 2013, Structural anatomy of the Ligurian accretionary wedge (Monferrato, NW Italy), and evolution of superposed melanges: Geological Society of America Bulletin, v. 125, no. 9-10, p. 1580-1598.

Festa, A., Dilek, Y., Gawlick, H.-J., and Missoni, S., 2014, Mass-transport deposits, olistostromes and soft-sediment deformation in modern and ancient continental margins, and associated natural hazards: Marine Geology, v. 356, p. 1-4.

Festa, A., Dilek, Y., Pini, G. A., Codegone, G., and Ogata, K., 2012, Mechanisms and processes of stratal disruption and mixing in the development of mélanges and broken formations: Redefining and classifying mélanges: Tectonophysics, v. 568-569, p. 7-24.

Festa, A., Ogata, K., Pini, G. A., Dilek, Y., and Alonso, J. L., 2016, Origin and significance of olistostromes in the evolution of orogenic belts: A global synthesis: Gondwana Research, v. 39, p. 180-203.

Festa, A., Pini, G. A., Ogata, K., and Dilek, Y., 2019, Diagnostic features and field-criteria in recognition of tectonic, sedimentary and diapiric mélanges in orogenic belts and exhumed subduction-accretion complexes: Gondwana Research, v. 74, p. 7-30.

Franke, D., 2013, Rifting, lithosphere breakup and volcanism: Comparison of magma-poor and volcanic rifted margins: Marine and Petroleum Geology, v. 43, p. 63-87.

Franke, D., Barckhausen, U., Baristeas, N., Engels, M., Ladage, S., Lutz, R., Montano, J., Pellejera, N., et al., 2011, The continent-ocean transition at the southeastern margin of the South China Sea: Marine and Petroleum Geology, v. 28, no. 6, p. 1187-1204.

Franke, D., Barckhausen, U., Heyde, I., Tingay, M., and Ramli, N., 2008, Seismic images of a collision zone offshore NW Sabah/Borneo: Marine and Petroleum Geology, v. 25, no. 7, p. 606-624.

Franke, D., Savva, D., Pubellier, M., Steuer, S., Mouly, B., Auxietre, J.-L., Meresse, F., and Chamot-Rooke, N., 2014, The final rifting evolution in the South China Sea: Marine and Petroleum Geology, v. 58, p. 704-720.

Fricaud, L., 1984, Etude géologique et structurale de la marge ouest Palawan (mer de Chine méridionale).

Fuller, M., Ali, J. R., Moss, S. J., Frost, G. M., Richter, B., and Mahfi, A., 1999, Paleomagnetism of Borneo: Journal of Asian Earth Sciences, v. 17, no. 1-2, p. 3-24.

Fuller, M., Haston, R., Lin, J.-L., Richter, B., Schmidtke, E., and Almasco, J., 1991, Tertiary paleomagnetism of regions around the South China Sea: Journal of Southeast Asian Earth Sciences, v. 6, no. 3-4, p. 161-184.

Fyhn, M. B. W., Boldreel, L. O., and Nielsen, L. H., 2009, Geological development of the Central and South Vietnamese margin: Implications for the establishment of the South China Sea, Indochinese escape tectonics and Cenozoic volcanism: Tectonophysics, v. 478, no. 3, p. 184-214.

Fyhn, M. B. W., Boldreel, L. O., Nielsen, L. H., Giang, T. C., Nga, L. H., Hong, N. T. M., Nguyen, N. D., and Abatzis, I., 2013, Carbonate platform growth and demise offshore Central Vietnam: Effects of Early Miocene transgression and subsequent onshore uplift: Journal of Asian Earth Sciences, v. 76, p. 152-168.

Gao, J., Bangs, N., Wu, S., Cai, G., Han, S., Ma, B., Wang, J., Xie, Y., et al., 2019, Post-seafloor spreading magmatism and associated magmatic hydrothermal systems in the Xisha uplift region, northwestern South China Sea: Basin Research, v. 31, no. 4, p. 688-708.

Gao, J., Wu, S., McIntosh, K., Mi, L., Liu, Z., and Spence, G., 2016, Crustal structure and extension mode in the northwestern margin of the South China Sea: Geochemistry, Geophysics, Geosystems, v. 17, no. 6, p. 2143-2167.

Gao, J., Wu, S., McIntosh, K., Mi, L., Yao, B., Chen, Z., and Jia, L., 2015, The continent–ocean transition at the mid-northern margin of the South China Sea: Tectonophysics, v. 654, p. 1-19.
Gautier, P., Brun, J.-P., Moriceau, R., Sokoutis, D., Martinod, J., and Jolivet, L., 1999, Timing, kinematics and cause of Aegean extension: a scenario based on a comparison with simple analogue experiments: Tectonophysics, v. 315, no. 1-4, p. 31-72.
Gautier, S., Tiberi, C., Lopez, M., Foix, O., Lallemand, S., Theunissen, T., Hwang, C., and Chang, E., 2019, Detailed lithospheric structure of an arc-continent collision beneath Taiwan revealed by joint inversion of seismological and gravity data: Geophysical Journal International.
Gee, J. S., and Kent, D. V., 2007, Source of oceanic magnetic anomalies and the geomagnetic polarity time scale, in Kono, M., ed., Treatise on Geophysics, Volume 5, Elsevier, Amsterdam, p. 455-507.
Gernigon, L., Gaina, C., Olesen, O., Ball, P. J., Péron-Pinvidic, G., and Yamasaki, T., 2012, The Norway Basin revisited: From continental breakup to spreading ridge extinction: Marine and Petroleum Geology, v. 35, no. 1, p. 1-19.
Gibbons, A. D., Zahirovic, S., Müller, R. D., Whittaker, J. M., and Yatheesh, V., 2015, A tectonic model reconciling evidence for the collisions between India, Eurasia and intra-oceanic arcs of the central-eastern Tethys: Gondwana Research, v. 28, no. 2, p. 451-492.
Gillard, M., Autin, J., Manatschal, G., Sauter, D., Munschy, M., and Schaming, M., 2015, Tectonomagmatic evolution of the final stages of rifting along the deep conjugate Australian-Antarctic magma-poor rifted margins: Constraints from seismic observations: Tectonics, v. 34, no. 4, p. 753-783.
Gong, Y., Lin, C., Zhang, Z., Zhang, B., Shu, L., Feng, X., Hong, F., Xing, Z., et al., 2019, Breakup unconformities at the end of the early Oligocene in the Pearl River Mouth Basin, South China Sea: significance for the evolution of basin dynamics and tectonic geography during rift–drift transition: Marine Geophysical Research.
Gozzard, S., Kusznir, N., Franke, D., Cullen, A., Reemst, P., and Henstra, G., 2018, South China Sea crustal thickness and oceanic lithosphere distribution from satellite gravity inversion: Petroleum Geoscience.
Granath, J. W., and Argakoesoemah, R. M. I., 1989, Variations in structural style along the eastern Central Range thrust belt, Irian Jaya: 18th Annual Convention Proceedings, v. 1, p. 79-89.
Guan, D. L., Ke, X. P., and Wang, Y., 2016, Basement structures of East and South China Seas and adjacent regions from gravity inversion: Journal of Asian Earth Sciences, v. 117, p. 242-255.
Hall, R., 2002, Cenozoic geological and plate tectonic evolution of SE Asia and the SW Pacific: computer-based reconstructions, model and animations: Journal of Asian Earth Sciences, v. 20, no. 4, p. 353-431.
-, 2012, Late Jurassic–Cenozoic reconstructions of the Indonesian region and the Indian Ocean: Tectonophysics, v. 570-571, p. 1-41.
-, 2013, Contraction and extension in northern Borneo driven by subduction rollback: Journal of Asian Earth Sciences, v. 76, p. 399-411.
Hall, R., and Breitfeld, H. T., 2017, Nature and demise of the Proto-South China Sea: Bulletin of the Geological Society of Malaysia, v. 63, p. 61-76.
Hall, R., and Spakman, W., 2015, Mantle structure and tectonic history of SE Asia: Tectonophysics, v. 658, p. 14-45.
Hall, R., van Hattum, M. W. A., and Spakman, W., 2008, Impact of India–Asia collision on SE Asia: The record in Borneo: Tectonophysics, v. 451, no. 1-4, p. 366-389.
Hamilton, W. B., 1979, Tectonics of the Indonesian region, 1078.
Han, J., Leng, J., and Wang, Y., 2016, Characteristics and genesis of the polygonal fault system in southern slope of the Qiongdongnan Basin, South China Sea: Marine and Petroleum Geology, v. 70, p. 163-174.
Hart, N. R., Stockli, D. F., Lavier, L. L., and Hayman, N. W., 2017, Thermal evolution of a hyperextended rift basin, Mauléon Basin, western Pyrenees: Tectonics, v. 36, no. 6, p. 1103-1128.
Hartono, U., 2006, Petrogenesis of the Sintang Intrusives and its implications for mineralization in Northwest Kalimantan: Jurnal Geol. Sumberdaya Min., v. 16, p. 210-219.

Hasterok, D., 2013, A heat flow based cooling model for tectonic plates: Earth and Planetary Science Letters, v. 361, p. 34-43.
Hawkins, J. W., and Evans, C. A., 1983, Geology of the Zambales Range, Luzon, Philippine Islands: Ophiolite derived from an island arc-back arc basin pair, v. 27, p. 95-123.
Hayes, D. E., and Nissen, S. S., 2005, The South China sea margins: Implications for rifting contrasts: Earth and Planetary Science Letters, v. 237, no. 3-4, p. 601-616.
Hennig-Breitfeld, J., Breitfeld, H. T., Hall, R., BouDagher-Fadel, M., and Thirlwall, M., 2019, A new upper Paleogene to Neogene stratigraphy for Sarawak and Labuan in northwestern Borneo: Paleogeography of the eastern Sundaland margin: Earth-Science Reviews, v. 190, p. 1-32.
Hesse, S., Back, S., and Franke, D., 2009, The deep-water fold-and-thrust belt offshore NW Borneo: Gravity-driven versus basement-driven shortening: Geological Society of America Bulletin, v. 121, no. 5-6, p. 939-953.
Hillier, J. K., and Watts, A., 2005, Relationship between depth and age in the North Pacific Ocean: Journal of Geophysical Research: Solid Earth, v. 110, no. B2.
Hoang, N., Shinjo, R., Phuc, L. T., Anh, L. D., Huong, T. T., Pécskay, Z. n., and Bac, D. T., 2019, Pleistocene basaltic volcanism in the Krông Nô area and vicinity, Dac Nong T Province (Vietnam).
Holloway, N. H., 1982, North Palawan Block, Philippines - Its Relation to Asian Mainland and Role in Evolution of South China Sea: Aapg Bulletin-American Association of Petroleum Geologists, v. 66, no. 9, p. 1355-1383.
Holm, R., and Richards, S., 2013, A re-evaluation of arc-continent collision and along-arc variation in the Bismarck Sea region, Papua New Guinea: Australian Journal of Earth Sciences, v. 60, p. 605-619.
Hsü, K. J., 1968, Principles of Mélanges and Their Bearing on the Franciscan-Knoxville Paradox: Geological Society of America Bulletin, v. 79, no. 8, p. 1063.
Hu, B., Wang, L., Yan, W., Liu, S., Cai, D., Zhang, G., Zhong, K., Pei, J., et al., 2013, The tectonic evolution of the Qiongdongnan Basin in the northern margin of the South China Sea: Journal of Asian Earth Sciences, v. 77, p. 163-182.
Hu, L., Zhang, P., Hao, T., Tian, Y., Zhang, D., Li, Z., and Li, X., 2019, Analysis of topography, heat flow against crustal age in the Southwest Subbasin, South China Sea: International Geology Review, p. 1-13.
Huang, H., Qiu, X., Pichot, T., Klingelhoefer, F., Zhao, M., Wang, P., and Hao, T., 2019, Seismic structure of the northwestern margin of the South China Sea: implication for asymmetric continental extension: Geophysical Journal International, v. 218, no. 2, p. 1246-1261.
Huang, X.-L., Niu, Y., Xu, Y.-G., Ma, J.-L., Qiu, H.-N., and Zhong, J.-W., 2012, Geochronology and geochemistry of Cenozoic basalts from eastern Guangdong, SE China: constraints on the lithosphere evolution beneath the northern margin of the South China Sea: Contributions to Mineralogy and Petrology, v. 165, no. 3, p. 437-455.
Huchon, P., and Khanbari, K., 2003, Rotation of the syn-rift stress field of the northern Gulf of Aden margin, Yemen: Tectonophysics, v. 364, no. 3-4, p. 147-166.
Hui, G., Li, S., Li, X., Guo, L., Suo, Y., Somerville, I. D., Zhao, S., Hu, M., et al., 2016, Temporal and spatial distribution of Cenozoic igneous rocks in the South China Sea and its adjacent regions: implications for tectono-magmatic evolution: Geological Journal, v. 51, p. 429-447.
Huismans, R., and Beaumont, C., 2011, Depth-dependent extension, two-stage breakup and cratonic underplating at rifted margins: Nature, v. 473, no. 7345, p. 74-78.
Hutchison, C. S., 2005, Geology of North-West Borneo: Sarawak, Brunei and Sabah, Elsevier.
Hutchison, C. S., 2010, The North-West Borneo Trough: Marine Geology, v. 271, no. 1-2, p. 32-43.
Hutchison, C. S., Bergman, S. C., Swauger, D. A., and Graves, J. E., 2000, A Miocene collisional belt in north Borneo: uplift mechanism and isostatic adjustment quantified by thermochronology: Journal of the Geological Society, v. 157, no. 4, p. 783.
Ilao, K. A., Morley, C. K., and Aurelio, M. A., 2018, 3D seismic investigation of the structural and stratigraphic characteristics of the Pagasa Wedge, Southwest Palawan Basin, Philippines, and their tectonic implications: Journal of Asian Earth Sciences, v. 154, p. 213-237.

Jamaludin, S. N. F., Pubellier, M., and Menier, D., 2017, Structural Restoration of Carbonate Platform in the Southern Part of Central Luconia, Malaysia: Journal of Earth Science, v. 29, no. 1, p. 155-168.
Jarvis, G. T., and McKenzie, D. P., 1980, Sedimentary basin formation with finite extension rates: Earth and Planetary Science Letters, v. 48, no. 1, p. 42-52.
Jasin, B., and Geologi, J., 1992, Significance of radiolarian' cherts from the Chert-Spilite Formation, Telupid, Sabah: Bulletin of the Geological Society of Malaysia, v. 31, p. 67-83.
Jasin, B., and S, H., 1993, Some radiolarians from the chert block of the Lubok Antu Melange, Sarawak: Warta Geologi, v. 19, p. 205-209.
Jasin, B., and Tongkul, F., 2013, Cretaceous radiolarians from Baliojong ophiolite sequence, Sabah, Malaysia: Journal of Asian Earth Sciences, v. 76, p. 258-265.
Ji, W.-Q., Wu, F.-Y., Chung, S.-L., Li, J.-X., and Liu, C.-Z., 2009, Zircon U–Pb geochronology and Hf isotopic constraints on petrogenesis of the Gangdese batholith, southern Tibet: Chemical Geology, v. 262, no. 3-4, p. 229-245.
Jiang, T., Gao, H., He, J., and Tian, D., 2018, Post-spreading volcanism in the central South China Sea: insights from zircon U–Pb dating on volcaniclastic breccia and seismic features: Marine Geophysical Research, v. 40, no. 2, p. 185-198.
Jiawei, X., Weixing, T., Guang, Z., Shoufa, L., and Goufeng, M., 1989, An outline of the pre-Jurassic tectonic framework in east Asia: Journal of Southeast Asian Earth Sciences, v. 3, no. 1-4, p. 29-45.
Jin, S., Wang, H., Cao, H., Chen, S., Lin, Z., Yu, J., and Pan, S., 2014, Sedimentation of the Paleogene Liushagang Formation and the response to regional tectonics in the Fushan Sag, Beibuwan Basin, South China Sea: Austrian Journal of Earth Sciences, v. 107, no. 2, p. 112-130.
Jolivet, L., Huchon, P., and Rangin, C., 1989, Tectonic setting of Western Pacific marginal basins: Tectonophysics, v. 160, no. 1-4, p. 23-47.
Karig, D., Anderson, R., and Bibee, L., 1978, Characteristics of back-arc spreading in the Mariana Trough: Journal of Geophysical Research, v. 83, p. 1213-1226.
Keenan, T. E., Encarnacion, J., Buchwaldt, R., Fernandez, D., Mattinson, J., Rasoazanamparany, C., and Luetkemeyer, P. B., 2016, Rapid conversion of an oceanic spreading center to a subduction zone inferred from high-precision geochronology: Proc Natl Acad Sci U S A, v. 113, no. 47, p. E7359-E7366.
Kessler, F. L., and Jong, J., 2016, The South China Sea: Sub-basins, Regional Unconformities and Uplift of the Peripheral Mountain Ranges since the Eocene: Berita Sedimentologi, v. 35.
Khan, A. A., 2018, An appraisal of the tectonic evolution of SW Borneo constraints from petrotectonic assemblage and gravity anomaly: Bulletin of the Geological Society of Malaysia, v. 66, p. 47-56.
Khanchuk, A. I., Grebennikov, A. V., and Ivanov, V. V., 2019, Albian–Cenomanian Orogenic Belt and Igneous Province of Pacific Asia: Russian Journal of Pacific Geology, v. 13, no. 3, p. 187-219.
Kirk, H., 1968, The igneous rocks of the Sarawak and Sabah: Geological Survey Borneo Region, Malaysia, Bull, v. 5, p. 201.
Korenaga, T., and Korenaga, J., 2008, Subsidence of normal oceanic lithosphere, apparent thermal expansivity, and seafloor flattening: Earth and Planetary Science Letters, v. 268, no. 1-2, p. 41-51.
Kosa, E., Warrlich, G. M. D., and Loftus, G., 2015, Wings, mushrooms, and Christmas trees: The carbonate seismic geomorphology of Central Luconia, Miocene–present, offshore Sarawak, northwest Borneo: AAPG Bulletin, v. 99, no. 11, p. 2043-2075.
Kudrass, H. R., Wiedicke, M., Cepek, P., Kreuzer, H., and Müller, P., 1986, Mesozoic and Cainozoic rocks dredged from the South China Sea (Reed Bank area) and Sulu Sea and their significance for plate-tectonic reconstructions: Marine and Petroleum Geology, v. 3, no. 1, p. 19-30.
Langford, R., 1989, Geology of the western New Territories: 1: 20 000 sheets 2, 5 & 6, Geotechnical Control Office, Civil Engineering Services Dept., v. 3.
Larsen, H. C., Mohn, G., Nirrengarten, M., Sun, Z., Stock, J., Jian, Z., Klaus, A., Alvarez-Zarikian, C. A., et al., 2018, Rapid transition from continental breakup to igneous oceanic crust in the South China Sea: Nature Geoscience, v. 11, no. 10, p. 782-789.

Lavier, L. L., Ball, P. J., Manatschal, G., Heumann, M. J., MacDonald, J., Matt, V. J., and Schneider, C., 2019, Controls on the Thermomechanical Evolution of Hyperextended Lithosphere at Magma-Poor Rifted Margins: The Example of Espirito Santo and the Kwanza Basins: Geochemistry, Geophysics, Geosystems, v. 20, no. 11, p. 5148-5176.

Lavier, L. L., and Manatschal, G., 2006, A mechanism to thin the continental lithosphere at magma-poor margins: Nature, v. 440, no. 7082, p. 324-328.

Le Pourhiet, L., Chamot-Rooke, N., Delescluse, M., May, D. A., Watremez, L., and Pubellier, M., 2018, Continental break-up of the South China Sea stalled by far-field compression: Nature Geoscience, v. 11, no. 8, p. 605-609.

Lee, T.-Y., and Lawver, L. A., 1995, Cenozoic plate reconstruction of Southeast Asia: Tectonophysics, v. 251, no. 1-4, p. 85-138.

Lei, C., Alves, T. M., Ren, J., Pang, X., Yang, L., and Liu, J., 2019a, Depositional architecture and structural evolution of a region immediately inboard of the locus of continental breakup (Liwan Sub-basin, South China Sea): GSA Bulletin, v. 131, no. 7-8, p. 1059-1074.

Lei, C., and Ren, J., 2016, Hyper-extended rift systems in the Xisha Trough, northwestern South China Sea: Implications for extreme crustal thinning ahead of a propagating ocean: Marine and Petroleum Geology, v. 77, p. 846-864.

Lei, C., Ren, J., and Pang, X., 2019b, Rift structures and its related unconformities on and adjacent the Dongsha Rise: insights into the nature of the high-velocity layer in the northern South China Sea: Marine Geophysical Research, v. 40, no. 2, p. 99-110.

Leloup, P. H., Arnaud, N., Lacassin, R., Kienast, J. R., Harrison, T. M., Trong, T. T. P., Replumaz, A., and Tapponnier, P., 2001, New constraints on the structure, thermochronology, and timing of the Ailao Shan-Red River shear zone, SE Asia: Journal of Geophysical Research, v. 106, no. B4, p. 6683.

Leong, K. M., 1999, Geological setting of Sabah, The Petroleum geology and resources of Malaysia.

Leong, K. M., and Anuar, A., 1999, Northeast Sabah Basin, The Petroleum geology and resources of Malaysia.

Lewis, S. D., and Hayes, D. E., 1984, A geophysical study of the Manila Trench, Luzon, Philippines: 2. Fore arc basin structural and stratigraphic evolution: Journal of Geophysical Research, v. 89, no. B11, p. 9196.

Li, C.-F., Li, J., Ding, W., Franke, D., Yao, Y., Shi, H., Pang, X., Cao, Y., et al., 2015, Seismic stratigraphy of the central South China Sea basin and implications for neotectonics: Journal of Geophysical Research: Solid Earth, v. 120, no. 3, p. 1377-1399.

Li, C.-F., Xu, X., Lin, J., Sun, Z., Zhu, J., Yao, Y., Zhao, X., Liu, Q., et al., 2014a, Ages and magnetic structures of the South China Sea constrained by deep tow magnetic surveys and IODP Expedition 349: Geochemistry, Geophysics, Geosystems, v. 15, no. 12, p. 4958-4983.

Li, C.-F., Zhou, Z., Li, J., Hao, H., and Geng, J., 2007, Structures of the northeasternmost South China Sea continental margin and ocean basin: geophysical constraints and tectonic implications: Marine Geophysical Researches, v. 28, no. 1, p. 59-79.

Li, F., Sun, Z., Pang, X., Liao, J., Yang, H., Xie, H., Zhuo, H., and Zhao, Z., 2019, Low-Viscosity Crustal Layer Controls the Crustal Architecture and Thermal Distribution at Hyperextended Margins: Modeling Insight and Application to the Northern South China Sea Margin: Geochemistry, Geophysics, Geosystems.

Li, F., Sun, Z., and Yang, H., 2018, Possible Spatial Distribution of the Mesozoic Volcanic Arc in the Present-Day South China Sea Continental Margin and Its Tectonic Implications: Journal of Geophysical Research: Solid Earth.

Li, L., Clift, P. D., Stephenson, R., and Nguyen, H. T., 2014b, Non-uniform hyper-extension in advance of seafloor spreading on the vietnam continental margin and the SW South China Sea: Basin Research, v. 26, no. 1, p. 106-134.

Li, Z.-X., Li, X.-H., Chung, S.-L., Lo, C.-H., Xu, X., and Li, W.-X., 2012, Magmatic switch-on and switch-off along the South China continental margin since the Permian: Transition from an Andean-type to a Western Pacific-type plate boundary: Tectonophysics, v. 532, p. 271-290.

Liang, Y., Delescluse, M., Qiu, Y., Pubellier, M., Chamot-Rooke, N., Wang, J., Nie, X., Watremez, L., et al., 2019, Décollements, Detachments, and Rafts in the Extended Crust of Dangerous Ground, South China Sea: The Role of Inherited Contacts: Tectonics, v. 38, no. 6, p. 1863-1883.

Ligi, M., Bonatti, E., Bosworth, W., Cai, Y., Cipriani, A., Palmiotto, C., Ronca, S., and Seyler, M., 2018, Birth of an ocean in the Red Sea: Oceanic-type basaltic melt intrusions precede continental rupture: Gondwana Research, v. 54, p. 150-160.

Lin, A. T., and Watts, A. B., 2002, Origin of the West Taiwan basin by orogenic loading and flexure of a rifted continental margin: Journal of Geophysical Research: Solid Earth, v. 107, no. B9, p. ETG 2-1-ETG 2-19.

Lin, A. T., Watts, A. B., and Hesselbo, S. P., 2003, Cenozoic stratigraphy and subsidence history of the South China Sea margin in the Taiwan region: Basin Research, v. 15, no. 4, p. 453-478.

Liu, W.-N., Li, C.-F., Li, J., Fairhead, D., and Zhou, Z., 2014, Deep structures of the Palawan and Sulu Sea and their implications for opening of the South China Sea: Marine and Petroleum Geology, v. 58, Part B, no. 0, p. 721-735.

Long, M. D., and Silver, P. G., 2008, The subduction zone flow field from seismic anisotropy: a global view: Science, v. 319, no. 5861, p. 315-318.

Lu, C.-Y., and Malavieille, J., 1994, Oblique convergence, indentation and rotation tectonics in the Taiwan Mountain Belt: Insights from experimental modelling: Earth and Planetary Science Letters, v. 121, no. 3-4, p. 477-494.

Lü, C., Hao, T., Lin, J., and Qiu, X., 2016, The role of rifting in the development of the continental margins of the southwest subbasin, South China Sea: Insights from an OBS experiment: Marine Geophysical Research, p. 1-19.

Lüdmann, T., and Wong, H. K., 1999, Neotectonic regime on the passive continental margin of the northern South China Sea: Tectonophysics, v. 311, no. 1-4, p. 113-138.

Lunt, P., 2019, A new view of integrating stratigraphic and tectonic analysis in South China Sea and north Borneo basins: Journal of Asian Earth Sciences, v. 177, p. 220-239.

Lunt, P., and Madon, M., 2017, Onshore to offshore correlation of northern Borneo; a regional perspective: Bulletin of the Geological Society of Malaysia, v. 64, p. 101 – 122.

Lymer, G., Cresswell, D. J. F., Reston, T. J., Bull, J. M., Sawyer, D. S., Morgan, J. K., Stevenson, C., Causer, A., et al., 2019, 3D development of detachment faulting during continental breakup: Earth and Planetary Science Letters, v. 515, p. 90-99.

Madon, M., Kim, C. L., and Wong, R., 2013, The structure and stratigraphy of deepwater Sarawak, Malaysia: Implications for tectonic evolution: Journal of Asian Earth Sciences, v. 76, p. 312-333.

Magni, V., Allen, M. B., van Hunen, J., and Bouilhol, P., 2017, Continental underplating after slab break-off: Earth and Planetary Science Letters, v. 474, p. 59-67.

Mahanjane, E. S., and Franke, D., 2014, The Rovuma Delta deep-water fold-and-thrust belt, offshore Mozambique: Tectonophysics, v. 614, p. 91-99.

Manighetti, I., Tapponnier, P., Courtillot, V., Gruszow, S., and Gillot, P.-Y., 1997, Propagation of rifting along the Arabia-Somalia Plate Boundary: The Gulfs of Aden and Tadjoura: Journal of Geophysical Research: Solid Earth, v. 102, no. B2, p. 2681-2710.

Maraquis, G., Roques, D., Huchon, P., Coulon, O., Chamot-Rooke, N., Rangin, C., and Le Pichon, X., 1997, Amount and timing of extension along the continental margin off central Vietnam: Bull. Soc. géol. Fr, v. 168, no. 6, p. 707-716.

Marchadier, Y., and Rangin, C., 1990, Polyphase tectonics at the southern tip of the Manila trench, Mindoro-Tablas Islands, Philippines: Tectonophysics, v. 183, no. 1-4, p. 273-287.

Masini, E., Manatschal, G., Mohn, G., Ghienne, J. F., and Lafont, F., 2011, The tectono-sedimentary evolution of a supra-detachment rift basin at a deep-water magma-poor rifted margin: the example of the Samedan Basin preserved in the Err nappe in SE Switzerland: Basin Research, v. 23, no. 6, p. 652-677.

Masini, E., Manatschal, G., Mohn, G., and Unternehr, P., 2012, Anatomy and tectono-sedimentary evolution of a rift-related detachment system: The example of the Err detachment (central Alps, SE Switzerland): Geological Society of America Bulletin, v. 124, no. 9-10, p. 1535-1551.

McCabe, R., Almasco, J., and Diegor, W., 1982, Geologic and paleomagnetic evidence for a possible Miocene collision in western Panay, central Philippines: Geology, v. 10, no. 6, p. 325-329.

McCabe, R., Harder, S., Cole, J. T., and Lumadyo, E., 1993, The use of paleomagnetic studies in understanding the complex Tertiary tectonic history of East and Southeast Asia: Journal of Southeast Asian Earth Sciences, v. 8, no. 1, p. 257-268.

McClay, K. R., Dooley, T., and Lewis, G., 1998, Analog modeling of progradational delta systems: Geology, v. 26, no. 9, p. 771.

McIntosh, K., Lavier, L., van Avendonk, H., Lester, R., Eakin, D., and Liu, C.-S., 2014, Crustal structure and inferred rifting processes in the northeast South China Sea: Marine and Petroleum Geology, v. 58, p. 612-626.

McKenzie, D., 1978, Some remarks on the development of sedimentary basins: Earth and Planetary Science Letters, v. 40, no. 1, p. 25-32.

Menant, A., Sternai, P., Jolivet, L., Guillou-Frottier, L., and Gerya, T., 2016, 3D numerical modeling of mantle flow, crustal dynamics and magma genesis associated with slab roll-back and tearing: The eastern Mediterranean case: Earth and Planetary Science Letters, v. 442, p. 93-107.

Menier, D., Mathew, M., Pubellier, M., Sapin, F., Delcaillau, B., Siddiqui, N., Ramkumar, M., and Santosh, M., 2017, Landscape response to progressive tectonic and climatic forcing in NW Borneo: Implications for geological and geomorphic controls on flood hazard: Scientific Reports, v. 7, no. 1.

Meresse, F., Savva, D., Wong, P., Pubellier, M., Chamot-Rooke, N., Steuer, S., Franke, D., Sapin, F., et al., 2012, Structural heritage as a key factor controlling the South China Sea opening, American Geophysical Union, Fall Meeting 2012, Volume T42A-06: San Francisco.

Metcalfe, I., 2011, Palaeozoic–Mesozoic history of SE Asia: Geological Society, London, Special Publications, v. 355, no. 1, p. 7-35.

Mitchell, A. H. G., Hernandez, F., and dela Cruz, A. P., 1986, Cenozoic evolution of the Philippine archipelago: Journal of Southeast Asian Earth Sciences, v. 1, no. 1, p. 3-22.

Mohn, G., Manatschal, G., Beltrando, M., Masini, E., and Kusznir, N., 2012, Necking of continental crust in magma-poor rifted margins: Evidence from the fossil Alpine Tethys margins: Tectonics, v. 31.

Morley, C. K., 2007, Development of crestal normal faults associated with deepwater fold growth: Journal of Structural Geology, v. 29, no. 7, p. 1148-1163.

Morley, C. K., 2009, Growth of folds in a deep-water setting: Geosphere, v. 5, no. 2, p. 59-89.

Morley, C. K., 2016, Major unconformities/termination of extension events and associated surfaces in the South China Seas: Review and implications for tectonic development: Journal of Asian Earth Sciences, v. 120, p. 62-86.

Morley, C. K., Back, S., Van Rensbergen, P., Crevello, P., and Lambiase, J. J., 2003, Characteristics of repeated, detached, Miocene–Pliocene tectonic inversion events, in a large delta province on an active margin, Brunei Darussalam, Borneo: Journal of Structural Geology, v. 25, no. 7, p. 1147-1169.

Morley, C. K., and Guerin, G., 1996, Comparison of gravity-driven deformation styles and behavior associated with mobile shales and salt: Tectonics, v. 15, no. 6, p. 1154-1170.

Morley, C. K., and Westaway, R., 2006, Subsidence in the super-deep Pattani and Malay basins of Southeast Asia: a coupled model incorporating lower-crustal flow in response to post-rift sediment loading: Basin Research, v. 18, no. 1, p. 51-84.

Moss, S. J., Carter, A., Baker, S., and Hurford, A. J., 1998, A Late Oligocene tectono-volcanic event in East Kalimantan and the implications for tectonics and sedimentation in Borneo: Journal of the Geological Society, v. 155, no. 1, p. 177-192.

Mourgues, R., Lecomte, E., Vendeville, B., and Raillard, S., 2009, An experimental investigation of gravity-driven shale tectonics in progradational delta: Tectonophysics, v. 474, no. 3-4, p. 643-656.

Nanni, U., Pubellier, M., Chan, L. S., and Sewell, R. J., 2017, Rifting and reactivation of a Cretaceous structural belt at the northern margin of the South China Sea: Journal of Asian Earth Sciences, v. 136, p. 110-123.

Nathan, S. A., and Leckie, R. M., Miocene planktonic foraminiferal biostratigraphy of sites 1143 and 1146, ODP Leg 184, South China Sea, in Proceedings Proceedings of the Ocean Drilling Program, Scientific Results2003, Volume 184, p. 1-43.

Nirrengarten, M., Mohn, G., Kusznir, N. J., Sapin, F., Despinois, F., Pubellier, M., Chang, S. P., Larsen, H. C., et al., 2020a, Extension modes and breakup processes of the southeast China-Northwest Palawan conjugate rifted margins: Marine and Petroleum Geology, v. 113, p. 104123.

Nirrengarten, M., Mohn, G., Schito, A., Corrado, S., Gutiérrez-García, L., Bowden, S. A., and Despinois, F., 2020b, The thermal imprint of continental breakup during the formation of the South China Sea: Earth and Planetary Science Letters, v. 531, p. 115972.
Noon, S. W., 2011, Biostratigraphic correlation wells Tiga Papan 1, 2, 3, and 4.
Oil Search, 2016, Oil Search Update report.
Okubo, Y., Ishihara, T., and Daigo, M. J. N., 1997, Magnetic anomalies of east and southeast Asia andtheir linear features: Journal of Asian Earth Sciences, v. 15, no. 2-3, p. 161-163.
Omang, S. A. K., and Barber, A. J., 1996, Origin and tectonic significance of the metamorphic rocks associated with the Darvel Bay Ophiolite, Sabah, Malaysia: Geological Society, London, Special Publications, v. 106, no. 1, p. 263-279.
Orange, D. L., 1990, Criteria helpful in recognizing shear-zone and diapiric mélanges: Examples from the Hoh accretionary complex, Olympic Peninsula, Washington: Geological Society of America Bulletin, v. 102, no. 7, p. 935-951.
Otofuji, Y.-i., Sasajima, S., Nishimura, S., Dharma, A., and Hehuwat, F., 1981, Paleomagnetic evidence for clockwise rotation of the northern arm of Sulawesi, Indonesia: Earth and Planetary Science Letters, v. 54, no. 2, p. 272-280.
Padrones, J. T., Tani, K., Tsutsumi, Y., and Imai, A., 2017, Imprints of Late Mesozoic tectono-magmatic events on Palawan Continental Block in northern Palawan, Philippines: Journal of Asian Earth Sciences, v. 142, p. 56-76.
Page, B. M., 1978, Franciscan melanges compared with olistostromes of Taiwan and Italy: Tectonophysics, v. 47, no. 3-4, p. 223-246.
Parsons, B., and Sclater, J. G., 1977, An analysis of the variation of ocean floor bathymetry and heat flow with age: Journal of Geophysical Research, v. 82, no. 5, p. 803-827.
Peltzer, G., and Tapponnier, P., 1988, Formation and evolution of strike-slip faults, rifts, and basins during the India-Asia Collision: An experimental approach: Journal of Geophysical Research: Solid Earth, v. 93, no. B12, p. 15085-15117.
Peng, X., Shen, C., Mei, L., Zhao, Z., and Xie, X., 2018, Rift–drift transition in the Dangerous Grounds, South China Sea: Marine Geophysical Research.
Péron-Pinvidic, G., and Manatschal, G., 2008, The final rifting evolution at deep magma-poor passive margins from Iberia-Newfoundland: a new point of view: International Journal of Earth Sciences, v. 98, no. 7, p. 1581-1597.
-, 2009, The final rifting evolution at deep magma-poor passive margins from Iberia-Newfoundland: a new point of view: International Journal of Earth Sciences, v. 98, no. 7, p. 1581-1597.
Péron-Pinvidic, G., Manatschal, G., Minshull, T. A., and Sawyer, D. S., 2007, Tectonosedimentary evolution of the deep Iberia-Newfoundland margins: Evidence for a complex breakup history: Tectonics, v. 26, no. 2, p. n/a-n/a.
Péron-Pinvidic, G., Manatschal, G., and Osmundsen, P. T., 2013, Structural comparison of archetypal Atlantic rifted margins: A review of observations and concepts: Marine and Petroleum Geology, v. 43, p. 21-47.
Petri, B., Duretz, T., Mohn, G., Schmalholz, S. M., Karner, G. D., and Müntener, O., 2019, Thinning mechanisms of heterogeneous continental lithosphere: Earth and Planetary Science Letters, v. 512, p. 147-162.
Pichot, T., Delescluse, M., Chamot-Rooke, N., Pubellier, M., Qiu, Y., Meresse, F., Sun, G., Savva, D., et al., 2014, Deep crustal structure of the conjugate margins of the SW South China Sea from wide-angle refraction seismic data: Marine and Petroleum Geology, v. 58, p. 627-643.
Pieters, P. E., Trail, D. S., and Supriatna, S., 1987, Correlation of Early Tertiary rocks across Kalimantan: Proceedings Indonesian Petroleum Association, 16th Annual Convention, v. 1, p. 291-306.
Prouteau, G., Maury, R. C., Pubellier, M., Cotten, J., and Bellon, H., 2001, Le magmatisme post-collisionnel du Nord-Ouest de Borneo, produit de la fusion d'un fragment de croute oceanique ancre dans le manteau superieur: Bulletin de la Societe Geologique de France, v. 172, no. 3, p. 319-332.
Prouteau, G., Maury, R. C., Rangin, C., Suparka, E., Bellon, H., Pubellier, M., and Gotten, J., 1996, Miocene adakites from northwest Borneo and their relation to the subduction of the Proto South China Sea: Comptes Rendus de l'Academie de Sciences - Serie IIa: Sciences de la Terre et des Planetes, v. 323, no. 11, p. 925-932.

Pubellier, M., Chamot-Rooke, N., Ego, F., Guézou, J. C., Konstantinovskaya, E., Rabaute, E., and Ringenbach, J.-C., 2008, Structural Map of Eastern Eurasia CCGM-CGMW scale 1/12,500,000.
Pubellier, M., Chamot-Rooke, N., Meresse, F., Savva, D., and Le Gal, V., 2014, South China Sea-GRI: Report on a joint study of ENS-CNRS, TOTAL and collaboration with BGR.
Pubellier, M., Ego, F., Chamotrooke, N., and Rangin, C., 2003, The building of pericratonic mountain ranges: structural and kinematic constraints applied to GIS-based reconstructions of SE Asia: Bulletin De La Societe Geologique De France, v. 174, no. 6, p. 561-584.
Pubellier, M., and Meresse, F., 2013, Phanerozoic growth of Asia: Geodynamic processes and evolution: Journal of Asian Earth Sciences, v. 72, p. 118-128.
Pubellier, M., Monnier, C., Maury, R., and Tamayo, R., 2004, Plate kinematics, origin and tectonic emplacement of supra-subduction ophiolites in SE Asia: Tectonophysics, v. 392, no. 1-4, p. 9-36.
Pubellier, M., and Morley, C. K., 2014, The basins of Sundaland (SE Asia): Evolution and boundary conditions: Marine and Petroleum Geology, v. 58, Part B, no. 0, p. 555-578.
Pubellier, M., Rangin, C., Cadet, J. P., and Tjashuri, I., 1992, L'île de Nias, un édifice polyphasé sur la bordure interne de la fosse de la Sonde (Archipel des Mentawai Indonésie): Les Comptes Rendus de l'Académie des sciences, v. 315, p. 1019-1026.
Pubellier, M., Rangin, C., Le Pichon, X., Ego, F., Nguyen, T. N. H., Nielsen, C., Rabaute, A., Sun, D. T. H., et al., 2001, DOTSEA: Deep Offshore Tectonics of South East Asia - A synthesis of deep marine data in South East Asia.
Pubellier, M., Savva, D., Sapin, F., and Aurelio, M., 2016, Structural map of the South China Sea, scale 1/4.4M: CGMW 2016.
Qiu, Y., Wang, Y., Huang, W., Li, W., Zhuo, H., Du, W., and Gong, C., 2016, Jump event of mid-ocean ridge during the eastern subbasin evolution of the South China Sea: Interpretation, v. 4, no. 3, p. SP67-SP77.
Queano, K. L., Ali, J. R., Milsom, J., Aitchison, J. C., and Pubellier, M., 2007, North Luzon and the Philippine Sea Plate motion model: Insights following paleomagnetic, structural, and age-dating investigations: Journal of Geophysical Research-Solid Earth, v. 112, no. B5.
Rahim, A. R., Konjing, Z., Asis, J., Nursyazwani, A. J., Muhamad, A. J., Ibrahim, N., Koraini, A. M., Kob, R. C., et al., 2017, Tectonostratigraphic terranes of Kudat Peninsula, Sabah: Bulletin of the Geological Society of Malaysia, v. 64, p. 123-139.
Rangin, C., 1989, The Sulu Sea, a back-arc basin setting within a Neogene collision zone: Tectonophysics, v. 161, no. 1-2, p. 119-141.
Rangin, C., Bellon, H., Benard, F., Letouzey, J., Muller, C., and Sanudin, T., 1990a, Neogene arc-continent collision in Sabah, Northern Borneo (Malaysia): Tectonophysics, v. 183, no. 1-4, p. 305-319.
Rangin, C., Jolivet, L., Pubellier, M., and group, t. T. P. w., 1990b, A simple model for the tectonic evolution of southeast Asia and Indonesia region for the past 43 m.y.: Bull. Soc. géol. Fr, v. 8, no. 6, p. 889-905.
Rangin, C., Silver, E. A., Berner, U., Bertrand, P., Betzler, C., Brass, G. W., Hsu, V., Huang, Z. F., et al., Forages dans les bassins marginaux du SE asiatique: résultats préliminaires du leg 124 (Ocean Drilling Program)1989.
Rangin, C., Spakman, W., Pubellier, M., and Bijwaard, H., 1999, Tomographic and geological constraints on subduction along the eastern Sundaland continental margin (South-East Asia): Bulletin de la Societe Geologique de France, v. 170, no. 6, p. 775.
Raymond, L. A., 1984, Melanges : their nature, origin, and significance, Boulder, Colo., Geological Society of America.
Ren, J., Zhang, D., Tong, D., Huang, A., Wang, Y., Lei, C., Zuo, Q., Zhao, Y., et al., 2014, Characterising the nature, evolution and origin of detachment fault in central depression belt, Qiongdongnan Basin of South China Sea: evidence from seismic reflection data: Acta Oceanologica Sinica, v. 33, no. 12, p. 118-126.
Richter, C., and Ali, J. R., 2015, Philippine Sea Plate motion history: Eocene-Recent record from ODP Site 1201, central West Philippine Basin: Earth and Planetary Science Letters, v. 410, p. 165-173.

Roques, D., Ranero, C., and Huchon, P., 1997, Geometry and sense of motion along the Vietnam continental margin: onshore/offshore Da Nang area: Bull. Soc. géol. Fr, v. 168, no. 4, p. 413-422.

Ros, E., Pérez-Gussinyé, M., Araújo, M., Thoaldo Romeiro, M., Andrés-Martínez, M., and Morgan, J. P., 2017, Lower Crustal Strength Controls on Melting and Serpentinization at Magma-Poor Margins: Potential Implications for the South Atlantic: Geochemistry, Geophysics, Geosystems, v. 18, no. 12, p. 4538-4557.

Rossman, D. L., Castañada, G. C., and Bacuta, G. C., 1989, Geology of the Zambales ophiolite, Luzon, Philippines: Tectonophysics, v. 168, no. 1-3, p. 1-22.

Ruh, J. B., Vergés, J., and Burg, J.-P., 2018, Shale-related minibasins atop a massive olistostrome in an active accretionary wedge setting: Two-dimensional numerical modeling applied to the Iranian Makran: Geology, v. 46, no. 9, p. 791-794.

Samuel, M. A., Harbury, N. A., Bakri, A., Banner, F. T., and Hartono, L., 1997, A new stratigraphy for the islands of the Sumatran Forearc, Indonesia: Journal of Asian Earth Sciences, v. 15, no. 4-5, p. 339-380.

Sapin, F., 2010, Impact du couple érosion/sédimentation sur la structuration d'un prisme d'accrétion: L'exemple du prisme NO Bornéo, Approche géologique, sismique et thermique [PhD: Université Paris VI.

Sapin, F., Hermawan, I., Pubellier, M., Vigny, C., and Ringenbach, J.-C., 2013, The recent convergence on the NW Borneo Wedge—a crustal-scale gravity gliding evidenced from GPS: Geophysical Journal International, v. 193, no. 2, p. 549-556.

Sapin, F., Pubellier, M., Lahfid, A., Janots, D., Aubourg, C., and Ringenbach, J.-C., 2011, Onshore record of the subduction of a crustal salient: example of the NW Borneo Wedge: Terra Nova, v. 23, no. 4, p. 232-240.

Sapin, F., Ringenbach, J.-C., Rives, T., and Pubellier, M., 2012, Counter-regional normal faults in shale-dominated deltas: Origin, mechanism and evolution: Marine and Petroleum Geology, v. 37, no. 1, p. 121-128.

Sautter, B., Pubellier, M., Králiková Schlögl, S., Matenco, L., Andriessen, P., and Mathew, M., 2019, Exhumation of west Sundaland: A record of the path of India?: Earth-Science Reviews, v. 198.

Savva, D., 2013, Variabilite des processus d'extension continentale en Mer de Chine du Sud [Doctorale: L'Université Pierre et Marie Curie, 389 p.

Savva, D., Meresse, F., Pubellier, M., Chamot-Rooke, N., Lavier, L., Po, K. W., Franke, D., Steuer, S., et al., 2013, Seismic evidence of hyper-stretched crust and mantle exhumation offshore Vietnam: Tectonophysics, v. 608, p. 72-83.

Savva, D., Pubellier, M., Franke, D., Chamot-Rooke, N., Meresse, F., Steuer, S., and Auxietre, J. L., 2014, Different expressions of rifting on the South China Sea margins: Marine and Petroleum Geology, v. 58, no. 0, p. 579-598.

Schellart, W. P., Chen, Z., Strak, V., Duarte, J. C., and Rosas, F. M., 2019, Pacific subduction control on Asian continental deformation including Tibetan extension and eastward extrusion tectonics: Nature Communications, v. 10, no. 1, p. 4480.

Schellart, W. P., and Moresi, L., 2013, A new driving mechanism for backarc extension and backarc shortening through slab sinking induced toroidal and poloidal mantle flow: Results from dynamic subduction models with an overriding plate: Journal of Geophysical Research: Solid Earth, v. 118, no. 6, p. 3221-3248.

Schlüter, H. U., Hinz, K., and Block, M., 1996, Tectono-stratigraphic terranes and detachment faulting of the South China Sea and Sulu Sea: Marine Geology, v. 130, no. 1-2, p. 39-78.

Schulmann, K., and Whitechurch, H., 2014, Plate Tectonics, in Amils, R., Gargaud, M., Cernicharo Quintanilla, J., Cleaves, H. J., Irvine, W. M., Pinti, D., and Viso, M., eds., Encyclopedia of Astrobiology: Berlin, Heidelberg, Springer Berlin Heidelberg, p. 1-13.

Seton, M., Müller, R. D., Zahirovic, S., Gaina, C., Torsvik, T., Shephard, G., Talsma, A., Gurnis, M., et al., 2012, Global continental and ocean basin reconstructions since 200Ma: Earth-Science Reviews, v. 113, no. 3-4, p. 212-270.

Shemenda, A. I., 1993, Subduction of the lithosphere and back arc dynamics: Insights from physical modeling: Journal of Geophysical Research, v. 98, no. B9, p. 16167.

Shi, X., Jiang, H., Yang, J., Yang, X., and Xu, H., 2017, Models of the rapid post-rift subsidence in the eastern Qiongdongnan Basin, South China Sea: implications for the development of the deep thermal anomaly: Basin Research, v. 29, no. 3, p. 340-362.
Shu, L. S., Zhou, X. M., Deng, P., Wang, B., Jiang, S. Y., Yu, J. H., and Zhao, X. X., 2009, Mesozoic tectonic evolution of the Southeast China Block: New insights from basin analysis: Journal of Asian Earth Sciences, v. 34, no. 3, p. 376-391.
Sibuet, J.-C., Yeh, Y.-C., and Lee, C.-S., 2016, Geodynamics of the South China Sea: Tectonophysics, v. 692, p. 98-119.
Silver, E. A., Abbott, L. D., Kirchoff-Stein, K. S., Reed, D. L., Bernstein-Taylor, B., and Hilyard, D., 1991, Collision propagation in Papua New Guinea and the Solomon Sea: Tectonics, v. 10, no. 5, p. 863-874.
Silver, E. A., and Rangin, C., 1991, Leg 124 Tectonic Synthesis, v. 124.
Sleep, N., and Toksoz, M. N., 1971, Evolution of marginal basins: Nature, v. 233, no. 5321, p. 548-550.
Soeria-Atmadja, R., Noeradi, D., and Priadi, B., 1999, Cenozoic magmatism in Kalimantan and its related geodynamic evolution: Journal of Asian Earth Sciences, v. 17, no. 1, p. 25-45.
Song, T., and Li, C.-F., 2015, Rifting to drifting transition of the Southwest Subbasin of the South China Sea: Marine Geophysical Research, v. 36, no. 2-3, p. 167-185.
Stampfli, G. M., and Borel, G. D., 2002, A plate tectonic model for the Paleozoic and Mesozoic constrained by dynamic plate boundaries and restored synthetic oceanic isochrons: Earth and Planetary Science Letters, v. 196, no. 1-2, p. 17-33.
Stein, C. A., and Stein, S., 1992, A model for the global variation in oceanic depth and heat flow with lithospheric age: Nature, v. 359, no. 6391, p. 123-129.
-, 1993, Constraints on Pacific midplate swells from global depth-age and heat flow-age models: The Mesozoic Pacific: Geology, Tectonics, and Volcanism, Geophys. Monogr. Ser, v. 77, p. 53-76.
Stern, R. J., 2002, Subduction zones: Reviews of Geophysics, v. 40, no. 4.
Stern, R. J., and Dickinson, W. R., 2010, The Gulf of Mexico is a Jurassic backarc basin: Geosphere, v. 6, no. 6, p. 739-754.
Steuer, S., Franke, D., Meresse, F., Savva, D., Pubellier, M., and Auxietre, J.-L., 2014, Oligocene–Miocene carbonates and their role for constraining the rifting and collision history of the Dangerous Grounds, South China Sea: Marine and Petroleum Geology, v. 58, no. 0, p. 644-657.
Steuer, S., Franke, D., Meresse, F., Savva, D., Pubellier, M., Auxietre, J.-L., and Aurelio, M., 2013, Time constraints on the evolution of southern Palawan Island, Philippines from onshore and offshore correlation of Miocene limestones: Journal of Asian Earth Sciences, v. 76, p. 412-427.
Sun, Z., Lin, J., Qiu, N., Jian, Z., Wang, P., Pang, X., Zheng, J., and Zhu, B., 2019, The role of magmatism in the thinning and breakup of the South China Sea continental margin: National Science Review, v. 6, no. 5, p. 871-876.
Surmont, J., Laj, C., Kissel, C., Rangin, C., Bellon, H., and Priadi, B., 1994, New paleomagnetic constraints on the Cenozoic tectonic evolution of the North Arm of Sulawesi, Indonesia: Earth and Planetary Science Letters, v. 121, no. 3-4, p. 629-638.
Svartman Dias, A. E., Lavier, L. L., and Hayman, N. W., 2015, Conjugate rifted margins width and asymmetry: The interplay between lithospheric strength and thermomechanical processes: Journal of Geophysical Research: Solid Earth, v. 120, no. 12, p. 8672-8700.
Swauger, D. A., Hutchison, C. S., Bergman, S. C., and Graves, J. E., 2000, Age and emplacement of the Mount Kinabalu pluton: Geological Society of Malaysia Bulletin, v. 44, p. 159–163.
Taguibao, K. J., Aurelio, M. A., Savva, D., and Pubellier, M., Onshore Palawan structures: implications on the evolution of the South China Sea., in Proceedings Proceedings of the 34th International Geological Congress, Brisbane, Australia, 5-10 August 2012.
Tan, D. N. K., 1975, Preliminary notes on the mélange in the Lupar Valley, West Sarawak: Malaysia Geological Survey, Annual Report, p. 219-227.
Tan, D. N. K., 1979, Lupar Valley, West Sarawak, Malaysia: Explanation of Sheets 1-111-14, 1-111-15, and Part of 1-111-16, National Printing Department.
Tan, D. N. K., 1982, The Lubok Antu Melange, Lupar Valley, West Sarawak: A Lower Tertiary Subduction Complex: Bulletin of the Geological Society of Malaysia, v. 15, p. 31-46.

Tang, X., Yang, S., Zhu, J., Long, Z., Jiang, G., Huang, S., and Hu, S., 2017, Tectonic subsidence of the Zhu 1 Sub-basin in the Pearl River Mouth Basin, northern South China Sea: Frontiers of Earth Science, v. 11, no. 4, p. 729-739.
Tapponnier, P., Peltzer, G., Le Dain, A. Y., Armijo, R., and Cobbold, P., 1982, Propagating extrusion tectonics in Asia: New insights from simple experiments with plasticine: Geology, v. 10, no. 12, p. 611.
Taylor, B., 1979, Bismarck Sea: Evolution of a back-arc basin: Geology, v. 7, no. 4, p. 171.
Taylor, B., Goodliffe, A. M., and Martinez, F., 1999, How continents break up: Insights from Papua New Guinea: Journal of Geophysical Research: Solid Earth, v. 104, no. B4, p. 7497-7512.
Taylor, B., and Hayes, D. E., 1980, The tectonic evolution of the South China Basin, v. 23, p. 89-104.
-, 1983, Origin and history of the South China Sea basin, v. 27, p. 23-56.
Teng, L. S., and Lin, A. T., 2004, Cenozoic tectonics of the China continental margin: insights from Taiwan: Geological Society, London, Special Publications, v. 226, no. 1, p. 313-332.
Tetreault, J. L., and Buiter, S. J. H., 2018, The influence of extension rate and crustal rheology on the evolution of passive margins from rifting to break-up: Tectonophysics, v. 746, p. 155-172.
Tokuyama, A., and Yoshida, S., 1984, Kinabalu fault, a large strike slip fault in Sabah, East Malaysia: Geology and Paleontology of Southeast Asia, v. 14, p. 171-188.
Tong, D., Ren, J., Liao, Y., Yao, Y., and Zhao, Y., 2019, Cenozoic tectonic events and their implications for constraining the structure and stratigraphic styles from rifting to collision at the southeastern margin of the South China Sea: Marine Geophysical Research, v. 40, no. 2, p. 145-161.
Tongkul, F., 1990, Structural Styles and Tectonics of Western and Northern Sabah: Bulletin Geological Society of Malaysia, v. 27, p. 227-240.
-, 2003, The structural style of Lower Miocene sedimentary rocks, Kudat Peninsula, Sabah.
-, 2017, Active tectonics in Sabah – seismicity and active faults: Bulletin of the Geological Society of Malaysia, v. 64, p. 27-36.
Torsvik, T. H., Van der Voo, R., Preeden, U., Mac Niocaill, C., Steinberger, B., Doubrovine, P. V., van Hinsbergen, D. J. J., Domeier, M., et al., 2012, Phanerozoic polar wander, palaeogeography and dynamics: Earth-Science Reviews, v. 114, no. 3-4, p. 325-368.
Tugend, J., Gillard, M., Manatschal, G., Nirrengarten, M., Harkin, C., Epin, M.-E., Sauter, D., Autin, J., et al., 2018, Reappraisal of the magma-rich versus magma-poor rifted margin archetypes: Geological Society, London, Special Publications.
Tugend, J., Manatschal, G., Kusznir, N. J., Masini, E., Mohn, G., and Thinon, I., 2014, Formation and deformation of hyperextended rift systems: Insights from rift domain mapping in the Bay of Biscay-Pyrenees: Tectonics, v. 33, no. 7, p. 1239-1276.
van Bemmelen, R. W., 1949, The geology of Indonesia.
van Hattum, M. W. A., Hall, R., Pickard, A. L., and Nichols, G. J., 2013, Provenance and geochronology of Cenozoic sandstones of northern Borneo: Journal of Asian Earth Sciences, v. 76, p. 266-282.
van Hunen, J., and Allen, M. B., 2011, Continental collision and slab break-off: A comparison of 3-D numerical models with observations: Earth and Planetary Science Letters, v. 302, no. 1-2, p. 27-37.
Vigny, C., Perfettini, H., Walpersdorf, A., Lemoine, A., Simons, W., van Loon, D., Ambrosius, B., Stevens, C., et al., 2002, Migration of seismicity and earthquake interactions monitored by GPS in SE Asia triple junction: Sulawesi, Indonesia: Journal of Geophysical Research: Solid Earth, v. 107, no. B10, p. ETG 7-1-ETG 7-11.
Vogt, E. T., and Flower, M. F. J., 1989, Genesis of the Kinabalu (Sabah) granitoid at a subduction-collision junction: Contributions to Mineralogy and Petrology, v. 103, no. 4, p. 493-509.
Vu, A. T., Wessel Fyhn, M. B., Xuan, C. T., Nguyen, T. T., Hoang, D. N., Pham, L. T., and Van, H. N., 2017, Cenozoic tectonic and stratigraphic development of the Central Vietnamese continental margin: Marine and Petroleum Geology, v. 86, p. 386-401.
Wajzer, M. R., Barber, A. J., Hidayat, S., and Suharsono, 1991, Accretion, collision and strike-slip faulting: the Woyla group as a key to the tectonic evolution of North Sumatra: Journal of Southeast Asian Earth Sciences, v. 6, no. 3-4, p. 447-461.
Wakita, K., Miyazaki, K., Zulkarnain, I., Sopaheluwakan, J., and Sanyoto, P., 1998, Tectonic implications of new age data for the Meratus Complex of south Kalimantan, Indonesia: The Island Arc, v. 7, no. 1-2, p. 202-222.

Wallace, L. M., Ellis, S., and Mann, P., 2009, Collisional model for rapid fore-arc block rotations, arc curvature, and episodic back-arc rifting in subduction settings: Geochemistry, Geophysics, Geosystems, v. 10, no. 5.

Wallace, L. M., McCaffrey, R., Beavan, J., and Ellis, S., 2005, Rapid microplate rotations and backarc rifting at the transition between collision and subduction: Geology, v. 33, no. 11, p. 857.

Walpersdorf, A., Vigny, C., Subarya, C., and Manurung, P., 1998, Monitoring of the Palu-Koro Fault (Sulawesi) by GPS: Geophysical Research Letters, v. 25, no. 13, p. 2313-2316.

Wang, D. W., Wu, S. G., Qin, Z. L., Spence, G., and Lu, F. L., 2013, Seismic characteristics of the Huaguang mass transport deposits in the Qiongdongnan Basin, South China Sea: Implications for regional tectonic activity: Marine Geology, v. 346, p. 165-182.

Wang, Y., Qiu, Y., Yan, P., Zheng, H., Liu, H., and Wang, J., 2016, Seismic evidence for Mesozoic strata in the northern Nansha waters, South China Sea: Tectonophysics, v. 677-678, p. 190-198.

Wei, X.-D., Ruan, A.-G., Zhao, M.-H., Qiu, X.-L., Li, J.-B., Zhu, J.-J., Wu, Z.-L., and Ding, W.-W., 2011, A Wide-Angle Obs Profile Across the Dongsha Uplift and Chaoshan Depression in the Mid-Northern South China Sea: Chinese Journal of Geophysics, v. 54, no. 6, p. 1149-1160.

Weissel, J. K., 1980, Evidence for Eocene oceanic crust in the Celebes Basin: The tectonic and geologic evolution of southeast Asian seas and islands, v. 23, p. 37-47.

Whitmarsh, R. B., Manatschal, G., and Minshull, T. A., 2001, Evolution of magma-poor continental margins from rifting to seafloor spreading: Nature, v. 413, no. 6852, p. 150-154.

Williams, P. R., and Harahap, B. H., 1987, Preliminary geochemical and age data from postsubduction intrusive rocks, northwest Borneo: Australian Journal of Earth Sciences, v. 34, no. 4, p. 405-415.

Wilson, R. A. M., 1961, The geology and mineral resources of the Banggi Island and Sugut River area North Borneo, [Kuching], Geological Survey, Borneo Region, Malaysia.

Wu, J., and Suppe, J., 2017, Proto-South China Sea plate tectonics using subducted slab constraints from tomography: Journal of Earth Science.

Wu, J., Suppe, J., Lu, R. Q., and Kanda, R., 2016, Philippine Sea and East Asian plate tectonics since 52 Ma constrained by new subducted slab reconstruction methods: Journal of Geophysical Research-Solid Earth, v. 121, no. 6, p. 4670-4741.

Wu, S. G., Yuan, S. Q., Zhang, G. C., Ma, Y. B., Mi, L. J., and Xu, N., 2009, Seismic characteristics of a reef carbonate reservoir and implications for hydrocarbon exploration in deepwater of the Qiongdongnan Basin, northern South China Sea: Marine and Petroleum Geology, v. 26, no. 6, p. 817-823.

Xia, S., Zhao, F., Zhao, D., Fan, C., Wu, S., Mi, L., Sun, J., Cao, J., et al., 2018, Crustal plumbing system of post-rift magmatism in the northern margin of South China Sea: New insights from integrated seismology: Tectonophysics, v. 744, p. 227-238.

Xiao, M., Yao, Y.-J., Cai, Y., Qiu, H.-N., Xu, Y.-G., Xu, X., Jiang, Y.-D., Li, Y.-B., et al., 2019, Evidence of Early Cretaceous lower arc crust delamination and its role in the opening of the South China Sea: Gondwana Research, v. 76, p. 123-145.

Xie, H., Zhou, D., Li, Y., Pang, X., Li, P., Chen, G., Li, F., and Cao, J., 2014, Cenozoic tectonic subsidence in deepwater sags in the Pearl River Mouth Basin, northern South China Sea: Tectonophysics, v. 615-616, p. 182-198.

Xie, X., Müller, R. D., Li, S., Gong, Z., and Steinberger, B., 2006, Origin of anomalous subsidence along the Northern South China Sea margin and its relationship to dynamic topography: Marine and Petroleum Geology, v. 23, no. 7, p. 745-765.

Xie, X., Ren, J., Pang, X., Lei, C., and Chen, H., 2019, Stratigraphic architectures and associated unconformities of Pearl River Mouth basin during rifting and lithospheric breakup of the South China Sea: Marine Geophysical Research, v. 40, no. 2, p. 129-144.

Xie, Z., Sun, L., Pang, X., Zheng, J., and Sun, Z., 2017, Origin of the Dongsha Event in the South China Sea: Marine Geophysical Research, v. 38, no. 4, p. 357-371.

Xu, C., Shi, H., Barnes, C. G., and Zhou, Z., 2015, Tracing a late Mesozoic magmatic arc along the Southeast Asian margin from the granitoids drilled from the northern South China Sea: International Geology Review, v. 58, no. 1, p. 71-94.

Xu, C., Zhang, L., Shi, H., Brix, M. R., Huhma, H., Chen, L., Zhang, M., and Zhou, Z., 2017, Tracing an Early Jurassic magmatic arc from South to East China Seas: Tectonics, v. 36, no. 3, p. 466-492.

Xu, J., Ren, J., and Luo, P., 2019, The evolution of a gravity-driven system accompanied by diapirism under the control of the prograding West Luconia Deltas in the Kangxi Depression, Southern South China Sea: Marine Geophysical Research, v. 40, no. 2, p. 199-221.

Xu, X. S., Suzuki, K., Liu, L., and Wang, D. Z., 2010, Petrogenesis and tectonic implications of Late Mesozoic granites in the NE Yangtze block, China: Further insights from the Jiuhuashan-Qingyang complex: Geological Magazine, v. 147, no. 2, p. 219-232.

Yamazaki, T., Takahashi, M., Iryu, Y., Sato, T., Oda, M., Takayanagi, H., Chiyonobu, S., Nishimura, A., et al., 2010, Philippine Sea Plate motion since the Eocene estimated from paleomagnetism of seafloor drill cores and gravity cores: Earth, planets and space, v. 62, no. 6, p. 495-502.

Yan, P., Deng, H., Liu, H., Zhang, Z., and Jiang, Y., 2006, The temporal and spatial distribution of volcanism in the South China Sea region: Journal of Asian Earth Sciences, v. 27, no. 5, p. 647-659.

Yan, P., Wang, L., and Wang, Y., 2014a, Late Mesozoic compressional folds in Dongsha Waters, the northern margin of the South China Sea: Tectonophysics, v. 615-616, p. 213-223.

Yan, P., Zhou, D., and Liu, Z., 2001a, A crustal structure profile across the northern continental margin of the South China Sea: Tectonophysics, v. 338, no. 1, p. 1-21.

Yan, P., Zhou, D., and Liu, Z. S., 2001b, A crustal structure profile across the northern continental margin of the South China Sea: Tectonophysics, v. 338, no. 1, p. 1-21.

Yan, Q., Shi, X., and Castillo, P. R., 2014b, The late Mesozoic-Cenozoic tectonic evolution of the South China Sea: A petrologic perspective: Journal of Asian Earth Sciences, v. 85, p. 178-201.

Yan, Q., Shi, X., Liu, J., Wang, K., and Bu, W., 2010, Petrology and geochemistry of Mesozoic granitic rocks from the Nansha micro-block, the South China Sea: Constraints on the basement nature: Journal of Asian Earth Sciences, v. 37, no. 2, p. 130-139.

Yang, F., Huang, X.-L., Xu, Y.-G., and He, P.-L., 2019, Plume-ridge interaction in the South China Sea: Thermometric evidence from Hole U1431E of IODP Expedition 349: Lithos, v. 324-325, p. 466-478.

Yao, Y., Liu, H., Yang, C., Han, B., Tian, J., Yin, Z., Gong, J., and Xu, Q., 2012, Characteristics and evolution of Cenozoic sediments in the Liyue Basin, SE South China Sea: Journal of Asian Earth Sciences, v. 60, p. 114-129.

Ye, Q., Mei, L., Shi, H., Du, J., Deng, P., Shu, Y., and Camanni, G., 2020, The influence of pre-existing basement faults on the Cenozoic structure and evolution of the proximal domain, northern South China Sea rifted margin: Tectonics.

Ye, Q., Mei, L., Shi, H., Shu, Y., Camanni, G., and Wu, J., 2018, A low-angle normal fault and basement structures within the Enping Sag, Pearl River Mouth Basin: Insights into late Mesozoic to early Cenozoic tectonic evolution of the South China Sea area: Tectonophysics, v. 731-732, p. 1-16.

Yu, J., Yan, P., Wang, Y., Zhang, J., Qiu, Y., Pubellier, M., and Delescluse, M., 2018a, Seismic Evidence for Tectonically Dominated Seafloor Spreading in the Southwest Sub-basin of the South China Sea: Geochemistry, Geophysics, Geosystems, v. 19, no. 9, p. 3459-3477.

Yu, M., Yan, Y., Huang, C.-Y., Zhang, X., Tian, Z., Chen, W.-H., and Santosh, M., 2018b, Opening of the South China Sea and Upwelling of the Hainan Plume: Geophysical Research Letters, v. 45, no. 6, p. 2600-2609.

Zahirovic, S., Seton, M., and Müller, R. D., 2014, The Cretaceous and Cenozoic tectonic evolution of Southeast Asia: Solid Earth, v. 5, no. 1, p. 227-273.

Zakaria, A. A., Johnson, H. D., Jackson, C. A. L., and Tongkul, F., 2013, Sedimentary facies analysis and depositional model of the Palaeogene West Crocker submarine fan system, NW Borneo: Journal of Asian Earth Sciences, v. 76, p. 283-300.

Zaw, K. L., Setijadji, L. D., Wardana, I. W., and Watanabe, K., 2011, Petrogenetic Interpretation of Granitoid Rocks Using Multicationic Parameters in The Sanggau Area, Kalimantan Island, Indonesia: Journal of South East Asian Applied Geologi, v. 3, no. 1, p. 45-53.

Zenonos, A., De Siena, L., Widiyantoro, S., and Rawlinson, N., 2019, P and S wave travel time tomography of the SE Asia-Australia collision zone: Physics of the Earth and Planetary Interiors.

Zhang, G., Shao, L., Qiao, P., Cao, L., Pang, X., Zhao, Z., Xiang, X., Cui, Y., et al., 2019a, Cretaceous–Palaeogene sedimentary evolution of the South China Sea region: A preliminary synthesis: Geological Journal.

Zhang, Q., Guo, F., Zhao, L., and Wu, Y., 2017, Geodynamics of divergent double subduction: 3-D numerical modeling of a Cenozoic example in the Molucca Sea region, Indonesia: Journal of Geophysical Research: Solid Earth, v. 122, no. 5, p. 3977-3998.

Zhang, X., Chung, S.-L., Lai, Y.-M., Ghani, A. A., Murtadha, S., Lee, H.-Y., and Hsu, C.-C., 2019b, A 6000-km-long Neo-Tethyan arc system with coherent magmatic flare-ups and lulls in South Asia: Geology, v. 47, no. 6, p. 573-576.

Zhang, Y., Sun, Z., Zhang, J., and Wang, L., 2019c, The structure, depositional style and accumulation characteristics of continental margin with diachronous breakup in the northern South China Sea: International Geology Review, p. 1-13.

Zhao, F., Alves, T. M., Wu, S., Li, W., Huuse, M., Mi, L., Sun, Q., and Ma, B., 2016, Prolonged post-rift magmatism on highly extended crust of divergent continental margins (Baiyun Sag, South China Sea): Earth and Planetary Science Letters, v. 445, p. 79-91.

Zhao, M., He, E., Sibuet, J.-C., Sun, L., Qiu, X., Tan, P., and Wang, J., 2018a, Postseafloor Spreading Volcanism in the Central East South China Sea and Its Formation Through an Extremely Thin Oceanic Crust: Geochemistry, Geophysics, Geosystems, v. 19, no. 3, p. 621-641.

Zhao, Y., Zhang, S.-H., Xu, G., Yang, Z., and Hu, J.-M., 2004, The Jurassic major tectonic events of the Yanshan intraplate deformation belt: Geological Bulletin of China, v. 23, p. 854-863.

Zhao, Z., Sun, Z., Sun, L., Wang, Z., and Sun, Z., 2018b, Cenozoic tectonic subsidence in the Qiongdongnan Basin, northern South China Sea: Basin Research, v. 30, p. 269-288.

Zhao, Z., Sun, Z., Wang, Z., Sun, Z., Liu, J., and Zhang, C., 2015, The high resolution sedimentary filling in Qiongdongnan Basin, Northern South China Sea: Marine Geology, v. 361, p. 11-24.

Zheng, H., Zhong, L.-F., Kapsiotis, A., Cai, G.-Q., Wan, Z.-F., and Xia, B., 2019, Post-spreading Basalts from the Nanyue Seamount: Implications for the Involvement of Crustal- and Plume-Type Components in the Genesis of the South China Sea Mantle: Minerals, v. 9, no. 6, p. 378.

Zhou, B., Du, B., Wang, Z. L., Tang, Y., and Du, B. D., 2006, Effects of various durations of noise exposure on auditory brainstem response and distortion product otoacoustic emissions in rats: Journal of Jilin University Medicine Edition, v. 32, no. 1, p. 26-30.

Zhou, D., 2014, Marginal Seas, in Harff, J., Meschede, M., Petersen, S., and Thiede, J., eds., Encyclopedia of Earth Sciences Series, Springer, Dordrecht, p. 1-7.

Zhou, D., Ru, K., and Chen, H.-z., 1995, Kinematics of Cenozoic extension on the South China Sea continental margin and its implications for the tectonic evolution of the region: Tectonophysics, v. 251, no. 1-4, p. 161-177.

Zhou, W., Gao, X., Wang, Y., Zhuo, H., Zhu, W., Xu, Q., and Wang, Y., 2015, Seismic geomorphology and lithology of the early Miocene Pearl River Deepwater Fan System in the Pearl River Mouth Basin, northern South China Sea: Marine and Petroleum Geology, v. 68, Part A, p. 449-469.

Zhuo, H., Wang, Y., Sun, Z., Wang, Y., Xu, Q., Hou, P., Wang, X., Zhao, Z., et al., 2018, Along-strike variability in shelf-margin morphology and accretion pattern: An example from the northern margin of the South China Sea: Basin Research, v. 31, no. 3, p. 431-460.

Appendix

A.1 Re-interpretation of MCS profiles in Pearl River Mouth Basin, Phu Khanh Basin, and Nam Con Son Basin

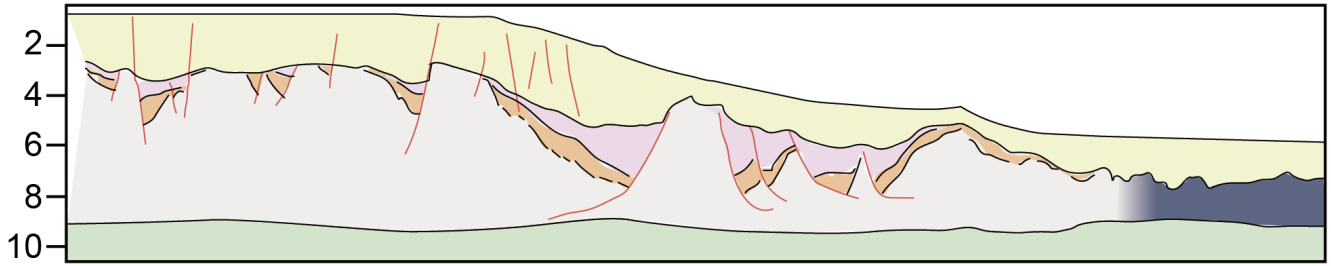

Figure A.1.1. Tectonostratigraphy in the Peral River Mouth Basin. Modified from Xie et al. (2019).

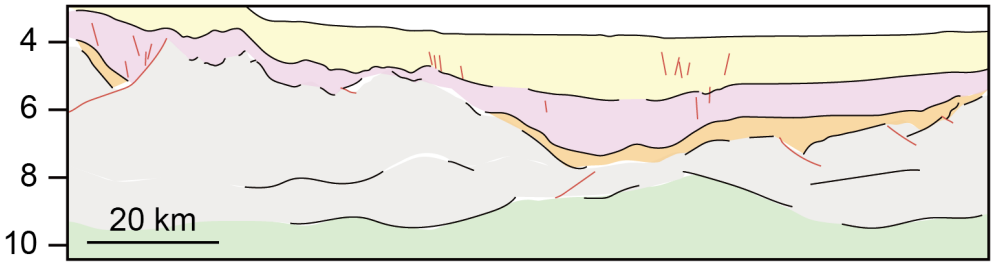

Figure A.1.2. Tectonostratigraphy in the Phu Khank Basin. Modified from Savva et al. (2013).

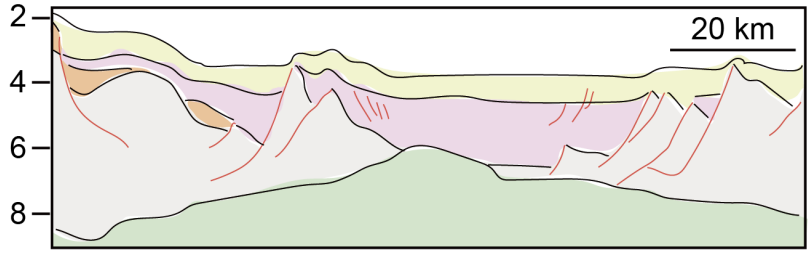

Figure A.1.3. Tectonostratigraphy in the Nam Con Son Basin (Clerc et al., 2018).

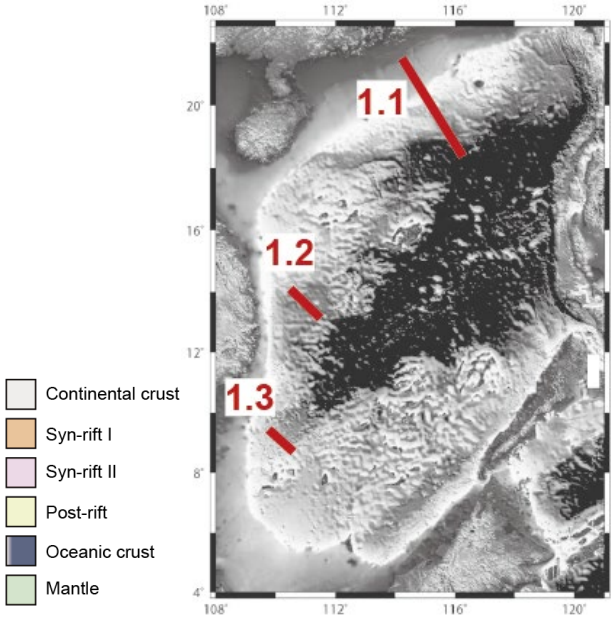

A.2 Bio-stratigraphy results in Kudat Peninsula

CLIENT:	UTP
FILE REF:	GS007_UTP
REPORT NO:	GS007_UTP
STATUS:	CONFIDENTIAL
DISTRIBUTION:	UTP

LABORATORY RESULTS REPORT

LABORATORY RESULTS REPORT
FOR
KUDAT OUTCROP, SARAWAK

PREPARED FOR
UNIVERSITI TEKNOLOGI PETRONAS

March, 2018

LABORATORY RESULTS REPORT

Our Ref : GS007_UTP
Date : 6th March 2017
Client : Universiti Teknologi PETRONAS

SAMPLE DESCRIPTION:
Three (3) outcrops samples were received with details as the following:

SAMPLE LABEL:

NO.	SAMPLE LABLE	LOCALITY
1.	KDT-04	KUDAT
2.	KDT-05	KUDAT
3.	KDT-06	KUDAT

Table 1: Sample list.

ANALYSIS CONDUCTED:
As requested by client, the purpose of this document is to report the results of the following analysis:

NO.	SAMPLE	ANALYSIS	
		NANNO	PALY
1.	KDT-04	1	1
2.	KDT-05	1	
3.	KDT-06	1	

Table 2: Number of samples & types analysis.

LABORATORY ANALYSIS RESULTS

NANNOFOSSILS ANALYSIS

Nannofossils Samples & Data

Samp No.	Samp Lable	Sample Type	Preservation	NANNOFOSSIL / NANNO ZONE						Total NN	Total no. of species (NN)
				NN21 / 20	NN15	NN12	NN6				
				Reticulofenestra minuta	*Sphenolithus abies*	*Ceratolithus acutus*	*Cyclicargolithus floridanus*	*Ceratolithus* spp.	*Sphenolithus* spp.		
1	KDT-04	OC	poor	1	1	1	1	1	2	7	6
2	KDT-05	OC	poor				1			1	1
3	KDT-06	OC	barren							0	0

*Note:
OC Outcrop
NN Nannofossils

Table 3: Nannofossils component of the Kudat outcrop

Nannofossils Results

Samples	Nanno NN zone	Age	Interpretation
KDT-04	NN6	Middle Miocene	Based on the occurrence of *Cyclicargolithus floridanus*.
KDT-05	NN6	Middle Miocene	Based on the occurrence of *Cyclicargolithus floridanus*.
KDT-06	indeterminate	indeterminate	Barren.

Table 4: Nannofossils interpretation.

PALYNOLOGY ANALYSIS

Palynology Samples & Data

Analysis of palynology was conducted on sample labeled KDT-04. Standard sample preparation was employed entailing acid digestion and heavy liquid preparation. High concentration of hydrofluoric acid was used to eliminate silicate mineral, followed by hydrochloric acid to eliminate carbonate minerals. The remaining residue after acid digestion was separated using heavy liquid to obtain organic residue which was further treated with low concentration of nitric acid and potassium hydroxide for oxidation processes.

Three prepared slides were scanned under transmitted light microscope for palynomorph identification. The sample failed to yield any palynomorph for further age determination and evaluation. In addition, no spore taxa were discovered which precluded thermal alteration index (TAI) interpretation. The sample is overwhelmed by dark to dark brown woody tissue including black and opaque phytoclast with various shape and size ranging from equidimensional, unstructured and blade in shape. This assemblage of organic material is equivalent to inertinite-vitrinite type of maceral.

Palynology Results

Samples	Paly Zone	Age
KDT-04	indeterminate	indeterminate

Table 5: Palynology interpretation.

1. KDT-04
2. KDT-05
3. KDT-06

Figure 1: Location map and sample labels.

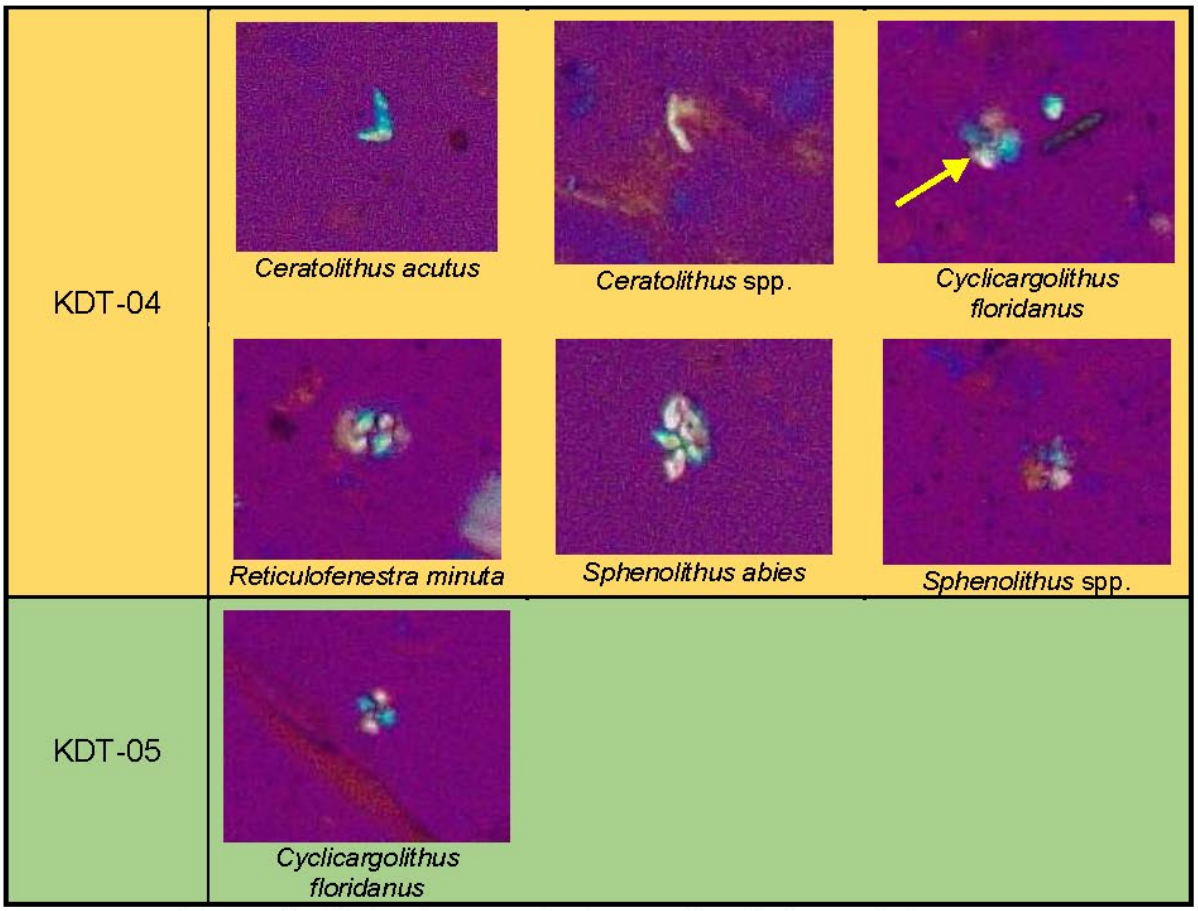

Figure 2: Photomicrograph of nannofossils from study area.

A.3 Sediment analyses in sedimentary mélange

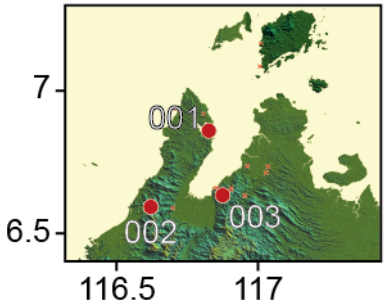

Sample no. 001

Table A.1.1. XRF analysis results.

Z	Formula	Concentration	Status	Line 1	Stat. error	Net int.LLD	Analyzed layer	XRF %	
14	Si	48.00%	XRF 1	Si KA1-HR-Tr	0.45%	161.7	142.8 PPM	3.7 um	47.98
26	Fe	20.70%	XRF 1	Fe KA1-HR-Tr	0.21%	720.5	183.1 PPM	37 um	20.68
13	Al	13.80%	XRF 1	Al KA1-HR-Tr	0.96%	34.71	147.4 PPM	3.5 um	13.8
19	K	10.40%	XRF 1	K KA1-HR-Tr	0.65%	76.64	90.2 PPM	8.3 um	10.4
22	Ti	1.76%	XRF 1	Ti KA1-HR-Tr	1.38%	17.37	99.6 PPM	14.7 um	1.76
20	Ca	1.65%	XRF 1	Ca KA1-HR-Tr	1.64%	12.26	237.5 PPM	8.9 um	1.65
12	Mg	1.48%	XRF 1	Mg KA1-HR-Tr	3.95%	2.766	276.0 PPM	2.40 um	1.48
15	P	0.99%	XRF 1	P KA1-HR-Tr	3.13%	3.617	171.2 PPM	2.28 um	0.994
11	Na	0.27%	XRF 1	Na KA1-HR-Tr	22.50%	0.1493	760.8 PPM	1.52 um	0.27
16	S	0.23%	XRF 1	S KA1-HR-Tr	5.38%	1.743	134.1 PPM	3.1 um	0.234
25	Mn	0.16%	XRF 1	Mn KA1-HR-Tr	3.55%	3.901	64.6 PPM	29.4 um	0.156
40	Zr	0.14%	XRF 2	Zr KA1-HR-Tr	1.86%	21.43	45.1 PPM	254 um	0.14
37	Rb	0.11%	XRF 1	Rb KA1-HR-Tr	1.82%	19.28	29.6 PPM	160 um	0.108

56	Ba	0.08%	XRF 1	Ba LA1-HR-Tr	13.30%	0.447	665.0 PPM	14.3 um	0.077
30	Zn	0.07%	XRF 1	Zn KA1-HR-Tr	3.91%	4.805	39.5 PPM	47 um	0.0744
38	Sr	0.06%	XRF 1	Sr KA1-HR-Tr	2.95%	10.97	24.5 PPM	188 um	0.0551
29	Cu	0.04%	XRF 1	Cu KA1-HR-Tr	7.16%	2.111	44.8 PPM	39 um	0.041
23	V	0.03%	XRF 1	V KA1-HR-Tr	20.90%	0.909	199.3 PPM	19.0 um	0.03
28	Ni	0.03%	XRF 1	Ni KA1-HR-Tr	11.20%	1.13	49.5 PPM	32 um	0.028
31	Ga	0.02%	XRF 1	Ga KA1-HR-Tr	13.50%	1.215	39.7 PPM	57 um	0.016
24	Cr	0.02%	XRF 1	Cr KA1-HR-Tr	17.10%	0.4515	115.2 PPM	23.2 um	0.015

SEM images:

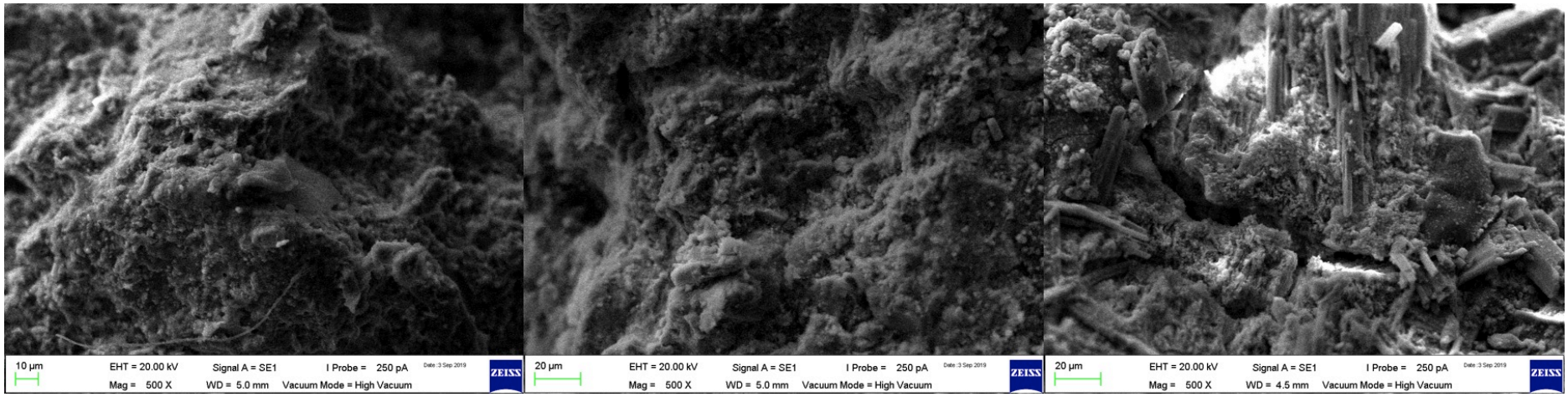

Sample no. 002 (XRD result)

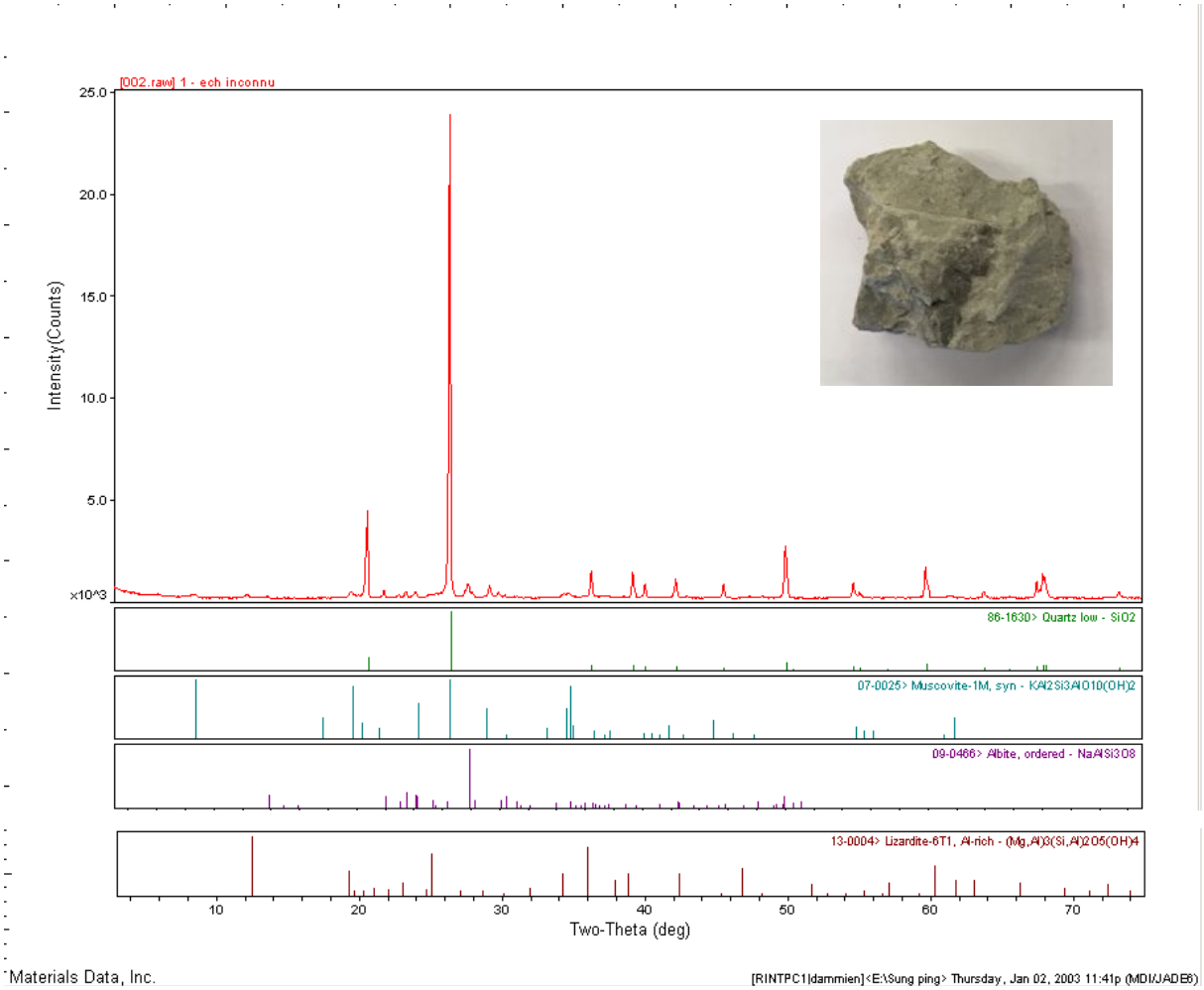

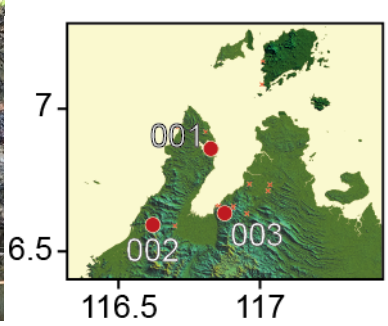

Sample no. 003 (XRD result)

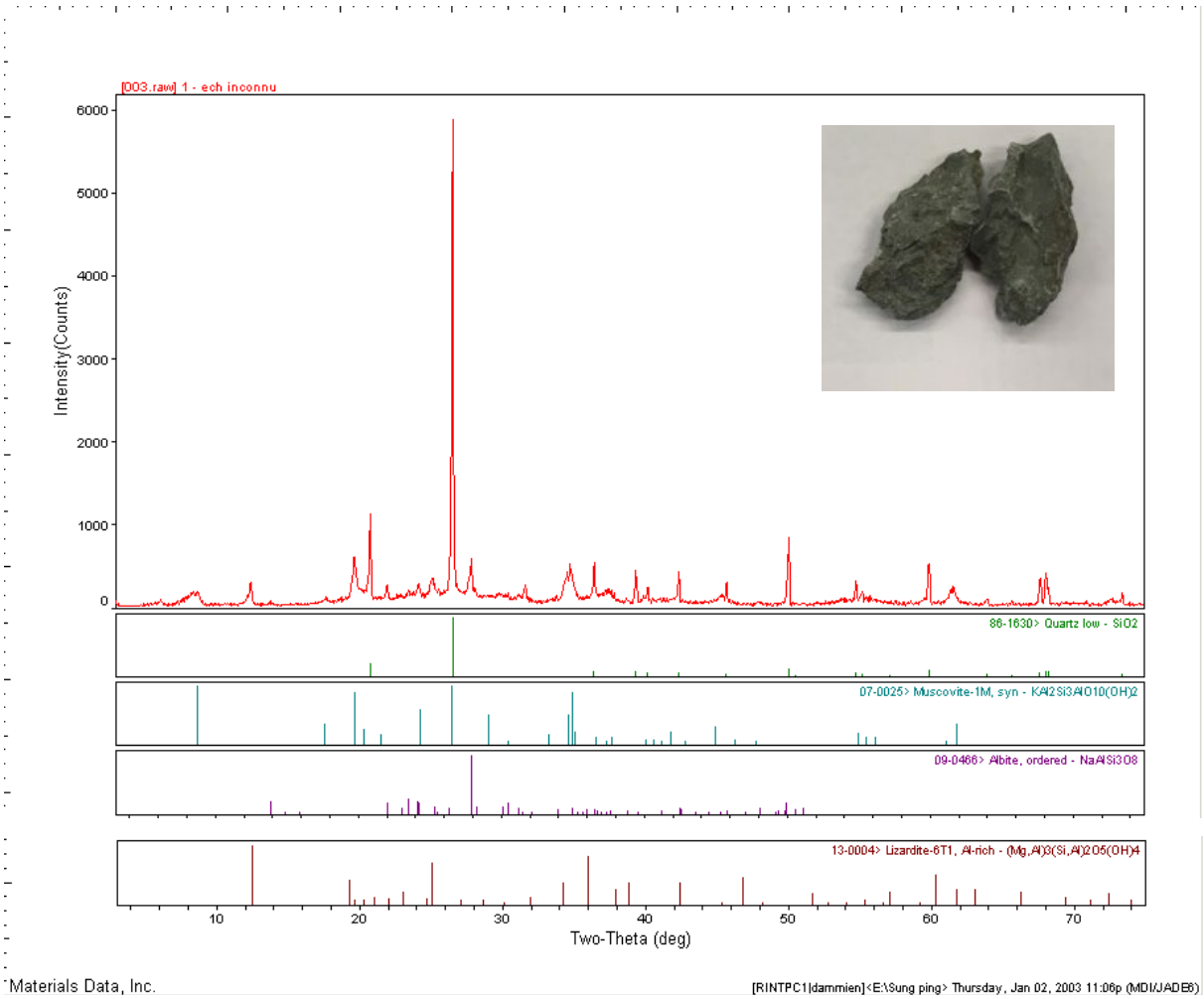

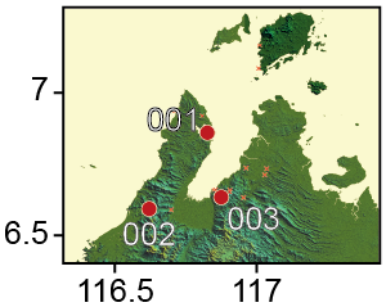

Plate convergence is accommodated by subduction process, and may in turn influence the downgoing plate and create new basins. This study focuses on the basin evolution of a unique marginal sea located in the South China Sea to evaluate the relation with the adjacent Proto-South China Sea subduction zone in terms of sedimentary infill and crustal structures in the Cenozoic time. The basin has a V shape and its rifted margins display a hyper-extended continental crust whose extensional direction varied from North-South to Northwest-Southeast. The coincident differential closure of the adjacent Proto South China Sea and the lateral variation of the crustal nature and thickness created a rotation of the continental margin. These observation allow us to explore some of the boundary forces which are inherent to geodynamics of subduction.

La convergence des plaques s'effectue par subduction, mais peut à son tour influencer la plaque plongeante et créer de nouveaux bassins. Cette étude se concentre sur l'évolution du bassin d'une mer marginale unique, la Mer de Chine Méridionale dont le contexte permet d'appréhender la relation avec la zone de subduction du bassin adjacente ; la Proto-Mer de Chine du Sud, en termes de remplissage sédimentaire et de structures crustales au Cénozoïque. Le bassin a une forme en V et ses marges déchirées présentent une croûte continentale hyper-étendue dont la direction d'extension varie du nord-sud au nord-ouest-sud-est. La fermeture différentielle coïncidente de la Proto-Mer de Chine concomitante, et la variation latérale de la nature et de l'épaisseur de la croûte, ont généré une rotation de la marge continentale sud de la MDC. Ces observations nous permettent d'explorer certaines des forces aux limites inhérentes à la géodynamique de la subduction.